Precision calculations for the low-energy dynamics of pions and nucleons

Dissertation

zur

Erlangung des Doktorgrades (Dr. rer. nat.)

der

Mathematisch-Naturwissenschaftlichen Fakultät

der

Rheinischen Friedrich-Wilhelms-Universität Bonn

vorgelegt von

Martin Hoferichter

aus

Bonn–Bad Godesberg

Bonn, Mai 2012

Angefertigt mit Genehmigung der
Mathematisch-Naturwissenschaftlichen Fakultät der
Rheinischen Friedrich-Wilhelms-Universität Bonn

Diese Dissertation ist auf dem Hochschulschriftenserver der ULB Bonn unter
`http://hss.ulb.uni-bonn.de/diss_online` elektronisch publiziert.

1. Gutachter: Prof. Dr. Ulf-G. Meißner

2. Gutachter: Prof. Dr. Hans-Werner Hammer

Tag der Promotion: 12.07.2012

Erscheinungsjahr: 2012

Abstract

QCD is strongly coupled at long distances and therefore non-perturbative methods are required to understand its low-energy properties, e.g. to answer such basic questions as of the origin of the nucleon mass. In this thesis we study the interplay of effective field theories and dispersion relations in the description of strong and electromagnetic interactions of pions and nucleons.

In the first part, we use chiral perturbation theory to calculate the π^-–deuteron scattering length to a few-percent accuracy including isospin-violating corrections. We apply the result to perform a combined analysis of data on pionic deuterium and pionic hydrogen atoms that leads to a precision determination of the isoscalar and isovector pion–nucleon scattering lengths, and discuss the consequences for the πN coupling constant and the pion–nucleon σ term.

In the second part, we derive a system of Roy–Steiner equations for pion Compton scattering that respects analyticity, unitarity, gauge invariance, and crossing symmetry, and thus maintains all symmetries of the underlying quantum field theory. To suppress the dependence on the high-energy input, we also consider subtracted versions of the equations, identifying the subtraction constants with pion polarizabilities. Based on the assumption of Mandelstam analyticity, we determine the kinematic range in which the equations are valid. We solve for the $\gamma\gamma \to \pi\pi$ partial waves using a Muskhelishvili–Omnès representation and derive a correlation between the two-photon coupling of the σ resonance and the isospin-zero pion polarizabilities, which, in combination with chiral perturbation theory, provides new rigorous constraints on the $\sigma \to \gamma\gamma$ coupling.

In the final part, we construct a similar system of Roy–Steiner equations for pion–nucleon scattering. We study the solution of the $\bar{N}N \to \pi\pi$ partial waves by Muskhelishvili–Omnès techniques, taking into account coupled-channel effects in the case of the S-wave, and apply the results to a two-channel dispersive calculation of the scalar form factor of the nucleon. We develop a solution strategy for the pion–nucleon s-channel partial waves and determine the corrections needed for the extraction of the pion–nucleon σ term from the extrapolation of the πN amplitude to the Cheng–Dashen point by means of a low-energy theorem.

Parts of this thesis have been published in the following articles:

- V. Baru, C. Hanhart, M. Hoferichter, B. Kubis, A. Nogga, and D. R. Phillips, *Precision calculation of the $\pi^- d$ scattering length and its impact on threshold πN scattering*, Phys. Lett. B **694** (2011) 473.

- V. Baru, C. Hanhart, M. Hoferichter, B. Kubis, A. Nogga, and D. R. Phillips, *Precision calculation of threshold $\pi^- d$ scattering, πN scattering lengths, and the GMO sum rule*, Nucl. Phys. A **872** (2011) 69.

- M. Hoferichter, D. R. Phillips, and C. Schat, *Roy–Steiner equations for $\gamma\gamma \to \pi\pi$*, Eur. Phys. J. C **71** (2011) 1743.

- C. Ditsche, M. Hoferichter, B. Kubis, and U.-G. Meißner, *Roy–Steiner equations for pion–nucleon scattering*, JHEP **1206** (2012) 043.

- M. Hoferichter, C. Ditsche, B. Kubis, and U.-G. Meißner, *Dispersive analysis of the scalar form factor of the nucleon*, JHEP **1206** (2012) 063.

Contents

Chapter 1

Introduction

Since its discovery nearly four decades ago, the Standard Model of particle physics has withstood innumerable challenges from experiment, both in direct searches at high-energy colliders and at the intensity frontier, e.g. in the study of CP asymmetries, rare decays, and searches for electric dipole moments. It is striking that despite this impressive success, quantum chromodynamics (QCD), the theory of strong interactions and one of the pillars of the Standard Model, is still poorly understood in the low-energy regime.

First written down by Fritzsch, Gell-Mann, and Leutwyler to realize the color degree of freedom of strong interactions in terms of a Yang–Mills gauge theory [1], it was subsequently shown that the Lagrangian of QCD fulfills the property of asymptotic freedom [2], i.e. its coupling constant α_s decreases with increasing energy. Put another way, the β-function of QCD

$$\beta_\mathrm{QCD} = -\left(11 - \frac{2n_\mathrm{f}}{3}\right)\frac{g^3}{16\pi^2} + \mathcal{O}\big(g^5\big) \,, \qquad \alpha_\mathrm{s} = \frac{g^2}{4\pi} \,, \tag{1.1}$$

is negative as long as the number of flavors n_f is not too large, a discovery for which the Nobel prize was awarded to Gross, Politzer, and Wilczek in 2004. Over the last forty years it has become unequivocally clear that QCD is indeed the correct theory of strong interactions (for a recent review, see [3]). In particular, the running coupling $\alpha_\mathrm{s}(\mu)$ has been extracted from a myriad of different processes, leading to the world average [4, 5]

$$\alpha_\mathrm{s}(M_\mathrm{Z}) = 0.1184 \pm 0.0007 \,, \tag{1.2}$$

where the renormalization scale μ has been chosen as the mass of the Z boson $\mu = M_\mathrm{Z}$. Moreover, the scale dependence of the coupling agrees well with its expected QCD running, as shown in Fig. 1.1 for the energy scale $\mu = Q$ varying over two orders of magnitude. In this sense, QCD is well understood at energies where α_s is sufficiently small to allow for a meaningful perturbative expansion. In contrast, the negative sign of the β-function (1.1) renders QCD strongly coupled at low energies, so that perturbation theory fails and non-perturbative, model-independent methods are called for.

A particularly instructive example for the prominent role of non-perturbative phenomena in low-energy QCD is provided by the origin of mass. In the limit of massless quarks, the QCD Lagrangian exhibits a classical scale invariance with conserved Noether current

$$J^\mu_\mathrm{scale} = x_\nu \theta^{\mu\nu} \,. \tag{1.3}$$

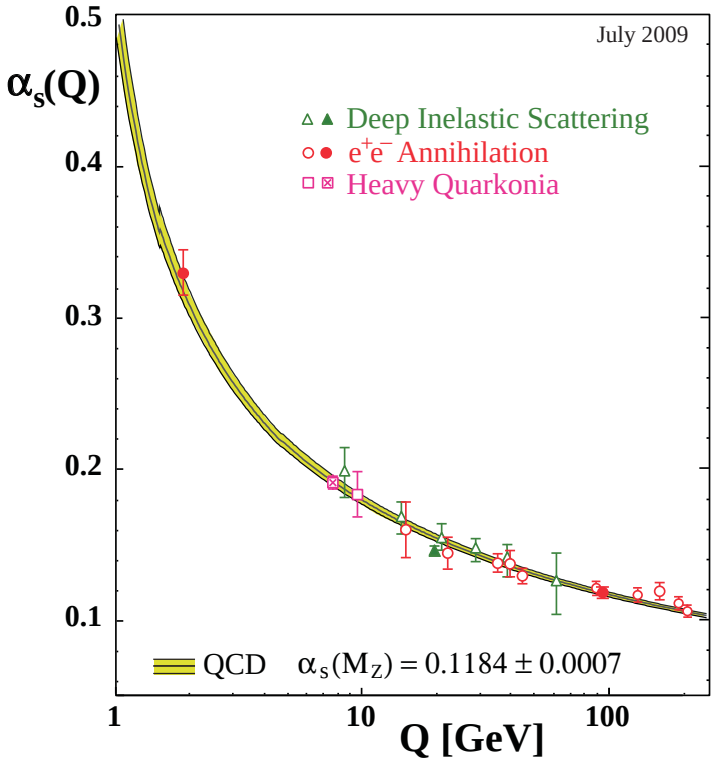

Figure 1.1: Running of the strong coupling α_s compared to determinations from deep inelastic scattering, e^+e^- annihilation, and heavy quarkonia. Figure taken from [4], with kind permission from Springer Science and Business Media.

Since the energy-momentum tensor $\theta^{\mu\nu}$ itself is conserved, this implies immediately that the trace θ^μ_μ and thus the masses of hadrons vanish as well. However, classical scale invariance is broken at the quantum level and the associated trace anomaly causes hadrons to remain massive even in the absence of quark masses. Indeed, switching on quark-mass effects again, the mass of the nucleon m can be decomposed as [6]

$$m = \frac{1}{2m}\langle N(p)|\theta^\mu_\mu|N(p)\rangle = \frac{1}{2m}\langle N(p)|\frac{\beta_{\rm QCD}}{2g}F^a_{\mu\nu}F^{\mu\nu}_a + m_{\rm u}\bar{u}u + m_{\rm d}\bar{d}d + m_{\rm s}\bar{s}s + \cdots|N(p)\rangle \ , \quad (1.4)$$

where $N(p)$ denotes the nucleon states, u, d, s the light quark fields with masses $m_{\rm u}$, $m_{\rm d}$, $m_{\rm s}$, and the ellipsis contributions from the heavy quarks. The trace anomaly thus manifests itself in the term involving the field strength tensor $F^{\mu\nu}_a$ and the QCD β-function. Although an accurate determination of the individual terms in (1.4), especially of the strangeness content due to $m_{\rm s}\bar{s}s$, is still an open problem, the overall hierarchy has been well established and constitutes an integral result of QCD: the bulk of the nucleon mass is generated by gluonic self-interactions, while strange and non-strange quarks vie for a distant second place.[1] In this way, the mass of matter surrounding us in our everyday life is not generated by the Higgs mechanism, but by the trace anomaly of the QCD energy-momentum tensor and thus non-perturbative QCD dynamics in form of the gluon field energy.

[1] At present, it is not possible to definitely settle the matter whether strange or non-strange contributions prevail. We will return to this issue in the context of the pion–nucleon σ term in part III of this thesis.

For lack of a perturbative expansion in the coupling constant, the loop expansion in α_s has to be substituted by systematic, non-perturbative methods to gain insights into the low-energy realm of QCD. To this end, three complementary ansätze have been developed over the last decades: effective field theories, which rely on symmetries and a separation of scales in the system at hand, dispersion relations, which exploit analyticity and unitarity requirements of the amplitude describing the system, and lattice QCD, an ab initio method aimed at solving a discretized version of the theory on a computer. In recent years, substantial progress in our knowledge of low-energy QCD has been achieved by realizing that frequently the applicability and accuracy of these techniques can be improved significantly if combined with one another. In this work, we concentrate on the interplay between effective field theories and dispersion relations in the description of the dynamics in the pion–nucleon (πN) system and $\gamma\gamma \to \pi\pi$ to pave the way towards a precise understanding of these fundamental processes in low-energy hadron physics.

The structure of this thesis is as follows: in Sects. 1.1 and 1.2 we give a brief introduction into effective field theories and dispersion relations. To illustrate the merits of combining both techniques we discuss the matching of $\pi\pi$ Roy equations and chiral perturbation theory (ChPT). Part I is devoted to a high-accuracy extraction of the S-wave πN scattering lengths from hadronic-atom data that relies on ChPT to calculate the required corrections to the πN and pion–deuteron (πd) amplitudes, as well as a determination of the πN coupling constant by means of the Goldberger–Miyazawa–Oehme (GMO) sum rule. In Part II we derive a system of Roy–Steiner (RS) equations for $\gamma\gamma \to \pi\pi$. On the one hand, this process bears several similarities to πN scattering and can thus be considered as a first step towards the construction (and solution) of RS equations for the πN case. On the other hand, $\gamma\gamma \to \pi\pi$ is interesting on its own, since RS equations in combination with ChPT can be used to derive rigorous constraints on the two-photon coupling of the σ meson and provide a framework to extract pion polarizabilities from forthcoming low-energy $\gamma\gamma \to \pi\pi$ cross-section data. In Part III we write down a system of RS equations for πN scattering. We solve the t-channel equations using one- and two-channel Muskhelishvili–Omnès (MO) methods and apply the results to perform a full two-channel dispersive analysis of the scalar form factor of the nucleon. Finally, we lay out a strategy to solve the s-channel equations involving sum rules for the πN threshold parameters as well as the hadronic-atom values for the S-wave scattering lengths, and show how the pion–nucleon σ term can be extracted from a full solution of the RS system.

1.1 Effective field theories

The starting point of any effective field theory (EFT) is Weinberg's conjecture [7] that field theory has no content besides analyticity, unitarity, cluster decomposition, and the assumed symmetry principles.[2] Accordingly, the Lagrangian of the EFT is constructed in terms of the low-energy degrees of freedom as the most general Lagrangian compatible with the symmetries of the theory. The expansion parameter of the EFT will be determined by the ratio of low- and high-energy scales, so that a good scale separation is crucial for the success of the EFT. Formally, this follows from the power-counting argument: the effective Lagrangian is organized as a series of operators suppressed by higher and higher powers in the expansion parameter, accompanied by a priori unknown low-energy constants (LECs) that parameter-

[2] It has been proven for Lorentz-invariant, anomaly-free theories that the effective Lagrangian can indeed be derived from the Ward identities of the theory [8].

ize the influence of high-energy degrees of freedom not explicitly included in the theory and have to be determined from experiment (or from lattice simulations). Evidently, the smaller the expansion parameter, the smaller the number of free parameters required for the desired accuracy, and thus the higher the predictive power. One particular strength of an EFT is that it relates different physical processes, so that the LECs determined in one process can subsequently be used to predict another. In addition, the EFT expansion is systematically improvable by calculating the next order in the power counting, while the parametrical suppression of the first order not included provides an accuracy estimate of the calculation. For a detailed introduction to the concept of effective field theories we refer to [9].

1.1.1 Chiral symmetry

The Lagrangian of QCD reads

$$\mathcal{L}_{\mathrm{QCD}} = \bar{q}\left(i\not{D} - \mathcal{M}\right) q - \frac{1}{4} F^a_{\mu\nu} F_a^{\mu\nu} + \theta \frac{g^2}{32\pi^2} F^a_{\mu\nu} \tilde{F}_a^{\mu\nu} \,, \tag{1.5}$$

where $q = (u, d, s, \ldots)^T$ contains the quark fields and $\mathcal{M} = \mathrm{diag}\,(m_{\mathrm{u}}, m_{\mathrm{d}}, m_{\mathrm{s}}, \ldots)$ the quark masses. The gauge bosons A^a_μ (in the adjoint representation of $SU(3)$, $a = 1 \ldots 8$) enter through the covariant derivative

$$D^\mu = \partial^\mu - ig \frac{\lambda_a}{2} A^\mu_a \tag{1.6}$$

and the field strength tensor

$$F^{\mu\nu}_a = \partial^\mu A^\nu_a - \partial^\nu A^\mu_a + g f_{abc} A^\mu_b A^\nu_c \,, \qquad \left[\lambda_a, \lambda_b\right] = 2i f_{abc} \lambda_c \,, \tag{1.7}$$

where λ_a are the Gell-Mann matrices and g denotes the coupling constant of QCD as introduced in (1.1). For completeness, we have included in (1.5) also the QCD θ-term, which involves the dual field strength tensor $\tilde{F}^{\mu\nu}_a = \frac{1}{2}\epsilon^{\mu\nu\alpha\beta} F^a_{\alpha\beta}$ and is related to strong CP violation, although in the following we will put $\theta = 0$.

Written in terms of left- and right-handed fields

$$q_{R/L} = \frac{1 \pm \gamma_5}{2} q \,, \tag{1.8}$$

it becomes manifest that the QCD Lagrangian

$$\mathcal{L}_{\mathrm{QCD}} = \bar{q}_L i\not{D} q_L + \bar{q}_R i\not{D} q_R - \bar{q}_L \mathcal{M} q_R - \bar{q}_R \mathcal{M} q_L - \frac{1}{4} F^a_{\mu\nu} F_a^{\mu\nu} \tag{1.9}$$

displays an additional symmetry, i.e. invariance under global rotations in flavor space

$$q_R \to U_R q_R \,, \qquad q_L \to U_L q_L \,, \qquad U_{R/L} \in U(n_{\mathrm{f}})_{R/L} \,, \tag{1.10}$$

in the chiral limit where the mass term is switched off. More precisely, these transformations factorize according to

$$U(n_{\mathrm{f}})_L \times U(n_{\mathrm{f}})_R \to SU(n_{\mathrm{f}})_L \times SU(n_{\mathrm{f}})_R \times U(1)_V \times U(1)_A \,, \tag{1.11}$$

where $U(1)_V$ corresponds to baryon number conservation and $U(1)_A$ is anomalously broken [10]. Finally, chiral symmetry is realized in the Goldstone rather than the Wigner–Weyl mode, as the remaining symmetry group is spontaneously broken to its vectorial subgroup

$$SU(n_{\mathrm{f}})_L \times SU(n_{\mathrm{f}})_R = SU(n_{\mathrm{f}})_V \times SU(n_{\mathrm{f}})_A \to SU(n_{\mathrm{f}})_V \,. \tag{1.12}$$

In practice, chiral symmetry is only meaningful for $n_\mathrm{f} = 2$ or $n_\mathrm{f} = 3$, while the heavy quarks are integrated out at low energies. The Goldstone bosons [11] corresponding to the broken generators of $SU(n_\mathrm{f})_A$ can be identified with the pion triplet or the pseudoscalar octet of pions, kaons, and η, respectively. Since chiral symmetry is only an approximate symmetry—the masses of the light quarks are small compared to the typical scale of chiral symmetry breaking $\Lambda_\chi \sim 1\,\mathrm{GeV}$—chiral symmetry is also explicitly broken and these mesons actually acquire a finite mass. In this thesis, we will mainly be concerned with the case $n_\mathrm{f} = 2$, where the mass of the strange quark is fixed at its physical value and only up and down quarks are retained as dynamical degrees of freedom.

1.1.2 Chiral perturbation theory

Chiral perturbation theory is the effective field theory of strong interactions. First developed by Weinberg, Gasser, and Leutwyler [7, 12, 13], it exploits chiral symmetry and provides an expansion of Green functions in terms of quark masses and soft particle momenta p.[3] The effective Lagrangian is constructed as the most general Lagrangian consistent with chiral symmetry. Its basic building blocks in the $SU(2)$ version of the theory are the pion fields

$$\boldsymbol{\tau}\cdot\boldsymbol{\pi} = \begin{pmatrix} \pi^0 & \sqrt{2}\,\pi^+ \\ \sqrt{2}\,\pi^- & -\pi^0 \end{pmatrix} \tag{1.13}$$

represented by a unitary matrix $U(\boldsymbol{\pi})$, e.g. in σ-model parameterization

$$U(\boldsymbol{\pi}) = \sqrt{1 - \frac{\boldsymbol{\pi}^2}{F^2}} + i\frac{\boldsymbol{\tau}\cdot\boldsymbol{\pi}}{F}\,, \tag{1.14}$$

where $\boldsymbol{\tau}$ are the Pauli matrices and F denotes the pion decay constant in the chiral limit. In addition, scalar (s), pseudoscalar (p), vector (v_μ), and axial-vector (a_μ) external sources may be introduced in the covariant derivative

$$d_\mu U = \partial_\mu U - i r_\mu U + i U l_\mu\,, \qquad r_\mu = v_\mu + a_\mu\,, \qquad l_\mu = v_\mu - a_\mu\,, \tag{1.15}$$

the field strength tensors

$$\mathcal{F}_\mathrm{R}^{\mu\nu} = \partial^\mu r^\nu - \partial^\nu r^\mu - i[r^\mu, r^\nu]\,, \qquad \mathcal{F}_\mathrm{L}^{\mu\nu} = \partial^\mu l^\nu - \partial^\nu l^\mu - i[l^\mu, l^\nu]\,, \tag{1.16}$$

and in

$$\chi = 2B(s + ip)\,, \qquad s = \mathcal{M} + \cdots\,. \tag{1.17}$$

In this way, the leading-order Lagrangian takes the form

$$\mathcal{L}_\pi^{(p^2)} = \frac{F^2}{4}\langle d^\mu U^\dagger d_\mu U + \chi^\dagger U + U^\dagger \chi\rangle\,, \tag{1.18}$$

where $\langle\ldots\rangle$ denotes the trace in flavor space. An immediate consequence of (1.18) is the Gell-Mann–Oakes–Renner relation $M_\pi^2 = B(m_\mathrm{u} + m_\mathrm{d})$ that relates the mass of the pion to the quark masses and the scalar quark condensate via $B = -\langle\bar{q}q\rangle/F^2$. In particular, it suggests that quark masses be counted as $\mathcal{O}(p^2)$, resulting in a simultaneous expansion in momenta

[3] A detailed review of various aspects of ChPT can be found in [14].

and quark masses.[4] Counting meson propagators as $\mathcal{O}(p^{-2})$ and loop integrations as $\mathcal{O}(p^4)$, Lorentz invariance dictates that only even powers of p will occur in the series. A given diagram with L loops and V_{2n} vertices from the $\mathcal{O}(p^{2n})$ Lagrangian can then be assigned a well-defined chiral dimension

$$\nu = 2 + 2L + \sum_{n=1}^{\infty} 2(n-1)V_{2n} \,, \tag{1.19}$$

so that only a finite number of diagrams will contribute at a given order in the chiral expansion, as required for the power counting to make sense. Finally, the rate of convergence depends on the expansion parameter p/Λ_χ, and thus on the scale of chiral symmetry breaking. Estimates range from the mass of the lowest-lying resonance to the generic loop factor of a tadpole diagram [17]

$$775\,\text{MeV} \approx M_\rho \lesssim \Lambda_\chi \lesssim 4\pi F_\pi \approx 1160\,\text{MeV} \,, \tag{1.20}$$

both consistent with $\Lambda_\chi \sim 1\,\text{GeV}$ given above.

While originally formulated to describe the interactions of light pseudoscalar mesons, important generalizations of ChPT concern the single-baryon sector and the coupling to electromagnetic interactions. The latter can be achieved relatively straightforwardly by coupling virtual photons to the vector currents in (1.15) and (1.16), and by supplementing the Lagrangian with operators associated with hard photons [18] (which are required for the renormalization of UV divergent photon loops). Thus, in particular isospin-violating effects, caused by differences in the up- and down-quark mass and electromagnetic interactions, can be addressed within the same framework in a consistent and systematic way.

In contrast, the extension to the single-baryon sector is hampered by the fact that the inclusion of baryons adds a new heavy scale to the problem: as explained in the introduction, the nucleon mass does not vanish in the chiral limit. In particular, no baryon–antibaryon creation/annihilation will be permitted, so that the effective Lagrangian in the nucleon sector takes the form

$$\mathcal{L}_\text{N} = \sum_i \bar\Psi \mathcal{O}_i \Psi \,, \qquad \Psi = \begin{pmatrix} p \\ n \end{pmatrix} \,, \tag{1.21}$$

with operators $\mathcal{O}_i$ covering the space of all structures allowed by chiral symmetry at a given chiral order. Due to the Dirac algebra associated with the spin of the nucleon also odd powers in p are permitted, in particular the leading-order contribution enters at $\mathcal{O}(p)$. Most importantly, though, it is no longer guaranteed that the loop graphs obey the naive power counting rules, since the integrals may pick up momenta $p \sim m$ as well [19]. Several methods have been proposed to circumvent this problem. In heavy-baryon ChPT [20], the nucleon fields are subject to a Foldy–Wouthuysen transformation in order to eliminate the nucleon mass from the leading Lagrangian. Taken together with the corresponding $1/m$ corrections, this procedure leads to a two-fold expansion in p/Λ_χ and p/m. More recently, baryon ChPT has also been formulated in a manifestly covariant way. The basic idea amounts to imposing a different renormalization condition for loop integrals that separates and subtracts the power-counting-violating part, which is regular in the quark masses, in favor of a redefinition of LECs (for more details, see [21–24]). In all variants of this approach, certain higher-order terms are resummed, however, the heavy-baryon result will always be reproduced in the limit of a strict chiral expansion—up to a redefinition of LECs.

[4] The modifications necessary if the leading contribution to the pion mass were not generated by the quark condensate are discussed in [15]. However, by now it has become apparent that the quark condensate is indeed the leading order parameter of the spontaneous breaking of chiral symmetry, see e.g. [16].

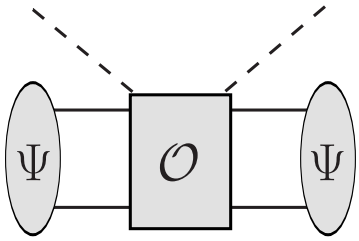

Figure 1.2: Schematic of the calculation of observables in the πd system in ChEFT. Solid/dashed lines denote nucleons/pions, the blobs refer to the deuteron wave function, and the box to the scattering operator $\mathcal{O}$.

1.1.3 Chiral effective field theory

Chiral effective field theory (ChEFT) is an extension of ChPT to systems with more than one nucleon, pioneered by Weinberg in [25, 26] and further refined in [27–30]. The main challenge in the few-nucleon system consists of accounting for the non-perturbative nature of nucleon–nucleon (NN) interactions, which stands in marked contrast to the perturbative nature of Goldstone-boson dynamics that underlies ChPT. The basic idea amounts to splitting a given diagram into so-called NN reducible and irreducible pieces, where only the irreducible part determines its contribution to the NN potential V. Over the last two decades, this idea has enabled a systematic construction of high-precision NN potentials consistent with chiral symmetry and thus a model-independent approach to nuclear forces, see [31] for recent reviews.

Furthermore, ChEFT is a powerful tool to describe the interaction of light nuclei with pions and photons. As a first step, one solves the Lippmann–Schwinger equation for the wave function Ψ

$$|\Psi\rangle = G_0 V |\Psi\rangle \,, \qquad G_0 = \frac{1}{E + i\epsilon - H} \,, \tag{1.22}$$

with Hamilton operator H and total energy E (shifted by a positive infinitesimal imaginary part). An observable can then be calculated by convolving the chiral expansion of the corresponding operator $\mathcal{O}$ with the wave function as determined from the Lippmann–Schwinger equation (cf. Fig. 1.2 for the example of πd scattering). While originally wave functions derived from phenomenological potentials were employed ("hybrid approach") [26], consistency of the method requires that the chiral expansion of $\mathcal{O}$ and the potential underlying the calculation of the wave functions be treated in exactly the same way, most notably that they be carried out to the same chiral order.

Finally, the non-perturbative nature of the NN system renders renormalization a highly contentious subject (see [32] for a sample of attitudes towards this issue). Nonetheless, the coupling of electromagnetic interactions proceeds in close analogy to ChPT, which makes ChEFT the ideal tool to study the $\pi^- d$ scattering length in a systematic manner including isospin-violating effects, as required for a high-accuracy extraction of the πN scattering lengths from hadronic atoms. As far as renormalization is concerned, we will take a pragmatic point of view and quote the scatter of wave-function integrals evaluated with various chiral and phenomenological wave functions as uncertainty estimate of the calculation.[5]

[5]The numerical evaluation of the wave-function averages is not part of this thesis. The corresponding integrals will be taken from [33].

1.2 Dispersion relations

Since ChPT is an effective field theory, the chiral expansion of a given quantity can, in principle, be systematically improved by including higher and higher orders in the calculation. However, the effect of degrees of freedom not included in the theory is parameterized in terms of LECs, whose number rapidly increases at subleading orders. Moreover, the strict chiral expansion is only valid at low energies, which, especially in the case of low-lying resonances, can significantly limit the range of applicability of ChPT. In recent years, it has become apparent that the predictive power of chiral symmetry can be vastly increased by combining ChPT with dispersive techniques, which exploit analyticity to arrive at a representation that relates the amplitude at an arbitrary point in the complex plane to an integral over its imaginary part. While the latter can be constrained by the respective unitarity relation, convergence of the dispersive integral often requires a certain number of a priori undetermined subtraction constants that, in turn, can frequently be pinned down by matching to ChPT. Once the subtraction constants are fixed, a dispersive representation provides the ideal framework to reliably perform an analytic continuation into the complex plane, which becomes of fundamental importance for broad resonances situated far away from the real axis. In the remainder of this section, we will illustrate these ideas for the case of $\pi\pi$ scattering.

1.2.1 Fixed-t dispersion relations

For simplicity, we consider the process $\pi(p_1)+\pi(p_2)\to\pi(p_3)+\pi(p_4)$ (ignoring isospin labels for the time being) with Mandelstam variables

$$s=(p_1+p_2)^2\,,\qquad t=(p_1-p_3)^2\,,\qquad u=(p_1-p_4)^2\,. \tag{1.23}$$

On the mass shell, they fulfill the relation

$$s+t+u=4M_\pi^2\,, \tag{1.24}$$

with the result that the scattering amplitude $T(s,t)$ reduces to a function of only two independent variables. The basic assumption in the construction of dispersion relations can be summarized as the principle of maximal analyticity: the amplitude $T(s,t)$ is represented by a complex function that exhibits no further singularities except for those required by general principles such as unitarity and crossing symmetry. The amplitude in the physical regions of the Mandelstam plane (cf. Fig. 1.3) is given as a particular limit of $T(s,t)$, e.g. for fixed $t=t_0$ the physical s-channel amplitude on the right-hand cut is defined as the limit from the upper half of the complex s-plane

$$T(s,t_0)=\lim_{\epsilon\to 0}T(s+i\epsilon,t_0)\,. \tag{1.25}$$

These assumptions can be justified in the framework of perturbation theory, e.g. the definition of the physical limit (1.25) corresponds to the $i\epsilon$ prescription in Feynman propagators (see, e.g., [34]). We will comment below on the issue to what extent analyticity can even be vindicated from axiomatic field theory.

Once analyticity is established, the powerful machinery of complex analysis may be invoked, primarily by means of Cauchy's integral formula. The corresponding integral equation for the scattering amplitude, itself a function of the *external kinematics* (s,t,u), will involve integrals over the *internal kinematics* (s',t',u'), which, a priori, can take arbitrary values in the Mandelstam plane. However, in order to write down a single-variable integral equation

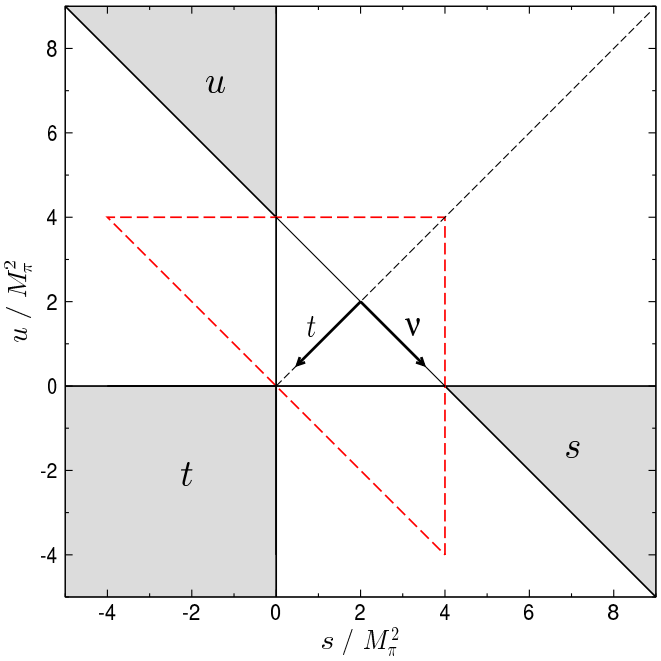

Figure 1.3: Mandelstam plane for $\pi\pi$ scattering. The filled areas mark the s-, t-, and u-channel physical regions, the red dashed line the subthreshold triangle, and the arrows the orientation of the plane in t and $\nu = s - u$.

the allowed range of these internal variables needs to be restricted appropriately. The standard choice that the on-shell condition (1.24) be valid for the internal kinematics as well is universal to all dispersion relations, while the second condition, relating external and internal kinematics, distinguishes different kinds thereof, e.g. the fixed-t version is characterized by $t' = t$ (but, in principle, any path through the Mandelstam plane would be adequate). In this case, Cauchy's theorem yields

$$T(s,t) = \frac{1}{2\pi i} \oint_{\mathcal{C}} \mathrm{d}s' \frac{T(s',t)}{s'-s} \,, \tag{1.26}$$

where the integration proceeds along the contour $\mathcal{C}$ as indicated in Fig. 1.4. If $T(s',t)$ vanishes for $|s'| \to \infty$, the contribution from the circle will vanish as well as soon as its radius is taken to infinity. The remaining integration around the cuts can be expressed in terms of the discontinuity

$$\operatorname{disc} T(s',t) = \lim_{\epsilon \to 0} \left[T(s'+i\epsilon,t) - T(s'-i\epsilon,t) \right] \,, \tag{1.27}$$

which, by virtue of hermitian analyticity [35], directly follows from unitarity. More precisely, hermitian analyticity—itself a fundamental consequence of the CPT theorem of quantum field theory—states that if the amplitude T_{ab} for a process $a \to b$ is the boundary value of an analytic function from above, cf. (1.25), the amplitude T^*_{ba} will be given by the limit of the same function from below. For time-invariant interactions this property permits the

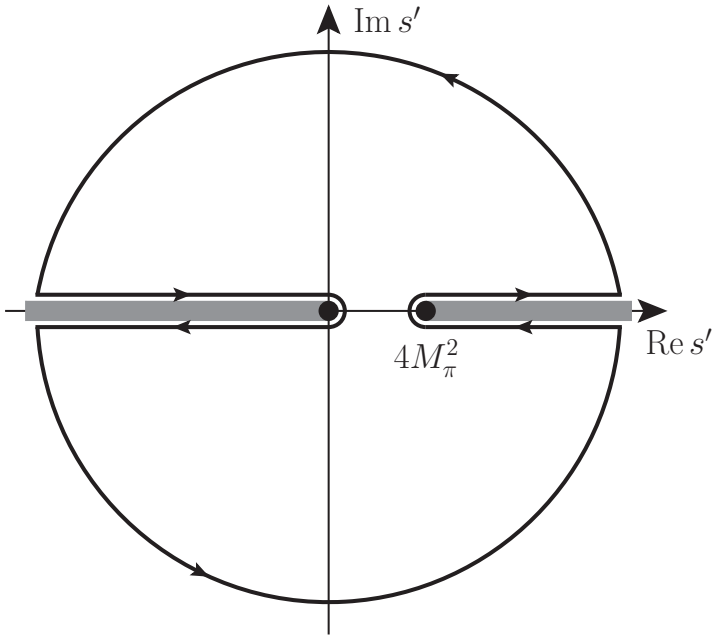

Figure 1.4: Integration contour $\mathcal{C}$ in the complex s'-plane for fixed $t = 0$. The grey bands denote left- and right-hand cuts, respectively, and the black dots the corresponding branch points.

identification[6]

$$\operatorname{disc} T(s',t) = 2i \operatorname{Im} T(s',t) \,, \tag{1.28}$$

and thus leads to

$$T(s,t) = \frac{1}{\pi} \int\limits_{4M_\pi^2}^{\infty} \mathrm{d}s' \left\{ \frac{1}{s'-s} + \frac{1}{s'-u} \right\} \operatorname{Im} T(s',t) \,. \tag{1.29}$$

In practice, the asymptotic behavior of $T(s',t)$ for large $|s'|$ does not allow for an unsubtracted dispersion relation, since the contribution from the contour at infinity cannot be discarded. Provided that $T(s',t)$ does not grow faster than a polynomial, this obstacle may be overcome by introducing so-called subtractions, i.e. by considering dispersion relations not for $T(s',t)$, but for $T(s',t)/P_n(s')$ instead, where

$$P_n(s') = \prod_{i=1}^{n} (s' - s_i) \tag{1.30}$$

involves the subtraction points $\{s_i\}$, and n is chosen sufficiently large to ensure convergence of the dispersive integral. In the application of Cauchy's theorem, the poles introduced by dividing by $P_n(s')$ can be dealt with using the residue theorem. Eventually, n additional powers of s' appear in the denominator of (1.29), but at the same time one also incurs a subtraction polynomial of degree $n-1$ with a priori unknown coefficients, which, in the case

[6] We exclude the possibility that a particle in the initial or final state of the reaction is kinematically allowed to decay into the other particles involved. In such a case, the discontinuity is not purely imaginary and cannot be simply related to the imaginary part [36].

of fixed-t dispersion relations, will actually depend on the value of t chosen. Therefore, we will refer to these coefficients as subtraction functions in the following.

The maximal number of subtractions necessary for the dispersive integrals to converge and the contour at infinity to be irrelevant is restricted by the Froissart–Martin bound [37, 38], which requires the total cross section not to increase faster than $\log^2 s$ for $s \to \infty$, and, by means of the optical theorem, implies that at most two subtractions are needed.[7] However, one may perform further subtractions to reduce the sensitivity of the integrals to the high-energy regime, where the imaginary part is often poorly known, of course at the expense of introducing additional undetermined parameters. Subtracting twice at $s = 0$, (1.29) becomes

$$T(s,t) = c(t) + \frac{1}{\pi} \int\limits_{4M_\pi^2}^{\infty} \mathrm{d}s' \left[\frac{s^2}{s'^2(s'-s)} + \frac{u^2}{s'^2(s'-u)} \right] \mathrm{Im}\, T(s',t) \,. \tag{1.31}$$

Here, we have taken advantage of crossing symmetry to discard terms proportional to $s - u$ in the subtraction polynomial, while terms proportional to $s + u = 4M_\pi^2 - t$ can be absorbed into $c(t)$. Indeed, the validity of a twice-subtracted dispersion relation for $|t| < 4M_\pi^2$ has been established from axiomatic field theory [39], which together with [38] for $t < 0$ rigorously vindicates (1.31) for all $t < 4M_\pi^2$.

Finally, one can try to go another step forward and drop the restriction of single-variable dispersion relations (keeping the internal kinematics on-shell). The corresponding assumption that $T(s,t)$ can be expressed in terms of double-spectral density functions ρ_{su}, ρ_{tu}, and ρ_{st} by double dispersive integrals of the form

$$\begin{aligned} T(s,t) = {} & \frac{1}{\pi^2} \iint \mathrm{d}s' \mathrm{d}u' \frac{\rho_{su}(s',u')}{(s'-s)(u'-u)} + \frac{1}{\pi^2} \iint \mathrm{d}t' \mathrm{d}u' \frac{\rho_{tu}(t',u')}{(t'-t)(u'-u)} \\ & + \frac{1}{\pi^2} \iint \mathrm{d}s' \mathrm{d}t' \frac{\rho_{st}(s',t')}{(s'-s)(t'-t)} \,, \end{aligned} \tag{1.32}$$

where the integration ranges extend over those regions in the Mandelstam plane where the corresponding double-spectral functions have support, is referred to as Mandelstam analyticity [40]. In either case, this concept can be justified in perturbation theory [40, 41], but while for $\pi\pi$ scattering the validity of the Mandelstam representation can at least be derived rigorously in a finite domain [42], for πN scattering only the uniqueness of amplitudes satisfying Mandelstam analyticity has been proven [43].

1.2.2 Roy equations

Roy equations are a coupled system of partial-wave dispersion relations (PWDRs) that respect analyticity, unitarity, and crossing symmetry of the scattering amplitude [44]. The starting point in the construction of these equations is the twice-subtracted fixed-t dispersion

[7] The appearance of the logarithm may be understood intuitively from a classical example already given in [37]: suppose, the scattering of two particles were described by a Yukawa-type interaction with probability density function $P(r) = P_0 e^{-br}$ and typical range b. Suppose further, that the energy dependence of the interaction probability were limited by a polynomial in s, i.e. $P(s,r) < P_0 (s/s_0)^N e^{-br}$. Then, the interaction would be exponentially suppressed for $r > r_0 = N/b \log s/s_0$ and the cross section bounded by $\sigma < \pi r_0^2 = \pi N^2/b^2 \log^2 s/s_0$.

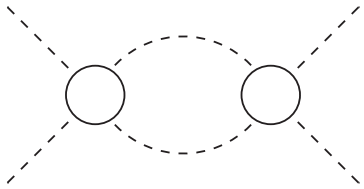

Figure 1.5: Elastic unitarity for $\pi\pi$ scattering. Dashed lines denote pions and the spheres the $\pi\pi$ scattering amplitude.

relation (1.31). First, Roy realized that the subtraction function $c(t)$ may be determined by means of $s \leftrightarrow t$ crossing symmetry

$$\begin{aligned} T(0,t) &= c(t) + \frac{1}{\pi}\int\limits_{4M_\pi^2}^{\infty} \mathrm{d}s' \frac{(4M_\pi^2 - t)^2}{s'^2(s' - 4M_\pi^2 + t)} \mathrm{Im}\, T(s',t) \\ = T(t,0) &= c(0) + \frac{1}{\pi}\int\limits_{4M_\pi^2}^{\infty} \mathrm{d}s' \left[\frac{t^2}{s'^2(s'-t)} + \frac{(4M_\pi^2 - t)^2}{s'^2(s' - 4M_\pi^2 + t)}\right] \mathrm{Im}\, T(s',0)\ . \end{aligned} \tag{1.33}$$

Second, the remaining subtraction constant $c(0)$ is intimately related to the amplitude at threshold, and thus the scattering length, via

$$T(4M_\pi^2, 0) = c(0) + \frac{1}{\pi}\int\limits_{4M_\pi^2}^{\infty} \mathrm{d}s' \frac{16M_\pi^4}{s'^2(s' - 4M_\pi^2)} \mathrm{Im}\, T(s',0)\ . \tag{1.34}$$

Third, the imaginary part of the amplitude that appears inside the dispersive integrals is expanded in partial waves, and finally the partial-wave projection of the resulting equation performed. Retrieving isospin indices again, one thus arrives at a system of integral equations for the $\pi\pi$ amplitudes $t_J^I(s)$

$$t_J^I(s) = k_J^I(s) + \sum_{I'=0}^{2} \sum_{J'=0}^{\infty} \int\limits_{4M_\pi^2}^{\infty} \mathrm{d}s' K_{JJ'}^{II'}(s,s') \mathrm{Im}\, t_{J'}^{I'}(s')\ , \tag{1.35}$$

that relates a partial wave of given angular momentum J and isospin I to all other partial waves via analytically calculable kinematic kernel functions $K_{JJ'}^{II'}(s,s')$. These kernels are composed of a singular Cauchy kernel and a regular remainder according to

$$K_{JJ'}^{II'}(s,s') = \frac{\delta_{JJ'}\delta_{II'}}{s' - s - i\epsilon} + \bar{K}_{JJ'}^{II'}(s,s')\ . \tag{1.36}$$

In particular, the construction that led to (1.35) ensures that the $t_J^I(s)$ automatically fulfill the analytic properties expected for the partial waves: while the Cauchy kernel implements the right-hand cut, $\bar{K}_{JJ'}^{II'}(s,s')$ will incorporate all analytic structure required from the left-hand cut. The only free parameters of the approach are hidden in the subtraction term $k_J^I(s)$ that depends on the S-wave scattering lengths a_0^0 and a_0^2. As long as elastic unitarity holds, i.e.

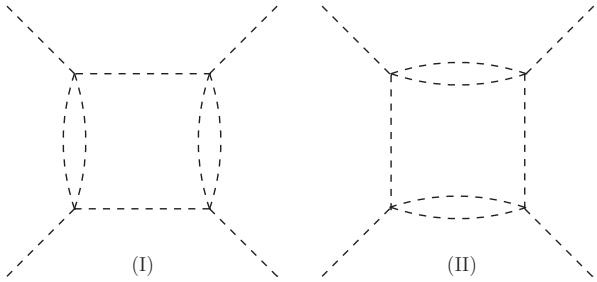

Figure 1.6: Box graphs constraining the boundaries of the double-spectral functions for $\pi\pi$ scattering.

only $\pi\pi$ intermediate states enter the unitarity relation (see Fig. 1.5), the $\pi\pi$ partial waves may be parameterized as

$$t_J^I(s) = \frac{e^{2i\delta_J^I(s)} - 1}{2i\sigma(s)} , \qquad \sigma(s) = \sqrt{1 - \frac{4M_\pi^2}{s}} , \tag{1.37}$$

with the result that the Roy equations (1.35) reduce to coupled integral equations for the phase shifts $\delta_J^I(s)$.

An important issue is the range of validity of the Roy equations. While the convergence of the fixed-t dispersion relations is guaranteed for all $t < 4M_\pi^2$ [37–39], the reduction to partial waves imposes further constraints on the domain of validity of the system. As a matter of fact, the partial-wave expansion of the imaginary part in the dispersive integral converges only for scattering angles z' that lie within the large Lehmann ellipse [45]. It has been derived from axiomatic field theory that this condition is met for all $s' \in [4M_\pi^2, \infty)$ if $-28M_\pi^2 \leq t \leq 4M_\pi^2$ [42]. By virtue of Bose symmetry, the partial-wave projection of the equations can be restricted onto $0 \leq z \leq 1$, which translates into a range in t of

$$-\frac{s - 4M_\pi^2}{2} \leq t \leq 0 . \tag{1.38}$$

Consequently, the Roy equations can be established from axiomatic field theory up to [44]

$$s_{\max} = 60M_\pi^2 = (1.08\,\text{GeV})^2 . \tag{1.39}$$

It is crucial to observe that the derivation of this result heavily relies on the fact that internal and external kinematics are related by $t' = t$, which allows for the translation of constraints originating from the Lehmann ellipse into a range of convergence in s. This is the essential part of the derivation that needs to be generalized in the analysis of different kinds of dispersion relations.

Since rigorous results from axiomatic field theory are rarely available for processes other than $\pi\pi$ scattering, we will assume that the analytic properties of the amplitude are correctly reproduced by Mandelstam analyticity in Parts II and III of this thesis. Therefore, it is instructive to compare the consequences of this relaxed assumption also for the $\pi\pi$ case to the axiomatic-field-theory result (1.39). The central objects of the analysis are the boundaries of the support of the double-spectral functions that determine the integration range in (1.32). These boundaries can be inferred from the box diagrams depicted in Fig. 1.6, which are to be understood as generalizations of four-propagator box diagrams (see, e.g., [46]), with one

or more lines replaced by a particle whose mass is equal to the input mass of the lowest-lying intermediate state accessible to the interacting particles.

Due to crossing symmetry, it suffices to investigate the boundary of ρ_{st}. From diagrams (I) and (II) in Fig. 1.6 we find that this boundary is defined by

$$\begin{aligned} b_{\mathrm{I}}(s,t) &= t(s-4M_\pi^2) - 16M_\pi^2 s = 0 \;, \\ b_{\mathrm{II}}(s,t) &= t(s-16M_\pi^2) - 4M_\pi^2 s = 0 \;, \end{aligned} \tag{1.40}$$

and thus obeys

$$t = T_{st}(s) = \min\left\{T_{\mathrm{I}}(s), T_{\mathrm{II}}(s)\right\} \;, \tag{1.41}$$

where T_{I} and T_{II} follow from solving (1.40) for t. The corresponding double-spectral regions, defined as the portions of the Mandelstam plane that obey $s+t+u = 4M_\pi^2$ and where any of the functions ρ_{st}, ρ_{su}, ρ_{tu} has support, are shown in the left panel of Fig. 1.7. By definition, the line in the Mandelstam plane corresponding to a fixed value of t must not enter the double-spectral regions if a single-variable dispersion relation with this value of t is supposed to hold. Moreover, the maximally allowed value of z' becomes

$$z'_{\max} = 1 + \frac{2T_{st}(s')}{s'-4M_\pi^2} \;, \tag{1.42}$$

and hence the Lehmann-ellipse constraint in the form $-z'_{\max} \le z' \le z'_{\max}$ restricts the allowed values of t to

$$\begin{aligned} &T'_{st}(s') \le t \le T_{st}(s') \;, \\ &T'_{st}(s') = 4M_\pi^2 - s' - T_{st}(s') \;, \qquad \forall\, s' \in \left[4M_\pi^2, \infty\right) \;. \end{aligned} \tag{1.43}$$

As illustrated in Fig. 1.7, both constraints actually yield the same range $-32M_\pi^2 \le t \le 4M_\pi^2$, and thus

$$s_{\max} = 68M_\pi^2 = (1.15\,\mathrm{GeV})^2 \;, \tag{1.44}$$

slightly larger than (1.39). Irrespective of the analyticity assumptions, the range of validity of the Roy equations can be extended significantly, at least up to $s_{\max} = 165M_\pi^2$, if dispersion relations in the manifestly crossing-symmetric variables

$$x = st + tu + us \;, \qquad y = stu \;, \tag{1.45}$$

instead of fixed-t dispersion relations are employed [47], however, at the expense of a substantial increase in complexity of the equations.

Due to the finite domain of validity, the Roy equations cannot be used up to infinity. Above a certain energy, referred to as the matching point s_{m}, input from experiment for the imaginary parts of the partial waves is required, so that in practice the equations are solved between threshold and s_{m}. Furthermore, the partial-wave expansion will be truncated at a certain angular momentum J and higher partial waves treated on the same footing as the lower partial waves above s_{m}. In fact, the existence and uniqueness of a solution depends on the value of the phases δ_i of the partial waves dynamically included in the calculation at the matching point [48–50]. More precisely, the situation is characterized by the multiplicity index m, which is given by

$$m = \sum_i m_i \;, \qquad m_i = \begin{cases} \left\lfloor \frac{2\delta_i(s_{\mathrm{m}})}{\pi} \right\rfloor & \text{if } \delta_i(s_{\mathrm{m}}) > 0 \;, \\ -1 & \text{if } \delta_i(s_{\mathrm{m}}) < 0 \;, \end{cases} \tag{1.46}$$

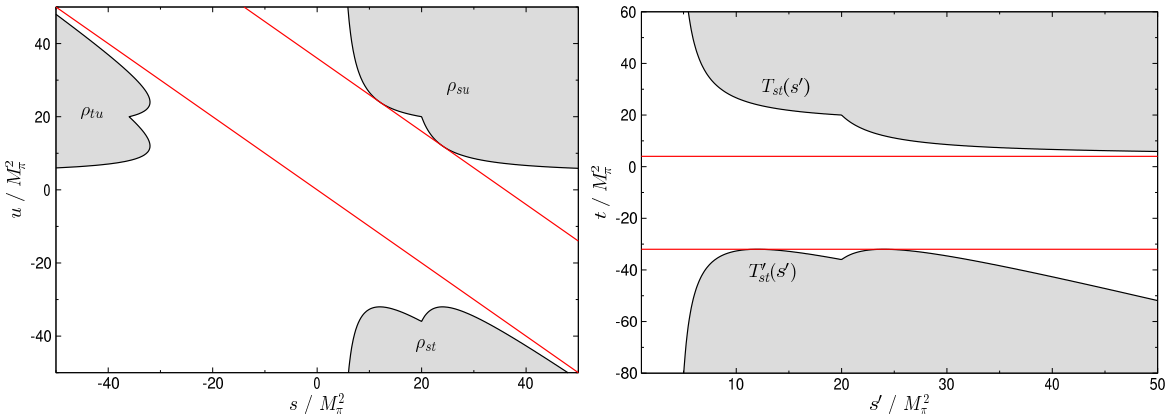

Figure 1.7: Double-spectral regions (left) and allowed range of t (right) for $\pi\pi$ scattering. The red lines refer to $t = 4M_\pi^2$ and $t = -32M_\pi^2$, respectively.

where $\lfloor x \rfloor$ denotes the largest integer $\leq x$ and we have assumed that $\delta_i(s_\mathrm{m}) > -\pi/2$ for all partial waves. If $m = 0$, a unique solution exists, while for $m > 0$ the neighborhood of each solution contains an m-parameter family of solutions and for $m < 0$ only for a specific choice (constrained by $|m|$ conditions) of the input, i.e. subtraction constants, imaginary parts above s_m, and higher partial waves, a solution can be found.

1.2.3 Matching to chiral perturbation theory

Shortly after Roy's article [44], a comprehensive phenomenological analysis of the $\pi\pi$ data available at that time was performed using the Roy-equation formalism [51]. Over the last years, there has been renewed interest in the Roy equations [52–57], mainly triggered by recognizing the full potential of the approach in combination with effective field theory, which has led to a determination of the low-energy $\pi\pi$ scattering amplitude with unprecedented accuracy. In the following, we will briefly summarize the strategy for the solution of the equations, especially focusing on the interplay with ChPT.

A typical truncation scheme for the numerical solution of the Roy equations proceeds as follows: in [53], the system was truncated at $J = 1$ and the matching point chosen as $s_\mathrm{m} = (0.8\,\mathrm{GeV})^2$, implying that $m = 0$. The effects of higher partial waves as well as higher energies, i.e. the part of (1.35) with $J' \geq 2$ and $s' \geq s_\mathrm{m}$, are accounted for in so-called driving terms, which are determined from experimental input for the intermediate-energy regime and from Regge theory for the high-energy behavior. A crucial result of [53] was that the amplitudes in the low-energy regime are remarkably insensitive to the details of the contributions from higher partial waves and higher energies, so that a very precise representation of the S- and P-wave amplitudes at low energies in terms of the scattering lengths a_0^0 and a_0^2 was achieved.

The simplest matching procedure between Roy equations and ChPT, matching at threshold, would amount to inserting the two-loop ChPT result for the scattering lengths into the Roy equations. However, this approach is unfavorable, since the chiral expansion at threshold converges rather slowly, caused by the onset of the unitarity cut, and further constraints in the whole low-energy region, where both the Roy-equation and the chiral parameterization are valid, would be ignored. Instead, the strategy put forward in [58] relies on the fact that ultimately the subtraction constants in the dispersive calculation and the LECs in the chiral

expansion can be identified. To this end, both parameterizations are brought into a form that proves that agreement at low energies is ensured if the polynomial parts match. In this way, by requiring consistency of both representations in the full low-energy regime, the slow convergence at threshold is avoided and the sensitivity to terms in the chiral expansion beyond two-loop order diminished. Thus, since the Roy equations have elastic unitarity fully built in—in contrast to ChPT that restores unitarity only perturbatively—they can be regarded as a means to unitarize the chiral expansion. Retaining only the LECs $\bar{l}_3$ and $\bar{l}_4$ (the latter eliminated in favor of the scalar pion radius $\langle r^2\rangle_\pi^S$), which measure the quark-mass dependence and thus cannot be determined dynamically in the matching of the polynomials parts, the scattering lengths can be expressed as [58]

$$\begin{aligned} a_0^0 &= 0.198 \pm 0.001 + 0.0443\,\mathrm{fm}^{-2}\langle r^2\rangle_\pi^S - 0.0017\,\bar{l}_3\ , \\ a_0^2 &= -0.0392 \pm 0.0003 - 0.0066\,\mathrm{fm}^{-2}\langle r^2\rangle_\pi^S - 0.0004\,\bar{l}_3\ , \end{aligned} \tag{1.47}$$

which together with $\bar{l}_3 = 2.9 \pm 2.4$, $\langle r^2\rangle_\pi^S = (0.61 \pm 0.04)\,\mathrm{fm}^2$ finally led to a very precise prediction of the $\pi\pi$ scattering lengths [58]

$$a_0^0 = 0.220 \pm 0.005\ , \qquad a_0^2 = -0.0444 \pm 0.0010\ . \tag{1.48}$$

Recently, these predictions have been tested in various high-precision experiments. First, the decay width of pionium is sensitive to $|a_0^0 - a_0^2|$, and has been measured by the DIRAC collaboration [59]. Next, a measurement of K_{l4} decays [60, 61] yields access to the phase-shift difference $\delta_0^0 - \delta_1^1$ of $\pi\pi$ S- and P-waves, which, combined with a numerical solution of the Roy equations, determines a_0^0 and a_0^2. Lastly, the scattering lengths may be extracted from a high-statistics analysis of $K \to 3\pi$ decays [62], where the rescattering of pions in the final state generates a cusp whose strength relates to the pertinent $\pi\pi$ scattering amplitude at threshold [63]. Presently, the most stringent constraints on a_0^0 and a_0^2 originate from K_{l4} and $K \to 3\pi$ decays. The NA48/2 collaboration quotes for the combination of both measurements [61]

$$a_0^0 = 0.2210 \pm 0.0047_{\mathrm{stat}} \pm 0.0040_{\mathrm{syst}}\ , \qquad a_0^2 = -0.0429 \pm 0.0044_{\mathrm{stat}} \pm 0.0028_{\mathrm{syst}}\ , \tag{1.49}$$

in beautiful agreement with (1.48). In fact, at this level of accuracy it is critical that isospin-violating corrections specific to each experiment be properly taken into account [64].

The importance of an accurate knowledge of the $\pi\pi$ scattering lengths, and thus of the low-energy phase shifts, is hard to overestimate. First of all, the scattering lengths are central parameters of low-energy QCD themselves, intimately related to the pattern of chiral symmetry breaking. Indeed, their precise determination was essential to confirm the role of the quark condensate as the leading order parameter of the spontaneous breaking of chiral symmetry [16]. Moreover, once the subtraction constants are fixed, the Roy equations automatically provide the analytic continuation of the $\pi\pi$ amplitude beyond the physical region. The domain of validity of the equations reaches sufficiently far into the complex plane to encompass the σ pole $m_\sigma = M_\sigma - i\Gamma_\sigma/2$, with the result that the combination of Roy equations and ChPT allowed for the first reliable determination of the pole parameters of the σ meson [65]

$$M_\sigma = 441^{+16}_{-8}\,\mathrm{MeV}\ , \qquad \Gamma_\sigma = 544^{+18}_{-25}\,\mathrm{MeV}\ . \tag{1.50}$$

Finally, the $\pi\pi$ phase shifts are crucial ingredients to describe $\pi\pi$ rescattering in innumerable processes in low-energy hadron physics. Examples are $\gamma\gamma \to \pi\pi$ and $\pi\pi \to \bar{N}N$, as discussed in Parts II and III of this thesis.

1.2.4 Beyond $\pi\pi$ scattering

Evidently, it would be of high interest to extend the successful program of a combined framework of Roy or Roy-like equations and ChPT to processes other than $\pi\pi$ scattering. An important step forward in this direction was taken in [66, 67], where Roy–Steiner equations for πK scattering were constructed. Unfortunately, the generalization beyond $\pi\pi$ scattering comes with plenty of complications, mainly rooted in unequal masses and more involved crossing properties, as we will demonstrate in the following using the example of πK scattering [66, 67].

First of all, a full system of PWDRs will include dispersion relations for two distinct physical processes, πK scattering (s-channel) and $\pi\pi \to \bar{K}K$ (t-channel). An immediate consequence concerns the applicability of fixed-t dispersion relations and the use of crossing symmetry to determine the subtraction function $c(t)$ in (1.33): $s \leftrightarrow t$ crossing symmetry will intertwine s- and t-channel equations, so that the equations for the s-channel partial waves will also involve t-channel dispersive integrals that extend over $t' \geq 4M_\pi^2$. Accordingly, the determination of the t-channel partial waves will require the partial-wave projection for $t > 4M_\pi^2$, which lies beyond the range of validity of fixed-t dispersion relations.

A convenient choice of dispersion relations that evade these limitations are so-called hyperbolic dispersion relations (HDRs) [68],[8] defined by

$$(s-a)(u-a) = (s'-a)(u'-a) \equiv b \,. \tag{1.51}$$

While $b = b(s,t,a)$ is fixed by the external kinematics, the hyperbola parameter a can be freely chosen. In particular, it can be used to optimize the range of validity of the resulting system of RS equations. HDRs are particularly suitable for processes such as πK scattering, since $s \leftrightarrow u$ crossing is manifest, so that all constraints by crossing symmetry are automatically fulfilled. The unsubtracted version of HDRs for a crossing-symmetric amplitude $T^+(s,t)$ reads

$$T^+(s,t) = \frac{1}{\pi}\int\limits_{s_+}^{\infty} \mathrm{d}s' \left[\frac{1}{s'-s} + \frac{1}{s'-u} - \frac{1}{s'-a}\right] \mathrm{Im}\, T^+(s',t') + \frac{1}{\pi}\int\limits_{4M_\pi^2}^{\infty} \mathrm{d}t' \frac{\mathrm{Im}\, T^+(s',t')}{t'-t} \,, \tag{1.52}$$

where

$$s_+ = (M_\pi + M_K)^2 \,, \tag{1.53}$$

and M_K denotes the mass of the kaon. The above integrals are understood in such a way that the integrands shall be expressed in terms of the integration variable and the external kinematics by virtue of (1.51) and

$$s' + t' + u' = 2M_\pi^2 + 2M_K^2 \,. \tag{1.54}$$

The first integral in (1.52) is reminiscent of fixed-t dispersion relations, but in that case $\mathrm{Im}\, T^+(s',t') \to \mathrm{Im}\, T^+(s',t)$ and the last term is removed. Thus, the key difference here is that t' depends not only on t, but on s and s' as well. The dispersion relation for an amplitude

[8] Even more, HDRs are the unique choice if one demands that the curves pass through all kinematic channels, avoid double-spectral regions, do not introduce ostensible kinematic cuts into the partial-wave amplitudes, and still yield manageable kernel functions [68]. In view of the efforts [68, 69] that led to s-channel PWDRs for πN scattering and thus provided the first step towards the construction of a Roy-equation analog for processes with πN crossing properties, the resulting full system of partial-wave hyperbolic dispersion relations (PWHDRs) is referred to as Roy–Steiner equations.

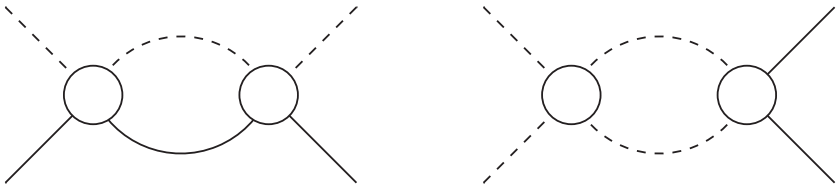

Figure 1.8: Elastic unitarity for πK scattering (left) and $\pi\pi \to \bar{K}K$ (right). Dashed/solid lines denote pions/kaons, and the spheres refer to the pertinent scattering amplitudes.

$T^-(s,t)$ that is odd under crossing may be constructed by considering $T^-(s,t)/\nu$, $\nu = s-u$, yielding

$$T^-(s,t) = \frac{1}{\pi}\int\limits_{s_+}^{\infty} \mathrm{d}s' \left[\frac{1}{s'-s} - \frac{1}{s'-u}\right] \mathrm{Im}\, T^-(s',t') + \frac{1}{\pi}\int\limits_{4M_\pi^2}^{\infty} \mathrm{d}t' \frac{\nu}{\nu'} \frac{\mathrm{Im}\, T^-(s',t')}{t'-t}\,. \tag{1.55}$$

In [67], a combination of fixed-t and hyperbolic dispersion relations (with $a = 0$) was used, arguing that the range of validity of fixed-t dispersion relations in the s-channel is slightly larger than for HDRs. We suspect that this advantage would dissolve if HDRs with general a were allowed (as is true, e.g., for πN scattering). Hence, we will bypass the fixed-t step and solely consider HDRs in this thesis.

The second major impediment concerns unitarity in the t-channel. While s-channel unitarity corresponds exactly to unitarity in $\pi\pi$ scattering, the t-channel unitarity relation does not. In particular, it is linear in the $\pi\pi \to \bar{K}K$ partial waves, and thus far less restrictive than s-channel unitarity, cf. Fig. 1.8. The resulting equations for the t-channel partial waves take the form of a Muskhelishvili–Omnès problem [70, 71], whose solution will require input for the $\pi\pi$ partial waves. However, once the t-channel equations are solved, the remaining s-channel problem will be amenable to the same methods that can be used to solve $\pi\pi$ Roy equations.

Last, $\pi\pi$ scattering is also exceptional in the matching to ChPT, since the number of LECs is small and neither potentially large $SU(3)$ corrections nor the presence of baryons threaten the rapid convergence of the chiral expansion. In contrast, the comparison of RS equations and ChPT in πK scattering is indeed hampered by large uncertainties in the chiral series [66, 67, 72].

Despite all drawbacks in the non-identical-particle case one should note that the important feature of the Roy-equation approach that the kernel functions will correctly incorporate the analytic properties of the partial waves prevails in the general case. As long as the dispersion relations on the amplitude level hold, the correct analytic structure of the partial waves will emerge automatically. Although the complications besetting the generalization of $\pi\pi$ Roy equations to other processes lead to a considerable increase in complexity, a full solution of the corresponding system of RS equations is highly rewarding nonetheless. After all, the result will maintain analyticity, unitarity, crossing symmetry, and, by matching to ChPT, chiral symmetry, and thus all symmetries of the underlying quantum field theory. In fact, RS equations for πK scattering have provided invaluable information on the πK scattering lengths, low-energy phase shifts, and the pole position of the κ meson [67, 73].

The construction and numerical solution of RS equations for $\gamma\gamma \to \pi\pi$ and πN scattering will be discussed in much more detail in Parts II and III of this thesis. In either case, the strategy will closely follow the recipe laid out in this section.

Part I

Extraction of the πN scattering lengths from hadronic atoms[#1]

[#1] The contents of this part have been published in [33].

Chapter 2

Precision calculation of the $\pi^- d$ scattering length

2.1 Introduction

Hadron–hadron scattering lengths are fundamental quantities characterizing strong interactions, especially the import of a precise knowledge of the scattering lengths for the simplest example, $\pi\pi$ scattering, for low-energy hadron physics cannot be overstated (see Sect. 1.2.3). More generally, pion–hadron scattering lengths are of considerable interest, as chiral symmetry and the Goldstone-boson nature of the pions dictate that they are small [74], while their non-vanishing size is linked to fundamental quantities such as the light quark masses and condensates. However, while slowly becoming accessible to ab initio calculations in lattice QCD [75], scattering lengths for reactions other than $\pi\pi$ scattering still defy a precision determination.

In the case of pion–nucleon scattering, chiral symmetry predicts that the isoscalar scattering length a^+ is suppressed compared to its isovector counterpart a^-.[1] In particular, the low-energy theorem for a^- [74, 76]

$$a^- = \frac{M_\pi}{8\pi(1+M_\pi/m_\mathrm{p})F_\pi^2} + \mathcal{O}\big(M_\pi^3\big) \approx 80\cdot 10^{-3} M_\pi^{-1} \tag{2.1}$$

receives corrections only at third order in the pion mass and its prediction is numerically very close to the full result. Meanwhile, the expansion of the isoscalar scattering length [76]

$$a^+ = 0 + \frac{M_\pi^2}{4\pi(1+M_\pi/m_\mathrm{p})F_\pi^2}\left\{ -\frac{g_\mathrm{A}^2}{4m_\mathrm{p}} + 2(c_2+c_3-2c_1)\right\} + \mathcal{O}\big(M_\pi^3\big) \approx 0\,, \tag{2.2}$$

with the pion decay constant F_π, the axial charge of the nucleon g_A, and LECs c_i, stands in marked contrast: the leading order vanishes—leaving a^+ as a measure of the explicit breaking of chiral symmetry—and at subleading orders poorly determined LECs and huge cancellations between individual terms limit the predictive power of the expansion. Experimentally, a measurement of a^+ is complicated by the lack of π^0 beams and neutron targets that makes direct pion–nucleon scattering experiments impossible in some charge channels. The best

[1] For the sake of brevity, we suppress the angular-momentum labels for the S-wave scattering lengths, i.e. $a^\pm = a^\pm_{0+}$ in the general notation introduced in Part III.

hope for access to a^+ therefore lies in future precision measurements of threshold neutral-pion photoproduction [77]. In the meantime, extractions of a^+ from πN scattering data suffer from large uncertainties. Different phase-shift analyses yield values covering a wide range from $-10 \cdot 10^{-3} M_\pi^{-1}$ to $+5 \cdot 10^{-3} M_\pi^{-1}$ [78]. For this reason, the combination of data and theory has even failed to provide sufficient evidence to establish definitely that $a^+ \neq 0$.

In view of the difficulties of the chiral expansion in the isoscalar sector (2.2), an independent, precise determination of the πN scattering lengths would be highly desirable. Along the lines of Sect. 1.2.3, this should prove valuable to help constraining subtraction constants in RS equations for πN scattering (see Part III). Besides that, a^+ and a^- serve as vital input parameters for dispersive analyses of the pion–nucleon σ term [79, 80] and the determination of the pion–nucleon coupling constant via the Goldberger–Miyazawa–Oehme sum rule [81], respectively. While the uncertainty in a^- is much smaller than that in a^+, it still contributes significantly to the overall error estimate in the sum-rule evaluation [82, 83], which renders a more accurate determination also of a^- highly welcome.

In recent years, data on hadronic atoms have become the primary source to gain information on the πN scattering lengths [84]. In these systems, strong interactions modify the spectrum compared to pure QED by shifting the energy levels and introducing a finite width to the states, both effects being sensitive to threshold pion–nucleon scattering. In this way, new information on pion–nucleon scattering lengths has become available due to recent high-accuracy measurements of pionic hydrogen (πH) and pionic deuterium (πD). In the case of πH, the latest experimental results [85] are

$$\epsilon_{1s} = (-7.120 \pm 0.012)\,\text{eV} \;, \qquad \Gamma_{1s} = (0.823 \pm 0.019)\,\text{eV} \;, \tag{2.3}$$

for the (attractive) shift of the $1s$ level of πH due to strong interactions and its width. The shift of the ground state is related to the $\pi^- p$ scattering length $a_{\pi^- p}$, while the width gives access to the charge-exchange scattering length $a^{\text{cex}}_{\pi^- p} \equiv a_{\pi^- p \to \pi^0 n}$ [84]. More precisely, ϵ_{1s} is related to $a_{\pi^- p}$ through an improved Deser formula [86]

$$\epsilon_{1s} = -2\alpha^3 \mu_H^2 a_{\pi^- p}(1 + K_\epsilon + \delta_\epsilon^{\text{vac}}) \;, \tag{2.4}$$

where $\alpha = e^2/4\pi$ denotes the fine-structure constant, μ_H refers to the reduced mass of πH, $K_\epsilon = 2\alpha(1 - \log\alpha)\mu_H a_{\pi^- p}$, and $\delta_\epsilon^{\text{vac}} = 2\delta\Psi_H(0)/\Psi_H(0) = 0.48\%$ is the effect of vacuum polarization on the wave function at the origin [87]. The width determines $a^{\text{cex}}_{\pi^- p}$ via [88]

$$\Gamma_{1s} = 4\alpha^3 \mu_H^2 p_1 \left(1 + \frac{1}{P}\right) \left(a^{\text{cex}}_{\pi^- p}\right)^2 \left(1 + K_\Gamma + \delta_\epsilon^{\text{vac}}\right) \;, \tag{2.5}$$

with $K_\Gamma = 4\alpha(1 - \log\alpha)\mu_H a_{\pi^- p} + 2\mu_H(m_\text{p} + M_\pi - m_\text{n} - M_{\pi^0})(a_{\pi^0 n})^2$, m_p, m_n, M_π, and M_{π^0} the masses of proton, neutron, charged and neutral pions, respectively, p_1 the momentum of the outgoing $n\pi^0$ pair, and the Panofsky ratio [89]

$$P = \frac{\sigma(\pi^- p \to \pi^0 n)}{\sigma(\pi^- p \to n\gamma)} = 1.546 \pm 0.009 \;. \tag{2.6}$$

Similarly, the (repulsive) strong shift ϵ_{1s}^D of the $1s$ level of πD yields the real part of the $\pi^- d$ scattering length $\text{Re}\, a_{\pi^- d}$ via [90]

$$\epsilon_{1s}^D = -2\alpha^3 \mu_D^2 \text{Re}\, a_{\pi^- d}(1 + K_{\epsilon^D} + \delta_{\epsilon^D}^{\text{vac}}) \;, \tag{2.7}$$

with reduced mass μ_D, second-order correction $K_{\epsilon^D} = 2\alpha(1-\log\alpha)\mu_D \mathrm{Re}\, a_{\pi^- d}$, and vacuum-polarization effect $\delta^{\rm vac}_{\epsilon^D} = 2\delta\Psi_D(0)/\Psi_D(0) = 0.51\%$ [87].

In the isospin limit, the level shift of πH is sensitive to $a^+ + a^-$, whereas the width is solely determined by a^-. In this way, data from πH alone permit, in principle, an extraction of the πN scattering lengths. However, the chiral suppression of a^+ makes it very sensitive to isospin-violating corrections (see Sect. 2.2), with the result that additional experimental information—in particular from isoscalar nuclei as they provide better access to a^+—are essential to check the systematics and potentially improve the accuracy of the scattering-length determination. To this end, we split the $\pi^- d$ scattering length into its two-(πN) and three-(πNN) body contributions

$$\mathrm{Re}\, a_{\pi^- d} = a^{(2)}_{\pi^- d} + a^{(3)}_{\pi^- d}\,, \tag{2.8}$$

where the former is related to a^+ via

$$a^{(2)}_{\pi^- d} = \frac{2\xi_{\rm p}}{\xi_{\rm d}}(\tilde{a}^+ + \Delta\tilde{a}^+)\,. \tag{2.9}$$

Here the difference between a^+ and $\tilde{a}^+$ as well as $\Delta\tilde{a}^+$ are determined by isospin-violating corrections (Sect. 2.2) and

$$\xi_{\rm p} = 1 + \frac{M_\pi}{m_{\rm p}}\,, \qquad \xi_{\rm d} = 1 + \frac{M_\pi}{m_{\rm d}}\,, \tag{2.10}$$

with the deuteron mass $m_{\rm d}$. Once isospin breaking in the two-body sector is under control, we therefore have to develop a theoretical description of $a^{(3)}_{\pi^- d}$ that finally allows one to exploit information on πD at the same level of accuracy as in πH, which requires a calculation of $a^{(3)}_{\pi^- d}$ to an accuracy of better than 10 %. As we will discuss in this chapter, this proves to be possible, and a combined analysis of the data (2.3) on πH and the recently remeasured level shift in πD [91]

$$\epsilon^D_{1s} = (2.356 \pm 0.031)\,\mathrm{eV} \tag{2.11}$$

then yields a determination of a^+ and a^- of unprecedented accuracy.[2] In this chapter, we present in detail the calculation of the three-body part of $a_{\pi^- d}$, which we decompose as

$$a^{(3)}_{\pi^- d} = a^{\rm str} + a^{\rm disp+\Delta} + a^{\rm EM}\,, \tag{2.12}$$

where $a^{\rm disp+\Delta}$ involves two-nucleon or Δ-isobar intermediate states, $a^{\rm EM}$ represents virtual-photon corrections, and $a^{\rm str}$ denotes "strong" diagrams, i.e. essentially all other contributions in the chiral expansion (the definition of each class of diagrams can be found in Sects. 2.4–2.6).

The analysis will proceed as follows: we first briefly review isospin-violating corrections to the πN scattering lengths in Sect. 2.2. Then, we summarize the hierarchy of diagrams contributing to $a^{(3)}_{\pi^- d}$ in both the isospin-conserving and the isospin-violating sector in Sect. 2.3, before discussing strong, virtual-photon, and dispersive + Δ contributions in detail in Sects. 2.4, 2.5, and 2.6. Sect. 2.7 summarizes our main conclusions concerning three-body contributions to the $\pi^- d$ scattering length. The consequences for the πN scattering lengths, the πN coupling constant, as well as some brief comments on the pion–nucleon σ term will be presented in Chapter 3.

[2] The width of πD is governed by $\pi^- d \to nn$ (BR = 73.9 %) and $\pi^- d \to nn\gamma$ (BR = 26.1 %) [92], so that no additional information on threshold πN physics is provided.

2.2 Isospin violation in the πN scattering lengths

Before turning to the calculation of $a^{(3)}_{\pi^- d}$, we review isospin-violating corrections to the πN scattering lengths, which provide an essential input to the present analysis. The scattering lengths in the isospin limit for all eight channels can be written in terms of a^+ and a^- as

$$\begin{aligned}
a_{\pi^- p} &\equiv a_{\pi^- p\to\pi^- p} = a_{\pi^+ n} \equiv a_{\pi^+ n\to\pi^+ n} = a^+ + a^- \,, \\
a_{\pi^+ p} &\equiv a_{\pi^+ p\to\pi^+ p} = a_{\pi^- n} \equiv a_{\pi^- n\to\pi^- n} = a^+ - a^- \,, \\
a^{\text{cex}}_{\pi^- p} &\equiv a_{\pi^- p\to\pi^0 n} = a^{\text{cex}}_{\pi^+ n} \equiv a_{\pi^+ n\to\pi^0 p} = -\sqrt{2}\, a^- \,, \\
a_{\pi^0 p} &\equiv a_{\pi^0 p\to\pi^0 p} = a_{\pi^0 n} \equiv a_{\pi^0 n\to\pi^0 n} = a^+ \,.
\end{aligned} \tag{2.13}$$

To extract a^+ and a^- from hadronic-atom data, we need to relate the scattering lengths in particular charge channels to those in the isospin limit, i.e. we need the corrections

$$\Delta a_{\pi^- p} = a_{\pi^- p} - (a^+ + a^-) \,, \qquad \Delta a_{\pi^- n} = a_{\pi^- n} - (a^+ - a^-) \,, \qquad \Delta a^{\text{cex}}_{\pi^- p} = a^{\text{cex}}_{\pi^- p} + \sqrt{2}\, a^- \,. \tag{2.14}$$

These corrections are generated by the quark mass difference $m_\text{d} - m_\text{u}$ and electromagnetic interactions. They can be calculated systematically in ChPT, and have been worked out at next-to-leading order (NLO) in the chiral expansion in [93, 94].

In those works, and throughout this thesis, the isospin limit is defined by the charged-particle masses, in particular the nucleon mass is identified with the mass of the proton. Moreover, the counting $m_\text{d} - m_\text{u} \sim e^2$ is used, i.e. electromagnetic and quark-mass effects are assumed to contribute at the same order. This counting is phenomenologically rather successful. The prime example is the nucleon mass difference, to which—according to the evaluation of the Cottingham sum rule [95] in [96, 97]—the quark mass difference and electromagnetic interactions contribute $(2.1 \pm 0.3)\,\text{MeV}$ and $(-0.8 \pm 0.3)\,\text{MeV}$, respectively.[3] A similar picture emerges from the kaon mass difference, where—depending on the assumptions about violation of Dashen's theorem [102–104]—quark-mass effects are a factor 2–3 larger than electromagnetic ones. It is also instructive to look at tree-level contributions to isospin violation in πN scattering [93]: $a_{\pi^- p} - a_{\pi^+ n}$ and $a_{\pi^+ p} - a_{\pi^- n}$ are purely electromagnetic, $a_{\pi^0 p} - a_{\pi^0 n}$ is solely due to $m_\text{d} - m_\text{u}$, while both effects are of the same size in $a^{\text{cex}}_{\pi^- p} - a^{\text{cex}}_{\pi^+ n}$. Similar conclusions can be drawn from tree-level isospin breaking in the πK scattering lengths [105], where the corrections for some channels are purely electromagnetic, for some purely quark-mass induced, and for some due to both effects, sometimes the former being a factor of 2 larger, sometimes the latter.

First of all, the major consequence of the leading-order (LO) isospin breaking in ChPT [106]

$$\begin{aligned}
\Delta a^{\text{LO}}_{\pi^- p} &= \frac{1}{4\pi\xi_\text{p}} \left\{ \frac{4\Delta_\pi}{F_\pi^2} c_1 - \frac{e^2}{2}(4f_1 + f_2) \right\} , \qquad \Delta a^{\text{cex LO}}_{\pi^- p} = \frac{\sqrt{2}}{4\pi\xi_\text{p}} \left\{ \frac{e^2 f_2}{2} + \frac{g_\text{A}^2 \Delta_\pi}{4F_\pi^2 m_\text{p}} \right\} , \\
\Delta a^{\text{LO}}_{\pi^- n} &= \frac{1}{4\pi\xi_\text{p}} \left\{ \frac{4\Delta_\pi}{F_\pi^2} c_1 - \frac{e^2}{2}(4f_1 - f_2) \right\} , \qquad \Delta_\pi = M_\pi^2 - M_{\pi^0}^2 \,,
\end{aligned} \tag{2.15}$$

[3] This result was critically re-examined in [98], where it was argued that the Cottingham sum rule in its unsubtracted form cannot be justified. Estimating the subtraction constant with nucleon polarizabilities as extracted from Compton-scattering reactions [99], the subtracted analysis yields an electromagnetic contribution of $(-1.3 \pm 0.5)\,\text{MeV}$ instead. In either case, the result is compatible with recent determinations from the lattice [100] and from charge symmetry breaking in $pn \to d\pi^0$ [101].

is that it is impossible to directly extract a^+ from hadronic atoms. Only the combination

$$\tilde{a}^+ \equiv a^+ + \frac{1}{4\pi\xi_\mathrm{p}}\left\{\frac{4\Delta_\pi}{F_\pi^2}c_1 - 2e^2 f_1\right\} \tag{2.16}$$

is accessible, and a^+ itself cannot be obtained absent input on the LECs c_1 and f_1 from other sources (the full list of LECs relevant for the present analysis is given in Appendix A.1). If the standard single-nucleon-sector counting $e \sim p$ is employed, then these isospin-violating effects are actually of the same size as the piece of $\tilde{a}^+$ that would be present in the isospin limit. c_1 enters as its contribution to a^+ is proportional to $M_{\pi^0}^2$, and f_1 features in the electromagnetic contributions to m_p and m_n. Estimates of these constants will be discussed in Sect. 3.1.

Since only $\tilde{a}^+$ can directly be extracted, it is convenient to work with

$$\Delta\tilde{a}_{\pi^-p} = a_{\pi^-p} - (\tilde{a}^+ + a^-)\,, \qquad \Delta\tilde{a}_{\pi^-n} = a_{\pi^-n} - (\tilde{a}^+ - a^-)\,, \tag{2.17}$$

instead of Δa_{π^-p} and Δa_{π^-n}. The results relevant for the scattering-length extraction may then be written as

$$\begin{aligned}
\Delta\tilde{a}_{\pi^-p} &= \Delta\tilde{a}^+ + \Delta a^-\,, \qquad \Delta\tilde{a}_{\pi^-n} = \Delta\tilde{a}^+ - \Delta a^-\,,\\
\Delta\tilde{a}^+ &= \frac{1}{4\pi\xi_\mathrm{p}}\left\{e^2 M_\pi\big(2g_6^\mathrm{r} + g_8^\mathrm{r}\big) - \frac{g_\mathrm{A}^2 M_\pi}{32\pi F_\pi^2}\left(\frac{33\Delta_\pi}{4F_\pi^2} + e^2\right)\right\}\,,\\
\Delta a^- &= -\frac{e^2 f_2}{8\pi\xi_\mathrm{p}} - \frac{M_\pi}{4\pi\xi_\mathrm{p}}\left\{\frac{\Delta_\pi}{32\pi^2 F_\pi^4}\left(3 + \log\frac{M_\pi^2}{\mu^2}\right) + \frac{8\Delta_\pi}{F_\pi^2}d_5^\mathrm{r}\right.\\
&\quad \left. + \frac{e^2 g_\mathrm{A}^2}{16\pi^2 F_\pi^2}\left(1 + 4\log 2 + 3\log\frac{M_\pi^2}{\mu^2}\right) - e^2 g_8^\mathrm{r} + \frac{10}{9}\frac{e^2}{F_\pi^2}\big(k_1^\mathrm{r} + k_2^\mathrm{r}\big)\right\}\,,\\
\Delta a_{\pi^-p}^\mathrm{cex} &= \frac{\sqrt{2}}{4\pi\xi_\mathrm{p}}\left\{\frac{e^2 f_2}{2} + \frac{g_\mathrm{A}^2\Delta_\pi}{4F_\pi^2 m_\mathrm{p}} - \frac{3M_\pi\Delta_\pi}{16F_\pi^2 m_\mathrm{p}^2} - \frac{M_\pi\Delta_\mathrm{N}}{4F_\pi^2 m_\mathrm{p}}\big(1 + 2g_\mathrm{A}^2\big) + \frac{M_\pi\Delta_\pi}{8F_\pi^2 m_\mathrm{p}^2}(1 + 4m_\mathrm{p}c_4)\right.\\
&\quad + \frac{M_\pi\Delta_\pi}{192\pi^2 F_\pi^4}\left(2 - 7g_\mathrm{A}^2 + \big(2 - 5g_\mathrm{A}^2\big)\log\frac{M_\pi^2}{\mu^2}\right) + \frac{e^2 M_\pi}{32\pi^2 F_\pi^2}\left(5 + 3\log\frac{M_\pi^2}{\mu^2}\right)\\
&\quad \left. + \frac{8M_\pi\Delta_\pi}{F_\pi^2}d_5^\mathrm{r} + \frac{e^2 M_\pi}{2F_\pi^2}\left(F_\pi^2 g_7^\mathrm{r} - 2k_3^\mathrm{r} + k_4^\mathrm{r} + \frac{20}{9}\big(k_1^\mathrm{r} + k_2^\mathrm{r}\big)\right)\right\}\,,
\end{aligned} \tag{2.18}$$

where

$$\Delta_\mathrm{N} = m_\mathrm{n} - m_\mathrm{p}\,. \tag{2.19}$$

The apparent dependence on the renormalization scale μ is canceled by the scale dependence of the LECs, whose definition is briefly reviewed in Appendix A.1 (for more details we refer to [94]). Estimating the LECs as in [93] yields

$$\begin{aligned}
\Delta\tilde{a}^+ &= (-3.3 \pm 0.3)\cdot 10^{-3} M_\pi^{-1}\,, \qquad \Delta a^- = (1.4 \pm 1.3)\cdot 10^{-3} M_\pi^{-1}\,,\\
\Delta\tilde{a}_{\pi^-p} &= (-2.0 \pm 1.3)\cdot 10^{-3} M_\pi^{-1}\,, \qquad \Delta a_{\pi^-p}^\mathrm{cex} = (0.4 \pm 0.9)\cdot 10^{-3} M_\pi^{-1}\,.
\end{aligned} \tag{2.20}$$

In principle, one could also define an $\tilde{a}^-$ that absorbs the LECs appearing in Δa^- and $\Delta a_{\pi^-p}^\mathrm{cex}$ in the same way (namely f_2, d_5^r, k_1^r, and k_2^r), similarly to the definition of $\tilde{a}^+$ with respect to c_1 and f_1. In this way, the constraints of πH and πD on $\tilde{a}^+$ and $\tilde{a}^-$ would be considered and only in the end the estimates for the LECs inserted. The advantage of this alternative

procedure is that the dependence on the LECs is more transparent and correlations between the three constraints better under control. However, we have checked that the results obtained in such an approach differ only marginally from what we present here. In order to keep the discussion as simple as possible we work in terms of $\tilde{a}^+$, $\Delta\tilde{a}^+$, a^-, and Δa^-.

2.3 Hierarchy of three-body operators

2.3.1 Isospin-conserving operators

So far no counting scheme is known that permits consistent, realistic, and simultaneous consideration of the two- and three-body operators that contribute to $\pi^- d$ scattering. For example, in the original power counting by Weinberg [26, 107] the leading two-body operator (proportional to a^+) appears formally at one order lower than the leading three-body terms shown in Table 2.1. However, it has been known for years (see e.g. [82, 114]) that the double-scattering diagram (the first diagram in the first row of Table 2.1) alone nearly saturates the experimental value of the scattering length, whereas the term proportional to a^+ is significantly smaller, in plain disagreement with Weinberg counting. On the other hand, practical calculations demonstrate that Weinberg power counting still works quite well once applied to two- and three-body operators separately—despite its difficulties in accounting for the relative size of these two classes of contribution. In particular, it was shown in [109] that an application of the Weinberg scheme allows for a systematic, high-accuracy calculation of the strong three-body contributions to $a_{\pi^- d}$. The aim of this chapter is to demonstrate that Weinberg counting can be used to account for the isospin-violating three-body contributions as well.

For this reason, we consider a power counting within the class of three-body operators, ordered in Weinberg counting relative to the leading, double-scattering term. The isospin-conserving three-body diagrams are illustrated in Table 2.1, where we have indicated their relative contribution according to the expansion parameter p. We note that the ordering in Table 2.1 goes beyond naive dimensional analysis, since known enhancements and contributions at fractional orders in the expansion parameter are already taken into account (see below). The goal is to include all three-body operators up to one order lower than the contribution of the leading unknown $(N^\dagger N)^2\pi\pi$ contact term, which appears at next-to-next-to-leading order ($\mathrm{N^2LO}$). Its contribution cannot easily be determined from data, and is a key source of uncertainty in our result. Identifying $\Lambda_\chi \sim m_\mathrm{p}$, the expansion parameter $\mathcal{O}(p) \sim \chi = M_\pi/m_\mathrm{p}$ leads us to anticipate an accuracy of a few percent for threshold $\pi^- d$ scattering.

This expectation is substantiated by the sensitivity of our integrals to the choice of the deuteron wave function (see Sect. 2.4.4). Convolving the operators of Table 2.1 with different wave functions derived from chiral and phenomenological NN potentials we find a variation in the results of about 5 %, in agreement with the power-counting estimate of the contact term. In fact, it has been demonstrated explicitly that, for deuteron wave functions based on the one-pion-exchange interaction, the results for the individual diagrams at LO and NLO become cutoff-independent in the limit of a large cutoff [115, 109].

Apart from the double-scattering diagram, there are also LO diagrams involving $3\pi N^\dagger N$ and 4π vertices, which individually depend on the parameterization of the pion fields, while only the sum is parameterization independent. Numerically, these diagrams are strongly suppressed [26, 108], which can be traced back to the spin-isospin matrix element that is more than one order of magnitude smaller in these diagrams than that in double scattering, although the momenta in the diagrams are in line with Weinberg counting [109].

Chiral order	Three-body operator	Reference
LO $= \mathcal{O}(1)$	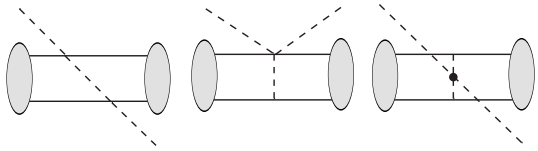	[26, 107]
NLO $= \mathcal{O}(p)$	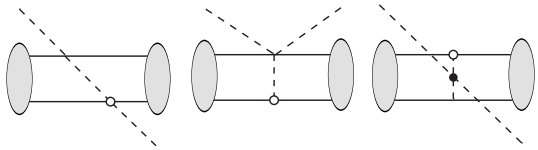	[108]
	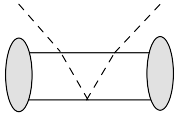	[108, 109]
	Effect of nucleon recoil in LO diagrams	[110, 111]
$\mathrm{N}^{3/2}\mathrm{LO} = \mathcal{O}\left(p^{3/2}\right)$	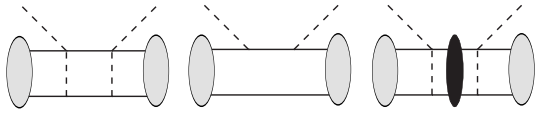	[112]
	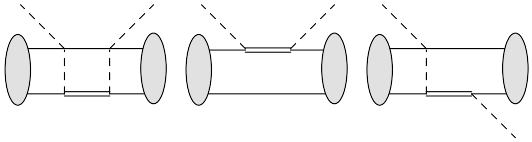	[113]
	Effect of nucleon recoil in LO diagrams	[110, 111]
$\mathrm{N}^{2}\mathrm{LO} = \mathcal{O}\left(p^{2}\right)$	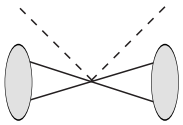 $+ \cdots$	

Table 2.1: Hierarchy of isospin-conserving three-body operators in Weinberg counting. Solid (open) circles correspond to leading (subleading) vertices, grey blobs indicate the deuteron wave functions, and the black ellipse corresponds to NN interactions in the intermediate state. Solid single, solid double, and dashed lines correspond to nucleons, $\Delta(1232)$-isobars, and pions, respectively.

The operators at NLO involve subleading vertices and were shown to cancel amongst themselves in [108]. In addition, the triple-scattering term should be included at NLO, since its contribution is enhanced due to its triangle topology. Indeed, it was shown in [109] that the long-ranged (infrared) part of this diagram is enhanced numerically by a factor of π^2, whereas the rest behaves in accord with Weinberg counting. The origin of this enhancement was associated in [109] with the special topology of the diagram consisting of two consecutive pion exchanges with Coulombic pion propagators. Similar enhancements by factors of π were already observed in triangle-type pion-loop contributions to the NN potential [116], the scalar form factor of the nucleon [22], the π^0 photoproduction amplitude [117], and even isospin violation in πN scattering [94, 93] itself, cf. (2.18). Evidently, this numerical (not parametric) enhancement, which results from a dimensionless integral not being $\mathcal{O}(1)$, cannot be captured by a power counting. For $\pi^- d$ scattering a similar effect may be expected from topologically analogous diagrams that belong to the so-called multiple-scattering series, which leads to concerns regarding the quadruple-scattering term: although it formally appears only at N^{4}LO, which is far beyond the edge of the theoretical accuracy, a potential numerical enhancement needs to be carefully investigated. However, the whole class of multiple-scattering diagrams can be summed up to all orders, and we find the effect from quadruple-scattering and higher diagrams to be entirely negligible, see Sect. 2.4.3.

In addition, starting from NLO, nucleon-recoil corrections to the leading, double-scattering operator have to be taken into account. The nucleon recoil has been extensively studied in the literature both phenomenologically, see e.g. [118], and within effective field theory [110, 111, 119]. While at leading order nucleons may be considered as infinitely heavy (fixed-center approximation), at NLO the kinetic energy of the nucleon matters, with the result that the static pion propagator needs to be replaced by the full propagator pertinent to the three-body πNN intermediate state. In the regime where all momenta in the diagram are of order of M_π, the nucleon-recoil effect is purely perturbative, can be calculated by expanding the nucleon kinetic energies using standard heavy-baryon techniques, and thus contributes at integer powers in the expansion. In contrast, there is also a non-perturbative regime—the regime of the three-body singularity—where the three-body propagator vanishes and the pion kinetic energy is of the order of the nucleon recoil. Consequently, pion momenta appear to be suppressed by $\sqrt{M_\pi/m_\mathrm{p}}$ compared to the typical momenta in the deuteron. Thus, the recoil effect generates half-integer powers of M_π/m_p in the expansion of the double-scattering diagram as well. Note that the potentially largest isovector recoil correction at order $\mathcal{O}(p^{1/2})$ vanishes exactly as a consequence of the Pauli principle, which prohibits the NN intermediate state to be in an S-wave in this case [110, 111]. Numerically, it was demonstrated in [111] that the recoil effect for $\pi^- d$ scattering is relevant only at orders $\mathcal{O}(p)$ and $\mathcal{O}(p^{3/2})$, in accordance with the power counting.

Besides the nucleon-recoil effect, there are further diagrams that may contribute at fractional orders due to the appearance of new scales. First, so-called dispersive corrections[4] due to the process $\pi d \to NN \to \pi d$ are characterized by the large momentum $p \sim \sqrt{M_\pi m_\mathrm{p}} \sim 360\,\mathrm{MeV}$ between the NN pair that corresponds to the threshold for pion production in NN collisions. Taking into account that the appropriate expansion parameter is $\sqrt{M_\pi/m_\mathrm{p}}$, one finds that these diagrams will enter at $\mathcal{O}(p^{3/2})$ in the calculation of the $\pi^- d$ scattering length [112]. Second, the typical momentum scale $p \sim \sqrt{(m_\Delta - m_\mathrm{p} - M_\pi)m_\mathrm{p}}$ for diagrams

[4]The name refers to the fact that the NN and $NN\gamma$ channels dominate the width of πD, which implies that diagrams with these intermediate states will indeed generate the imaginary part of the scattering length.

with explicit treatment of the $\Delta(1232)$ resonance (with mass m_Δ) is numerically very close to $\sqrt{M_\pi m_\mathrm{p}}$, which indicates that these contributions will become relevant at $\mathcal{O}(p^{3/2})$ as well [113]. Indeed, both effects must be included for a full calculation at $\mathcal{O}(p^{3/2})$, which is necessary to achieve the desired accuracy for the scattering-length extraction, see Sect. 2.6.

In the Δ-less theory the influence of the Δ-resonance is parameterized by the LECs c_i of πN scattering and contributes to $\pi^- d$ scattering through the so-called boost (Fermi motion) correction,[5] which was shown to be large but considerably model-dependent [108, 109]. Once the Δ is included explicitly, the value of the relevant LEC c_2 is significantly reduced [121], so that the residual boost correction is negligible in the Δ-full theory [109].

2.3.2 Isospin-violating operators

The two-body isospin-violating corrections relevant for $\pi^- d$ scattering have already been summarized in Sect. 2.2. Here, we delineate the hierarchy of isospin-violating three-body operators relative to each other, as well as their relative suppression compared to the leading-order isospin-conserving operators.

There are three classes of isospin-violating three-body contributions: first, isospin-breaking corrections appear in πNN propagators due to pion and nucleon mass differences. Second, isospin-violating πN interactions can occur in the diagrams introduced in Sect. 2.3.1. The operators corresponding to these two classes of isospin-violating mechanisms are marked as crossed circles in Table 2.2. Since isospin violation in hadron masses and πN interactions can occur due to both electromagnetic and quark-mass effects both these classes could be either $\sim m_\mathrm{d} - m_\mathrm{u}$ or $\sim e^2$. The third class is a purely electromagnetic effect: a new set of diagrams involving (low-energy) virtual photons (see Table 2.2 and Sect. 2.5 for more details).

At leading order in isospin violation, diagrams of this third class that involve a virtual photon and one insertion of the isospin-conserving πN vertex occur. These are represented by the first row of diagrams in Table 2.2. At the same order effects due to the pion mass difference in the leading-order isospin-conserving diagrams enter (the second row of diagrams in Table 2.2). These effects can be computed by working on the particle basis for the pion intermediate states in the leading-order three-body diagrams (see first row of Table 2.1), and explicitly keeping track of charged and neutral pion masses there. However, when this is done the double-scattering diagram must be treated in a special way, as its πNN intermediate state, and associated three-body cut, implies that the pion-mass-difference effect in this graph generates contributions not only at $\mathcal{O}(e^2)$, but at all subleading orders. The double-scattering graph with one insertion of the pion mass difference is therefore shown in Table 2.2 at LO, N$^{1/2}$LO, and NLO. The piece of this graph which is LO in isospin violation is suppressed by $e^2F_\pi^2/M_\pi^2$ compared to the corresponding isospin-conserving diagrams at LO, as are the other diagrams listed in the first two rows of Table 2.2. Diagrams involving $NN\gamma$ intermediate states are also of this size (see third line of Table 2.2), but these are included in the calculation of the dispersive corrections in [112], and so will be accounted for in Sect. 2.6.

The first contribution at subleading orders originates from the non-analytic terms due to the inclusion of the pion mass difference in the πNN propagator of the double-scattering diagram. These yield the N$^{1/2}$LO contribution of Table 2.2, in full analogy with the effect

[5] Note that the LEC c_1 and the linear combination of LECs $c_2 + c_3$ contribute to the πN scattering length a^+ and through that also to $\pi^- d$ scattering. However, neither c_1 nor $c_2 + c_3$ are affected by the Δ-isobar up to order $\mathcal{O}(p^2)$ [120], although the values of c_2 and c_3 individually are strongly saturated by the Δ and thus change significantly when considering the Δ as an explicit degree of freedom [120, 121].

Chiral order	Three-body operator	Reference
LO $= \mathcal{O}(e^2)$	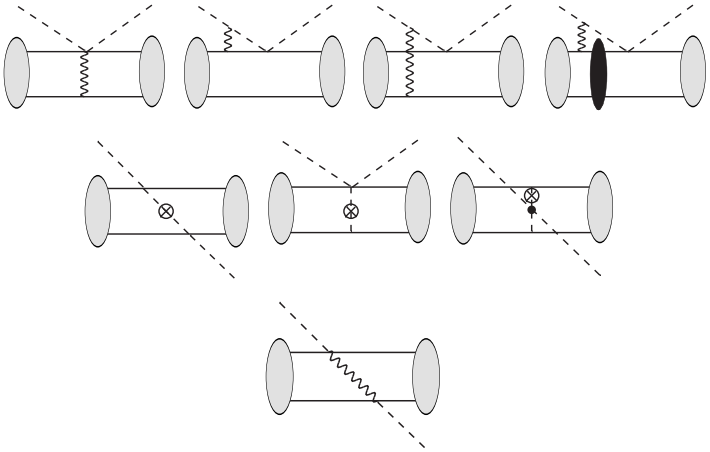	[112]
N$^{1/2}$LO $= \mathcal{O}(e^2 p^{1/2})$	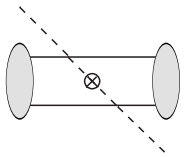	
NLO $= \mathcal{O}(e^2 p)$	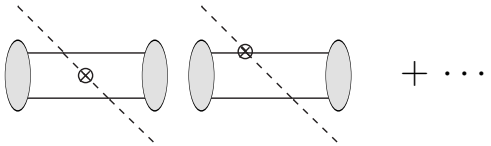	
N^{2}LO $= \mathcal{O}(e^2 p^2)$	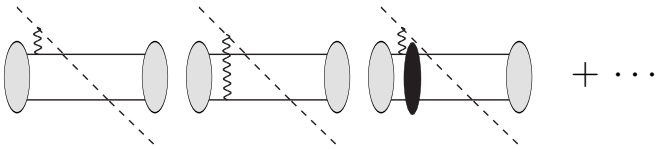	

Table 2.2: Hierarchy of isospin-violating three-body operators in Weinberg counting. The suppression of these operators is given with respect to the isospin-conserving diagrams at LO (cf. Table 2.1). Isospin violation appears either due to the inclusion of virtual photons (wiggly lines) or due to mass differences and electromagnetic effects (crossed circles). Note that diagrams with intermediate $NN\gamma$ states were already considered in [112] and are thus included in the dispersive corrections, cf. Sect. 2.6.

of nucleon recoil in the isospin-conserving case. Next, the operators at NLO are suppressed by $\mathcal{O}(e^2p)$ compared to the three-body isospin-conserving operators at LO, and, given the smallness of the expansion parameter, are already irrelevant numerically.[6] Therefore, we may, in principle, restrict the analysis to all isospin-violating mechanisms up to $\mathrm{N}^{1/2}\mathrm{LO}$.

However, due to the appearance of new scales in the three-body problem, certain higher-order operators might be enhanced, even though formally they only appear beyond $\mathcal{O}(e^2p^{1/2})$. Therefore, we investigate several higher-order effects:

1) To account for all effects related to the three-body cut in the double-scattering diagram we keep all terms proportional to the pion and nucleon mass differences in the πNN propagator unexpanded (see Sect. 2.4). In particular, we include the nucleon mass difference in the propagators to have the $\pi^0 nn$ and $\pi^- pn$ thresholds at the proper places, although this is formally an NLO effect.[7]

2) Due to the large size of the double-scattering diagram in the isospin-conserving case we include isospin violation in the πN vertices in this diagram. This effect also starts at NLO.

3) We study certain virtual-photon corrections to the double-scattering process (formally appearing at $\mathrm{N}^2\mathrm{LO}$). The presence of virtual photons enhances the region of small momenta in these diagrams, so that the integrals become infrared divergent in the limit of vanishing deuteron binding energy. The finite binding energy of the deuteron renders these diagrams finite, but the resulting contribution is potentially enhanced. In view of the fact that double scattering is numerically by far the dominant contribution to $\pi^- d$ scattering, these virtual-photon corrections could become relevant despite their being suppressed by yet another order in the power counting. This effect is discussed in detail in Sect. 2.5.

Note that the isospin-violating three-body mechanisms up to $\mathrm{N}^{1/2}\mathrm{LO}$ are of purely electromagnetic origin, while isospin violation due to the quark mass difference appears only in higher-order corrections, e.g. in 1) and 2). In particular, isospin violation in the pion mass difference is predominantly an electromagnetic, not a quark-mass effect (there is no term $\sim m_\mathrm{d} - m_\mathrm{u}$ at LO in isospin violation), while nucleon-mass-difference effects enter only at $\mathcal{O}(e^2p)$. In the case of 2), the isospin-violating πN interactions which appear there include terms proportional to the quark mass difference—as reviewed in Sect. 2.2—but this whole class of diagrams involving isospin-breaking pion–nucleon vertices does not start until NLO. We demonstrate in the subsequent sections that it is indeed the case that the additional corrections 1)–3) beyond $\mathrm{N}^{1/2}\mathrm{LO}$ are significantly smaller than the estimated theoretical uncertainty of the full analysis. Hence, the explicit calculation of these higher-order corrections provides an additional test of our counting scheme and uncertainty estimate.

[6] Furthermore, for full consistency with the power counting, the inclusion of NLO corrections to the three-body isospin-violating operators would require the calculation of $\mathrm{N}^2\mathrm{LO}$ isospin-violating two-body corrections, which have yet to be worked out.

[7] At first order in isospin breaking we have $\Delta_\mathrm{N} = -4Bc_5(m_\mathrm{d} - m_\mathrm{u}) + f_2 e^2 F_\pi^2$ and $\Delta_\pi = 2Ze^2F_\pi^2$, with $c_5 \sim f_2 \sim 1/m_\mathrm{p}$ and $Z = \mathcal{O}(1)$. These quantities then enter the πNN propagator in the combination $\rho = 2M_\pi\Delta_\mathrm{N} - \Delta_\pi$, cf. (2.21). Assuming that the electromagnetic and quark-mass-induced contributions to Δ_N are of the same size, one finds $M_\pi\Delta_\mathrm{N}/\Delta_\pi \sim M_\pi/m_\mathrm{p} \sim \mathcal{O}(p)$. Therefore, the nucleon-mass-difference contribution to ρ is suppressed by one chiral order compared to that coming from Δ_π. After accounting for the modification of the chiral counting due to the presence of the πNN cut, we find that Δ_N contributes to a^cut at $\mathcal{O}(e^2p)$, whereas Δ_π affects the scattering length already at $\mathcal{O}(e^2)$.

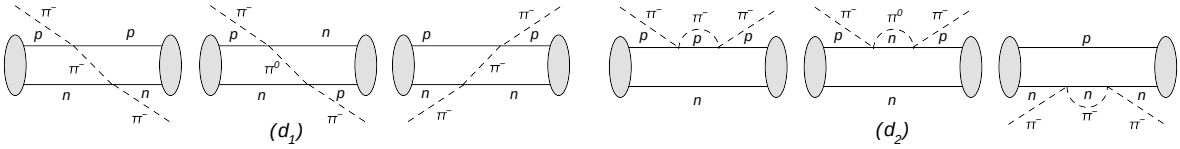

Figure 2.1: Double-scattering contributions to $\pi^- d$ scattering.

2.4 Strong contributions to $\pi^- d$ scattering

2.4.1 Double scattering

We start our discussion with the double-scattering diagrams (d_1) and (d_2) (cf. Fig. 2.1). While diagram (d_1) enters already at LO and contributes to all higher orders due to the nucleon-recoil effect, diagram (d_2) gives rise to a three-body contribution only if nucleons are not treated as static. Indeed, in the limit of infinitely heavy nucleons the pion loops in diagram (d_2) are already subsumed in the πN scattering lengths, since in this limit (d_2) is nothing but an ordinary loop correction in their chiral expansion. In this way, the contribution to $\pi^- d$ scattering from the part of (d_2) corresponding to static nucleons is always included in the two-body term $a^{(2)}_{\pi^- d}$ proportional to a^+, see (2.8) and (2.9). Thus, to obtain an additional three-body correction we need to investigate the effect of embedding the πN amplitude into the πNN system. In this procedure, established for the isospin-conserving case in [110, 111], the proper treatment of three-body dynamics demands that the contribution of the two-body (πN) cut be replaced by that of the three-body (πNN) cut. The goal of this section is to extend this formalism to the isospin-violating case.

First, we note that in the calculation of the double-scattering diagrams one can safely omit all isoscalar terms, since the term proportional to $(\tilde{a}^+)^2$ is tiny compared to $(a^-)^2$, while the term proportional to the combination $\tilde{a}^+ a^-$ cancels. Therefore, we calculate the diagrams of Fig. 2.1 keeping only the isovector πN scattering amplitude, but retaining the isospin-violating correction Δa^-. Following the procedure described in [110], we obtain

$$\begin{aligned}
a^{(d_1)+(d_2)} &= a^{\text{static}} + a^{\text{static}}_{\text{NLO}} + a^{\text{cut}} + \Delta a^{(2)} \,, \\
a^{\text{static}} &= -\bar{a}^2 \left\langle \frac{1}{\mathbf{q}^2} \right\rangle , \qquad a^{\text{static}}_{\text{NLO}} = \bar{a}^2 \left\langle \frac{1}{\mathbf{q}^2} \left(\frac{\omega_{\mathbf{q}}}{\omega_{\mathbf{q}} + m_{\text{p}}} \right) \right\rangle , \\
a^{\text{cut}} &= \int \mathrm{d}^3 p \, \mathrm{d}^3 q \big(\Psi^\dagger(\mathbf{p}) - \Psi^\dagger(\mathbf{p} - \mathbf{q}) \big) \Psi(\mathbf{p}) \\
&\qquad \times \left\{ \bar{a}^2 \left[\frac{1}{\mathbf{q}^2 + \delta} - \frac{1}{\mathbf{q}^2 + \tilde{\delta}} \right] - \bar{a}^2_{\text{cex}} \left[\frac{1}{\mathbf{q}^2 + \delta} - \frac{1}{\mathbf{q}^2 + \delta + \rho} \right] \right\} , \\
\Delta a^{(2)} &= \bar{a}^2_{\text{cex}} \int \mathrm{d}^3 q \, \left[\frac{1}{\mathbf{q}^2 + \tilde{\delta}} - \frac{1}{\mathbf{q}^2 + \tilde{\delta} + \rho} \right] ,
\end{aligned} \tag{2.21}$$

where

$$\begin{aligned}
&\delta_{\mathbf{p}_1, \mathbf{p}_2} = 2\omega_{\mathbf{p}_1 - \mathbf{p}_2} \left(\epsilon + \frac{\mathbf{p}_1^2 + \mathbf{p}_2^2}{2 m_{\text{p}}} \right) , \qquad \delta = \delta_{\mathbf{p}, \mathbf{p} - \mathbf{q}} \,, \qquad \tilde{\delta} = \frac{\omega_{\mathbf{q}} \mathbf{q}^2}{m_{\text{p}}} \,, \qquad \rho = 2 M_\pi \Delta_{\text{N}} - \Delta_\pi \,, \\
&\omega_{\mathbf{q}} = \sqrt{M_\pi^2 + \mathbf{q}^2} \,, \qquad \langle f(\mathbf{q}) \rangle = \int \mathrm{d}^3 p \, \mathrm{d}^3 q \, \Psi^\dagger(\mathbf{p} - \mathbf{q}) f(\mathbf{q}) \Psi(\mathbf{p}) \,,
\end{aligned} \tag{2.22}$$

and ϵ is the deuteron binding energy. The πN scattering lengths in (2.21) are defined as

$$\bar{a}^2 = \frac{\xi_\mathrm{p}^2}{\pi^2\xi_\mathrm{d}}\left((a^- + \Delta a^-)^2 + \frac{1}{2}\left(a^{\mathrm{cex}}_{\pi^- p}\right)^2\right) = \frac{\xi_\mathrm{p}^2}{\pi^2\xi_\mathrm{d}}\left(2(a^-)^2 + 2a^-\Delta a^- - \sqrt{2}\,a^-\Delta a^{\mathrm{cex}}_{\pi^- p} + \cdots\right),$$
$$\bar{a}^2_{\mathrm{cex}} = \frac{\xi_\mathrm{p}^2}{2\pi^2\xi_\mathrm{d}}\left(a^{\mathrm{cex}}_{\pi^- p}\right)^2 = \frac{\xi_\mathrm{p}^2}{\pi^2\xi_\mathrm{d}}\left((a^-)^2 - \sqrt{2}\,a^-\Delta a^{\mathrm{cex}}_{\pi^- p} + \cdots\right), \tag{2.23}$$

where the ellipses contain higher orders in isospin violation. We use a normalization of the deuteron wave functions $\Psi(\mathbf{p})$ where

$$\int \mathrm{d}^3p\,\Psi^\dagger(\mathbf{p})\Psi(\mathbf{p}) = 1\,. \tag{2.24}$$

The individual terms in (2.21) can be interpreted as follows: a^{static} corresponds to (d_1) evaluated with a static pion propagator, and is numerically by far the dominant contribution. Recoil corrections to the static pion propagator are incorporated in $a^{\mathrm{static}}_{\mathrm{NLO}}$, while a^{cut} comprises effects due to the three-body $\pi^0 nn$ and $\pi^- pn$ cuts. $\Delta a^{(2)}$ emerges as an isospin-violating correction in this rearrangement, which in the end does not constitute a true three-body effect—as indicated by the absence of the deuteron wave function. In the isospin limit $\rho = \Delta_\pi = \Delta_N = \Delta a^- = \Delta a^{\mathrm{cex}}_{\pi^- p} = 0$ (2.21) reduces to the result derived in [110].

As alluded to in Sect. 2.3.1, the power counting is complicated by the fact that the integrals in (2.21) involve scales other than M_π: $\sqrt{M_\pi\epsilon}$ and $\sqrt{M_\pi/m_\mathrm{p}}\,M_\pi$ due to the three-body cut, and $\sqrt{m_\mathrm{p}\epsilon}$ by means of the deuteron wave functions. Accordingly, it may seem at first glance that the presence of a three-body cut renders the integral for a^{cut} enhanced compared to its naive ChPT order by $\sqrt{m_\mathrm{p}/M_\pi}$ [119]. Indeed, it was shown in [111] that the full result for the double-scattering diagrams can be expanded in half-integer powers of χ as

$$a^{(d1)+(d2)} = a^{\mathrm{static}} + a_1\,\chi^{1/2} + a_2\,\chi + a_3\,\chi^{3/2} + \cdots\,, \tag{2.25}$$

where non-integer powers appear due to the presence of the three-body cut. However, the leading non-integer recoil correction at order $\chi^{1/2}$ vanishes, since the Pauli principle and the isovector character of the leading πN scattering operator ensure that the intermediate NN state is projected onto a P-wave [110]. Explicitly, the $\chi^{1/2}$ contribution to a^{cut} can be derived by neglecting small pion momenta $\mathbf{q}$ with respect to $\mathbf{p}$ in the wave functions, which immediately proves that $a_1 = 0$, see (2.21). In consequence, the scales $\sqrt{M_\pi\epsilon}$, $\sqrt{M_\pi/m_\mathrm{p}}\,M_\pi$, and $\sqrt{m_\mathrm{p}\epsilon}$ do not enter at this order: all potentially enhanced contributions cancel due to a subtle interplay between the two diagrams (d_1) and (d_2) ultimately dictated by the Pauli principle. Therefore, the combined integral is indeed dominated by momenta of order M_π, as assumed in the power counting. Half-integer corrections at order $\chi^{3/2}$ and above may contain the additional scales as well, but still momenta of order of M_π will have the largest impact on a_3 in (2.25).

In principle, there are also diagrams with P-wave interactions between nucleons in the intermediate state. Examination of the integrand for $a_{\pi^- d}$ in this case shows that the size of the effect can be estimated as [33]

$$\chi^{3/2}\left|\delta_{^3P_J}\right| a^{\mathrm{static}} \sim 0.2\cdot 10^{-3} M_\pi^{-1}\,, \tag{2.26}$$

where $J \in \{0,1,2\}$, and the NN phase shifts $\delta_{^3P_J}$ provide a further suppression beyond the ChEFT counting that ensures that this class of diagrams does not have to be considered any further.

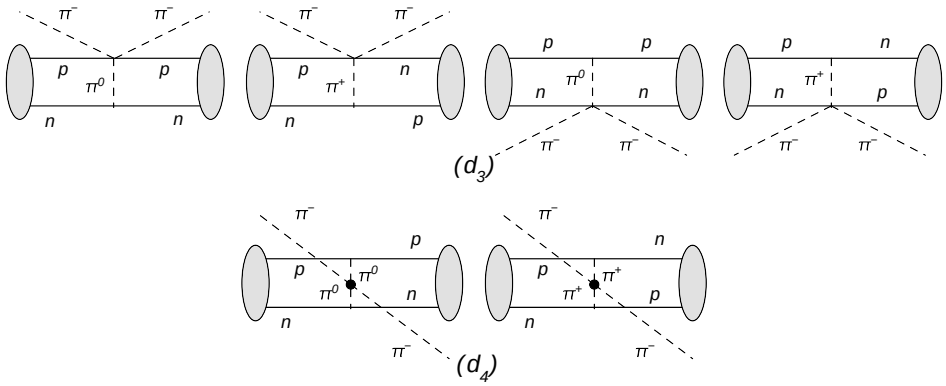

Figure 2.2: Isospin violation in (d_3) and (d_4).

2.4.2 Further leading-order diagrams

Although the diagrams (d_3) and (d_4) (cf. Fig. 2.2) are suppressed by accidentally small spin-isospin factors [109], we have calculated the full isospin-violating corrections to this class of diagrams, as required by the power counting

$$a^{\pi\pi} = \frac{g_\mathrm{A}^2 M_{\pi^0}^2}{128\pi^4 \xi_\mathrm{d} F_\pi^4} \left\{ \left\langle \frac{\mathbf{q}\cdot\boldsymbol{\sigma}_1 \mathbf{q}\cdot\boldsymbol{\sigma}_2}{(\mathbf{q}^2+M_{\pi^0}^2)^2} \right\rangle - \frac{4\Delta_\pi}{M_{\pi^0}^2} \left\langle \frac{\mathbf{q}\cdot\boldsymbol{\sigma}_1 \mathbf{q}\cdot\boldsymbol{\sigma}_2}{(\mathbf{q}^2+M_\pi^2)^2} \right\rangle \right\} . \tag{2.27}$$

We find that isospin breaking due to the pion mass difference amounts to $4\Delta_\pi/M_{\pi^0}^2 \approx 28\,\%$. This is a large isospin-violating effect, which is, however, of little practical relevance given the overall suppression of this contribution. As was shown in [108], NLO contributions to the leading-order diagrams vanish in the isospin limit. As isospin-breaking corrections to this are suppressed by another two orders, subleading corrections to (d_1)–(d_4) may therefore be safely ignored.

2.4.3 Triple scattering and the multiple-scattering series

Despite its nominal suppression by p^2 relative to the double-scattering operator (see Table 2.1), it was shown in [108, 109] that the triple-scattering diagram is enhanced by a factor of π^2 over its power-counting estimate and hence has to be included in order to achieve the desired accuracy. Neglecting isoscalar contributions as well as isospin-breaking corrections, one finds

$$a^\mathrm{triple} = \frac{(\xi_\mathrm{p} a^-)^3}{\pi \xi_\mathrm{d}} \left\langle \frac{1}{|\mathbf{q}|} \right\rangle . \tag{2.28}$$

The enhancement can be traced back to the occurrence of two Coulombic propagators, which produces a dimensionless integral that is not $\mathcal{O}(1)$, as assumed in dimensional analysis, but instead yields a factor π^2. Similar enhancements occur at higher orders in the multiple-scattering series as well, potentially jeopardizing the convergence of the perturbative expansion. However, an explicit numerical evaluation shows that the result for the full multiple-scattering series resummed in configuration space [122]

$$a^\mathrm{ms} = -\frac{4}{\xi_\mathrm{d}} \left\langle \frac{\frac{(\xi_\mathrm{p} a^-)^2}{r} - \frac{(\xi_\mathrm{p} a^-)^3}{r^2}}{1 + \frac{(\xi_\mathrm{p} a^-)^2}{r^2} - 2\frac{(\xi_p a^-)^3}{r^3}} \right\rangle = -\frac{4(\xi_\mathrm{p} a^-)^2}{\xi_\mathrm{d}} \left\langle \frac{r}{r^2 + r\xi_\mathrm{p} a^- + 2(\xi_\mathrm{p} a^-)^2} \right\rangle \tag{2.29}$$

model	$\Lambda/\tilde{\Lambda}$	$\langle 1/\mathbf{q}^2\rangle$	$I^{\rm NLO}$	$I^{\rm cut}$	$\langle 1/\lvert\mathbf{q}\rvert\rangle$	$a^{\pi\pi}$	$I^{\rm EM}$
AV 18	—	12.7	1.94	−2.68	7.4	−0.00050	9.92
CD-Bonn	—	12.8	2.04	−2.47	8.7	−0.00037	9.85
ChEFT N^{2}LO	450/500	13.0	2.12	−2.29	9.7	−0.00007	9.85
ChEFT N^{2}LO	600/500	12.8	2.04	−2.43	8.8	−0.00025	9.94
ChEFT N^{2}LO	550/600	12.9	2.09	−2.39	9.5	−0.00020	9.91
ChEFT N^{2}LO	450/700	13.2	2.15	−2.30	9.9	−0.00007	9.95
ChEFT N^{2}LO	600/700	12.9	2.09	−2.43	9.4	−0.00025	9.85

Table 2.3: Matrix elements for phenomenological as well as N^{2}LO chiral wave functions in appropriate powers of M_π [33]. The cutoffs $\Lambda/\tilde{\Lambda}$ are given in MeV and specify the version of the chiral interaction as given in [29]. $I^{\rm EM}$ is defined in Sect. 2.4.4 and needed for diagrams involving virtual photons.

differs from the first two terms (double and triple scattering) by only $0.1\cdot 10^{-3} M_\pi^{-1}$ [33], significantly less than the estimated uncertainty due to the contact term of about $1\cdot 10^{-3} M_\pi^{-1}$. Hence, the multiple-scattering series converges sufficiently fast that quadruple scattering and higher orders can be neglected in the calculation of $a_{\pi^- d}$. For a more detailed discussion of the multiple-scattering series in meson–nucleus scattering we refer to [123].

2.4.4 Numerical results

In Table 2.3 we quote the results given in [33] for the wave-function averages for two different modern phenomenological interactions, AV18 [124] and CD-Bonn [125], as well as N^{2}LO chiral interactions [29]. As the isospin-breaking corrections to the πN scattering lengths in (2.23) are relevant only for $a^{\rm static}$, to which they contribute about 1%, we may write the integrals for the contribution of $a^{\rm cut}$ and the NLO correction to the static πNN propagator as

$$a^{\rm cut} = \frac{2\xi_{\rm p}^2}{\pi^2\xi_{\rm d}}(a^-)^2 I^{\rm cut}\,, \qquad a^{\rm static}_{\rm NLO} = \frac{2\xi_{\rm p}^2}{\pi^2\xi_{\rm d}}(a^-)^2 I^{\rm NLO}\,, \tag{2.30}$$

with

$$I^{\rm cut} = \int \mathrm{d}^3p\,\mathrm{d}^3q\big(\Psi^\dagger(\mathbf{p}) - \Psi^\dagger(\mathbf{p}-\mathbf{q})\big)\Psi(\mathbf{p})\left\{\frac{1}{\mathbf{q}^2+\delta} - \frac{1}{\mathbf{q}^2+\tilde{\delta}} - \frac{1}{2}\left[\frac{1}{\mathbf{q}^2+\delta} - \frac{1}{\mathbf{q}^2+\delta+\rho}\right]\right\},$$
$$I^{\rm NLO} = \left\langle \frac{1}{\mathbf{q}^2}\left(\frac{\omega_{\mathbf{q}}}{\omega_{\mathbf{q}}+m_{\rm p}}\right)\right\rangle, \tag{2.31}$$

and δ, $\tilde{\delta}$, and ρ defined in (2.22).

While the statistical uncertainties of the numerical results are not significant, an appreciably larger uncertainty is introduced by the different short-distance ($r \ll 1/M_\pi$) physics of the NN wave functions used. To combine the results for the different deuteron wave functions, we take the average of all seven potentials as our mean value, while the uncertainty is taken to be the maximum deviation from this average. In this way, we obtain the individual contributions

a^{static}	-24.1 ± 0.7	$a^{\text{static}}_{\text{NLO}}$	3.8 ± 0.2	a^{cut}	-4.8 ± 0.5
a^{triple}	2.6 ± 0.5	$a^{\pi\pi}$	-0.2 ± 0.3	$\Delta a^{(2)}$	0.2

Table 2.4: Strong contributions to $a^{(3)}_{\pi^- d}$ in units of $10^{-3} M_\pi^{-1}$ for $a^- = 86.1 \cdot 10^{-3} M_\pi^{-1}$.

to a^{str} given in Table 2.4 (note that $\Delta a^{(2)}$ is independent of the deuteron wave function). Summing all contributions to a^{str}, we find

$$a^{\text{str}} = (-22.6 \pm 1.1 \pm 0.4) \cdot 10^{-3} M_\pi^{-1} \,, \tag{2.32}$$

where the first error refers to the model dependence of the matrix elements and the second to the uncertainty in the isospin-breaking shifts in the πN scattering lengths.[8]

2.5 Virtual photons

The improved Deser formula (2.7) is derived in an EFT that resums the effects of the photon ladder in pionic deuterium. In particular, this calculation already includes effects characterized by virtual-photon momenta $|\mathbf{k}| \sim r_{\text{B}}^{-1}$ with the Bohr radius $r_{\text{B}} = (\alpha M_\pi)^{-1}$. The virtual-photon corrections to $a_{\pi^- d}$ should therefore include all contributions above this scale, a requirement that can in fact be regarded as a definition of the $\pi^- d$ scattering lengths in the presence of electromagnetic interactions (see Sect. 3.2.1). In the chiral regime where momenta are assumed to be of order M_π, photons are perturbative and the leading contributions due to the exchange of (Coulomb) photons between the π^- and the proton are given by the diagrams shown in Fig. 2.3: (d_6), (d_7), and (d_8) (cf. Table 2.2).

However, diagrams (d_6) and (d_8)–(d_{10}) involve πNN intermediate states with relative momenta $\sim \sqrt{M_\pi \epsilon} \ll M_\pi$. Even more, these diagrams are "would-be infrared singular" in the sense that in the limit $\epsilon \to 0$ (and for static nucleons) they entail the (singular) matrix elements $\langle 1/\mathbf{q}^4 \rangle$. This leads to a potential enhancement $\sim \sqrt{M_\pi/\epsilon}$ for physical values of ϵ. Furthermore, the intermediate NN pair can be in an S-wave, so that NN interactions cannot be ignored. In particular, in the isoscalar partial wave, where the intermediate NN Green function includes the deuteron pole, the contribution of a point-like deuteron already accounted for in the improved Deser formula needs to be carefully subtracted (see Appendix A.2).

In the remainder of this section, we will discuss all these effects in some detail. As the appearance of additional scales might require modifications of the ChPT counting rules, we will also consider the higher-order diagrams (d_9) and (d_{10}).

2.5.1 Diagrams without intermediate-state NN rescattering

As a first step, we consider the diagrams depicted in Fig. 2.3 without intermediate-state NN interactions. For (d_6) and (d_8) we obtain

$$a^{(d_6)+(d_8)} = \frac{2\alpha M_\pi \xi_{\text{p}}}{\pi^2 \xi_{\text{d}}} \int \mathrm{d}^3 p \, \mathrm{d}^3 q \frac{a_{\pi^- n} \Psi^\dagger(\mathbf{p}-\mathbf{q}) \Psi(\mathbf{p}) + a_{\pi^- p} \Psi^\dagger(\mathbf{p}) \Psi(\mathbf{p})}{|\mathbf{q}| \big(|\mathbf{q}| + \delta/2\omega_{\mathbf{q}}\big) \big(\mathbf{q}^2 + \delta\big)} \,, \tag{2.33}$$

[8] These results are quoted for $a^- = 86.1 \cdot 10^{-3} M_\pi^{-1}$. However, for the final result in Fig. 3.1 the full a^- dependence of a^{str} is taken into account.

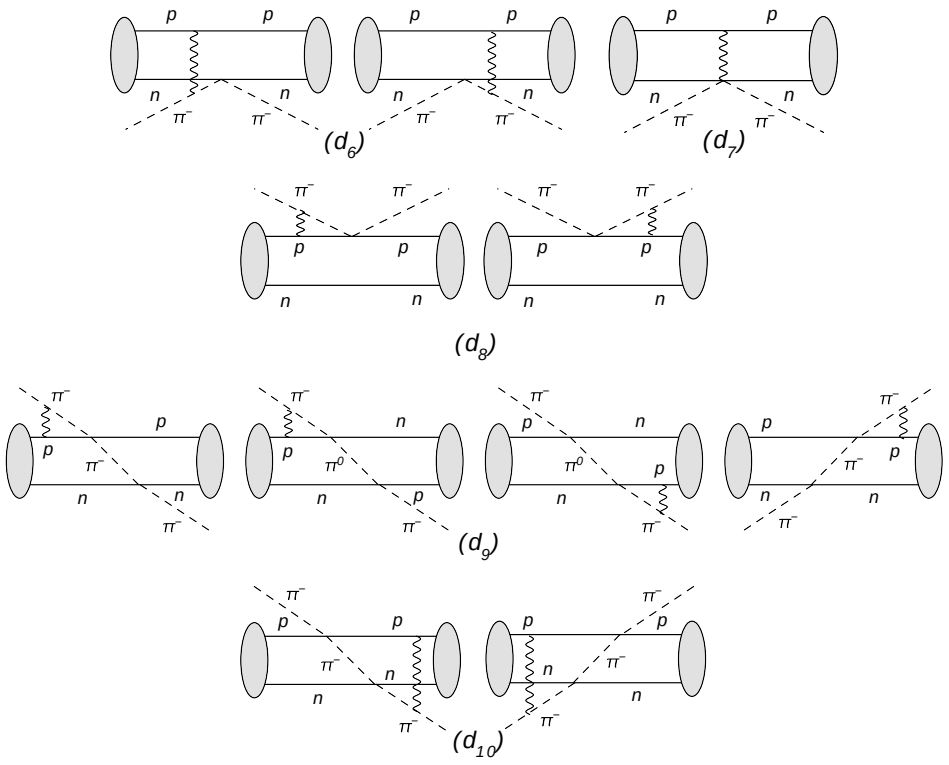

Figure 2.3: Virtual-photon diagrams in $\pi^- d$ scattering. Charged and neutral pions as well as protons and neutrons are shown explicitly to illustrate how the photon couples to the charged particles. The effect of mass differences between charged and neutral particles is not considered, since it is higher order in isospin breaking.

where we have used time-ordered perturbation theory to include the nucleon recoil both in the photon and the pion propagator. It is now convenient to split this expression into isovector and isoscalar πN interactions. Dropping isospin violation in the scattering lengths, the isospin $T = 1$ part becomes

$$a_{T=1}^{(d_6)+(d_8)} = \frac{2\alpha M_\pi \xi_\mathrm{p} a^-}{\pi^2 \xi_\mathrm{d}} \int \mathrm{d}^3p\, \mathrm{d}^3q \frac{\big(\Psi^\dagger(\mathbf{p}) - \Psi^\dagger(\mathbf{p}-\mathbf{q})\big)\Psi(\mathbf{p})}{|\mathbf{q}|\big(|\mathbf{q}| + \delta/2\omega_\mathbf{q}\big)\big(\mathbf{q}^2 + \delta\big)} \,. \tag{2.34}$$

Similar to the double-scattering diagram the expansion of (d_6) and (d_8) in M_π/m_p induces non-analytic terms due to nucleon recoil. However, contrary to a^cut in (2.21) the region of small momenta in (2.34) is significantly enhanced due to the presence of the photon. As a consequence, the expansion[9] of (d_6) and (d_8) starts from $\chi^{-1/2}$

$$a^{(d_6)+(d_8)} = b_0\, \chi^{-1/2} + b_\mathrm{static} + b_1\, \chi^{1/2} + \cdots \,. \tag{2.35}$$

Indeed, at leading order in M_π/m_p, which appears from the non-perturbative regime of the three-body cut ($|\mathbf{q}| \sim \sqrt{M_\pi/m_\mathrm{p}}|\mathbf{p}| \ll |\mathbf{p}|$), the contributions of (d_6) and (d_8) are equal and

[9]Note that this concerns only the aforementioned expansion in M_π/m_p, whereas the scale of the individual contributions is hidden in the coefficients b_i. For example, $b_0 \sim M_\pi/\gamma$ is dominated by momenta $\sim \gamma = \sqrt{m_\mathrm{p}\epsilon}$, which together with $\chi^{-1/2}$ from (2.35) produces $\sqrt{M_\pi/\epsilon}$ in (2.38).

both involve the integral

$$\int \mathrm{d}^3p\,\mathrm{d}^3q \frac{\Psi^\dagger(\mathbf{p})\Psi(\mathbf{p})}{\mathbf{q}^2\big(\mathbf{q}^2+2M_\pi(\epsilon+\mathbf{p}^2/m_\mathrm{p})\big)} = \frac{\sqrt{2}\,\pi^2}{\sqrt{\chi}}\int \mathrm{d}^3p\,\frac{\Psi^\dagger(\mathbf{p})\Psi(\mathbf{p})}{\sqrt{\mathbf{p}^2+\gamma^2}}\,. \tag{2.36}$$

If we use asymptotic deuteron wave functions

$$\Psi(\mathbf{p}) = \frac{\sqrt{\gamma}}{\pi(\mathbf{p}^2+\gamma^2)} \tag{2.37}$$

to perform the integral, we find at leading order

$$a_{T=1}^{(d_8)} = -a_{T=1}^{(d_6)} = \frac{2\alpha M_\pi \xi_\mathrm{p} a^-}{\pi^2\xi_\mathrm{d}}\frac{8\pi}{3\sqrt{2}}\frac{1}{\sqrt{M_\pi\epsilon}} = a^-\frac{16\alpha\xi_\mathrm{p}}{3\pi\xi_\mathrm{d}}\sqrt{\frac{M_\pi}{2\epsilon}}\,. \tag{2.38}$$

In this way, we see that indeed the individual diagrams are enhanced by $\sqrt{M_\pi/\epsilon}$, but these contributions cancel in the sum of (d_6) and (d_8), with the result that $b_0 = 0$ in (2.35) (in close analogy to $a_1 = 0$ in (2.25)). The physical explanation for this cancellation is again provided by the Pauli principle: as the πN interaction does not change the spin, it implies that for the isovector case the intermediate NN pair must be in a P-wave, which is reflected by the relative sign between the wave functions in (2.34). As P-wave NN interactions are small, the only non-vanishing isovector contribution is therefore generated by the residual effects in (2.34).

The calculation of the gauged Weinberg–Tomozawa diagram (d_7) including the nucleon recoil in the photon propagator proceeds along the same lines as the decomposition of (d_1) and (d_2). Subtracting the appropriate two-body diagram, we obtain

$$\begin{aligned} a^{(d_7)} &= -\frac{\alpha}{16\pi^3F_\pi^2\xi_\mathrm{d}}\left\langle\frac{1}{\mathbf{q}^2}\right\rangle + \frac{\alpha}{16\pi^3F_\pi^2\xi_\mathrm{d}}\left\langle\frac{1}{|\mathbf{q}|(2m_\mathrm{p}+|\mathbf{q}|)}\right\rangle \\ &\quad + \frac{\alpha}{16\pi^3F_\pi^2\xi_\mathrm{d}}\int \mathrm{d}^3p\,\mathrm{d}^3q\big(\Psi^\dagger(\mathbf{p})-\Psi^\dagger(\mathbf{p}-\mathbf{q})\big)\Psi(\mathbf{p})\left\{\frac{1}{|\mathbf{q}|(|\mathbf{q}|+\delta/2\omega_\mathbf{q})}-\frac{1}{|\mathbf{q}|(|\mathbf{q}|+\mathbf{q}^2/2m_\mathrm{p})}\right\}, \end{aligned} \tag{2.39}$$

where the second and third terms are analogs of $a_\mathrm{NLO}^\mathrm{static}$ and a^cut, respectively. For momenta $\sim M_\pi$, the recoil correction in the photon propagator is, in principle, a higher-order effect. Indeed, numerical evaluation [33] shows that the corrections to the static photon propagator are very small, only about $-0.045\cdot10^{-3}M_\pi^{-1}$, and may therefore be safely neglected.

In contrast, the Pauli principle allows for S-wave NN interactions in the isoscalar part of (d_6) and (d_8). These will be discussed in Sect. 2.5.2, while the numerical results are summarized in Sect. 2.5.4. However, if the $T=0$ part of these diagrams were significant, then one would also be concerned about virtual-photon exchange within the more sizeable double-scattering diagram. For this reason, we also give the expressions for (d_9) and (d_{10}). Neglecting the nucleon recoil in the photon propagator, the result reads

$$a^{(d_9)+(d_{10})} = -\frac{\alpha M_\pi(\xi_\mathrm{p}a^-)^2}{\pi^4\xi_\mathrm{d}}\left\langle\frac{3}{\mathbf{q}^2}\int\frac{\mathrm{d}^3l}{\mathbf{l}^2\big(\mathbf{l}^2+\delta_{\mathbf{p},\mathbf{p}+\mathbf{l}}\big)}+\int\frac{\mathrm{d}^3l}{(\mathbf{q}+\mathbf{l})^2\,\mathbf{l}^2\big(\mathbf{l}^2+\delta_{\mathbf{p},\mathbf{p}+\mathbf{l}}\big)}\right\rangle, \tag{2.40}$$

which can be separated into its isoscalar and isovector pieces as follows

$$\begin{aligned} a_{T=0}^{(d_9)+(d_{10})} &= -\frac{2\alpha M_\pi(\xi_\mathrm{p}a^-)^2}{\pi^4\xi_\mathrm{d}}\left\langle\frac{1}{\mathbf{q}^2}\int\frac{\mathrm{d}^3l}{\mathbf{l}^2\big(\mathbf{l}^2+\delta_{\mathbf{p},\mathbf{p}+\mathbf{l}}\big)}+\int\frac{\mathrm{d}^3l}{(\mathbf{q}+\mathbf{l})^2\,\mathbf{l}^2\big(\mathbf{l}^2+\delta_{\mathbf{p},\mathbf{p}+\mathbf{l}}\big)}\right\rangle, \\ a_{T=1}^{(d_9)+(d_{10})} &= -\frac{\alpha M_\pi(\xi_\mathrm{p}a^-)^2}{\pi^4\xi_\mathrm{d}}\left\langle\frac{1}{\mathbf{q}^2}\int\frac{\mathrm{d}^3l}{\mathbf{l}^2\big(\mathbf{l}^2+\delta_{\mathbf{p},\mathbf{p}+\mathbf{l}}\big)}-\int\frac{\mathrm{d}^3l}{(\mathbf{q}+\mathbf{l})^2\,\mathbf{l}^2\big(\mathbf{l}^2+\delta_{\mathbf{p},\mathbf{p}+\mathbf{l}}\big)}\right\rangle. \end{aligned} \tag{2.41}$$

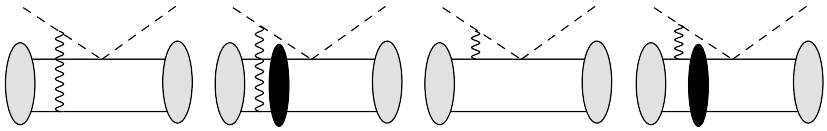

Figure 2.4: Leading virtual-photon diagrams with the black blobs indicating intermediate-state NN interactions. The time-reversed diagrams are not shown explicitly, but are included in the calculation (time flows from left to right).

Again, the leading, potentially enhanced contribution in the isovector case cancels in accordance with the Pauli principle. The isoscalar case, including intermediate-state NN interactions, will be addressed in Sect. 2.5.3.

2.5.2 The role of rescattering I: single scattering with photon exchange

The isoscalar contribution of (d_6) and (d_8) including intermediate-state NN interactions (ISI) (see Fig. 2.4) is given by

$$a_{T=0}^{(d_6)+(d_8)} + a_{T=0,\,\mathrm{ISI}}^{(d_6)+(d_8)} = -\frac{8\pi\alpha\xi_\mathrm{p}a^+}{(2\pi)^6\xi_\mathrm{d}}\int\frac{\mathrm{d}^3k}{\mathbf{k}^2}\int\mathrm{d}^3q\,\mathrm{d}^3q'\Psi^\dagger(\mathbf{q}')$$
$$\times\left\{G_s\Big(\mathbf{q}'-\frac{\mathbf{k}}{2},\mathbf{q}-\frac{\mathbf{k}}{2};-\epsilon-\frac{\mathbf{k}^2}{2M_\pi},-\mathbf{k}\Big)+G_s\Big(\mathbf{q}'-\frac{\mathbf{k}}{2},-\mathbf{q}+\frac{\mathbf{k}}{2};-\epsilon-\frac{\mathbf{k}^2}{2M_\pi},-\mathbf{k}\Big)\right.$$
$$\left.-\frac{2(2\pi)^3\Psi(\mathbf{q}')\Psi^\dagger(\mathbf{q})}{-\mathbf{k}^2/2\mu_D+i\eta}\right\}\Psi(\mathbf{q})\,, \tag{2.42}$$

where $G_s(\mathbf{p}',\mathbf{p};E,\mathbf{P})$ is the isoscalar NN Green function for initial (final) relative momentum $\mathbf{p}$ ($\mathbf{p}'$) and a state of total energy E and momentum $\mathbf{P}$. Note that to obtain this result we have neglected the nucleon recoil in the photon propagator and treated the pion as a non-relativistic particle. In the regime relevant for this section, where the pion momentum is much less than its mass, both approximations amount to perturbative corrections to the main result. Therefore, we may neglect these effects for the time being, and focus on the infrared enhancement of these graphs. The two Green functions may be interpreted as direct and exchange contributions, i.e. the photon can couple either to the nucleon that undergoes the πN interaction or to the other one. The last term subtracts the deuteron pole ($\eta\to 0^+$), as this part is already accounted for in the modified Deser formula, cf. Fig. 2.5 for a graphical illustration of this piece. The shift of the $1s$ level in pionic deuterium is proportional to the convolution of the $\pi^- d$ scattering length with the Coulombic wave function of the atom, which diagrammatically correspond to an infinite ladder of Coulomb photons. The simplest example shown in Fig. 2.5 thus needs to be subtracted in (2.42) in order to avoid double counting. The details of the derivation of (2.42) are relegated to Appendix A.2.1.

The isoscalar propagator G_s is real for energies below the NN threshold and constructed out of continuum states normalized as[10]

$$\int\frac{\mathrm{d}^3q}{(2\pi)^3}\Psi_\mathbf{p}^{s\,\dagger}(\mathbf{q})\Psi_{\mathbf{p}'}^s(\mathbf{q}) = (2\pi)^3\delta^{(3)}(\mathbf{p}'-\mathbf{p})\,, \tag{2.43}$$

[10]Note that this implies a different normalization of continuum and deuteron wave functions (merely owed to the choice of conventions).

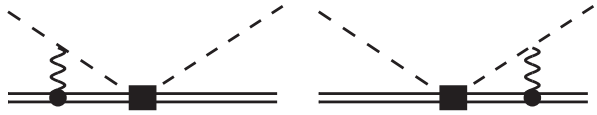

Figure 2.5: Contribution to the modified Deser formula in the πD atom due to the part of the Coulomb-photon ladder that is subtracted in (2.42) and (2.59). The double line labels the deuteron, the box corresponds to $\pi^- d$ scattering, and the circle to the photon coupling of the deuteron.

with $\Psi^s_{\mathbf{p}}(\mathbf{q})$ obeying

$$\left(\frac{\mathbf{p}^2}{m_\mathrm{p}} - \frac{\mathbf{q}^2}{m_\mathrm{p}}\right)\Psi^s_{\mathbf{p}}(\mathbf{q}) = \int \frac{\mathrm{d}^3 q'}{(2\pi)^3} V_s(\mathbf{q},\mathbf{q}')\Psi^s_{\mathbf{p}}(\mathbf{q}') \,, \tag{2.44}$$

where V_s is the isoscalar projection of the NN potential. The free part of G_s is therefore

$$G^{(0)}(\mathbf{q}',\mathbf{q};E,\mathbf{P}) = \frac{(2\pi)^3\delta^{(3)}(\mathbf{q}'-\mathbf{q})}{E+i\eta-\mathbf{P}^2/4m_\mathrm{p}-\mathbf{q}^2/m_\mathrm{p}} \,, \tag{2.45}$$

while the total Green function can be related to the NN scattering T-matrix as

$$\begin{aligned} G_s(\mathbf{q}',\mathbf{q};E,\mathbf{P}) &= G^{(0)}(\mathbf{q}',\mathbf{q};E,\mathbf{P}) \\ &\quad + \frac{T(\mathbf{q}',\mathbf{q};E,\mathbf{P})}{(E+i\eta-\mathbf{P}^2/4m_\mathrm{p}-\mathbf{q}^2/m_\mathrm{p})(E+i\eta-\mathbf{P}^2/4m_\mathrm{p}-\mathbf{q}'^2/m_\mathrm{p})} \,, \end{aligned} \tag{2.46}$$

where T is connected to the NN phase shifts via

$$T(\mathbf{k},\mathbf{k};E,\mathbf{P}) = -\frac{4\pi}{m_\mathrm{p}}\frac{1}{k\cot\delta(k)-ik} \tag{2.47}$$

with $k=|\mathbf{k}|=\sqrt{m_\mathrm{p}(E-\mathbf{P}^2/4m_\mathrm{p})}$. Alternatively, G_s can be rewritten in terms of the bound- and continuum-state wave functions

$$G_s(\mathbf{q}',\mathbf{q};E,\mathbf{P}) = \frac{(2\pi)^3\Psi(\mathbf{q}')\Psi^\dagger(\mathbf{q})}{E+i\eta+\epsilon-\mathbf{P}^2/4m_\mathrm{p}} + \int\frac{\mathrm{d}^3 p}{(2\pi)^3}\frac{\Psi^s_{\mathbf{p}}(\mathbf{q}')\Psi^{s\,\dagger}_{\mathbf{p}}(\mathbf{q})}{E+i\eta-\mathbf{p}^2/m_\mathrm{p}-\mathbf{P}^2/4m_\mathrm{p}} \,. \tag{2.48}$$

The additional factor $(2\pi)^3$ for the deuteron-pole part is due to our conventions for the deuteron wave functions (2.24). Inserting the free part of the Green function (2.45) into (2.42) reproduces the expressions for the structureless diagrams discussed in Sect. 2.5.1 up to higher-order terms neglected in the derivation of (2.42). Using the decomposition (2.48), the isoscalar contributions can be cast into the form

$$\begin{aligned} a_{T=0}^{(d_6)+(d_8)} + a_{T=0,\,\mathrm{ISI}}^{(d_6)+(d_8)} &= \frac{16\pi\alpha\xi_\mathrm{p}a^+}{\xi_\mathrm{d}}\int\frac{\mathrm{d}^3 k}{(2\pi)^3}\frac{1}{\mathbf{k}^2}\Bigg\{\frac{|F(\mathbf{k})|^2-1}{\mathbf{k}^2/2\mu_D-i\eta} \\ &\quad + \int\frac{\mathrm{d}^3 p}{(2\pi)^6}\frac{1}{\epsilon+\mathbf{p}^2/m_\mathrm{p}+\mathbf{k}^2/2\mu_D-i\eta}G^s_{\mathbf{p}}(\mathbf{k})\frac{1}{2}\big(G^{s\,\dagger}_{\mathbf{p}}(\mathbf{k})+G^{s\,\dagger}_{\mathbf{p}}(-\mathbf{k})\big)\Bigg\} \,, \end{aligned} \tag{2.49}$$

where

$$F(\mathbf{k}) = \int \mathrm{d}^3 q\,\Psi^\dagger(\mathbf{q})\Psi(\mathbf{q}-\mathbf{k}/2) \,, \qquad G^s_{\mathbf{p}}(\mathbf{k}) = \int \mathrm{d}^3 q\,\Psi^\dagger(\mathbf{q})\Psi^s_{\mathbf{p}}(\mathbf{q}-\mathbf{k}/2) \,. \tag{2.50}$$

From the normalization condition of $\Psi(\mathbf{q})$ and the orthogonality of $\Psi(\mathbf{q})$ and $\Psi^s_{\mathbf{p}}(\mathbf{q})$ for vanishing momentum transfer, it follows that

$$|F(\mathbf{k})|^2 - 1 = \mathcal{O}\big(\mathbf{k}^2\big) \,, \qquad G^s_{\mathbf{p}}(\mathbf{k}) = \mathcal{O}(\mathbf{k}) \,. \tag{2.51}$$

In this way, we conclude that also in the isoscalar case no terms enhanced by $\sqrt{M_\pi/\epsilon}$ remain. Due to the chiral suppression of a^+ the subleading corrections can simply be dropped. The reasoning used here—based on exploiting orthogonality of bound state and continuum wave functions—follows the calculation of recoil corrections to $\bar{K}d$ scattering in [111].

Alternatively, the cancellation can be derived within heavy-pion effective field theory (HπEFT) [126]. In this case, it is also convenient to split the total effect into parts without and parts with ISI. The portion without ISI gives (cf. (2.35) and (2.38))

$$\begin{aligned} a^{(d_8)}_{T=0} &= a^+ \frac{16\alpha}{3\pi}\sqrt{\frac{M_\pi}{2\epsilon}}\left(1 + \mathcal{O}\left(\frac{M_\pi}{m_\mathrm{p}}\right)\right) \,, \\ a^{(d_6)}_{T=0} &= a^+ \frac{16\alpha}{3\pi}\sqrt{\frac{M_\pi}{2\epsilon}}\left(1 - \frac{3\pi}{8\sqrt{2}}\sqrt{\frac{M_\pi}{m_\mathrm{p}}} + \mathcal{O}\left(\frac{M_\pi}{m_\mathrm{p}}\right)\right) \,. \end{aligned} \tag{2.52}$$

Again, these expressions show the anticipated infrared enhancement.

The diagrams with ISI can be evaluated using the leading-order form of the NN scattering amplitude in pionless EFT [127]

$$T_{s,NN}(\mathbf{q}', \mathbf{q}; E, \mathbf{P}) = \frac{4\pi}{m_\mathrm{p}} \frac{1}{\gamma + i\sqrt{m_\mathrm{p}\left(E - \frac{\mathbf{P}^2}{4m_\mathrm{p}}\right)}} \,. \tag{2.53}$$

Indeed, after removing the deuteron pole already accounted for in the Deser formula, one finds [33]

$$a^{(d_6)+(d_8)}_{T=0,\,\mathrm{ISI}} = -\frac{32\alpha}{3\pi} a^+ \sqrt{\frac{M_\pi}{2\epsilon}} \,, \tag{2.54}$$

which precisely cancels the leading piece of the free part of the diagrams in (2.52). Furthermore, any contributions from momenta $|\mathbf{k}| \sim \sqrt{M_\pi \epsilon}$ may only appear in the non-integer terms in the expansion (2.35) and thus are suppressed by an additional power of M_π/m_p (i.e. they correspond to the third term in (2.35)). These contributions thus have an overall size

$$\frac{32\alpha}{3\pi}\frac{M_\pi}{m_\mathrm{p}}\sqrt{\frac{M_\pi}{2\epsilon}} a_+ \approx 2.8\,\alpha a^+ \,, \tag{2.55}$$

and are therefore well beyond the accuracy we claim for our calculation.

Nevertheless, there are still possible contributions from diagrams with ISI and momenta of order γ. These would be enhanced by M_π/γ compared to their naive ChPT order, and hence could be relevant for the present analysis. Decomposing the Green function according to

$$\begin{aligned} G_s(\mathbf{q}', \mathbf{q}; E, \mathbf{P}) &= G^{(0)}(\mathbf{q}', \mathbf{q}; E, \mathbf{P}) + \frac{(2\pi)^3 \Psi(\mathbf{q}')\Psi^\dagger(\mathbf{q})}{E + i\eta + \epsilon - \mathbf{P}^2/4m_\mathrm{p}} \\ &\quad + \frac{1}{E + i\eta - \mathbf{P}^2/4m_\mathrm{p} - \mathbf{q}'^2/m_\mathrm{p}} T^{\mathrm{np}}_{s,NN}(\mathbf{q}', \mathbf{q}; E, \mathbf{P}) \frac{1}{E + i\eta - \mathbf{P}^2/4m_\mathrm{p} - \mathbf{q}^2/m_\mathrm{p}} \,, \end{aligned} \tag{2.56}$$

i.e. into its free part, the deuteron pole, and the non-pole isoscalar NN T-matrix $T^{\rm np}_{s,NN}$, the additional contributions due to ISI are given by

$$a^{(d_6)+(d_8)}_{T=0,\,\rm ISI} = -\frac{8\pi\alpha\xi_{\rm p}a^+}{\xi_{\rm d}}\int\frac{{\rm d}^3k}{(2\pi)^3}\frac{1}{\mathbf{k}^2}\Bigg\{\int\frac{{\rm d}^3q\,{\rm d}^3q'}{(2\pi)^3}\Psi^\dagger(\mathbf{q}')\frac{1}{-\epsilon-\mathbf{k}^2/2\mu_D-(\mathbf{q}'-\mathbf{k}/2)^2/m_{\rm p}} \times T^{\rm np}_{s,NN}\frac{1}{-\epsilon-\mathbf{k}^2/2\mu_D-(\mathbf{q}-\mathbf{k}/2)^2/m_{\rm p}}\Psi(\mathbf{q}) + 2\frac{|F(\mathbf{k})|^2-1}{-\mathbf{k}^2/2\mu_D+i\eta}\Bigg\}\,, \quad (2.57)$$

with

$$T^{\rm np}_{s,NN} = T^{\rm np}_{s,NN}\Big(\mathbf{q}'-\frac{\mathbf{k}}{2},\mathbf{q}-\frac{\mathbf{k}}{2};-\epsilon-\frac{\mathbf{k}^2}{2M_\pi},-\mathbf{k}\Big)+T^{\rm np}_{s,NN}\Big(\mathbf{q}'-\frac{\mathbf{k}}{2},-\mathbf{q}+\frac{\mathbf{k}}{2};-\epsilon-\frac{\mathbf{k}^2}{2M_\pi},-\mathbf{k}\Big)\,. \quad (2.58)$$

We will present the results of an explicit numerical evaluation of this equation in Sect. 2.5.4. Finally, the part of the integral involving momenta $|\mathbf{k}|\sim M_\pi$ only contributes at the naive chiral order of the pertinent diagrams. For that effect it suffices to evaluate (d_6)–(d_8) without any ISI, keeping only the $T=1$ pieces of the free parts of these graphs, cf. (2.34) and (2.39).

2.5.3 The role of rescattering II: double scattering with photon exchange

If only momenta $|\mathbf{k}|\sim M_\pi$ were important, there would be no need to consider (d_9) and (d_{10}). However, the full isoscalar contribution to these diagrams reads (for the derivation see Appendix A.2.2)

$$a^{(d_9)+(d_{10})}_{T=0} + a^{(d_9)+(d_{10})}_{T=0,\,\rm ISI} = \frac{32\pi^2\alpha(\xi_{\rm p}a^-)^2}{\xi_{\rm d}}\int\frac{{\rm d}^3k}{(2\pi)^3}\int\frac{{\rm d}^3l}{(2\pi)^3}\frac{1}{\mathbf{k}^2\mathbf{l}^2}\int\frac{{\rm d}^3q\,{\rm d}^3q'}{(2\pi)^3}\Psi^\dagger(\mathbf{q}') \times\Bigg\{2G_s\Big(\mathbf{q}'-\frac{\mathbf{k}}{2},\mathbf{q}-\frac{\mathbf{k}}{2}+\mathbf{l};-\epsilon-\frac{\mathbf{k}^2}{2M_\pi},-\mathbf{k}\Big)+2G_s\Big(\mathbf{q}'-\frac{\mathbf{k}}{2},-\mathbf{q}+\frac{\mathbf{k}}{2}-\mathbf{l};-\epsilon-\frac{\mathbf{k}^2}{2M_\pi},-\mathbf{k}\Big) - \frac{4(2\pi)^3\Psi(\mathbf{q}')\Psi^\dagger(\mathbf{q}-\mathbf{l})}{-\mathbf{k}^2/2\mu_D+i\eta}\Bigg\}\Psi(\mathbf{q})\,. \quad (2.59)$$

The same arguments as for single scattering yield that the leading contributions from momenta $|\mathbf{k}|\sim\sqrt{M_\pi\epsilon}$ cancel, but again momenta of order γ could yield terms enhanced by M_π/γ that might compromise the accuracy of our calculation. To evaluate these contributions explicitly we have checked that the free part of the Green function reproduces (2.41), while ISI lead to

$$a^{(d_9)+(d_{10})}_{T=0,\,\rm ISI} = \frac{32\pi^2\alpha(\xi_{\rm p}a^-)^2}{\xi_{\rm d}}\int\frac{{\rm d}^3k}{(2\pi)^3}\int\frac{{\rm d}^3l}{(2\pi)^3}\frac{1}{\mathbf{k}^2\mathbf{l}^2}\Bigg\{\int\frac{{\rm d}^3q\,{\rm d}^3q'}{(2\pi)^3}\Psi^\dagger(\mathbf{q}') \times\frac{1}{-\epsilon-\mathbf{k}^2/2\mu_D-(\mathbf{q}'-\mathbf{k}/2)^2/m_{\rm p}}\tilde{T}^{\rm np}_{s,NN}\frac{1}{-\epsilon-\mathbf{k}^2/2\mu_D-(\mathbf{q}-\mathbf{k}/2+\mathbf{l})^2/m_{\rm p}}\Psi(\mathbf{q}) + 4\frac{F(\mathbf{k})F(\mathbf{k}-2\mathbf{l})-F(2\mathbf{l})}{-\mathbf{k}^2/2\mu_D+i\eta}\Bigg\}\,, \quad (2.60)$$

with

$$\tilde{T}^{\rm np}_{s,NN} = 2T^{\rm np}_{s,NN}\Big(\mathbf{q}'-\frac{\mathbf{k}}{2},\mathbf{q}-\frac{\mathbf{k}}{2}+\mathbf{l};-\epsilon-\frac{\mathbf{k}^2}{2M_\pi},-\mathbf{k}\Big)+2T^{\rm np}_{s,NN}\Big(\mathbf{q}'-\frac{\mathbf{k}}{2},-\mathbf{q}+\frac{\mathbf{k}}{2}-\mathbf{l};-\epsilon-\frac{\mathbf{k}^2}{2M_\pi},-\mathbf{k}\Big)\,, \quad (2.61)$$

where we have used repeatedly that $\Psi(\mathbf{p})=\Psi(-\mathbf{p})$.

2.5.4 Numerical evaluations

In [33], the expressions for the isoscalar contributions to single and double scattering (2.42) and (2.59) were evaluated using a separable NN potential (the integrals are dominated by low-momentum modes, so that details of the potential do not matter)

$$V(\mathbf{p},\mathbf{p}') = \lambda g(\mathbf{p}) g(\mathbf{p}') \,, \qquad g(\mathbf{p}) = \frac{1}{\mathbf{p}^2+\beta^2} \,, \tag{2.62}$$

where λ is a constant tuned to reproduce the binding momentum $\gamma = \sqrt{m_\mathrm{p}\epsilon}$, and $\beta = 1.4\,\mathrm{fm}^{-1}$ is introduced to parameterize the effective range of pn scattering, which enters into realistic potentials through the one-pion exchange. Solving the Schrödinger equation (2.44) for the bound state, one obtains the deuteron wave function of the Hulthén type [128]

$$\Psi(\mathbf{p}) = N \frac{g(\mathbf{p})}{\mathbf{p}^2+\gamma^2} \,, \qquad N = \frac{1}{\pi}\sqrt{\gamma\beta(\gamma+\beta)^3} \,. \tag{2.63}$$

In this way, (2.42) with G_s from (2.46) leads to [33]

$$a_{T=0}^{(d_6)+(d_8)} + a_{T=0,\,\mathrm{ISI}}^{(d_6)+(d_8)} = -0.034\, a^+ \,. \tag{2.64}$$

In fact, the individual contributions $a_{T=0}^{(d_6)+(d_8)}$ and $a_{T=0,\,\mathrm{ISI}}^{(d_6)+(d_8)}$ are 5–6 times larger than their sum, which attests to the cancellation derived in Sect. 2.5.2: at leading order both $a_{T=0}^{(d_6)+(d_8)}$ and $a_{T=0,\,\mathrm{ISI}}^{(d_6)+(d_8)}$ acquire large contributions from momenta of order $\sqrt{M_\pi\epsilon}$ which, however, cancel completely in the sum. If the dominant effect in the result (2.64) was indeed due to momenta of order γ, it should also be accessible in HπEFT. From (2.52) we see that the free piece of the isoscalar contribution to (d_6) is

$$a_{T=0}^{(d_6)+(d_8)} = -\alpha a^+ \frac{M_\pi}{2\gamma}\left[1+\mathcal{O}\left(\sqrt{\frac{M_\pi}{m_\mathrm{p}}}\right)\right] \approx -0.022 a^+ \,. \tag{2.65}$$

This number is actually quite close to (2.64), which suggests that indeed momenta of order γ are largely responsible for this contribution.[11]

Similarly, the numerical evaluation of (2.59) with the pionful wave functions based on the separable NN interaction described above yields [33]

$$a_{T=0}^{(d_9)+(d_{10})} + a_{T=0,\,\mathrm{ISI}}^{(d_9)+(d_{10})} = 0.3\cdot 10^{-3} M_\pi^{-1} \,. \tag{2.66}$$

Again, this result is nearly saturated by residual contributions of the free diagrams from scales above $\sqrt{M_\pi\epsilon}$. Contrary to (d_6) and (d_8), which are dominated by momenta of order γ, in this case also momenta of order M_π contribute significantly to the diagrams.

These evaluations show that despite their ostensible infrared enhancement the isoscalar parts of (d_6) and (d_8)–(d_{10}) receive contributions from momenta of order γ that result in corrections to $a_{\pi^- d}$ which are still significantly smaller than the theoretical uncertainty of the full calculation. We will therefore simply drop the isoscalar contributions in the following.

Finally, the numerical evaluation in [33] shows that—after the Pauli-principle-enforced cancellation of terms of order $\sqrt{M_\pi/\epsilon}$—isovector contributions to (d_9) and (d_{10}) are very

[11] Taking into account the wave-function-renormalization factor $Z = 1.690$ from [129] changes (2.65) to $-0.037 a^+$, which is even closer to (2.64).

small, only about $-0.1 \cdot 10^{-3} M_\pi^{-1}$. Thus, the same sort of cancellations that preclude the existence of a $\chi^{1/2}$ contribution due to recoil in the double-scattering diagrams also enforces the smallness of this $T = 1$ part of (d_9) and (d_{10}), which may therefore be omitted altogether. Indeed, had we found that (d_9) and (d_{10}) were necessary for a precision evaluation of $a_{\pi^- d}$, we would have been forced to consider all photon diagrams at this order, since (d_9) and (d_{10}) do not, on their own, form a gauge-invariant set of diagrams.

In fact, these results are very important, as the cancellations guarantee that the original ChPT counting, which assesses the impact of momenta $\sim M_\pi$ on the integrals, provides a reasonable estimate of diagrams involving virtual photons, since the remaining infrared enhancement is too weak to severely violate the ChPT estimates. In this way, we are left with the diagrams (d_6)–(d_8)

$$\begin{aligned} a^{\mathrm{EM}} &= \frac{2\alpha M_\pi \xi_{\mathrm{p}} a^-}{\pi^2 \xi_{\mathrm{d}}} I^{\mathrm{EM}} - \frac{\alpha}{16\pi^3 F_\pi^2 \xi_{\mathrm{d}}} \left\langle \frac{1}{\mathbf{q}^2} \right\rangle , \\ I^{\mathrm{EM}} &= \int \mathrm{d}^3 p \, \mathrm{d}^3 q \frac{\big(\Psi^\dagger(\mathbf{p}) - \Psi^\dagger(\mathbf{p}-\mathbf{q})\big)\Psi(\mathbf{p})}{|\mathbf{q}|\big(|\mathbf{q}| + \delta/2\omega_{\mathbf{q}}\big)\big(\mathbf{q}^2 + \delta\big)} . \end{aligned} \tag{2.67}$$

With the numerical results from Sect. 2.4.4 and $a^- = 86.1 \cdot 10^{-3} M_\pi^{-1}$, we obtain

$$a^{\mathrm{EM}} = (0.94 \pm 0.01) \cdot 10^{-3} M_\pi^{-1} , \tag{2.68}$$

where the error again reflects the wave-function dependence as follows from Table 2.3. Thus, virtual photons increase $\mathrm{Re}\, a_{\pi^- d}$ by about 4 %.

In summary, we may conclude that there are no infrared-enhanced photon contributions from momenta $\sim \sqrt{\epsilon M_\pi}$—due to subtle cancellations both for isoscalar and isovector πN interactions—and that the infrared enhancement provided by momenta $\sim \gamma$ is too weak to generate effects that significantly exceed the estimates for momenta $\sim M_\pi$. The size of the virtual-photon corrections is thus roughly in line with the original ChPT power counting.

2.6 Dispersive and Δ corrections

There are two additional contributions to the $\pi^- d$ scattering length that have not been mentioned so far. First, diagrams with pure NN or $NN\gamma$ intermediate states yield so-called dispersive corrections. It is this class of diagrams that produces the imaginary part of $a_{\pi^- d}$, although here their leading contribution to the real part of $a_{\pi^- d}$ is suppressed by $p^{3/2}$ relative to (d_1) [112]. Second, diagrams with explicit Δ degrees of freedom enter at the same order [113]. The $\Delta(1232)$ contribution is a true three-body effect, since the nucleon recoil is needed if this P-wave resonance is to contribute to S-wave $\pi^- d$ scattering. Typical examples for each of these two effects are depicted in Table 2.1. Both classes were computed in [112,113] using a calculation for $NN \to d\pi$ up to NLO in ChEFT [130] in which all integrals were cut off at 1 GeV. However, varying this cutoff does not introduce additional uncertainty [33], so that the combined effect in $a_{\pi^- d}$ amounts to [113]

$$a^{\mathrm{disp}+\Delta} = (-0.6 \pm 1.5) \cdot 10^{-3} M_\pi^{-1} . \tag{2.69}$$

Since this contribution is only $\mathcal{O}(p^{1/2})$ larger than the contact term, we need not include isospin-violating corrections to $a^{\mathrm{disp}+\Delta}$, which, counting $e \sim p$, would be suppressed by another two orders.

2.7 Summary of three-body contributions

In this section, we briefly summarize the results of Sects. 2.3–2.6, list the three-body corrections that finally have to be included, and comment on the uncertainty estimate of the calculation. First of all, we may conclude from the discussion in Sect. 2.3 that indeed all isospin-conserving three-body corrections can be reliably calculated up to $\mathcal{O}(p^{3/2})$, i.e. up to a relative accuracy of $(M_\pi/m_\mathrm{p})^{3/2}$, half an order below the leading $(N^\dagger N)^2\pi\pi$ contact term. Dimensional analysis for the contact term, the sensitivity of the integrals to the choice of the deuteron wave function, and the investigation of higher-order terms in the multiple-scattering series all point towards a final uncertainty of a few percent. However, at this accuracy it is mandatory to account for three-body isospin-violating corrections, which are suppressed by e^2 compared to the leading isospin-conserving terms. Therefore, we also performed a complete calculation of the isospin-violating corrections up to $\mathcal{O}(e^2p^{1/2})$. To this order, the three-body isospin-violating corrections are of purely electromagnetic origin, while the quark mass difference starts to contribute only at $\mathcal{O}(e^2p)$.

In Sect. 2.4 we have considered the diagrams of a multiple-scattering topology as well as those that involve $3\pi N^\dagger N$ and 4π vertices (cf. Fig. 2.1). In particular, we have generalized the decomposition of the leading, double-scattering diagram into the LO static term, its NLO correction, and the contribution from the three-body cut to the isospin-violating case. While nucleon recoil leads to important corrections in the calculation of double scattering, higher diagrams with a multiple-scattering topology are sufficiently small that they may be evaluated in the approximation of static nucleons, and terms beyond triple scattering can be discarded altogether, cf. Sect. 2.4.3. Similarly, isospin-violating corrections are irrelevant for all terms in the multiple-scattering series beyond double scattering.

The combination of all these effects defines the strong contribution to the $\pi^- d$ scattering length a^str. For the numerical evaluation we took the wave-function integrals from [33], which gives (with $a^- = 86.1 \cdot 10^{-3} M_\pi^{-1}$)

$$a^\mathrm{str} = (-22.6 \pm 1.1 \pm 0.4) \cdot 10^{-3} M_\pi^{-1} \,, \tag{2.70}$$

where the first uncertainty arises from the different short-distance physics of the deuteron wave functions, and the second from the isospin-breaking shifts in the πN scattering lengths. The variation in the results due to the use of different wave functions is about 5 %, completely in line with the power-counting estimate for the contact term. The combined effect of the dispersive and the $\Delta(1232)$ corrections that enter at $\mathcal{O}(p^{3/2})$ was discussed in Sect. 2.6 and taken from [112, 113]

$$a^{\mathrm{disp}+\Delta} = (-0.6 \pm 1.5) \cdot 10^{-3} M_\pi^{-1} \,. \tag{2.71}$$

Finally, Sect. 2.5 was devoted to a thorough investigation of the effects related to virtual photons. Due to the presence of photon and pion propagators some of these diagrams are infrared enhanced. Therefore, keeping the full dynamical structure of the πNN propagator (including the nucleon recoil) is mandatory to avoid infrared-divergent integrals. To the order we are working, it is sufficient to consider the diagrams (d_6)–(d_8), which form a gauge-invariant set of diagrams at $\mathcal{O}(e^2)$, leading to

$$a^\mathrm{EM} = (0.94 \pm 0.01) \cdot 10^{-3} M_\pi^{-1} \,, \tag{2.72}$$

with only a $\sim 1\,\%$ wave-function dependence. Despite the dominance of the double-scattering term we found that associated virtual-photon corrections, cf. diagrams (d_9) and (d_{10}), do not have to be included.

The three pieces $a^{\rm str}$, $a^{\rm disp+\Delta}$, and $a^{\rm EM}$, when added together, constitute the three-body contribution to the $\pi^- d$ scattering length. In fact, to a large extent, the novel three-body effects accidentally cancel

$$\Delta a^{(2)} + a^{\rm static}_{\rm NLO} + a^{\rm cut} + a^{\rm EM} = (0.1 \pm 0.7) \cdot 10^{-3} M_\pi^{-1} \,. \tag{2.73}$$

This cancellation is, in itself, rather remarkable, since, e.g., $a^{\rm static}_{\rm NLO}$ is ~ 40 times larger than the final central value. The effect of the cancellation is that the main impact of our analysis on the extraction of pion–nucleon scattering lengths is the consideration of NLO isospin-breaking corrections—in particular the large shift $\Delta\tilde{a}^+ = (-3.3 \pm 0.3) \cdot 10^{-3} M_\pi^{-1}$—in the πN amplitude [131].

Chapter 3

πN scattering lengths and the Goldberger–Miyazawa–Oehme sum rule

3.1 Pion–nucleon scattering lengths

The detailed analysis of the $\pi^- d$ scattering length presented in Chapter 2 now permits a high-accuracy extraction of the πN scattering lengths from a combined analysis of πH and πD. The resulting constraints due to the dependence of the $\pi^- d$ scattering length on $\tilde{a}^+$ and a^- and the results for πH discussed in Sect. 2.1 are depicted in Fig. 3.1. The combined 1σ error ellipse yields

$$\tilde{a}^+ = (1.9 \pm 0.8) \cdot 10^{-3} M_\pi^{-1} \,, \qquad a^- = (86.1 \pm 0.9) \cdot 10^{-3} M_\pi^{-1} \,, \tag{3.1}$$

with a correlation coefficient $\rho_{a^- \tilde{a}^+} = -0.21$. At this point, the merits of an additional constraint besides πH data become apparent, as the inclusion of the πD energy shift reduces the uncertainty of $\tilde{a}^+$ by more than a factor of 2 and the correlation between $\tilde{a}^+$ and a^- by more than a factor of 3. As far as the error analysis is concerned, we observe that in the case of the πH level shift the width of the band is dominated by the theoretical uncertainty in $\Delta\tilde{a}_{\pi^- p}$, whereas for the πH width the experimental error is about 50 % larger than the theoretical one. Moreover, Table 3.1 shows the individual contributions to the πD error band: as with the πH level shift, the experimental error is much smaller than the combined theoretical uncertainty, whose largest individual contribution is produced by the uncertainty in $a^{\mathrm{disp}+\Delta}$. The wave-function averages contribute about $0.5 \cdot 10^{-3} M_\pi^{-1}$ to the overall uncertainty in $\tilde{a}^+$, which is in line with the estimated impact on $a_{\pi^- d}$ of the $\mathcal{O}(p^2)$ contact term. It is striking that—apart from the πH width—any improvement of the experimental results would be in vain without significant progress on the theoretical side, which, however, would require additional information on LECs both in the πH and πD system.

To deduce a value for a^+ itself, further input on c_1 and f_1 is needed according to (2.16). c_1 is related to the πN σ term: $\sigma_{\pi N} = (45 \pm 8)\,\mathrm{MeV}$ as quoted in [80][1] corresponds to

[1] This value is consistent with recent determinations of $\sigma_{\pi N}$ from the lattice, e.g. $\sigma_{\pi N} = (50 \pm 10)\,\mathrm{MeV}$ [132], $\sigma_{\pi N} = (59 \pm 2 \pm 17)\,\mathrm{MeV}$ [133], $\sigma_{\pi N} = (39 \pm 4^{+18}_{-7})\,\mathrm{MeV}$ [134], $\sigma_{\pi N} = (38 \pm 12)\,\mathrm{MeV}$ [135]. Note that all these indirect extractions of $\sigma_{\pi N}$ from the derivative of the nucleon mass by means of the Feynman–Hellmann theorem [136] suffer from significant systematic uncertainties inherent in the chiral extrapolations, see e.g. [137].

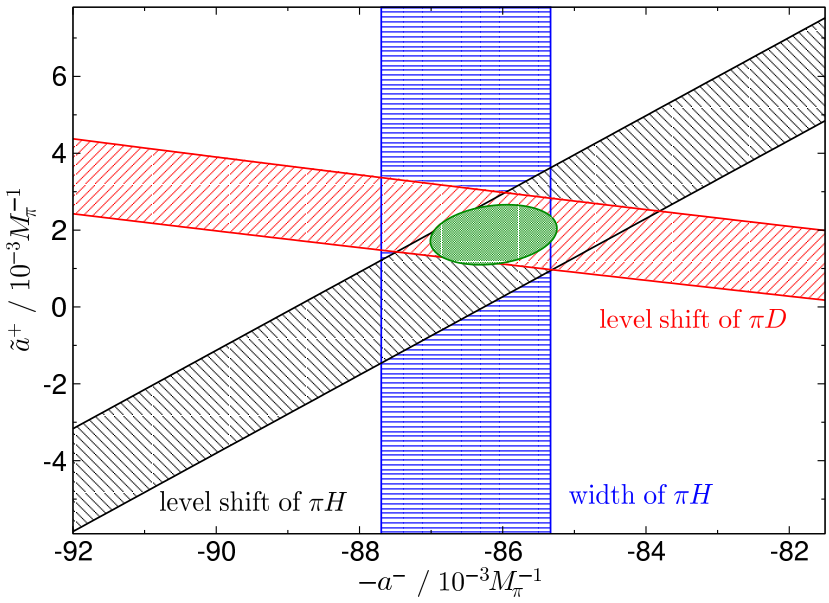

Figure 3.1: Combined constraints in the $\tilde{a}^+$–a^- plane from data on the width and energy shift of πH, as well as the πD energy shift.

$c_1 = (-0.9 \pm 0.1)\,\mathrm{GeV}^{-1}$ and $c_1 = (-1.0 \pm 0.2)\,\mathrm{GeV}^{-1}$ at third and fourth chiral order, respectively [138]. Recent determinations based on πN threshold parameters yield $c_1 = (-0.93 \pm 0.07)\,\mathrm{GeV}^{-1}$ [94] and $c_1 = (-1.2 \pm 0.3)\,\mathrm{GeV}^{-1}$ [84], while an investigation of πN scattering inside the Mandelstam triangle led to $c_1 = (-0.81 \pm 0.12)\,\mathrm{GeV}^{-1}$ [139]. Finally, fits of ChPT amplitudes to phase-shift analyses with and without explicit Δ degrees of freedom provide values in the range $c_1 = -(0.8 \ldots 1.0)\,\mathrm{GeV}^{-1}$ [140] and $c_1 = -(1.2 \ldots 1.4)\,\mathrm{GeV}^{-1}$ [78], respectively.[2] In conclusion, we consider

$$c_1 = (-1.0 \pm 0.3)\,\mathrm{GeV}^{-1} \tag{3.2}$$

as a reasonable average of the present knowledge on this LEC. Taken together with the rough estimate $|f_1| \leq 1.4\,\mathrm{GeV}^{-1}$ [94, 141], this value for c_1 and (3.1) yield a non-zero a^+ at better than the 95 % confidence level

$$a^+ = (7.6 \pm 3.1) \cdot 10^{-3} M_\pi^{-1}\,. \tag{3.3}$$

The fact that the final result for a^+ (or even more for $\tilde{a}^+$) is of the same order of magnitude as several of the individual contributions considered in Chapter 2 emphasizes the necessity of a systematic ordering scheme as well as a careful treatment of isospin violation and three-body dynamics. A reduction of the theoretical uncertainty beyond that of the present analysis is hard to conceive absent further QCD input that helps determine the unknown contact-term contributions in both the πN and πNN sectors.

Finally, we can combine our values for the scattering lengths in the isospin limit with the isospin-breaking corrections [93] to arrive at the πN scattering lengths for the physical

[2] Note that c_1 is not saturated by the Δ [120]. Therefore, the spread in the results reflects rather the substantial uncertainties in the chiral expansion of the isoscalar amplitude, cf. (2.2) for the expansion of the isoscalar S-wave scattering length.

ϵ_{1s}^D	$\Delta a^-, \Delta a_{\pi^- p}^{\rm cex}$	$a^{\rm disp+\Delta}$	$\Delta\tilde{a}^+$	Wave-function averages
16 %	21 %	75 %	30 %	53 %

Table 3.1: Individual contributions to the error on $\tilde{a}^+$, which, added in quadrature, yield the total uncertainty depicted in the band for the πD level shift in Fig. 3.1. The impact of each source of error is given as a percentage of the total (the second column gives the uncertainty in the isospin-breaking shifts of πN scattering lengths that occur in $a^{\rm str}$, cf. (2.23)).

channels summarized in Table 3.2. Note that the difference between scattering lengths in the same isospin channel is better known than their individual values, since the scattering lengths in the isospin limit and the associated uncertainties drop out. For example, the difference between $a_{\pi^0 p}$ and $a_{\pi^0 n}$ at NLO is given by [93]

$$\begin{aligned} a_{\pi^0 p} - a_{\pi^0 n} &= \frac{1}{4\pi\xi_{\rm p}}\left\{\frac{4c_5 B(m_{\rm d}-m_{\rm u})}{F_\pi^2} - \frac{M_\pi^2}{8\pi F_\pi^4}\Big(\sqrt{\Delta_\pi + 2M_\pi\Delta_{\rm N}} - \sqrt{\Delta_\pi - 2M_\pi\Delta_{\rm N}}\Big)\right\} \\ &= (-3.4 \pm 0.4)\cdot 10^{-3} M_\pi^{-1}\,, \end{aligned} \tag{3.4}$$

with c_5 being related to the strong contribution to the proton–neutron mass difference. Although it is formally of higher chiral order, here the contribution from the cusp due to $\pi^+ n$ and $\pi^- p$ intermediate states has been kept, since it is enhanced by half an order in the isospin-breaking parameter $\delta = \{e^2, m_{\rm d} - m_{\rm u}\}$. Indeed, it ultimately contributes about 30 % to the number quoted in (3.4).

3.2 Goldberger–Miyazawa–Oehme sum rule

The GMO sum rule [81] relates the charged-pion–nucleon coupling constant $g_c^2/4\pi$ to the scattering-length combination $a_{\pi^- p} - a_{\pi^+ p}$ and the integral over the cross-section difference $\sigma_{\pi^- p}^{\rm tot} - \sigma_{\pi^+ p}^{\rm tot}$ measured in the laboratory frame for pion momenta $|\mathbf{k}|$ from zero to infinity

$$\begin{aligned} \frac{g_c^2}{4\pi} &= \left(\left(\frac{m_{\rm p}+m_{\rm n}}{M_\pi}\right)^2 - 1\right)\left\{\left(1+\frac{M_\pi}{m_{\rm p}}\right)\frac{M_\pi}{4}(a_{\pi^- p} - a_{\pi^+ p}) - \frac{M_\pi^2}{2}J^-\right\}\,, \\ J^- &= \frac{1}{4\pi^2}\int_0^\infty d|\mathbf{k}|\frac{\sigma_{\pi^- p}^{\rm tot}(|\mathbf{k}|) - \sigma_{\pi^+ p}^{\rm tot}(|\mathbf{k}|)}{\sqrt{M_\pi^2 + \mathbf{k}^2}}\,. \end{aligned} \tag{3.5}$$

This result is derived by writing down dispersion relations for $\pi^\pm p \to \pi^\pm p$ for fixed t (see Sect. 1.2.1), assuming that the amplitudes are analytic functions of s with a right-hand cut starting at $s_{\rm thr} = (m_{\rm p} + M_\pi)^2$ and a left-hand cut starting at $s = (m_{\rm p} - M_\pi)^2 - t$. These dispersion relations are then evaluated at threshold. The scattering lengths enter as the πN amplitude at threshold, while the coupling constant g_c is related to the residue of the nucleon pole. Finally, one employs the optical theorem in the laboratory frame to replace the imaginary part of the amplitude by the total cross section.

3.2.1 Isospin violation

There are two ways in which isospin violation affects the derivation of the GMO sum rule: mass effects and virtual photons. The proton–neutron mass difference enters through the

isospin limit	channel	scattering length	channel	scattering length
$a^+ + a^-$	$\pi^- p \to \pi^- p$	86.1 ± 1.8	$\pi^+ n \to \pi^+ n$	85.2 ± 1.8
$a^+ - a^-$	$\pi^+ p \to \pi^+ p$	-88.1 ± 1.8	$\pi^- n \to \pi^- n$	-89.0 ± 1.8
$-\sqrt{2}\, a^-$	$\pi^- p \to \pi^0 n$	-121.4 ± 1.6	$\pi^+ n \to \pi^0 p$	-119.5 ± 1.6
a^+	$\pi^0 p \to \pi^0 p$	2.1 ± 3.1	$\pi^0 n \to \pi^0 n$	5.5 ± 3.1

Table 3.2: πN scattering lengths for the physical channels in units of $10^{-3} M_\pi^{-1}$, including isospin-breaking corrections both due to mass effects and virtual photons [93].

intermediate neutron in the nucleon-pole diagram, which is already taken into account in (3.5). Additionally, the threshold for $\pi^- p \to \pi^0 n$ lies below $s_{\rm thr}$, with the result that the right-hand cut for $\pi^- p$ already starts at $(m_{\rm n} + M_{\pi^0})^2$. Thus, the total cross section for $\pi^- p$ diverges at threshold due to the lower threshold of $\pi^0 n$. However, this divergence corresponds just to the right half of a principal-value integral: the dispersion integral for the reaction $\pi^- p$ really starts at $s = (m_{\rm n} + M_{\pi^0})^2$, and the resulting pole at $s_{\rm thr}$ can be taken care of in the usual way by the principal-value prescription. To estimate the remaining effect, one may use the fact that the imaginary part of the amplitude for $s < (m_{\rm p} + M_\pi)^2$ can be well approximated by the imaginary part of the $\pi^- p$ scattering length due to the $\pi^0 n$ intermediate state [93]. In this way, we find a shift in J^- by about $-0.005\,$mb, which we will take into account in our uncertainty estimate for J^- below. In conclusion, mass effects do not invalidate the GMO sum rule and the necessary modifications are quite well under control.

In contrast, we cannot write down the GMO sum rule in the presence of virtual photons, as e.g. the nucleon pole is not separated any more from the γN cut. Therefore, (3.5) is only applicable if all ingredients are purified from virtual-photon effects to ensure that the analytic structure of the corresponding amplitude coincides with what was assumed in the original derivation. For this reason, we will adopt the following point of view: we assume that the removal of electromagnetic effects in the cross sections using the Tromborg procedure [142] works sufficiently well that the resulting value for J^- is compatible with the above analyticity assumptions. Moreover, we subtract virtual-photon effects in the scattering lengths based on [93], but keep isospin-violating effects due to the nucleon and pion mass difference (we will dwell on this procedure in Sect. 3.2.3). In this way, our final result for g_c consistently refers to the scenario where all particle masses are fixed at their physical value, but virtual photons are switched off.

Finally, we comment on the definition of scattering lengths and coupling constants in the presence of electromagnetic interactions. Even in principle, the calculation of electromagnetic corrections is a scale-dependent procedure [143], which, however, can only be systematically addressed if the underlying theory is known. Within an effective theory, ChPT in our case, a consistent treatment of electromagnetic corrections is possible, apart from the fact that the ambiguities in the separation of photon effects present in full QCD should be reflected in additional uncertainties in the LECs. To the best of our knowledge, the practical consequences of [143] for ChPT calculations have yet to be explored. However, the study of the linear σ model in [143] suggests that such effects are not relevant at the level of accuracy at which the LECs can be usually pinned down. In addition, the definition of a scattering length for charged particles is a subtle matter [144], and recent attempts to define a strong proton–

proton scattering length yield only scale-dependent quantities [145]. An effect analogous to that discussed in these works is also present in the calculation of the πN scattering lengths, but, due to the perturbative nature of πN dynamics, this effect is negligible as we will show in the following. Removing the Coulomb phase $\theta_{\mathrm{C}}(|\mathbf{p}|)$, the behavior of the $\pi^- p$ scattering amplitude $T_{\pi^- p}$ at threshold is given by [86]

$$e^{-2i\alpha\theta_{\mathrm{C}}(|\mathbf{p}|)}T_{\pi^- p} = \frac{B_1}{|\mathbf{p}|} + B_2 \log\frac{|\mathbf{p}|}{\mu_H} + T^{\mathrm{thr}}_{\pi^- p} + \mathcal{O}(|\mathbf{p}|)\ , \tag{3.6}$$

where

$$4\pi\xi_{\mathrm{p}} a_{\pi^- p} = T^{\mathrm{thr}}_{\pi^- p}\ , \qquad B_1 = 4\pi^2\alpha M_\pi a_{\pi^- p}\ , \qquad B_2 = -8\pi\alpha M_\pi \big(a_{\pi^- p}\big)^2\ . \tag{3.7}$$

The scale ambiguity represented by the presence of $\log\mu_H$ is not induced by an ultraviolet divergence, but by a kinematic singularity at threshold. While the $1/|\mathbf{p}|$ term (the leading approximation to the Gamow–Sommerfeld factor [146]) can be unambiguously separated, the $\log|\mathbf{p}|$ requires the choice of a scale in order to define the strong threshold amplitude $T^{\mathrm{thr}}_{\pi^- p}$. In (3.6) that scale has been chosen to be μ_H. However, B_2 differs from zero only at two-loop level, i.e. it is suppressed by two chiral orders compared to the accuracy at which the isospin-breaking corrections [93] are known. Thus, choosing the mass of the ρ meson rather than the reduced mass μ_H shifts $a_{\pi^- p}$ by

$$\frac{B_2}{4\pi\xi_{\mathrm{p}}}\log\frac{M_\rho}{\mu_H} = -2\alpha\mu_H\big(a_{\pi^- p}\big)^2\log\frac{M_\rho}{\mu_H} = -0.2\cdot 10^{-3} M_\pi^{-1}\ , \tag{3.8}$$

an effect fully in line with its two-loop estimate that can therefore be safely neglected.

One might worry that our definition of g_c is not exactly what is measured in experiment, because, despite the application of electromagnetic corrections, the full range of virtual-photon effects is not captured by present-day analyses. For this reason, one could try to add a certain class of virtual-photon diagrams in order to obtain a quantity that corresponds better to the experimentally accessible one. In fact, this is quite a difficult enterprise: to extract the coupling constant, we need the amplitude at $s = m_{\mathrm{n}}^2$, where threshold ambiguities as in the case of the scattering lengths do not occur. However, the cancellation of infrared divergences that is ensured at threshold by phase-space arguments no longer works, which makes the inclusion of bremsstrahlung inevitable. In order to estimate the size of such effects, one may in a first rough approximation consider only the leading bremsstrahlung contribution that involves logarithms of the detector resolution $E_{\max}$. In this naive approach—described in more detail in Appendix A.3.2—we find a shift of about 0.07 in $g_c^2/4\pi$ for $E_{\max} = 10\,\mathrm{MeV}$, which is significantly below the accuracy we claim for our final result (see Sect. 3.2.3) and therefore does not alter the overall uncertainty estimate. We conclude that, in order to address virtual-photon effects systematically, one is forced to perform the full radiative corrections for a given process, which is beyond the scope of this work.

3.2.2 Evaluation of J^-

The evaluation of J^- has recently been discussed in great detail in [82] and [83], hereafter referred to as ELT and AMS. The main difference between both analyses is that the former relies on phase-shift solutions to determine the cross sections, while the latter uses data directly. Both investigations apply the Tromborg procedure [142] to remove electromagnetic

effects.[3] The quoted results

$$J^-_{\rm ELT} = (-1.083 \pm 0.032)\,\text{mb}\ , \qquad J^-_{\rm AMS} = (-1.060 \pm 0.030)\,\text{mb}\ , \tag{3.9}$$

are consistent within the uncertainties and we take the discrepancy between the mean values as an indication of the final accuracy one can hope to achieve in an evaluation of J^-. In order to obtain an average value of J^- that combines ELT and AMS, we now compare both analyses in the low-momentum ($|\mathbf{k}| \leq 2\,\text{GeV}/c$), the high-momentum ($2\,\text{GeV}/c \leq |\mathbf{k}| \leq 240\,\text{GeV}/c$), and the Regge regime ($|\mathbf{k}| \geq 240\,\text{GeV}/c$) separately. In general, we employ the uncertainties quoted by ELT, whose error estimates tend to be more conservative than those of AMS.

In the low-momentum region, we average the mean of the results for the SM95 [82, 148], SM99 [82, 149], and FA02 [150, 151] phase-shift solutions with AMS. In these determinations, the threshold region constitutes an additional source of uncertainty due to the lack of very low-energy data. Therefore, for the interval (0–80) MeV/c an interpolation between the cross sections at threshold

$$\Delta\sigma(0) = \sigma^{\rm tot}_{\pi^- p}(0) - \sigma^{\rm tot}_{\pi^+ p}(0) = 4\pi\Big((a_{\pi^- p})^2 + (a^{\rm cex}_{\pi^- p})^2 - (a_{\pi^+ p})^2\Big) \tag{3.10}$$

and the available scattering data is needed. To estimate the impact of the scattering lengths on J^-, we consider the S-wave part of this interpolation, which changes by about 0.009 mb if one varies $\Delta\sigma(0)$ by 30 %. In view of the fact that the difference between our value for $\Delta\sigma(0)$ and those of AMS and ELT lies below 20 %, this should provide a conservative estimate of the additional uncertainties to be expected in the threshold region. Adding in quadrature this estimation, the uncertainty quoted by ELT, and the effect due to the lower $\pi^0 n$ threshold discussed in Sect. 3.2.1, yields the ± 0.023 error given in Table 3.3. In the high-momentum region we use the mean of AMS and ELT with the ELT error, while the contributions from the Regge regime above $240\,\text{GeV}/c$ are determined as the average of the five models employed in AMS and ELT with an error chosen generously to encompass all models (cf. Table 3.3). In this way, we finally obtain for our average

$$J^- = (-1.073 \pm 0.034)\,\text{mb}\ . \tag{3.11}$$

3.2.3 Results for the pion–nucleon coupling constant

Inspired by [82], we adopt the following strategy to determine $a_{\pi^- p} - a_{\pi^+ p}$. Writing

$$\begin{aligned} a_{\pi^- p} - a_{\pi^+ p} &= 2a_{\pi^- p} - \big(a_{\pi^- p} + a_{\pi^- n}\big) + a_{\pi^- n} - a_{\pi^+ p} \\ &= 2a_{\pi^- p} - 2\big(\tilde{a}^+ + \Delta\tilde{a}^+\big) + a_{\pi^- n} - a_{\pi^+ p}\ , \end{aligned} \tag{3.12}$$

we can take

$$a_{\pi^- p} = (85.66 \pm 0.14) \cdot 10^{-3} M_\pi^{-1} \tag{3.13}$$

directly from the level shift in πH, $\tilde{a}^+$ from (3.1), and

$$a_{\pi^- n} - a_{\pi^+ p} = \frac{e^2}{4\pi\xi_{\rm p}}\Big\{f_2 + 2M_\pi\big(2g_6^{\rm r} + g_8^{\rm r}\big)\Big\} \tag{3.14}$$

[3] Above the energy range where the Tromborg corrections are available the effect due to the Coulomb barrier is accounted for following the potential-model calculation [147].

$\|\mathbf{k}\|$ in GeV/c			
0–2	SM95 [82, 148]	SM99 [82, 149]	FA02 [150, 151]
	-1.302	-1.314	-1.3043
	AMS	average	
	-1.3003	-1.304 ± 0.023	
2–240	ELT [82]	AMS [83]	average
	0.197	0.2149	0.206 ± 0.024
240–∞	Höhler [152]	Donnachie–Landshoff [153]	Gauron–Nicolescu [154]
	0.0222	0.0294	0.0244
	Regge94 [155]	Regge98 [156]	average
	0.030	0.018	0.025 ± 0.007

Table 3.3: Contributions to J^- from different momentum regions in mb. For the detailed comparison, we use that the regions (2–2.03) GeV/c and (240–350) GeV/c yield a contribution of 0.0027 mb and 0.0043 mb to J^-, respectively [150].

from [93]. As the $g_i^{\rm r}$ cancel between $a_{\pi^- n} - a_{\pi^+ p}$ and $2\Delta\tilde{a}^+$ (cf. (2.18) and (3.14)), so that only the rather well-determined LEC f_2 remains, this procedure is particularly stable with respect to unknown LECs. We find

$$a_{\pi^- p} - a_{\pi^+ p} = (173.4 \pm 1.6) \cdot 10^{-3} M_\pi^{-1} \,. \tag{3.15}$$

However, these scattering lengths still contain virtual-photon effects that should be removed for the application in the sum rule. Subtracting the corresponding contribution (cf. Appendix A.3.1)

$$a^\gamma_{\pi^- p} - a^\gamma_{\pi^+ p} = (2.1 \pm 1.8) \cdot 10^{-3} M_\pi^{-1} \tag{3.16}$$

from (3.15), we obtain for the virtual-photon-subtracted scattering lengths

$$a^{\not\gamma}_{\pi^- p} - a^{\not\gamma}_{\pi^+ p} = (171.3 \pm 2.4) \cdot 10^{-3} M_\pi^{-1} \,. \tag{3.17}$$

Together with the input (3.11) for J^-, the GMO sum rule (3.5) then yields

$$\frac{g_c^2}{4\pi} = 13.69 \pm 0.12 \pm 0.15 \,, \tag{3.18}$$

where the first error gives the uncertainty due to the scattering lengths and the second that due to J^-. This value is in agreement with determinations from NN ($g_c^2/4\pi = 13.54 \pm 0.05$ [157]) and πN ($g_c^2/4\pi = 13.75 \pm 0.10$ [151], $g_c^2/4\pi = 13.76 \pm 0.01$ [158]) scattering data. We stress that the errors quoted in [151,157,158] mainly reflect statistical uncertainties. The systematic subtleties associated with isospin violation that have been discussed in Sect. 3.2.1 were not quantified in these studies.[4]

[4] In the nucleon–nucleon case electromagnetic corrections to the one-pion-exchange potential were calculated in [159, 160]. The renormalization procedure chosen in [159] implies that electromagnetic corrections to g_c are small. However, it is unclear how these conventions could be translated to πN scattering.

3.3 Implications for the pion–nucleon σ term

The isospin-symmetric part of the scalar form factor of the nucleon is defined as

$$\sigma(t) = \frac{1}{2m}\langle N(p')|\hat{m}(\bar{u}u + \bar{d}d)|N(p)\rangle \ , \qquad t = (p'-p)^2 \ , \qquad \hat{m} = \frac{m_\mathrm{u} + m_\mathrm{d}}{2} \ . \tag{3.19}$$

Its value at vanishing momentum transfer $t = 0$, the pion–nucleon σ term $\sigma_{\pi N}$, measures the contribution from the light quarks to the mass of the nucleon. The standard procedure to extract $\sigma_{\pi N}$ from πN scattering data [79, 80] involves the venerable low-energy theorem that relates the Born-term-subtracted isoscalar πN scattering amplitude $\bar{D}^+$ at the Cheng–Dashen point to $\sigma(2M_\pi^2)$ [161, 162]. Later on, it was shown that the correction Δ_R to this low-energy theorem is very small, in particular it is free of chiral logarithms at full one-loop order in ChPT [163, 138]. The extraction of $\sigma_{\pi N}$ itself thus requires knowledge of the difference

$$\Delta_\sigma = \sigma(2M_\pi^2) - \sigma_{\pi N} \ , \tag{3.20}$$

which can be determined by means of a dispersive representation of $\sigma(t)$ [164]. Moreover, by defining another correction Δ_D as the difference between $\bar{D}^+$ evaluated at the Cheng–Dashen point and the first two terms in the subthreshold expansion

$$\Delta_D = F_\pi^2\big(\bar{D}^+ - d_{00}^+ - 2M_\pi^2 d_{01}^+\big) \ , \tag{3.21}$$

the σ term may be written as

$$\sigma_{\pi N} = \Sigma_d + \Delta_D - \Delta_\sigma - \Delta_\mathrm{R} \ , \qquad \Sigma_d = F_\pi^2\big(d_{00}^+ + 2M_\pi^2 d_{01}^+\big) \ . \tag{3.22}$$

In Part III, we will address the determination of Δ_D and Δ_σ in the framework of RS equations in much more detail, but for the moment we merely mention the estimate [164]

$$\Delta_D - \Delta_\sigma = -(3.3 \pm 0.2)\,\mathrm{MeV} \ , \tag{3.23}$$

where the error only includes the uncertainty in the parameterization of the $\pi\pi$ phase shift that served as input for the dispersive calculation.

Finally, πN scattering lengths enter as subtraction constants in a dispersive representation of the subthreshold parameters [79]. First, we have

$$d_{00}^+ = \bar{D}^+(0) \ , \qquad d_{01}^+ = \bar{E}^+(0) \ , \tag{3.24}$$

where

$$\begin{aligned} D^+(\omega) &= \big[A^+ + \omega B^+\big]_{s=s(w),t=0} \ , \qquad s = m^2 + M_\pi^2 + 2m\omega \ , \\ E^+(\omega) &= \left[\frac{\partial}{\partial t}\big(A^+(s,t) + \omega B^+(s,t)\big)\right]_{s=s(w),t=0} \ , \end{aligned} \tag{3.25}$$

and the bar indicates the subtraction of the pseudovector Born terms (for the precise definition of the πN invariant amplitudes A^+, B^+, and D^+ see Sect. 6.2). Second, $D^+(\omega)$ and $E^+(\omega)$ fulfill once-subtracted fixed-t dispersion relations that involve a^+ and the P-wave scattering length a_{1+}^+ as subtraction constants. In analogy to the evaluation of the GMO sum rule,

	KH80 [152, 165]	FA01 [166]	this work	[167]	ChPT [78]
a^+	-7	0	-0.7 ± 0.7		$-7.3 \ldots +3.6$
a^+_{1+}	352	351			$344 \ldots 348$
J^+	-91	-88		-88.9 ± 0.3	
$\tilde{J}^+$	-72	-69			
g_c	-133	-127	-125.2 ± 1.8		
Σ_d^c	50	67			

Table 3.4: Individual contributions to the sum rule (3.27) for Σ_d^c as indicated in the first column (all in MeV). The values for KH80 are quoted as given in [166].

we identify the isoscalar quantities with the pertinent linear combination of π^+p and π^-p amplitudes for the time being, i.e. we consider

$$\Sigma_d^c = F_\pi^2 \Big\{ \bar{D}^c(0) + 2M_\pi^2 \bar{E}^c(0) \Big\} \,, \qquad D^c = \frac{1}{2}(D_{\pi^-p} + D_{\pi^+p}) \,, \qquad E^c = \frac{1}{2}(E_{\pi^-p} + E_{\pi^+p}) \,. \tag{3.26}$$

The dispersive representation for Σ_d^c in terms of S- and P-wave scattering lengths then reads

$$\begin{aligned}
\Sigma_d^c &= F_\pi^2 \Bigg\{ 2\pi\xi_\mathrm{p}(a_{\pi^-p} + a_{\pi^+p}) + \frac{2g_c^2 M_\pi^2}{(m_\mathrm{p}+m_\mathrm{n})\big[(m_\mathrm{p}+m_\mathrm{n})^2 - M_\pi^2\big]} - J^+ \\
&\quad + 2M_\pi^2 \bigg[3\pi\xi_\mathrm{p}(a_{1+}^{\pi^-p} + a_{1+}^{\pi^+p}) - \frac{g_c^2}{(M_\pi + m_\mathrm{n} - m_\mathrm{p})(m_\mathrm{p}+m_\mathrm{n}-M_\pi)^2} - \tilde{J}^+ \bigg] \Bigg\} \,, \\
J^+ &= \frac{M_\pi^2}{\pi} \int\limits_0^\infty \mathrm{d}|\mathbf{k}'| \frac{\sigma^\mathrm{tot}_{\pi^-p}(|\mathbf{k}'|) + \sigma^\mathrm{tot}_{\pi^+p}(|\mathbf{k}'|)}{M_\pi^2 + \mathbf{k}'^2} \,, \qquad \omega' = \sqrt{\mathbf{k}'^2 + M_\pi^2} \,, \\
\tilde{J}^+ &= \frac{2M_\pi^2}{\pi} \int\limits_{M_\pi}^\infty \mathrm{d}\omega' \frac{\mathrm{Im}\, E^c(\omega')}{\omega'(\omega'^2 - M_\pi^2)} + \frac{1}{2\pi m_\mathrm{p}} \int\limits_{M_\pi}^\infty \mathrm{d}\omega' \mathrm{Im}\, D^c(\omega') \bigg(\frac{1}{\omega'^2} - \frac{1}{(\omega'+M_\pi)^2} \bigg) \\
&\quad - \frac{1}{2\pi m_\mathrm{p}} \int\limits_{M_\pi}^\infty \mathrm{d}\omega' \mathrm{Im}\, B^c(\omega') \bigg(\frac{1}{\omega'} - \frac{1}{\omega'+M_\pi} \bigg) \,.
\end{aligned} \tag{3.27}$$

Although J^+ could still be evaluated directly by means of cross-section data, the calculation of $\tilde{J}^+$ has to rely on phase-shift solutions. In either case, it seems more accurate to relate the outcome of the sum rule to the $\pi^\pm p$ channels instead of the strict isospin limit, bearing in mind that also the phase-shift analyses are largely based on elastic $\pi^\pm p$ scattering.

The individual contributions to (3.27) are summarized for the KH80 partial-wave solution [152,165] and the GWU FA01 solution [166] in the second and third column of Table 3.4, illustrating the origin of the discrepancy in the resulting values for $\sigma_{\pi N}$. For comparison, we also show the results using the hadronic-atom constraints for $a^{\not\gamma}_{\pi^-p} + a^{\not\gamma}_{\pi^+p}$ from (A.28) as input for the S-wave scattering lengths and (3.18) for the coupling constant, as well as the results for J^+ from [167] and for the scattering lengths from a fourth-order ChPT calculation [78].

These results show that the dispersive approach [79,80] to the determination of Σ_d suffers from the inherent difficulty that huge cancellations between individually sizeable terms occur. In this way, all input quantities need to be known to a very good relative accuracy for the final result to be accurate. While the uncertainty due to a^+ is now essentially under control, thanks to the precise hadronic-atom data, the accuracy in the evaluation of (3.27) is limited by our knowledge of a_{1+}^+, which produces by far the largest individual contribution. Given that already the moderate deviations between [166]

$$a_{1+}^+ = 133 \cdot 10^{-3} M_\pi^{-3} \tag{3.28}$$

and the ChPT result [78]

$$a_{1+}^+ = (130.4 \ldots 131.8) \cdot 10^{-3} M_\pi^{-3} \tag{3.29}$$

impact the final result for Σ_d significantly, we conclude that the uncertainty in a_{1+}^+ presently precludes an evaluation of (3.27) at the same level of accuracy as for the GMO sum rule.

Finally, we comment on the issue of isospin breaking in the pion–nucleon σ term, since—as exemplified by the chiral expansion of a^+—isospin-violating effects may play an important role for isoscalar πN amplitudes. Starting from the chiral expansion of the nucleon mass in the isospin limit [19]

$$m = m_0 - 4c_1 M_\pi^2 - \frac{3g_\mathrm{A}^2 M_\pi^3}{32\pi F^2} + \mathcal{O}\big(M_\pi^4\big) \,, \tag{3.30}$$

the Feynman–Hellmann theorem [136] yields

$$\sigma_{\pi N} = \hat{m}\frac{\partial m}{\partial \hat{m}} = -4c_1 M_\pi^2 - \frac{9g_\mathrm{A}^2 M_\pi^3}{64\pi F^2} + \mathcal{O}\big(M_\pi^4\big) \,. \tag{3.31}$$

However, the full expansion of the proton and neutron mass [168,94]

$$\begin{aligned} m_\mathrm{p} &= m_0 - 4c_1 M_{\pi^0}^2 + 2Bc_5(m_\mathrm{d} - m_\mathrm{u}) - \frac{e^2F_\pi^2}{2}(f_1 + f_2 + f_3) - \frac{g_\mathrm{A}^2(2M_\pi^3 + M_{\pi^0}^3)}{32\pi F_\pi^2} + \mathcal{O}\big(M_\pi^4\big) \,, \\ m_\mathrm{n} &= m_0 - 4c_1 M_{\pi^0}^2 - 2Bc_5(m_\mathrm{d} - m_\mathrm{u}) - \frac{e^2F_\pi^2}{2}(f_1 - f_2 + f_3) - \frac{g_\mathrm{A}^2(2M_\pi^3 + M_{\pi^0}^3)}{32\pi F_\pi^2} + \mathcal{O}\big(M_\pi^4\big) \,, \end{aligned} \tag{3.32}$$

leads to

$$\sigma_\mathrm{p} = \hat{m}\frac{\partial m_\mathrm{p}}{\partial \hat{m}} = \sigma_\mathrm{n} = \hat{m}\frac{\partial m_\mathrm{n}}{\partial \hat{m}} = -4c_1 M_{\pi^0}^2 - \frac{3g_\mathrm{A}^2}{64\pi F_\pi^2} M_{\pi^0}^2 (2M_\pi + M_{\pi^0}) + \mathcal{O}\big(M_\pi^4\big) \,, \tag{3.33}$$

and thus

$$\sigma_\mathrm{p} - \sigma_{\pi N} = \sigma_\mathrm{n} - \sigma_{\pi N} = 4c_1\Delta_\pi + \frac{21g_\mathrm{A}^2 M_\pi \Delta_\pi}{128\pi F_\pi^2} = (-3.3 \pm 1.5)\,\mathrm{MeV} \,. \tag{3.34}$$

In fact, the same large correction alongside c_1, which on its own shifts the σ term by $-5\,\mathrm{MeV}$, appears in the relation of (3.27) to its isospin limit

$$F_\pi^2 4\pi\xi_\mathrm{p}\left(\frac{a_{\pi^- p}^{\not{\gamma}} + a_{\pi^+ p}^{\not{\gamma}}}{2} - a^+\right) = 4c_1\Delta_\pi - \frac{e^2F_\pi^2}{2}(4f_1 + f_2) - \frac{33g_\mathrm{A}^2 M_\pi \Delta_\pi}{128\pi F_\pi^2} \,, \tag{3.35}$$

which suggests that the σ term as determined from (3.27) should be identified with σ_p rather than $\sigma_{\pi N}$. To clarify these relations as well as the potential impact of isospin-violating corrections on a precise determination of the σ term, it might be worthwhile to revisit the derivation of the underlying low-energy theorem in the presence of isospin violation.

Part II

Roy–Steiner equations for $\gamma\gamma \to \pi\pi$[#2]

[#2]The contents of this part have been published in [169].

Chapter 4

Partial-wave dispersion relations

4.1 Introduction

The reaction $\gamma\gamma \to \pi\pi$ is of particular interest in the realm of non-perturbative QCD, as it probes the dynamics of strong interactions in the 0^{++} channel, which has the same quantum numbers as the QCD vacuum. Nonetheless, a detailed theoretical understanding of this channel has proven to be a rather demanding endeavor. The rescattering of the pions produced in two-photon collisions will dominate the reaction dynamics, with the result that a reliable description of $\pi\pi$ scattering is a prerequisite for understanding $\gamma\gamma \to \pi\pi$. As highlighted in Sect. 1.2.3, a major step forward in this direction was taken by combining analyticity, unitarity, and crossing symmetry in form of the Roy equations with chiral symmetry of QCD, culminating in a very precise prediction of the pole parameters of the σ resonance, the lowest-lying resonance in QCD, cf. (1.50).

This resonance influences the cross sections in $\gamma\gamma \to \pi\pi$, which therefore provides an alternative to meson–meson scattering reactions for its excitation. Experimentally, $\gamma\gamma \to \pi\pi$ is accessible in e^+e^- colliders via the reaction $e^+e^- \to e^+e^-\pi\pi$, where both the incoming electron and positron radiate one photon [170–174]. However, due to its very large width, the σ is either entirely overshadowed by the QED Born terms in the charged reaction $\gamma\gamma \to \pi^+\pi^-$ or manifests itself only as a broad bump in the $\gamma\gamma \to \pi^0\pi^0$ cross section, which makes it difficult to directly extract information on the resonance from these data. In particular, theoretical input is needed to perform the analytic continuation into the complex plane in order to establish contact to the properties of the σ.

Moreover, the two-photon coupling of the σ enters the description of Compton scattering off the proton by means of the exchange of degrees of freedom between the incoming photon and the target proton that can be identified with the σ [175, 176]. Besides its relation to nucleon polarizabilities, there has been particular interest in the two-photon width of the σ in the context of elucidating the nature of this state. Apart from an interpretation as a $q\bar{q}$ state, possibilities such as a tetraquark state, a meson–meson molecule, or a gluonic resonance have been put forward in the literature. The coupling to two photons has been used to discriminate between different scenarios (see e.g. [177–179] and references therein). A recent K-matrix-based extraction of the σ width from $\gamma\gamma \to \pi\pi$ data can be found in [178, 180]. Alternatively, a model-independent approach using dispersion relations and Muskhelishvili–Omnès techniques [70, 71] for describing this reaction was pursued in [176, 177, 181–188]. In the most sophisticated such treatment [188], motivated by the fact that most of the Belle data

lie above 1 GeV, a MO representation was constructed that dynamically includes the $\bar{K}K$ channel, in order to obtain a description of $\gamma\gamma \to \pi\pi$ valid up to 1.3 GeV.

Here, we consider a more general approach, namely a complete system of Roy–Steiner equations for $\gamma\gamma \to \pi\pi$ and the crossed reaction $\gamma\pi \to \gamma\pi$ that, in analogy to the $\pi\pi$ Roy equations, fully respects analyticity, unitarity, and crossing symmetry of the scattering amplitude. We find that—at a similar level of rigor at which the Roy equations for $\pi\pi$ scattering hold—our $\gamma\gamma \to \pi\pi$ equations are valid up to 1 GeV. We compare our equations for the $\gamma\gamma \to \pi\pi$ partial waves to existing dispersive descriptions of this process, and find, in particular, that a numerically important coupling between S- and D-waves has been previously neglected. Furthermore, our equations lead to sum rules for the isospin-two partial waves, which we use to improve the ChPT prediction of the charged-pion quadrupole polarizability.

As an application of these results, we study the constraints of our equations on the two-photon coupling of the σ. The subtraction constants necessary to ensure sufficiently fast convergence of the dispersion integrals can be directly related to the pion polarizabilities, which therefore play a similar role to that of the $\pi\pi$ scattering lengths in the case of $\pi\pi$ Roy equations. As the tension between various experimental determinations of the dipole polarizability of the charged pion (based on Primakov measurements [189] or radiative pion production [190]) and ChPT predictions [191–193] is far from being resolved, we provide the two-photon width of the σ as a function of the pertinent polarizabilities. We are confident that the ongoing measurements at COMPASS [194], in combination with ChPT predictions, will clarify the situation in the near future.

Finally, we stress that the construction of RS equations for $\gamma\gamma \to \pi\pi$ already displays all the complications that emerge both due to more involved crossing properties and less restrictive unitarity in the t-channel, see Sect. 1.2.4. Since the structure of the partial-wave expansions is still considerably simpler, the investigation of $\gamma\gamma \to \pi\pi$ can be benefited from to gain valuable insights for the construction and solution of RS equations for πN scattering.

The analysis is organized as follows: having specified our conventions in Sect. 4.2, we present the detailed derivation of the RS system in Sect. 4.3. The domain of validity of these equations is studied in Sect. 4.4. In Chapter 5, we then concentrate on the equations for the $\gamma\gamma \to \pi\pi$ partial waves, whose solution in terms of Omnès functions is discussed in Sect. 5.1. Establishing the connection to the two-photon width of the σ in Sect. 5.2, we then discuss the input we use and present our numerical results in Sects. 5.3 and 5.4.

4.2 Formalism

4.2.1 Kinematics

We first consider the Compton-scattering process

$$\gamma(q_1, \lambda_1) + \pi^a(p_1) \to \gamma(q_2, \lambda_2) + \pi^b(p_2) \tag{4.1}$$

with momenta as indicated, photon helicities λ_1, λ_2, and pion isospin indices a, b. For on-shell particles, the Mandelstam variables defined as

$$s = (p_1 + q_1)^2 \,, \qquad t = (q_1 - q_2)^2 \,, \qquad u = (q_1 - p_2)^2 \,, \tag{4.2}$$

are subject to the constraint

$$s + t + u = 2M_\pi^2 \,. \tag{4.3}$$

In the center-of-mass frame (CMS), we have

$$t = -2\mathbf{q}^2(1 - z_s) \,, \qquad z_s = \cos\theta_s \,, \qquad \mathbf{q}^2 = \frac{(s - M_\pi^2)^2}{4s} \,. \tag{4.4}$$

The S-matrix for the charged process can be written as

$$\begin{aligned} {}_{\rm out}\langle\gamma(q_2,\lambda_2)\pi^\pm(p_2)|\gamma(q_1,\lambda_1)\pi^\pm(p_1)\rangle_{\rm in} &= (2\pi)^4\delta^4(q_2 + p_2 - q_1 - p_1) \\ &\quad \times \Big\{\delta_{\lambda_1\lambda_2} + ie^2 F^{\rm c}_{\lambda_1\lambda_2}(s,t)e^{i(\lambda_1-\lambda_2)\varphi}\Big\} \,, \end{aligned} \tag{4.5}$$

with azimuthal angle φ, and similarly for the neutral amplitude $F^{\rm n}_{\lambda_1\lambda_2}$. Separating the photon polarization vectors,[1]

$$F_{\lambda_1\lambda_2}(s,t) = \epsilon_\mu(q_1,\lambda_1)\epsilon^*_\nu(q_2,\lambda_2)W^{\mu\nu}(s,t) \,, \tag{4.6}$$

we can use gauge and Lorentz invariance to decompose the amplitude as

$$\begin{aligned} W_{\mu\nu}(s,t) &= A(s,t)\Big(\frac{t}{2}g_{\mu\nu} + q_{2\mu}q_{1\nu}\Big) \\ &\quad + B(s,t)\Big(2t\Delta_\mu\Delta_\nu - (s-u)^2 g_{\mu\nu} + 2(s-u)(\Delta_\mu q_{1\nu} + \Delta_\nu q_{2\mu})\Big) \,, \end{aligned} \tag{4.7}$$

where $\Delta_\mu = p_{1\mu} + p_{2\mu}$ and we have dropped terms that vanish in $F_{\lambda_1\lambda_2}$ due to $\epsilon(q_i,\lambda_i)\cdot q_i = 0$. In the conventions of [195] for the polarization vectors, one obtains

$$\begin{aligned} F_{++}(s,t) &= F_{--}(s,t) = 4(M_\pi^4 - su)B(s,t) \,, \\ F_{+-}(s,t) &= F_{-+}(s,t) = -\frac{t}{2}A(s,t) + t(t - 4M_\pi^2)B(s,t) \,. \end{aligned} \tag{4.8}$$

The Born-term contributions are

$$\begin{aligned} A^{\rm Born}(s,t) \equiv A^{\rm c,\,Born}(s,t) &= \frac{1}{M_\pi^2 - s} + \frac{1}{M_\pi^2 - u} \\ &= 2tB^{\rm c,\,Born}(s,t) \equiv 2tB^{\rm Born}(s,t) \,. \end{aligned} \tag{4.9}$$

In these conventions, the differential cross section is given by

$$\frac{{\rm d}\sigma}{{\rm d}\Omega} = \frac{\alpha^2}{4s}\big(|F_{++}(s,t)|^2 + |F_{+-}(s,t)|^2\big) \,. \tag{4.10}$$

The analytic continuation of $F_{+\pm}(s,t)$ to the kinematical region where $t \geq 4M_\pi^2$ describes the crossed-channel process $\gamma\gamma \to \pi\pi$, so that the cross section reads

$$\left.\frac{{\rm d}\sigma}{{\rm d}\Omega}\right|_{\gamma\gamma\to\pi^+\pi^-} = \frac{\alpha^2}{8t}\sigma(t)\big(|F^{\rm c}_{++}(s,t)|^2 + |F^{\rm c}_{+-}(s,t)|^2\big) \tag{4.11}$$

($\sigma(t)$ was defined in (1.37)). The same formula with an additional factor of 1/2 on the right-hand side holds for the case of neutral pions. The kinematics for the crossed reaction

$$\gamma(q_1,\lambda_1) + \gamma(-q_2,\lambda_2) \to \pi^a(-p_1) + \pi^b(p_2) \tag{4.12}$$

[1] Here and throughout Chapters 4 and 5, we suppress isospin indices whenever possible.

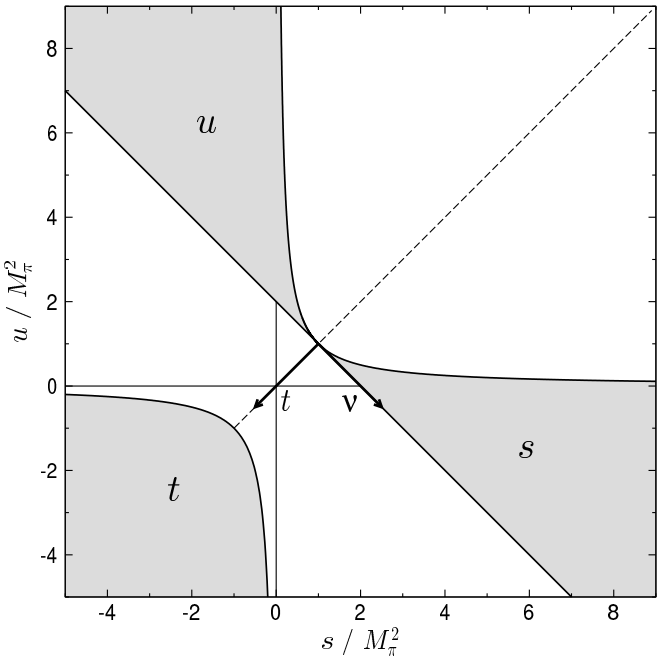

Figure 4.1: Mandelstam plane for $\gamma\pi \to \gamma\pi$. The filled areas mark the s-, t-, and u-channel physical regions, and the arrows the orientation of the plane in t and ν.

in terms of the Mandelstam variables (4.2) lead to different CMS momenta for initial and final states

$$\mathbf{q}_t^2 = \frac{t}{4}\,, \qquad \mathbf{p}_t^2 = \frac{t}{4} - M_\pi^2 = \frac{t - t_\pi}{4}\,, \qquad t_\pi = 4M_\pi^2\,, \tag{4.13}$$

and to the CMS scattering angle

$$z_t = \cos\theta_t = \frac{\nu}{4p_t q_t}\,, \qquad \nu = s - u\,, \qquad p_t = |\mathbf{p}_t|\,, \qquad q_t = |\mathbf{q}_t|\,. \tag{4.14}$$

The physical regions for pion Compton scattering and $\gamma\gamma \to \pi\pi$ are depicted in Fig. 4.1.

4.2.2 Partial-wave expansion and pion polarizabilities

The partial-wave expansion of the amplitudes for pion Compton scattering reads [196]

$$F_{+\pm}(s,t) = \sum_{J=1}^{\infty}(2J+1) f_{J,\pm}(s) d^J_{1,\pm1}(z_s)\,, \tag{4.15}$$

with the Wigner d-functions [197][2]

$$d^J_{1,\pm1}(z) = \frac{1 \mp z}{J(J+1)} P'_J(z) \pm P_J(z) \tag{4.16}$$

[2]For convenience, we write $d^J_{m,m'}(\cos\theta)$ instead of $d^J_{m,m'}(\theta)$. A comprehensive review on Wigner functions may be found in [198].

and the inversion

$$f_{J,\pm}(s) = \frac{1}{2}\int_{-1}^{1} \mathrm{d}z_s d^J_{1,\pm1}(z_s) F_{+\pm}(s,t)\Big|_{t=-2\mathbf{q}^2(1-z_s)} . \tag{4.17}$$

The expansion (4.15) can be mapped onto the multipole expansion [199] via[3]

$$f_{J,\pm}(s) = \pm\frac{2\sqrt{s}}{\alpha(2J+1)}\big(E_J(\omega) \pm M_J(\omega)\big) , \tag{4.18}$$

where ω denotes the energy of the photon. Defining the pion polarizabilities as the leading terms of the Born-term-subtracted multipoles $\hat{E}_J(\omega)$, $\hat{M}_J(\omega)$ in an expansion in ω [199],

$$\alpha_J = \frac{2J[(2J-1)!!]^2}{J+1}\frac{\hat{E}_J(\omega)}{\omega^{2J}}\bigg|_{\omega=0} , \qquad \beta_J = \frac{2J[(2J-1)!!]^2}{J+1}\frac{\hat{M}_J(\omega)}{\omega^{2J}}\bigg|_{\omega=0} , \tag{4.19}$$

we can read off α_J and β_J from an expansion of the Born-term-subtracted amplitudes $\hat{F}_{+\pm}(s,t)$ in t at fixed $s = M_\pi^2$

$$\begin{aligned} \frac{2\alpha}{M_\pi t}\hat{F}_{++}(s=M_\pi^2,t) &= \alpha_1+\beta_1+\frac{t}{12}(\alpha_2+\beta_2)+\mathcal{O}\big(t^2\big) , \\ -\frac{2\alpha}{M_\pi t}\hat{F}_{+-}(s=M_\pi^2,t) &= \alpha_1-\beta_1+\frac{t}{12}(\alpha_2-\beta_2)+\mathcal{O}\big(t^2\big) . \end{aligned} \tag{4.20}$$

4.2.3 Relation to $\gamma\gamma \to \pi\pi$

To establish connection to the notation of the crossed process [188, 192], which we will refer to as the t-channel reaction, we briefly discuss

$$\gamma(q_1,\lambda_1) + \gamma(q_2,\lambda_2) \to \pi^a(p_1) + \pi^b(p_2) \tag{4.21}$$

in terms of the Mandelstam variables

$$\tilde{s} = (q_1+q_2)^2 , \qquad \tilde{t} = (q_1-p_1)^2 , \qquad \tilde{u} = (q_1-p_2)^2 , \tag{4.22}$$

and the amplitudes

$${}_{\text{out}}\langle\pi(p_1)\pi(p_2)|\gamma(q_1,\lambda_1)\gamma(q_2,\lambda_2)\rangle_{\text{in}} = ie^2(2\pi)^4\delta^4(q_2+p_2-q_1-p_1)H_{\lambda_1\lambda_2}(\tilde{s},\tilde{t})e^{i(\lambda_1-\lambda_2)\varphi} . \tag{4.23}$$

They are related to the s-channel amplitudes by

$$H_{++}(s,t) = -F_{+-}(t,s) , \qquad H_{+-}(s,t) = -F_{++}(t,s) , \tag{4.24}$$

and their polarizability expansion therefore reads

$$\begin{aligned} \frac{2\alpha}{M_\pi\tilde{s}}\hat{H}_{++}(\tilde{s},\tilde{t}=M_\pi^2) &= \alpha_1-\beta_1+\frac{\tilde{s}}{12}(\alpha_2-\beta_2)+\mathcal{O}\big(\tilde{s}^2\big) , \\ -\frac{2\alpha}{M_\pi\tilde{s}}\hat{H}_{+-}(\tilde{s},\tilde{t}=M_\pi^2) &= \alpha_1+\beta_1+\frac{\tilde{s}}{12}(\alpha_2+\beta_2)+\mathcal{O}\big(\tilde{s}^2\big) . \end{aligned} \tag{4.25}$$

[3] The covariant amplitudes in [199] are related to ours by $A_{\text{GR}} = -e^2A$, $B_{\text{GR}} = 16e^2B$.

Furthermore, the partial-wave amplitudes $h_{J\pm}$ follow from $F_{+\pm}$ via

$$\begin{aligned} F_{++}(s,t) &= -\sum_J (2J+1) h_{J,-}(t) d^J_{20}(z_t) \,, \\ F_{+-}(s,t) &= -\sum_J (2J+1) h_{J,+}(t) d^J_{00}(z_t) \,, \end{aligned} \tag{4.26}$$

where due to Bose symmetry the sum extends over even values of J only, and

$$d^J_{00}(z) = P_J(z) \,, \qquad d^J_{20}(z) = \frac{2P'_{J-1}(z) - J(J-1)P_J(z)}{\sqrt{(J-1)J(J+1)(J+2)}} \,. \tag{4.27}$$

In our conventions, the transition between isospin and particle basis is achieved by

$$\begin{pmatrix} H^{\mathrm{c}} \\ H^{\mathrm{n}} \end{pmatrix} = \begin{pmatrix} \frac{1}{\sqrt{3}} & \frac{1}{\sqrt{6}} \\ \frac{1}{\sqrt{3}} & -\sqrt{\frac{2}{3}} \end{pmatrix} \begin{pmatrix} H^0 \\ H^2 \end{pmatrix} \,. \tag{4.28}$$

4.3 Roy–Steiner equations

4.3.1 Hyperbolic dispersion relations

We start the derivation of RS equations by writing down unsubtracted HDRs for the amplitudes A and B, which can be constructed following [68]. The advantage of using dispersion relations for A and B instead of $F_{+\pm}$ is that all constraints by gauge invariance that lead to the decomposition (4.8) are automatically built in. In particular, the equations for F_{++} and F_{+-} do not decouple, as gauge invariance dictates that the same invariant function B contributes to both amplitudes. The dispersion relations for A and B read

$$\begin{aligned} A(s,t) &= \bar{A}^{\mathrm{B}}(s,t) + \frac{1}{\pi}\int\limits_{t_\pi}^{\infty} \mathrm{d}t' \frac{\mathrm{Im}\, A(s',t')}{t'-t} + \frac{1}{\pi}\int\limits_{M_\pi^2}^{\infty} \mathrm{d}s' \mathrm{Im}\, A(s',t') \left[\frac{1}{s'-s} + \frac{1}{s'-u} - \frac{1}{s'-a}\right] \,, \\ B(s,t) &= \bar{B}^{\mathrm{B}}(s,t) + \frac{1}{\pi}\int\limits_{t_\pi}^{\infty} \mathrm{d}t' \frac{\mathrm{Im}\, B(s',t')}{t'-t} + \frac{1}{\pi}\int\limits_{M_\pi^2}^{\infty} \mathrm{d}s' \mathrm{Im}\, B(s',t') \left[\frac{1}{s'-s} + \frac{1}{s'-u} - \frac{1}{s'-a}\right] \,, \end{aligned} \tag{4.29}$$

with the Born terms

$$\bar{A}^{\mathrm{B}}(s,t) = A^{\mathrm{Born}}(s,t) - \frac{1}{M_\pi^2 - a} \,, \qquad \bar{B}^{\mathrm{B}}(s,t) = B^{\mathrm{Born}}(s,t) \tag{4.30}$$

only contributing to the charged-pion process. As discussed in Sect. 1.2.4, the primed set of Mandelstam variables is constrained to lie on the hyperbola

$$(s'-a)(u'-a) = (s-a)(u-a) \equiv b \,, \tag{4.31}$$

where the hyperbola parameter a is tuned to maximize the range of validity of the RS system (cf. Sect. 4.4) and $b = b(s,t,a)$ is determined by a and the external variables. The integrands are expressed in terms of the integration variable and the external kinematics using (4.31) and

$$s' + t' + u' = 2M_\pi^2 \,. \tag{4.32}$$

Although in the HDR setup t' depends not only on t, but on s and s' as well, the limit of fixed-t may be recovered by sending a to infinity. This can be shown explicitly based on the relation between z_s and z'_s in (B.5) (the primed variable always refers to the internal kinematics).

4.3.2 Sum rules and subtracted dispersion relations

The most economical way to obtain a subtracted version of HDRs is to derive sum rules from the original dispersion relation and then subtract them from it. We will choose the subtraction point on-shell at $s = M_\pi^2$, $t = 0$, with the result that the subtraction constants coincide with the pion polarizabilities. With knowledge of the dipole pion polarizabilities $\alpha_1 \pm \beta_1$ we can implement one subtraction, while for a second subtraction the quadrupole polarizabilities $\alpha_2 \pm \beta_2$ are also needed. For example, choosing $s = M_\pi^2$ and taking the limit $t \to 0$, we can compare (4.29) with (4.8) and (4.20) in order to obtain[4]

$$\frac{M_\pi}{2\alpha}(\alpha_1+\beta_1) = \frac{4M_\pi^2}{\pi}\int\limits_{t_\pi}^{\infty}\mathrm{d}t'\frac{[\mathrm{Im}\,B(s',t')]_0}{t'} + \frac{4M_\pi^2}{\pi}\int\limits_{M_\pi^2}^{\infty}\mathrm{d}s'\,\big[\mathrm{Im}\,B(s',t')\big]_0\left[\frac{2}{s'-M_\pi^2}-\frac{1}{s'-a}\right],$$

which, together with similar sum rules, may be used to write down subtracted versions of (4.29).

4.3.3 *s*-channel projection

The RS system is obtained by expanding the integrands into partial waves and subsequently performing the s- and t-channel partial-wave projection of each equation. To this end, we make use of (4.15) and (4.26) as well as their inversions. Moreover, it is useful to note that

$$4(M_\pi^4 - su) = 8s\mathbf{q}^2(1+z_s) = -t(t-t_\pi)(1-z_t^2) \tag{4.33}$$

to identify the relevant kinematic dependencies.

We start with the projection onto $\gamma\pi \to \gamma\pi$ partial waves, which can be written as

$$\begin{aligned}
f_{J,+}(s) &= N_J^+(s) + \frac{1}{\pi}\int\limits_{M_\pi^2}^{\infty}\mathrm{d}s'\sum_{J'=1}^{\infty}K_{JJ'}^{++}(s,s')\mathrm{Im}\,f_{J',+}(s') \\
&\quad + \frac{1}{\pi}\int\limits_{t_\pi}^{\infty}\mathrm{d}t'\sum_{J'\,\mathrm{even}}G_{JJ'}^{+-}(s,t')\mathrm{Im}\,h_{J',-}(t')\,, \\
f_{J,-}(s) &= N_J^-(s) + \frac{1}{\pi}\int\limits_{M_\pi^2}^{\infty}\mathrm{d}s'\sum_{J'=1}^{\infty}\Big(K_{JJ'}^{-+}(s,s')\mathrm{Im}\,f_{J',+}(s') + K_{JJ'}^{--}(s,s')\mathrm{Im}\,f_{J',-}(s')\Big) \\
&\quad + \frac{1}{\pi}\int\limits_{t_\pi}^{\infty}\mathrm{d}t'\sum_{J'\,\mathrm{even}}\Big(G_{JJ'}^{-+}(s,t')\mathrm{Im}\,h_{J',+}(t') + G_{JJ'}^{--}(s,t')\mathrm{Im}\,h_{J',-}(t')\Big)\,,
\end{aligned} \tag{4.34}$$

where $N_J^\pm(s)$ includes Born terms and—in case subtractions were performed—pion polarizabilities. The kernel functions for the unsubtracted case read

$$K_{JJ'}^{++}(s,s') = \frac{s\,\mathbf{q}^2}{s'\mathbf{q}'^2}\frac{2J'+1}{2}\int\limits_{-1}^{1}\mathrm{d}z_s(1+z_s)d_{11}^J(z_s)\frac{d_{11}^{J'}(z_s')}{1+z_s'}\left[\frac{1}{s'-s}+\frac{1}{s'-u}-\frac{1}{s'-a}\right],$$

[4]Note that s' and t', respectively, depend on the integration variable as well as on s and t. The subscript 0 indicates evaluation at $s = M_\pi^2$ and $t = 0$.

$$G^{+-}_{JJ'}(s,t') = \frac{8s\mathbf{q}^2}{t'(t'-t_\pi)}\frac{2J'+1}{2}\int\limits_{-1}^{1}\mathrm{d}z_s(1+z_s)d^J_{11}(z_s)\frac{d^{J'}_{20}(z'_t)}{1-z'^2_t}\frac{1}{t'-t}\,,$$

$$K^{-+}_{JJ'}(s,s') = \frac{\mathbf{q}^2}{4s'\mathbf{q}'^2}\frac{2J'+1}{2}\int\limits_{-1}^{1}\mathrm{d}z_s(1-z_s)d^J_{1,-1}(z_s)\frac{d^{J'}_{11}(z'_s)}{1+z'_s}(t'-t)\left[\frac{1}{s'-s}+\frac{1}{s'-u}-\frac{1}{s'-a}\right],$$

$$K^{--}_{JJ'}(s,s') = \frac{\mathbf{q}^2}{\mathbf{q}'^2}\frac{2J'+1}{2}\int\limits_{-1}^{1}\mathrm{d}z_s(1-z_s)d^J_{1,-1}(z_s)\frac{d^{J'}_{1,-1}(z'_s)}{1-z'_s}\left[\frac{1}{s'-s}+\frac{1}{s'-u}-\frac{1}{s'-a}\right],$$

$$G^{-+}_{JJ'}(s,t') = 2\mathbf{q}^2\frac{2J'+1}{2}\int\limits_{-1}^{1}\mathrm{d}z_s\frac{1-z_s}{t'(t'-t)}d^J_{1,-1}(z_s)P_{J'}(z'_t)\,,$$

$$G^{--}_{JJ'}(s,t') = 2\mathbf{q}^2\frac{2J'+1}{2}\int\limits_{-1}^{1}\mathrm{d}z_s\frac{1-z_s}{t'(t'-t_\pi)}d^J_{1,-1}(z_s)\frac{d^{J'}_{20}(z'_t)}{1-z'^2_t}\,. \tag{4.35}$$

Explicit expressions for $J, J' \leq 2$ as well as the modifications for the subtracted case are given in Appendix B.1. It is important to note that while we have consistently suppressed isospin indices for the partial-wave amplitudes, all kernel functions are independent of isospin.

4.3.4 *t*-channel projection

Similarly, the projection onto $\gamma\gamma \to \pi\pi$ amplitudes has the form

$$\begin{aligned}
h_{J,+}(t) &= \tilde{N}^+_J(t) + \frac{1}{\pi}\int\limits_{M_\pi^2}^{\infty}\mathrm{d}s'\sum_{J'=1}^{\infty}\Big(\tilde{G}^{++}_{JJ'}(t,s')\mathrm{Im}\,f_{J',+}(s') + \tilde{G}^{+-}_{JJ'}(t,s')\mathrm{Im}\,f_{J',-}(s')\Big)\\
&\quad + \frac{1}{\pi}\int\limits_{t_\pi}^{\infty}\mathrm{d}t'\sum_{J'\,\mathrm{even}}\Big(\tilde{K}^{++}_{JJ'}(t,t')\mathrm{Im}\,h_{J',+}(t') + \tilde{K}^{+-}_{JJ'}(t,t')\mathrm{Im}\,h_{J',-}(t')\Big)\,,\\
h_{J,-}(t) &= \tilde{N}^-_J(t) + \frac{1}{\pi}\int\limits_{M_\pi^2}^{\infty}\mathrm{d}s'\sum_{J'=1}^{\infty}\tilde{G}^{-+}_{JJ'}(t,s')\mathrm{Im}\,f_{J',+}(s')\\
&\quad + \frac{1}{\pi}\int\limits_{t_\pi}^{\infty}\mathrm{d}t'\sum_{J'\,\mathrm{even}}\tilde{K}^{--}_{JJ'}(t,t')\mathrm{Im}\,h_{J',-}(t')\,,
\end{aligned} \tag{4.36}$$

where, in the unsubtracted case,

$$\tilde{G}^{++}_{JJ'}(t,s') = \frac{t}{8s'\mathbf{q}'^2}\frac{2J'+1}{2}\int\limits_{-1}^{1}\mathrm{d}z_t(t'-t)P_J(z_t)\frac{d^{J'}_{11}(z'_s)}{1+z'_s}\left[\frac{1}{s'-s}+\frac{1}{s'-u}-\frac{1}{s'-a}\right],$$

$$\tilde{G}^{+-}_{JJ'}(t,s') = \frac{t}{2\mathbf{q}'^2}\frac{2J'+1}{2}\int\limits_{-1}^{1}\mathrm{d}z_tP_J(z_t)\frac{d^{J'}_{1,-1}(z'_s)}{1-z'_s}\left[\frac{1}{s'-s}+\frac{1}{s'-u}-\frac{1}{s'-a}\right],$$

# subtractions	0	1	2
$K_{11}^{++}(s,s'), K_{12}^{++}(s,s')$	$\mathcal{O}(s'^{-3})$	$\mathcal{O}(s'^{-4})$	$\mathcal{O}(s'^{-5})$
$K_{21}^{++}(s,s'), K_{22}^{++}(s,s')$	$\mathcal{O}(s'^{-4})$	$\mathcal{O}(s'^{-4})$	$\mathcal{O}(s'^{-5})$
$G_{12}^{+-}(s,t')$	$\mathcal{O}(t'^{-3})$	$\mathcal{O}(t'^{-4})$	$\mathcal{O}(t'^{-5})$
$G_{22}^{+-}(s,t')$	$\mathcal{O}(t'^{-4})$	$\mathcal{O}(t'^{-4})$	$\mathcal{O}(t'^{-5})$
$\tilde{G}_{21}^{-+}(t,s'), \tilde{G}_{22}^{-+}(t,s')$	$\mathcal{O}(s'^{-3})$	$\mathcal{O}(s'^{-4})$	$\mathcal{O}(s'^{-5})$
$\tilde{K}_{22}^{--}(t,t')$	$\mathcal{O}(t'^{-3})$	$\mathcal{O}(t'^{-4})$	$\mathcal{O}(t'^{-5})$

Table 4.1: Asymptotics of the kernel functions in the equations for $f_{J,+}(s)$ and $h_{J,-}(t)$.

$$\tilde{K}_{JJ'}^{++}(t,t') = \frac{t}{t'(t'-t)}\frac{2J'+1}{2}\int_{-1}^{1}\mathrm{d}z_t P_J(z_t)P_{J'}(z_t') \,,$$

$$\tilde{K}_{JJ'}^{+-}(t,t') = \frac{t}{t'(t'-t_\pi)}\frac{2J'+1}{2}\int_{-1}^{1}\mathrm{d}z_t P_J(z_t)\frac{d_{20}^{J'}(z_t')}{1-z_t'^2} \,,$$

$$\tilde{G}_{JJ'}^{-+}(t,s') = \frac{t(t-t_\pi)}{8s'\mathbf{q}'^2}\frac{2J'+1}{2}\int_{-1}^{1}\mathrm{d}z_t(1-z_t^2)d_{20}^{J}(z_t)\frac{d_{11}^{J'}(z_s')}{1+z_s'}\left[\frac{1}{s'-s}+\frac{1}{s'-u}-\frac{1}{s'-a}\right] ,$$

$$\tilde{K}_{JJ'}^{--}(t,t') = \frac{t(t-t_\pi)}{t'(t'-t_\pi)(t'-t)}\frac{2J'+1}{2}\int_{-1}^{1}\mathrm{d}z_t(1-z_t^2)d_{20}^{J}(z_t)\frac{d_{20}^{J'}(z_t')}{1-z_t'^2} \,.$$

Explicit expressions for $J, J' \leq 2$ are provided in Appendix B.2.

4.3.5 Threshold and asymptotic behavior of the kernel functions

In order to check our kernel functions and determine the convergence properties of the dispersive integrals, we study the behavior of the kernels at threshold and for $s', t' \to \infty$.

Based on (4.26), one can show that for $t \to 0$

$$\begin{aligned}\hat{H}_{++}(t,M_\pi^2) &= \hat{h}_{0,+}(t) - \frac{5}{2}\hat{h}_{2,+}(t) + \mathcal{O}(t^3) \,,\\ \hat{H}_{+-}(t,M_\pi^2) &= -\frac{5\sqrt{6}\,M_\pi^2}{t-t_\pi}\hat{h}_{2,-}(t) + \mathcal{O}(t^2) \,,\end{aligned} \tag{4.37}$$

where the hat indicates the subtraction of the Born terms. By comparing to (4.20) and (B.12), (4.37) implies that

$$\begin{aligned}
&\tilde{G}_{JJ'}^{+\pm}\big|^{\text{1-sub}}(t,s') = \mathcal{O}(t^2) \,, && \tilde{K}_{JJ'}^{+\pm}\big|^{\text{1-sub}}(t,t') = \mathcal{O}(t^2) \,,\\
&\tilde{G}_{0J'}^{+\pm}\big|^{\text{2-sub}}(t,s') - \frac{5}{2}\tilde{G}_{2J'}^{+\pm}\big|^{\text{2-sub}}(t,s') = \mathcal{O}(t^3) \,, && \tilde{K}_{0J'}^{+\pm}\big|^{\text{2-sub}}(t,t') - \frac{5}{2}\tilde{K}_{2J'}^{+\pm}\big|^{\text{2-sub}}(t,t') = \mathcal{O}(t^3) \,,\\
&\tilde{G}_{2J'}^{-+}\big|^{\text{1-sub}}(t,s') = \mathcal{O}(t^2) \,, && \tilde{K}_{2J'}^{--}\big|^{\text{1-sub}}(t,t') = \mathcal{O}(t^2) \,,\\
&\tilde{G}_{2J'}^{-+}\big|^{\text{2-sub}}(t,s') = \mathcal{O}(t^2) \,, && \tilde{K}_{2J'}^{--}\big|^{\text{2-sub}}(t,t') = \mathcal{O}(t^2) \,,
\end{aligned} \tag{4.38}$$

# subtractions	0	1	2
$K_{11}^{-+}(s,s'), K_{12}^{-+}(s,s')$	$\mathcal{O}(s'^{-2})$	$\mathcal{O}(s'^{-3})$	$\mathcal{O}(s'^{-4})$
$K_{21}^{-+}(s,s'), K_{22}^{-+}(s,s')$	$\mathcal{O}(s'^{-4})$	$\mathcal{O}(s'^{-3})$	$\mathcal{O}(s'^{-4})$
$K_{11}^{--}(s,s'), K_{12}^{--}(s,s')$	$\mathcal{O}(s'^{-2})$	$\mathcal{O}(s'^{-3})$	$\mathcal{O}(s'^{-4})$
$K_{21}^{--}(s,s'), K_{22}^{--}(s,s')$	$\mathcal{O}(s'^{-3})$	$\mathcal{O}(s'^{-3})$	$\mathcal{O}(s'^{-4})$
$G_{10}^{-+}(s,t'), G_{12}^{-+}(s,t')$	$\mathcal{O}(t'^{-2})$	$\mathcal{O}(t'^{-3})$	$\mathcal{O}(t'^{-4})$
$G_{20}^{-+}(s,t'), G_{22}^{-+}(s,t')$	$\mathcal{O}(t'^{-3})$	$\mathcal{O}(t'^{-3})$	$\mathcal{O}(t'^{-4})$
$G_{12}^{--}(s,t')$	$\mathcal{O}(t'^{-2})$	$\mathcal{O}(t'^{-3})$	$\mathcal{O}(t'^{-4})$
$G_{22}^{--}(s,t')$		$\mathcal{O}(t'^{-3})$	$\mathcal{O}(t'^{-4})$
$\tilde{G}_{01}^{+\pm}(t,s'), \tilde{G}_{02}^{+\pm}(t,s')$	$\mathcal{O}(s'^{-2})$	$\mathcal{O}(s'^{-3})$	$\mathcal{O}(s'^{-4})$
$\tilde{G}_{21}^{+\pm}(t,s'), \tilde{G}_{22}^{+\pm}(t,s')$	$\mathcal{O}(s'^{-4})$	$\mathcal{O}(s'^{-4})$	$\mathcal{O}(s'^{-4})$
$\tilde{K}_{00}^{++}(t,t'), \tilde{K}_{02}^{++}(t,t')$	$\mathcal{O}(t'^{-2})$	$\mathcal{O}(t'^{-3})$	$\mathcal{O}(t'^{-4})$
$\tilde{K}_{22}^{++}(t,t')$	$\mathcal{O}(t'^{-4})$	$\mathcal{O}(t'^{-4})$	$\mathcal{O}(t'^{-4})$
$\tilde{K}_{02}^{+-}(t,t')$	$\mathcal{O}(t'^{-2})$	$\mathcal{O}(t'^{-3})$	$\mathcal{O}(t'^{-4})$

Table 4.2: Asymptotics of the kernel functions in the equations for $f_{J,-}(s)$ and $h_{J,+}(t)$.

with the number of subtractions as indicated in the superscript. We have checked that the explicit expressions in Appendix B.2 fulfill these relations.

Furthermore, is clear from (4.34) and (4.36) that the dependence of the kernel functions on s and t must reproduce the correct threshold behavior of the partial-wave amplitudes

$$\begin{aligned} f_{J,+}(s) &= \mathcal{O}(\mathbf{q}^{2J}) , & f_{J,-}(s) &= \mathcal{O}(\mathbf{q}^{2J}) , \\ \hat{h}_{J,+}(t) &= \mathcal{O}(q_t^2 (q_t p_t)^J) , & \hat{h}_{J,-}(t) &= \mathcal{O}((q_t p_t)^J) . \end{aligned} \tag{4.39}$$

The additional factor of q_t^2 in $\hat{h}_{J,+}(t)$ is a manifestation of Low's theorem for low-energy QED [200], which requires the full scattering amplitude to be equal to the Born terms at the threshold for Compton scattering. We have checked explicitly that the expressions provided in Appendices B.1 and B.2 indeed fulfill

$$\begin{aligned} K_{JJ'}^{++}(s,s') &= \mathcal{O}(\mathbf{q}^{2J}) , & G_{JJ'}^{+-}(s,t') &= \mathcal{O}(\mathbf{q}^{2J}) , \\ K_{JJ'}^{-\pm}(s,s') &= \mathcal{O}(\mathbf{q}^{2J}) , & G_{JJ'}^{-\pm}(s,t') &= \mathcal{O}(\mathbf{q}^{2J}) , \\ \tilde{G}_{JJ'}^{+\pm}(t,s') &= \mathcal{O}(q_t^2 (q_t p_t)^J) , & \tilde{K}_{JJ'}^{+\pm}(t,t') &= \mathcal{O}(q_t^2 (q_t p_t)^J) , \\ \tilde{G}_{JJ'}^{-+}(t,s') &= \mathcal{O}((q_t p_t)^J) , & \tilde{K}_{JJ'}^{--}(t,t') &= \mathcal{O}((q_t p_t)^J) . \end{aligned} \tag{4.40}$$

Similarly, the asymptotic behavior of the kernel functions for $s' \to \infty$ and $t' \to \infty$, respectively, determines the convergence properties of the dispersion integrals. In particular, one can directly read off which rate of convergence can be achieved when working with a certain number of subtractions. The corresponding behavior of the kernels for large values of the respective integration variable is summarized in Tables 4.1 and 4.2. Although in some cases the leading power vanishes, one can see that in general the kernels for $f_{J,-}(s)$ and $h_{J,+}(t)$ drop

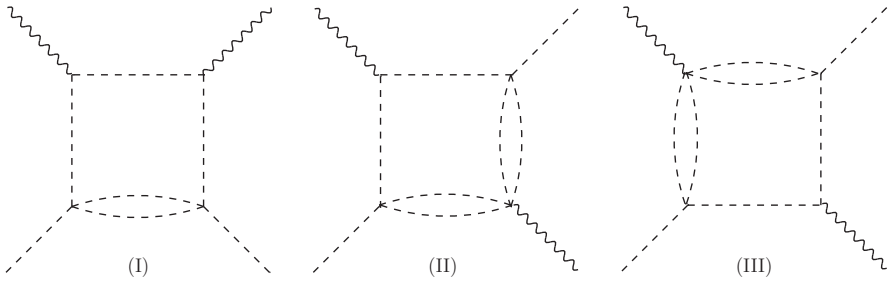

Figure 4.2: Box graphs constraining the boundaries of the double-spectral functions. Dashed/wiggly lines denote pions/photons.

as the second, third, and fourth power in the integration variable, while the integrals related to $f_{J,+}(s)$ and $h_{J,-}(t)$ will converge one order faster.

4.4 Domain of validity

In this section, we derive the limits on the domain of validity of the system of RS equations constructed in Sect. 4.3 that follow from the assumption of Mandelstam analyticity [40]. For more details of the derivation we refer to similar work on πK and πN scattering [68,67,73,152].

If we neglect the possibility of photons in intermediate states, the box diagrams that determine the boundaries of the double-spectral functions[5] involve one- and two-pion states, cf. Fig. 4.2. Diagram (I) represents the mechanism that produces the boundary of the support of ρ_{st}, while (II) and (III) are relevant for ρ_{su}. From (I) we find that

$$b_{\rm I}(s,t) = t(s-9M_\pi^2) - 4M_\pi^2(s-M_\pi^2) = 0 \tag{4.41}$$

defines the st boundary of support as well as, with $s \leftrightarrow u$, the tu boundary. Likewise,

$$b_{\rm II}(s,t) = b_{\rm III}(s,t) = su + M_\pi^2(9t-M_\pi^2) = 0 \tag{4.42}$$

gives the boundary of ρ_{su}. In particular, the boundary of ρ_{st} may be described by

$$t = T_{st}(s) = T_{\rm I}(s)\ , \tag{4.43}$$

where $t = T_{\rm I}(s)$ follows from solving $b_{\rm I}(s,t) = 0$ for t, and similarly for ρ_{tu} and ρ_{su}.

These domains of support restrict the range of validity of the RS equations in two ways:

1) The partial-wave expansion of the imaginary parts in the dispersion integrals converges only for scattering angles z that lie within the large Lehmann ellipse [45,42]. This ellipse can be constructed as the largest ellipse in the complex z-plane which does not reach into the double-spectral regions. Given a value of a, this constraint can be translated into an allowed range for the parameter b, since (4.31) relates b to the angle z.

2) A specific value of b is only allowed if the hyperbola $(s-a)(u-a) = b$ does not enter the double-spectral regions.

[5]The double-spectral functions ρ_{su}, ρ_{tu}, and ρ_{st} are defined as given in (1.32).

The allowed values of b (for a given a) must respect both constraints in the integrals for both the $\gamma\pi \to \gamma\pi$ and $\gamma\gamma \to \pi\pi$ amplitudes. Once the constraints on the allowed values of b are derived, limits of the domain of validity of the full RS system follow from the partial-wave projection of the dispersion relations. For example, in the s-channel we need $-1 \leq z_s \leq 1$, so that the maximally allowed $s_{\rm max}$ is the largest value of s for which both

$$(s-a)(2M_\pi^2 - s - a) \tag{4.44}$$

and

$$(s-a)\left(2M_\pi^2 - s - a + \frac{(s-M_\pi^2)^2}{s}\right) \tag{4.45}$$

lie within the allowed range for b. In a similar fashion the requirement that $0 \leq z_t^2 \leq 1$ determines $t_{\rm max}$ in the t-channel projection.

We begin with the Lehmann-ellipse constraint in the s-channel. The partial-wave expansion converges in an ellipse with foci at $z_s' = \pm 1$

$$\frac{(\mathrm{Re}\, z_s')^2}{A_s^2} + \frac{(\mathrm{Im}\, z_s')^2}{B_s^2} = 1 \,, \tag{4.46}$$

so that the semimajor and semiminor axis A_s and B_s are related by

$$A_s^2 - B_s^2 = 1 \,. \tag{4.47}$$

The maximal value of z_s' that does not enter the region where $\rho_{st} \neq 0$ is given by

$$z_{s'}^{\rm max} = 1 + \frac{2s' T_{st}(s')}{(s'-M_\pi^2)^2} \,, \tag{4.48}$$

cf. (1.42), which results in

$$-z_{s'}^{\rm max} \leq z_s' \leq z_{s'}^{\rm max} \tag{4.49}$$

for the Lehmann-ellipse constraint of the st boundary. Translating this into a restriction on t', we find

$$\begin{aligned} &T_{st}'(s') \leq t' \leq T_{st}(s') \,, \\ &T_{st}'(s') = -\frac{(s'-M_\pi^2)^2}{s'} - T_{st}(s') \,, \qquad \forall\, s' \in \left[M_\pi^2, \infty\right) \,, \end{aligned} \tag{4.50}$$

in the s-channel integral of the dispersion relations. As (4.31) defines a linear relation between b and t', (4.50) translates into a condition on b

$$b_s^-(s',a) \leq b \leq b_s^+(s',a) \,, \tag{4.51}$$

where

$$\begin{aligned} b_s^+(s',a) &= (s'-a)(2M_\pi^2 - s' - T_{st}'(s') - a) \,, \\ b_s^-(s',a) &= (s'-a)(2M_\pi^2 - s' - T_{st}(s') - a) \,. \end{aligned} \tag{4.52}$$

We may then define

$$b_s^+(a) = \min_{s' \in [M_\pi^2, \infty)} b_s^+(s',a) \,, \qquad b_s^-(a) = \max_{s' \in [M_\pi^2, \infty)} b_s^-(s',a) \tag{4.53}$$

as the minimum/maximum of $b_s^{\pm}(s',a)$ within the domain of integration. Similar restrictions are provided by ρ_{tu} and ρ_{su}, and the intersection of the resulting constraints on b defines the limitations imposed by condition 1) due to the s-channel part of the dispersion relation.

The same argument in the case of the t-channel reaction is slightly more involved, since in this case the relation between the CMS angle z_t' and b is not linear

$$z_t'^2 = \frac{(t' - 2M_\pi^2 + 2a)^2 - 4b}{16 q_t'^2 p_t'^2} \,. \tag{4.54}$$

Consequently, we need to consider the Lehmann ellipse for $z_t'^2$

$$\frac{\left(\mathrm{Re}\, z_t'^2 - \frac{1}{2}\right)^2}{\tilde{A}_t^2} + \frac{\left(\mathrm{Im}\, z_t'^2\right)^2}{\tilde{B}_t^2} = 1 \,, \tag{4.55}$$

where the parameters are related to those of the ellipse for z_t' by

$$\tilde{A}_t = A_t^2 - \frac{1}{2} \,, \qquad \tilde{B}_t = A_t B_t \,. \tag{4.56}$$

Rewriting (4.41) in terms of ν and t and inserting the result in (4.14), we obtain the boundary of the double-spectral region in terms of z_t'

$$z_{t'}^{\max} = \frac{N(t')}{4 q_t' p_t'} \,, \qquad N(t') = \frac{t'(t' + 12M_\pi^2)}{t' - t_\pi} \,, \tag{4.57}$$

so that ρ_{st} imposes the restriction

$$b_t^-(t',a) \le b \le b_t^+(t',a) \,, \qquad \forall\, t' \in \left[t_\pi, \infty\right) \,, \tag{4.58}$$

with

$$\begin{aligned} b_t^-(t',a) &= \frac{1}{4}(t' - 2M_\pi^2 + 2a)^2 - \frac{1}{4}N(t')^2 \,, \\ b_t^+(t',a) &= \frac{1}{4}(t' - 2M_\pi^2 + 2a)^2 + \frac{1}{4}N(t')^2 - 4 q_t'^2 p_t'^2 \,, \end{aligned} \tag{4.59}$$

and similarly for ρ_{tu} and ρ_{su}. Together with

$$b_t^+(a) = \min_{t' \in [t_\pi, \infty)} b_t^+(t',a) \,, \qquad b_t^-(a) = \max_{t' \in [t_\pi, \infty)} b_t^-(t',a) \,, \tag{4.60}$$

the constraints

$$b_s^-(a) \le b \le b_s^+(a) \,, \qquad b_t^-(a) \le b \le b_t^+(a) \tag{4.61}$$

then provide, for a given a, the range of allowed values for b that satisfies the Lehmann-ellipse constraint for both the s-channel and t-channel integrals. If the associated hyperbolae in the external variables s and u do not cross the double-spectral regions either, as required by condition 2), then this determines the kinematic regime in which the partial-wave projection is valid.

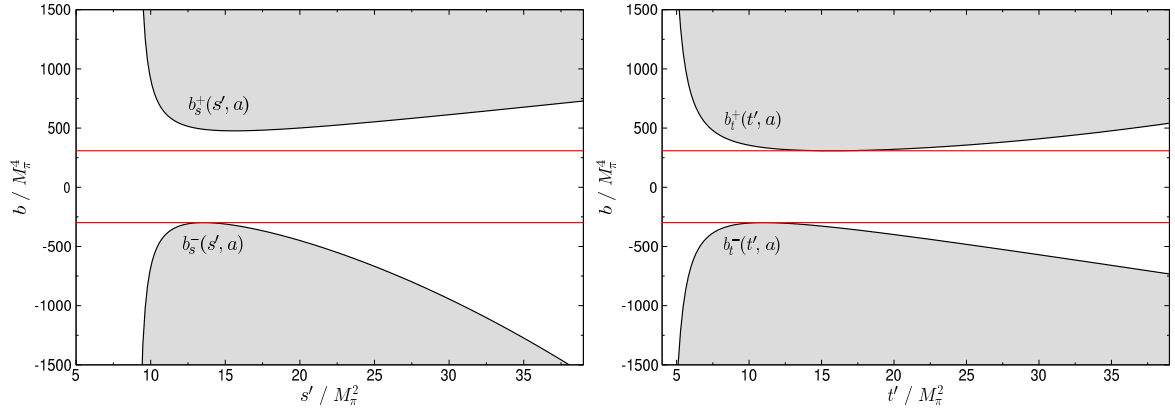

Figure 4.3: Allowed range of b for $a = -9.8M_\pi^2$ in the s-channel projection due to s-channel (left) and t-channel (right) constraints. The red lines correspond to $b_t^+(a) = 308.4M_\pi^4$ and $b_t^-(a) = -298.1M_\pi^4$, respectively.

4.4.1 *s*-channel projection

As a first step, we consider the restrictions due to ρ_{st} in the s-channel part only. The strategy to find the optimal value of a proceeds as follows: the Lehmann-ellipse constraint imposes the condition that all allowed values of b must fulfill $b_s^-(a) \leq b \leq b_s^+(a)$. As t varies only within

$$-\frac{(s-M_\pi^2)^2}{s} \leq t \leq 0 \,, \tag{4.62}$$

this limits the range of values of b that are needed for a given s. The maximal value of s possible, $s_{\max}$, can be determined by the condition that the smallest b coincide with $b_s^-(a)$, and the largest b with $b_s^+(a)$, i.e. $s_{\max}$ will be given as the value of s that ensures that the solutions of

$$\begin{aligned} (s-a)(2M_\pi^2 - s - a) &= b_s^-(a) \,, \\ (s-a)\left(2M_\pi^2 - s - a + \frac{(s-M_\pi^2)^2}{s}\right) &= b_s^+(a) \end{aligned} \tag{4.63}$$

coincide. This procedure results in

$$\begin{aligned} a = -41.3M_\pi^2 \,, \qquad & s_{\max} = 27.8M_\pi^2 \,, \\ b_s^+(a) = 2852M_\pi^4 \,, \qquad & b_s^-(a) = 1071M_\pi^4 \,. \end{aligned} \tag{4.64}$$

ρ_{su} and ρ_{tu} do not yield additional constraints.

The investigation of the t-channel contribution proceeds along the same lines: demanding that the solutions of the two equations

$$\begin{aligned} (s-a)(2M_\pi^2 - s - a) &= b_t^-(a) \,, \\ (s-a)\left(2M_\pi^2 - s - a + \frac{(s-M_\pi^2)^2}{s}\right) &= b_t^+(a) \end{aligned} \tag{4.65}$$

coincide, we find

$$\begin{aligned} a = -9.8M_\pi^2 \,, \qquad & s_{\max} = 21.4M_\pi^2 \,, \\ b_t^+(a) = 308.4M_\pi^4 \,, \qquad & b_t^-(a) = -298.1M_\pi^4 \,. \end{aligned} \tag{4.66}$$

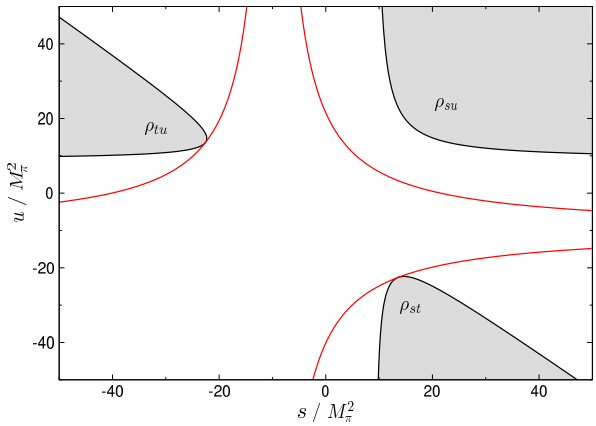

Figure 4.4: Double-spectral regions and hyperbolae for $a = -9.8M_\pi^2$, $b_t^+(a) = 308.4M_\pi^4$, and $b_t^-(a) = -298.1M_\pi^4$.

Thus, the s-channel constraint (4.64) is weaker than the t-channel restriction (4.66), as can be deduced from Fig. 4.3, where the situation for $a = -9.8M_\pi^2$ is displayed: both b_t^+ and b_t^- also lie within the allowed region for the s-channel. Since the hyperbolae resulting from (4.66) do not enter the double-spectral regions either (see Fig. 4.4), (4.66) constitutes the final answer for the range of validity of the s-channel projection.

4.4.2 *t*-channel projection

As we may start from a different set of HDRs to project onto the t-channel partial waves (4.36), it is not mandatory to use the same value of a as in the s-channel, so that the domain of validity can be separately optimized. To perform the t-channel projection we need to consider

$$0 \leq z_t^2 = \frac{(t - 2M_\pi^2 + 2a)^2 - 4b}{16 q_t^2 p_t^2} \leq 1 \,. \tag{4.67}$$

Similarly to the s-channel case, the optimal choice of a is determined in such a way that the solutions for t with $z_t^2 = 0$ and $z_t^2 = 1$ coincide, which yields

$$\begin{aligned} a &= -7.5M_\pi^2 \,, \qquad -17.4M_\pi^2 \leq t \leq 51.6M_\pi^2 = 1\,\mathrm{GeV}^2 \,, \\ b_t^+(a) &= 298.4M_\pi^4 \,, \qquad b_t^-(a) = -316.8M_\pi^4 \,. \end{aligned} \tag{4.68}$$

Again, the most stringent restriction originates from the t-channel Lehmann ellipse, which provides a stronger constraint than that involving $b_s^+(a)$ and $b_s^-(a)$. We will use the value $a = -7.5M_\pi^2$ in the following.

As we eventually aim to investigate the properties of the σ, we also need to consider the domain of convergence in the complex plane. We will restrict our analysis to the value of the hyperbola parameter $a = -7.5M_\pi^2$. Then, the constraints from both s-channel and t-channel Lehmann ellipses yield ellipses of allowed values for b in the complex b-plane. As the ellipse for the s-channel contains the ellipse for the t-channel, it suffices to consider the latter. The resulting permitted region of the complex t-plane is depicted in Fig. 4.5. It safely encompasses the position of the σ pole, and marginally that of the $f_0(980)$.

The result that the equations for the t-channel are rigorously valid up to $t_{\mathrm{max}} = 1\,\mathrm{GeV}^2$ seems to shed doubt on recent dispersive fits [188] to high-statistics $\gamma\gamma \to \pi\pi$ data [173,174] in

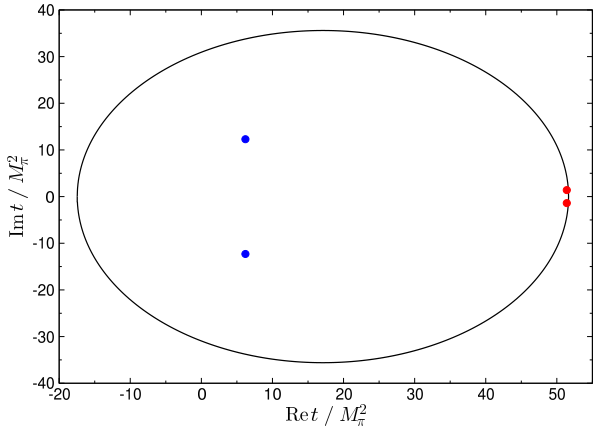

Figure 4.5: Domain of validity in the complex t-plane for $a = -7.5\ M_\pi^2$. The blue dots refer to the position of the σ pole at $t = (6.2 \pm i12.3)M_\pi^2$ and the red dots to that of the f_0 at $t = (51.4 \pm i1.4)M_\pi^2$ [65].

the energy region up to 1.28 GeV, where a lot of effort was put into building a good description of $\bar{K}K$ dynamics above 1 GeV. However, one possible way to obtain a higher upper limit on the range of validity of the RS equations would be to relax the assumptions about the boundaries of the double-spectral functions: if one assumed that the spectral strength of the 2π intermediate states depicted in Fig. 4.2 only set in at an effective mass larger than $2M_\pi$, the domain of validity would be extended accordingly. For instance, a threshold of $m_{\text{eff}} = 3M_\pi$ would produce $t_{\max} = 82.8M_\pi^2 = (1.27\,\text{GeV})^2$ at $a = -12.0M_\pi^2$. In any case, the validity of a system of PWHDRs above 1 GeV entails analyticity assumptions that go beyond Mandelstam analyticity.

Chapter 5

Two-photon coupling of the σ resonance

5.1 Muskhelishvili–Omnès problem for $\gamma\gamma \to \pi\pi$

We now turn to the resolution of the equations for $\gamma\gamma \to \pi\pi$. We truncate the system at $J = 2$ both for s- and t-channel contributions (the generalization to higher partial waves is straightforward). In this approximation, the equations can be brought into the form

$$\begin{aligned}
h_{0,+}(t) &= \Delta_{0,+}\big|^{n\text{-sub}}(t) + \frac{t^{1+n}}{\pi}\int\limits_{t_\pi}^{\infty} \mathrm{d}t' \frac{\mathrm{Im}\, h_{0,+}(t')}{t'^{1+n}(t'-t)}\,, \\
h_{2,+}(t) &= \Delta_{2,+}(t) + \frac{t^2(t-t_\pi)}{\pi}\int\limits_{t_\pi}^{\infty} \mathrm{d}t' \frac{\mathrm{Im}\, h_{2,+}(t')}{t'^{2}(t'-t_\pi)(t'-t)}\,, \\
h_{2,-}(t) &= \Delta_{2,-}\big|^{n\text{-sub}}(t) + \frac{t^{1+n}(t-t_\pi)}{\pi}\int\limits_{t_\pi}^{\infty} \mathrm{d}t' \frac{\mathrm{Im}\, h_{2,-}(t')}{t'^{1+n}(t'-t_\pi)(t'-t)}\,,
\end{aligned} \tag{5.1}$$

where $n \in \{0,1,2\}$ indicates the number of subtractions, and $\Delta_{J,\pm}(t)$, also referred to as MO inhomogeneity in the following, includes the Born terms, subtraction constants, and integrals involving the imaginary parts of the other partial waves

$$\begin{aligned}
\Delta_{0,+}\big|^{n\text{-sub}}(t) &= \frac{1}{\pi}\int\limits_{M_\pi^2}^{\infty} \mathrm{d}s' \sum_{J'=1,2} \Big(\tilde{G}^{++}_{0J'}\big|^{n\text{-sub}}(t,s')\mathrm{Im}\, f_{J',+}(s') + \tilde{G}^{+-}_{0J'}\big|^{n\text{-sub}}(t,s')\mathrm{Im}\, f_{J',-}(s')\Big) \\
&\quad + \tilde{N}_0^+\big|^{n\text{-sub}}(t) + \frac{1}{\pi}\int\limits_{t_\pi}^{\infty} \mathrm{d}t' \Big(\tilde{K}^{++}_{02}\big|^{n\text{-sub}}(t,t')\mathrm{Im}\, h_{2,+}(t') + \tilde{K}^{+-}_{02}\big|^{n\text{-sub}}(t,t')\mathrm{Im}\, h_{2,-}(t')\Big)\,, \\
\Delta_{2,+}(t) &= \tilde{N}_2^+(t) + \frac{1}{\pi}\int\limits_{M_\pi^2}^{\infty} \mathrm{d}s' \sum_{J'=1,2} \Big(\tilde{G}^{++}_{2J'}(t,s')\mathrm{Im}\, f_{J',+}(s') + \tilde{G}^{+-}_{2J'}(t,s')\mathrm{Im}\, f_{J',-}(s')\Big)\,, \\
\Delta_{2,-}\big|^{n\text{-sub}}(t) &= \tilde{N}_2^-\big|^{n\text{-sub}}(t) + \frac{1}{\pi}\int\limits_{M_\pi^2}^{\infty} \mathrm{d}s' \sum_{J'=1,2} \tilde{G}^{-+}_{2J'}\big|^{n\text{-sub}}(t,s')\mathrm{Im}\, f_{J',+}(s')\,.
\end{aligned} \tag{5.2}$$

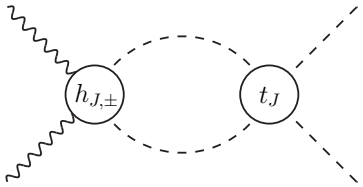

Figure 5.1: Elastic unitarity for $\gamma\gamma \to \pi\pi$. Dashed/wiggly lines denote pions/photons.

Several comments are in order: first, the equation for $h_{2,+}(t)$ is not affected by subtractions. Second, the equations for the D-waves decouple, as the corresponding kernel functions relating them to the S-wave or to each other vanish. Conversely, the S-wave does not decouple from the D-waves: both D-waves are needed as input to solve for $h_{0,+}(t)$. The consequence of these observations for the numerical evaluation is obvious: we first solve the equations for the D-waves separately, and then use these solutions as input for $\Delta_{0,+}\big|^{n\text{-sub}}(t)$.

Assuming elastic unitarity (cf. Fig. 5.1),

$$\operatorname{Im} h_{J,\pm}(t) = \sigma(t)\big(t_J(t)\big)^* h_{J,\pm}(t) \,, \tag{5.3}$$

with $\pi\pi$ partial waves $t_J(t)$ in the normalization (1.37), the phase of $h_{J,\pm}(t)$ coincides with the $\pi\pi$ phase $\delta_J(t)$ ("Watson's theorem" [201]), and (5.1) takes the form of a Muskhelishvili–Omnès problem [70, 71], whose resolution we will review in the following section.

5.1.1 Muskhelishvili–Omnès problem with finite matching point

As argued in Sect. 4.4, the domain of validity of (5.1) is restricted to the energy range below 1 GeV. We will follow here the strategy of [53,67], namely to assume that the imaginary parts of the amplitudes are known above a matching point t_m, and solve the equations in the regime between threshold and t_m. The input that we will use both for the s-channel contributions and the high-energy regime above t_m will be discussed in detail in Sect. 5.3.

In this finite-matching-point setup, the solution in terms of Omnès functions reads

$$\begin{aligned}
h_{0,+}(t) &= \Delta_{0,+}\big|^{n\text{-sub}}(t) + \frac{t^{1+n}\Omega_0(t)}{\pi} \\
&\quad\times\left\{\int_{t_\pi}^{t_\mathrm{m}} \mathrm{d}t' \frac{\sin\delta_0(t')\Delta_{0,+}\big|^{n\text{-sub}}(t')}{t'^{1+n}(t'-t)|\Omega_0(t')|} + \int_{t_\mathrm{m}}^{\infty} \mathrm{d}t' \frac{\operatorname{Im} h_{0,+}(t')}{t'^{1+n}(t'-t)|\Omega_0(t')|}\right\}, \\
h_{2,+}(t) &= \Delta_{2,+}(t) + \frac{t^2(t-t_\pi)\Omega_2(t)}{\pi} \\
&\quad\times\left\{\int_{t_\pi}^{t_\mathrm{m}} \mathrm{d}t' \frac{\sin\delta_2(t')\Delta_{2,+}(t')}{t'^{2}(t'-t_\pi)(t'-t)|\Omega_2(t')|} + \int_{t_\mathrm{m}}^{\infty} \mathrm{d}t' \frac{\operatorname{Im} h_{2,+}(t')}{t'^{2}(t'-t_\pi)(t'-t)|\Omega_2(t')|}\right\}, \\
h_{2,-}(t) &= \Delta_{2,-}\big|^{n\text{-sub}}(t) + \frac{t^{1+n}(t-t_\pi)\Omega_2(t)}{\pi} \\
&\quad\times\left\{\int_{t_\pi}^{t_\mathrm{m}} \mathrm{d}t' \frac{\sin\delta_2(t')\Delta_{2,-}\big|^{n\text{-sub}}(t')}{t'^{1+n}(t'-t_\pi)(t'-t)|\Omega_2(t')|} + \int_{t_\mathrm{m}}^{\infty} \mathrm{d}t' \frac{\operatorname{Im} h_{2,-}(t')}{t'^{1+n}(t'-t_\pi)(t'-t)|\Omega_2(t')|}\right\},
\end{aligned} \tag{5.4}$$

where

$$\Omega_J(t) = \exp\left\{\frac{t}{\pi}\int\limits_{t_\pi}^{t_\mathrm{m}} \mathrm{d}t' \frac{\delta_J(t')}{t'(t'-t)}\right\}. \tag{5.5}$$

Defining the physical amplitude by the limit $t \to t + i\epsilon$, (5.4) can be rewritten as

$$\begin{aligned}|h_{0,+}(t)| = \Delta_{0,+}\big|^{n\text{-sub}}(t)\cos\delta_0(t) + \frac{t^{1+n}|\Omega_0(t)|}{\pi} \\ \times\left\{\int\limits_{t_\pi}^{t_\mathrm{m}} \mathrm{d}t' \frac{\sin\delta_0(t')\Delta_{0,+}\big|^{n\text{-sub}}(t')}{t'^{1+n}(t'-t)|\Omega_0(t')|} + \int\limits_{t_\mathrm{m}}^{\infty} \mathrm{d}t' \frac{\mathrm{Im}\, h_{0,+}(t')}{t'^{1+n}(t'-t)|\Omega_0(t')|}\right\},\end{aligned} \tag{5.6}$$

where the dash denotes the principal value of the integral, and similarly for the D-waves. There are several subtleties related to the behavior of $|\Omega_J(t)|$ for $t \to t_\mathrm{m}$ [67]

$$|\Omega_J(t)| \sim |t_\mathrm{m} - t|^{\frac{\delta_J(t_\mathrm{m})}{\pi}}, \tag{5.7}$$

in particular the integrals in (5.6) diverge for $\delta_J(t_\mathrm{m}) > \pi$. In such a case, there are non-trivial homogeneous solutions whose coefficients can be used to absorb these divergences, but, of course, the presence of such solutions introduces undetermined constants in the result for $h_{J,\pm}(t)$. For instance, the solution for $h_{0,+}(t)$ for $\pi < \delta_0(t_\mathrm{m}) < 2\pi$ involves one free parameter α,

$$\begin{aligned}|h_{0,+}(t)| = \Delta_{0,+}\big|^{n\text{-sub}}(t)\cos\delta_0(t) + \frac{t^{1+n}|\Omega_0(t)|}{(t_\mathrm{m}-t)\pi} \\ \times\left\{\alpha + t\int\limits_{t_\pi}^{t_\mathrm{m}} \mathrm{d}t' \frac{(t_\mathrm{m}-t')\sin\delta_0(t')\Delta_{0,+}\big|^{n\text{-sub}}(t')}{t'^{2+n}(t'-t)|\Omega_0(t')|} + t\int\limits_{t_\mathrm{m}}^{\infty} \mathrm{d}t' \frac{(t_\mathrm{m}-t')\mathrm{Im}\, h_{0,+}(t')}{t'^{2+n}(t'-t)|\Omega_0(t')|}\right\}.\end{aligned} \tag{5.8}$$

α can be fixed if one assumes, in addition, knowledge of the derivative of $h_{0,+}(t)$ at t_m. Conversely, the fact that the phases of the $I = 2$ partial waves are negative induces different complications, which we will address in Sect. 5.1.2.

The part of the integrals in (5.4) involving the pion polarizabilities can be explicitly performed based on the spectral representation of the Omnès functions

$$\begin{aligned}\Omega_J^{-1}(t) &= -\frac{1}{\pi}\int\limits_{t_\pi}^{t_\mathrm{m}} \mathrm{d}t' \frac{\sin\delta_J(t')}{(t'-t)|\Omega_J(t')|}, \qquad \Omega_J^{-1}(t) = 1 - \frac{t}{\pi}\int\limits_{t_\pi}^{t_\mathrm{m}} \mathrm{d}t' \frac{\sin\delta_J(t')}{t'(t'-t)|\Omega_J(t')|}, \\ \Omega_J^{-1}(t) &= 1 - t\,\dot{\Omega}_J(0) - \frac{t^2}{\pi}\int\limits_{t_\pi}^{t_\mathrm{m}} \mathrm{d}t' \frac{\sin\delta_J(t')}{t'^2(t'-t)|\Omega_J(t')|},\end{aligned} \tag{5.9}$$

where the dot denotes the derivative with respect to t. The results of this modification, which, in particular, only involve integrals over

$$\tilde{\Delta}_{J,\pm}(t) = \Delta_{J,\pm}(t) - \Delta\tilde{N}_J^{\pm}(t), \tag{5.10}$$

are summarized in Appendix B.3.1 (with $\Delta\tilde{N}_J^{\pm}(t)$ defined in Appendix B.2).[1]

[1] In this procedure, e.g. the constant terms proportional to $(M_\pi^2 - a)^{-1}$ in the unsubtracted version of the

5.1.2 Sum rules for $I = 2$

If $\delta_0(t_\mathrm{m}) < 0$, $\Omega_0(t)$ diverges at t_m, so that (5.4) breaks down. However, we may rewrite the solution as

$$h_{0,+}(t) = \Delta_{0,+}\big|^{n\text{-sub}}(t) + \tilde{\alpha}^{(n)}\left(\frac{t}{t_\mathrm{m}}\right)^{1+n}\Omega_0(t) + \frac{t^{1+n}\Omega_0(t)(t_\mathrm{m}-t)}{\pi} \times\left\{\int\limits_{t_\pi}^{t_\mathrm{m}}\mathrm{d}t'\frac{\sin\delta_0(t')\Delta_{0,+}\big|^{n\text{-sub}}(t')}{t'^{1+n}(t_\mathrm{m}-t')(t'-t)|\Omega_0(t')|} + \int\limits_{t_\mathrm{m}}^{\infty}\mathrm{d}t'\frac{\mathrm{Im}\,h_{0,+}(t')}{t'^{1+n}(t_\mathrm{m}-t')(t'-t)|\Omega_0(t')|}\right\}, \quad (5.11)$$

where

$$\tilde{\alpha}^{(n)} = \frac{t_\mathrm{m}^{1+n}}{\pi}\int\limits_{t_\pi}^{t_\mathrm{m}}\mathrm{d}t'\frac{\sin\delta_0(t')\Delta_{0,+}\big|^{n\text{-sub}}(t')}{t'^{1+n}(t'-t_\mathrm{m})|\Omega_0(t')|} + \frac{t_\mathrm{m}^{1+n}}{\pi}\int\limits_{t_\mathrm{m}}^{\infty}\mathrm{d}t'\frac{\mathrm{Im}\,h_{0,+}(t')}{t'^{1+n}(t'-t_\mathrm{m})|\Omega_0(t')|}\,. \quad (5.12)$$

Demanding continuity at the matching point implies that $\tilde{\alpha}^{(n)} = 0$, since otherwise $h_{0,+}(t)$ would diverge at t_m. Indeed, multiplying the first equation of (5.4) with $\Omega_0^{-1}(t)$ and subsequently evaluating the result at $t = t_\mathrm{m}$ explicitly proves that $\tilde{\alpha}^{(n)} = 0$ must hold in order for $h_{0,+}(t_\mathrm{m})$ to be finite. The final solutions for all amplitudes as well as the explicit form of all possible sum rules which could be obtained are given in Appendix B.3.2.

One case that is of particular interest is the $I = 2$ S-waves, where the $\pi\pi$ phase shift is substantial, and negative, at the matching point. Thus, we obtain from the once- and twice-subtracted versions of the MO representation

$$\begin{aligned} 0 &= \frac{M_\pi}{2\alpha}t_\mathrm{m}(\alpha_1-\beta_1)^{I=2} + I^{(1)}\,,\\ 0 &= \frac{M_\pi}{2\alpha}t_\mathrm{m}(1-t_\mathrm{m}\,\dot{\Omega}_0(0))(\alpha_1-\beta_1)^{I=2} + \frac{M_\pi}{24\alpha}t_\mathrm{m}^2(\alpha_2-\beta_2)^{I=2} + I^{(2)}\,, \end{aligned} \quad (5.13)$$

where

$$I^{(n)} = \frac{t_\mathrm{m}^{1+n}}{\pi}\left\{\int\limits_{t_\pi}^{t_\mathrm{m}}\mathrm{d}t'\frac{\sin\delta_0(t')\tilde{\Delta}_{0,+}\big|^{n\text{-sub}}(t')}{t'^{1+n}(t'-t_\mathrm{m})|\Omega_0(t')|} + \int\limits_{t_\mathrm{m}}^{\infty}\mathrm{d}t'\frac{\mathrm{Im}\,h_{0,+}(t')}{t'^{1+n}(t'-t_\mathrm{m})|\Omega_0(t')|}\right\}, \qquad n\in\{1,2\}\,. \quad (5.14)$$

As we shall see below, the second sum rule, in particular, provides a novel constraint on $(\alpha_2-\beta_2)^{I=2}$.

5.1.3 Uniqueness and comparison to $\pi\pi$ Roy equations

The pattern in which free parameters emerge in the Omnès solutions is reminiscent of the results concerning the uniqueness properties of the solutions of $\pi\pi$ Roy equations presented

Born terms (4.30) cancel. In fact, this has to be the case, as these (unphysical) contributions do not vanish asymptotically and generate an unphysical behavior on a. Hence, the dispersive integrals for the unsubtracted case both for the MO solution (5.4) and the spectral representation of the Omnès function are strictly speaking not correct and should be supplemented by terms from the integration contour at infinity. In practice, this problem can be circumvented most easily by removing the pertinent parts of the inhomogeneities by means of (5.9), which ensures that all potential contributions from the contour at infinity vanish.

in [48–50]. There, an additional free parameter occurs each time the phase at the matching point crosses an integer multiple of $\pi/2$. Indeed, to derive this result the Roy equations are linearized, and in the one-channel approximation one finds that the difference

$$\phi(s) = \frac{\delta'(s) - \delta(s)}{\sigma(s)} \tag{5.15}$$

between two solutions $\delta(s)$ and $\delta'(s)$ for the $\pi\pi$ phase shift must fulfill [49]

$$\cos 2\delta(s)\,\phi(s) = \frac{s - 4M_\pi^2}{\pi} \int\limits_{4M_\pi^2}^{s_\mathrm{m}} \mathrm{d}s' \frac{\sin 2\delta(s')\,\phi(s')}{(s' - 4M_\pi^2)(s' - s)} \,, \tag{5.16}$$

where s_m is the matching point. In the $\pi\pi$ case the phase shift is the quantity that is to be determined, while in $\gamma\gamma \to \pi\pi$ that phase is input and the modulus of the amplitude $|h(t)|$ unknown, but the mathematical structure is the same up to a factor of 2.

As an example we consider the unsubtracted equation for the S-wave. In $\gamma\gamma \to \pi\pi$ the difference

$$\psi_{0,+}(t) = |h'_{0,+}(t)| - |h_{0,+}(t)| \tag{5.17}$$

between two solutions of (5.1) obeys

$$\cos\delta_0(t)\,\psi_{0,+}(t) = \frac{t}{\pi} \int\limits_{t_\pi}^{t_\mathrm{m}} \mathrm{d}t' \frac{\sin\delta_0(t')\,\psi_{0,+}(t')}{t'(t' - t)} \,. \tag{5.18}$$

The presence of $\sin\delta_0(t')$, rather than the $\sin 2\delta(s')$ of the $\pi\pi$ case, explains why the multiplicity of solutions in $\pi\pi$ scattering is $\lfloor 2\delta(s_\mathrm{m})/\pi \rfloor$ instead of $\lfloor \delta_0(t_\mathrm{m})/\pi \rfloor$ in $\gamma\gamma \to \pi\pi$.

In addition, there is also an analog of the sum rules discussed in Sect. 5.1.2 in $\pi\pi$ Roy equations. In the single-channel approximation $\phi(s)$ vanishes if $\delta(s_\mathrm{m}) < \pi/2$. If the effects of the coupling to other partial waves are taken into account, the phase-shift difference for a channel i with $\delta_i(s_\mathrm{m}) < \pi/2$ may be written as [50]

$$\phi_i(s) = (s - 4M_\pi^2) G_i(s) H_i(s) \,, \qquad G_i(s) = \exp\left\{ \frac{2}{\pi} \int\limits_{4M_\pi^2}^{s_\mathrm{m}} \mathrm{d}s' \frac{\delta_i(s')}{s' - s} \right\} , \tag{5.19}$$

where $H_i(s)$ includes information on other partial waves. Once again, $G_i(s_\mathrm{m})$ diverges if $\delta_i(s_\mathrm{m}) < 0$, with the result that

$$H_i(s_\mathrm{m}) = 0 \tag{5.20}$$

in this case. The difference as compared to $\gamma\gamma \to \pi\pi$ is that in $\pi\pi$ the MO representation is only available for phase-shift differences and not for the phase shifts themselves. Thus, the constraint manifests itself rather subtly by reducing the number of free parameters in the manifold of solutions. However, the mathematical input that leads to this constraint, namely continuity of the MO representation at the matching point, is the same.

5.1.4 Comparison to previous work

One key result of the derivation of RS equations for $\gamma\gamma \to \pi\pi$ is the existence of a term that couples S- and D-waves, cf. (5.2). In all previous dispersive treatments of $\gamma\gamma \to \pi\pi$ each partial wave was considered separately. Moreover, to the best of our knowledge, this is the first time that a finite-matching-point representation has been employed for $\gamma\gamma \to \pi\pi$. The practical consequences of both these developments will be discussed in Sects. 5.3 and 5.4. However, we can consider the limit $t_\mathrm{m} \to \infty$ in our equations in order to delineate the differences between our formalism and the recent works [177,185,188], which are also based on dispersive techniques.

In [177], a once-subtracted[2] dispersion relation for the S-wave is considered. The subtraction constant is fixed by assuming $h_{0,+}(t) \propto t_0(t)$ and using ChPT information on the Adler zero of the $\pi\pi$ amplitude. This representation depends quite strongly on the details of the $\pi\pi$ phase above the $\bar{K}K$ threshold already at energies $\gtrsim 0.5\,\mathrm{GeV}$. For this reason, another subtraction was performed in [185] at the energy t_1 where the $\pi\pi$ phase crosses π, the subtraction constant being fixed by the requirement that the cross section at t_1 does not become outrageously large. The Born terms as well as vector and axial-vector resonances were used to approximate the left-hand cut.

In [188], a MO representation for S- and D-waves is constructed that explicitly takes into account the $\bar{K}K$ channel, and in addition includes tensor resonances in the description of the left-hand cut. For the S-waves two subtractions are performed, while the D-waves are treated differently for the two isospin channels: for $I = 2$, no subtraction constants for $h_{2,+}$ and $h_{2,-}$ are provided (in our conventions this corresponds to the unsubtracted case for $h_{2,-}$), while for $I = 0$ an additional subtraction in both partial waves is performed. Thus, the treatment of $I = 0$ corresponds to our once-subtracted case for $h_{2,-}$. However, the RS analysis shows that the subtraction constant for $h_{2,+}$ cannot be related to dipole and quadrupole polarizabilities, as the equations for this partial wave are not affected by the corresponding subtractions. For this reason, the subtraction constants in [188] determined by fits to data (together with several chiral constraints) can be translated into pion polarizabilities, but in general not vice versa, unless even higher terms in the polarizability expansion are included. We have checked explicitly that our results agree with [188] in the limit $t_\mathrm{m} \to \infty$, once the $\bar{K}K$ channel is switched off and the additional subtraction in $h_{2,+}$ dropped.

5.2 Photon coupling of the σ resonance

We define the $\sigma\pi\pi$ coupling constant $g_{\sigma\pi\pi}$ in such a way that the full isospin $I = 0$ $\pi\pi$ scattering amplitude on the second Riemann sheet T^0_II near the position of the σ pole

$$t_\sigma = \left(M_\sigma - i\frac{\Gamma_\sigma}{2}\right)^2 \tag{5.21}$$

can be written as

$$T^0_\mathrm{II} = 32\pi \sum_{J=0}^{\infty} (2J+1) t^0_{J,\mathrm{II}}(t) P_J(z_t) = \frac{g^2_{\sigma\pi\pi}}{t_\sigma - t}\,. \tag{5.22}$$

[2]Here, we do not count powers of t' or $t' - t_\pi$ that are present for kinematical reasons alone and thus do not require any subtraction constants. This is not always the convention employed in the literature.

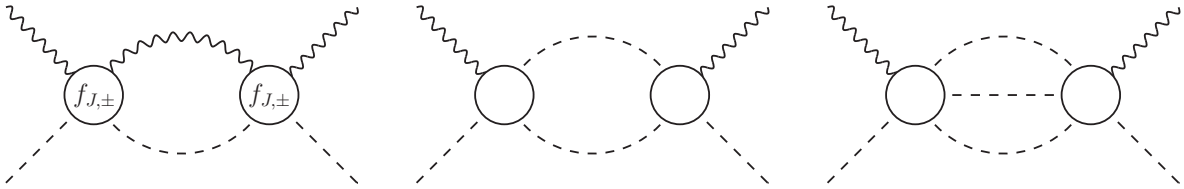

Figure 5.2: Elastic unitarity for $\gamma\pi \to \gamma\pi$ (left) and diagrams for 2- and 3-pion intermediate states.

As the σ pole occurs in the S-wave, all other partial waves only contribute to the background. Similarly, in $\gamma\gamma \to \pi\pi$ we take

$$e^2 H^0_{++,\mathrm{II}} = \frac{e^2 g_{\sigma\pi\pi} g_{\sigma\gamma\gamma}}{t_\sigma - t} \,. \tag{5.23}$$

In these conventions, the widths in the narrow-width approximation are

$$\Gamma_{\sigma\pi\pi} = \frac{|g_{\sigma\pi\pi}|^2}{32\pi M_\sigma}\sqrt{1-\frac{4M_\pi^2}{M_\sigma^2}} \,, \qquad \Gamma_{\sigma\gamma\gamma} = \frac{\pi\alpha^2 |g_{\sigma\gamma\gamma}|^2}{M_\sigma} \,. \tag{5.24}$$

Note that since the large strong width of the σ renders the applicability of these relations questionable, we use $g_{\sigma\pi\pi}$ as determined from the residue of the pole. Although the formula for $\Gamma_{\sigma\gamma\gamma}$ and $g_{\sigma\gamma\gamma}$ suffers from the same deficiency, it is conventionally employed in the literature to illustrate the relation between the two quantities. As the direct determination of $\Gamma_{\sigma\gamma\gamma}$ from the position of the pole is not possible in view of the large strong width, we follow this convention. The coupling constant itself can always be recovered by means of (5.24).

The analytic continuation of $h^0_{0,+}(t)$ into the complex plane is given by [185][3]

$$h^0_{0,+,\mathrm{II}}(t) = (1 - 2i\sigma(t) t^0_{0,\mathrm{II}}(t)) h^0_{0,+,\mathrm{I}}(t) \,, \tag{5.25}$$

and thus

$$\frac{g^2_{\sigma\gamma\gamma}}{g^2_{\sigma\pi\pi}} = -\left(\frac{\sigma(t_\sigma)}{16\pi}\right)^2 (h^0_{0,+}(t_\sigma))^2 \,, \tag{5.26}$$

where $h^0_{0,+}$ is evaluated on the first Riemann sheet. Assuming the position of the σ pole and its coupling constant to two pions to be known, we can infer $g_{\sigma\gamma\gamma}$ (and hence $\Gamma_{\sigma\gamma\gamma}$) from the value of the $I = 0$ S-wave of $\gamma\gamma \to \pi\pi$ evaluated at t_σ.

5.3 Input

To solve the RS equations for the $\gamma\gamma \to \pi\pi$ partial waves we must specify the input for $\mathrm{Im}\, f_{J,\pm}(s)$ in the whole energy range and for $\mathrm{Im}\, h_{J,\pm}(t)$ above the matching point. One could, in the spirit of the RS analysis for πK scattering [67], consider the equations for s- and t-channel partial waves simultaneously, and determine a solution of the whole system

[3] We neglect $\gamma\gamma$ intermediate states in the unitarity relation. This is the same approximation as used in [65], where the σ pole is deduced from $\pi\pi$ scattering with electromagnetic interactions switched off. Since the width corresponding to the $\gamma\gamma$ channel amounts only to a few keV, the ensuing shift of the pole is much smaller than the uncertainty of its position as quoted in [65].

	M_σ	Γ_σ	$g_{\sigma\pi\pi}/\sqrt{2}$
CCL [65]	441^{+16}_{-8} MeV	544^{+18}_{-25} MeV	$3.31^{+0.17}_{-0.08}$ GeV
GKPRY [202]	457^{+14}_{-13} MeV	558^{+22}_{-14} MeV	$3.59^{+0.11}_{-0.13}$ GeV

Table 5.1: Mass, width, and $\pi\pi$ coupling constant of the σ. The coupling for CCL obtained from [203] is quoted in [186].

by an iterative procedure. However, the RS equations for $\gamma\pi \to \gamma\pi$ are less powerful than those for $\pi K \to \pi K$, since the only contributions that can be obtained in the s-channel without additional input are determined by elastic unitarity, cf. Fig. 5.2. In the $\gamma\pi$ case, $\gamma\pi$ intermediate states are suppressed by e^2 and thus expected to be numerically negligible. By comparison, πK intermediate states dominate the unitarity relation in πK scattering at least up to 1 GeV [67].

For this reason, we will drop $\gamma\pi$ intermediate states altogether and content ourselves with the resonance description of the imaginary parts of the Compton-scattering amplitudes constructed in [188], where the resonance contributions are eventually included in a spectral representation with an integration cutoff of $-5\,\text{GeV}^2$. In our framework, the effect of the resonance description of $\operatorname{Im} f_{J,\pm}(s)$ on $h_{J,\pm}(t)$ can be directly read off from (4.36) or (5.2), cf. Sect. 5.3.1. Physically, one can understand this summation of resonances as an effective description of multi-pion states in the s-channel for $\gamma\pi \to \gamma\pi$, or, equivalently, in the t-channel for $\gamma\gamma \to \pi\pi$, which amounts to approximating the multi-pion cuts by a sum of poles. As a future extension, this description could be improved upon at low energies by explicitly incorporating the 2- and 3-pion intermediate states based on the pertinent ChPT amplitudes.[4]

We now turn to the input for $\operatorname{Im} h_{J,\pm}(t)$. We choose the matching point as

$$\sqrt{t_\text{m}} = 0.98\,\text{GeV}\,, \tag{5.27}$$

which, on the one hand, ensures that $\delta_0(t_\text{m}) < \pi$, avoiding a free parameter in the MO solution, and, on the other hand, extends the energy range as far as possible. As the cross section above 1 GeV is dominated by the $f_2(1270)$ resonance, we put $h_{J,\pm}(t) = 0$ above t_m for all partial waves except for $h^{I=0}_{2,-}(t)$, which we match to a Breit–Wigner ansatz for the $f_2(1270)$, cf. Sect. 5.3.2. As we will show in Sect. 5.4, this approximation already allows for a reasonable description of the cross section. Since we are ultimately interested in the properties of the σ, a more detailed analysis of the high-energy region is not necessary for the present application.

As input for the $\pi\pi$ phases we use the results of an extended Roy-equation analysis of $\pi\pi$ scattering [57], which in particular ensures that the phases and the pole position of the σ are consistent, since [57] coincides perfectly with the older analysis [58] at low energies.[5] To estimate the uncertainties due to the $\pi\pi$ input, we also consider the $\pi\pi$ phases determined in a recent study of Roy-like equations [55]. The parameters of the σ resonances corresponding to both approaches, which we will refer to as CCL and GKPRY, respectively, are given in Table 5.1, and are consistent within errors.

Finally, our results depend on the input chosen for the pion polarizabilities. For definiteness, we will consider the two sets of parameters compiled in Table 5.2, which we refer to

[4] These intermediate states enter the $\gamma\pi$ amplitude at $\mathcal{O}(e^2p^6)$ and $\mathcal{O}(e^2p^4)$ in the chiral counting, respectively, where the 2-pion case even requires two anomalous $\gamma\pi \to \pi\pi$ vertices, see Fig. 5.2.

[5] The impact of the high-energy region on the σ pole position was shown to be negligible in [65].

	ChPT [192, 193]	GMM [188]
$(\alpha_1-\beta_1)^{\pi^0}$	-1.9 ± 0.2	-1.25 ± 0.17
$(\alpha_1+\beta_1)^{\pi^0}$	1.1 ± 0.3	1.22 ± 0.12
$(\alpha_2-\beta_2)^{\pi^0}$	37.6 ± 3.3	32.1 ± 2.1
$(\alpha_2+\beta_2)^{\pi^0}$	0.037 ± 0.003	-0.19 ± 0.02
$(\alpha_1-\beta_1)^{\pi^\pm}$	5.7 ± 1.0	4.7
$(\alpha_1+\beta_1)^{\pi^\pm}$	0.16 [0.16]	0.19 ± 0.09
$(\alpha_2-\beta_2)^{\pi^\pm}$	16.2 [21.6]	14.7 ± 2.1
$(\alpha_2+\beta_2)^{\pi^\pm}$	-0.001 [-0.001]	0.11 ± 0.03

Table 5.2: Dipole and quadrupole pion polarizabilities in units of 10^{-4}fm^3 and 10^{-4}fm^5, respectively. The numbers in brackets refer to the LECs from [103].

as ChPT and GMM, respectively. The polarizabilities in the isospin basis follow from (4.28). Note that in [188] the dipole polarizability of the charged pion was only allowed to vary within the range of the ChPT prediction. Unfortunately, the charged-pion quadrupole polarizability $\alpha_2 - \beta_2$ is rather sensitive to LECs: the first number, $16.2 \cdot 10^{-4}\,\text{fm}^5$, corresponds to the resonance-saturation model of [193], while taking the LECs from [103] yields $21.6 \cdot 10^{-4}\,\text{fm}^5$.

5.3.1 Resonances in $\gamma\pi \to \gamma\pi$

We use the resonance model constructed in [188], with the contribution of vector (V), axial-vector (A), tensor (T), and axial-tensor (T_A) resonances to the Compton-scattering partial waves in the narrow-width approximation, to define the imaginary part of the $\gamma\pi \to \gamma\pi$ amplitudes

$$\begin{aligned}
\text{Im}\, f^{\text{V}}_{J,\pm}(s) &= \pm\frac{2}{3}\pi C_\text{V}(m_\text{V}^2 - M_\pi^2)^2\delta(s-m_\text{V}^2)\delta_{J1}\,, \\
\text{Im}\, f^{\text{A}}_{J,\pm}(s) &= \frac{2}{3}\pi C_\text{A}(m_\text{A}^2 - M_\pi^2)^2\delta(s-m_\text{A}^2)\delta_{J1}\,, \\
\text{Im}\, f^{\text{T}}_{J,\pm}(s) &= \pm\frac{2}{5}\pi C_\text{T}\frac{(m_\text{T}^2 - M_\pi^2)^4}{m_\text{T}^2}\delta(s-m_\text{T}^2)\delta_{J2}\,, \\
\text{Im}\, f^{\text{T}_\text{A}}_{J,\pm}(s) &= \frac{2}{5}\pi C_{\text{T}_\text{A}}\frac{(m_{\text{T}_\text{A}}^2 - M_\pi^2)^4}{m_{\text{T}_\text{A}}^2}\delta(s-m_{\text{T}_\text{A}}^2)\delta_{J2}\,,
\end{aligned} \tag{5.28}$$

where m_i, $i \in \{\text{V}, \text{A}, \text{T}, \text{T}_\text{A}\}$, denotes the mass of the resonance, and the coupling constants C_i are related to the widths Γ_i by

$$\begin{aligned}
\Gamma_\text{V} &= \alpha C_\text{V}\frac{(m_\text{V}^2 - M_\pi^2)^3}{3m_\text{V}^3}\,, \qquad \Gamma_\text{A} = \alpha C_\text{A}\frac{(m_\text{A}^2 - M_\pi^2)^3}{3m_\text{A}^3}\,, \\
\Gamma_\text{T} &= \alpha C_\text{T}\frac{(m_\text{T}^2 - M_\pi^2)^5}{5m_\text{T}^5}\,, \qquad \Gamma_{\text{T}_\text{A}} = \alpha C_{\text{T}_\text{A}}\frac{(m_{\text{T}_\text{A}}^2 - M_\pi^2)^5}{5m_{\text{T}_\text{A}}^5}\,.
\end{aligned} \tag{5.29}$$

Inserting (5.28) into (4.36) yields

$$
\begin{aligned}
h^{\mathrm{V}}_{J,+}(t) &= \frac{2}{3}C_{\mathrm{V}}(m_{\mathrm{V}}^2-M_\pi^2)^2\Big(\tilde{G}^{++}_{J1}(t,m_{\mathrm{V}}^2)-\tilde{G}^{+-}_{J1}(t,m_{\mathrm{V}}^2)\Big)\,,\\
h^{\mathrm{V}}_{J,-}(t) &= \frac{2}{3}C_{\mathrm{V}}(m_{\mathrm{V}}^2-M_\pi^2)^2\tilde{G}^{-+}_{J1}(t,m_{\mathrm{V}}^2)\,,\\
h^{\mathrm{A}}_{J,+}(t) &= \frac{2}{3}C_{\mathrm{A}}(m_{\mathrm{A}}^2-M_\pi^2)^2\Big(\tilde{G}^{++}_{J1}(t,m_{\mathrm{A}}^2)+\tilde{G}^{+-}_{J1}(t,m_{\mathrm{A}}^2)\Big)\,,\\
h^{\mathrm{A}}_{J,-}(t) &= \frac{2}{3}C_{\mathrm{A}}(m_{\mathrm{A}}^2-M_\pi^2)^2\tilde{G}^{-+}_{J1}(t,m_{\mathrm{A}}^2)\,,\\
h^{\mathrm{T}}_{J,+}(t) &= \frac{2}{5}C_{\mathrm{T}}\frac{(m_{\mathrm{T}}^2-M_\pi^2)^4}{m_{\mathrm{T}}^2}\Big(\tilde{G}^{++}_{J2}(t,m_{\mathrm{T}}^2)-\tilde{G}^{+-}_{J2}(t,m_{\mathrm{T}}^2)\Big)\,,\\
h^{\mathrm{T}}_{J,-}(t) &= \frac{2}{5}C_{\mathrm{T}}\frac{(m_{\mathrm{T}}^2-M_\pi^2)^4}{m_{\mathrm{T}}^2}\tilde{G}^{-+}_{J2}(t,m_{\mathrm{T}}^2)\,,\\
h^{\mathrm{T_A}}_{J,+}(t) &= \frac{2}{5}C_{\mathrm{T_A}}\frac{(m_{\mathrm{T_A}}^2-M_\pi^2)^4}{m_{\mathrm{T_A}}^2}\Big(\tilde{G}^{++}_{J2}(t,m_{\mathrm{T_A}}^2)+\tilde{G}^{+-}_{J2}(t,m_{\mathrm{T_A}}^2)\Big)\,,\\
h^{\mathrm{T_A}}_{J,-}(t) &= \frac{2}{5}C_{\mathrm{T_A}}\frac{(m_{\mathrm{T_A}}^2-M_\pi^2)^4}{m_{\mathrm{T_A}}^2}\tilde{G}^{-+}_{J2}(t,m_{\mathrm{T_A}}^2)\,.
\end{aligned}
\tag{5.30}
$$

We include all resonances listed in [188]. Moreover, we have checked that (5.30) agrees with the results quoted in [188]: once the ambiguous term linear in t in $h_{0,+}(t)$ in [188] is removed, we recover that result by taking the limit $a\to\infty$ of our unsubtracted kernel functions.

5.3.2 Including the $f_2(1270)$

To incorporate the D-wave resonance $f_2(1270)$ we follow [182]. Starting from

$$
\mathcal{L}_{\mathrm{TPP}} = C_{\mathrm{T}}^{\pi} T^{\mu\nu}\partial_\mu P\partial_\nu P\,,\qquad \mathcal{L}_{\mathrm{T}\gamma\gamma} = e^2 C_{\mathrm{T}}^{\gamma} T^{\mu\nu}F_{\mu\alpha}F_{\nu}{}^{\alpha}
\tag{5.31}
$$

to describe the coupling of a tensor resonance to pseudoscalars and photons, respectively, we find

$$
A = -\frac{C_{\mathrm{T}}^{\pi}C_{\mathrm{T}}^{\gamma}}{6(t-m_{\mathrm{T}}^2)}\left\{4M_\pi^2\left(4-\frac{t}{m_{\mathrm{T}}^2}\right)-t\left(5-\frac{2t^2}{m_{\mathrm{T}}^4}\right)\right\}\,,\qquad B=\frac{C_{\mathrm{T}}^{\pi}C_{\mathrm{T}}^{\gamma}}{4(t-m_{\mathrm{T}}^2)}\,,
\tag{5.32}
$$

and thus

$$
\begin{aligned}
H_{++} &= -\frac{C_{\mathrm{T}}^{\pi}C_{\mathrm{T}}^{\gamma}t}{6m_{\mathrm{T}}^4}\Big(t(t+m_{\mathrm{T}}^2)-2m_{\mathrm{T}}^2M_\pi^2\Big)\,,\\
H_{+-} &= \frac{C_{\mathrm{T}}^{\pi}C_{\mathrm{T}}^{\gamma}}{4}\frac{t^2\sigma(t)^2}{t-m_{\mathrm{T}}^2}(1-z_t^2)\,.
\end{aligned}
\tag{5.33}
$$

Accordingly, a resonant contribution only occurs in $h_{2,-}(t)$, while the non-resonant background in $h_{0,+}(t)$ can be discarded. Taking the full width of the $f_2(1270)$ into account and dropping the non-resonant background, we obtain

$$
h^{f_2}_{2,-}(t) = \frac{C_{f_2}^{\pi}C_{f_2}^{\gamma}}{5\sqrt{6}}\frac{m_{f_2}^4\sigma(m_{f_2}^2)^2}{t-m_{f_2}^2+im_{f_2}\Gamma_{f_2}}\,.
\tag{5.34}
$$

	full	$a \to \infty$	no resonances
$I^{(1)}$, CCL	-0.62	-1.15	0.61
$I^{(1)}$, GKPRY	-0.63	-1.17	0.60
$I^{(2)}$, CCL	3.45	3.58	2.08
$I^{(2)}$, GKPRY	3.40	3.53	2.03

Table 5.3: Integrals in the $I = 2$ sum rule for the full left-hand cut, in the limit $a \to \infty$, and with resonances switched off.

	$\alpha_1 - \beta_1$	$\alpha_2 - \beta_2$	total
ChPT	1.03 ± 0.14	-4.29 ± 0.78	0.18 ± 0.85
GMM	0.80 ± 0.14	-3.49 ± 0.60	0.76 ± 0.68

Table 5.4: Individual contribution to (5.13) from the polarizabilities (first two columns) and total value of the right-hand side of the sum rule (third column).

In fact, in Sect. 5.4.2 we will restore the background in order to describe the cross section for $\gamma\gamma \to \pi^+\pi^-$ above the matching point. The coupling constants can be determined from the partial widths

$$\Gamma_{f_2\to\pi\pi} = \frac{\left(C^\pi_{f_2}\right)^2}{960\pi}\frac{\left(m_{f_2}^2 - 4M_\pi^2\right)^{\frac{5}{2}}}{m_{f_2}^2}\,, \qquad \Gamma_{f_2\to\gamma\gamma} = \frac{\pi}{5}\alpha^2\left(C^\gamma_{f_2}\right)^2 m_{f_2}^3\,. \tag{5.35}$$

For the f_2 parameters we use as input [3]

$$\begin{aligned} m_{f_2} &= 1275.1\,\text{MeV}\,, & \Gamma_{f_2} &= 185.1\,\text{MeV}\,,\\ \Gamma_{f_2\to\pi\pi} &= 156.9\,\text{MeV}\,, & \Gamma_{f_2\to\gamma\gamma} &= 3.03\,\text{keV}\,, \end{aligned} \tag{5.36}$$

leading to

$$|C^\pi_{f_2}| = 16.06\,\text{GeV}^{-1}\,, \qquad |C^\gamma_{f_2}| = 0.21\,\text{GeV}^{-1}\,. \tag{5.37}$$

However, the relative sign of the couplings cannot be inferred and must be fitted to experiment.

5.4 Numerical results

5.4.1 Sum rules

First, we turn to the numerical evaluation of the sum rules for $I = 2$ derived in Sect. 5.1.2. As the $I = 2$ D-wave $\pi\pi$ phase is very small, in practice no meaningful constraint results in these partial waves and we therefore restrict the analysis to the S-wave. These sum rules are given explicitly in (5.13) (see also Appendix B.3.2). The results for $I^{(1)}$ and $I^{(2)}$ and both input $\pi\pi$ phases are shown in the first column of Table 5.3. The difference between using CCL and GKPRY $\pi\pi$ phases is very small in both cases.

Evaluating the sum-rule integrals involves several approximations, in particular, we have put $\text{Im}\, h_{0,+}(t)$ to zero above the matching point, neglected partial waves with $J > 2$, and

used a resonance approximation for $\mathrm{Im}\, f_{J,\pm}(s)$. Therefore, we need to ascertain that the dependence on the high-energy part of the integrals $I^{(1)}$ and $I^{(2)}$, higher partial waves, and details of the resonance description of the left-hand cut is sufficiently small for the sum-rule constraint to be meaningful. We can estimate the accuracy of these approximations by sending the hyperbola parameter $a \to \infty$, as the original HDRs are valid independent of a. Thus, any residual dependence on a provides a measure of the impact of the approximations made. The corresponding results are shown in the second column of Table 5.3: the once-subtracted integral depends strongly on the value of a, but the twice-subtracted version is already rather stable under $a \to \infty$. Doubling the effect of taking $a \to \infty$ to get a conservative estimate of the uncertainty in $I^{(2)}$, we conclude that

$$I^{(2)} = 3.45 \pm 0.30 \; . \tag{5.38}$$

In order to further test the sensitivity of the sum rule to the modeling of the left-hand cut by a set of resonances we can check the impact of switching off resonance contributions completely. In the case of $I^{(2)}$ even this crude approximation entails a relatively modest shift in the result. As shown in the third column of Table 5.3, the resonances contribute less than 50 % to the full result, so that their contribution would have to be drastically wrong to exceed the error estimate given in (5.38). The stability of $I^{(2)}$ under these changes in high-energy input makes it worth taking (5.38) seriously as a constraint on a particular linear combination of $(\alpha_1 - \beta_1)^{I=2}$ and $(\alpha_2 - \beta_2)^{I=2}$. Thus, we will now consider the resulting sum rule that arises from the twice-subtracted MO representation in more detail.

First of all, we test if the parameter sets of Table 5.2 fulfill the sum rule. The error analysis is complicated by the fact that in the GMM set no uncertainty estimate is given for $(\alpha_1 - \beta_1)^{\pi^\pm}$, while in the ChPT set the error induced by the LEC dependence of $(\alpha_2 - \beta_2)^{\pi^\pm}$ is difficult to assess. To obtain a rough estimate, we use the ChPT error for $(\alpha_1 - \beta_1)^{\pi^\pm}$ also for GMM, and vice versa for $(\alpha_2 - \beta_2)^{\pi^\pm}$. This, together with the number (5.38), leads to the results summarized in Table 5.4. We conclude that the sum rule is fulfilled for both sets, although rather marginally in the case of GMM, which is mainly due to the fact that $(\alpha_2 - \beta_2)^{\pi^0}$ differs quite substantially between ChPT and GMM. The largest uncertainty in the sum rule is driven by lack of knowledge of the quadrupole polarizability.

Observing that both dipole polarizabilities as well as $(\alpha_2 - \beta_2)^{\pi^0}$ have an accurate ChPT prediction, we can turn around the argument and use the sum rule to derive an improved value for $(\alpha_2 - \beta_2)^{\pi^\pm}$. Using (5.38) and the ChPT prediction for the isospin-two dipole polarizability, (5.13) leads to

$$(\alpha_2 - \beta_2)^{I=2} = (-18.2 \pm 1.3) \cdot 10^{-4} \mathrm{fm}^5 \; . \tag{5.39}$$

Resorting, in addition, to the ChPT prediction for $(\alpha_2 - \beta_2)^{\pi^0}$, we find

$$\begin{aligned} (\alpha_2 - \beta_2)^{\pi^\pm} &= (15.3 \pm 3.7) \cdot 10^{-4} \mathrm{fm}^5 \; , \\ (\alpha_2 - \beta_2)^{I=0} &= (39.4 \pm 6.0) \cdot 10^{-4} \mathrm{fm}^5 \; , \end{aligned} \tag{5.40}$$

where the increase in uncertainty compared to (5.39) is due to the ChPT uncertainty in $(\alpha_2 - \beta_2)^{\pi^0}$. In the remainder of this chapter, we will make use of the improved value (5.40) when referring to the ChPT predictions for pion polarizabilities. Note that, as expected given the results of Table 5.4, the sum-rule value of $(\alpha_2 - \beta_2)^{\pi^\pm}$ is consistent with the first ChPT number quoted in Table 5.2, but not with the larger number found when the LECs of [103] are taken as input.

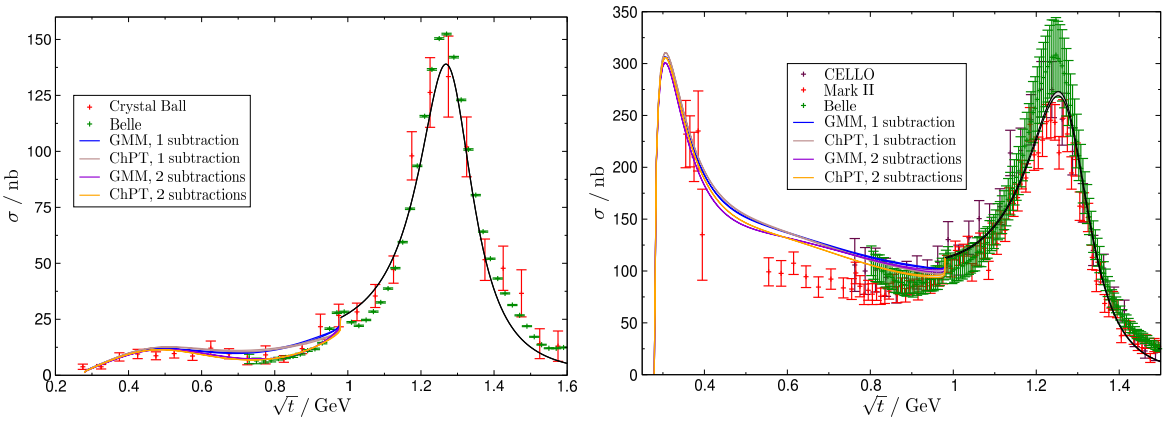

Figure 5.3: Total cross section for $\gamma\gamma \to \pi^0\pi^0$ [170, 174] and $\gamma\gamma \to \pi^+\pi^-$ [171–173] for $|\cos\theta| \leq 0.8$ and $|\cos\theta| \leq 0.6$, respectively.

5.4.2 Total cross section

Before performing the analytic continuation to the σ pole, we need to demonstrate that the amplitude on the real axis is reasonably well described—at least up to $\sqrt{t} = 1\,\text{GeV}$, which we assess to be the region which will influence the analytic continuation to the σ pole. The results for the cross section are depicted in Figs. 5.3 and 5.4. Below the matching point, the results for the once- and twice-subtracted formulation are provided for both ChPT and GMM polarizabilities. The uncertainty due to $\pi\pi$ input, represented by the grey band, is estimated by the variation between CCL and GKPRY phases and proves to be very small. The low-energy region is totally dominated by the Born terms in the charged process, but it is very sensitive to the σ in the neutral reaction. The prediction of the twice-subtracted dispersion relation is in especially good agreement with $\gamma\gamma \to \pi^0\pi^0$ data (see Fig. 5.4), with the level of agreement comparable to that obtained in the coupled-channel fit of [188].

Above the matching point, we exploit the fact that the cross section is dominated by the $f_2(1270)$, and thus can be well approximated by employing a Breit–Wigner description of this resonance in $h_{2,-}^{I=0}(t)$ and putting all other partial waves to zero. In this way, (5.34) alone yields a good description of the neutral cross section above the matching point. In contrast, in the charged case an additional background is necessary. As observed in [182], this can be most easily achieved by adding the Born terms and the off-shell contributions dropped in the transition from (5.33) to (5.34) back into the charged-channel amplitude for $h_{2,-}(t)$. Moreover, after the transition to the isospin basis, we add a constant background phase to ensure matching with the $\pi\pi$ phase below the matching point. However, if $C_{f_2}^{\pi} C_{f_2}^{\gamma}$ is chosen to be negative, the mismatch of the phases is very small: we find a correction of $\delta_{\text{corr}} = -0.09$ and $\delta_{\text{corr}} = -0.04$ in order to obtain agreement with the CCL and GKPRY phases, respectively.

Finally, we comment on the analyticity properties of the partial waves at the matching point. As shown in the appendix of [67], the solutions in terms of Omnès functions automatically fulfill continuity at the matching point, but the derivative at t_{m} is not determined. Therefore, in general, strong cusps can occur at the matching point. For example, if the background in the charged reaction is dropped, the neutral cross section above t_{m} is still correctly reproduced, but the input for the $I = 0$ component changes, which affects the neutral cross section below t_{m}: the result for $|h_{2,-}^{I=0}(t)|$ exhibits a strong cusp below t_{m}, which translates

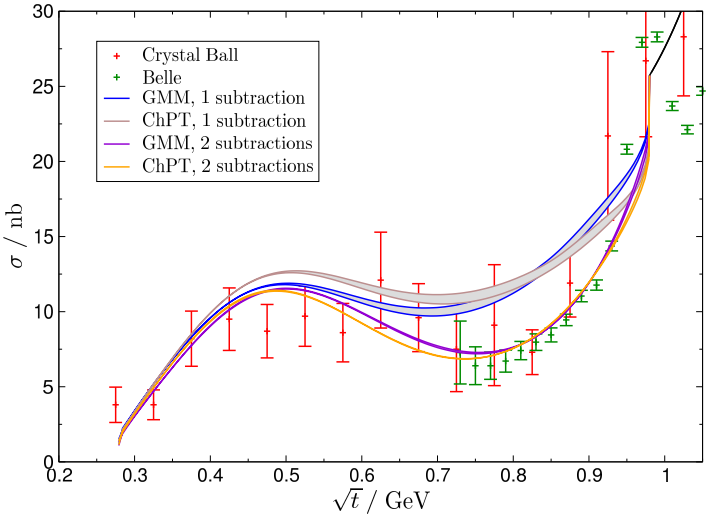

Figure 5.4: Total cross section for $\gamma\gamma \to \pi^0\pi^0$ for $|\cos\theta| \leq 0.8$ in the low-energy region.

into an (unphysical) sharp peak of about 15 nb in the neutral cross section directly below t_m. The fact that this effect is much smaller in the full solution provides evidence that our model for the high-energy region is reasonably accurate, as only a specific input of $\pi\pi$ phases, polarizabilities, and imaginary parts above t_m will yield a smooth solution for $h_{2-}^{I=0}(t)$ around $t = t_\mathrm{m}$. In the language of [49] such a solution corresponds to an "analytic input." If the input above the matching point were sufficiently well known, one could thus derive constraints on the polarizabilities by requiring a no-cusp condition. These constraints would be similar to those derived in [53, 67] for $\pi\pi$ and πK scattering lengths. However, the input above the matching point is not very well known in $\gamma\gamma \to \pi\pi$, and so we content ourselves with demanding that the cusp at t_m is not too large, which indicates that the input is reasonably close to being "analytic."

5.4.3 Two-photon coupling of the σ

Finally, we present our results for the two-photon width $\Gamma_{\sigma\gamma\gamma}$ as a function of the pion polarizabilities. $(\alpha_1+\beta_1)$ and $(\alpha_2+\beta_2)$ only feature as subtraction constants in the D-waves, which, in turn, influence $\Gamma_{\sigma\gamma\gamma}$ only indirectly via the corresponding coupling to the S-wave in (5.2). Moreover, the imaginary part of these D-waves is dominated to a large extent by the $f_2(1270)$, and the dependence of $|h_{2,-}^{I=0}(t)|$ on the number of subtractions is very weak, see Fig. 5.5 for the results using the ChPT polarizabilities. The variation between the $|h_{2-}^{I=0}(t)|$ solutions for different numbers of subtractions is so small that the uncertainty in the $\pi\pi$ phases (estimated as the difference between CCL and GKPRY) becomes of comparable size. Consequently, the dependence of $\Gamma_{\sigma\gamma\gamma}$ on $(\alpha_1+\beta_1)^{I=0}$ and $(\alpha_2+\beta_2)^{I=0}$ is entirely negligible, with the result that we end up with the dipole polarizability $(\alpha_1-\beta_1)^{I=0}$ as the only free parameter that affects $\Gamma_{\sigma\gamma\gamma}$ in the once-subtracted version of the equations, while a second subtraction additionally requires the quadrupole polarizability $(\alpha_2-\beta_2)^{I=0}$ as input. The resulting model-independent correlation between $\Gamma_{\sigma\gamma\gamma}$ and the pion polarizabilities depicted in Fig. 5.6 represents the main result of this chapter.

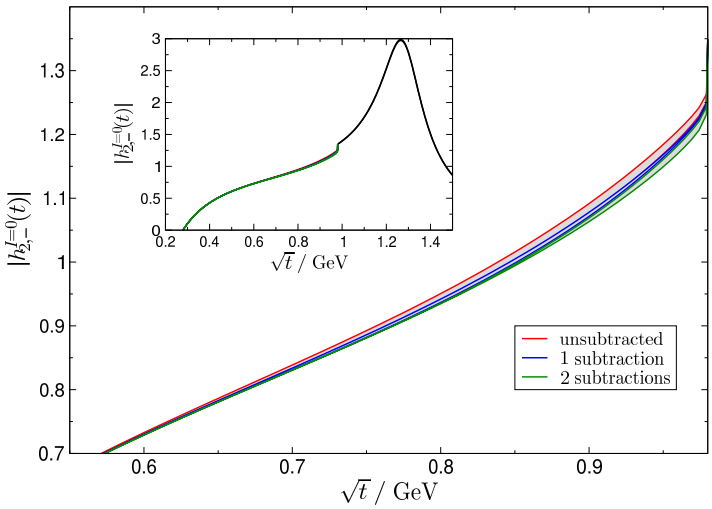

Figure 5.5: Dependence of $|h_{2,-}^{I=0}(t)|$ on the number of subtractions. The grey bands indicate the difference between CCL and GKPRY phases.

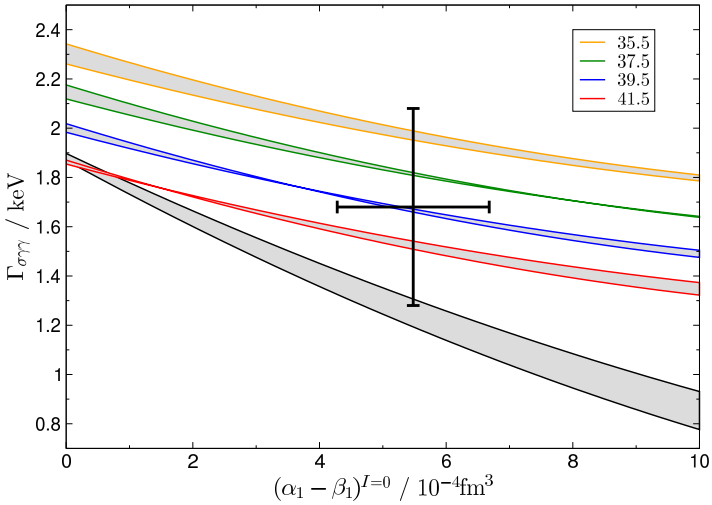

Figure 5.6: $\Gamma_{\sigma\gamma\gamma}$ as a function of the $I = 0$ pion polarizabilities. The black line refers to the unsubtracted case and the colored lines to the twice-subtracted version with $(\alpha_2 - \beta_2)^{I=0}$ as indicated (in units of 10^{-4}fm^5). The grey band for the uncertainty in the $\pi\pi$ input is estimated by the variation found when CCL and GKPRY phases and σ parameters are chosen. The cross corresponds to the twice-subtracted case plus ChPT input.

The role of the different contributions to the left-hand cut is illustrated in Fig. 5.7: starting from the Born-term approximation (black line), we add resonances in the limit $a \to \infty$ (red line), the additional terms for finite $a = -7.5M_\pi^2$ (blue line), and D-wave contributions (green line). The twice-subtracted version (solid lines) is hardly affected by any of these changes. In the once-subtracted case (dashed lines) we see that D-wave and resonance contributions are of comparable size. We therefore expect that, as soon as resonances yield a significant contribution to the left-hand cut, the coupling between S- and D-waves should also become numerically important in any description of data that is based on a MO representation.

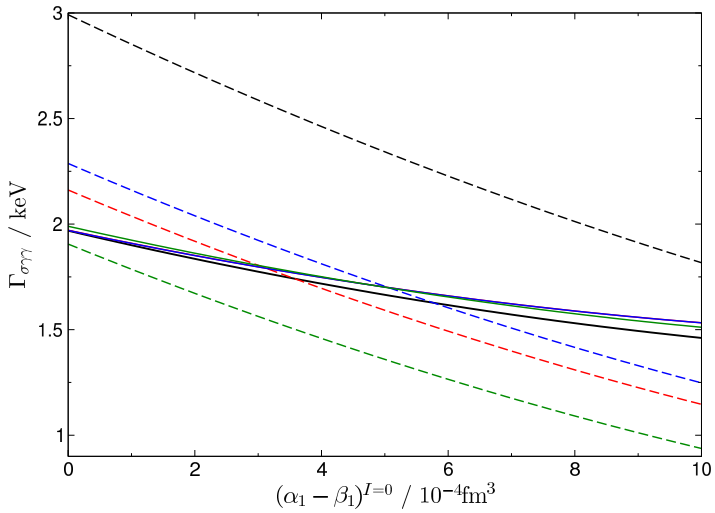

Figure 5.7: Individual contributions to $\Gamma_{\sigma\gamma\gamma}$ for CCL phases and σ parameters. The dashed lines refer to the once-subtracted version, and the solid lines to the twice-subtracted version with input for $(\alpha_2-\beta_2)^{I=0}$ from (5.40). The black lines denote the results for a left-hand cut modeled solely by the Born terms, while the red, blue, and green lines are obtained by successively adding resonances in the limit $a\to\infty$, terms for finite a, and D-wave contributions.

	1 subtraction	2 subtractions
ChPT	1.3 ± 0.1	1.7 ± 0.4
GMM	1.4 ± 0.1	2.0 ± 0.2

Table 5.5: Prediction for $\Gamma_{\sigma\gamma\gamma}$ in keV based on ChPT and GMM polarizabilities for CCL phases and σ parameters.

The results for $\Gamma_{\sigma\gamma\gamma}$ given ChPT and GMM choices for the polarizabilities are summarized in Table 5.5, where the errors only include the uncertainties from the pion polarizabilities. We have checked that these numbers are insensitive to the details of the input above the matching point. While for the ChPT parameters the results from the once- and twice-subtracted equations are consistent, there is significant tension between these two results in the case of GMM. This issue seems to be related to the relatively small value of $(\alpha_2-\beta_2)^{\pi^0}$ in that polarizability set: increasing this polarizability and thus bringing it closer to the ChPT prediction would both improve the fulfillment of the $I=2$ sum rule (cf. Sect. 5.4.1) and bring $\Gamma_{\sigma\gamma\gamma}$ down from the (2.0 ± 0.2) keV result given in Table 5.5.

In view of Fig. 5.7, we consider the outcome for the twice-subtracted system of RS equations as the most reliable one, despite the fact that input for the quadrupole polarizability is required. Although the result based on the GMM parameters is ostensibly more precise, the MO representation used in [188] is, for the reasons explained in Sect. 5.1.4, not fully consistent with the RS equations derived here. For this reason, we follow the philosophy of [58] and combine the strict predictions of the RS equations with ChPT input for the pion polarizabilities to obtain our final result

$$\Gamma_{\sigma\gamma\gamma}=(1.7\pm0.4)\,\text{keV}\ , \tag{5.41}$$

Reference		$\Gamma_{\sigma\gamma\gamma}$
Penn. 06	[177]	4.1 ± 0.3
MNO 08	[178]	3.9 ± 0.6
MNW 11	[180]	3.08 ± 0.82
FK 06	[183]	0.62
Penn. *et al.* 08	[184], sol B	2.4 ± 0.4
ORS 08	[185]	1.8 ± 0.4
OR 08	[186]	1.68 ± 0.15
BP 08	[176]	1.20 ± 0.40
Mao *et al.* 09	[187]	2.08
Mouss. 11	[56]	$2.08 \pm 0.20^{+0.07}_{-0.04}$

Table 5.6: Previous results for $\Gamma_{\sigma\gamma\gamma}$ in keV.

which is depicted by the cross in Fig. 5.6. We note that the uncertainty here is broad enough to encompass all the central values in Table 5.5. A comparison with previous results for $\Gamma_{\sigma\gamma\gamma}$ is shown in Table 5.6 and Fig. 5.8.

5.5 Summary and conclusion

In this part, we have constructed a complete set of Roy–Steiner equations for pion Compton scattering and the crossed reaction $\gamma\gamma \to \pi\pi$. In particular, we have worked out all necessary integral kernels for zero, one, and two subtractions explicitly up to D-waves, and identified the subtraction constants with pion polarizabilities. Assuming Mandelstam analyticity, we studied the range of validity of the system, and found that the equations for the $\gamma\gamma \to \pi\pi$ partial waves are rigorously valid up to 1 GeV—a domain that comfortably includes the σ pole. Truncating the system at $J = 2$, we then concentrated on the equations for $\gamma\gamma \to \pi\pi$, whose solution in terms of a Muskhelishvili–Omnès representation with a finite matching point was discussed. Comparing our equations with existing approaches in the literature, we found a coupling between S- and D-waves, which has previously been neglected in dispersive calculations of $\gamma\gamma \to \pi\pi$, but seems to be numerically comparable to the contributions of resonances in $\gamma\gamma \to \pi\pi$ to the left-hand cut.

Demanding continuity of the Muskhelishvili–Omnès representation at the matching point, we derived sum rules for the $I = 2$ partial waves that relate dipole and quadrupole polarizabilities to integrals over the left-hand cut. We used the S-wave sum rule, together with ChPT input for the neutral-pion quadrupole polarizability and the dipole polarizabilities, to obtain a new, more accurate, prediction for the charged-pion quadrupole polarizability

$$(\alpha_2 - \beta_2)^{\pi^\pm} = (15.3 \pm 3.7) \cdot 10^{-4} \text{fm}^5 \,. \tag{5.42}$$

The central value is hardly shifted compared to [193], but the error estimate is difficult to obtain in ChPT alone due to a strong dependence on poorly known LECs. In fact, the

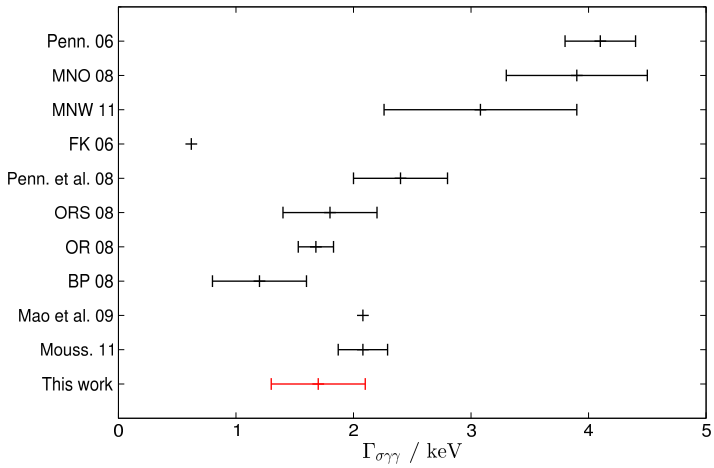

Figure 5.8: Previous results for $\Gamma_{\sigma\gamma\gamma}$ with acronyms defined in Table 5.6. The red point corresponds to our result. For [183, 187] we only show the central value, as no errors are provided in these references.

outcome of the present calculation can be interpreted as support for the resonance-saturation model of [193], while disfavoring the set of LECs from [103].

The main application of our formalism concerns the two-photon width of the σ resonance. To this end, we first showed that the cross section for both the charged and neutral channel can be accurately reproduced by approximating the high-energy region above 1 GeV by a Breit–Wigner ansatz for the $f_2(1270)$ resonance and employing a suitably chosen background amplitude in the charged case. With this input, the Muskhelishvili–Omnès representation yields a good description of the available data in the low-energy region.

Finally, we presented the results of the analytic continuation to the σ pole as a correlation plot between the pertinent pion polarizabilities and $\Gamma_{\sigma\gamma\gamma}$. We stress that the corresponding correlation between the $I = 0$ pion polarizabilities and $\Gamma_{\sigma\gamma\gamma}$ results solely from analyticity, unitarity, crossing symmetry, gauge invariance, and the accurately known $\pi\pi$ phases in the region below 1 GeV. We also provided a specific result for $\Gamma_{\sigma\gamma\gamma}$ that corresponds to the ChPT predictions for the pertinent pion polarizabilities. As a future application, Roy–Steiner equations, once extended to include $\bar{K}K$ effects in a two-channel formalism, should provide a valuable framework to extract pion polarizabilities from low-energy measurements of the cross section for $\gamma\gamma \to \pi^0\pi^0$ currently analyzed by the KLOE collaboration [204], which would be complementary to the more direct Primakoff approach at COMPASS [194]. In the future, the results of these ongoing efforts to accurately determine the pion polarizabilities, will—as shown here—directly translate into improved knowledge of $\Gamma_{\sigma\gamma\gamma}$.

Part III

Roy–Steiner equations for pion–nucleon scattering

Chapter 6

Partial-wave dispersion relations[#3]

6.1 Introduction

Pion–nucleon scattering has been of primary interest in low-energy QCD for decades. Despite the large data base and innumerable theoretical investigations based on a variety of different methods, it is still the insufficient knowledge of low-energy πN physics that prevents progress on our understanding of fundamental properties of strong interactions. Most notably, a precise determination of the isoscalar πN amplitude would yield access to the pion–nucleon σ term $\sigma_{\pi N}$, which measures the contribution from the light quarks to the nucleon mass and can, by means of $SU(3)$ ChPT, even be related to the strangeness content of the nucleon [206, 207]. In this respect, its value is intimately connected to the decomposition of the nucleon mass into the fractions originating from gluonic self interactions and the different quark species, cf. (1.4). Moreover, the σ term is an essential input quantity for the investigation of nuclear matter, in particular the in-medium properties of the quark condensate [208], as well as for dark matter searches, where it determines the scattering cross section of dark matter candidates off nuclei [209]. Eventually, $\sigma_{\pi N}$ should be calculable from first principles in lattice QCD, but while the direct approach still lacks the required accuracy due to the presence of disconnected diagrams, the indirect extraction from the derivative of the nucleon mass by means of the Feynman–Hellmann theorem [136] is afflicted with substantial uncertainties in the chiral extrapolation, see [132–135, 137]. The goal of the final part of this thesis is to lay out a path how the σ term can be extracted from a precise determination of the πN scattering amplitude at low energies within the framework of Roy–Steiner equations. In the pursuit of this program, the S-wave scattering lengths deserve special attention, as their precise values inferred from hadronic-atom data provide powerful constraints on low-energy πN scattering. In particular, their extraction from pionic hydrogen and deuterium (see Part I) indicates that ultimately even isospin violation cannot be ignored in the isoscalar amplitude.

The construction of a complete system of RS equations will proceed in close analogy to the derivation presented in Part II. With the starting point provided by HDRs for the invariant πN amplitudes, the pertinent partial-wave expansions as well as unitarity relations are used to derive a closed system of PWHDRs that fully respects analyticity, unitarity, and crossing symmetry. Subtractions will be performed at the so-called subthreshold point, which proves convenient for the extrapolation to the Cheng–Dashen point [161], and thus for establishing the relation to $\sigma_{\pi N}$ by means of a low-energy theorem [161–163, 138]. In fact, it has been pointed

[#3] The contents of this chapter have been published in [205].

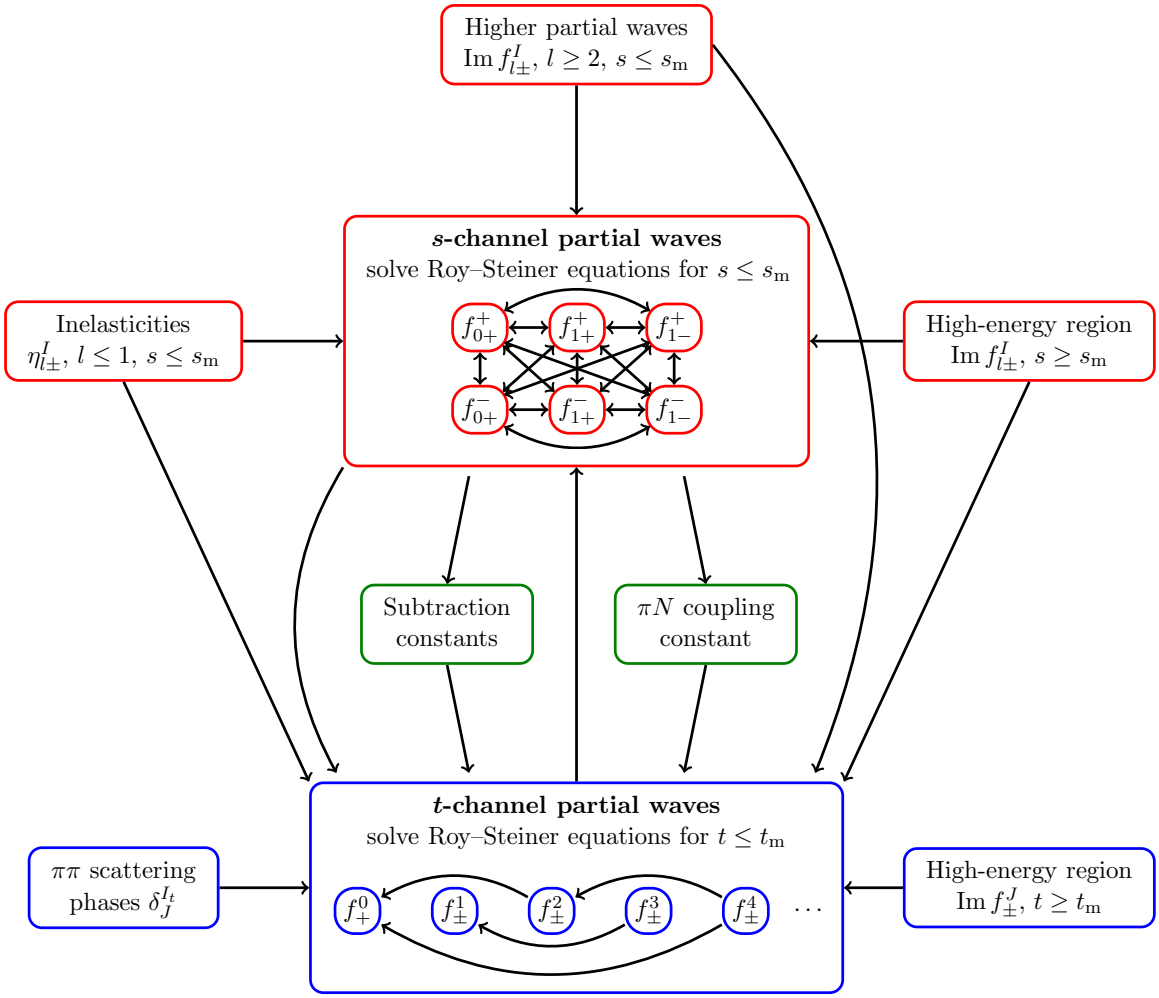

Figure 6.1: Solution strategy for Roy–Steiner equations in πN scattering.

out previously that a reliable extrapolation to the subthreshold region requires additional input from the t-channel ($\pi\pi \to \bar{N}N$) partial waves [210–212], a requirement that is straightforward to comply with in the RS formalism, as HDRs by construction intertwine all physical regions. The PWHDRs for the s-channel (πN) partial waves in their unsubtracted form were already written down in [68], while the t-channel equations that are necessary to obtain a closed system of equations were omitted, as was the issue of subtractions. In the end, both the s- and t-channel equations will involve the subtraction constants and the πN coupling constant as free parameters.

The strategy for the solution of the RS equations is outlined in Fig. 6.1: in the s-channel, the six S- and P-waves $f^\pm_{0+}$, $f^\pm_{1+}$, $f^\pm_{1-}$, with superscript $I = \pm$ for isospin, $l \in \{0, 1\}$ in the subscript for orbital angular momentum, and the $\pm$ for the total angular momentum $j = |l \pm 1/2|$, are considered dynamically below the matching point s_m, whereas the imaginary parts of higher partial waves for all s, the imaginary parts of the S- and P-waves above s_m, and, potentially, inelasticities below s_m are required as input. In contrast, there are only three S- and P-waves in the t-channel, f^0_+ and $f^1_\pm$, with the superscript referring to total angular momentum J and the subscript to parallel/antiparallel antinucleon–nucleon

helicities. The equations for the t-channel partial waves take the form of a Muskhelishvili–Omnès problem [70, 71], whose solution requires—in addition to higher partial waves and the imaginary parts above the matching point t_m—input for the $\pi\pi$ phase shifts. Once the t-channel problem is solved, the resulting t-channel partial waves are used as input for the s-channel problem, which then reduces to the form of conventional $\pi\pi$ Roy equations, rendering known results on the existence and uniqueness of solutions [48–50] as well as known solution techniques [53] applicable. Eventually, a full solution of the system is obtained by iterating this procedure until all partial waves and parameters are determined self-consistently.

Next, we comment on the structure of the equations. Contrary to $\gamma\pi \to \gamma\pi$, the s-channel unitarity relation in πN scattering is indeed dominated by elastic unitarity at low energies, so that new constraints on the low-energy πN phase shifts should ensue. However, inelasticities due to $\pi\pi N$ intermediate states set in rather early, especially in the partial wave corresponding to the Roper resonance $P_{11}(1440)$ the inelasticity cannot be neglected and has to be taken as input. While the s-channel partial waves are all mutually coupled, the t-channel problem actually decouples to a certain degree, as the equation for an amplitude with even/odd J only depends on partial waves with even/odd J' larger than J, cf. Fig. 6.1. Nonetheless, the solution of the t-channel equations is subject to an additional complication as compared to $\pi\pi \to \bar{K}K$ [66] that is related to the large pseudophysical region in $\pi\pi \to \bar{N}N$. In either case, intermediate states besides $\pi\pi$ become relevant in the unitarity relation around 1 GeV, most notably in the S-wave, where $\bar{K}K$ intermediate states account for the occurrence of the $f_0(980)$ resonance. While in $\pi\pi \to \bar{K}K$ these effects can simply be included by choosing t_m around 1 GeV and using phase-shift solutions above, physical input for $\pi\pi \to \bar{N}N$ becomes only available at the two-nucleon threshold, which leaves a large fraction of the pseudophysical region unconstrained by the single-channel approximation. Since for similar reasons no reliable input information for higher partial waves is available, we also solve for D-waves in the t-channel problem. In the end, we consider a full two-channel MO problem for the S-wave to reproduce the $f_0(980)$ dynamics, a single-channel solution for P- and D-waves, and put higher partial waves as well as the imaginary parts above t_m to zero. Evidently, this implies that we need to introduce a sufficient number of subtractions that ensure that the dispersive integrals are already insensitive to the energy regime where the associated uncertainties set in.

Besides its coupling to the s-channel equations, the solution of the t-channel problem is interesting on its own, since the S- and P-wave amplitudes constitute crucial input for a dispersive analysis of the scalar and electromagnetic form factors of the nucleon, respectively. Due to its impact on the σ-term extraction, we will discuss the case of the scalar form factor in detail in Sect. 7.4. Presently, dispersive analyses of nucleon form factors still rely on the KH80 solution [152,165], or variants thereof [213], which, however, does not include more recent data and contradicts modern determinations of the πN coupling constant. In addition, the KH80 solution has been reported to suffer from internal inconsistencies [211, 214, 215], and does not provide estimates for the theoretical uncertainties of the calculation (apart from a vague iteration uncertainty). For these reasons, a consistent set of partial waves and subtractions constants that fulfills the complete system of RS equations would be immensely valuable.

The outline of the presentation is as follows: we first describe the complete system of RS equations together with the corresponding unitarity relations in the remainder of this chapter. Then, we discuss the solution of the t-channel equations using one- and two-channel MO techniques in Chapter 7, which we apply to a dispersive calculation of the scalar form factor of the nucleon. Finally, we comment on the solution of the s-channel problem and the extraction of the pion–nucleon σ term in Chapter 8.

6.2 Kinematics and conventions

We consider the reaction[1]

$$\pi^a(q) + N(p) \to \pi^b(q') + N(p') \,, \tag{6.1}$$

with pion isospin labels a, b, and Mandelstam variables

$$s = (p+q)^2 \,, \qquad t = (q-q')^2 \,, \qquad u = (p-q')^2 \,, \tag{6.2}$$

which fulfill

$$s + t + u = 2m^2 + 2M_\pi^2 \equiv \Sigma \,. \tag{6.3}$$

Again, the masses of the nucleon (m), the pion (M_π), and, later, the kaon (M_K) are identified with the charged-particle masses [3]. Furthermore, we will need the definitions

$$s = W^2 \,, \qquad \nu = \frac{s-u}{4m} \,, \qquad s_\pm = W_\pm^2 = (m \pm M_\pi)^2 \,, \qquad s_0 = \frac{\Sigma}{2} \,. \tag{6.4}$$

The kinematics for the s-channel reaction may be described by the CMS momentum $\mathbf{q}$, nucleon energy E, and scattering angle $z_s = \cos\theta_s$

$$\mathbf{q}^2 = \frac{(s-s_+)(s-s_-)}{4s} \,, \qquad E = \sqrt{m^2+\mathbf{q}^2} = \frac{s+m^2-M_\pi^2}{2W} \,, \qquad z_s = 1 + \frac{t}{2\mathbf{q}^2} \,. \tag{6.5}$$

Similarly, the t-channel reaction is determined by CMS momenta $q_t = |\mathbf{q}_t|$, $p_t = |\mathbf{p}_t|$, and scattering angle $z_t = \cos\theta_t$

$$\begin{aligned} q_t &= \sqrt{\frac{t}{4} - M_\pi^2} = \sqrt{\frac{t-t_\pi}{4}} = \frac{\sqrt{t}}{2}\sigma_t^\pi = iq_- \,, \qquad z_t = \frac{s-u}{4p_tq_t} = \frac{m\nu}{p_tq_t} \,, \\ p_t &= \sqrt{\frac{t}{4} - m^2} = \sqrt{\frac{t-t_N}{4}} = \frac{\sqrt{t}}{2}\sigma_t^N = ip_- \,, \end{aligned} \tag{6.6}$$

where the phases between q_t, p_t, and

$$q_- = \sqrt{M_\pi^2 - \frac{t}{4}} \,, \qquad p_- = \sqrt{m^2 - \frac{t}{4}} \,, \tag{6.7}$$

have been fixed by convention. The physical regions for πN scattering, determined by the requirement that the Kibble function Φ [216]

$$\Phi = t\Big[su - (m^2 - M_\pi^2)^2\Big] \tag{6.8}$$

be non-negative, are shown in Fig. 6.2. Points of special interest in the Mandelstam plane are the Cheng–Dashen point at $(s = u = m^2, t = 2M_\pi^2)$ for the relation to the σ term, the subthreshold point at $(s = u = s_0, t = 0)$ as starting point for the subthreshold expansion, and the s-channel threshold point $(s = s_+, t = 0, u = s_-)$ for the definition of the threshold expansion.

[1] For a comprehensive review of πN kinematics and conventions we refer to [152]. Most of the variables defined here will appear in a primed version as well to denote the corresponding quantity in the internal kinematics, e.g. z_s', q_t', ν', etc.

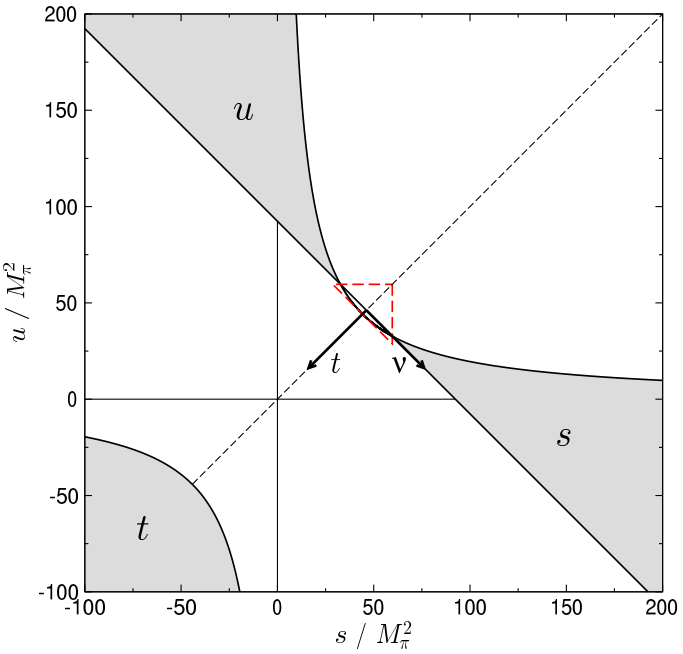

Figure 6.2: Mandelstam plane for πN scattering. The filled areas mark the s-, t-, and u-channel physical regions, the red dashed line the subthreshold triangle, and the arrows the orientation of the plane in t and ν.

The scattering amplitude may be expressed in terms of Lorentz-invariant amplitudes A, B, and D according to

$$\begin{aligned} T^{ba}(s,t) &= \delta^{ba}T^{+}(s,t) + \frac{1}{2}[\tau^b,\tau^a]T^{-}(s,t)\,, \\ T^{I}(s,t) &= \bar{u}(p')\left\{A^I(s,t) + \frac{\not{q}'+\not{q}}{2}B^I(s,t)\right\}u(p) = \bar{u}(p')\left\{D^I(s,t) - \frac{[\not{q}',\not{q}]}{4m}B^I(s,t)\right\}u(p)\,, \\ D^{I}(s,t) &= A^I(s,t) + \nu B^I(s,t)\,, \end{aligned} \tag{6.9}$$

where $I = \pm$, τ^a denotes the Pauli matrices, and the spinors are normalized as $\bar{u}u = 2m$. The pertinent crossing properties become most transparent when the amplitudes are written as functions of ν and t

$$A^{\pm}(\nu,t) = \pm A^{\pm}(-\nu,t)\,, \qquad B^{\pm}(\nu,t) = \mp B^{\pm}(-\nu,t)\,, \qquad D^{\pm}(\nu,t) = \pm D^{\pm}(-\nu,t)\,. \tag{6.10}$$

Moreover, isospin symmetry leaves only two independent amplitudes that are needed to describe all ten πN scattering reactions, characterized by total s-channel isospin $I_s \in \{1/2, 3/2\}$. In agreement with [152], we choose the isospin-doublets of nucleons and antinucleons according to

$$|p\rangle = \left|\frac{1}{2},\frac{1}{2}\right\rangle\,, \qquad |n\rangle = \left|\frac{1}{2},-\frac{1}{2}\right\rangle\,, \qquad |\bar{n}\rangle = \left|\frac{1}{2},\frac{1}{2}\right\rangle\,, \qquad |\bar{p}\rangle = \left|\frac{1}{2},-\frac{1}{2}\right\rangle\,, \tag{6.11}$$

and the isospin-triplet of the pions as

$$|\pi^+\rangle = |1,1\rangle\,, \qquad |\pi^0\rangle = |1,0\rangle\,, \qquad |\pi^-\rangle = |1,-1\rangle\,. \tag{6.12}$$

These conventions imply for the relation between the spherical and the Cartesian components of the pion-multiplet

$$|\pi^{\pm}\rangle = \mp\frac{1}{\sqrt{2}}\big(|\pi_1\rangle \pm i|\pi_2\rangle\big) \,, \qquad |\pi^0\rangle = |\pi_3\rangle \,, \tag{6.13}$$

and for the crossing properties

$$C|p\rangle = |\bar{p}\rangle \,, \qquad C|n\rangle = -|\bar{n}\rangle \,, \qquad C|\pi^{\pm}\rangle = -|\pi^{\mp}\rangle \,, \qquad C|\pi^0\rangle = |\pi^0\rangle \,. \tag{6.14}$$

In this way, the physical πN amplitudes read

$$\begin{aligned}
&\mathcal{A}(\pi^+p\to\pi^+p) = \mathcal{A}(\pi^-n\to\pi^-n) = \mathcal{A}^+ - \mathcal{A}^- = \mathcal{A}^{3/2} \,, \\
&\mathcal{A}(\pi^-p\to\pi^-p) = \mathcal{A}(\pi^+n\to\pi^+n) = \mathcal{A}^+ + \mathcal{A}^- = \frac{1}{3}(2\mathcal{A}^{1/2} + \mathcal{A}^{3/2}) \,, \\
&\mathcal{A}(\pi^-p\to\pi^0n) = \mathcal{A}(\pi^+n\to\pi^0p) = -\sqrt{2}\mathcal{A}^- = -\frac{\sqrt{2}}{3}(\mathcal{A}^{1/2} - \mathcal{A}^{3/2}) \,, \\
&\mathcal{A}(\pi^0p\to\pi^0p) = \mathcal{A}(\pi^0n\to\pi^0n) = \mathcal{A}^+ = \frac{1}{3}(\mathcal{A}^{1/2} + 2\mathcal{A}^{3/2}) \,,
\end{aligned} \tag{6.15}$$

where $\mathcal{A} \in \{A, B, D\}$. These relations can be summarized in matrix notation as

$$\begin{pmatrix}\mathcal{A}^+\\ \mathcal{A}^-\end{pmatrix} = C_{\nu s}\begin{pmatrix}\mathcal{A}^{1/2}\\ \mathcal{A}^{3/2}\end{pmatrix} \,, \qquad \begin{pmatrix}\mathcal{A}^{1/2}\\ \mathcal{A}^{3/2}\end{pmatrix} = C_{s\nu}\begin{pmatrix}\mathcal{A}^+\\ \mathcal{A}^-\end{pmatrix} \,, \qquad C_{\nu s} = \frac{1}{3}C_{s\nu} = \frac{1}{3}\begin{pmatrix}1 & 2\\ 1 & -1\end{pmatrix} \,. \tag{6.16}$$

Similarly, the amplitudes with definite u-channel isospin $I_u \in \{1/2 = N, 3/2 = \Delta\}$ obey the $s \leftrightarrow u$ crossing relations

$$\begin{pmatrix}\mathcal{A}^{1/2}\\ \mathcal{A}^{3/2}\end{pmatrix} = C_{su}\begin{pmatrix}\mathcal{A}^N\\ \mathcal{A}^\Delta\end{pmatrix} \,, \qquad \begin{pmatrix}\mathcal{A}^N\\ \mathcal{A}^\Delta\end{pmatrix} = C_{us}\begin{pmatrix}\mathcal{A}^{1/2}\\ \mathcal{A}^{3/2}\end{pmatrix} \,, \qquad C_{su} = C_{us} = \frac{1}{3}\begin{pmatrix}-1 & 4\\ 2 & 1\end{pmatrix} \,, \tag{6.17}$$

and, in combination with (6.16),

$$\begin{pmatrix}\mathcal{A}^+\\ \mathcal{A}^-\end{pmatrix} = C_{\nu u}\begin{pmatrix}\mathcal{A}^N\\ \mathcal{A}^\Delta\end{pmatrix} \,, \qquad C_{\nu u} = C_{\nu s}C_{su} = \frac{1}{3}\begin{pmatrix}1 & 2\\ -1 & 1\end{pmatrix} \,, \qquad C_{u\nu} = C_{\nu u}^{-1} = \begin{pmatrix}1 & -2\\ 1 & 1\end{pmatrix} \,. \tag{6.18}$$

The t-channel $|\bar{N}N\rangle$ isospin states may be decomposed into states with definite t-channel isospin $|I_t = 1, (I_t)_3\rangle$ and $|I_t = 0, 0\rangle$ according to

$$|\bar{n}p\rangle = |1,1\rangle \,, \qquad |\bar{n}n\rangle = \frac{1}{\sqrt{2}}\big(|1,0\rangle + |0,0\rangle\big) \,, \qquad |\bar{p}p\rangle = \frac{1}{\sqrt{2}}\big(|1,0\rangle - |0,0\rangle\big) \,, \qquad |\bar{p}n\rangle = |1,-1\rangle \,, \tag{6.19}$$

with the inversion

$$|1,0\rangle = \frac{1}{\sqrt{2}}(|\bar{n}n\rangle + |\bar{p}p\rangle) \,, \qquad |0,0\rangle = \frac{1}{\sqrt{2}}(|\bar{n}n\rangle - |\bar{p}p\rangle) \,. \tag{6.20}$$

Using the decomposition of the physical $|\pi\pi\rangle$ states

$$\begin{aligned}
|\pi^+\pi^0\rangle &= \frac{1}{\sqrt{2}}(|2,1\rangle + |1,1\rangle) \,, & |\pi^+\pi^-\rangle &= \frac{1}{\sqrt{6}}|2,0\rangle + \frac{1}{\sqrt{2}}|1,0\rangle + \frac{1}{\sqrt{3}}|0,0\rangle \,, \\
|\pi^-\pi^0\rangle &= \frac{1}{\sqrt{2}}(|2,-1\rangle - |1,-1\rangle) \,, & |\pi^0\pi^0\rangle &= \sqrt{\frac{2}{3}}|2,0\rangle - \frac{1}{\sqrt{3}}|0,0\rangle \,,
\end{aligned} \tag{6.21}$$

we find

$$\begin{aligned}
\mathcal{A}(\bar{p}p \to \pi^+\pi^-) &= -\mathcal{A}^+ + \mathcal{A}^- = -\mathcal{A}^{3/2} = -\frac{1}{\sqrt{6}}\mathcal{A}^0 + \frac{1}{2}\mathcal{A}^1 \,, \\
\mathcal{A}(\bar{p}p \to \pi^-\pi^+) &= -\mathcal{A}^+ - \mathcal{A}^- = -\frac{1}{3}(2\mathcal{A}^{1/2} + \mathcal{A}^{3/2}) = -\frac{1}{\sqrt{6}}\mathcal{A}^0 - \frac{1}{2}\mathcal{A}^1 \,, \\
\mathcal{A}(\bar{n}p \to \pi^+\pi^0) &= \sqrt{2}\mathcal{A}^- = \frac{\sqrt{2}}{3}(\mathcal{A}^{1/2} - \mathcal{A}^{3/2}) = \frac{1}{\sqrt{2}}\mathcal{A}^1 \,, \\
\mathcal{A}(\bar{p}p \to \pi^0\pi^0) &= \mathcal{A}^+ = \frac{1}{3}(\mathcal{A}^{1/2} + 2\mathcal{A}^{3/2}) = \frac{1}{\sqrt{6}}\mathcal{A}^0 \,,
\end{aligned} \tag{6.22}$$

which can be summarized in the $s \leftrightarrow t$ crossing relations

$$\begin{pmatrix}\mathcal{A}^{1/2}\\ \mathcal{A}^{3/2}\end{pmatrix} = C_{st}\begin{pmatrix}\mathcal{A}^0\\ \mathcal{A}^1\end{pmatrix} \,, \qquad \begin{pmatrix}\mathcal{A}^0\\ \mathcal{A}^1\end{pmatrix} = C_{ts}\begin{pmatrix}\mathcal{A}^{1/2}\\ \mathcal{A}^{3/2}\end{pmatrix} \,, \qquad \begin{pmatrix}\mathcal{A}^+\\ \mathcal{A}^-\end{pmatrix} = C_{\nu t}\begin{pmatrix}\mathcal{A}^0\\ \mathcal{A}^1\end{pmatrix} \,, \tag{6.23}$$

with crossing matrices

$$C_{st} = \begin{pmatrix}\frac{1}{\sqrt{6}} & 1\\ \frac{1}{\sqrt{6}} & -\frac{1}{2}\end{pmatrix} \,, \qquad C_{ts} = \frac{2}{3}\begin{pmatrix}\sqrt{\frac{3}{2}} & \sqrt{6}\\ 1 & -1\end{pmatrix} \,, \qquad C_{\nu t} = C_{\nu s}C_{st} = \begin{pmatrix}\frac{1}{\sqrt{6}} & 0\\ 0 & \frac{1}{2}\end{pmatrix} \,. \tag{6.24}$$

This result shows that the amplitudes $\mathcal{A}^+$ and $\mathcal{A}^-$ have well-defined t-channel isospin $I_t = 0$ and $I_t = 1$, respectively. Since the G-parity of the pion is negative, the antinucleon–nucleon initial state in $\bar{N}N \to \pi\pi$ has to have positive G-parity, so that this state can only couple to an even number of pions. Moreover, since

$$G|\bar{N}N\rangle = (-1)^{J+I_t}|\bar{N}N\rangle \,, \tag{6.25}$$

only the combinations of even angular momentum J with $I_t = 0$ and odd J with $I_t = 1$ are permitted. The same selection rules follow from the $\pi\pi$ system, where Bose symmetry gives rise to the same factor $(-1)^{J+I_t}$ due to the parity $(-1)^L$ for an orbital state with total angular momentum $J = L$ and the symmetry/antisymmetry of the pion isosinglet/isotriplet state. These observations are crucial for the t-channel partial-wave expansion of $\mathcal{A}^{I=\pm}$ or $\mathcal{A}^{I_t=0,1}$, which contains only partial waves with even/odd J. According to (6.24), the transition between the $I = \pm$ or $I_t = 0, 1$ bases involves the isospin crossing coefficients c_J

$$c_J = \begin{cases} \frac{1}{\sqrt{6}} & \text{for even } J \,, \\ \frac{1}{2} & \text{for odd } J \,. \end{cases} \tag{6.26}$$

6.3 Roy–Steiner equations

6.3.1 Hyperbolic dispersion relations

The unsubtracted set of HDRs for the πN amplitudes as derived in [68] reads

$$A^+(s,t) = \frac{1}{\pi}\int\limits_{s_+}^{\infty} \mathrm{d}s' \left[\frac{1}{s'-s} + \frac{1}{s'-u} - \frac{1}{s'-a}\right] \mathrm{Im}\, A^+(s',t') + \frac{1}{\pi}\int\limits_{t_\pi}^{\infty} \mathrm{d}t' \, \frac{\mathrm{Im}\, A^+(s',t')}{t'-t} \,,$$

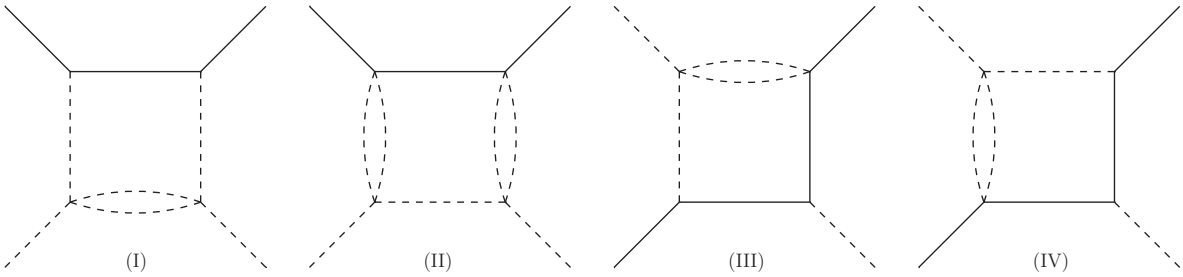

Figure 6.3: Box graphs constraining the boundaries of the double-spectral regions for πN scattering. Solid/dashed lines denote nucleons/pions.

$$
\begin{aligned}
A^-(s,t) &= \frac{1}{\pi}\int\limits_{s_+}^{\infty} \mathrm{d}s' \left[\frac{1}{s'-s}-\frac{1}{s'-u}\right] \mathrm{Im}\, A^-(s',t') + \frac{1}{\pi}\int\limits_{t_\pi}^{\infty} \mathrm{d}t'\, \frac{\nu}{\nu'}\frac{\mathrm{Im}\, A^-(s',t')}{t'-t}\,, \\
B^+(s,t) &= N^+(s,t) + \frac{1}{\pi}\int\limits_{s_+}^{\infty} \mathrm{d}s' \left[\frac{1}{s'-s}-\frac{1}{s'-u}\right] \mathrm{Im}\, B^+(s',t') + \frac{1}{\pi}\int\limits_{t_\pi}^{\infty} \mathrm{d}t'\, \frac{\nu}{\nu'}\frac{\mathrm{Im}\, B^+(s',t')}{t'-t}\,, \\
B^-(s,t) &= N^-(s,t) + \frac{1}{\pi}\int\limits_{s_+}^{\infty} \mathrm{d}s' \left[\frac{1}{s'-s}+\frac{1}{s'-u}-\frac{1}{s'-a}\right] \mathrm{Im}\, B^-(s',t') \\
&\quad + \frac{1}{\pi}\int\limits_{t_\pi}^{\infty} \mathrm{d}t'\, \frac{\mathrm{Im}\, B^-(s',t')}{t'-t}\,,
\end{aligned}
\tag{6.27}
$$

cf. (1.52) and (1.55), with Born-term contributions

$$
N^+(s,t) = g^2\left[\frac{1}{m^2-s}-\frac{1}{m^2-u}\right]\,, \qquad N^-(s,t) = g^2\left[\frac{1}{m^2-s}+\frac{1}{m^2-u}-\frac{1}{m^2-a}\right]\,. \tag{6.28}
$$

We will take $g^2/4\pi = 13.7$ as our central value, cf. (3.18), but adopt $g^2/4\pi = 14.28$ [217] when comparing our results to the KH80 solution. The derivation of a RS system for πN scattering given the HDRs (6.27) proceeds in close analogy to the calculation in Part II, but is considerably more involved due to the more complicated form of the partial-wave expansions for πN scattering. Before we turn to the structure of these equations, we briefly comment on the range of convergence of the final system. Assuming Mandelstam analyticity, the investigation of the box diagrams depicted in Fig. 6.3 along the lines of Sect. 4.4 shows that for the s-channel

$$
\begin{aligned}
a = -23.2 M_\pi^2 \qquad &\Rightarrow \qquad s \in \left[s_+ = (m+M_\pi)^2, 97.3 M_\pi^2\right] = \left[59.6 M_\pi^2, 97.3 M_\pi^2\right] \\
&\Leftrightarrow \qquad W \in [W_+ = 1.08\,\mathrm{GeV}, 1.38\,\mathrm{GeV}]\,,
\end{aligned}
\tag{6.29}
$$

and for the t-channel

$$
\begin{aligned}
a = -2.7 M_\pi^2 \qquad &\Rightarrow \qquad t \in [t_\pi = 4M_\pi^2, 205.5 M_\pi^2] \\
&\Leftrightarrow \qquad \sqrt{t} \in [\sqrt{t_\pi} = 0.28\,\mathrm{GeV}, 2.00\,\mathrm{GeV}]\,,
\end{aligned}
\tag{6.30}
$$

yield the largest domain of validity (for more details of the derivation we refer to [205]). In the following, we will constrain a to the values given in (6.29) and (6.30) for the s- and t-channel part of the system, respectively.

6.3.2 Partial-wave projection

The s-channel partial-wave amplitudes $f_{l\pm}^I(W)$ with isospin index $I = \pm$, orbital angular momentum l, and total angular momentum $j = |l \pm 1/2|$ are defined as [218]

$$f_{l\pm}^I(W) = \frac{1}{16\pi W}\Big\{(E+m)\big[A_l^I(s) + (W-m)B_l^I(s)\big] + (E-m)\big[-A_{l\pm1}^I(s) + (W+m)B_{l\pm1}^I(s)\big]\Big\}\,, \tag{6.31}$$

where

$$X_l^I(s) = \int_{-1}^{1} \mathrm{d}z_s\; P_l(z_s) X^I(s,t)\Big|_{t=-2q^2(1-z_s)}\,, \qquad X \in \{A,B\}\,. \tag{6.32}$$

They fulfill the MacDowell symmetry relation [219] in the complex W-plane

$$f_{l+}^I(W) = -f_{(l+1)-}^I(-W)\,, \tag{6.33}$$

which allows us to restrict the analysis to $f_{l+}^I(W)$ for the time being. Performing the partial-wave expansion of the integrands of (6.27) and subsequent projection onto the s-channel partial waves yields [68]

$$\begin{aligned} f_{l+}^I(W) = N_{l+}^I(W) &+ \frac{1}{\pi}\int_{t_\pi}^{\infty} \mathrm{d}t' \sum_J \Big\{G_{lJ}(W,t')\,\mathrm{Im}\, f_+^J(t') + H_{lJ}(W,t')\,\mathrm{Im}\, f_-^J(t')\Big\} \\ &+ \frac{1}{\pi}\int_{W_+}^{\infty} \mathrm{d}W' \sum_{l'=0}^{\infty}\Big\{K_{ll'}^I(W,W')\,\mathrm{Im}\, f_{l'+}^I(W') + K_{ll'}^I(W,-W')\,\mathrm{Im}\, f_{(l'+1)-}^I(W')\Big\}\,, \end{aligned} \tag{6.34}$$

where $N_{l\pm}^I(W)$ corresponds to the projection of the nucleon pole terms. As mentioned in Sect. 6.1, each partial wave $f_{l\pm}^I(W)$ is coupled to all other s-channel partial waves by means of the kernel functions $K_{ll'}^I(W,W')$. Moreover, the equations involve the t-channel partial waves $f_\pm^J(t)$, with subscript $\pm$ for parallel/antiparallel antinucleon–nucleon helicities and total momentum J, via the kernels $G_{lJ}(W,t')$ and $H_{lJ}(W,t')$. The summation is restricted to even/odd values of J for $I = \pm$. Explicit expressions for $N_{l\pm}^I(W)$ and the kernel functions are provided in Appendix C.1.

The t-channel partial-wave projection reads [220]

$$\begin{aligned} f_+^J(t) &= -\frac{1}{4\pi}\int_0^1 \mathrm{d}z_t\; P_J(z_t)\left\{\frac{p_t^2}{(p_t q_t)^J} A^I(s,t)\Big|_{s=s(t,z_t)} - \frac{m}{(p_t q_t)^{J-1}} z_t B^I(s,t)\Big|_{s=s(t,z_t)}\right\}, \\ f_-^J(t) &= \frac{1}{4\pi}\frac{\sqrt{J(J+1)}}{2J+1}\frac{1}{(p_t q_t)^{J-1}}\int_0^1 \mathrm{d}z_t\Big[P_{J-1}(z_t) - P_{J+1}(z_t)\Big] B^I(s,t)\Big|_{s=s(t,z_t)}\,, \end{aligned} \tag{6.35}$$

where the integration has been restricted to half the angular interval by virtue of Bose symmetry, and again $I = \pm$ corresponds to even/odd J. The result for the t-channel equations

takes the form

$$
\begin{aligned}
f_+^J(t) &= \tilde{N}_+^J(t) + \frac{1}{\pi}\int\limits_{W_+}^{\infty} \mathrm{d}W' \sum_{l=0}^{\infty} \Big\{ \tilde{G}_{Jl}(t,W')\,\mathrm{Im}\, f_{l+}^I(W') + \tilde{G}_{Jl}(t,-W')\,\mathrm{Im}\, f_{(l+1)-}^I(W') \Big\} \\
&\quad + \frac{1}{\pi}\int\limits_{t_\pi}^{\infty} \mathrm{d}t' \sum_{J'} \Big\{ \tilde{K}^1_{JJ'}(t,t')\,\mathrm{Im}\, f_+^{J'}(t') + \tilde{K}^2_{JJ'}(t,t')\,\mathrm{Im}\, f_-^{J'}(t') \Big\} \,, \\
f_-^J(t) &= \tilde{N}_-^J(t) + \frac{1}{\pi}\int\limits_{W_+}^{\infty} \mathrm{d}W' \sum_{l=0}^{\infty} \Big\{ \tilde{H}_{Jl}(t,W')\,\mathrm{Im}\, f_{l+}^I(W') + \tilde{H}_{Jl}(t,-W')\,\mathrm{Im}\, f_{(l+1)-}^I(W') \Big\} \\
&\quad + \frac{1}{\pi}\int\limits_{t_\pi}^{\infty} \mathrm{d}t' \sum_{J'} \tilde{K}^3_{JJ'}(t,t')\,\mathrm{Im}\, f_-^{J'}(t') \,,
\end{aligned}
\tag{6.36}
$$

where the sum over J' runs over even/odd values of J' if J is even/odd. In contrast to the s-channel equations, we have $\tilde{K}^{1,2,3}_{JJ'}(t,t') = 0$ for all $J' < J$, which implies that a given t-channel partial wave only receives contributions from the absorptive parts of higher partial waves. Explicit expressions for Born terms and kernel functions are relegated to Appendix C.2.

In order to combine analyticity with partial-wave unitarity, the equations have to be cast into a form that permits diagonal s-channel partial-wave unitarity relations (see Sect. 6.4). Therefore, we work in the s-channel isospin basis $I_s \in \{1/2, 3/2\}$ instead of the $I = \pm$ basis. Using the definitions

$$
\begin{pmatrix} X^{1/2} \\ X^{3/2} \end{pmatrix} = C_{s\nu} \begin{pmatrix} X^+ \\ X^- \end{pmatrix} \,, \qquad \begin{pmatrix} X^+ \\ X^- \end{pmatrix} = C_{\nu s} \begin{pmatrix} X^{1/2} \\ X^{3/2} \end{pmatrix} \,, \qquad X \in \{ f_{l\pm}, N_{l\pm}, K_{ll'} \} \,,
\tag{6.37}
$$

and

$$
K_{ll'}^{1/2+3/2}(W,W') = K_{ll'}^{1/2}(W,W') + K_{ll'}^{3/2}(W,W') = 2K_{ll'}^{+}(W,W') + K_{ll'}^{-}(W,W') \,,
\tag{6.38}
$$

the complete system of RS equations becomes

$$
\begin{aligned}
f_{l+}^{1/2}(W) &= N_{l+}^{1/2}(W) \\
&\quad + \frac{1}{\pi}\int\limits_{W_+}^{\infty} \mathrm{d}W' \sum_{l'=0}^{\infty} \frac{1}{3} \Big\{ K_{ll'}^{1/2}(W,W')\,\mathrm{Im}\, f_{l'+}^{1/2}(W') + 2K_{ll'}^{3/2}(W,W')\,\mathrm{Im}\, f_{l'+}^{3/2}(W') \\
&\qquad + K_{ll'}^{1/2}(W,-W')\,\mathrm{Im}\, f_{(l'+1)-}^{1/2}(W') + 2K_{ll'}^{3/2}(W,-W')\,\mathrm{Im}\, f_{(l'+1)-}^{3/2}(W') \Big\} \\
&\quad + \frac{1}{\pi}\int\limits_{t_\pi}^{\infty} \mathrm{d}t' \sum_{J=0}^{\infty} \frac{\big(3-(-1)^J\big)}{2} \Big\{ G_{lJ}(W,t')\,\mathrm{Im}\, f_+^J(t') + H_{lJ}(W,t')\,\mathrm{Im}\, f_-^J(t') \Big\} \,, \\
f_{l+}^{3/2}(W) &= N_{l+}^{3/2}(W) \\
&\quad + \frac{1}{\pi}\int\limits_{W_+}^{\infty} \mathrm{d}W' \sum_{l'=0}^{\infty} \frac{1}{3} \Big\{ K_{ll'}^{3/2}(W,W')\,\mathrm{Im}\, f_{l'+}^{1/2}(W') + K_{ll'}^{1/2+3/2}(W,W')\,\mathrm{Im}\, f_{l'+}^{3/2}(W') \\
&\qquad + K_{ll'}^{3/2}(W,-W')\,\mathrm{Im}\, f_{(l'+1)-}^{1/2}(W') + K_{ll'}^{1/2+3/2}(W,-W')\,\mathrm{Im}\, f_{(l'+1)-}^{3/2}(W') \Big\}
\end{aligned}
$$

$$
\begin{aligned}
&+\frac{1}{\pi}\int\limits_{t_\pi}^{\infty}\mathrm{d}t'\sum_{J=0}^{\infty}(-1)^J\Big\{G_{lJ}(W,t')\,\mathrm{Im}\,f_+^J(t')+H_{lJ}(W,t')\,\mathrm{Im}\,f_-^J(t')\Big\}\,,\\
f^{1/2}_{(l+1)-}(W)&=N^{1/2}_{(l+1)-}(W)\\
&-\frac{1}{\pi}\int\limits_{W_+}^{\infty}\mathrm{d}W'\sum_{l'=0}^{\infty}\frac{1}{3}\Big\{K^{1/2}_{ll'}(-W,W')\,\mathrm{Im}\,f^{1/2}_{l'+}(W')+2K^{3/2}_{ll'}(-W,W')\,\mathrm{Im}\,f^{3/2}_{l'+}(W')\\
&\qquad+K^{1/2}_{ll'}(-W,-W')\,\mathrm{Im}\,f^{1/2}_{(l'+1)-}(W')+2K^{3/2}_{ll'}(-W,-W')\,\mathrm{Im}\,f^{3/2}_{(l'+1)-}(W')\Big\}\\
&-\frac{1}{\pi}\int\limits_{t_\pi}^{\infty}\mathrm{d}t'\sum_{J=0}^{\infty}\frac{\big(3-(-1)^J\big)}{2}\Big\{G_{lJ}(-W,t')\,\mathrm{Im}\,f_+^J(t')+H_{lJ}(-W,t')\,\mathrm{Im}\,f_-^J(t')\Big\}\,,\\
f^{3/2}_{(l+1)-}(W)&=N^{3/2}_{(l+1)-}(W)\\
&-\frac{1}{\pi}\int\limits_{W_+}^{\infty}\mathrm{d}W'\sum_{l'=0}^{\infty}\frac{1}{3}\Big\{K^{3/2}_{ll'}(-W,W')\,\mathrm{Im}\,f^{1/2}_{l'+}(W')+K^{1/2+3/2}_{ll'}(-W,W')\,\mathrm{Im}\,f^{3/2}_{l'+}(W')\\
&\qquad+K^{3/2}_{ll'}(-W,-W')\,\mathrm{Im}\,f^{1/2}_{(l'+1)-}(W')+K^{1/2+3/2}_{ll'}(-W,-W')\,\mathrm{Im}\,f^{3/2}_{(l'+1)-}(W')\Big\}\\
&-\frac{1}{\pi}\int\limits_{t_\pi}^{\infty}\mathrm{d}t'\sum_{J=0}^{\infty}(-1)^J\Big\{G_{lJ}(-W,t')\,\mathrm{Im}\,f_+^J(t')+H_{lJ}(-W,t')\,\mathrm{Im}\,f_-^J(t')\Big\}\,,
\end{aligned}
\tag{6.39}
$$

and

$$
\begin{aligned}
f_+^J(t)&=\tilde N_+^J(t)+\frac{1}{\pi}\int\limits_{W_+}^{\infty}\mathrm{d}W'\sum_{l=0}^{\infty}\frac{1}{3}\Big\{\tilde G_{Jl}(t,W')\Big[\mathrm{Im}\,f^{1/2}_{l+}(W')+\frac{1+3(-1)^J}{2}\mathrm{Im}\,f^{3/2}_{l+}(W')\Big]\\
&\qquad+\tilde G_{Jl}(t,-W')\Big[\mathrm{Im}\,f^{1/2}_{(l+1)-}(W')+\frac{1+3(-1)^J}{2}\mathrm{Im}\,f^{3/2}_{(l+1)-}(W')\Big]\Big\}\\
&\quad+\frac{1}{\pi}\int\limits_{t_\pi}^{\infty}\mathrm{d}t'\sum_{J'=J}^{\infty}\frac{1+(-1)^{J+J'}}{2}\Big\{\tilde K^1_{JJ'}(t,t')\,\mathrm{Im}\,f_+^{J'}(t')+\tilde K^2_{JJ'}(t,t')\,\mathrm{Im}\,f_-^{J'}(t')\Big\}\,,\\
f_-^J(t)&=\tilde N_-^J(t)+\frac{1}{\pi}\int\limits_{W_+}^{\infty}\mathrm{d}W'\sum_{l=0}^{\infty}\frac{1}{3}\Big\{\tilde H_{Jl}(t,W')\Big[\mathrm{Im}\,f^{1/2}_{l+}(W')+\frac{1+3(-1)^J}{2}\mathrm{Im}\,f^{3/2}_{l+}(W')\Big]\\
&\qquad+\tilde H_{Jl}(t,-W')\Big[\mathrm{Im}\,f^{1/2}_{(l+1)-}(W')+\frac{1+3(-1)^J}{2}\mathrm{Im}\,f^{3/2}_{(l+1)-}(W')\Big]\Big\}\\
&\quad+\frac{1}{\pi}\int\limits_{t_\pi}^{\infty}\mathrm{d}t'\sum_{J'=J}^{\infty}\frac{1+(-1)^{J+J'}}{2}\tilde K^3_{JJ'}(t,t')\,\mathrm{Im}\,f_-^{J'}(t')\,.
\end{aligned}
\tag{6.40}
$$

In these equations, all sums run over both even and odd values, but those over J' in the t-channel part (6.40) are restricted to $J'\geq J$ due to (C.39). The equations for $f^I_{(l+1)-}(W)$ are given here merely for convenience, as they could be obtained by means of MacDowell symmetry (6.33).

	parameters		1-sub	2-sub	3-sub	ex 3-sub
M_π^{-1}	$a_{00}^+ = d_{00}^+$		d_{00}^+	d_{00}^+	d_{00}^+	d_{00}^+
M_π^{-2}	$a_{00}^- = d_{00}^- - b_{00}^-$		b_{00}^-	b_{00}^-, a_{00}^-	b_{00}^-, a_{00}^-	b_{00}^-, a_{00}^-
M_π^{-3}	$a_{01}^+ = d_{01}^+$,	$a_{10}^+ = d_{10}^+ - b_{00}^+$		d_{01}^+, b_{00}^+	d_{01}^+, b_{00}^+, a_{10}^+	d_{01}^+, b_{00}^+, a_{10}^+
M_π^{-4}	$a_{01}^- = d_{01}^- - b_{01}^-$,	$a_{10}^- = d_{10}^- - b_{10}^-$		b_{01}^-	b_{01}^-, a_{01}^-	b_{01}^-, a_{01}^-, b_{10}^-, a_{10}^-

Table 6.1: Subthreshold parameters in the different subtraction schemes.

6.3.3 Subtractions

The introduction of subtractions is essential to suppress the high-energy regime and derive constraints that solely involve low-energy physics. The most convenient choice for the subtraction point is provided by the subthreshold point at $(\nu = 0, t = 0)$, since the relation to the Cheng–Dashen point and the pion–nucleon σ term can be established in a straightforward manner, while the subtraction constants are given directly in terms of subthreshold parameters. In addition, this choice of the subtraction point should prove favorable for matching to ChPT, which is expected to be most reliable in the subthreshold region (for an application of heavy-baryon ChPT to πN scattering inside the Mandelstam triangle see [139]).

The subthreshold expansion in πN scattering is conventionally applied to the pseudovector-Born-term-subtracted amplitudes

$$\begin{aligned} \bar{A}^+(s,t) &= A^+(s,t) - \frac{g^2}{m}\,, & \bar{B}^+(s,t) &= B^+(s,t) - g^2\left[\frac{1}{m^2-s} - \frac{1}{m^2-u}\right]\,, \\ \bar{A}^-(s,t) &= A^-(s,t)\,, & \bar{B}^-(s,t) &= B^-(s,t) - g^2\left[\frac{1}{m^2-s} + \frac{1}{m^2-u}\right] + \frac{g^2}{2m^2}\,. \end{aligned} \tag{6.41}$$

Separating factors of ν that are required by crossing symmetry, these amplitudes allow for the expansions

$$\begin{aligned} \bar{A}^+(\nu,t) &= \sum_{m,n=0}^{\infty} a_{mn}^+ \nu^{2m} t^n\,, & \bar{B}^+(\nu,t) &= \sum_{m,n=0}^{\infty} b_{mn}^+ \nu^{2m+1} t^n\,, \\ \bar{A}^-(\nu,t) &= \sum_{m,n=0}^{\infty} a_{mn}^- \nu^{2m+1} t^n\,, & \bar{B}^-(\nu,t) &= \sum_{m,n=0}^{\infty} b_{mn}^- \nu^{2m} t^n\,, \end{aligned} \tag{6.42}$$

and similarly for $\bar{D}^\pm = \bar{A}^\pm + \nu\bar{B}^\pm$. The corresponding subthreshold parameters fulfill the relations

$$d_{mn}^+ = a_{mn}^+ + b_{m-1,n}^+\,, \qquad d_{mn}^- = a_{mn}^- + b_{mn}^-\,, \qquad d_{0n}^+ = a_{0n}^+\,. \tag{6.43}$$

The implementation of subtractions into the RS system again proceeds in close analogy to Part II. Expanding (6.27) around $(s = s_0, t = 0)$ and equating the coefficients to the subthreshold expansion yields sum rules for the subthreshold parameters that, once subtracted from (6.27), lead to a subtracted version of the RS equations. We will consider several variants thereof: first, we perform a simultaneous expansion around $s = s_0$ and $t = 0$ up to first and second order in both variables, which we will refer to as "1-sub" and "2-sub", respectively. Moreover, we implement a partial third subtraction ("3-sub") that involves two additional

subthreshold parameters only affected at third order in the (s,t) expansion. For the s-channel projection, we consider an extended version of this scenario including two further parameters ("ex 3-sub"). Table 6.1 delineates which subthreshold parameters, ordered by their dimension in inverse powers of M_π, are required for a particular subtraction scheme.

The motivation to deviate from the strict expansion in s and t originates from the observation that this counting favors certain subthreshold parameters of higher dimension. For instance, the twice-subtracted version includes the $\mathcal{O}(M_\pi^{-4})$ parameter b_{01}^-, while the $\mathcal{O}(M_\pi^{-3})$ parameter a_{10}^+ is not yet included. Furthermore, apart from a_{0n}^+ all subthreshold parameters can be canonically ordered in pairs, as shown in the second column of Table 6.1, which suggests that if b_{01}^- is incorporated, a_{01}^- or, equivalently, d_{01}^-, should be as well. Both of these amendments are reflected in the "3-sub" version. Indeed, we will see in Chapter 7 that this scenario translates into PWDRs for the t-channel partial waves with the same number of subtractions for a given angular momentum J. In contrast, for the once- and twice-subtracted versions, the equations for $f_+^J(t)$ and $f_-^J(t)$ involve a different number of subtractions. Finally, counting the multiplicity of solutions for the s-channel RS equations shows that if the hadronic-atom values for the S-wave scattering lengths are imposed as constraints on the solution, two additional parameters may be introduced, cf. Chapter 8. Table 6.1 suggests to choose these as b_{10}^- and a_{10}^-, since then all subthreshold parameters of dimension $\mathcal{O}(M_\pi^{-4})$ are incorporated into the system, which motivates to consider the "ex 3-sub" version for the s-channel problem.

The explicit form of the sum rules for the subthreshold parameters listed in Table 6.1, the subtracted version of the HDRs (6.27), and the necessary modifications of the kernel functions are summarized in Appendix C.3.

6.4 Partial-wave unitarity relations

Unitarity of the S-matrix $S = \mathbb{1} + i\,T$ demands that, evaluated between initial and final states $|i\rangle$ and $|f\rangle$, the T-matrix must fulfill

$$\langle f|T|i\rangle - \langle f|T^\dagger|i\rangle = i \sum_{\{j\}} \int \mathrm{d}\Pi_{n_j}^{(j)} \langle f|T^\dagger|j\rangle\langle j|T|i\rangle \;, \tag{6.44}$$

where the sum extends over all intermediate states $|j\rangle$, and $\mathrm{d}\Pi_{n_j}^{(j)}$ denotes the n_j-particle phase space.[2] For interactions invariant under time reversal, such as strong interactions, (6.44) amounts to the following condition for the invariant amplitudes T_{fi}

$$\mathrm{Im}\, T_{fi} = \frac{1}{2} \sum_{\{j\}} \int \mathrm{d}\Pi_{n_j}^{(j)} (2\pi)^4 \delta^{(4)}(\Sigma p_j - \Sigma p_i) T_{fj}^* T_{ji} \;, \tag{6.45}$$

once energy-momentum conservation $\delta^{(4)}(\Sigma p_f - \Sigma p_i)$ is separated (p_i, p_f, and p_j denote initial-, final-, and intermediate-state momenta, respectively). For a generic two-by-two scattering process with two-particle intermediate state $|j\rangle$, (6.45) reduces to

$$\mathrm{Im}\, T_{fi} = \frac{1}{S_j} \frac{|\mathbf{p}_j|}{8\pi\sqrt{s}} \int \frac{\mathrm{d}\Omega_j}{4\pi} T_{fj}^* T_{ji} \;, \tag{6.46}$$

[2] The phase space is understood to be implicitly supplemented with a symmetry factor $1/n_j!$ for each set of n_j identical intermediate-state particles.

with CMS momentum $\mathbf{p}_j$ and symmetry factor $S_j = 2$ or $S_j = 1$ in the case of identical/non-identical particles. In these conventions, the differential cross section becomes

$$\frac{\mathrm{d}\sigma_{fi}}{\mathrm{d}\Omega} = \frac{|\mathbf{p}_f|}{|\mathbf{p}_i|}\left|\frac{T_{fi}}{8\pi\sqrt{s}}\right|^2 , \tag{6.47}$$

where $\mathbf{p}_i$ and $\mathbf{p}_f$ are the CMS momenta for the initial and final state.

Unitarity in the form (6.46) still involves amplitudes $T_{fi}(s,t)$ with the full kinematic dependence of the scattering process and leaves the angular integration $\mathrm{d}\Omega_j$ to be performed. Therefore, the explicit restrictions from unitarity are most conveniently derived invoking a partial-wave decomposition of T_{fi}, which leads to separate unitarity relations for the single-variable partial-wave amplitudes corresponding to a given angular momentum J. In the helicity formalism, the general partial-wave expansion for a process $a+b \to c+d$ with particle helicities λ_P reads [196]

$$T_{fi}^{\lambda_c,\lambda_d;\lambda_a,\lambda_b}(s,t) = \sqrt{S_f S_i}16\pi \sum_J (2J+1) T^J_{\lambda_c,\lambda_d;\lambda_a,\lambda_b}(s) d^J_{\lambda_a-\lambda_b,\lambda_c-\lambda_d}(\theta) , \tag{6.48}$$

with CMS scattering angle θ, azimuthal angle φ set to zero, and final-/initial-state symmetry factors S_f and S_i defined in analogy to S_j. The ensuing partial-wave unitarity relations become particularly simple if the matrix $T^J(s)$ in helicity space is diagonal, which e.g. for πN scattering holds true for the s-channel isospin basis $I_s \in \{1/2, 3/2\}$, but not for the $I = \pm$ basis. Assuming further that $|i\rangle = |f\rangle$, elastic unitarity in the form (6.46) yields for each diagonal element $T^J_\lambda(s)$ of $T^J(s)$

$$\mathrm{Im}\, T^J_\lambda(s) = \frac{2|\mathbf{p}|}{\sqrt{s}}\left|T^J_\lambda(s)\right|^2 \tag{6.49}$$

(with CMS momentum $\mathbf{p}$). In this normalization, $T^J_\lambda(s)$ may be expressed in terms of phase shifts $\delta^J_\lambda(s)$ according to

$$T^J_\lambda(s) = \frac{\sqrt{s}}{2|\mathbf{p}|}\sin\delta^J_\lambda(s) e^{i\delta^J_\lambda(s)} , \tag{6.50}$$

and related to the S-matrix elements by

$$S^J_\lambda(s) = e^{2i\delta^J_\lambda(s)} = 1 + i\frac{4|\mathbf{p}|}{\sqrt{s}} T^J_\lambda(s) . \tag{6.51}$$

Inelastic contributions are accounted for by introducing inelasticity parameters $0 \leq \eta^J_\lambda(s) \leq 1$ into these parameterizations.

The partial waves for s-channel πN scattering are conventionally parameterized in terms of phase shifts $\delta^{I_s}_{l\pm}$ and inelasticities $\eta^{I_s}_{l\pm}$ as

$$f^{I_s}_{l\pm}(W) = \frac{\left[S^{I_s}_{l\pm}(W)\right]_{\pi N\to\pi N} - 1}{2i|\mathbf{q}|} = \frac{\eta^{I_s}_{l\pm}(W) e^{2i\delta^{I_s}_{l\pm}(W)} - 1}{2i|\mathbf{q}|} \overset{W<W_{\mathrm{inel}}}{=} \frac{e^{i\delta^{I_s}_{l\pm}(W)}\sin\delta^{I_s}_{l\pm}(W)}{|\mathbf{q}|} , \tag{6.52}$$

where the first inelastic threshold due to $\pi\pi N$ intermediate states occurs at $W_{\mathrm{inel}} = W_+ + M_\pi$. In this normalization, the unitarity relation becomes

$$\mathrm{Im}\, f^{I_s}_{l\pm}(W) = |\mathbf{q}|\left|f^{I_s}_{l\pm}(W)\right|^2 \theta\big(W - W_+\big) + \frac{1 - \big(\eta^{I_s}_{l\pm}(W)\big)^2}{4|\mathbf{q}|}\,\theta\big(W - W_{\mathrm{inel}}\big) . \tag{6.53}$$

The derivation of the t-channel unitarity relations is complicated by the fact that the the corresponding reaction is necessarily inelastic. For instance, the contribution from $\pi\pi$ intermediate states alone yields

$$\mathrm{Im}\, f_\pm^J(t) = \sigma_t^\pi \big(t_J^{I_t}(t)\big)^* f_\pm^J(t)\, \theta\big(t - t_\pi\big) \tag{6.54}$$

(with $\pi\pi$ partial waves $t_J^{I_t}(t)$), which proves Watson's theorem [201] for $f_\pm^J(t)$. However, (6.54) is invariant under rescaling of $f_\pm^J(t)$ with arbitrary real factors, so that the correct normalization and relation to the S-matrix element can only be inferred relative to the pertinent elastic reactions. In the following, we will illustrate this procedure for a coupled system of $\pi\pi$, $\bar{K}K$, and $\bar{N}N$ states.

First, we collect all the partial-wave amplitudes involved in the full system. The precise definition of the $\pi\pi$ partial waves $t_J^{I_t}(t)$ is provided by

$$T^{I_t}(s,t) = 32\pi \sum_{J=0}^{\infty} (2J+1) t_J^{I_t}(t) P_J(\cos\theta^{\pi\pi}) \,, \tag{6.55}$$

with CMS scattering angle $\theta^{\pi\pi}$ and normalization

$$\frac{\mathrm{d}\sigma_{\pi\pi\to\pi\pi}^{I_t}}{\mathrm{d}\Omega} = \left| \frac{T^{I_t}(s,t)}{8\pi\sqrt{t}} \right|^2 \,. \tag{6.56}$$

Elastic unitarity then implies

$$\mathrm{Im}\, t_J^{I_t}(t) = \sigma_t^\pi \big| t_J^{I_t}(t) \big|^2 \theta\big(t - t_\pi\big) \,, \qquad t_J^{I_t}(t) = \frac{e^{i\delta_J^{I_t}(t)} \sin\delta_J^{I_t}(t)}{\sigma_t^\pi} \,. \tag{6.57}$$

The t-channel partial waves $f_\pm^J(t)$ are related to the helicity amplitudes $F_{\bar{\lambda}\lambda}(s,t)$ by [220]

$$\begin{aligned}
F_{++}(s,t) = F_{--}(s,t) &= \frac{4\pi\sqrt{t}}{q_t} \sum_{J=0}^{\infty} (2J+1) F_+^J(t) P_J(\cos\theta_t) \,, \\
F_{+-}(s,t) = -F_{-+}(s,t) &= \frac{4\pi\sqrt{t}}{q_t} \sum_{J=1}^{\infty} \frac{2J+1}{\sqrt{J(J+1)}} F_-^J(t) \sin\theta_t P_J'(\cos\theta_t) \,, \\
F_+^J(t) = \frac{q_t}{p_t} (p_t q_t)^J \frac{2}{\sqrt{t}} f_+^J(t) \,, &\qquad F_-^J(t) = \frac{q_t}{p_t} (p_t q_t)^J f_-^J(t) \,,
\end{aligned} \tag{6.58}$$

with normalization of the spin-averaged cross section

$$\frac{\mathrm{d}\bar{\sigma}_{\pi\pi\to\bar{N}N}}{\mathrm{d}\Omega} = \frac{p_t}{q_t} \sum_{\bar{\lambda},\lambda} \left| \frac{F_{\bar{\lambda}\lambda}(s,t)}{8\pi\sqrt{t}} \right|^2 = \frac{2p_t}{q_t} \left\{ \left| \frac{F_{++}(s,t)}{8\pi\sqrt{t}} \right|^2 + \left| \frac{F_{+-}(s,t)}{8\pi\sqrt{t}} \right|^2 \right\} \,. \tag{6.59}$$

The partial waves for $\pi\pi \to \bar{K}K$ are defined by

$$G^{I_t}(s,t) = 16\pi\sqrt{2} \sum_{J=0}^{\infty} (2J+1) (k_t q_t)^J g_J^{I_t}(t) P_J(\cos\theta_t^{\pi K}) \,, \qquad k_t = \sqrt{\frac{t}{4} - M_K^2} = \frac{\sqrt{t}}{2} \sigma_t^K \,, \tag{6.60}$$

and

$$\frac{\mathrm{d}\sigma^{I_t}_{\pi\pi\to\bar{K}K}}{\mathrm{d}\Omega} = \frac{k_t}{q_t}\left|\frac{G^{I_t}(s,t)}{8\pi\sqrt{t}}\right|^2 . \tag{6.61}$$

Finally, we need the $\bar{K}K$ partial waves $r_J^{I_t}(t)$

$$R^{I_t}(s,t) = 16\pi\sum_{J=0}^{\infty}(2J+1)r_J^{I_t}(t)P_J(\cos\theta_t^{\bar{K}K}) , \qquad \frac{\mathrm{d}\sigma^{I_t}_{\bar{K}K\to\bar{K}K}}{\mathrm{d}\Omega} = \left|\frac{R^{I_t}(s,t)}{8\pi\sqrt{t}}\right|^2 , \tag{6.62}$$

and the $\bar{K}K \to \bar{N}N$ amplitudes $h_\pm^J(t)$, the KN analogs of $f_\pm^J(t)$. Our conventions for these partial waves are summarized in Appendix C.4.

With the T-matrix elements $T_{11} = T_{\pi\pi\to\pi\pi}$, $T_{12} = T_{\bar{K}K\to\pi\pi}$, $T_{13} = T_{\bar{N}N\to\pi\pi}$ etc., unitarity in the multi-channel case requires

$$S^*_{fj}S_{ji} = \delta_{fi} , \qquad S_{fi} = \delta_{fi} + iT_{fi} = \delta_{if} + iT_{if} = S_{if} . \tag{6.63}$$

In particular, one finds

$$|S_{11}|^2 + |S_{12}|^2 + |S_{13}|^2 = 1 \quad \Rightarrow \quad 2\,\mathrm{Im}\,T_{11} = |T_{11}|^2 + |T_{12}|^2 + |T_{13}|^2 , \tag{6.64}$$

and

$$S^*_{11}S_{13} + S^*_{12}S_{23} + S^*_{13}S_{33} = 0 \quad \Rightarrow \quad 2\,\mathrm{Im}\,T_{13} = T^*_{11}T_{13} + T^*_{12}T_{23} + T^*_{13}T_{33} . \tag{6.65}$$

Taking into account the different helicity projections, (6.64) in the t-channel isospin basis becomes

$$\left|\left[S_J^{I_t}(t)\right]_{\pi\pi\to\pi\pi}\right|^2 + \left|\left[S_J^{I_t}(t)\right]_{\pi\pi\to\bar{K}K}\right|^2 + 2\left\{\left|\left[S_+^J(t)\right]^{I_t}_{\pi\pi\to\bar{N}N}\right|^2 + \left|\left[S_-^J(t)\right]^{I_t}_{\pi\pi\to\bar{N}N}\right|^2\right\} = 1 , \tag{6.66}$$

while the explicit form of (6.46) for $\pi\pi$ scattering with $\pi\pi$, $\bar{K}K$, and $\bar{N}N$ intermediate states leads to

$$\begin{aligned}\mathrm{Im}\,t_J^{I_t}(t) = {}& \sigma_t^\pi\left|t_J^{I_t}(t)\right|^2\theta\big(t-t_\pi\big) + (k_tq_t)^{2J}\sigma_t^K\left|g_J^{I_t}(t)\right|^2\theta\big(t-t_K\big) \\ & + \frac{t}{16q_t^2}\frac{\sigma_t^N}{c_J^2}\left\{\left|F_+^J(t)\right|^2 + \left|F_-^J(t)\right|^2\right\}\theta\big(t-t_N\big) .\end{aligned} \tag{6.67}$$

In this way, the comparison of (6.66) and (6.67), successively for $t < t_K$, $t < t_N$, and $t > t_N$ determines the relation between S-matrix elements and partial waves

$$\begin{aligned}&\left[S_J^{I_t}(t)\right]_{\pi\pi\to\pi\pi} = 1 + i\frac{4q_t}{\sqrt{t}}t_J^{I_t}(t)\,\theta\big(t-t_\pi\big) , \qquad \left[S_J^{I_t}(t)\right]_{\pi\pi\to\bar{K}K} = i\frac{4(k_tq_t)^{J+\frac{1}{2}}}{\sqrt{t}}g_J^{I_t}(t)\,\theta\big(t-t_K\big) , \\ &\left[S_\pm^J(t)\right]^{I_t}_{\pi\pi\to\bar{N}N} = \frac{i}{c_J\sqrt{2}}\sqrt{\frac{p_t}{q_t}}F_\pm^J(t)\,\theta\big(t-t_N\big) .\end{aligned} \tag{6.68}$$

In fact, these relations already imply interesting constraints on the partial waves that follow from the unitarity bound $|S_{ij}| \le 1$, e.g. the asymptotic behavior of $f_\pm^J(t)$ for $t\to\infty$ will be restricted by

$$f_+^J(t) = \mathcal{O}\big(t^{-J+\frac{1}{2}}\big) , \qquad f_-^J(t) = \mathcal{O}\big(t^{-J}\big) . \tag{6.69}$$

Similarly, unitarity for $\bar{K}K$ scattering

$$\begin{aligned}\operatorname{Im} r_J^{I_t}(t) = (k_t q_t)^{2J}\sigma_t^\pi \left|g_J^{I_t}(t)\right|^2 \theta\big(t-t_\pi\big) + \sigma_t^K \left|r_J^{I_t}(t)\right|^2 \theta\big(t-t_K\big) \\ + \frac{t}{8k_t^2}\frac{\sigma_t^N}{(c_J^{KN})^2}\Big\{\left|H_+^J(t)\right|^2 + \left|H_-^J(t)\right|^2\Big\}\theta\big(t-t_N\big)\end{aligned} \tag{6.70}$$

settles the normalization of the remaining partial waves

$$\big[S_J^{I_t}(t)\big]_{\bar{K}K\to\bar{K}K} = 1 + i\frac{4k_t}{\sqrt{t}} r_J^{I_t}(t)\,\theta\big(t-t_K\big)\,, \qquad \big[S_\pm^J(t)\big]^{I_t}_{\bar{K}K\to\bar{N}N} = \frac{i}{c_J^{KN}}\sqrt{\frac{p_t}{k_t}} H_\pm^J(t)\,\theta\big(t-t_N\big)\,. \tag{6.71}$$

Once the relations between S-matrix elements and partial-wave amplitudes are established, the unitarity relations for $f_\pm^J(t)$ and $h_\pm^J(t)$ including $\pi\pi$ and $\bar{K}K$ intermediate states follow from (6.65) and its analog for $\operatorname{Im} T_{23}$

$$\begin{aligned}\operatorname{Im} f_\pm^J(t) &= \sigma_t^\pi \big(t_J^{I_t}(t)\big)^* f_\pm^J(t)\,\theta\big(t-t_\pi\big) + \frac{\sqrt{2}\,c_J}{c_J^{KN}} k_t^{2J}\sigma_t^K \big(g_J^{I_t}(t)\big)^* h_\pm^J(t)\,\theta\big(t-t_K\big)\,, \\ \operatorname{Im} h_\pm^J(t) &= \sigma_t^K \big(r_J^{I_t}(t)\big)^* h_\pm^J(t)\,\theta\big(t-t_K\big) + \frac{c_J^{KN}}{\sqrt{2}\,c_J}\,\sigma_t^\pi q_t^{2J} \big(g_J^{I_t}(t)\big)^* f_\pm^J(t)\,\theta\big(t-t_\pi\big)\,.\end{aligned} \tag{6.72}$$

The factors c_J and c_J^{KN} originate from the transition between the $I_t = 0, 1$ and the $I = \pm$ bases in πN and KN scattering, since the derivation of the unitarity relations proceeds in the isospin basis, whereas the t-channel πN and KN partial waves are defined from the $I = \pm$ amplitudes. Moreover, the additional factor $\sqrt{2}$ is a remnant from a symmetry factor in the $\pi\pi$ system that occurs since this factor is not included in the conventional definition of the $\pi\pi \to \bar{N}N$ partial waves (6.58). In contrast, these symmetry factors as required by the general result (6.48) are included in the definition of the $\pi\pi$ and $\pi\pi \to \bar{K}K$ partial waves in (6.55) and (6.60), otherwise they would occur in (6.72) as well.

The structure of (6.72) can be made more apparent by noting that by virtue of unitarity in the $\pi\pi/\bar{K}K$ system the pertinent T-matrix becomes

$$T_J(t) = \begin{pmatrix} \frac{\eta_J^{I_t}(t) e^{2i\delta_J^{I_t}(t)} - 1}{2i\sigma_t^\pi q_t^{2J}} & \left|g_J^{I_t}(t)\right| e^{i\psi_J^{I_t}(t)} \\ \left|g_J^{I_t}(t)\right| e^{i\psi_J^{I_t}(t)} & \frac{\eta_J^{I_t}(t) e^{2i\left(\psi_J^{I_t}(t) - \delta_J^{I_t}(t)\right)} - 1}{2i\sigma_t^K k_t^{2J}} \end{pmatrix}\,, \tag{6.73}$$

where $\psi_J^{I_t}(t)$ denotes the phase of $g_J^{I_t}(t)$, the inelasticity parameter is given by

$$\eta_J^{I_t}(t) = \sqrt{1 - \left|\big[S_J^{I_t}(t)\big]_{\pi\pi\to\bar{K}K}\right|^2} = \sqrt{1 - 4\sigma_t^\pi\sigma_t^K (k_t q_t)^{2J}\left|g_J^{I_t}(t)\right|^2 \theta\big(t-t_K\big)}\,, \tag{6.74}$$

and the $\bar{K}K$ partial waves may be identified as

$$r_J^{I_t}(t) = \frac{\eta_J^{I_t}(t) e^{2i\left(\psi_J^{I_t}(t) - \delta_J^{I_t}(t)\right)} - 1}{2i\sigma_t^K}\,. \tag{6.75}$$

Together with the phase-space factor

$$\Sigma_J(t) = \operatorname{diag}\Big(\sigma_t^\pi q_t^{2J}\theta\big(t-t_\pi\big), \sigma_t^K k_t^{2J}\theta\big(t-t_K\big)\Big)\,, \tag{6.76}$$

the t-channel unitarity relation (6.72) then takes the form

$$\operatorname{Im}\mathbf{f}_{\pm}^{J}(t) = T_J^*(t)\Sigma_J(t)\mathbf{f}_{\pm}^{J}(t)\;, \qquad \mathbf{f}_{\pm}^{J}(t) = \begin{pmatrix} f_{\pm}^{J}(t) \\ \frac{\sqrt{2}\,c_J}{c_J^{K\!N}} h_{\pm}^{J}(t) \end{pmatrix}\;. \tag{6.77}$$

This equation will serve as starting point for a full two-channel treatment of the coupled system of $f_+^0(t)$ and $h_+^0(t)$ in Sect. 7.3.

Chapter 7

Solution of the t-channel equations[#4]

7.1 Muskhelishvili–Omnès problem for $\pi\pi \to \bar{N}N$

7.1.1 Single-channel Muskhelishvili–Omnès solution

In the single-channel approximation where only $\pi\pi$ intermediate states are considered in the unitarity relation the MO solution for $f_\pm^J(t)$ can be derived from the RS equations (6.40) following the strategy laid out in Sect. 5.1 for $\gamma\gamma \to \pi\pi$. However, it is advantageous to rearrange the equations first in such a way that the behavior of $f_\pm^J(t)$ at the two-nucleon threshold is properly taken into account.

Starting from the partial-wave expansion (6.35) one can show that the S-wave vanishes for $t \to t_N$ according to

$$f_+^0(t) = \mathcal{O}\big(p_t^2\big) \,. \tag{7.1}$$

Although higher partial waves with $J \geq 1$ individually take a finite value

$$f_+^J(t) = \mathcal{O}(1) \,, \qquad f_-^J(t) = \mathcal{O}(1) \,, \tag{7.2}$$

the linear combination

$$\Gamma^J(t) = m\sqrt{\frac{J}{J+1}} f_-^J(t) - f_+^J(t) \tag{7.3}$$

again vanishes at threshold [222]

$$\Gamma^J(t) = \mathcal{O}(p_t^2) \,. \tag{7.4}$$

Indeed, the leading terms in the t-channel partial-wave expansion (C.16)

$$\begin{aligned} \frac{A^+(\nu,t)}{4\pi} &= -\frac{f_+^0(t)}{p_t^2} + \frac{15}{2} m^2\nu^2 \frac{\Gamma^2(t)}{p_t^2} + \frac{5}{2} q_t^2 f_+^2(t) + \dots \,, & \frac{A^-(\nu,t)}{4\pi} &= 3m\nu \frac{\Gamma^1(t)}{p_t^2} + \dots \,, \\ \frac{B^+(\nu,t)}{4\pi} &= \frac{15}{\sqrt{6}} m\nu f_-^2(t) + \dots \,, & \frac{B^-(\nu,t)}{4\pi} &= \frac{3}{\sqrt{2}} f_-^1(t) + \dots \,, \end{aligned} \tag{7.5}$$

already demonstrate that (7.1) and (7.4) are indispensable for the invariant amplitudes to remain finite.

[#4] The contents of this chapter have been published in [205, 221].

In strict analogy to (5.1) the t-channel equations in their unsubtracted form read

$$
\begin{aligned}
f_+^0(t) &= \Delta_+^0(t) - \frac{1}{\pi}\int\limits_{t_\pi}^{\infty} \mathrm{d}t' \frac{\operatorname{Im} f_+^0(t')}{t'-t_N} + \frac{1}{\pi}\int\limits_{t_\pi}^{\infty} \mathrm{d}t' \frac{\operatorname{Im} f_+^0(t')}{t'-t} \,, \\
f_+^J(t) &= \Delta_+^J(t) + \frac{1}{\pi}\int\limits_{t_\pi}^{\infty} \mathrm{d}t' \frac{\operatorname{Im} \Gamma^J(t')}{t'-t_N} + \frac{1}{\pi}\int\limits_{t_\pi}^{\infty} \mathrm{d}t' \frac{\operatorname{Im} f_+^J(t')}{t'-t} \,, \\
f_-^J(t) &= \Delta_-^J(t) + \frac{1}{\pi}\int\limits_{t_\pi}^{\infty} \mathrm{d}t' \frac{\operatorname{Im} f_-^J(t')}{t'-t} \,,
\end{aligned}
\tag{7.6}
$$

where

$$
\begin{aligned}
\Delta_\pm^J(t) &= \tilde{N}_\pm^J(t) + \bar{\Delta}_\pm^J(t) \,, \\
\bar{\Delta}_+^J(t) &= \frac{1}{\pi}\int\limits_{W_+}^{\infty} \mathrm{d}W' \sum_{l=0}^{\infty} \Big\{ \tilde{G}_{Jl}(t,W') \operatorname{Im} f_{l+}^I(W') + \tilde{G}_{Jl}(t,-W') \operatorname{Im} f_{(l+1)-}^I(W') \Big\} \\
&\quad + \frac{1}{\pi}\int\limits_{t_\pi}^{\infty} \mathrm{d}t' \sum_{J'=J+2}^{\infty} \frac{1+(-1)^{J+J'}}{2} \Big\{ \tilde{K}_{JJ'}^1(t,t') \operatorname{Im} f_+^{J'}(t') + \tilde{K}_{JJ'}^2(t,t') \operatorname{Im} f_-^{J'}(t') \Big\} \,, \\
\bar{\Delta}_-^J(t) &= \frac{1}{\pi}\int\limits_{W_+}^{\infty} \mathrm{d}W' \sum_{l=0}^{\infty} \Big\{ \tilde{H}_{Jl}(t,W') \operatorname{Im} f_{l+}^I(W') + \tilde{H}_{Jl}(t,-W') \operatorname{Im} f_{(l+1)-}^I(W') \Big\} \\
&\quad + \frac{1}{\pi}\int\limits_{t_\pi}^{\infty} \mathrm{d}t' \sum_{J'=J+2}^{\infty} \frac{1+(-1)^{J+J'}}{2} \tilde{K}_{JJ'}^3(t,t') \operatorname{Im} f_-^{J'}(t') \,.
\end{aligned}
\tag{7.7}
$$

Again, the convergence of the t-independent integrals in (7.6) is ensured by the threshold behavior (7.1) and (7.4). In particular, the fact that the numerator in the case of $f_+^J(t)$ coincides with $\operatorname{Im}\Gamma^J(t')$ is a manifestation of the general property of the kernel functions

$$
\begin{aligned}
\operatorname{Res}\Big[H_{lJ}(W,t'),t'=t_N\Big] &= -m\sqrt{\frac{J}{J+1}}\operatorname{Res}\Big[G_{lJ}(W,t'),t'=t_N\Big] \,, \\
\operatorname{Res}\Big[\tilde{K}_{JJ'}^2(t,t'),t'=t_N\Big] &= -m\sqrt{\frac{J'}{J'+1}}\operatorname{Res}\Big[\tilde{K}_{JJ'}^1(t,t'),t'=t_N\Big] \,,
\end{aligned}
\tag{7.8}
$$

which induces the cancellation of ostensible $p_t'^{-2}$ divergences in the t-channel dispersive integrals in (6.39) and (6.40). In addition, the structure of (7.6) suggests to reformulate the problem in terms of $\Gamma^J(t)$ as

$$
\begin{aligned}
f_+^0(t) &= \Delta_+^0(t) + \frac{t-t_N}{\pi}\int\limits_{t_\pi}^{\infty} \mathrm{d}t' \frac{\operatorname{Im} f_+^0(t')}{(t'-t_N)(t'-t)} \,, \qquad f_-^J(t) = \Delta_-^J(t) + \frac{1}{\pi}\int\limits_{t_\pi}^{\infty} \mathrm{d}t' \frac{\operatorname{Im} f_-^J(t')}{t'-t} \,, \\
\Gamma^J(t) &= \Delta_\Gamma^J(t) + \frac{t-t_N}{\pi}\int\limits_{t_\pi}^{\infty} \mathrm{d}t' \frac{\operatorname{Im} \Gamma^J(t')}{(t'-t_N)(t'-t)} \,, \qquad \Delta_\Gamma^J(t) = m\sqrt{\frac{J}{J+1}}\Delta_-^J(t) - \Delta_+^J(t) \,.
\end{aligned}
\tag{7.9}
$$

	$f_+^0(t)$	$\Gamma^1(t)$	$f_-^1(t)$	$\Gamma^2(t)$	$f_-^2(t)$
1-sub	1	0	1	0	0
2-sub	2	1	2	0	1
3-sub	2	2	2	1	1

Table 7.1: Number of subtractions in the MO solution for the t-channel partial waves with $J \leq 2$ for once- and twice-subtracted HDRs as well as a partial third subtraction.

In this way, the equations decouple in the sense that the integral equation for a given partial-wave amplitude only depends on the s-channel partial waves as well as t-channel partial waves with higher angular momentum, and thus reduce to a form directly accessible to MO techniques. Once the solutions for $\Gamma^J(t)$ and $f_-^J(t)$ are obtained, the result for $f_+^J(t)$ can be recovered by means of (7.3). With the Omnès function as defined in (5.5), $\hat{N}_\pm^J(t)$ from (C.25), and

$$\tilde{\Delta}_\pm^J(t) = \hat{N}_\pm^J(t) + \bar{\Delta}_\pm^J(t)\,, \qquad \tilde{\Delta}_\Gamma^J(t) = m\sqrt{\frac{J}{J+1}}\tilde{\Delta}_-^J(t) - \tilde{\Delta}_+^J(t)\,, \tag{7.10}$$

the solutions for the unsubtracted case become

$$\begin{aligned}
f_+^0(t) &= \tilde{\Delta}_+^0(t) \\
&\quad + \frac{(t-t_N)\Omega_0(t)}{\pi}\left\{\int_{t_\pi}^{t_\mathrm{m}} \mathrm{d}t' \frac{\tilde{\Delta}_+^0(t')\sin\delta_0(t')}{(t'-t_N)(t'-t)|\Omega_0(t')|} + \int_{t_\mathrm{m}}^{\infty} \mathrm{d}t' \frac{\operatorname{Im} f_+^0(t')}{(t'-t_N)(t'-t)|\Omega_0(t')|}\right\}, \\
\Gamma^J(t) &= \tilde{\Delta}_\Gamma^J(t) \\
&\quad + \frac{(t-t_N)\Omega_J(t)}{\pi}\left\{\int_{t_\pi}^{t_\mathrm{m}} \mathrm{d}t' \frac{\tilde{\Delta}_\Gamma^J(t')\sin\delta_J(t')}{(t'-t_N)(t'-t)|\Omega_J(t')|} + \int_{t_\mathrm{m}}^{\infty} \mathrm{d}t' \frac{\operatorname{Im}\Gamma^J(t')}{(t'-t_N)(t'-t)|\Omega_J(t')|}\right\}, \\
f_-^J(t) &= \tilde{\Delta}_-^J(t) + \frac{\Omega_J(t)}{\pi}\left\{\int_{t_\pi}^{t_\mathrm{m}} \mathrm{d}t' \frac{\tilde{\Delta}_-^J(t')\sin\delta_J(t')}{(t'-t)|\Omega_J(t')|} + \int_{t_\mathrm{m}}^{\infty} \mathrm{d}t' \frac{\operatorname{Im} f_-^J(t')}{(t'-t)|\Omega_J(t')|}\right\},
\end{aligned} \tag{7.11}$$

where in analogy to (5.6) the phase can be explicitly separated by virtue of Watson's theorem [201] and the generalization for subtracted RS equations as introduced in Sect. 6.3.3 is deferred to Appendix C.5. The general pattern how subtractions in the original HDRs affect (7.11) is summarized in Table 7.1. In the once- and twice-subtracted version the equation for $\Gamma^1(t)$ always involves one subtraction less than the one for $f_-^1(t)$, while the equations for the D-waves remain unchanged in the once-subtracted case, and in the twice-subtracted version lack one subtraction compared to their P-wave analogs. The partial third subtraction is constructed in such a way that the equations for $\Gamma^1(t)$ and $\Gamma^2(t)$ receive an additional subtraction, with the result that in this scheme all partial waves with the same $J \leq 2$ are treated on an equal footing.

7.1.2 Input

We now collect all the input quantities needed for an explicit evaluation of (7.11) and (C.77). Most importantly, we will consider the results of the Karlsruhe–Helsinki partial-wave analysis

KH80 [152,165] both as input for the s-channel partial waves and the subthreshold parameters, in order to compare our results for the t-channel partial waves with KH80 and thereby demonstrate the viability of our approach. Throughout this consistency check with KH80, we will leave the πN coupling constant at $g^2/4\pi = 14.28$. The KH80 partial-wave solution—based on Pietarinen's expansion method [223] and incorporating various analyticity constraints—is still the only analysis that provides s- and t-channel partial waves as well as a complete set of subthreshold parameters within a common framework.[1] In this respect, available updates of KH80, for instance the Karlsruhe KA84 solution [225] or, more recently, the analysis of forward πN scattering in [167, 226], are incomplete. Similarly, the VPI/GWU(SAID) solution, see e.g. [158, 227–229], only pertains to the s-channel partial waves, the πN coupling constant, and certain subthreshold parameters. Although the results for the t-channel partial waves prove remarkably insensitive to the precise input for the s-channel amplitudes that is used to evaluate the inhomogeneities $\tilde{\Delta}^J_\pm(t)$, indicating that the iteration of the full system of RS equations depicted in Fig. 6.1 should converge quickly, we will stick to the KH80 solution in the present context. More precisely, we integrate all the s-channel partial waves up to $l \leq l_{\max}$ for $W_+ \leq W' \leq W_\mathrm{a} = 2.5\,\mathrm{GeV}$, while for even higher energies we rely on a the Regge model for backward πN scattering [230], which provides expressions for the full invariant amplitudes in the limit

$$s' \to \infty \quad \Rightarrow \quad t' \to -\infty\,, \qquad u' \to a\,. \tag{7.12}$$

Summing the partial waves up to $l_{\max} = 4$ encompasses all 4-star resonances quoted in [3] that lie entirely within the relevant energy range $W_+ \leq W' \leq W_\mathrm{a}$ and ensures a decent matching to the Regge model [230] (for more details, see [205]).

As already mentioned in Sect. 6.1, the solution of the t-channel equations suffers from the inherent difficulty that the single-channel approximation breaks down around 1 GeV, most distinctly in the S-wave due to the occurrence of the $f_0(980)$ resonance, while input from partial-wave analyses [231] only becomes available starting at the two-nucleon threshold. In principle, inelastic contributions from intermediate states other than $\pi\pi$ can be included in a single-channel MO formalism [232], but only provided that these inelasticities are sufficiently well known. Hence, this approach fails for $f^0_+(t)$ absent reliable input for the $\bar{K}K \to \bar{N}N$ S-wave. Alternatively, one might try to include the $f_0(980)$ using a Flatté-like parameterization [233], similarly to the Breit–Wigner ansatz for the $f_2(1270)$ in Sect. 5.3.2. However, while the $f_0\pi\pi$ coupling is known rather accurately [202], the f_0NN coupling ist not, with different meson-exchange models dissenting substantially on the coupling and the continuation to the physical pole [234]. For these reasons, we conclude that a reliable incorporation of the $f_0(980)$ dynamics can only be achieved in a full two-channel $\pi\pi/\bar{K}K$ MO description, which we will address in Sect. 7.3. Even if the $\bar{K}K$ channel is included, the two-channel representation will break down around $\sqrt{t_0} = 1.3\,\mathrm{GeV}$, where inelasticities from 4π intermediate states are expected to become important. Moreover, this strategy to extend the energy range by means of a two-channel treatment is only applicable if the inelasticities can be attributed entirely to one (effective) two-particle intermediate state and if the pertinent two-channel S-matrix is sufficiently well known. As these requirements thwart an extension of the two-channel formalism to other partial waves, P- and D-waves will be considered solely within the single-channel

[1] The t-channel partial waves are determined from an analytic continuation of the s-channel amplitude by means of a discrepancy-function method [220,224,213]. The extrapolation is stabilized using Watson's theorem for the phases of the t-channel amplitudes, assuming that only $\pi\pi$ intermediate states enter in the unitarity relation, and therefore becomes unreliable once significant inelastic contributions appear around $\sqrt{t} = 1\,\mathrm{GeV}$. For this reason, the results as quoted in [152] are given only up to $t = 40M_\pi^2 = (0.88\,\mathrm{GeV})^2$.

	KH80	St(KA84)	St(SP98)	Oa(KH80)	Oa(SP98)	Fe(KA84)
$d_{00}^{+}\ [M_\pi^{-1}]$	−1.46(10)	−1.39(2)	−1.32(2)	−1.46(4)	−1.29(2)	−1.58
$b_{00}^{-}\ [M_\pi^{-2}]$	10.36(10)	10.35(2)	10.45(1)	10.84(18)	10.37(8)	10.34
$a_{00}^{-}\ [M_\pi^{-2}]$	−8.83(10)	−8.82(4)	−8.97(1)	−9.26(17)	−8.92(7)	−8.47
$d_{01}^{+}\ [M_\pi^{-3}]$	1.14(2)	1.14(1)	1.15(2)	1.15(11)	1.23(4)	1.36
$b_{00}^{+}\ [M_\pi^{-3}]$	−3.54(6)	−3.49(3)	−3.48(2)	−3.56(10)	−3.42(4)	−7.90
$a_{10}^{+}\ [M_\pi^{-3}]$	4.66	4.63(3)	4.57(3)	4.84(20)	4.58(8)	9.14
$b_{01}^{-}\ [M_\pi^{-4}]$	0.24(1)	0.22(1)	0.24(1)	0.26(22)	0.26(10)	0.14
$a_{01}^{-}\ [M_\pi^{-4}]$	−0.37(2)	−0.38(1)	−0.38(1)	−0.44(21)	−0.38(9)	−0.46
$b_{10}^{-}\ [M_\pi^{-4}]$	1.08(5)	1.05(1)	1.01(1)	0.89(5)	1.04(2)	0.81
$a_{10}^{-}\ [M_\pi^{-4}]$	−1.25(5)	−1.24(4)	−1.18(1)	−1.09(6)	−1.20(2)	−1.46

Table 7.2: Subthreshold parameters as given by KH80/Höhler [152], Stahov [210], Oades [235], and Fettes [236]. The numbers in brackets refer to the uncertainty in the last significant digit.

approximation and inelasticities in these partial waves, which e.g. in the P-wave slowly set in starting around the $\pi\omega$ threshold at $\sqrt{t} = 0.92\,\text{GeV}$ due to 4π intermediate states, will be completely ignored. In view of the uncertainties associated with inelastic contributions to the unitarity relation in the pseudophysical region we simply put the t-channel imaginary parts to zero above the matching point, which, in this section, will be chosen at $\sqrt{t_\text{m}} = 0.98\,\text{GeV}$, slightly below the opening of the $\bar{K}K$ channel.

The determination of subthreshold parameters from πN scattering data requires an analytic continuation to the subthreshold point ($\nu = 0, t = 0$). The corresponding results within the KH80 framework are compared to more recent determinations in Table 7.2. In [210], the extrapolation is performed based on a combination of interior and fixed-t dispersion relations, with input for the s-channel partial waves from KA84 and VPI/SP98 [149, 227] and for the t-channel partial waves from KH80. Similarly, the subthreshold parameters are derived from finite-contour dispersion relations in [235], using as s-channel input the KH80 and VPI/SP98 solutions. In particular for the case of [235], the results for the subthreshold parameters depend critically on the input for the s-channel partial waves, in so far as KH80 s-channel input yields values close to the KH80 subthreshold parameters and SP98 input values close to [227]

$$d_{00}^{+} = -1.30 M_\pi^{-1}\,, \qquad d_{01}^{+} = 1.27 M_\pi^{-3}\,. \tag{7.13}$$

For [210] such a correlation is less distinct, which, however, may well be due to the fact that the t-channel input required in this analysis stems solely from KH80. In all cases one should note that the quoted uncertainties merely refer to statistical fit errors or consistency considerations, they do not reflect the total systematic uncertainties.[2] In the last column of Table 7.2 we show for comparison the predictions from a third-order calculation in heavy-baryon ChPT [236, 237], where the LECs are fitted to reproduce the low-energy KA84 phase shifts. As argued in [78, 236], the discrepancies between the ChPT and the KH80 subthreshold

[2] According to [152], the error estimates for the KH80 subthreshold parameters are "based on deviations from the internal consistency," while the total uncertainty is "somewhat larger."

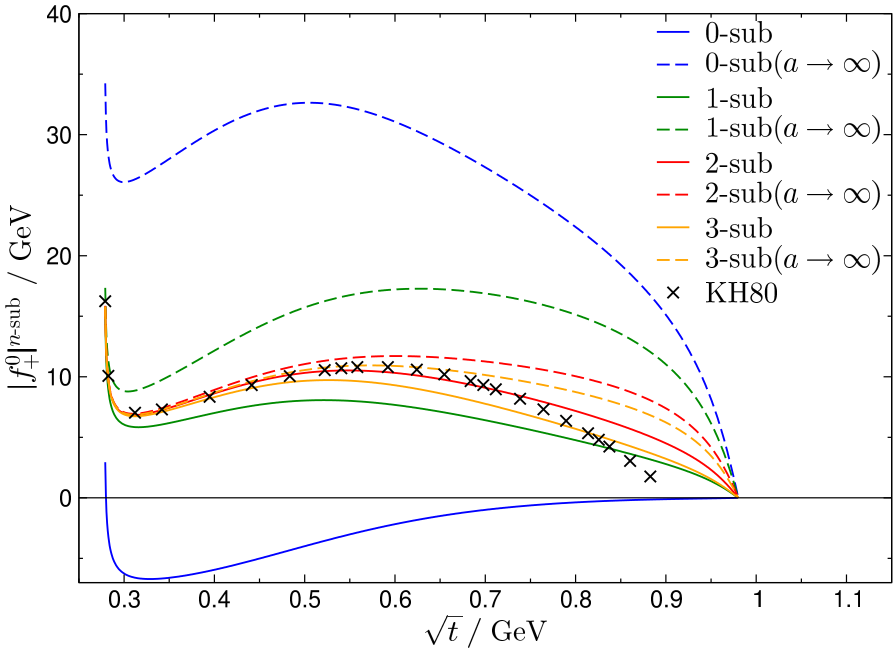

Figure 7.1: MO solutions for the S-wave.

parameters can be traced back to the fact that the ChPT amplitude does not sufficiently respect the analytic structure of the πN amplitude to reliably perform the extrapolation into the unphysical region. In particular, a fourth-order calculation does not improve the results any more, and in some cases even deteriorates the agreement with KH80 [78, 236].

Finally, we take the $\pi\pi$ phase shifts from the extended Roy-equation analysis of [57]. The variation of the final results for $f_\pm^J(t)$ due to the uncertainty in the $\pi\pi$ phases is negligible compared to the uncertainties introduced by the input for partial waves and subthreshold parameters (see also Sect. 5.4).

7.1.3 Results

The results for the t-channel partial waves using the input discussed in Sect. 7.1.2, the optimal hyperbola parameter $a = -2.7M_\pi^2$, cf. (6.30), and the matching point $\sqrt{t_\mathrm{m}} = 0.98\,\mathrm{GeV}$, for the different subtraction schemes introduced in Sect. 6.3.3, are depicted in Figs. 7.1–7.3, while Figs. 7.4 and 7.5 show the P- and D-wave results for the higher matching point $\sqrt{t_\mathrm{m}} = 1.1\,\mathrm{GeV}$. Apart from our central solutions, Figs. 7.1–7.3 also comprise the curves for the limit where the hyperbola parameter is taken to infinity, which should give a rough estimate of the sensitivity to the approximations concerning the high-energy input and higher partial waves (see also Sect. 5.4.1).[3] In these results, the coupling of the D-waves to the S-wave equation via the kernel functions $\tilde{K}^1_{02}(t,t')$ and $\tilde{K}^2_{02}(t,t')$—except for the $a \to \infty$ limit in the unsubtracted case, for which these kernels diverge, cf. (C.41)—as well as asymptotic contributions to the s-channel integrals for energies $W' \geq W_\mathrm{a}$ by means of the Regge model [230] have been taken

[3]The first subtraction does not affect the equations for the D-waves, while the partial third subtraction leaves $f_-^1(t)$ and $f_-^2(t)$ unchanged. Therefore, the corresponding curves are omitted in Figs. 7.2–7.5. Moreover, we actually take the limit $a \to -\infty$ to assess the a-dependence, as suggested by range-of-convergence considerations [205].

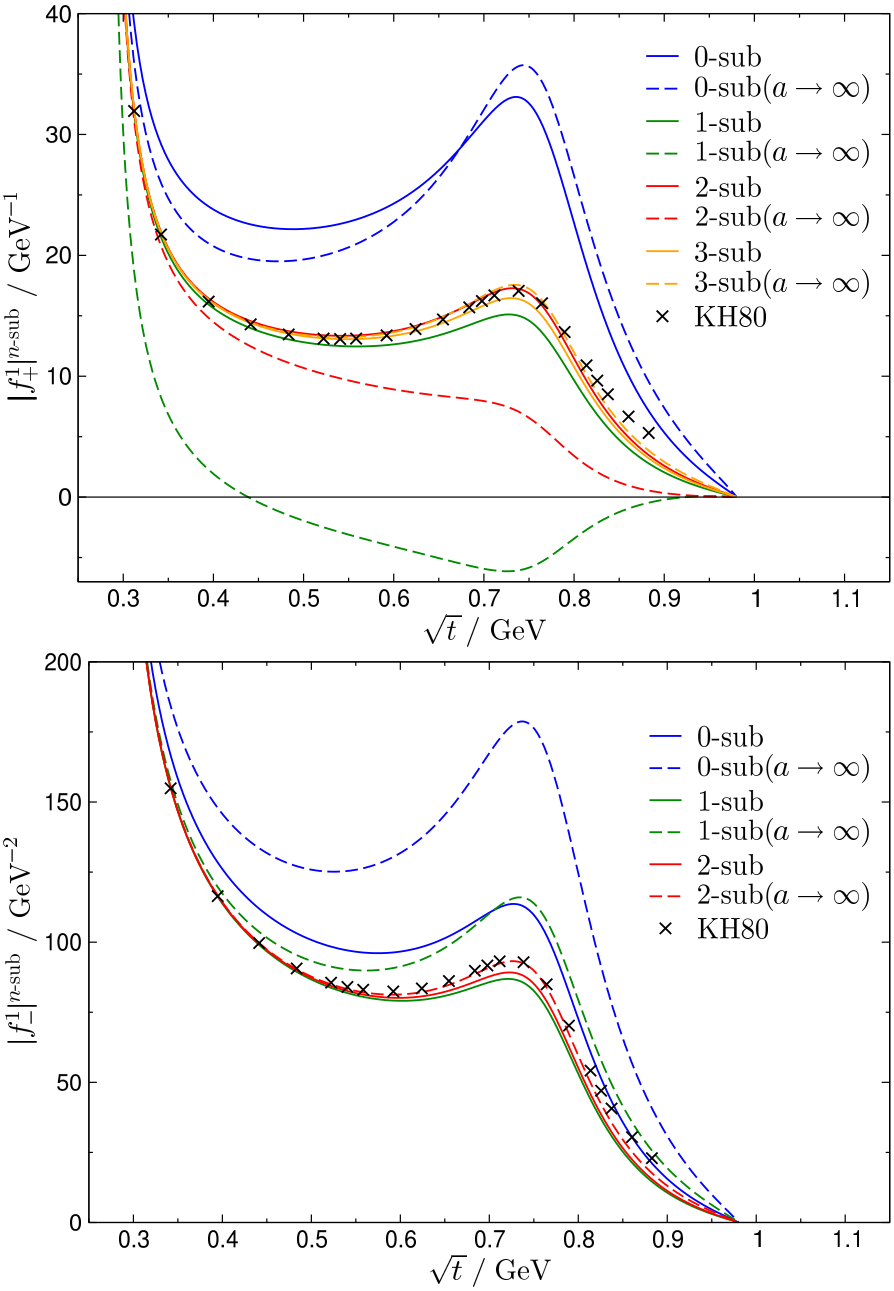

Figure 7.2: MO solutions for the P-waves.

into account, although both effects prove to be numerically irrelevant. In the vicinity of t_π all amplitudes $f_\pm^J(t)$ with $J \geq 1$ are dominated by the nucleon pole term and therefore agree by construction with KH80 as the same πN coupling constant is used. For this reason, we concentrate on the energy range where discrepancies are most significant in Figs. 7.1–7.5.

Figs. 7.1–7.3 demonstrate that the a-dependence decreases rapidly with increasing number of subtractions. In particular, the small residual sensitivity of the results to the choice of a for the curves with the respective highest number of subtractions provides evidence that for this version of the RS system the uncertainties originating from the high-energy input are indeed

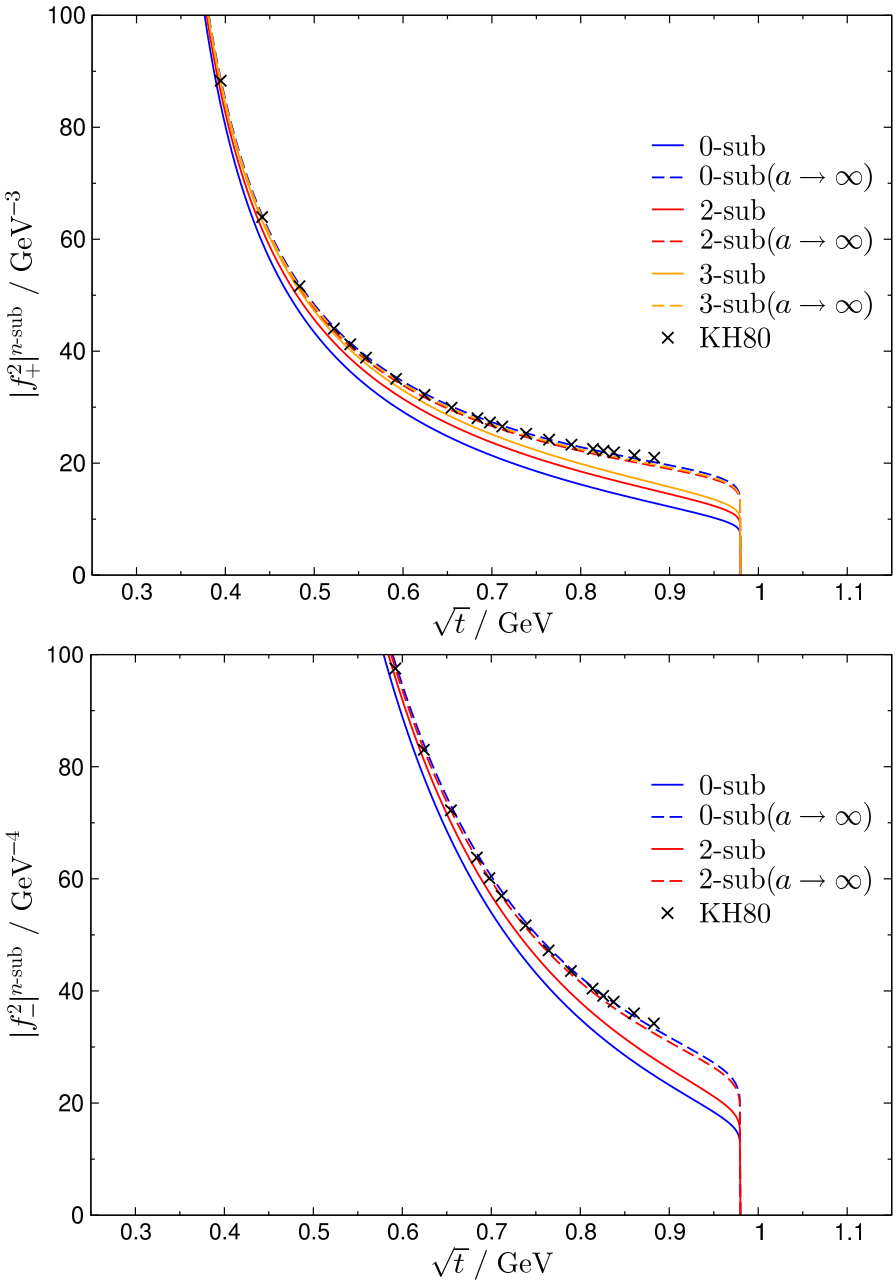

Figure 7.3: MO solutions for the D-waves.

appreciably suppressed. In addition, we conclude that the KH80 solution is accurately reproduced provided that a sufficient number of subtractions is introduced. We do not consider the deviations from KH80 that do emerge in the S-wave at higher energies as particularly disturbing, since at some point effects of the $\bar{K}K$ dynamics will in any case invalidate the single-channel approximation. For this partial wave, the partial third subtraction does not further improve the solution (as expected from Table 7.1), so that the twice-subtracted version proves already adequate and is actually favorable given the fact that fewer subthreshold parameters enter the solution. Nonetheless, the S-wave is considerably more sensitive to the

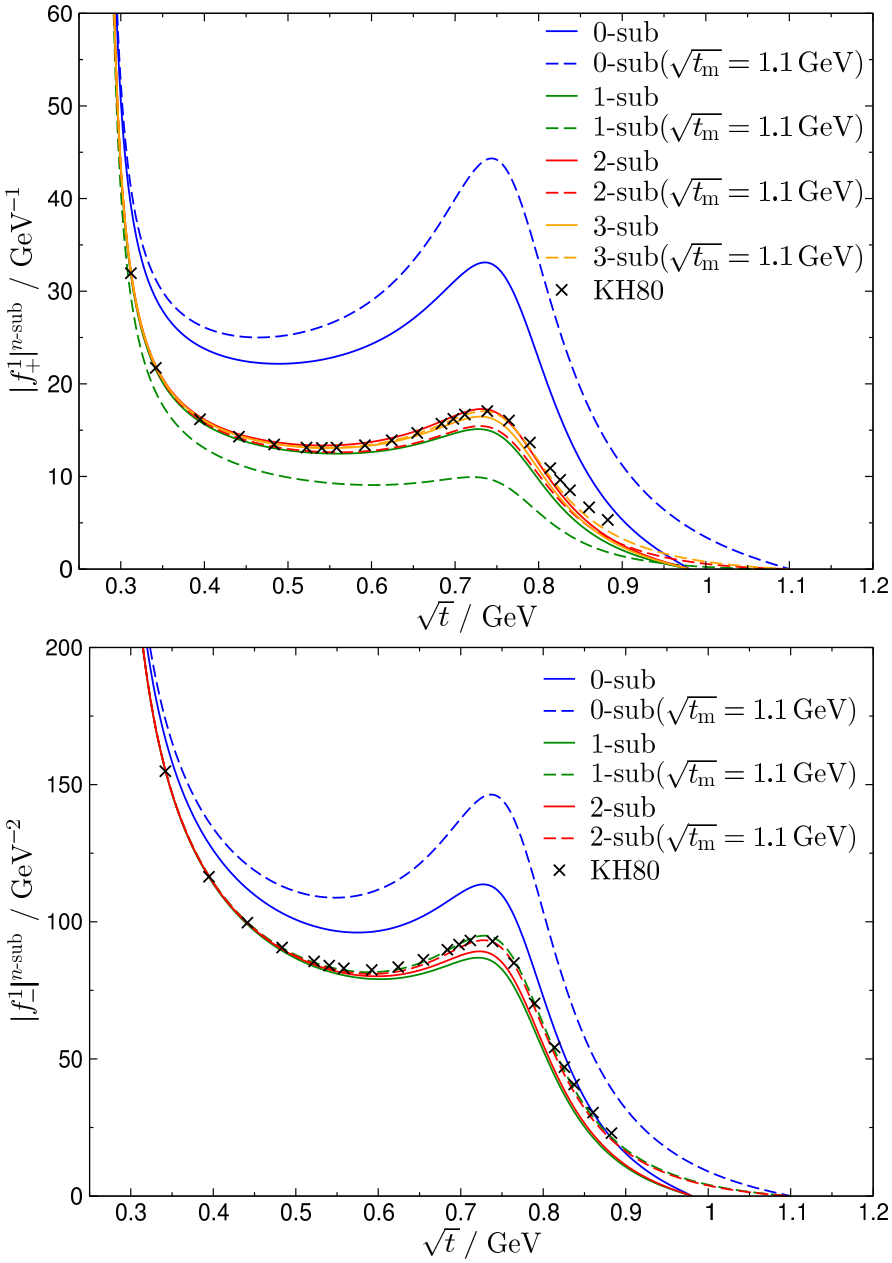

Figure 7.4: MO solutions for the P-waves with $\sqrt{t_m} = 1.1\,\text{GeV}$.

input for the subthreshold parameters than higher partial waves as the nucleon-pole contribution vanishes at t_π, with the result that not the Born terms, but subthreshold parameters dominate the low-energy behavior. In the same way, the solutions for $\Gamma^J(t)$, which occur in an intermediate step in the calculation of $f_+^J(t)$, involve the combination of Born terms

$$m\sqrt{\frac{J}{J+1}}\hat{N}_-^J(t) - \hat{N}_+^J(t)\,, \tag{7.14}$$

that vanishes at t_π as can be inferred from (C.28). For this reason, the solutions for $f_+^J(t)$ are systematically more sensitive to the subthreshold-parameter input than those for $f_-^J(t)$.

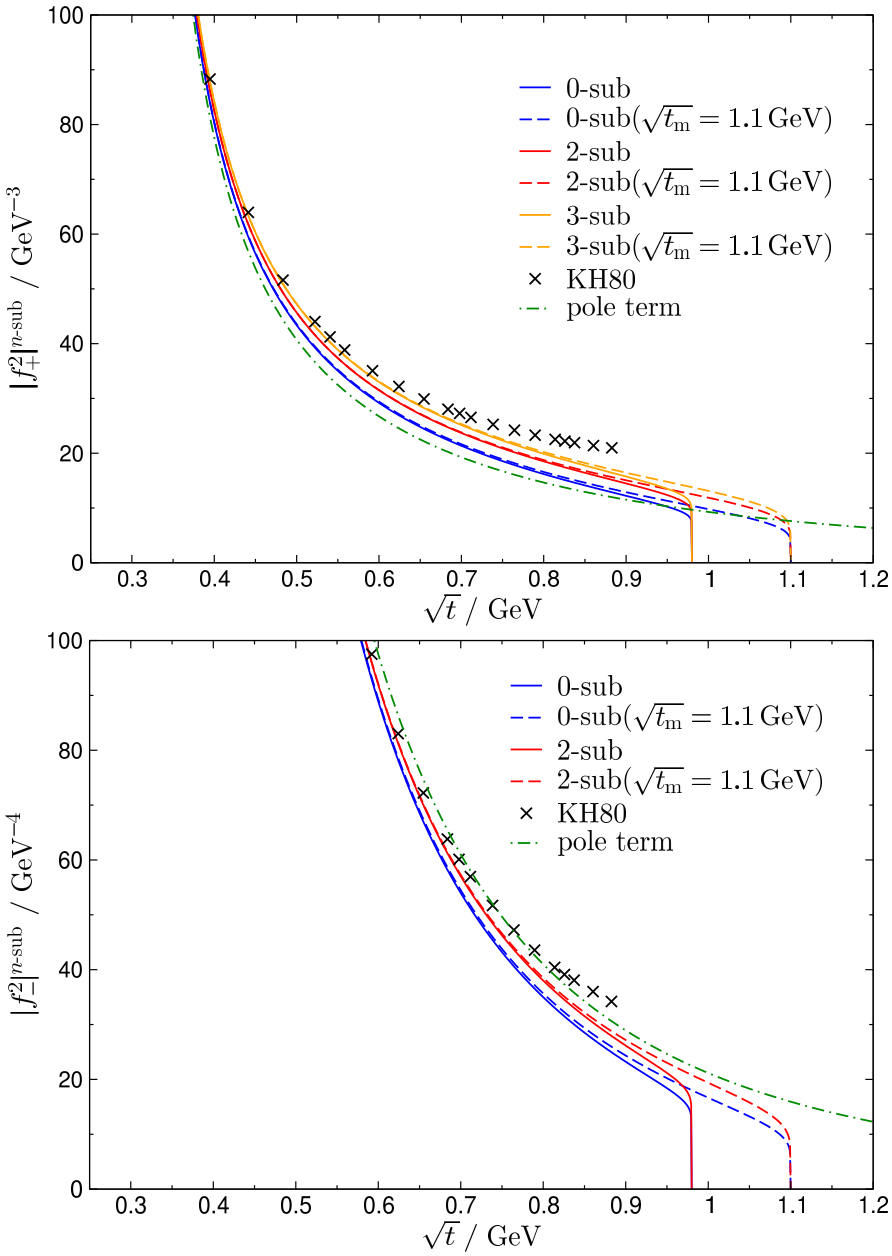

Figure 7.5: MO solutions for the D-waves with $\sqrt{t_m} = 1.1\,\text{GeV}$.

It is striking that for all partial waves, at the respective highest level of subtractions considered, the agreement with KH80 appears to be even better in the limit $a \to \infty$. This observation can be interpreted in such a way that this procedure implements the limit of fixed-t dispersion relations on the level of the original HDRs, since (6.27) reduces to the fixed-t limit once a is taken to infinity and the t-channel integrals are discarded. Although this limit and the partial-wave projection may not be interchanged—there would be no equations for the t-channel partial waves to begin with—it seems plausible that a treatment emulating the fixed-t approach improves the agreement with the KH80 solution, as fixed-t analyticity constitutes an integral part of the KH80 framework.

Furthermore, we observe that especially for the P-waves the solutions in the higher-matching-point scenario reproduce the high-energy tail of the KH80 results more accurately. This behavior is due to the fact that the solutions for the partial waves are forced to vanish at the matching point as a consequence of putting the imaginary parts above t_m to zero (see also the discussion in Sect. 5.4.2). Obviously, a higher matching point permits more freedom to account for the finite values of the amplitudes at the highest KH80 point.

Finally, Fig. 7.5 shows the comparison of the D-wave solutions with the nucleon pole terms. While the KH80 results for $f_-^2(t)$ are almost perfectly described by the pertinent Born term, $f_+^2(t)$ is underestimated by roughly a factor of 2 at the boundary of the KH80 energy range. In either case, the general form of the solution resembles closely the nucleon-pole contribution, in marked contrast to the P-waves where the peak associated with the $\rho(770)$ is clearly visible.

7.2 Two-channel Muskhelishvili–Omnès problem

Before turning to the calculation of $f_+^0(t)$, we first consider the generic coupled-channel integral equation

$$\mathbf{f}(t) = \mathbf{\Delta}(t) + \frac{1}{\pi}\int\limits_{t_\pi}^{t_\mathrm{m}} \mathrm{d}t' \frac{T^*(t')\Sigma(t')\mathbf{f}(t')}{t'-t} + \frac{1}{\pi}\int\limits_{t_\mathrm{m}}^{\infty} \mathrm{d}t' \frac{\mathrm{Im}\,\mathbf{f}(t')}{t'-t}\ , \tag{7.15}$$

where bold-faced quantities are two-dimensional vectors in channel space, representing pion and kaon intermediate states, and the imaginary part of $\mathbf{f}(t)$ is assumed to be known above the matching point t_m. In particular, $f_1(t)$ and $f_2(t)$ can be thought of as $f_+^0(t)$ and $h_+^0(t)$.[4] The function $\mathbf{\Delta}(t)$ contains at most left-hand cuts and is therefore real for $t \geq t_\pi$. The unitarity relation is written in the form

$$\mathrm{Im}\,\mathbf{f}(t) = T^*(t)\Sigma(t)\mathbf{f}(t)\ , \tag{7.16}$$

cf. (6.77), with T-matrix $T(t)$ and phase-space factor $\Sigma(t)$ parameterized as

$$T(t) = \begin{pmatrix} \frac{\eta(t)e^{2i\delta(t)}-1}{2i\sigma_t^\pi} & |g(t)|e^{i\psi(t)} \\ |g(t)|e^{i\psi(t)} & \frac{\eta(t)e^{2i(\psi(t)-\delta(t))}-1}{2i\sigma_t^K} \end{pmatrix}\ , \qquad \Sigma(t) = \mathrm{diag}\Big(\sigma_t^\pi\theta\big(t-t_\pi\big), \sigma_t^K\theta\big(t-t_K\big)\Big)\ . \tag{7.17}$$

The scattering phases $\delta(t)$ and $\psi(t)$ are required as input for $t_\pi \leq t \leq t_\mathrm{m}$, where Watson's theorem demands $\psi(t) = \delta(t)$ for $t \leq t_K$. Moreover, the modulus of $g(t)$ is needed in the full range $t_\pi \leq t \leq t_\mathrm{m}$, and thus has to be analytically continued into the pseudophysical region $t_\pi \leq t \leq t_K$. Finally, the inleasticity parameter $\eta(t)$ can be related to $|g(t)|$ via

$$\eta(t) = \sqrt{1 - 4\sigma_t^\pi\sigma_t^K|g(t)|^2\theta\big(t-t_K\big)}\ , \tag{7.18}$$

and the relation between S- and T-matrix reads

$$S(t) = \mathbb{1} + 2i\,\Sigma^{1/2}(t)T(t)\Sigma^{1/2}(t)\ . \tag{7.19}$$

[4] Accordingly, we take $J = 0$ in the following. The general case can always be recovered by introducing the correct phase-space factors according to $\sigma_t^\pi \to \sigma_t^\pi q_t^{2J}$ and $\sigma_t^K \to \sigma_t^K k_t^{2J}$.

7.2.1 Formal solution

We define the Omnès matrix $\Omega(t)$ by

$$\left\{\begin{array}{c}\operatorname{Im}\Omega(t) = T^*(t)\Sigma(t)\Omega(t)\\ \operatorname{Im}\Omega(t) = 0\end{array}\right\} \qquad \text{for} \qquad \left\{\begin{array}{c}t_\pi \le t \le t_{\mathrm{m}}\\ \text{otherwise}\end{array}\right\} \tag{7.20}$$

and choose the normalization $\Omega(0) = \mathbb{1}$. Writing

$$\mathbf{F}(t) = \mathbf{f}(t) - \mathbf{\Delta}(t) = \Omega(t)\mathbf{G}(t)\ , \tag{7.21}$$

it follows that for $t \ge t_\pi$

$$\big(\mathbb{1} - 2i\,T^*(t)\Sigma(t)\big)\Omega(t_+)\big(\mathbf{G}(t_+) - \mathbf{G}(t_-)\big) = 2i\,T^*(t)\Sigma(t)\mathbf{\Delta}(t)\ , \tag{7.22}$$

where $t_\pm = t \pm i\epsilon$ and the physical limit is given by t_+. Using unitarity in the form

$$\big(\mathbb{1} - 2i\,T^*(t)\Sigma(t)\big)^{-1} = \mathbb{1} + 2i\,T(t)\Sigma(t)\ , \tag{7.23}$$

which in particular holds for $t \le t_K$ by virtue of Watson's theorem, we find

$$\mathbf{G}(t_+) - \mathbf{G}(t_-) = 2i\,\Omega^{-1}(t)T(t)\Sigma(t)\mathbf{\Delta}(t)\ , \tag{7.24}$$

and hence

$$\begin{aligned}\mathbf{f}(t) &= \mathbf{\Delta}(t) + \frac{\Omega(t)}{\pi}\int\limits_{t_\pi}^{t_{\mathrm{m}}} \mathrm{d}t' \frac{\Omega^{-1}(t')T(t')\Sigma(t')\mathbf{\Delta}(t')}{t'-t} + \frac{\Omega(t)}{\pi}\int\limits_{t_{\mathrm{m}}}^{\infty} \mathrm{d}t' \frac{\Omega^{-1}(t')\operatorname{Im}\mathbf{f}(t')}{t'-t}\\ &= \mathbf{\Delta}(t) - \frac{\Omega(t)}{\pi}\int\limits_{t_\pi}^{t_{\mathrm{m}}} \mathrm{d}t' \frac{\operatorname{Im}\Omega^{-1}(t')\mathbf{\Delta}(t')}{t'-t} + \frac{\Omega(t)}{\pi}\int\limits_{t_{\mathrm{m}}}^{\infty} \mathrm{d}t' \frac{\Omega^{-1}(t')\operatorname{Im}\mathbf{f}(t')}{t'-t}\ .\end{aligned} \tag{7.25}$$

The problem is thus reduced to finding a matrix $\Omega(t)$ that fulfills (7.20). For $t_\pi \le t \le t_K$ we have

$$\Omega(t_+) = \big(\mathbb{1} + 2i\,T(t)\Sigma(t)\big)\Omega(t_-)\ . \tag{7.26}$$

Taking the determinant on both sides yields, again using Watson's theorem for $t \le t_K$,

$$\det\Omega(t_+) = e^{2i\psi(t)}\det\Omega(t_-)\ , \tag{7.27}$$

and thus [238]

$$\det\Omega(t) = \exp\left\{\frac{t}{\pi}\int\limits_{t_\pi}^{t_{\mathrm{m}}} \mathrm{d}t' \frac{\psi(t')}{t'(t'-t)}\right\}\ . \tag{7.28}$$

Although the determinant allows for an analytic solution in the same way as in the single-channel case [71], there is in general no analytic solution for the Omnès matrix itself even for an infinite matching point, which therefore has to be calculated numerically, either by an iterative procedure [239] or a discretization method, i.e. solving a matrix equation [238, 240] (for a mathematician's point of view see [70]). Similarly to the single-channel case, we expect

a cusp at t_m, which has to be taken into account in the numerical evaluation of the integrals in (7.25) (see [67, 205]). Indeed, for $t \to t_\mathrm{m}$ the determinant behaves as

$$\det \Omega(t) \sim |t_\mathrm{m} - t|^x \,, \qquad x = \frac{\psi(t_\mathrm{m})}{\pi} \,. \tag{7.29}$$

Accordingly, we write for $t \to t_\mathrm{m}$ from below

$$\det \Omega(t) = \det \bar{\Omega}(t_\mathrm{m}) e^{i\pi x} |t_\mathrm{m} - t|^x \,, \qquad \Omega_{ij}(t) = \bar{\Omega}_{ij}(t_\mathrm{m}) e^{i\delta_{ij}(t_\mathrm{m})} |t_\mathrm{m} - t|^{x_{ij}} \,, \tag{7.30}$$

and from above

$$\det \Omega(t) = \det \bar{\Omega}(t_\mathrm{m}) |t_\mathrm{m} - t|^x \,, \qquad \Omega_{ij}(t) = \bar{\Omega}_{ij}(t_\mathrm{m}) |t_\mathrm{m} - t|^{x_{ij}} \,, \tag{7.31}$$

since $\Omega(t)$ is real above t_m. Here, we have assumed that the (real) functions $\bar{\Omega}_{ij}(t)$ are continuous at t_m. The strength of the cusp in each component $\Omega_{ij}(t)$ of the Omnès matrix is determined by the numbers x_{ij}, whose relation to the S-matrix parameters will be established in the following sections. Throughout this section we will consider the case $0 < x_{ij} < 1$, which is relevant for the coupled-channel S-wave system of $\pi\pi$ and $\bar{K}K$ intermediate states. The extension to arbitrary values of x_{ij} can then be done along the lines described in [67] and Sect. 5.1.

7.2.2 Dispersive representation of the Omnès matrix

For $0 < x_{ij} < 1$ we may write down a dispersive representation

$$\Omega(t) = \Big(1 - \frac{t}{t_\mathrm{m}}\Big)\mathbb{1} + \frac{t(t-t_\mathrm{m})}{\pi} \int\limits_{t_\pi}^{t_\mathrm{m}} \mathrm{d}t' \frac{T^*(t')\Sigma(t')\Omega(t')}{t'(t'-t_\mathrm{m})(t'-t)} \,, \tag{7.32}$$

where the subtraction constants have been fixed in such a way that $\Omega(0) = \mathbb{1}$ and $\Omega(t_\mathrm{m}) = 0$. In particular, we can investigate the limit $t \to t_\mathrm{m}$ to obtain information on x_{ij}. Using the asymptotic form of the integrals [67]

$$\begin{aligned}
\frac{|t_\mathrm{m} - t|^x}{\pi} \int\limits_{t_\mathrm{m}-\epsilon}^{t_\mathrm{m}} \frac{\mathrm{d}t'}{(t'-t)|t_\mathrm{m} - t'|^x} &\overset{\epsilon\to 0,\, t\to t_\mathrm{m}}{\longrightarrow} \frac{1}{\pi} \int\limits_0^\infty \frac{\mathrm{d}v}{v^x(1-v)} = -\cot \pi x \,, \\
\frac{|t_\mathrm{m} - t|^x}{\pi} \int\limits_{t_\mathrm{m}}^{t_\mathrm{m}+\epsilon} \frac{\mathrm{d}t'}{(t'-t)|t_\mathrm{m} - t'|^x} &\overset{\epsilon\to 0,\, t\to t_\mathrm{m}}{\longrightarrow} \frac{1}{\pi} \int\limits_0^\infty \frac{\mathrm{d}v}{v^x(1+v)} = \frac{1}{\sin \pi x} \,,
\end{aligned} \tag{7.33}$$

we obtain for $t \to t_\mathrm{m}$ from below

$$\begin{aligned}
\bar{\Omega}_{11}|t_\mathrm{m} - t|^{x_{11}} e^{i\delta_{11}} &= \bar{\Omega}_{11}|t_\mathrm{m} - t|^{x_{11}} e^{i\delta_{11}} s_{11} \frac{1 - \eta e^{-2i\delta}}{2i} + \bar{\Omega}_{21}|t_\mathrm{m} - t|^{x_{21}} e^{i\delta_{21}} s_{21} |g| \sigma_{t_\mathrm{m}}^K e^{-i\psi} \,, \\
\bar{\Omega}_{12}|t_\mathrm{m} - t|^{x_{12}} e^{i\delta_{12}} &= \bar{\Omega}_{12}|t_\mathrm{m} - t|^{x_{12}} e^{i\delta_{12}} s_{12} \frac{1 - \eta e^{-2i\delta}}{2i} + \bar{\Omega}_{22}|t_\mathrm{m} - t|^{x_{22}} e^{i\delta_{22}} s_{22} |g| \sigma_{t_\mathrm{m}}^K e^{-i\psi} \,, \\
\bar{\Omega}_{21}|t_\mathrm{m} - t|^{x_{21}} e^{i\delta_{21}} &= \bar{\Omega}_{11}|t_\mathrm{m} - t|^{x_{11}} e^{i\delta_{11}} s_{11} |g| \sigma_{t_\mathrm{m}}^\pi e^{-i\psi} + \bar{\Omega}_{21}|t_\mathrm{m} - t|^{x_{21}} e^{i\delta_{21}} s_{21} \frac{1 - \eta e^{-2i(\psi-\delta)}}{2i} \,, \\
\bar{\Omega}_{22}|t_\mathrm{m} - t|^{x_{22}} e^{i\delta_{22}} &= \bar{\Omega}_{12}|t_\mathrm{m} - t|^{x_{12}} e^{i\delta_{12}} s_{12} |g| \sigma_{t_\mathrm{m}}^\pi e^{-i\psi} + \bar{\Omega}_{22}|t_\mathrm{m} - t|^{x_{22}} e^{i\delta_{22}} s_{22} \frac{1 - \eta e^{-2i(\psi-\delta)}}{2i} \,,
\end{aligned} \tag{7.34}$$

where

$$s_{ij} = \frac{e^{i\pi x_{ij}}}{\sin \pi x_{ij}} \,, \tag{7.35}$$

and for $t \to t_{\rm m}$ from above

$$\begin{aligned}
\bar\Omega_{11}|t_{\rm m}-t|^{x_{11}} &= \bar\Omega_{11}|t_{\rm m}-t|^{x_{11}} \frac{e^{i\delta_{11}}}{\sin\pi x_{11}} \frac{1-\eta e^{-2i\delta}}{2i} + \bar\Omega_{21}|t_{\rm m}-t|^{x_{21}} \frac{e^{i\delta_{21}}}{\sin\pi x_{21}} |g| \sigma^K_{t_{\rm m}} e^{-i\psi} \,, \\
\bar\Omega_{12}|t_{\rm m}-t|^{x_{12}} &= \bar\Omega_{12}|t_{\rm m}-t|^{x_{12}} \frac{e^{i\delta_{12}}}{\sin\pi x_{12}} \frac{1-\eta e^{-2i\delta}}{2i} + \bar\Omega_{22}|t_{\rm m}-t|^{x_{22}} \frac{e^{i\delta_{22}}}{\sin\pi x_{22}} |g| \sigma^K_{t_{\rm m}} e^{-i\psi} \,, \\
\bar\Omega_{21}|t_{\rm m}-t|^{x_{21}} &= \bar\Omega_{11}|t_{\rm m}-t|^{x_{11}} \frac{e^{i\delta_{11}}}{\sin\pi x_{11}} |g| \sigma^\pi_{t_{\rm m}} e^{-i\psi} + \bar\Omega_{21}|t_{\rm m}-t|^{x_{21}} \frac{e^{i\delta_{21}}}{\sin\pi x_{21}} \frac{1-\eta e^{-2i(\psi-\delta)}}{2i} \,, \\
\bar\Omega_{22}|t_{\rm m}-t|^{x_{22}} &= \bar\Omega_{12}|t_{\rm m}-t|^{x_{12}} \frac{e^{i\delta_{12}}}{\sin\pi x_{12}} |g| \sigma^\pi_{t_{\rm m}} e^{-i\psi} + \bar\Omega_{22}|t_{\rm m}-t|^{x_{22}} \frac{e^{i\delta_{22}}}{\sin\pi x_{22}} \frac{1-\eta e^{-2i(\psi-\delta)}}{2i} \,,
\end{aligned} \tag{7.36}$$

where we have suppressed the evaluation at $t_{\rm m}$ wherever possible. If we assume that $g(t_{\rm m}) \neq 0$ and $\bar\Omega_{ij}(t_{\rm m}) \neq 0$ (which can always be achieved by choosing the matching point appropriately), we can conclude from the first line of (7.34) that $x_{21} \geq x_{11}$, since otherwise g or $\bar\Omega_{21}$ would have to vanish at $t_{\rm m}$. Conversely, the third line requires $x_{21} \leq x_{11}$ by the same argument, and hence $x_{11} = x_{21}$. Similarly, we find $x_{12} = x_{22}$. Moreover, as the determinant behaves according to (7.29), we can conclude that $x_{11} + x_{12} = x$, again provided that $\det \bar\Omega(t_{\rm m}) \neq 0$. Dividing the first line of (7.34) by the first line of (7.36), we find

$$e^{i\delta_{11}} \left(1 - \frac{e^{i\pi x_{11}}}{\sin\pi x_{11}} \frac{1-\eta e^{-2i\delta}}{2i} \right) = e^{i\pi x_{21}} \left(1 - \frac{e^{i\delta_{11}}}{\sin\pi x_{11}} \frac{1-\eta e^{-2i\delta}}{2i} \right) , \tag{7.37}$$

which for $x_{21} = x_{11}$ reduces to

$$e^{i\delta_{11}} = e^{i\pi x_{11}} \,, \tag{7.38}$$

and thus $\pi x_{11} = \delta_{11}$ up to integer multiples of 2π. Arguing analogously for x_{12}, these results can be summarized as

$$x_{11} = x_{21} \,, \qquad x_{12} = x_{22} \,, \qquad x_{ij} = \frac{\delta_{ij}}{\pi} \,, \qquad x_{11} + x_{12} = x \,. \tag{7.39}$$

By virtue of (7.39), (7.34) and (7.36) take the form

$$\begin{aligned}
\begin{pmatrix} \frac{e^{i\pi x_{11}}}{\sin\pi x_{11}} \frac{1-\eta e^{-2i\delta}}{2i} - 1 & \frac{e^{i\pi x_{11}}}{\sin\pi x_{11}} |g| \sigma^K_{t_{\rm m}} e^{-i\psi} \\ \frac{e^{i\pi x_{11}}}{\sin\pi x_{11}} |g| \sigma^\pi_{t_{\rm m}} e^{-i\psi} & \frac{e^{i\pi x_{11}}}{\sin\pi x_{11}} \frac{1-\eta e^{-2i(\psi-\delta)}}{2i} - 1 \end{pmatrix} \begin{pmatrix} \bar\Omega_{11} \\ \bar\Omega_{21} \end{pmatrix} = 0 \,, \\
\begin{pmatrix} \frac{e^{i\pi x_{12}}}{\sin\pi x_{12}} \frac{1-\eta e^{-2i\delta}}{2i} - 1 & \frac{e^{i\pi x_{12}}}{\sin\pi x_{12}} |g| \sigma^K_{t_{\rm m}} e^{-i\psi} \\ \frac{e^{i\pi x_{12}}}{\sin\pi x_{12}} |g| \sigma^\pi_{t_{\rm m}} e^{-i\psi} & \frac{e^{i\pi x_{12}}}{\sin\pi x_{12}} \frac{1-\eta e^{-2i(\psi-\delta)}}{2i} - 1 \end{pmatrix} \begin{pmatrix} \bar\Omega_{12} \\ \bar\Omega_{22} \end{pmatrix} = 0 \,.
\end{aligned} \tag{7.40}$$

To ensure the existence of non-trivial solutions the determinants of the coefficient matrices must vanish. This leads to

$$\cos\pi(2x_{11}-x) - \eta\cos\pi(2y-x) = 0 \,, \qquad \cos\pi(2x_{12}-x) - \eta\cos\pi(2y-x) = 0 \,, \qquad y = \frac{\delta(t_{\rm m})}{\pi} \,. \tag{7.41}$$

These conditions are invariant under $x_{11} \to x - x_{11}$, i.e. there is an ambiguity between x_{11} and x_{12}. However, demanding that x_{11} coincide with x in the single-channel limit yields

$$x_{11} = \frac{1}{2}\Big\{x + \frac{1}{\pi}\arccos(\eta\cos\pi(2y-x))\Big\}\,, \qquad x_{12} = \frac{1}{2}\Big\{x - \frac{1}{\pi}\arccos(\eta\cos\pi(2y-x))\Big\}\,. \tag{7.42}$$

Finally, (7.40) together with (7.42) and

$$\begin{aligned}
\sin\pi x_{11} &= \sin\frac{\pi x}{2}\sqrt{\frac{1+z}{2}} + \cos\frac{\pi x}{2}\sqrt{\frac{1-z}{2}}\,, \qquad \cos\pi x_{11} = \cos\frac{\pi x}{2}\sqrt{\frac{1+z}{2}} - \sin\frac{\pi x}{2}\sqrt{\frac{1-z}{2}}\,,\\
\sin\pi x_{12} &= \sin\frac{\pi x}{2}\sqrt{\frac{1+z}{2}} - \cos\frac{\pi x}{2}\sqrt{\frac{1-z}{2}}\,, \qquad \cos\pi x_{12} = \cos\frac{\pi x}{2}\sqrt{\frac{1+z}{2}} + \sin\frac{\pi x}{2}\sqrt{\frac{1-z}{2}}\,,\\
z &= \eta\cos\pi(2y-x)\,,
\end{aligned} \tag{7.43}$$

can be used to derive constraints on $\bar{\Omega}_{ij}$. We find

$$\frac{\bar{\Omega}_{21}}{\bar{\Omega}_{11}} = \frac{N}{2|g|\sigma^K_{t_\mathrm{m}}}\,, \qquad \frac{\bar{\Omega}_{12}}{\bar{\Omega}_{22}} = -\frac{N}{2|g|\sigma^\pi_{t_\mathrm{m}}}\,, \qquad N = \sqrt{1-\eta^2\cos^2\pi(2y-x)} - \eta\sin\pi(2y-x)\,. \tag{7.44}$$

In the single-channel case one can show that, using the integrals (7.33), the MO solution is automatically continuous at t_m [67]. In fact, the same statement holds true also in the two-channel case. The relations (7.44) are essential in the proof, as demonstrated in Appendix C.6.

7.2.3 Construction of the Omnès matrix

Infinite matching point

Our construction of the two-channel Omnès matrix with finite matching point will heavily rely on the solution for its infinite-matching-point analog $\Omega^\infty(t)$, whose defining property can be stated as

$$\begin{Bmatrix} \operatorname{Im}\Omega^\infty(t) = T^*(t)\Sigma(t)\Omega^\infty(t) \\ \operatorname{Im}\Omega^\infty(t) = 0 \end{Bmatrix} \qquad \text{for} \qquad \begin{Bmatrix} t \geq t_\pi \\ \text{otherwise} \end{Bmatrix}\,. \tag{7.45}$$

For its calculation we follow [238] and discretize the unsubtracted dispersion relation

$$\operatorname{Re}\Omega^\infty(t) = \frac{1}{\pi}\fint_{t_\pi}^{\infty}\mathrm{d}t'\,\frac{\operatorname{Im}\Omega^\infty(t')}{t'-t} \tag{7.46}$$

on a set of Gauß–Legendre integration points. Note that an unsubtracted dispersion relation converges provided that the phase-shift at infinity is positive. In the one-channel case this can be directly deduced from the explicit solution

$$\Omega^\infty(t) = \exp\left\{\frac{t}{\pi}\fint_{t_\pi}^{\infty}\mathrm{d}t'\,\frac{\delta(t')}{t'(t'-t)}\right\}\,, \tag{7.47}$$

which behaves as

$$\Omega^\infty(t) \sim t^{-\frac{\delta(\infty)}{\pi}} \tag{7.48}$$

for large t. The unitarity condition (7.45) can be rewritten as

$$\operatorname{Im}\mathbf{\Omega}_i^\infty = \begin{pmatrix} \frac{\eta\sin(2\delta-\psi)+\sin\psi}{\eta\cos(2\delta-\psi)+\cos\psi} & \frac{2|g|\sigma_t^K\theta(t-t_K)}{\eta\cos(2\delta-\psi)+\cos\psi} \\ \frac{2|g|\sigma_t^\pi}{\eta\cos(2\delta-\psi)+\cos\psi} & -\frac{\eta\sin(2\delta-\psi)-\sin\psi}{\eta\cos(2\delta-\psi)+\cos\psi} \end{pmatrix} \operatorname{Re}\mathbf{\Omega}_i^\infty \,, \qquad i\in\{1,2\}\,, \tag{7.49}$$

with

$$\mathbf{\Omega}_1^\infty = \begin{pmatrix}\Omega_{11}^\infty\\ \Omega_{21}^\infty\end{pmatrix}\,, \qquad \mathbf{\Omega}_2^\infty = \begin{pmatrix}\Omega_{12}^\infty\\ \Omega_{22}^\infty\end{pmatrix}\,, \tag{7.50}$$

which below the two-kaon threshold reduces to

$$\operatorname{Im}\mathbf{\Omega}_i^\infty = \begin{pmatrix}\tan\delta & 0\\ \frac{|g|\sigma_t^\pi}{\cos\delta} & 0\end{pmatrix}\operatorname{Re}\mathbf{\Omega}_i^\infty\,. \tag{7.51}$$

The details of the numerical solution of the corresponding integral equation for $\operatorname{Re}\mathbf{\Omega}_i^\infty$ are described in [238, 240].

Finite matching point, single-channel case

An Omnès function with a finite matching point does not allow for an unsubtracted dispersion relation, since the solution (7.28) tends to a constant for $t\to\infty$, and consequently one picks up contributions at infinity. Moreover, the cusp at the matching point renders both the discretization method and an iterative procedure involving subtracted dispersion relations inappropriate, as neither is able to accurately reproduce the analytic behavior around t_m. For this reason, the aim of this section is to establish a method that relies on the known solution in the infinite-matching-point scenario.

We first observe that the function

$$\xi(t) = \left(\frac{t_\mathrm{m}-t}{t_\mathrm{m}}\right)^{x(t)} = \left|\frac{t_\mathrm{m}-t}{t_\mathrm{m}}\right|^{x(t)} e^{-i\pi x(t)\theta(t-t_\mathrm{m})} \tag{7.52}$$

has the correct properties to cancel an imaginary part above t_m. Indeed, the function

$$\Omega(t) = \Omega^\infty(t)\xi(t)\,, \tag{7.53}$$

with $\Omega^\infty(t)$ from (7.47), fulfills

$$\left\{\begin{array}{c}\operatorname{Im}\Omega(t) = T^*(t)\Sigma(t)\Omega(t)\\ \operatorname{Im}\Omega(t) = \Omega^\infty(t)|\xi(t)|\Big(e^{i(\pi x(t)-\delta(t))}\sin\delta(t)-\sin\pi x(t)\Big)\end{array}\right\} \qquad \text{for} \qquad \left\{\begin{array}{c}t_\pi\le t\le t_\mathrm{m}\\ t\ge t_\mathrm{m}\end{array}\right\}\,, \tag{7.54}$$

and with the choice

$$\left\{\begin{array}{c}x(t)=\frac{\delta(t_\mathrm{m})}{\pi}\\ x(t)=\frac{\delta(t)}{\pi}\end{array}\right\} \qquad \text{for} \qquad \left\{\begin{array}{c}t\le t_\mathrm{m}\\ t\ge t_\mathrm{m}\end{array}\right\} \tag{7.55}$$

the defining property (7.20) holds. Since we know the analytic solution, we can study the properties of this construction in more detail

$$\Omega(t) = \exp\left\{\frac{t}{\pi}\int\limits_{t_\pi}^{t_\mathrm{m}}\mathrm{d}t'\frac{\delta(t')}{t'(t'-t)}\right\}\exp\left\{\frac{t}{\pi}\int\limits_{t_\mathrm{m}}^{\infty}\mathrm{d}t'\frac{\delta(t')-\pi x(t)}{t'(t'-t)}\right\}\,. \tag{7.56}$$

The first term coincides with the expected result for the single-channel case, while the second factor is new. It is indeed real, and thus preserves all defining properties, in particular the normalization $\Omega(0) = 1$. This example shows that we would exactly recover the result (7.28) if we did not know the solution for a finite matching point, constructed it according to (7.53), and chose $\delta(t) = \delta(t_\mathrm{m})$ for t above the matching point. Obviously, (7.56) implies that "the" Omnès function is not unique. The derivation of (7.25), however, only relies on the defining properties and is therefore independent of such modifications.

Finite matching point, two-channel case

To generalize the preceding considerations to the two-channel case we define a matrix

$$\xi_{ij}(t) = \bar{\xi}_{ij}(t)\left(\frac{t_\mathrm{m} - t}{t_\mathrm{m}}\right)^{x_{ij}(t)} \tag{7.57}$$

with real functions $\bar{\xi}_{ij}(t)$. In view of the results of the previous section we take phases and inelasticities constant above t_m and thus can ignore the t-dependence of x_{ij} and $\bar{\xi}_{ij}$, which in the following will always be understood to be evaluated at t_m. It is straightforward to show that

$$\left.\begin{matrix}\Omega(t) = a(t)\Omega^\infty(t)\xi(t)\\ \Omega(t) = a(t)(\Omega^\infty)^T(t)\xi(t)\end{matrix}\right\} \qquad \text{for} \qquad \left\{\begin{matrix}t \le t_\mathrm{m}\\ t \ge t_\mathrm{m}\end{matrix}\right\} , \tag{7.58}$$

with infinite-matching-point solution $\Omega^\infty(t)$ and a real matrix $a(t)$, fulfills (7.20) provided that

$$\begin{aligned}\operatorname{Im}\xi^T(t) + \xi^T(t)T(t)\Sigma(t) = 0 \qquad & \text{for } t \ge t_\mathrm{m} ,\\ \big[a(t), T^*(t)\Sigma(t)\big] = 0 \qquad & \text{for } t \le t_\mathrm{m} .\end{aligned} \tag{7.59}$$

Imposing $x_{11} = x_{21} = x - x_{12} = x - x_{22}$, the first condition corresponds to

$$\begin{aligned}&\begin{pmatrix} \frac{e^{i\pi x_{11}}}{\sin\pi x_{11}}\frac{1-\eta e^{-2i\delta}}{2i} - 1 & \frac{e^{i\pi x_{11}}}{\sin\pi x_{11}}|g|\sigma^\pi_{t_\mathrm{m}} e^{-i\psi} \\ \frac{e^{i\pi x_{11}}}{\sin\pi x_{11}}|g|\sigma^K_{t_\mathrm{m}} e^{-i\psi} & \frac{e^{i\pi x_{11}}}{\sin\pi x_{11}}\frac{1-\eta e^{-2i(\psi-\delta)}}{2i} - 1 \end{pmatrix}\begin{pmatrix}\bar{\xi}_{11}\\ \bar{\xi}_{21}\end{pmatrix} = 0 ,\\ &\begin{pmatrix} \frac{e^{i\pi x_{12}}}{\sin\pi x_{12}}\frac{1-\eta e^{-2i\delta}}{2i} - 1 & \frac{e^{i\pi x_{12}}}{\sin\pi x_{12}}|g|\sigma^\pi_{t_\mathrm{m}} e^{-i\psi} \\ \frac{e^{i\pi x_{12}}}{\sin\pi x_{12}}|g|\sigma^K_{t_\mathrm{m}} e^{-i\psi} & \frac{e^{i\pi x_{12}}}{\sin\pi x_{12}}\frac{1-\eta e^{-2i(\psi-\delta)}}{2i} - 1 \end{pmatrix}\begin{pmatrix}\bar{\xi}_{12}\\ \bar{\xi}_{22}\end{pmatrix} = 0 .\end{aligned} \tag{7.60}$$

Non-trivial solutions of (7.60) again exist for x_{11} and x_{12} given by (7.42), while the components of $\xi(t)$ are related by

$$\frac{\bar{\xi}_{21}}{\bar{\xi}_{11}} = \frac{N}{2|g|\sigma^\pi_{t_\mathrm{m}}} , \qquad \frac{\bar{\xi}_{12}}{\bar{\xi}_{22}} = -\frac{N}{2|g|\sigma^K_{t_\mathrm{m}}} . \tag{7.61}$$

For definiteness, we take

$$\bar{\xi}_{11} = 1 , \qquad \bar{\xi}_{22} = \left(1 + \frac{N^2}{1-\eta^2}\right)^{-1} , \tag{7.62}$$

which ensures that

$$\det\xi(t) = \left(\frac{t_\mathrm{m} - t}{t_\mathrm{m}}\right)^x , \tag{7.63}$$

and thus, by the results of the previous section, would preserve the form (7.28) of the determinant of the Omnès function if $\det a(t) = 1$. The condition (7.59) on $a(t)$ requires

$$a_{21} = a_{12}\frac{\sigma_t^\pi}{\sigma_t^K}\,, \qquad a_{22} = a_{11} - a_{12}\frac{\eta\sin(2\delta-\psi)}{|g|\sigma_t^K}\,, \tag{7.64}$$

while a_{11} and a_{12} can be chosen freely.

Finally, $\Omega(t)$ should fulfill the normalization $\Omega(0) = \mathbb{1}$, which can be achieved by modifying the normalization in the calculation of $\Omega^\infty(t)$ appropriately. Assuming $a(0) = \mathbb{1}$, the corresponding condition

$$\Omega^\infty(0)\xi(0) = \begin{pmatrix} \bar\xi_{11}\big(\Omega^\infty_{11}(0) + \frac{N}{2|g|\sigma^\pi_{t_\mathrm{m}}}\Omega^\infty_{12}(0)\big) & \bar\xi_{22}\big(\Omega^\infty_{12}(0) - \frac{N}{2|g|\sigma^K_{t_\mathrm{m}}}\Omega^\infty_{11}(0)\big) \\ \bar\xi_{11}\big(\Omega^\infty_{21}(0) + \frac{N}{2|g|\sigma^\pi_{t_\mathrm{m}}}\Omega^\infty_{22}(0)\big) & \bar\xi_{22}\big(\Omega^\infty_{22}(0) - \frac{N}{2|g|\sigma^K_{t_\mathrm{m}}}\Omega^\infty_{21}(0)\big) \end{pmatrix} = \mathbb{1} \tag{7.65}$$

leads to

$$\Omega^\infty(0) = \left(1 + \frac{N^2}{1-\eta^2}\right)^{-1} \begin{pmatrix} \bar\xi_{11}^{-1} & \bar\xi_{11}^{-1}\frac{N}{2|g|\sigma^K_{t_\mathrm{m}}} \\ -\bar\xi_{22}^{-1}\frac{N}{2|g|\sigma^\pi_{t_\mathrm{m}}} & \bar\xi_{22}^{-1} \end{pmatrix}\,. \tag{7.66}$$

The above construction (7.58) ensures that $\Omega_{ij}(t)$ has the expected behavior for $t \to t_\mathrm{m}$, that the factors of $(1 - t/t_\mathrm{m})^{x_{ij}}$ factorize in (7.60) (which have therefore already been canceled there), and that $\det\bar\Omega(t)$ is continuous at t_m. However, in general, $\bar\Omega_{ij}(t)$ itself will not be continuous at t_m and the condition (7.44) will be violated.

In order to remove these shortcomings we make use of the freedom in choosing $a(t)$. In fact, a particular choice of $a(t)$ can enforce continuity of either $\bar{\boldsymbol\Omega}_1(t)$ or $\bar{\boldsymbol\Omega}_2(t)$, but not of both simultaneously. This impediment can be circumvented by noting that (7.58) may be regarded as separate equations for $\bar{\boldsymbol\Omega}_1(t)$ and $\bar{\boldsymbol\Omega}_2(t)$. We can thus derive an $\bar{\boldsymbol\Omega}_1^{(1)}(t)$ from a construction with an $a_1(t)$ tailored for this component (discarding $\bar{\boldsymbol\Omega}_2^{(1)}(t)$ in this case), $\bar{\boldsymbol\Omega}_2^{(2)}(t)$ from a different $a_2(t)$ (discarding $\bar{\boldsymbol\Omega}_1^{(2)}(t)$), and finally join these two vectors into the final Omnès matrix $\Omega(t) = \big\{\bar{\boldsymbol\Omega}_1^{(1)}(t), \bar{\boldsymbol\Omega}_2^{(2)}(t)\big\}$.

Below the two-kaon threshold we take $a_1(t) = a_2(t) = \mathbb{1}$, while for $t \geq t_K$

$$\begin{aligned} a_1(t) &= \begin{pmatrix} 1 & \frac{N(t)}{2|g(t)|\sigma_t^\pi}f(t) \\ \frac{N(t)}{2|g(t)|\sigma_t^K}f(t) & 1 - f(t) + \frac{N^2(t)}{1-\eta^2(t)}f(t) \end{pmatrix}\,, \\ a_2(t) &= \begin{pmatrix} 1 & -\frac{2|g(t)|\sigma_t^K}{N(t)}f(t) \\ -\frac{2|g(t)|\sigma_t^\pi}{N(t)}f(t) & 1 - f(t) + \frac{1-\eta^2(t)}{N^2(t)}f(t) \end{pmatrix}\,, \end{aligned} \tag{7.67}$$

with

$$N(t) = \sqrt{1 - \eta(t)^2\cos^2(2\delta(t) - \psi(t))} - \eta(t)\sin(2\delta(t) - \psi(t))\,, \tag{7.68}$$

cf. (7.44), and a function $f(t)$ fulfilling $f(t_K) = 0$, $f(t_\mathrm{m}) = 1$, proves adequate. This construction makes sure that $\bar\Omega_{ij}(t)$ is continuous at t_m and that the relations (7.44) hold.

As we have seen in the previous section, the Omnès function is not unique, and therefore there is a priori no reason why the determinant of the resulting $\Omega(t)$ should match the single-channel expectation: we can always multiply $\bar{\boldsymbol\Omega}_i(t)$ with a real function $g(t)$ with $g(0) = 1$

without vitiating the above construction. Since the unitarity condition in its form analogous to (7.49) alone implies that

$$\det\Omega = \frac{2e^{i\psi}}{\eta\cos(2\delta-\psi)+\cos\psi}\big(\mathrm{Re}\,\Omega_{11}\mathrm{Re}\,\Omega_{22}-\mathrm{Re}\,\Omega_{12}\mathrm{Re}\,\Omega_{21}\big)\,, \tag{7.69}$$

and thus ensures the correct phase, this could be used to make the modulus of the determinant coincide with (7.28). We simply take

$$f(t) = \left(\frac{t-t_K}{t_\mathrm{m}-t_K}\right)^6 . \tag{7.70}$$

This choice of the exponent ensures that $f(t)$ decreases rapidly below t_m, but not so fast as to cause numerical problems in the matching-point region. In this way, the single-channel result for the determinant is accurately reproduced except for the energy region close to t_m.

7.3 Coupled-channel analysis of $\pi\pi \to \bar{N}N$ and $\bar{K}K \to \bar{N}N$

The $\pi\pi \to \bar{N}N$ and $\bar{K}K \to \bar{N}N$ S-waves fulfill the unitarity relation

$$\mathrm{Im}\,\mathbf{f}(t) = T^*(t)\Sigma(t)\mathbf{f}(t)\,, \qquad \mathbf{f}(t) = \begin{pmatrix} f_+^0(t) \\ \frac{2}{\sqrt{3}}h_+^0(t)\end{pmatrix}\,, \tag{7.71}$$

cf. (6.77), while RS equations provide a dispersion relation of the form

$$\mathbf{f}(t) = \mathbf{\Delta}(t) + (\mathbf{a}+\mathbf{b}\,t)(t-t_N) + \frac{t^2(t-t_N)}{\pi}\int\limits_{t_\pi}^{\infty}\mathrm{d}t'\frac{\mathrm{Im}\,\mathbf{f}(t')}{t'^2(t'-t_N)(t'-t)}\,. \tag{7.72}$$

In view of the results of Sect. 7.1.3, we only consider the twice-subtracted version of the RS system. The corresponding inhomogeneity $\Delta_1(t)$ for the πN part equals $\tilde{\Delta}_+^0(t)$ as defined in (7.10), although here we will neglect the contributions from higher t-channel partial waves, which are numerically insignificant (see [205]). In fact, the corresponding equation for $\Delta_2(t)$ is very similar, as long as we restrict ourselves to combinations of isospin and angular momentum that couple to $\pi\pi$ (cf. Appendix C.4): the nucleon pole terms need to be replaced by the hyperon-pole contributions (C.72), M_π by M_K, and the Clebsch–Gordan coefficients in the relation between the s-channel amplitudes in $I = \pm$ and $I_s = 0, 1$ bases are different from πN. In particular, the kernel functions $\tilde{G}_{0l}(t, W)$ require no further modification besides $M_\pi \to M_K$. Finally, the subtraction constants a_1 and b_1 can be related to the πN subthreshold parameters according to

$$a_1 = -\frac{1}{16\pi}\left(d_{00}^+ + \frac{g^2}{m} + b_{00}^+\frac{M_\pi^2}{3}\right)\,, \qquad b_1 = -\frac{1}{16\pi}\left(d_{01}^+ - \frac{b_{00}^+}{12}\right)\,, \tag{7.73}$$

cf. (C.56), and similarly for a_2, b_2, and KN subthreshold parameters.

Starting from the dispersion relation (7.72), the solution for $\mathbf{f}(t)$ can be derived along the lines that led to (7.25). In addition, we may use the spectral representation of the inverse of the Omnès matrix

$$\Omega^{-1}(t) = \mathbb{1} + \frac{t}{\pi}\int\limits_{t_\pi}^{t_\mathrm{m}}\mathrm{d}t'\frac{\mathrm{Im}\,\Omega^{-1}(t')}{t'(t'-t)} = \mathbb{1} - t\,\dot{\Omega}(0) + \frac{t^2}{\pi}\int\limits_{t_\pi}^{t_\mathrm{m}}\mathrm{d}t'\frac{\mathrm{Im}\,\Omega^{-1}(t')}{t'^2(t'-t)} \tag{7.74}$$

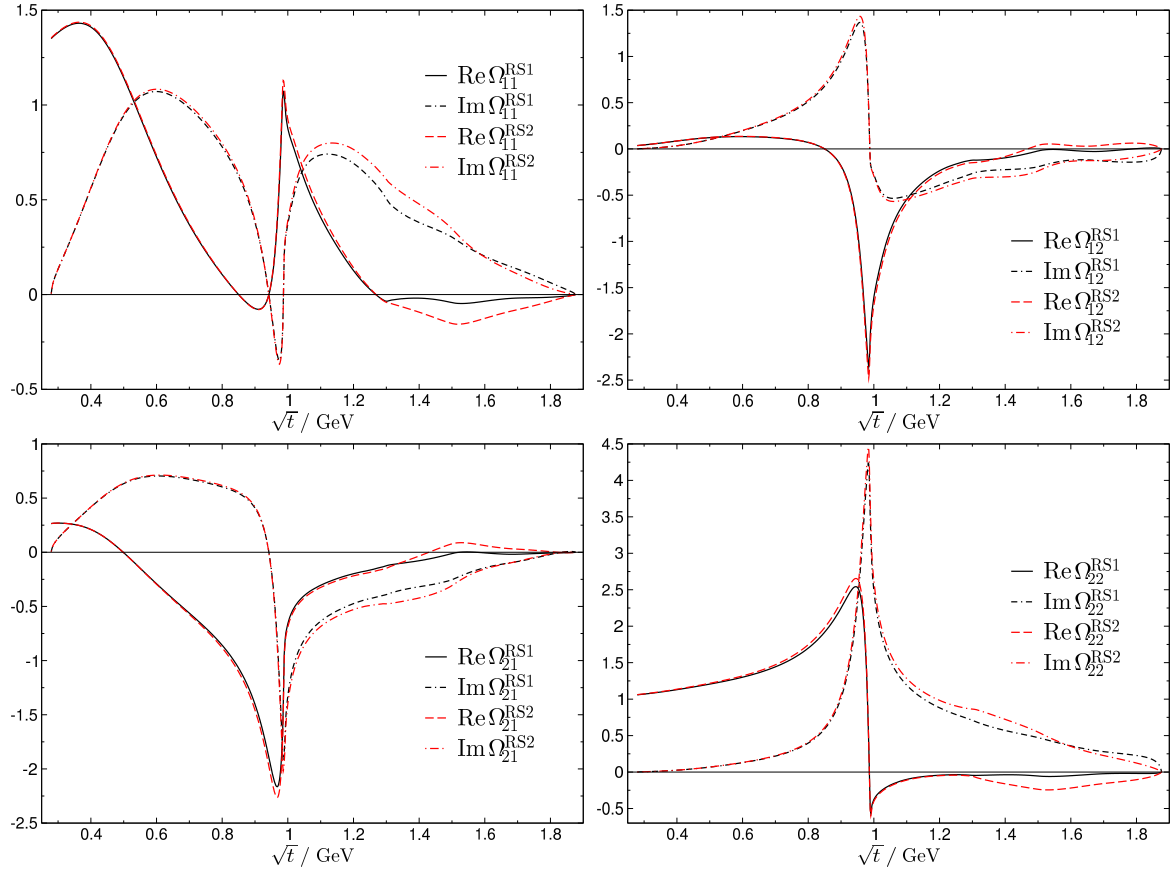

Figure 7.6: Results for real and imaginary part of the components of the Omnès matrix for the input phases RS1 and RS2 as described in the main text.

to perform the integrals involving $\mathbf{a}$ and $\mathbf{b}$, cf. (5.9). In this way, we arrive at

$$\mathbf{f}(t) = \mathbf{\Delta}(t) + (t-t_N)\Omega(t)(\mathbb{1} - t\,\dot{\Omega}(0))\mathbf{a} + t(t-t_N)\Omega(t)\mathbf{b} \tag{7.75}$$
$$- \frac{t^2(t-t_N)}{\pi}\Omega(t)\int_{t_\pi}^{t_{\rm m}} {\rm d}t' \frac{{\rm Im}\,\Omega^{-1}(t')\mathbf{\Delta}(t')}{t'^2(t'-t_N)(t'-t)} + \frac{t^2(t-t_N)}{\pi}\Omega(t)\int_{t_{\rm m}}^{\infty} {\rm d}t' \frac{\Omega^{-1}(t'){\rm Im}\,\mathbf{f}(t')}{t'^2(t'-t_N)(t'-t)}\,.$$

We now collect the additional input needed for the explicit evaluation of (7.75). We take the $\pi\pi$ phase and inelasticity up to $\sqrt{t_0} = 1.3\,$GeV from the extended Roy-equation analysis of [57] and the $\pi\pi \to \bar{K}K$ partial wave from [67], where, in the pseudophysical region $t_\pi \le t \le t_K$, the modulus $|g(t)|$ is determined as the solution of RS equations for πK scattering, while above the two-kaon threshold phase-shift solutions [241] are used.[5] Putting again ${\rm Im}\,\mathbf{f} = \mathbf{0}$ above $t_{\rm m}$, continuity of the MO solution at the matching point implies that the solution for $\mathbf{f}$ will vanish at $t_{\rm m}$ as well. We take advantage of the fact that for kinematic reasons $f_+^0(t)$ and $h_+^0(t)$ have a zero at the physical threshold t_N and choose the matching point accordingly as $t_{\rm m} = t_N$, which should allow for a reasonably smooth matching. To evaluate

[5] We are indebted to Bachir Moussallam for providing a version of the solution for $g(t)$ consistent with the $\pi\pi$ phase shift of [57].

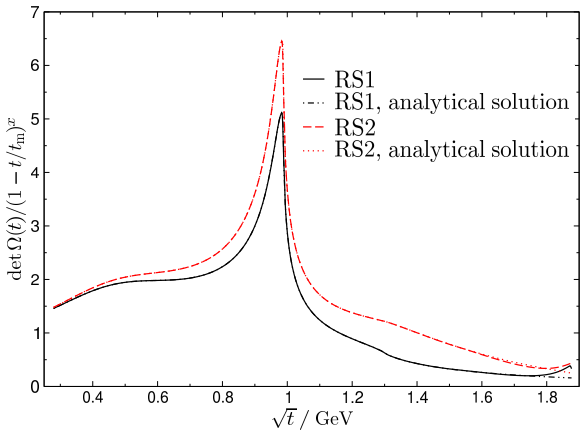

Figure 7.7: Comparison between numerical and analytical result for the determinant of the Omnès matrix.

the inhomogeneity Δ_2 we rely on the s-channel KN partial-wave solution from [229, 242], integrating the partial waves with $l \leq 4$ up to 2 GeV, and use the conventions for the KN Born terms given in Appendix C.4.

In the remainder of this chapter we will consider three variants of the input described above. First, we take δ and ψ to be constant above t_0 ("RS1"), second, we guide δ and ψ smoothly to 2π above t_0 by means of [238]

$$\delta(t) = 2\pi + (\delta(t_0) - 2\pi)\hat{f}\left(\frac{t}{t_0}\right), \qquad \hat{f}(x) = \frac{2}{1+x^{3/2}}, \tag{7.76}$$

keeping the phase constant above t_m ("RS2"), and third, we modify RS1 in such a way that $\Delta_2 = 0$ ("RS3"). In all three cases, $|g(t)|$ is led smoothly to zero above t_m by a prescription similar to (7.76). The choice of these variants is motivated as follows. As indicated above, the model for the $\pi\pi/\bar{K}K$ S-matrix is only meaningful roughly up to t_0, and ideally our results should be insensitive to variations of this input above t_0, the simplest choice of course being to keep the phases constant. However, in the calculation of the scalar meson form factors (see Sect. 7.4.1), the phase ψ must tend to an asymptotic value of 2π to ensure the correct asymptotic behavior [238], which, phenomenologically, also suggests to guide δ to 2π. Thus, RS1 and RS2 are convenient choices to assess the sensitivity to the high-energy input for the phase shifts. The results for the Omnès matrix corresponding to these two scenarios are depicted in Fig. 7.6. In addition, we compare the results for $\det\Omega(t)/(1-t/t_\mathrm{m})^x$ to the analytically known results in Fig. 7.7. As expected, the only deviations occur in the proximity of t_m, where the modifications originating from $f(t)$ according to (7.70) set in. Note that the difference between RS1 and RS2 appears slightly exaggerated here, since x differing in both cases leads to a different factor being divided out.

For the remaining πN input we take $g^2/4\pi = 14.28$ and the KH80 subthreshold parameters as reference point. In contrast, we are not aware of reliable input for the KN subthreshold parameters, and simply put $a_2 = b_2 = 0$. In fact, this approximation gives reason to investigate RS3, since the results from the πN sector show that the contributions from the corresponding parameters will certainly not be larger than the sum of KN Born terms and s-channel integrals. The difference between RS1 and RS3 thus serves as an estimate of the uncertainty induced by neglecting the KN subthreshold parameters.

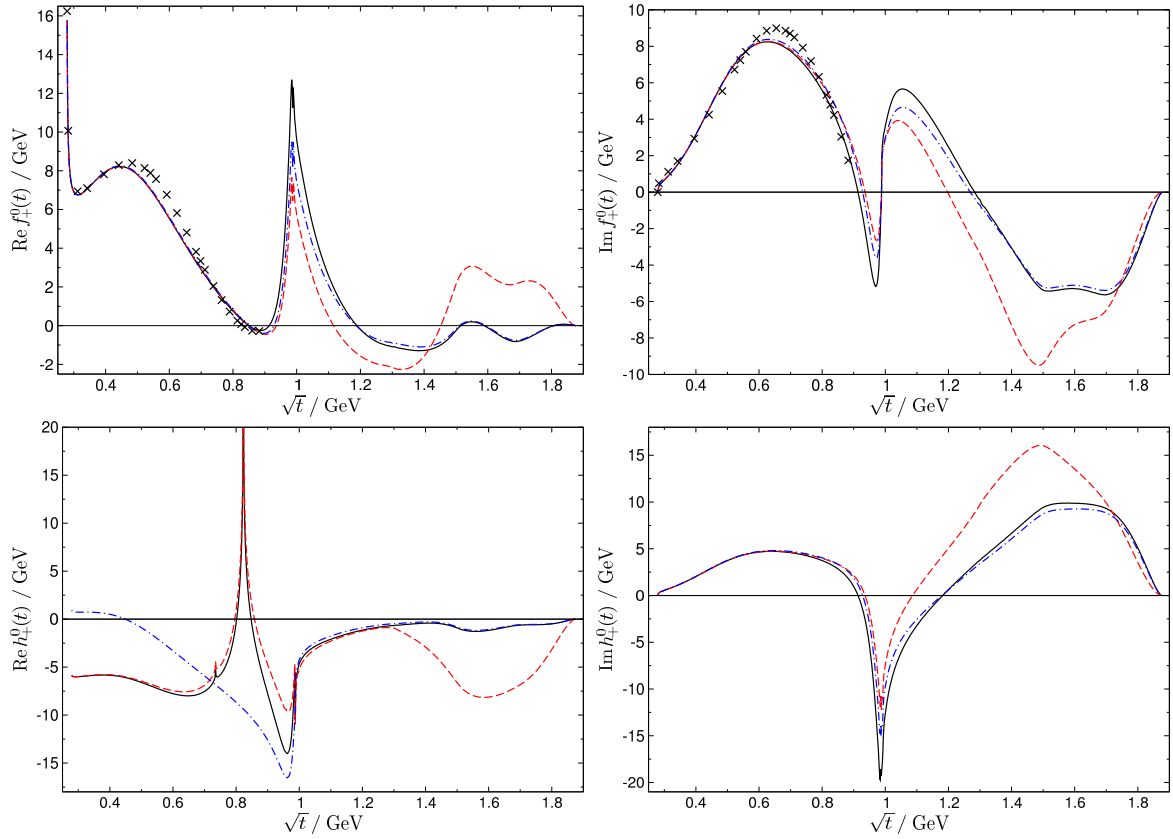

Figure 7.8: Results for real and imaginary part of $f_+^0(t)$ and $h_+^0(t)$. The solid, dashed, and dot-dashed lines refer to the input RS1, RS2, and RS3 as described in the main text. For $f_+^0(t)$ the black crosses indicate the results of [152].

The results for $f_+^0(t)$ and $h_+^0(t)$ are shown in Fig. 7.8. In the case of $f_+^0(t)$ the agreement between the different parameter sets is very good up to 1 GeV. It is striking that the difference between RS1 and RS2 is much larger than between RS1 and RS3, which indicates that the results are much more sensitive to the choice of the phases above t_0 than to the details of the KN amplitude. The real part of $h_+^0(t)$ exhibits two distinct divergences below 1 GeV that correspond to the pole-term contributions from the Λ (large peak at 0.82 GeV) and Σ (small peak at 0.73 GeV) hyperon, strictly analogous to the nucleon pole in $f_+^0(t)$ that emerges slightly below t_π, cf. Appendix C.2.1. These divergences, which disappear in RS3 by construction, do not pose a problem in practice, e.g. in a dispersive analysis of the scalar form factor of the nucleon (see Sect. 7.4.2), since $h_+^0(t)$ only contributes to the spectral function above t_K. Apart from these poles below the two-kaon threshold the conclusion is very similar to $f_+^0(t)$: the uncertainty in the phase shifts outweighs the uncertainty in the KN input.

7.4 Dispersive analysis of the scalar form factor of the nucleon

The results of the previous section for $f_+^0(t)$ and $h_+^0(t)$ may be applied to write down a dispersive representation for the scalar form factor of the nucleon that fully includes $\bar{K}K$ intermediate states, and thereby to update the result from [164] for the correction Δ_σ, which

is needed for the extraction of the pion–nucleon σ term from πN scattering (cf. Sect. 3.3). The leading contribution to the imaginary part of $\sigma(t)$ originates from $\pi\pi$ intermediate states, so that, upon neglecting higher terms in the spectral function, $\operatorname{Im}\sigma(t)$ can be expressed in terms of the scalar pion form factor $F_\pi^S(t)$ and $f_+^0(t)$. Relying on the results of [239] for $F_\pi^S(t)$ and of [152] for $f_+^0(t)$ led to the estimate [164]

$$\Delta_\sigma = (15.2 \pm 0.4)\,\text{MeV} \,, \tag{7.77}$$

where the error only includes the uncertainty in the parameterization of the $\pi\pi$ phase available at that time. In particular, one should note that the contributions from $\bar{K}K$ intermediate states in the determination of $f_+^0(t)$ and the unitarity relation for $\sigma(t)$ were neglected, while being included in the calculation of $F_\pi^S(t)$. Although the dominant effect may indeed be expected in the pion form factor, such a treatment is strictly speaking inconsistent and leads to an additional uncertainty in (7.77) that is difficult to quantify. Moreover, the results for $f_+^0(t)$ from [152] and thus for Δ_σ from [164] correspond to a πN coupling constant $g^2/4\pi = 14.28$ and KH80 subthreshold parameters, both of which will need to be updated in a full solution of the RS system.

7.4.1 Scalar pion and kaon form factors

We define the scalar pion and kaon form factors as

$$F_\pi^S(t) = \langle \pi(p')|\hat{m}(\bar{u}u + \bar{d}d)|\pi(p)\rangle \,, \qquad F_K^S(t) = \langle K(p')|\hat{m}(\bar{u}u + \bar{d}d)|K(p)\rangle \,, \qquad t = (p'-p)^2 \,. \tag{7.78}$$

In the two-channel approximation they fulfill the unitarity relation [239]

$$\operatorname{Im}\mathbf{F}^S(t) = T^*(t)\Sigma(t)\mathbf{F}^S(t) \,, \qquad \mathbf{F}^S(t) = \begin{pmatrix} F_\pi^S(t) \\ \frac{2}{\sqrt{3}} F_K^S(t) \end{pmatrix} \,, \tag{7.79}$$

and thus

$$\mathbf{F}^S(t) = \alpha\,\mathbf{\Omega}_1^\infty + \beta\,\mathbf{\Omega}_2^\infty \,, \tag{7.80}$$

with the infinite-matching-point Omnès solutions $\mathbf{\Omega}_i^\infty$ defined in (7.50). The phases δ and ψ are guided smoothly to their assumed asymptotic value of 2π according to (7.76). Using the normalization $\Omega^\infty(0) = \mathbb{1}$ of the Omnès matrix to pin down the coefficients α, β, we find

$$\begin{aligned} F_\pi^S(t) &= F_\pi^S(0)\Omega_{11}^\infty(t) + \frac{2}{\sqrt{3}} F_K^S(0)\Omega_{12}^\infty(t) \,, \\ F_K^S(t) &= \frac{\sqrt{3}}{2} F_\pi^S(0)\Omega_{21}^\infty(t) + F_K^S(0)\Omega_{22}^\infty(t) \,. \end{aligned} \tag{7.81}$$

The form factors at $t = 0$ can be determined via the Feynman–Hellmann theorem [136]

$$F_\pi^S(0) = \hat{m}\frac{\partial}{\partial\hat{m}} M_\pi^2 \,, \qquad F_K^S(0) = \hat{m}\frac{\partial}{\partial\hat{m}} M_K^2 \,, \tag{7.82}$$

from the quark-mass dependence of the meson masses. For the pion form factor the result at $\mathcal{O}(p^4)$ in the chiral expansion reads [12]

$$F_\pi^S(0) = M_\pi^2 - \frac{M_\pi^4}{32\pi^2 F_\pi^2}(\bar{l}_3 - 1) = (0.984 \pm 0.006) M_\pi^2 \,, \tag{7.83}$$

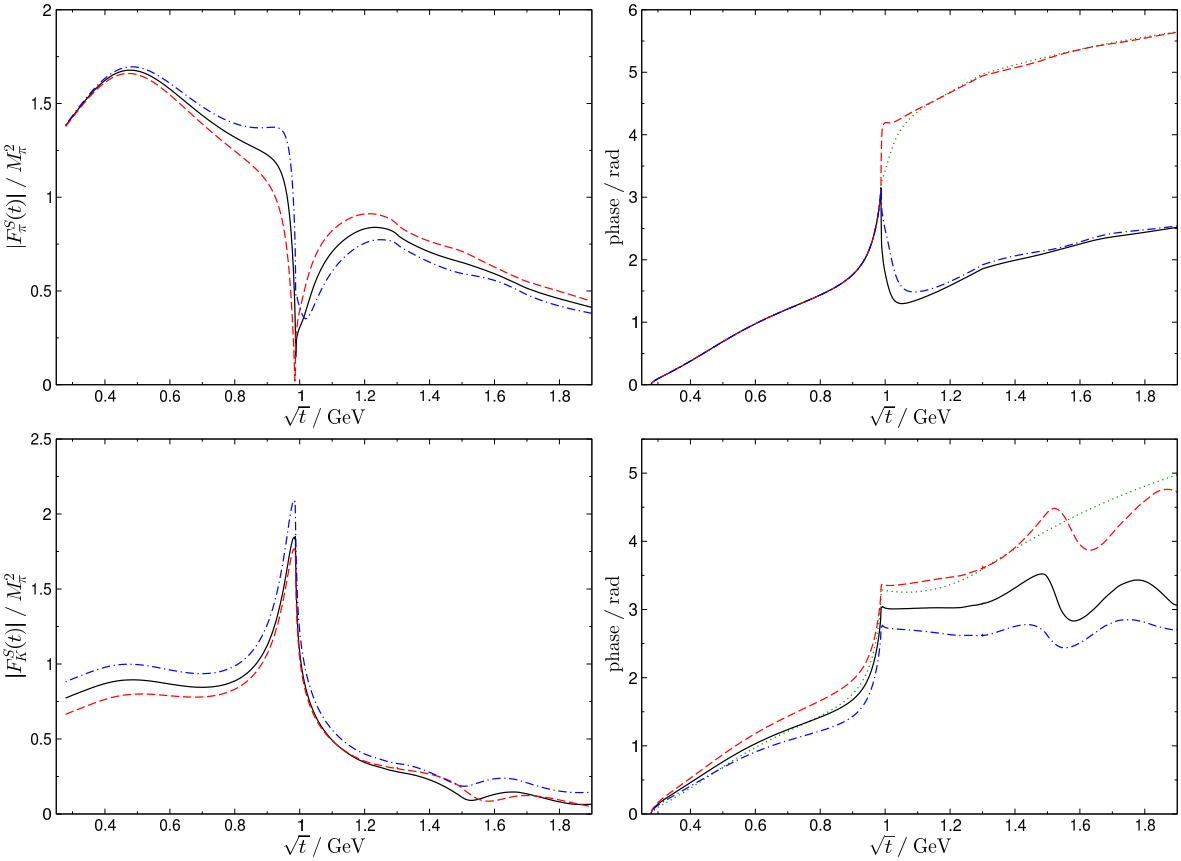

Figure 7.9: Modulus (left) and phase (right) of the scalar pion and kaon form factors. The solid, dashed, and dot-dashed lines refer to $F_K^S(0) = M_\pi^2/2$, $0.4M_\pi^2$, and $0.6M_\pi^2$. The phases of $F_\pi^S(t)$ and $F_K^S(t)$ are compared to δ and ψ, respectively, as indicated by the dotted lines.

where we have used $\bar{l}_3 = 3.2 \pm 0.8$ [102]. The leading-order result for the kaon form factor

$$F_K^S(0) = \frac{M_\pi^2}{2} \tag{7.84}$$

is subject to potentially large $SU(3)$ corrections, which in the isospin limit amount to [13]

$$F_K^S(0) = \frac{M_\pi^2}{2}\left\{1 + \frac{M_\eta^2}{32\pi^2 F_\pi^2}\log\frac{M_\eta^2}{\mu^2} + \frac{M_K^2}{72\pi^2 F_\pi^2}\left(\log\frac{M_\eta^2}{\mu^2} + 1\right) - \frac{M_\pi^2}{32\pi^2 F_\pi^2}\log\frac{M_\pi^2}{\mu^2} + \frac{8(2M_K^2 - M_\pi^2)}{F_\pi^2}\big(2L_8^{\mathrm{r}} - L_5^{\mathrm{r}}\big) + \frac{32M_K^2}{F_\pi^2}\big(2L_6^{\mathrm{r}} - L_4^{\mathrm{r}}\big)\right\}, \tag{7.85}$$

where M_η denotes the mass of the η. Varying the LECs in the range [102]

$$2L_8^{\mathrm{r}} - L_5^{\mathrm{r}} = (-0.35\ldots + 0.1)\cdot 10^{-3}\,, \qquad 2L_6^{\mathrm{r}} - L_4^{\mathrm{r}} = (0\ldots + 0.2)\cdot 10^{-3}\,, \tag{7.86}$$

corresponds to $F_K^S(0) = (0.4\ldots 0.6)M_\pi^2$. In the following, we will restrict $F_K^S(0)$ to lie within these boundaries, while adopting $F_K^S(0) = M_\pi^2/2$ as our central solution.

$F_K^S(0)$	$0.4M_\pi^2$	$M_\pi^2/2$	$0.6M_\pi^2$
$\langle r^2\rangle_\pi^S$ [fm^2]	0.575	0.584	0.592
$\langle r^2\rangle_K^S$ [fm^2]	0.835	0.710	0.626

Table 7.3: Dependence of the scalar pion and kaon radii on $F_K^S(0)$.

The corresponding results for the form factors are depicted in Fig. 7.9. The phase of $F_\pi^S(t)$ coincides with δ below t_K, as required by unitarity, cf. (7.51) and (7.81). Above t_K, the behavior of the phase actually depends on the assumption for $F_K^S(0)$, it either largely follows δ or abruptly drops by π. The appearance of the first scenario is surprising in view of the results of [243] (see also [244]), where only the second behavior is mentioned (the assumption for $F_K^S(0)$ agrees with our central solution). The reason for this discrepancy can be understood as follows. The S-matrix used in [243] involves a phase δ that fulfills $\delta(t_K) < \pi$. In this case, the phase δ_t of the full $\pi\pi$ partial wave t_0^0 itself displays the characteristic drop above t_K, reflecting the fact that the phase arrives at the two-kaon threshold immediately before completing a full circle in the Argand diagram. However, in recent years, it seems to have become consensus that $\delta(t_K) > \pi$ is more likely [55–57], which implies that δ_t by no means exhibits a sharp drop above t_K. We conclude that the behavior of the phase cannot simply be deduced from the phase of t_0^0, it crucially depends on the relative strength $F_\pi^S(0)/F_K^S(0)$ in the superposition of the two terms involving different components of the Omnès matrix as given in (7.81), thus attesting to the inherent two-channel nature of the problem.[6] From this point of view, it is not surprising that the phase may behave differently if $F_K^S(0)$ is varied. In contrast, the phase of $F_K^S(t)$ roughly follows the shape of ψ for all three solutions. Note that in this case (7.51) does not impose any additional constraints on the phase below t_K.

Finally, we can express the scalar radii in terms of the form factors at $t = 0$ and the derivative of the Omnès matrix

$$\begin{aligned}\langle r^2\rangle_\pi^S &= 6\left\{\dot\Omega_{11}^\infty(0) + \frac{2}{\sqrt{3}}\frac{F_K^S(0)}{F_\pi^S(0)}\dot\Omega_{12}^\infty(0)\right\},\\ \langle r^2\rangle_K^S &= 6\left\{\frac{\sqrt{3}}{2}\frac{F_\pi^S(0)}{F_K^S(0)}\dot\Omega_{21}^\infty(0) + \dot\Omega_{22}^\infty(0)\right\}.\end{aligned} \tag{7.87}$$

In this way, the derivative of the Omnès matrix, e.g. for our central solution

$$\dot\Omega^\infty(0) = \begin{pmatrix}2.31 & 0.32\\ 1.26 & 0.89\end{pmatrix}\ \text{GeV}^{-2}\,, \tag{7.88}$$

leads to the results for the scalar radii summarized in Table 7.3. Our results for the scalar pion radius are in good agreement with $\langle r^2\rangle_\pi^S = (0.61 \pm 0.04)\,\text{fm}^2$ from [58] and the range $\langle r^2\rangle_\pi^S = (0.583\ldots 0.653)\,\text{fm}^2$ found in [238]. Albeit attached with a fairly large uncertainty, the values for $\langle r^2\rangle_K^S$ lie systematically higher than its ChPT expectation $\langle r^2\rangle_K^S \sim 0.3\,\text{fm}^2$ [245] (for a more detailed comparison of the dispersive and the ChPT result see [246]). In both approaches the uncertainties are substantial, either due to the large sensitivity to the specific

[6] One immediate consequence is that an effective single-channel Omnès description of $F_\pi^S(t)$ in terms of the phase of $F_\pi^S(t)$ will only be applicable for certain ranges in $F_\pi^S(0)/F_K^S(0)$, unless the phase is supplemented by hand with an additional term $-\pi\theta(t - t_K)$.

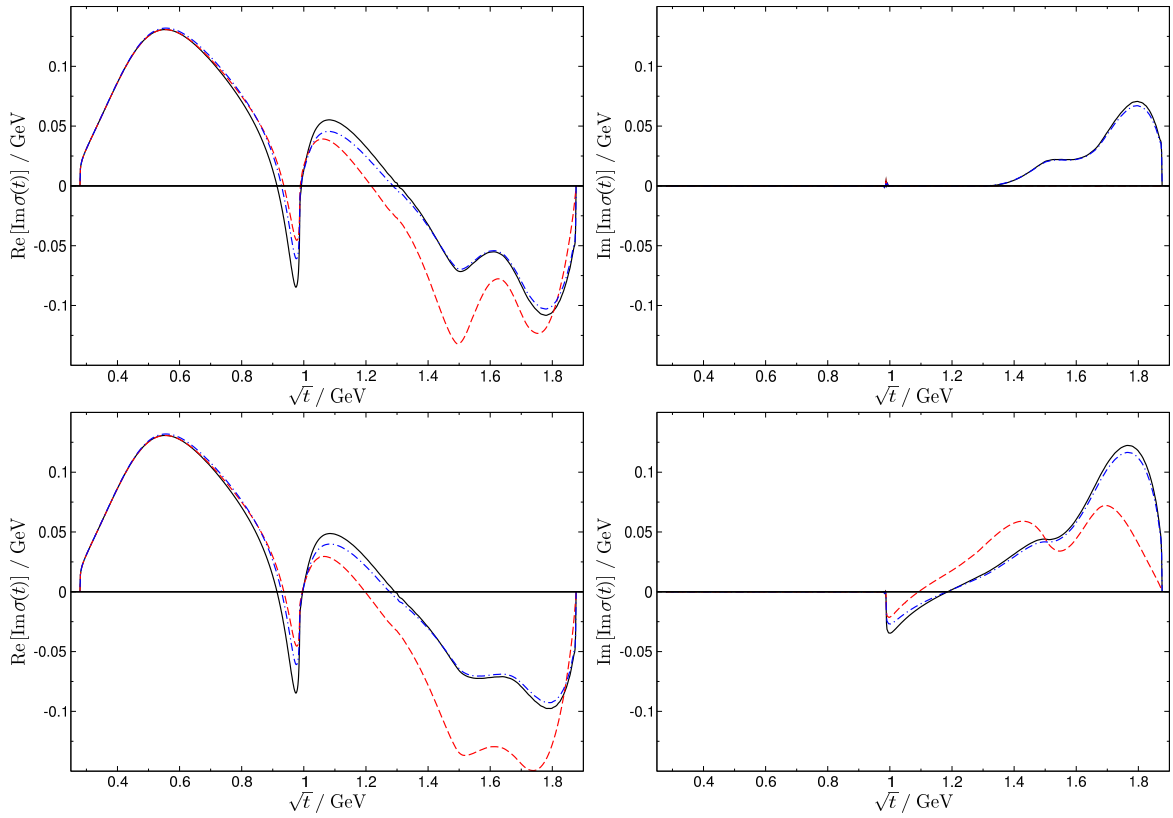

Figure 7.10: Real and imaginary part of $\mathrm{Im}\,\sigma(t)$ for our full solution (top) and with $h_+^0(t)$ set to zero (bottom). The solid, dashed, and dot-dashed lines refer to the input RS1, RS2, and RS3 as described in Sect. 7.3.

input in the dispersive calculation or due to insufficient knowledge of LECs. As the precise value of the scalar kaon radius is irrelevant for the present study, we do not consider this issue any further.

7.4.2 Scalar form factor of the nucleon

The scalar form factor of the nucleon fulfills the once-subtracted dispersion relation

$$\sigma(t) = \sigma_{\pi N} + \frac{t}{\pi}\int\limits_{t_\pi}^{\infty} \mathrm{d}t' \frac{\mathrm{Im}\,\sigma(t')}{t'(t'-t)}\,, \tag{7.89}$$

where the pion–nucleon σ term $\sigma_{\pi N} = \sigma(0)$ acts as subtraction constant. In this way, evaluation at $t = 2M_\pi^2$ gives access to Δ_σ as defined in (3.20), provided that the imaginary part is sufficiently well constrained to perform the dispersive integral. Generalizing the result quoted in [164] by including $\bar{K}K$ intermediate states, the spectral function becomes

$$\mathrm{Im}\,\sigma(t) = -\frac{1}{p_t^2\sqrt{t}}\left\{\frac{3}{4}q_t\big(F_\pi^S(t)\big)^* f_+^0(t)\,\theta\big(t-t_\pi\big) + k_t\big(F_K^S(t)\big)^* h_+^0(t)\,\theta\big(t-t_K\big)\right\}. \tag{7.90}$$

The corresponding results using the input RS1, RS2, and RS3 as discussed in Sect. 7.3 as well as our central solution for the scalar pion and kaon form factors are depicted in Fig. 7.10.

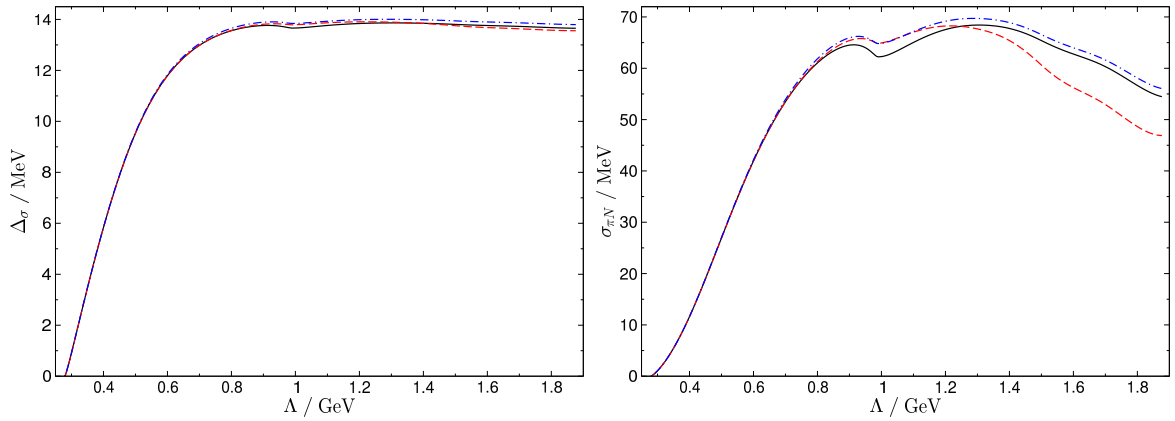

Figure 7.11: Δ_σ and $\sigma_{\pi N}$ as a function of the integral cutoff Λ. Line code as in Fig. 7.10.

We also show a variant of the spectral function where the second term in the above unitarity relation (7.90) due to $\bar{K}K$ intermediate states is neglected. While the impact on the real part is moderate, we see that the spectral function develops an imaginary part starting at t_K. In contrast, our full solution stays real as long as the input for the phases is treated in the same way in the calculation of the meson–nucleon partial waves and the scalar meson form factors. For this reason, the results for RS1 and RS3 become complex around t_0, while RS2 is real in the full energy range (apart from some numerical noise at the two-kaon threshold). These findings emphasize the importance of treating inelastic channels consistently in all contributions to the unitarity relation, in particular the necessity to explicitly include the intermediate states that are responsible for the inelasticities.

The dependence of Δ_σ on the cutoff Λ of the dispersive integral is shown in Fig. 7.11. We see that the dispersion relation converges quickly and the results hardly change above 1 GeV. We quote the outcome for $\Lambda = \sqrt{t_0}$ and input RS2 as our final result, estimating the uncertainty by the variation induced by changing the cutoff to $2m$ and varying the input set or the assumption for $F_K^S(0)$ (cf. Table 7.4). Moreover, $f_+^0(t)$ and $h_+^0(t)$ depend linearly on the πN coupling constant and the subthreshold parameters, so that the corresponding corrections for changing them can be determined straightforwardly. Putting everything together, we find

$$\begin{aligned}
\Delta_\sigma &= (13.9 \pm 0.3)\,\text{MeV} \\
&\quad + Z_1\left(\frac{g^2}{4\pi} - 14.28\right) + Z_2\Big(d_{00}^+\, M_\pi + 1.46\Big) + Z_3\Big(d_{01}^+\, M_\pi^3 - 1.14\Big) + Z_4\Big(b_{00}^+\, M_\pi^3 + 3.54\Big)\,, \\
Z_1 &= 0.36\,\text{MeV}\,, \qquad Z_2 = 0.57\,\text{MeV}\,, \qquad Z_3 = 12.0\,\text{MeV}\,, \qquad Z_4 = -0.81\,\text{MeV}\,.
\end{aligned} \tag{7.91}$$

These results are in reasonable agreement with [164], and remarkably close to the $\mathcal{O}(p^4)$ ChPT analysis of [22] (for earlier work in ChPT on Δ_σ see [247, 97, 19, 76])

$$\Delta_\sigma = 14.0\,\text{MeV} + 2M_\pi^4\,\bar{e}_2\,, \tag{7.92}$$

where $\bar{e}_2$ is an $\mathcal{O}(p^4)$ low-energy constant. The potentially largest correction in (7.91) originates from d_{01}^+, e.g. taking $d_{01}^+ = 1.27\,M_\pi^{-3}$ from [227] increases Δ_σ by 1.6 MeV. In contrast, adjusting the coupling constant to $g^2/4\pi = 13.7$ [33] only leads to a correction of -0.2 MeV. Indeed, this result is not surprising, as it is d_{01}^+ that controls the slope of the scalar form factor of the nucleon.

$(F_K^S(0),\, \Lambda)$	$(0.4M_\pi^2,\, 1.3\,\mathrm{GeV})$	$(M_\pi^2/2,\, 1.3\,\mathrm{GeV})$	$(0.6M_\pi^2,\, 1.3\,\mathrm{GeV})$	$(M_\pi^2/2,\, 2m)$
RS1	13.81	13.86	13.91	13.65
RS2	13.75	13.89	14.04	13.56
RS3	13.92	14.00	14.09	13.80

Table 7.4: Results for Δ_σ in MeV for various combinations of $F_K^S(0)$, integral cutoff Λ, and input.

Finally, it is of course tempting to evaluate the dispersive integral not only to determine Δ_σ, but also in its unsubtracted form

$$\sigma_{\pi N} = \frac{1}{\pi}\int\limits_{t_\pi}^{\infty} \mathrm{d}t' \frac{\mathrm{Im}\,\sigma(t')}{t'} \tag{7.93}$$

to constrain the σ term itself. Unfortunately, it is clear from Fig. 7.11 that the integral does not converge fast enough and is still sensitive to energies where the two-channel model for the spectral function is not trustworthy anymore. Nevertheless, we may conclude that large values of $\sigma_{\pi N}$ seem to be possible.

Chapter 8

Solution strategy for the *s*-channel problem

8.1 Parameterizations of the *s*-channel partial waves

Once the t-channel equations are solved, the structure of the s-channel problem resembles the form of $\pi\pi$ Roy equations, and should be amenable to similar solution techniques. The basic idea can be summarized in such a way that the phase shifts at low energies are represented in a suitable parameterization whose free parameters, together with the subtraction constants, are determined by minimizing the difference between the left- and right-hand side of (6.39).

The phase shifts $\delta_{l\pm}^{I_s}$ and inelasticities $\eta_{l\pm}^{I_s}$ for the S- and P-waves as given by the SAID [229] and KH80 [152] partial-wave solutions in the low-energy region, i.e. below the maximally allowed matching point $W_\mathrm{m} = 1.38\,\mathrm{GeV}$, cf. (6.30), are depicted in Figs. 8.1 and 8.2, while Fig. 8.3 shows the imaginary parts up to $W_\mathrm{a} = 2.5\,\mathrm{GeV}$. In particular, Fig. 8.2 suggests that inelasticities may be ignored in the S_{31}-, P_{13}-, and P_{33}-waves.[1] Inspired by [57], we find that in the remaining partial waves the inelasticity can be well described by a parameterization of the form

$$\eta_{l\pm}^{I_s} = \frac{1-\alpha_{l\pm}^{I_s}(s-s_\mathrm{inel})^{r_{l\pm}^{I_s}}(s-s_+)^{r_{l\pm}^{I_s}}}{1+\alpha_{l\pm}^{I_s}(s-s_\mathrm{inel})^{r_{l\pm}^{I_s}}(s-s_+)^{r_{l\pm}^{I_s}}}\,, \qquad s_\mathrm{inel} = (m+2M_\pi)^2\,, \tag{8.1}$$

with $r_{0+}^{1/2} = r_{1-}^{3/2} = 3/2$, $r_{1-}^{1/2} = 5/2$,[2] and

$$\alpha_{0+}^{1/2} = 0.0412\,\mathrm{GeV}^{-6}\,, \qquad \alpha_{1-}^{3/2} = 0.066\,\mathrm{GeV}^{-6}\,, \qquad \alpha_{1-}^{1/2} = 3.716\,\mathrm{GeV}^{-10}\,, \tag{8.2}$$

which have been determined by fitting to the SAID inelasticities. The main advantage of the parameterization (8.1) concerns the analytic continuation for $s_+ \le s \le s_\mathrm{inel}$. In this kinematic range $\eta_{l\pm}^{I_s}$ becomes a complex number of magnitude 1 and can thus be regarded as a modification of the phase shift $\delta_{l\pm}^{I_s}$. Indeed, (8.1) below s_inel gives rise to the phase

$$\hat\delta_{l\pm}^{I_s} = \pm\arctan\left\{\alpha_{l\pm}^{I_s}(s_\mathrm{inel}-s)^{r_{l\pm}^{I_s}}(s-s_+)^{r_{l\pm}^{I_s}}\right\}, \tag{8.3}$$

[1] In these figures, we have also introduced the spectroscopic notation $L_{2I_s\,2J}$ to label the partial waves. Several amplitudes of the KH80 solution exhibit peaks or oscillatory tendencies that should be considered an artifact of the calculation. In particular, we will discard the presumptive outliers for the inelasticities that appear in some partial waves between 1.3 GeV and the matching point.

[2] These powers have been chosen on purely phenomenological grounds to accurately reproduce the experimental inelasticities. However, the threshold behavior of the phase shifts demands that $r_{l\pm}^{I_s} \ge l + 1/2$.

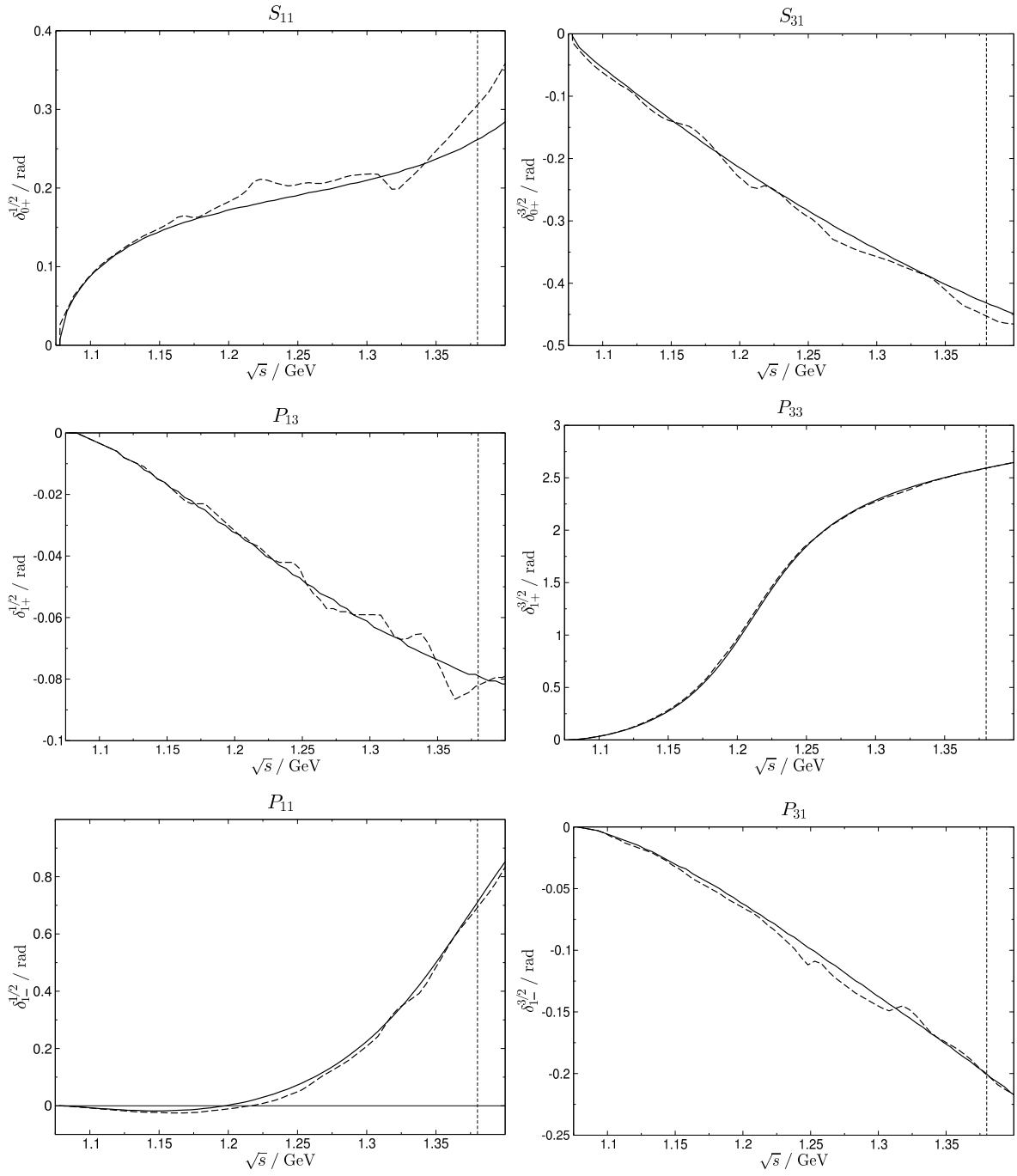

Figure 8.1: Phase shifts of the s-channel partial waves from the SAID [229] (solid line) and KH80 [152] (dashed line) partial-wave solutions in the low-energy region. The short-dashed line refers to $W_{\rm m} = 1.38\,{\rm GeV}$.

where the upper/lower sign applies to $r^{I_s}_{l\pm} = 3/2$ and $r^{I_s}_{l\pm} = 5/2$. In this way, (8.1) is applicable in the whole low-energy region and hence respects manifestly the requirement that the S-matrix be described by an analytic function. As indicated in Fig. 6.1, the inelasticities cannot be determined from an iterative solution of the RS system, but have to be taken as input.

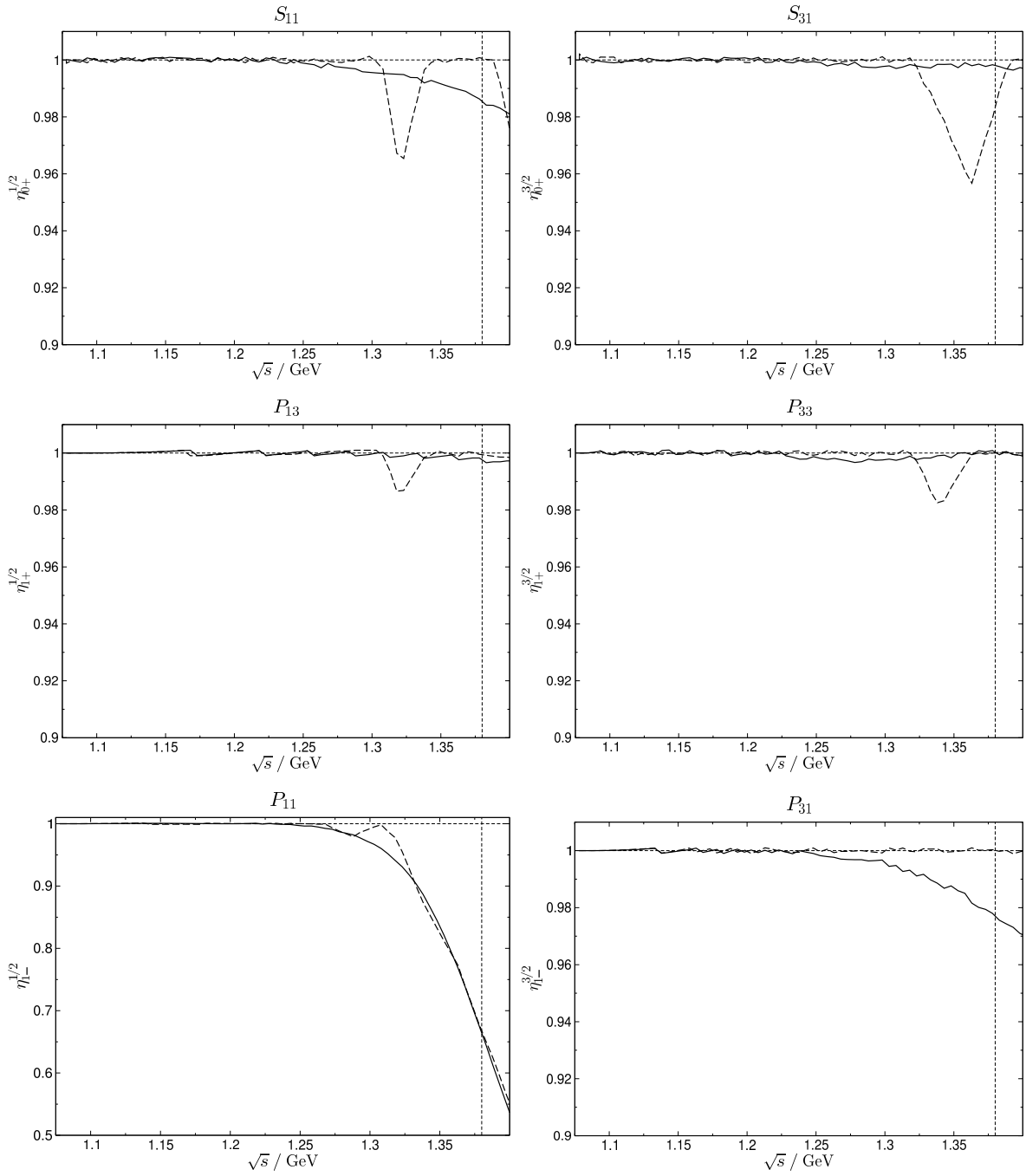

Figure 8.2: Inelasticity parameters of the s-channel partial waves in the low-energy region. Line code as in Fig. 8.1.

In view of Fig. 8.2 one would be inclined to consider the variation between $\alpha_{l\pm}^{I_s} = 0$ and the values given in (8.2) as the uncertainty range for S_{11} and P_{31}, while the inelasticity parameters for the P_{11}-wave from both partial-wave solutions agree reasonably well.

The obtain a parameterization for the full phase shifts we write

$$\delta_{l\pm}^{I_s} = \bar{\delta}_{l\pm}^{I_s} + \hat{\delta}_{l\pm}^{I_s} \,, \tag{8.4}$$

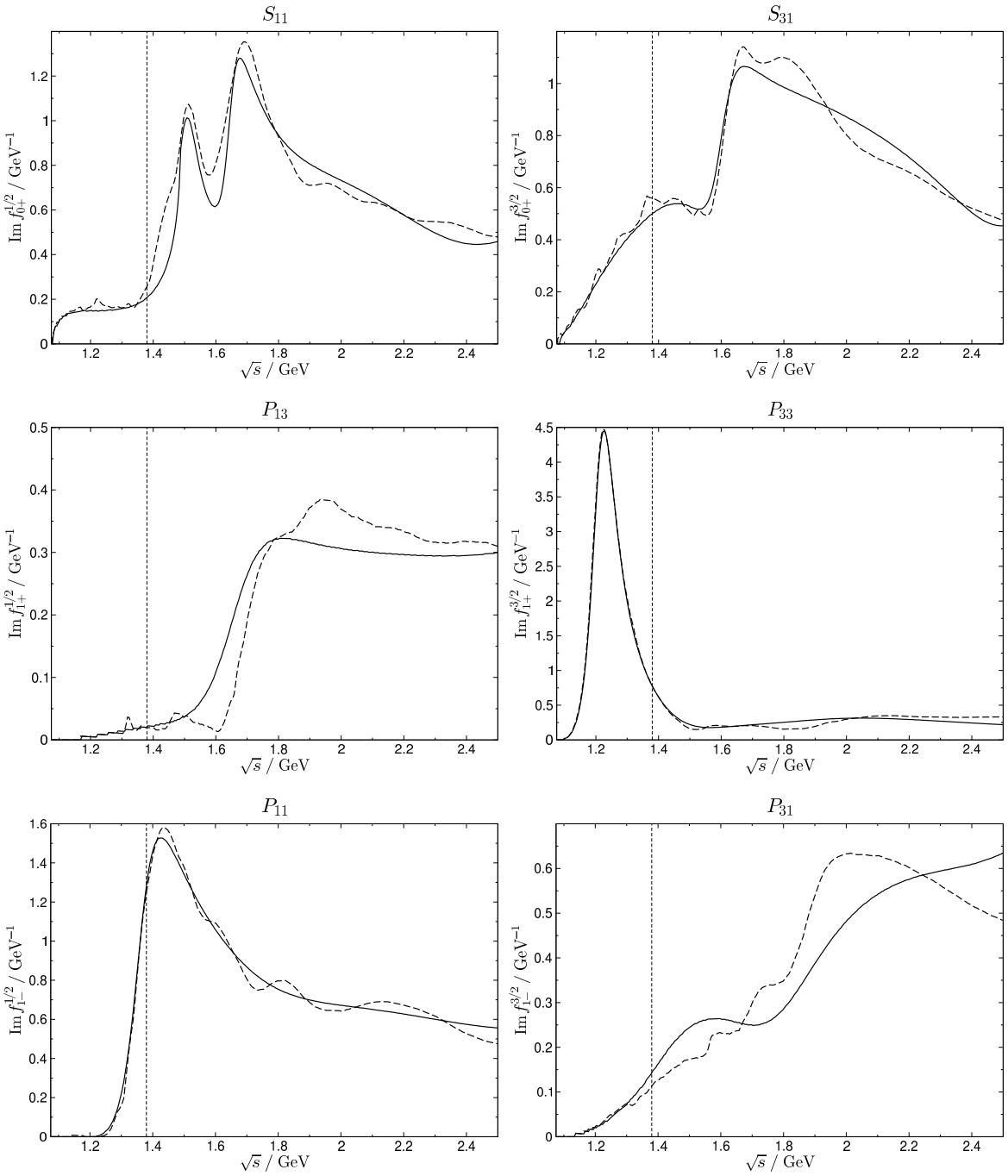

Figure 8.3: Imaginary parts of the s-channel partial waves up to $W_\mathrm{a} = 2.5\,\mathrm{GeV}$. Line code as in Fig. 8.1.

with $\hat{\delta}^{I_s}_{l\pm} = 0$ above s_inel. For the SAID low-energy phase shifts most of the partial waves may be accurately described by a Schenk-like parameterization of the form [248]

$$\tan\bar{\delta}^{I_s}_{l\pm} = |\mathbf{q}|^{2l+1}\Big\{A^{I_s}_{l\pm} + B^{I_s}_{l\pm}\mathbf{q}^2 + C^{I_s}_{l\pm}\mathbf{q}^4 + D^{I_s}_{l\pm}\mathbf{q}^6\Big\}\frac{s_+ - s^{I_s}_{l\pm}}{s - s^{I_s}_{l\pm}}\,, \tag{8.5}$$

except for the P_{33}-wave where a parameterization of the form [55]

$$\cot\bar{\delta}^{I_s}_{l\pm} = \frac{1}{|\mathbf{q}|^{2l+1}}\frac{s-s^{I_s}_{l\pm}}{s_+-s^{I_s}_{l\pm}}\left\{\frac{1}{\tilde{A}^{I_s}_{l\pm}}+\tilde{B}^{I_s}_{l\pm}\big(w(s)-w(s_+)\big)+\tilde{C}^{I_s}_{l\pm}\big(w(s)-w(s_+)\big)^2\right\},$$
$$w(s) = \frac{\sqrt{s}-\sqrt{\bar{s}^{I_s}_{l\pm}-s}}{\sqrt{s}+\sqrt{\bar{s}^{I_s}_{l\pm}-s}}, \tag{8.6}$$

proves more adequate to reproduce the phase shift above the resonance. In contrast, we conclude from Fig. 8.1 that the KH80 partial waves are not sufficiently smooth to allow for similar low-energy parameterizations.

8.2 Sum rules for the πN threshold parameters

In order to exploit the constraints on the S-wave scattering lengths from hadronic atoms for a solution of the RS system it is advantageous to first derive the relation to the threshold expansion. The threshold parameters are defined as the expansion coefficients in

$$\mathrm{Re}\, f^I_{l\pm}(s) = \mathbf{q}^{2l}\Big\{a^I_{l\pm}+b^I_{l\pm}\mathbf{q}^2+c^I_{l\pm}\mathbf{q}^4+d^I_{l\pm}\mathbf{q}^6+\mathcal{O}\big(\mathbf{q}^8\big)\Big\}. \tag{8.7}$$

The leading terms are the scattering lengths as introduced for the S-waves in Part I, while the first correction is determined by the effective ranges $b^I_{l\pm}$ and even higher terms are referred to as shape parameters.

As a direct calculation of these parameters from derivatives of the partial waves is numerically rather delicate, the most promising framework for a stable evaluation is based on sum rules involving dispersive integrals over the pertinent amplitudes, see [53, 249] for the case of $\pi\pi$ scattering. Such sum rules could be derived directly from (6.39) by taking derivatives with respect to $\mathbf{q}^2$ and identifying the results with the coefficients in (8.7). However, this procedure is unfavorable from a technical point of view since a substantial part of the effort in calculating the derivatives is wasted on reproducing the kinematic structure of the partial-wave expansion (6.31), i.e. its decomposition into invariant amplitudes A^I and B^I with known, $\mathbf{q}$-dependent prefactors.

For this reason, we will consider an approach that is directly based on the threshold expansion of the projections (6.32). Suppressing isospin indices for the time being, we have

$$X_l(s) = X^{(l)}_l\mathbf{q}^{2l}+X^{(l+1)}_l\mathbf{q}^{2l+2}+X^{(l+2)}_l\mathbf{q}^{2l+4}+\mathcal{O}\big(\mathbf{q}^{2l+6}\big), \qquad X\in\{A,B\}, \tag{8.8}$$

and the inversion

$$X^{(n)}_l = \frac{1}{n!}\Big[\partial^n_{\mathbf{q}^2}X_l(s)\Big]_{\mathbf{q}^2=0}. \tag{8.9}$$

By means of the expansion

$$X(s,t) = X(s,0)+t\,[\partial_t X(s,t)]_{t=0}+\frac{t^2}{2}\big[\partial_t^2X(s,t)\big]_{t=0}+\cdots, \tag{8.10}$$

the lowest coefficients in (8.8) are given by

$$X^{(0)}_0 = 2\,[X(s,0)]_{\mathbf{q}^2=0}, \qquad X^{(1)}_0 = 2\,\big[\partial_{\mathbf{q}^2}X(s,0)\big]_{\mathbf{q}^2=0}-4\,[\partial_tX(s,t)]_{t=0,\mathbf{q}^2=0}, \tag{8.11}$$
$$X^{(1)}_1 = \frac{4}{3}\,[\partial_tX(s,t)]_{t=0,\mathbf{q}^2=0}, \qquad X^{(2)}_1 = \frac{4}{3}\,\big[\partial_{\mathbf{q}^2}\partial_tX(s,t)\big]_{t=0,\mathbf{q}^2=0}-\frac{8}{3}\,\big[\partial_t^2X(s,t)\big]_{t=0,\mathbf{q}^2=0},$$

and expanding (6.31) in $\mathbf{q}^2$ then shows

$$\begin{aligned}
a_{0+} &= \frac{m}{8\pi W_+}\Big(A_0^{(0)} + M_\pi B_0^{(0)}\Big)\,,\\
b_{0+} &= \frac{1}{32\pi m M_\pi W_+}\Big(-A_0^{(0)}(2m-M_\pi) + B_0^{(0)}(2m^2+M_\pi^2)\Big) + \frac{m}{8\pi W_+}\Big(A_0^{(1)} + M_\pi B_0^{(1)}\Big)\,,\\
a_{1+} &= \frac{m}{8\pi W_+}\Big(A_1^{(1)} + M_\pi B_1^{(1)}\Big)\,,\\
b_{1+} &= \frac{1}{32\pi m M_\pi W_+}\Big(-A_1^{(1)}(2m-M_\pi) + B_1^{(1)}(2m^2+M_\pi^2)\Big) + \frac{m}{8\pi W_+}\Big(A_1^{(2)} + M_\pi B_1^{(2)}\Big)\,,\\
a_{1-} &= a_{1+} + \frac{1}{32\pi m W_+}\Big(-A_0^{(0)} + B_0^{(0)}(2m+M_\pi)\Big)\,,\\
b_{1-} &= b_{1+} + \frac{1}{128\pi m^3 M_\pi W_+}\Big(A_0^{(0)}(2m+M_\pi) - B_0^{(0)}(2m^2+2mM_\pi+M_\pi^2)\Big)\\
&\quad + \frac{1}{32\pi m W_+}\Big(-A_0^{(1)} + B_0^{(1)}(2m+M_\pi)\Big)\,.
\end{aligned} \tag{8.12}$$

In combination with the HDRs (6.27) as well as the subtracted versions thereof these equations lead to sum rules for the threshold parameters, e.g. for the S- and P-wave scattering lengths

$$\begin{aligned}
a_{0+}^{\pm} &= \frac{m}{4\pi W_+}\Big(\big[A^{\pm}(s,0)\big]_{\mathbf{q}^2=0} + M_\pi\big[B^{\pm}(s,0)\big]_{\mathbf{q}^2=0}\Big)\,,\\
a_{1+}^{\pm} &= \frac{m}{6\pi W_+}\Big(\big[\partial_t A^{\pm}(s,t)\big]_{t=0,\mathbf{q}^2=0} + M_\pi\big[\partial_t B^{\pm}(s,t)\big]_{t=0,\mathbf{q}^2=0}\Big)\,,\\
a_{1-}^{\pm} &= a_{1+}^{\pm} + \frac{1}{16\pi m W_+}\Big(-\big[A^{\pm}(s,0)\big]_{\mathbf{q}^2=0} + (2m+M_\pi)\big[B^{\pm}(s,0)\big]_{\mathbf{q}^2=0}\Big)\,,
\end{aligned} \tag{8.13}$$

and the S-wave effective ranges

$$\begin{aligned}
b_{0+}^{\pm} &= \frac{1}{16\pi m M_\pi W_+}\Big(-\big[A^{\pm}(s,0)\big]_{\mathbf{q}^2=0}(2m-M_\pi) + \big[B^{\pm}(s,0)\big]_{\mathbf{q}^2=0}(2m^2+M_\pi^2)\Big)\\
&\quad + \frac{m}{4\pi W_+}\Big(\big[\partial_{\mathbf{q}^2}A^{\pm}(s,0)\big]_{\mathbf{q}^2=0} - 2\big[\partial_t A^{\pm}(s,t)\big]_{t=0,\mathbf{q}^2=0}\\
&\qquad + M_\pi\Big[\big[\partial_{\mathbf{q}^2}B^{\pm}(s,0)\big]_{\mathbf{q}^2=0} - 2\big[\partial_t B^{\pm}(s,t)\big]_{t=0,\mathbf{q}^2=0}\Big]\Big)\,.
\end{aligned} \tag{8.14}$$

Thus, the equations for the effective ranges involve, in addition, the derivatives with respect to $\mathbf{q}^2$. However, integration and differentiation may only be exchanged after the threshold singularity has been removed, see e.g. [53], since otherwise the integral over

$$\left[\partial_{\mathbf{q}^2}\frac{\operatorname{Im} f_{0+}^{I_s}(W')}{s'-s}\right]_{\mathbf{q}^2=0} \sim \frac{W_+}{\sqrt{mM_\pi}}\frac{\big(a_{0+}^{I_s}\big)^2}{(s'-s_+)^{3/2}} \qquad \text{for} \qquad s' \to s_+ \tag{8.15}$$

would diverge at threshold. This divergence can be removed by adding a suitable term proportional to

$$\fint_{s_+}^{\infty}\frac{\mathrm{d}s'}{(s'-s)\sqrt{s'-s_+}} = 0 \qquad \text{for} \qquad s > s_+ \tag{8.16}$$

before taking the derivative.

		1-sub	2-sub	3-sub	ex 3-sub	KH80	SP98
S_{11}	$a_{0+}^{1/2}\ [10^{-3}M_\pi^{-1}]$	-40.9	146.0	175.0	175.9	173 ± 3	176.6
S_{31}	$a_{0+}^{3/2}\ [10^{-3}M_\pi^{-1}]$	-72.3	-132.4	-103.5	-103.9	-101 ± 4	-88.3
P_{13}	$a_{1+}^{1/2}\ [10^{-3}M_\pi^{-3}]$	-43.5	-30.9	-28.9	-29.2	-30 ± 2	-13.4
P_{33}	$a_{1+}^{3/2}\ [10^{-3}M_\pi^{-3}]$	200.7	207.7	208.8	208.9	214 ± 2	210.7
P_{11}	$a_{1-}^{1/2}\ [10^{-3}M_\pi^{-3}]$	-87.7	-74.3	-72.4	-71.5	-81 ± 2	-73.3
P_{31}	$a_{1-}^{3/2}\ [10^{-3}M_\pi^{-3}]$	-53.0	-43.8	-42.8	-43.3	-45 ± 2	-43.3
S_{11}	$b_{0+}^{1/2}\ [10^{-3}M_\pi^{-3}]$	-150.7	-65.1	-35.0	-33.5	-18 ± 12	-46.9
S_{31}	$b_{0+}^{3/2}\ [10^{-3}M_\pi^{-3}]$	-34.8	-78.3	-45.6	-46.3	-58 ± 9	-49.0

Table 8.1: Threshold parameters from the HDR sum rules compared to the results of the KH80 and SP98 partial-wave solutions as quoted in [152] and [78], respectively.

The sum rules for the covariant amplitudes and their derivatives required for the explicit evaluation of (8.13) and (8.14) are summarized in Appendix C.7. Using $a = -23.2 M_\pi^2$, cf. (6.29), KH80 subthreshold parameters, $g^2/4\pi = 13.7$, and SAID s-channel partial waves, we find for the threshold parameters in the different subtraction schemes, cf. Sect. 6.3.3, the results summarized in Table 8.1. For the t-channel amplitudes we have employed the two-channel result for the S-wave, with input RS2 as defined in Sect. 7.3, terminating the integration at $\sqrt{t_0} = 1.3\,\text{GeV}$, and for the P- and D-waves the "3-sub" single-channel solution with matching point $\sqrt{t_\text{m}} = 1.1\,\text{GeV}$, using in both cases the same coupling constant and s-channel partial waves as for the s-channel contributions.[3] The convergence pattern of the threshold parameters for an increasing number of subtractions as displayed in Table 8.1 indicates that the partial third subtraction is crucial for a reliable determination of the S-wave parameters, whereas for the P-wave scattering lengths also less subtractions might be sufficient. In any case, these results demonstrate that both subtraction schemes that go beyond the twice-subtracted version provide an appreciable suppression of the high-energy region in the integrals and ensure reasonable agreement with the threshold parameters deduced from partial-wave analyses.

8.3 *s*-channel Roy equations

8.3.1 Multiplicity of solutions

The existence and uniqueness of solutions for a particular choice of the matching point W_m depend on the value of the phase shifts at W_m and may be inferred from the multiplicity index m as defined in (1.46). Using the phases of the SAID amplitudes to determine the indices

[3] Strictly speaking, this input is inconsistent, as the KH80 subthreshold parameters would call for a different coupling constant and s-channel input, which e.g. manifests itself by the fact that the results for $a_{1+}^{3/2}$ and $a_{1-}^{1/2}$ are closer to the SAID than to the KH80 values. However, the implementation of the accordingly modified input is hampered by the convergence of the s-channel integrals near threshold. Especially for the S-wave effective ranges the cancellation of individually singular pieces required to render the integrals finite demands that the integrands near threshold be given in a suitable parameterization that makes their threshold behavior explicit. In view of the difficulties to cast the low-energy KH80 imaginary parts into such a parameterization, see Sect. 8.1, we refrain from repeating the calculation for strict KH80 input.

	$m_{f_{0+}^{1/2}}$	$m_{f_{0+}^{3/2}}$	$m_{f_{1+}^{1/2}}$	$m_{f_{1+}^{3/2}}$	$m_{f_{1-}^{1/2}}$	$m_{f_{1-}^{3/2}}$	m
$W_+ \leq W_\mathrm{m} \leq 1.20\,\mathrm{GeV}$	0	-1	-1	0	-1	-1	-4
$1.20\,\mathrm{GeV} \leq W_\mathrm{m} \leq 1.23\,\mathrm{GeV}$	0	-1	-1	0	0	-1	-3
$1.23\,\mathrm{GeV} \leq W_\mathrm{m} \leq 1.52\,\mathrm{GeV}$	0	-1	-1	1	0	-1	-2
$1.52\,\mathrm{GeV} \leq W_\mathrm{m} \leq 1.69\,\mathrm{GeV}$	0	-1	-1	1	1	-1	-1
$1.69\,\mathrm{GeV} \leq W_\mathrm{m} \leq 1.80\,\mathrm{GeV}$	1	-1	-1	1	1	-1	0

Table 8.2: Multiplicity index m as a function of W_m.

m_i for each partial wave leads to the pattern displayed in Table 8.2. The total multiplicity index m for the system of S- and P-wave Roy equations is negative for $W_\mathrm{m} < 1.69\,\mathrm{GeV}$, i.e. in general no solution exists unless the input satisfies $|m|$ additional conditions. Moreover, a physical solution is characterized by the requirement of a smooth matching. In this way, one expects another constraint on the input due to the no-cusp condition in each partial wave, which, altogether, amounts to 8 conditions for $W_\mathrm{m} = 1.38\,\mathrm{GeV}$. In fact, the partial third subtraction introduced in Sect. 6.3.3 was constructed in such a way that this matches exactly the number of degrees of freedom as reflected by the 8 subthreshold parameters involved in this version of the RS equations. In this "3-sub" setup one should be able to find a unique solution for the low-energy phase shifts and subthreshold parameters devoid of cusps at W_m.

In case the hadronic-atom values for the S-wave scattering lengths are imposed as further constraints on the solution two additional degrees of freedom need to be provided to guarantee the existence of a solution. For the reasons described in Sect. 6.3.3 we choose b_{10}^- and a_{10}^- and thus arrive at the "ex 3-sub" scenario. Following the reasoning in Chapter 3 we identify the scattering lengths with the virtual-photon subtracted versions of $a_{\pi^\pm p}$, which leads to

$$a_{0+}^{1/2} = (170.5 \pm 2.0) \cdot 10^{-3} M_\pi^{-1}\,, \qquad a_{0+}^{3/2} = (-86.5 \pm 1.8) \cdot 10^{-3} M_\pi^{-1}\,, \tag{8.17}$$

see Appendix A.3.1. For the potential issues regarding isospin violation that may ensue for the extraction of the pion–nucleon σ term we refer to the discussion in Sect. 3.3.

8.3.2 Towards a solution of the s-channel equations

As a first step we decompose the s-channel RS system (6.39) into the equations for the real and imaginary parts. Defining the physical limit by $W \to W + i\epsilon$ and collecting the imaginary pieces that follow from the principal-value prescription for the Cauchy kernels shows that the equations for the imaginary parts are trivially fulfilled, while those for the real parts are identical to (6.39) upon replacing $f_{l\pm}^{I_s}(W)$ by $\mathrm{Re}\, f_{l\pm}^{I_s}(W)$ and the integrals by their principal-value analogs. In order to investigate to what extent these equations are fulfilled for the SAID and KH80 s-channel amplitudes we compare their left- and right-hand side in Fig. 8.4 both for the "3-sub" and "ex 3-sub" versions of the RS equations, using $a = -23.2 M_\pi^2$, KH80 subthreshold parameters, and $g^2/4\pi = 13.7\,(14.28)$ for the SAID (KH80) partial waves, respectively, as well as t-channel amplitudes as described in Sect. 8.2 calculated with the pertinent input for the coupling constant and the s-channel partial waves. Fig. 8.4 shows that the equations are fulfilled for KH80 in the threshold region, while deviations emerge at higher energies in nearly all partial waves, most notably in the P_{13} and P_{31} phase shifts, while the discrepancy in the

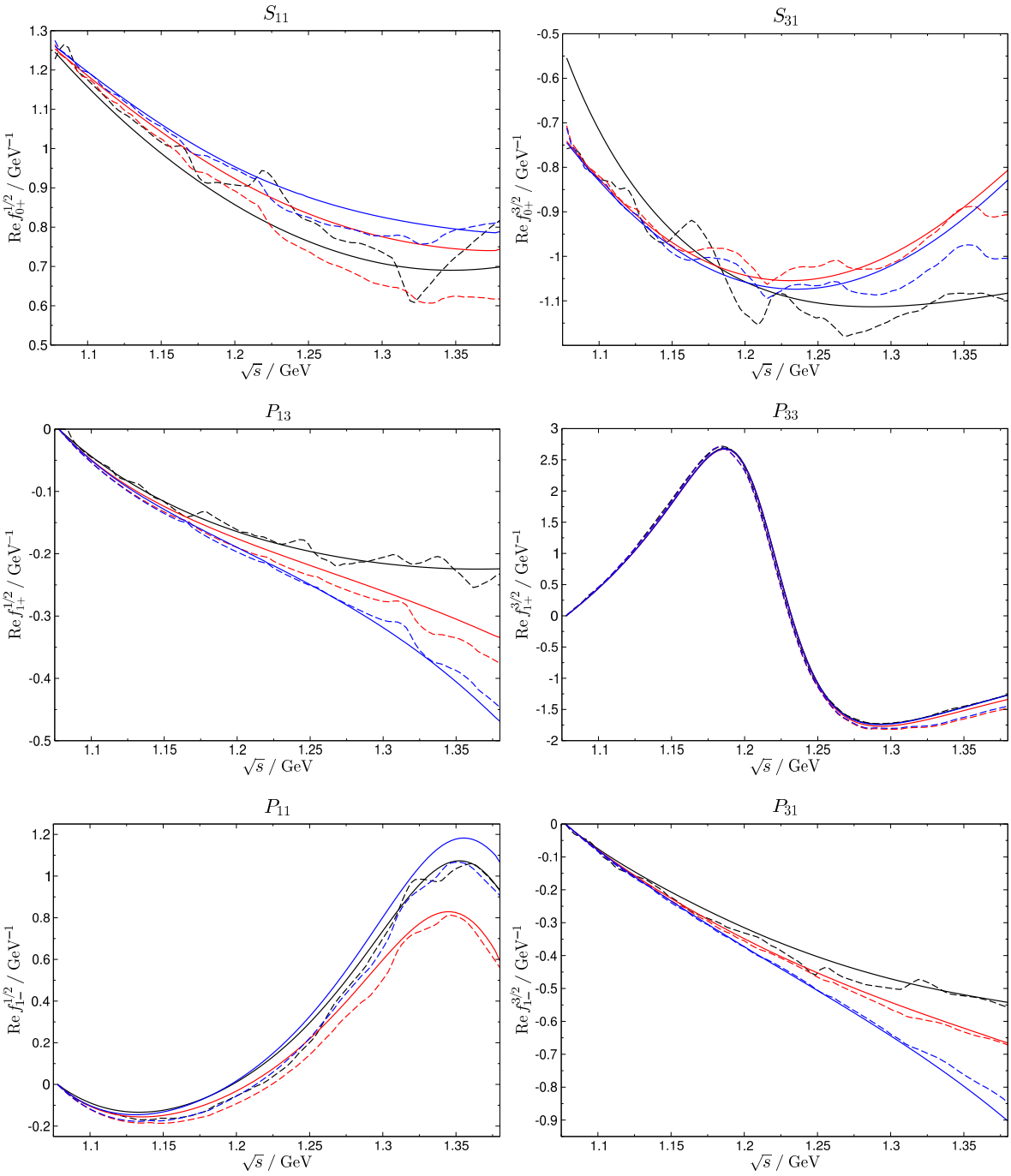

Figure 8.4: Left- (black) and right-hand side of the "3-sub" (red) and "ex 3-sub" (blue) versions of the RS equations for Re $f_{l\pm}^{I_s}(W)$. Solid/dashed lines refer to SAID/KH80 input as described in the main text.

case of the "3-sub" P_{11}-wave becomes cured in the "ex 3-sub" version. As far as the S-waves are concerned, one may argue that within the uncertainties induced by the oscillatory behavior of the KH80 phase shifts the combination of KH80 partial waves, coupling constant, and subthreshold parameters can still be regarded as essentially consistent.

	d_{00}^+	b_{00}^-	a_{00}^-	d_{01}^+	b_{00}^+	a_{10}^+	b_{01}^-	a_{01}^-	b_{10}^-	a_{10}^-
3-sub	−1.39	10.22	−8.71	1.20	−3.44	4.58	0.20	−0.34		
ex 3-sub	−1.33	10.12	−8.70	1.19	−3.43	4.56	0.26	−0.39	1.04	−1.20
KH80	−1.46	10.36	−8.83	1.14	−3.54	4.66	0.24	−0.37	1.08	−1.25

Table 8.3: Subthreshold parameters derived from RS equations in comparison with the KH80 values (units as in Table 7.2). See main text for details.

Whereas for the other partial waves the pattern follows roughly the KH80 precedent, we find a significant deviation for the SAID S_{31}-wave already in the threshold region. In fact, this discrepancy is not surprising since the KH80 subthreshold parameters are tailored in such a way as to reproduce the KH80 scattering lengths, and the KH80 and SAID values for $a_{0+}^{3/2}$ differ substantially, cf. Table 8.1. These observations lead to the conclusion that the main task in the solution of the s-channel RS equations will amount to reconciling a smoothed version of the KH80 partial waves with modern input for the coupling constant and scattering lengths.

The basic idea for the solution of the s-channel problem involves the minimization of the χ^2 function

$$\chi^2 = \sum_{l,I_s,\pm} \sum_{j=1}^{N} \Big(\mathrm{Re}\, f_{l\pm}^{I_s}(W_j) - F\big[f_{l\pm}^{I_s}\big](W_j) \Big)^2 \tag{8.18}$$

that sums the quadratic difference between $\mathrm{Re}\, f_{l\pm}^{I_s}$ and the right-hand side of the corresponding integral equation (6.39), denoted by $F\big[f_{l\pm}^{I_s}\big]$, over all dynamically included amplitudes on a grid of N points W_j between W_+ and W_m, so that an exact solution of the RS equations would fulfill $\chi^2 = 0$. An approximate solution may be found by casting the phase shifts below W_m into suitable parameterizations, e.g. (8.5) and (8.6), and minimizing (8.18) with respect to the parameters in these equations as well as the subtraction constants.[4] In order to illustrate this procedure we consider here a simplified approach that leaves the s-channel partial waves unaltered (we will take the SAID amplitudes) and only performs the minimization with respect to the subthreshold parameters. Distributing $N = 25$ grid points equidistantly between W_+ and W_m and using the KH80 subthreshold parameters as starting point, we obtain the subthreshold parameters given in Table 8.3. As demanded by the discussion in Sect. 8.3.1, the χ^2 function is augmented by an additional term in the case of the "ex 3-sub" version that enforces that the S-wave scattering lengths coincide with the values given in (8.17) by means of the sum rule (8.13). Moreover, once the correct S-wave scattering lengths are imposed as a global constraint, one should also adjust the first parameter in (8.5) in such a way that the requirement $A_{0+}^{I_s} = a_{0+}^{I_s}$ is exactly fulfilled. For this reason, we have used a slightly modified version of the SAID S-wave phase shifts for the "ex 3-sub" fit.

The quality of the thus determined solution is illustrated in Fig. 8.5. The agreement between the left- and right-hand side, especially for the "ex 3-sub" version, is already quite good for the P_{33}- and P_{11}-waves, whereas the equations for the S-waves and also the repulsive P-waves are not yet satisfactorily fulfilled. For further improvement in these partial waves the parameterizations of the s-channel amplitudes will have to be explicitly included in the fit.

[4] In principle it should be possible to consider also the πN coupling constant as a free parameter that ought to be determined self-consistently, although in the following we will keep the coupling fixed at $g^2/4\pi = 13.7$.

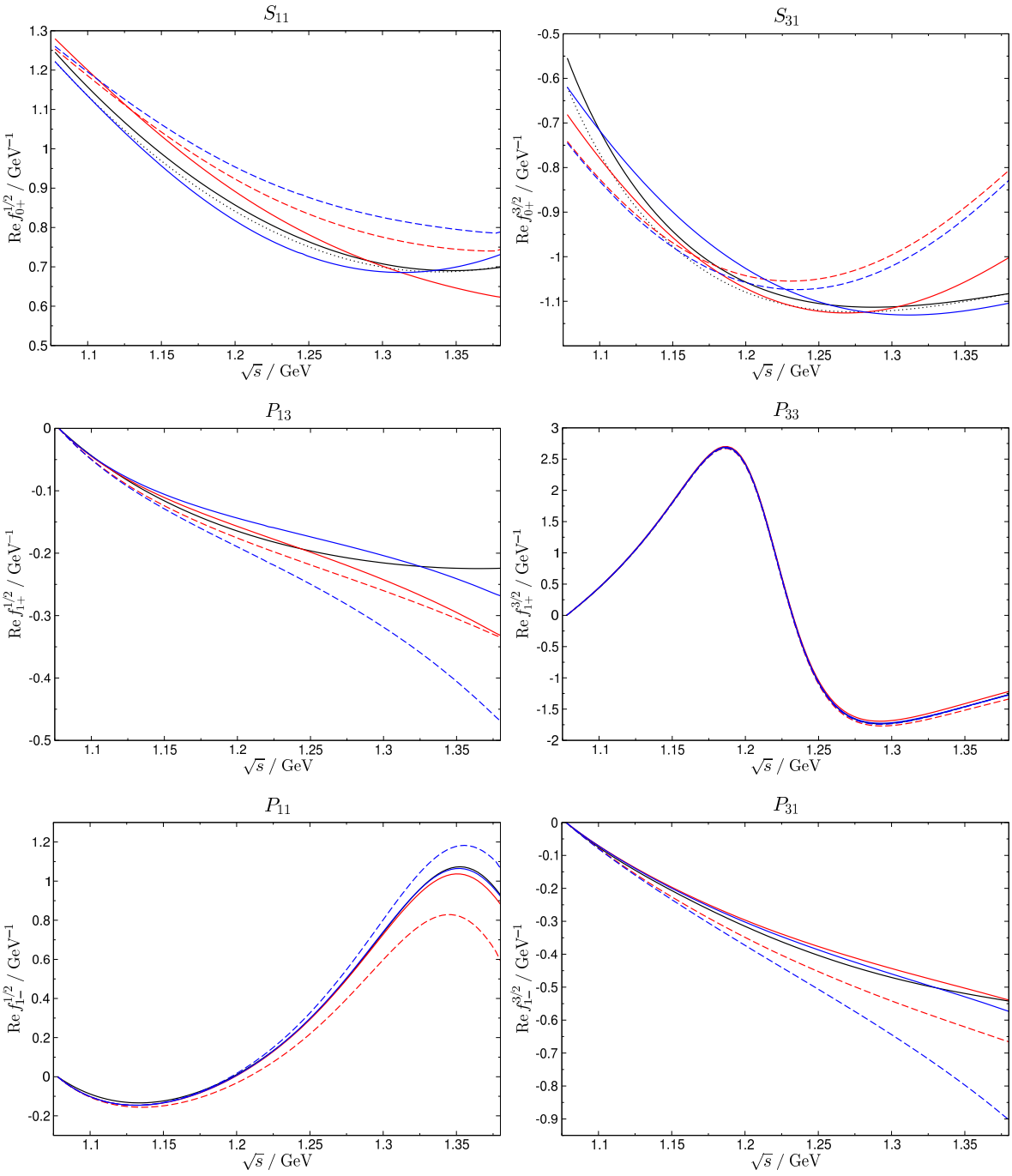

Figure 8.5: Left- (black) and right-hand side of the "3-sub" (red) and "ex 3-sub" (blue) versions of the RS equations for $\mathrm{Re}\, f_{l\pm}^{I_s}(W)$. Solid/dashed lines refer to the fitted/original subthreshold parameters, while the dotted lines for the S-waves denote the scattering-length-adjusted version of the SAID amplitudes, as explained in the main text.

Finally, we note that by construction the amended SAID S-wave (dotted line) and the "ex 3-sub" right-hand side coincide at threshold, as in both cases the same constraints for the scattering lengths have been imposed. This condition is expected to be of great value also

	$a_{0+}^{1/2}$	$a_{0+}^{3/2}$	$a_{1+}^{1/2}$	$a_{1+}^{3/2}$	$a_{1-}^{1/2}$	$a_{1-}^{3/2}$	$b_{0+}^{1/2}$	$b_{0+}^{3/2}$
3-sub	178.6	−95.1	−26.6	211.3	−71.2	−38.9	−41.0	−51.9
ex 3-sub	170.5	−86.5	−26.3	210.8	−71.2	−39.2	−45.0	−51.2
KH80	173	−101	−30	214	−81	−45	−18	−58

Table 8.4: Threshold parameters corresponding to the fit results displayed in Table 8.3 in comparison with the KH80 values (units as in Table 8.1).

in a full solution of the s-channel equations, since in this way the notoriously fragile S-waves are stabilized by precise experimental input. Similarly, one might consider synchronizing the sum-rule values of higher threshold parameters, collected for the present results in Table 8.4, with the appropriate terms in the phase-shift parameterizations.

8.4 Relation to the pion–nucleon σ term

In order to establish the relation of a solution of the s-channel equations to the pion–nucleon σ term we first return to the determination of the various corrections introduced in Sect. 3.3. The scalar form factor of the nucleon has already been investigated in some detail in Sect. 7.4.2, leading to the result (7.91) for Δ_σ. In a similar way we may use the solutions of the t-channel equations to determine Δ_D. Starting from the expansion

$$\bar{D}^+(\nu=0,t) = 4\pi\bigg\{ -\frac{1}{p_t^2}\bar{f}_+^0(t) + \frac{5}{2}q_t^2\bar{f}_+^2(t) - \frac{27}{8}p_t^2q_t^4\bar{f}_+^4(t) + \frac{65}{16}p_t^4q_t^6\bar{f}_+^6(t) + \cdots \bigg\}\,, \quad (8.19)$$

where $\bar{f}_+^J(t)$ denotes the Born-term-subtracted fraction of $f_+^J(t)$, and neglecting the imaginary parts of $f_\pm^J(t)$ for $J \geq 4$, the RS equations for $f_+^J(t)$ yield

$$\begin{aligned}
\bar{D}^+(\nu=0,t) &= d_{00}^+ + d_{01}^+ t - 16t^2 \int\limits_{t_\pi}^{\infty} \mathrm{d}t' \frac{\mathrm{Im}\, f_+^0(t')}{t'^2(t'-4m^2)(t'-t)} \\
&\quad - \frac{4}{p_t^2}\big(I_0^t(t)+I_0^s(t)\big) + 10q_t^2\big(I_2^t(t)+I_2^s(t)\big) - \frac{27}{2}p_t^2q_t^4 I_4^s(t) + \frac{65}{4}p_t^4q_t^6 I_6^s(t) + \cdots\,, \\
I_J^t(t) &= \int\limits_{t_\pi}^{\infty} \mathrm{d}t' \bigg\{ \tilde{K}_{J2}^1\big|^{\text{3-sub}}(t,t')\mathrm{Im}\, f_+^2(t') + \tilde{K}_{J2}^2\big|^{\text{3-sub}}(t,t')\mathrm{Im}\, f_-^2(t') \bigg\}\,, \\
I_J^s(t) &= \int\limits_{W_+}^{\infty} \mathrm{d}W' \sum_{l=0}^{\infty} \frac{1}{3}\bigg\{ \tilde{G}_{Jl}\big|^{\text{3-sub}}(t,W')\Big(\mathrm{Im}\, f_{l+}^{1/2}(W') + 2\mathrm{Im}\, f_{l+}^{3/2}(W')\Big) \\
&\qquad + \tilde{G}_{Jl}\big|^{\text{3-sub}}(t,-W')\Big(\mathrm{Im}\, f_{(l+1)-}^{1/2}(W') + 2\mathrm{Im}\, f_{(l+1)-}^{3/2}(W')\Big)\bigg\}\,,
\end{aligned} \quad (8.20)$$

and evaluation of this formula at $t = 2M_\pi^2$ immediately provides an expression for Δ_D. Using the same input as for the calculation of Δ_σ as well as the "3-sub" results for the t-channel D-waves we find the individual contributions to Δ_D summarized in Table 8.5. In particular,

f_+^0	$f_\pm^2$	I_0^s	I_2^s	I_4^s	I_6^s	full
14.74	0.10	1.02	−4.14	0.38	−0.01	12.08

Table 8.5: Individual contributions to Δ_D as inferred from (8.20) in MeV.

the convergence with increasing J shows that higher terms neglected in (8.20) can indeed be safely ignored. Estimating the sensitivity of the full result to the integral cutoff, the input for the solution of the t-channel problem, and the πN parameters in close analogy to the error analysis for Δ_σ, we find[5]

$$\begin{aligned}\Delta_D &= (12.1 \pm 0.3)\,\text{MeV} \\ &\quad + \tilde{Z}_1\left(\frac{g^2}{4\pi} - 14.28\right) + \tilde{Z}_2\Big(d_{00}^+ M_\pi + 1.46\Big) + \tilde{Z}_3\Big(d_{01}^+ M_\pi^3 - 1.14\Big) + \tilde{Z}_4\Big(b_{00}^+ M_\pi^3 + 3.54\Big)\,, \\ \tilde{Z}_1 &= 0.42\,\text{MeV}\,, \qquad \tilde{Z}_2 = 0.67\,\text{MeV}\,, \qquad \tilde{Z}_3 = 12.0\,\text{MeV}\,, \qquad \tilde{Z}_4 = -0.77\,\text{MeV}\,. \end{aligned} \tag{8.21}$$

In fact, the coefficients $\tilde{Z}_i$ are very close to the Z_i in (7.91), with the result that the dependence on subthreshold parameters and the πN coupling constant cancels almost completely in the difference $\Delta_D - \Delta_\sigma$. Similarly, it was already pointed out in [164] that Δ_σ and Δ_D themselves are considerably more sensitive to the details of the $\pi\pi$ phase shifts than their difference, which was traced back to the fact that the physical effect that dominates the scalar form factor of the nucleon is also largely responsible for the t-dependence of $\bar{D}^+(0,t)$. Apparently, the same mechanism suppresses the sensitivity to the πN parameters as well.

Last, we are left with the remainder $\Delta_\text{R} = F_\pi^2 \bar{D}^+(0, 2M_\pi^2) - \sigma(2M_\pi^2)$ at the Cheng–Dashen point. This correction was investigated in detail in the framework of heavy-baryon ChPT at fourth chiral order in [163], where it was first proven that even at $\mathcal{O}(p^4)$ chiral logarithms are absent. Moreover, the size of the analytic pieces was estimated considering various mechanisms, e.g. tree-level $\Delta(1232)$-isobar exchange produces a contribution of 0.6 MeV, leading to a final estimate of

$$|\Delta_\text{R}| \lesssim 2\,\text{MeV}\,. \tag{8.22}$$

Using a covariant formulation of baryon ChPT, the conclusion regarding chiral logarithms was confirmed more recently in [138], where Δ_R is also given explicitly in terms of $\mathcal{O}(p^2)$ and $\mathcal{O}(p^4)$ LECs, arguing that crude estimates for these constants indicate that Δ_R is "of order 1 MeV." Both values imply that the uncertainty in Δ_R clearly outweighs any remaining uncertainties in $\Delta_D - \Delta_\sigma$, in particular the small residual dependence on subthreshold parameters and the πN coupling constant. Adopting the more conservative estimate (8.22), we obtain

$$\begin{aligned}\sigma_{\pi N} &= \Sigma_d + \Delta_D - \Delta_\sigma - \Delta_\text{R}\,, \\ \Sigma_d &= F_\pi^2\big(d_{00}^+ + 2M_\pi^2 d_{01}^+\big)\,, \qquad \Delta_D - \Delta_\sigma - \Delta_\text{R} = (-1.8 \pm 2.0)\,\text{MeV}\,, \end{aligned} \tag{8.23}$$

so that the subthreshold parameters from a solution of the s-channel RS equations may be translated directly into an updated value of $\sigma_{\pi N}$. For completeness, the results for Σ_d that follow from the fits in Sect. 8.3.2 are displayed in Table 8.6. Although both values are closer

[5] In principle, the result for Δ_D also depends on a_{10}^+ via the input for $f_+^2(t)$, but the corresponding contribution is numerically entirely negligible.

	3-sub	ex 3-sub	KH80	[80]	[166]
Σ_d [MeV]	61.2	63.8	50.0	$48 \pm 4 \pm 4 \pm 4$ (sol. A)	67 ± 6
				$50 \pm 3 \pm 7 \pm 4$ (sol. B)	

Table 8.6: Values for Σ_d corresponding to the subthreshold parameters from Table 8.3 in comparison with the results from [80, 166].

to the scenario of a large σ term [166], we stress that these results are by no means definitive. It remains to be seen whether this inclination withstands a full solution of the RS system that includes the s-channel partial waves in the Roy-equation fit as well as the iteration between the s- and t-channel equations.

Finally, we comment on the relation between $\sigma_{\pi N}$ and the strangeness content of the nucleon y,

$$y = \frac{2\langle N(p)|\bar{s}s|N(p)\rangle}{\langle N(p)|\bar{u}u + \bar{d}d|N(p)\rangle} , \qquad \frac{1}{2m}\langle N(p)|m_{\rm s}\bar{s}s|N(p)\rangle = \sigma_{\pi N}\frac{m_{\rm s}}{2\hat{m}}y . \tag{8.24}$$

Rewriting the σ term as

$$\sigma_{\pi N} = \frac{\hat{\sigma}}{1-y} , \qquad \hat{\sigma} = \frac{\hat{m}}{2m}\langle N(p)|\bar{u}u + \bar{d}d - 2\bar{s}s|N(p)\rangle , \tag{8.25}$$

one may infer y from $\sigma_{\pi N}$ provided that $\hat{\sigma}$ can be determined from elsewhere. In the standard procedure $\hat{\sigma}$ would be taken from an analysis of baryon mass splittings in the framework of $SU(3)$ baryon ChPT, for instance $\hat{\sigma} = (36 \pm 7)\,\text{MeV}$ [207], so that e.g. $\sigma_{\pi N} = (45 \pm 8)\,\text{MeV}$ from [80] would translate into a strangeness content of $y = 0.2 \pm 0.2$, which already illustrates the difficulty inherent in this approach: even if this value for $\sigma_{\pi N}$ were exact, the uncertainty in $\hat{\sigma}$ would still cause an error of $\Delta y = \Delta\hat{\sigma}/\sigma_{\pi N} = 0.16$ in the strangeness content. In this way, a precise determination of y from πN scattering would require firm control over the $SU(3)$ expansion of the baryon masses.[6]

8.5 Summary and conclusion

We have derived a complete system of Roy–Steiner equations for pion–nucleon scattering as well as the associated partial-wave unitarity relations. In order to arrive at a system of integral equations that interrelates only low-energy degrees of freedom we have introduced various subtractions by means of suitable sum rules for the πN subthreshold parameters. The solution of the t-channel equations using Muskhelishvili–Omnès techniques was discussed in some detail for the lowest partial waves, demonstrating that with a sufficient number of subtractions the t-channel results of the old KH80 partial-wave analysis can be accurately reproduced. For the S-wave we have also extended the formalism beyond the single-channel approximation and

[6] The difficulties concerning the chiral expansion have already been mentioned in Sect. 6.1 in the context of lattice determinations of $\sigma_{\pi N}$. Lattice values for the strangeness content, e.g. $y = 0.20 \pm 0.07^{+0.13}_{-0.17}$ [134], $y < 0.14$ [135], $y = 0.050 \pm 0.012 \pm 0.034$ [250], $y = 0.082 \pm 0.016 \pm 0.002$ [251], in general point towards small strangeness effects. Recently, it has even been claimed that contributions from $\bar{c}c$ operators might be of equal importance [252].

included $\bar{K}K$ effects in the unitarity relation. To this end, we have developed a method to construct a two-channel MO solution with a finite matching point. Subsequently, we have applied the solutions of the t-channel partial waves to a two-channel dispersive calculation of the scalar form factor of the nucleon and updated the values of several corrections required for an extraction of the pion–nucleon σ term from the πN amplitude at the Cheng–Dashen point. With the t-channel problem solved for a given input of s-channel amplitudes and πN parameters, we have analyzed the structure of the resulting s-channel equations and developed a strategy towards their solution, arguing how the hadronic-atom values for the πN scattering lengths discussed in Part I can be used to stabilize the solution for the S-wave equations by means of sum rules for the πN threshold parameters. Within a simplified scenario where the s-channel partial waves are kept fixed we have illustrated how a solution of the s-channel problem can be found by minimizing the difference between left- and right-hand side of the s-channel equations with respect to the free parameters of the approach, and how an updated value of the σ term follows immediately from the results for certain subthreshold parameters, which, ultimately, are to be determined self-consistently from the full RS system.

Several results at intermediate steps of the calculation should prove valuable beyond their role in the RS system, e.g. the P-wave t-channel partial waves are crucial input for a dispersive analysis of the electromagnetic form factors of the nucleon, in a similar way as the S-wave for the scalar form factor as described in Sect. 7.4.2. In addition, the formalism developed here for including $\bar{K}K$ effects could be used to incorporate the $f_0(980)$ resonance into the RS representation for $\gamma\gamma \to \pi\pi$ derived in Part II. Although a full solution of the coupled s- and t-channel problem for pion–nucleon scattering is rather involved, already due to the mere number of partial-wave amplitudes that need to be considered, we are confident that the RS framework will lead to improved s-channel amplitudes at low energies and permit a reliable extrapolation to the Cheng–Dashen point.

Appendix A

Isospin violation in πN and $\pi^- d$ scattering

A.1 Effective Lagrangians

For the sake of completeness, we review here the effective Lagrangian for nucleons, pions, and virtual photons taken from [94] (see also [168]). The following terms are needed for the analysis in Part I

$$
\begin{aligned}
\mathcal{L}_{\rm eff} &= \mathcal{L}_\pi^{(p^2)} + \mathcal{L}_\pi^{(e^2)} + \mathcal{L}_\pi^{(e^2p^2)} + \mathcal{L}_{\rm N}^{(p)} + \mathcal{L}_{\rm N}^{(p^2)} + \mathcal{L}_{\rm N}^{(p^3)} + \mathcal{L}_{\rm N}^{(e^2)} + \mathcal{L}_{\rm N}^{(e^2p)} + \mathcal{L}_\gamma \ , \\
\mathcal{L}_\pi^{(p^2)} &= \frac{F^2}{4}\langle d^\mu U^\dagger d_\mu U + \chi^\dagger U + U^\dagger \chi\rangle \ , \\
\mathcal{L}_\pi^{(e^2)} &= ZF^4\langle \mathcal{Q}U\mathcal{Q}U^\dagger\rangle \ , \qquad \mathcal{L}_\gamma = -\frac{1}{4}F_{\mu\nu}F^{\mu\nu} - \frac{1}{2}\big(\partial_\mu A^\mu\big)^2 \ , \\
\mathcal{L}_\pi^{(e^2p^2)} &= F^2\Big\{\langle d^\mu U^\dagger d_\mu U\rangle\big(k_1\langle\mathcal{Q}^2\rangle + k_2\langle \mathcal{Q}U\mathcal{Q}U^\dagger\rangle\big) + k_4\langle d^\mu U^\dagger \mathcal{Q}U\rangle\langle d_\mu U\mathcal{Q}U^\dagger\rangle \\
&\quad + k_3\big(\langle d^\mu U^\dagger\mathcal{Q}U\rangle\langle d_\mu U^\dagger\mathcal{Q}U\rangle + \langle d^\mu U\mathcal{Q}U^\dagger\rangle\langle d_\mu U\mathcal{Q}U^\dagger\rangle\big)\Big\} \ , \\
\mathcal{L}_{\rm N}^{(p)} &= \bar\Psi\Big\{i\not{D} - m_0 + \frac{1}{2}g_0\not{u}\gamma_5\Big\}\Psi \ , \\
\mathcal{L}_{\rm N}^{(p^2)} &= \bar\Psi\Big\{c_1\langle\chi_+\rangle - \frac{c_2}{4m_0^2}\langle u_\mu u_\nu\rangle D^\mu D^\nu + \text{h.c.} + \frac{c_3}{2}\langle u_\mu u^\mu\rangle + \frac{i}{4}c_4\sigma^{\mu\nu}[u_\mu,u_\nu] + c_5\hat\chi_+\Big\}\Psi \ , \\
\mathcal{L}_{\rm N}^{(p^3)} &= \frac{i}{2m_0}\bar\Psi\Big\{d_5[\chi_-,u_\mu]D^\mu\Big\}\Psi + \text{h.c.} \ , \\
\mathcal{L}_{\rm N}^{(e^2)} &= F^2\bar\Psi\Big\{f_1\langle\hat Q_+^2 - Q_-^2\rangle + f_2\langle Q_+\rangle\hat Q_+ + f_3\langle\hat Q_+^2 + Q_-^2\rangle\Big\}\Psi \ , \\
\mathcal{L}_{\rm N}^{(e^2p)} &= \frac{F^2}{2}\bar\Psi\Big\{g_1\langle Q_+^2 - Q_-^2\rangle\gamma^\mu\gamma_5 u_\mu + g_2\langle Q_+\rangle^2\gamma^\mu\gamma_5 u_\mu\Big\}\Psi \\
&\quad + \frac{iF^2}{2m_0}\bar\Psi\Big\{g_6\langle Q_+\rangle\langle Q_- u_\mu\rangle D^\mu + g_7\langle Q_+u_\mu\rangle Q_- D^\mu + g_8\langle Q_- u_\mu\rangle Q_+ D^\mu\Big\}\Psi + \text{h.c.} \ , \qquad \text{(A.1)}
\end{aligned}
$$

where $\langle A\rangle$ denotes the trace of a matrix A, $\hat A = A - \langle A\rangle/2$ its traceless part, $\bar\Psi(\mathcal{O} + \text{h.c.})\Psi \equiv \bar\Psi\mathcal{O}\Psi + \text{h.c.}$ for an operator $\mathcal{O}$ and

$$
d_\mu U = \partial_\mu U - iA_\mu[\mathcal{Q},U] \ , \qquad \chi = 2B\,\text{diag}(m_{\rm u},m_{\rm d}) \ , \qquad U = u^2 \ , \qquad \mathcal{Q} = \frac{e}{3}\,\text{diag}(2,-1) \ ,
$$

$$F_{\mu\nu} = \partial_\mu A_\nu - \partial_\nu A_\mu \,, \qquad Q = e\,\mathrm{diag}(1,0) \,, \qquad Q_\pm = \frac{1}{2}(uQu^\dagger \pm u^\dagger Q u) \,,$$
$$D_\mu = \partial_\mu + \Gamma_\mu \,, \qquad \Gamma_\mu = \frac{1}{2}\Big(u^\dagger(\partial_\mu - iQA_\mu)u + u(\partial_\mu - iQA_\mu)u^\dagger\Big) \,, \qquad \chi_\pm = u^\dagger\chi u^\dagger \pm u\chi^\dagger u \,,$$
$$u_\mu = i\Big(u^\dagger(\partial_\mu - iQA_\mu)u - u(\partial_\mu - iQA_\mu)u^\dagger\Big) \,, \qquad [D_\mu, u_\nu] = \partial_\mu u_\nu + [\Gamma_\mu, u_\nu] \,. \tag{A.2}$$

Ψ and U collect nucleon and pion fields as discussed in Sect. 1.1.2. F, g_0, and m_0 are the pion decay constant, the axial charge, and the mass of the nucleon in the chiral limit, respectively, which in the main text are always eliminated in favor of the physical quantities F_π, g_A, and the physical nucleon mass (identified with the mass of the proton). The renormalized LECs are denoted by a superscript r.

A.2 Photon diagrams in chiral effective field theory

A.2.1 Single scattering with photon exchange

To begin with we discuss the case that the $\pi NN \to \pi NN$ operator contains only the nominally leading isoscalar contribution. Writing the isoscalar threshold πN amplitude as $T^+ = 4\pi\xi_\mathrm{p} a^+$, we find

$$i\mathcal{M}^{(d_6)+(d_8)} = 2\int\frac{\mathrm{d}^4k}{(2\pi)^4}\int\frac{\mathrm{d}^3q\,\mathrm{d}^3q'}{(2\pi)^3}\Psi^\dagger(\mathbf{q}')i2T^+\frac{i}{(M_\pi v+k)^2 - M_\pi^2 + i\eta}(-ie\,2M_\pi)\Big(i\frac{e}{2}\Big)\frac{i}{\mathbf{k}^2}$$
$$\times\left\{iG_s\Big(\mathbf{q}' - \frac{\mathbf{k}}{2}, \mathbf{q} - \frac{\mathbf{k}}{2}; -\epsilon - k_0, -\mathbf{k}\Big) + iG_s\Big(\mathbf{q}' - \frac{\mathbf{k}}{2}, -\mathbf{q} + \frac{\mathbf{k}}{2}; -\epsilon - k_0, -\mathbf{k}\Big)\right\}\Psi(\mathbf{q}) \,, \tag{A.3}$$

where $v = (1, \mathbf{0})$ and we have already used the fact that $k_0 \sim \mathbf{k}^2/M_\pi \ll \mathbf{k}$ and therefore can be neglected in the photon propagator. The factor of 2 multiplying T^+ is present as the pion can interact with either the neutron or the proton, while the overall factor of 2 includes the time-reversed diagram. The factor $e/2$ in the first line occurs since we include only one of the two possible interactions of the nucleons inside the deuteron with the photon. The other is accounted for via the exchange term, which is represented by the second Green function. In that portion we have reversed the initial-state relative momentum as compared to the direct piece of the amplitude. More specifically, we can rewrite $\mathcal{M}$ as

$$\mathcal{M} = \langle\Psi|QG(E)\frac{1}{2}(1 - P_{12})T_{\pi^- N}|\Psi\rangle \,, \tag{A.4}$$

where

$$T_{\pi^- N} = \Big(T^+\mathbb{1}^{(1)} + T^-\tau_3^{(1)}\Big)\otimes\mathbb{1}^{(2)} + (1 \leftrightarrow 2) \,, \qquad Q = \frac{e}{2}\Big(\mathbb{1}^{(1)} + \tau_3^{(1)}\Big)\otimes\mathbb{1}^{(2)} + (1 \leftrightarrow 2) \,, \tag{A.5}$$

the superscript referring to nucleon 1 and 2, respectively. In (A.4) $G(E) = 1/(E + i\eta - H)$ denotes the Green function describing the propagation of the NN pair from the πNN interaction to the photon coupling, and the projector $(1 - P_{12})/2$ has been introduced to impose the Pauli principle (P_{12} interchanges nucleons 1 and 2). Note that the operators in round brackets in (A.5) are implicitly understood to be accompanied by shift operators $\mathcal{S}^{(i)}$ indicating the momentum shift induced by the pion–nucleon or photon–nucleon interaction, which has to be taken into account when the symmetry properties of the individual terms are analyzed.

Inserting (A.5) into (A.4), we obtain two distinct contributions (all terms with a single $\tau_3^{(i)}$ involve $\langle T=0|\tau_3^{(i)}|T=0\rangle = 0$ and may thus be dropped). First, the isoscalar piece reads

$$\langle\Psi|\frac{e}{2}G(1-P_{12})2T^+|\Psi\rangle \equiv \langle\Psi|\frac{e}{2}(G_s+\tilde{G}_s)2T^+|\Psi\rangle\ , \tag{A.6}$$

and since the isospin wave function of the isospin-zero state is already antisymmetric under particle exchange, this isoscalar "direct-minus-exchange" $G(1-P_{12}) \equiv G_{\rm D} - G_{\rm E}$ prescription (in (A.6) $\tilde{G}_s$ denotes the outcome for the exchange part) produces the sum of two G_s terms in (A.3). Second, the "direct-minus-exchange" contribution to $\mathcal{M}$ that results from the isovector part of the pion's interaction with the NN system discussed below only contributes for odd partial waves due to the Pauli principle. This can already be inferred from the isospin structure: $\tau_3^{(i)}|T=0\rangle \propto |T=1,T_3=0\rangle$, and since spin is conserved, the Pauli principle in the form $(-1)^{L+S+T}=-1$ requires an odd partial wave.

In fact, the presence of the deuteron pole renders the expression (A.3) infrared divergent. This divergence reflects our neglecting of effects due to the atomic binding energy $B_{\rm at}$: if we included these, the integral would be regulated at scale $\sqrt{M_\pi B_{\rm at}} \sim \alpha M_\pi$. However, the physics associated with this momentum scale was already included in the atomic-physics calculation that led to the improved Deser formula (2.7). Put another way, we must subtract the expression for the diagram evaluated in non-relativistic effective field theory (NREFT), which corresponds to a structureless deuteron. Using the fact that the normalization of any deuteron wave function equals 1, it may be written as

$$\begin{aligned} i\mathcal{M}_{\rm IR} = 2\int\frac{{\rm d}^4k}{(2\pi)^4}\int{\rm d}^3q\,{\rm d}^3q'\Psi^\dagger(\mathbf{q}')i2T^+\Psi(\mathbf{q}')\frac{i}{-k_0-\mathbf{k}^2/2m_{\rm d}+i\eta}\frac{i}{k_0-\mathbf{k}^2/2M_\pi+i\eta} \\ \times\Psi^\dagger(\mathbf{q})(-ie)(ie)\frac{i}{\mathbf{k}^2}\Psi(\mathbf{q})\ . \end{aligned} \tag{A.7}$$

From the difference of (A.3) and (A.7), we can obtain an expression that is safe in the infrared and includes only the effects not already accounted for in the NREFT computation

$$\begin{aligned} \mathcal{M}_{\rm IR\ safe}^{(d_6)+(d_8)} = -2e^2T^+\int\frac{{\rm d}^3k}{(2\pi)^3}\frac{1}{\mathbf{k}^2}\int\frac{{\rm d}^3q\,{\rm d}^3q'}{(2\pi)^3}\Psi^\dagger(\mathbf{q}') \\ \times\Bigg\{\int\frac{{\rm d}k_0}{2\pi}\Big[iG_s\Big(\mathbf{q}'-\frac{\mathbf{k}}{2},\mathbf{q}-\frac{\mathbf{k}}{2};-\epsilon-k_0,-\mathbf{k}\Big)+iG_s\Big(\mathbf{q}'-\frac{\mathbf{k}}{2},-\mathbf{q}+\frac{\mathbf{k}}{2};-\epsilon-k_0,-\mathbf{k}\Big)\Big] \\ \times\frac{2M_\pi}{(M_\pi v+k)^2-M_\pi^2+i\eta}-\frac{2(2\pi)^3\Psi(\mathbf{q}')\Psi^\dagger(\mathbf{q})}{-\mathbf{k}^2/2\mu_D+i\eta}\Bigg\}\Psi(\mathbf{q})\ . \end{aligned} \tag{A.8}$$

Now, since we are prepared to ignore $\pi\pi NN$ cuts (they only lead to higher-order effects), we drop the "backward-going pion" contribution. The evaluation of the k_0 integral in the first term can then be done by picking up the pion pole. This yields

$$\begin{aligned} \mathcal{M}_{\rm IR\ safe}^{(d_6)+(d_8)} = -2e^2T^+\int\frac{{\rm d}^3k}{(2\pi)^3}\frac{1}{\mathbf{k}^2}\int\frac{{\rm d}^3q\,{\rm d}^3q'}{(2\pi)^3}\Psi^\dagger(\mathbf{q}')\Big\{G_s\Big(\mathbf{q}'-\frac{\mathbf{k}}{2},\mathbf{q}-\frac{\mathbf{k}}{2};-\epsilon-\frac{\mathbf{k}^2}{2M_\pi},-\mathbf{k}\Big) \\ +G_s\Big(\mathbf{q}'-\frac{\mathbf{k}}{2},-\mathbf{q}+\frac{\mathbf{k}}{2};-\epsilon-\frac{\mathbf{k}^2}{2M_\pi},-\mathbf{k}\Big)-\frac{2(2\pi)^3\Psi(\mathbf{q}')\Psi^\dagger(\mathbf{q})}{-\mathbf{k}^2/2\mu_D+i\eta}\Big\}\Psi(\mathbf{q})\ , \end{aligned} \tag{A.9}$$

where we have neglected terms that are higher order in $\mathbf{k}$, and so replaced $\omega_{\mathbf{k}}$ by M_π and the kinetic energy of the pion by its non-relativistic form. From this result, we can now read

off (2.42) via

$$a_{NN}^{(d_6)+(d_8)} = \frac{\mathcal{M}_{\text{IR safe}}^{(d_6)+(d_8)}}{4\pi\xi_{\text{d}}} \,. \tag{A.10}$$

Finally, the isovector P-wave part produces a contribution corresponding to

$$\begin{aligned} a_{T=1}^{(d_6)+(d_8)} = &-\frac{8\pi\alpha\xi_{\text{p}}a^-}{(2\pi)^6\xi_{\text{d}}}\int\frac{\mathrm{d}^3k}{\mathbf{k}^2}\int\mathrm{d}^3q\,\mathrm{d}^3q'\Psi^\dagger(\mathbf{q}') \\ &\times\left\{G_v\Big(\mathbf{q}'-\frac{\mathbf{k}}{2},\mathbf{q}-\frac{\mathbf{k}}{2};-\epsilon-\frac{\mathbf{k}^2}{2M_\pi},-\mathbf{k}\Big)-G_v\Big(\mathbf{q}'-\frac{\mathbf{k}}{2},-\mathbf{q}+\frac{\mathbf{k}}{2};-\epsilon-\frac{\mathbf{k}^2}{2M_\pi},-\mathbf{k}\Big)\right\}\Psi(\mathbf{q}) \,, \end{aligned} \tag{A.11}$$

where the isovector Green function G_v is defined analogously to G_s with the deuteron pole removed and $T_{s,NN}^{\text{np}} \to T_{v,NN}^{\text{np}}$ (the relative sign is due to the symmetry of the $|T=1,T_3=0\rangle$ state). Although we do not consider isovector NN interactions, it is a valuable check of the calculation that the free part of the Green function reproduces the expressions of Sect. 2.5.1.

A.2.2 Double scattering with photon exchange

We now generalize the previous discussion to a πNN kernel given by double πN scattering. Let us first consider the case where the photon is exchanged after the πNN interaction. Two distinct processes contribute to the πNN interaction: the exchange of a π^- corresponds to double elastic $\pi^- N$ scattering, while an intermediate π^0 requires two charge-exchange reactions. The amplitudes can be written as

$$\begin{aligned} \mathcal{M}^{\pi^-} &= \langle\Psi|QG\frac{1}{2}(1-P_{12})T_{\pi^-N}T_{\pi^-N}|\Psi\rangle \,, \\ \mathcal{M}^{\pi^0} &= \langle\Psi|QG\frac{1}{2}(1-P_{12})T_{\pi^0N\to\pi^-N}T_{\pi^-N\to\pi^0N}|\Psi\rangle \,, \end{aligned} \tag{A.12}$$

where

$$\begin{aligned} T_{\pi^-N\to\pi^0N} &= (-\sqrt{2}\,T^-)\tau_-^{(1)}\otimes\mathbb{1}^{(2)}+(1\leftrightarrow 2) \,, \\ T_{\pi^0N\to\pi^-N} &= (-\sqrt{2}\,T^-)\tau_+^{(1)}\otimes\mathbb{1}^{(2)}+(1\leftrightarrow 2) \,, \end{aligned} \tag{A.13}$$

with raising and lowering operators

$$\tau_\pm^{(i)} = \frac{1}{2}\left(\tau_1^{(i)}\pm i\tau_2^{(i)}\right) \,, \tag{A.14}$$

and T_{π^-N} and Q are defined in (A.5). Again, the momentum shifts are understood to be taken into account implicitly. The evaluation of $\mathcal{M}^{\pi^-}$ proceeds in close analogy to (A.4), once the contributions for which both πN interactions happen to the same nucleon are excluded. Neglecting isoscalar πN scattering terms (which are of higher order), we obtain

$$\mathcal{M}^{\pi^-} = -2(T^-)^2\langle\Psi|\frac{e}{2}G\frac{1}{2}(1-P_{12})|\Psi\rangle = -2(T^-)^2\langle\Psi|\frac{e}{2}(G_s+\tilde{G}_s)|\Psi\rangle \,. \tag{A.15}$$

The expression for $\mathcal{M}^{\pi^0}$ requires a bit more care, the crucial observation being that the states $\tau_+^{(2)}\tau_-^{(1)}|T=0\rangle$, $\tau_+^{(1)}\tau_-^{(2)}|T=0\rangle$, $(1+\tau_3^{(1)})|T=0\rangle$, and $(1+\tau_3^{(2)})|T=0\rangle$ are actually a

superposition of $|T=0,T_3=0\rangle$ and $|T=1,T_3=0\rangle$, with the result that both even and odd partial waves contribute. We find that the former give rise to

$$\mathcal{M}^{\pi^0}_{T=0} = -(-\sqrt{2}\,T^-)^2\langle\Psi|(G_s+\tilde{G}_s)\frac{e}{2}|\Psi\rangle\ , \tag{A.16}$$

while the latter lead to

$$\mathcal{M}^{\pi^0}_{T=1} = -(-\sqrt{2}\,T^-)^2\langle\Psi|(G_v-\tilde{G}_v)\frac{e}{2}|\Psi\rangle\ . \tag{A.17}$$

Therefore, the analog of (A.3) becomes

$$\begin{aligned}
i\mathcal{M}^{(d_9)+(d_{10})} &= 2\int\frac{\mathrm{d}^4k}{(2\pi)^4}\int\frac{\mathrm{d}^4l}{(2\pi)^4}\int\frac{\mathrm{d}^3q\,\mathrm{d}^3q'}{(2\pi)^3}\Psi^\dagger(\mathbf{q}')(-2)(iT^-)^2(-ie2M_\pi)\Big(i\frac{e}{2}\Big)\frac{i}{\mathbf{k}^2}\\
&\quad\times\bigg\{iG_s\Big(\mathbf{q}'-\frac{\mathbf{k}}{2},\mathbf{q}-\frac{\mathbf{k}}{2}+\mathbf{l};-\epsilon-k_0,-\mathbf{k}\Big)+iG_s\Big(\mathbf{q}'-\frac{\mathbf{k}}{2},-\mathbf{q}+\frac{\mathbf{k}}{2}-\mathbf{l};-\epsilon-k_0,-\mathbf{k}\Big)\bigg\}\\
&\qquad\times\frac{i}{-v\cdot l+i\eta}\frac{i}{(M_\pi v+l)^2-M_\pi^2+i\eta}\frac{i}{(M_\pi v+k)^2-M_\pi^2+i\eta}\Psi(\mathbf{q})\\
&\quad+2\int\frac{\mathrm{d}^4k}{(2\pi)^4}\int\frac{\mathrm{d}^4l}{(2\pi)^4}\int\frac{\mathrm{d}^3q\,\mathrm{d}^3q'}{(2\pi)^3}\Psi^\dagger(\mathbf{q}')(-1)(-i\sqrt{2}\,T^-)^2(-ie2M_\pi)\Big(i\frac{e}{2}\Big)\frac{i}{\mathbf{k}^2}\\
&\quad\times\bigg\{iG_s\Big(\mathbf{q}'-\frac{\mathbf{k}}{2},\mathbf{q}-\frac{\mathbf{k}}{2}+\mathbf{l};-\epsilon-k_0,-\mathbf{k}\Big)+iG_s\Big(\mathbf{q}'-\frac{\mathbf{k}}{2},-\mathbf{q}+\frac{\mathbf{k}}{2}-\mathbf{l};-\epsilon-k_0,-\mathbf{k}\Big)\bigg\}\\
&\qquad\times\frac{i}{-v\cdot l+i\eta}\frac{i}{(M_\pi v+l)^2-M_\pi^2+i\eta}\frac{i}{(M_\pi v+k)^2-M_\pi^2+i\eta}\Psi(\mathbf{q})\ ,
\end{aligned}\tag{A.18}$$

where again the overall factor of 2 accounts for the time-reversed diagram. Performing the l^0 and k^0 integrations yields

$$\begin{aligned}
\mathcal{M}^{(d_9)+(d_{10})} &= 2e^2(T^-)^2\int\frac{\mathrm{d}^3k}{(2\pi)^3}\int\frac{\mathrm{d}^3l}{(2\pi)^3}\int\frac{\mathrm{d}^3q\,\mathrm{d}^3q'}{(2\pi)^3}\Psi^\dagger(\mathbf{q}')\frac{1}{\mathbf{k}^2\mathbf{l}^2}\\
&\quad\times\bigg\{2G_s\Big(\mathbf{q}'-\frac{\mathbf{k}}{2},\mathbf{q}-\frac{\mathbf{k}}{2}+\mathbf{l};-\epsilon-\frac{\mathbf{k}^2}{2M_\pi},-\mathbf{k}\Big)\\
&\qquad+2G_s\Big(\mathbf{q}'-\frac{\mathbf{k}}{2},-\mathbf{q}+\frac{\mathbf{k}}{2}-\mathbf{l};-\epsilon-\frac{\mathbf{k}^2}{2M_\pi},-\mathbf{k}\Big)\bigg\}\Psi(\mathbf{q})\ .
\end{aligned}\tag{A.19}$$

To generalize (A.7) we must replace the isoscalar two-body contribution to the $\pi^- d$ scattering length $2T^+$ by the double-scattering analog

$$-4(T^-)^2\int\frac{\mathrm{d}^3p\,\mathrm{d}^3q}{(2\pi)^3}\Psi^\dagger(\mathbf{p}-\mathbf{q})\frac{1}{\mathbf{q}^2}\Psi(\mathbf{p})\ , \tag{A.20}$$

so that the infrared-safe amplitude is given by

$$\begin{aligned}
\mathcal{M}^{(d_9)+(d_{10})}_{\text{IR safe}} &= 2e^2(T^-)^2\int\frac{\mathrm{d}^3k}{(2\pi)^3}\int\frac{\mathrm{d}^3l}{(2\pi)^3}\frac{1}{\mathbf{k}^2\mathbf{l}^2}\int\frac{\mathrm{d}^3q\,\mathrm{d}^3q'}{(2\pi)^3}\\
&\quad\times\Psi^\dagger(\mathbf{q}')\bigg\{2G_s\Big(\mathbf{q}'-\frac{\mathbf{k}}{2},\mathbf{q}-\frac{\mathbf{k}}{2}+\mathbf{l};-\epsilon-\frac{\mathbf{k}^2}{2M_\pi},-\mathbf{k}\Big)\\
&\qquad+2G_s\Big(\mathbf{q}'-\frac{\mathbf{k}}{2},-\mathbf{q}+\frac{\mathbf{k}}{2}-\mathbf{l};-\epsilon-\frac{\mathbf{k}^2}{2M_\pi},-\mathbf{k}\Big)-\frac{4(2\pi)^3\Psi(\mathbf{q}')\Psi^\dagger(\mathbf{q}-\mathbf{l})}{-\mathbf{k}^2/2\mu_D+i\eta}\bigg\}\Psi(\mathbf{q})\ ,
\end{aligned}\tag{A.21}$$

which finally proves (2.59).

A.3 Subtraction of virtual-photon effects

A.3.1 πN scattering lengths

The isospin-violating corrections to the $\pi^\pm p$ scattering lengths calculated in [93] involve contributions due to the pion mass difference $\sim e^2 Z$ as well as virtual-photon corrections $\sim e^2$, where $Z = (M_\pi^2 - M_{\pi^0}^2)/2e^2F_\pi^2 = 0.81$. Retaining only the e^2 part that we indicate by $a^\gamma_{\pi^\pm p}$, we obtain the following correction [93]

$$a^\gamma_{\pi^- p} - a^\gamma_{\pi^+ p} = -\frac{M_\pi}{2\pi\xi_\mathrm{p}}\left\{\frac{e^2 g_\mathrm{A}^2}{16\pi^2 F_\pi^2}\left(1 + 4\log 2 + 3\log\frac{M_\pi^2}{\mu^2}\right) - 2e^2\left(\tilde{g}_6^\mathrm{r} + \tilde{g}_8^\mathrm{r} - \frac{5}{9F_\pi^2}\tilde{k}_1^\mathrm{r}\right)\right\}\,, \tag{A.22}$$

where $\tilde{g}_i^\mathrm{r}$ and $\tilde{k}_i^\mathrm{r}$ denote the e^2 piece of g_i^r and k_i^r, respectively. The relation between both sets of LECs can be established by means of their β-functions σ_i and η_i. It is convenient to define scale-independent LECs $\bar{g}_i$ and $\bar{k}_i$ by

$$k_i^\mathrm{r} = \frac{\sigma_i}{16\pi^2}\left(\bar{k}_i + \log\frac{M_\pi}{\mu}\right)\,, \qquad g_i^\mathrm{r} = \frac{\eta_i}{16\pi^2 F_\pi^2}\left(\bar{g}_i + \log\frac{M_\pi}{\mu}\right)\,, \tag{A.23}$$

and thus

$$\tilde{k}_i^\mathrm{r} = \frac{\sigma_i|_{Z=0}}{16\pi^2}\left(\bar{k}_i + \log\frac{M_\pi}{\mu}\right)\,, \qquad \tilde{g}_i^\mathrm{r} = \frac{\eta_i|_{Z=0}}{16\pi^2 F_\pi^2}\left(\bar{g}_i + \log\frac{M_\pi}{\mu}\right)\,, \tag{A.24}$$

which leads to

$$\tilde{k}_i^\mathrm{r} = \frac{\sigma_i|_{Z=0}}{\sigma_i}k_i^\mathrm{r}\,, \qquad \tilde{g}_i^\mathrm{r} = \frac{\eta_i|_{Z=0}}{\eta_i}g_i^\mathrm{r}\,. \tag{A.25}$$

Estimating the LECs as in [93] yields the result quoted in (3.16).

Similarly, virtual photons contribute to the sum of $a_{\pi^- p}$ and $a_{\pi^+ p}$ according to

$$a^\gamma_{\pi^- p} + a^\gamma_{\pi^+ p} = -\frac{1}{4\pi\xi_\mathrm{p}}\left\{\frac{e^2 g_\mathrm{A}^2 M_\pi}{16\pi F_\pi^2}\right\}\,. \tag{A.26}$$

Writing

$$a_{\pi^- p} + a_{\pi^+ p} = 2\big(\tilde{a}^+ + \Delta\tilde{a}^+\big) - a_{\pi^- n} + a_{\pi^+ p}\,, \tag{A.27}$$

we find, together with (2.18) and (3.14), for the virtual-photon-subtracted combination

$$a^{\not\gamma}_{\pi^- p} + a^{\not\gamma}_{\pi^+ p} = 2\tilde{a}^+ - \frac{1}{4\pi\xi_\mathrm{p}}\left\{e^2 f_2 + \frac{33 g_\mathrm{A}^2 M_\pi \Delta_\pi}{64\pi F_\pi^4}\right\} = (-1.6 \pm 1.6)\cdot 10^{-3} M_\pi^{-1}\,. \tag{A.28}$$

Finally, the associated virtual-photon-subtracted scattering lengths in the isospin basis are

$$\begin{aligned}
a^{1/2}_{\not\gamma} &= 2a_{\pi^- p} - \tilde{a}^+ + \frac{1}{8\pi\xi_\mathrm{p}}\left\{e^2 f_2 + \frac{33 g_\mathrm{A}^2 M_\pi \Delta_\pi}{64\pi F_\pi^4} + \frac{e^2 g_\mathrm{A}^2 M_\pi}{8\pi F_\pi^2}\right\} \\
&\quad + \frac{M_\pi}{2\pi\xi_\mathrm{p}}\left\{\frac{e^2 g_\mathrm{A}^2}{16\pi^2 F_\pi^2}\left(1 + 4\log 2 + 3\log\frac{M_\pi^2}{\mu^2}\right) - 2e^2\left(\tilde{g}_6^\mathrm{r} + \tilde{g}_8^\mathrm{r} - \frac{5}{9F_\pi^2}\tilde{k}_1^\mathrm{r}\right)\right\} \\
&= (170.5 \pm 2.0)\cdot 10^{-3} M_\pi^{-1}\,, \\
a^{3/2}_{\not\gamma} &= -a_{\pi^- p} + 2\tilde{a}^+ - \frac{1}{4\pi\xi_\mathrm{p}}\left\{e^2 f_2 + \frac{33 g_\mathrm{A}^2 M_\pi \Delta_\pi}{64\pi F_\pi^4} + \frac{e^2 g_\mathrm{A}^2 M_\pi}{32\pi F_\pi^2}\right\} \\
&\quad - \frac{M_\pi}{4\pi\xi_\mathrm{p}}\left\{\frac{e^2 g_\mathrm{A}^2}{16\pi^2 F_\pi^2}\left(1 + 4\log 2 + 3\log\frac{M_\pi^2}{\mu^2}\right) - 2e^2\left(\tilde{g}_6^\mathrm{r} + \tilde{g}_8^\mathrm{r} - \frac{5}{9F_\pi^2}\tilde{k}_1^\mathrm{r}\right)\right\} \\
&= (-86.5 \pm 1.8)\cdot 10^{-3} M_\pi^{-1}\,.
\end{aligned} \tag{A.29}$$

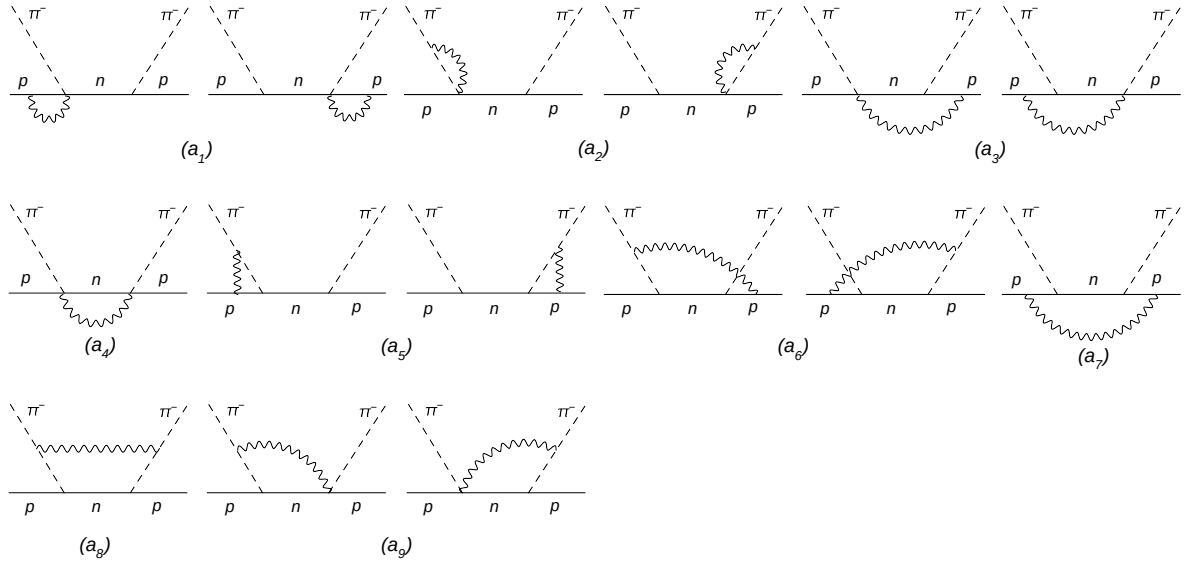

Figure A.1: Virtual-photon corrections to the nucleon-pole diagram in $\pi^- p$ scattering at $\mathcal{O}(p^3)$ [93].

A.3.2 πN coupling constant

The full set of virtual-photon corrections to the nucleon-pole diagram in $\pi^- p$ scattering at third chiral order is depicted in Fig. A.1. Based on the discussion of these diagrams in [93], the shift of g_c due to virtual photons can be read off from the residue of the scattering amplitude at $s = m_{\rm n}^2$. To obtain an idea how large these effects are, we consider here the diagrams (a_1), (a_2), and (a_5), which is motivated by the expectation that it ought to be possible to absorb this subset of diagrams into a simple redefinition of g_c. And indeed, we find that these diagrams, together with the pertinent contact terms and the wave-function renormalization, represent a scale-independent quantity: all ultraviolet divergences cancel between loops and contact terms. In a strict chiral expansion, we find that (a_1), (a_2), and (a_5) yield (after renormalization) a shift in g_c^2 of

$$\frac{\Delta g_c^2}{4\pi} = \frac{e^2 g_{\rm A}^2 m_{\rm p}^2}{4\pi F_\pi^2}\left\{\frac{2F_\pi^2}{g_{\rm A}}\big(\tilde{g}_1^{\rm r}+\tilde{g}_2^{\rm r}\big) - \frac{20}{9}\tilde{k}_1^{\rm r} - \frac{1}{8\pi^2}\left(3+\log\frac{M_\pi^2}{\mu^2}\right) + \frac{1}{4\pi^2}\log\frac{M_\pi^2}{4E_{\rm max}^2}\right\}. \quad \text{(A.30)}$$

The last term is present since infrared divergences only cancel at threshold. To remove these singularities (regulated by a finite photon mass m_γ in the actual calculation of the diagrams), we use the leading, logarithmically enhanced part of the bremsstrahlung calculated in [93], which effectively eliminates m_γ in favor of twice the detector resolution $E_{\rm max}$. Numerically, this amounts to

$$\frac{\Delta g_c^2}{4\pi} = 0.07 \pm 0.03 \pm 0.04\,, \quad \text{(A.31)}$$

where we take $E_{\rm max} = 10\,\text{MeV}$ and the errors are, respectively, due to the LECs and a variation of $E_{\rm max}$ by a factor of 2. Dropping the term due to bremsstrahlung, the shift in $g_c^2/4\pi$ is reduced to -0.01 ± 0.03. We stress that these estimates can by no means replace a full analysis of radiative corrections, but should merely be taken as indicative of the size of virtual-photon effects.

Appendix B

Roy–Steiner equations for $\gamma\gamma \to \pi\pi$

B.1 Kernel functions for the s-channel projection

The functions $N_J^{\pm}(s)$ for $J \leq 2$ are given by

$$
\begin{aligned}
N_1^+(s) &= \frac{s}{M_\pi^2 - s} - \frac{M_\pi^2}{\mathbf{q}^2}\Big\{d_{11}^1(y)Q_0(y) - \frac{1}{2}\Big\} + \Delta N_1^+(s)\,, \qquad y = -\frac{s+M_\pi^2}{s-M_\pi^2} \\
N_2^+(s) &= -\frac{1}{3}\frac{s}{M_\pi^2 - s} - \frac{M_\pi^2}{\mathbf{q}^2}\Big\{d_{11}^2(y)Q_0(y) - \frac{1}{2} - y\Big\} + \Delta N_2^+(s)\,, \\
N_1^-(s) &= -\frac{M_\pi^2}{M_\pi^2 - s} + \frac{M_\pi^2}{\mathbf{q}^2}\Big\{d_{1,-1}^1(y)Q_0(y) + \frac{1}{2}\Big\} + \Delta N_1^-(s)\,, \\
N_2^-(s) &= -\frac{1}{3}\frac{M_\pi^2}{M_\pi^2 - s} + \frac{M_\pi^2}{\mathbf{q}^2}\Big\{d_{1,-1}^2(y)Q_0(y) - \frac{1}{2} + y\Big\} + \Delta N_2^-(s)\,,
\end{aligned}
\tag{B.1}
$$

where

$$
Q_0(z) = \frac{1}{2}\int_{-1}^{1}\frac{\mathrm{d}x}{z-x}\,, \qquad Q_0(z \pm i\epsilon) = \frac{1}{2}\log\left|\frac{1+z}{1-z}\right| \mp i\frac{\pi}{2}\theta(1-z^2)\,, \tag{B.2}
$$

denotes the lowest Legendre polynomial of the second kind. The remainders $\Delta N_J^{\pm}(s)$

$$
\begin{aligned}
&\Delta N_1^+\big|^{\text{0-sub}}(s) = 0\,, \qquad \Delta N_1^+\big|^{\text{1-sub}}(s) = \frac{2s}{3M_\pi\alpha}(\alpha_1+\beta_1)\mathbf{q}^2\,, \\
&\Delta N_1^+\big|^{\text{2-sub}}(s) = \Delta N_1^+\big|^{\text{1-sub}}(s) - \frac{s}{18M_\pi\alpha}(\alpha_2+\beta_2)\mathbf{q}^4\,, \\
&\Delta N_2^+\big|^{\text{0-sub}}(s) = \Delta N_2^+\big|^{\text{1-sub}}(s) = 0\,, \qquad \Delta N_2^+\big|^{\text{2-sub}}(s) = \frac{s}{30M_\pi\alpha}(\alpha_2+\beta_2)\mathbf{q}^4\,, \\
&\Delta N_1^-\big|^{\text{0-sub}}(s) = -\frac{2\mathbf{q}^2}{3(M_\pi^2-a)}\,, \qquad \Delta N_1^-\big|^{\text{1-sub}}(s) = \frac{2M_\pi}{3\alpha}(\alpha_1-\beta_1)\mathbf{q}^2 + \frac{1}{2M_\pi\alpha}(\alpha_1+\beta_1)\mathbf{q}^4\,, \\
&\Delta N_1^-\big|^{\text{2-sub}}(s) = \frac{2M_\pi}{3\alpha}(\alpha_1-\beta_1)\mathbf{q}^2 - \frac{M_\pi}{6\alpha}(\alpha_2-\beta_2)\mathbf{q}^4 - \frac{2}{15M_\pi\alpha}(\alpha_2+\beta_2)\mathbf{q}^6\,, \\
&\Delta N_2^-\big|^{\text{0-sub}}(s) = 0\,, \qquad \Delta N_2^-\big|^{\text{1-sub}}(s) = -\frac{1}{10M_\pi\alpha}(\alpha_1+\beta_1)\mathbf{q}^4\,, \\
&\Delta N_2^-\big|^{\text{2-sub}}(s) = \frac{M_\pi}{30\alpha}(\alpha_2-\beta_2)\mathbf{q}^4 + \frac{2}{45M_\pi\alpha}(\alpha_2+\beta_2)\mathbf{q}^6\,,
\end{aligned}
\tag{B.3}
$$

contain the pion polarizabilities according to the number of subtractions indicated by the superscript.

B.1.1 *s*-channel

The kernels for the unsubtracted case read

$$K_{11}^{++}(s,s') = \frac{s\,\mathbf{q}^2}{s'\mathbf{q}'^2}\left\{\frac{1}{s'-s}-\frac{1}{s'-a}-\frac{3}{2\mathbf{q}^2}\left[\frac{(1+x_s)^2}{4}Q_0(x_s)-\frac{2+x_s}{4}\right]\right\},$$

$$K_{12}^{++}(s,s') = \frac{s\,\mathbf{q}^2}{s'\mathbf{q}'^2}\left\{\left[\frac{1}{s'-s}-\frac{1}{s'-a}\right]\frac{5}{3}(2\beta+\alpha-1)\right.$$
$$\left.-\frac{5}{2\mathbf{q}^2}\left[\frac{(1+x_s)^2}{4}(2x_s'-1)Q_0(x_s)-\left(\frac{2}{3}\alpha+\beta-\frac{1}{2}\right)-\left(\alpha+\frac{\beta}{2}-\frac{1}{4}\right)x_s-\frac{\alpha}{2}x_s^2\right]\right\},$$

$$K_{21}^{++}(s,s') = -\frac{s}{s'\mathbf{q}'^2}\frac{3}{2}\left\{\frac{(1+x_s)^2}{4}(2x_s-1)Q_0(x_s)-\frac{1}{6}-\frac{3x_s}{4}-\frac{x_s^2}{2}\right\},$$

$$K_{22}^{++}(s,s') = \frac{s\,\mathbf{q}^2}{s'\mathbf{q}'^2}\left\{\left[\frac{1}{s'-s}-\frac{1}{s'-a}\right]\alpha-\frac{5}{2\mathbf{q}^2}\left[\frac{(1+x_s)^2}{4}(2x_s-1)(2x_s'-1)Q_0(x_s)\right.\right.$$
$$\left.\left.-\left(\frac{\beta}{3}-\frac{1}{6}\right)-\left(\frac{\alpha}{3}+\frac{3}{2}\beta-\frac{3}{4}\right)x_s-\left(\beta+\frac{3}{2}\alpha-\frac{1}{2}\right)x_s^2-\alpha x_s^3\right]\right\},$$

$$K_{11}^{-+}(s,s') = \frac{\mathbf{q}^2}{2s'\mathbf{q}'^2}\left\{\left[\frac{1}{s'-s}-\frac{1}{s'-a}\right]\left(\frac{3}{2}\mathbf{q}^2-\frac{1}{2}\mathbf{q}'^2(\alpha-2\beta+2)\right)-\frac{s'-s}{2(s'-a)}\right\},$$

$$K_{12}^{-+}(s,s') = \frac{\mathbf{q}^2}{2s'\mathbf{q}'^2}\left\{\left[\frac{1}{s'-s}-\frac{1}{s'-a}\right]\left\{\left(5\beta-3\alpha-\frac{5}{2}\right)\mathbf{q}^2\right.\right.$$
$$\left.\left.+\frac{\mathbf{q}'^2}{6}\left(8\alpha^2+5\alpha(3-4\beta)+10\left(1-3\beta+2\beta^2\right)\right)\right\}+\frac{5}{6}\frac{s'-s}{s'-a}(1+\alpha-2\beta)\right\},$$

$$K_{21}^{-+}(s,s') = -\frac{\mathbf{q}^2}{2s'\mathbf{q}'^2}\left[\frac{1}{s'-s}-\frac{1}{s'-a}\right]\frac{3}{10}(\mathbf{q}^2-\mathbf{q}'^2\alpha),$$

$$K_{22}^{-+}(s,s') = \frac{\mathbf{q}^2}{2s'\mathbf{q}'^2}\left\{\left[\frac{1}{s'-s}-\frac{1}{s'-a}\right]\right.$$
$$\left.\times\left(\left(\frac{1}{2}+\frac{5\alpha}{3}-\beta\right)\mathbf{q}^2-\mathbf{q}'^2\frac{\alpha}{6}(9+4\alpha-12\beta)\right)-\frac{\alpha}{2}\frac{s'-s}{s'-a}\right\},$$

$$K_{11}^{--}(s,s') = \frac{\mathbf{q}^2}{\mathbf{q}'^2}\left\{\frac{1}{s'-s}-\frac{1}{s'-a}-\frac{3}{2\mathbf{q}^2}\left[\frac{(1-x_s)^2}{4}Q_0(x_s)+\frac{2-x_s}{4}\right]\right\},$$

$$K_{12}^{--}(s,s') = \frac{\mathbf{q}^2}{\mathbf{q}'^2}\left\{\left[\frac{1}{s'-s}-\frac{1}{s'-a}\right]\frac{5}{3}(2\beta-\alpha+1)-\frac{5}{2\mathbf{q}^2}\left[\frac{(1-x_s)^2}{4}(2x_s'+1)Q_0(x_s)\right.\right.$$
$$\left.\left.-\left(\frac{2}{3}\alpha-\beta-\frac{1}{2}\right)-\left(\frac{\beta}{2}-\alpha+\frac{1}{4}\right)x_s-\frac{\alpha}{2}x_s^2\right]\right\},$$

$$
\begin{aligned}
K_{21}^{--}(s,s') &= -\frac{1}{\mathbf{q}'^2}\frac{3}{2}\left\{\frac{(1-x_s)^2}{4}(2x_s+1)Q_0(x_s) - \frac{1}{6} + \frac{3x_s}{4} - \frac{x_s^2}{2}\right\}, \\
K_{22}^{--}(s,s') &= \frac{\mathbf{q}^2}{\mathbf{q}'^2}\left\{\left[\frac{1}{s'-s} - \frac{1}{s'-a}\right]\alpha - \frac{5}{2\mathbf{q}^2}\left[\frac{(1-x_s)^2}{4}(2x_s+1)(2x'_s+1)Q_0(x_s)\right.\right. \\
&\qquad \left.\left. - \Big(\frac{\beta}{3}+\frac{1}{6}\Big) - \Big(\frac{\alpha}{3} - \frac{3}{2}\beta - \frac{3}{4}\Big)x_s - \Big(\beta - \frac{3}{2}\alpha + \frac{1}{2}\Big)x_s^2 - \alpha x_s^3\right]\right\},
\end{aligned}
\tag{B.4}
$$

where

$$
\begin{aligned}
&\alpha = \frac{\mathbf{q}^2}{\mathbf{q}'^2}\frac{s-a}{s'-a}, \qquad \beta = 1-\alpha-\frac{s'-s}{s'-a}\frac{s+s'-2M_\pi^2}{2\mathbf{q}'^2}, \qquad z'_s = \alpha z_s + \beta, \\
&x_s = 1 - \frac{s+s'-2M_\pi^2}{2\mathbf{q}^2}, \qquad x'_s = \alpha x_s + \beta.
\end{aligned}
\tag{B.5}
$$

The corresponding versions for the once- and twice- subtracted case can be obtained by adding

$$
\begin{aligned}
\Delta K_{JJ'}^{++}\big|^{\text{1-sub}}(s,s') &= -\frac{s\,\mathbf{q}^2}{s'\mathbf{q}'^2}(2J'+1)\frac{2}{3}\delta_{J1}h_0(s')\left[\frac{d_{11}^{J'}(z'_s)}{1+z'_s}\right]_0, \\
\Delta K_{JJ'}^{++}\big|^{\text{2-sub}}(s,s') &= \Delta K_{JJ'}^{++}\big|^{\text{1-sub}} + \frac{2s\,\mathbf{q}^4}{s'\mathbf{q}'^2}(2J'+1)\Big(\frac{\delta_{J1}}{3} - \frac{\delta_{J2}}{5}\Big) \\
&\qquad \times\left\{h_0(s')\left[\partial_t\frac{d_{11}^{J'}(z'_s)}{1+z'_s}\right]_0 - \frac{1}{(s'-M_\pi^2)^2}\left[\frac{d_{11}^{J'}(z'_s)}{1+z'_s}\right]_0\right\}, \\
\Delta K_{JJ'}^{-+}\big|^{\text{1-sub}}(s,s') &= -\frac{\mathbf{q}^2}{4s'\mathbf{q}'^2}(2J'+1)h_0(s')\left[\frac{d_{11}^{J'}(z'_s)}{1+z'_s}\right]_0 \\
&\qquad \times\Big\{-2\mathbf{q}'^2\big(1-\big[z'_s\big]_0\big)\frac{2}{3}\delta_{J1} + 2\mathbf{q}^2\Big(\delta_{J1} - \frac{\delta_{J2}}{5}\Big)\Big\}, \\
\Delta K_{JJ'}^{-+}\big|^{\text{2-sub}}(s,s') &= \Delta K_{JJ'}^{-+}\big|^{\text{1-sub}} + \frac{\mathbf{q}^4}{2s'\mathbf{q}'^2}(2J'+1)\left\{\left[2\mathbf{q}^2\Big(\frac{8}{5}\delta_{J1} - \frac{8}{15}\delta_{J2} + \frac{8}{105}\delta_{J3}\Big)\right.\right. \\
&\qquad \left.+ 4M_\pi^2\Big(\delta_{J1} - \frac{\delta_{J2}}{5}\Big)\right]\left\{h_0(s')\left[\partial_t\frac{d_{11}^{J'}(z'_s)}{1+z'_s}\right]_0 - \frac{1}{(s'-M_\pi^2)^2}\left[\frac{d_{11}^{J'}(z'_s)}{1+z'_s}\right]_0\right\} \\
&\quad + \Big(\delta_{J1} - \frac{\delta_{J2}}{5}\Big)\left\{h_0(s')\left[\partial_t(t'-t_\pi)\frac{d_{11}^{J'}(z'_s)}{1+z'_s}\right]_0 - \frac{1}{(s'-M_\pi^2)^2}\left[(t'-t_\pi)\frac{d_{11}^{J'}(z'_s)}{1+z'_s}\right]_0\right\}\Bigg\}, \\
\Delta K_{JJ'}^{--}\big|^{\text{1-sub}}(s,s') &= -\frac{\mathbf{q}^2}{\mathbf{q}'^2}(2J'+1)\frac{2}{3}\delta_{J1}h_0(s')\left[\frac{d_{1,-1}^{J'}(z'_s)}{1-z'_s}\right]_0, \\
\Delta K_{JJ'}^{--}\big|^{\text{2-sub}}(s,s') &= \Delta K_{JJ'}^{--}\big|^{\text{1-sub}} + \frac{2\mathbf{q}^4}{\mathbf{q}'^2}(2J'+1)\Big(\delta_{J1} - \frac{\delta_{J2}}{5}\Big) \\
&\qquad \times\left\{h_0(s')\left[\partial_t\frac{d_{1,-1}^{J'}(z'_s)}{1-z'_s}\right]_0 - \frac{1}{(s'-M_\pi^2)^2}\left[\frac{d_{1,-1}^{J'}(z'_s)}{1-z'_s}\right]_0\right\},
\end{aligned}
\tag{B.6}
$$

with

$$
\big[z'_s\big]_0 = -\frac{s'+a}{s'-a}, \qquad \big[\partial_t z'_s\big]_0 = \frac{M_\pi^2 - a}{2\mathbf{q}'^2(s'-a)}, \qquad h_0(s') = \frac{2}{s'-M_\pi^2} - \frac{1}{s'-a}.
\tag{B.7}
$$

B.1.2 *t*-channel

The non-vanishing unsubtracted kernel functions are

$$
\begin{aligned}
G_{12}^{+-}(s,t') &= \frac{5\sqrt{6}\,s}{2t'\,(t'-t_\pi)}\Big\{(1+x_t)^2Q_0(x_t)-2-x_t\Big\}\,, \qquad G_{12}^{--}(s,t') = \frac{5\sqrt{6}\,\mathbf{q}^2}{3t'\,(t'-t_\pi)}\,,\\
G_{22}^{+-}(s,t') &= \frac{5\sqrt{6}\,s}{2t'\,(t'-t_\pi)}\Big\{(1+x_t)^2(2x_t-1)Q_0(x_t)-\frac{2}{3}-3x_t-2x_t^2\Big\}\,, \qquad G_{22}^{--}(s,t') = 0\,,\\
G_{10}^{-+}(s,t') &= \frac{1}{2t'}\Big\{(1-x_t)^2Q_0(x_t)+2-x_t\Big\}\,,\\
G_{20}^{-+}(s,t') &= \frac{1}{2t'}\Big\{(1-x_t)^2(2x_t+1)Q_0(x_t)-\frac{2}{3}+3x_t-2x_t^2\Big\}\,,\\
G_{12}^{-+}(s,t') &= \frac{5}{2t'}\Big\{(1-x_t)^2P_2(x_t')Q_0(x_t)-(1+2\gamma-3\delta)+\Big(\frac{1}{2}+3\gamma-\frac{3\delta}{2}\Big)x_t-\frac{3\gamma x_t^2}{2}\Big\}\,,\\
G_{22}^{-+}(s,t') &= \frac{5}{2t'}\Big\{(1-x_t)^2(2x_t+1)P_2(x_t')Q_0(x_t)-\Big(\delta-\frac{1}{3}\Big)-\Big(\gamma-\frac{9}{2}\delta+\frac{3}{2}\Big)x_t\\
&\qquad -\Big(3\delta-\frac{9}{2}\gamma-1\Big)x_t^2-3\gamma x_t^3\Big\}\,,
\end{aligned}
\tag{B.8}
$$

where

$$
\begin{aligned}
&\gamma = \frac{8\mathbf{q}^2(s-a)}{t'(t'-t_\pi)}\,, \qquad \delta = \frac{(t'-2M_\pi^2+2a)^2-4(s-a)(2\mathbf{q}^2+2M_\pi^2-s-a)}{t'(t'-t_\pi)}\,,\\
&z_t' = \sqrt{\gamma z_s+\delta}\,, \qquad x_t = 1+\frac{t'}{2\mathbf{q}^2}\,, \qquad x_t' = \sqrt{\gamma x_t+\delta}\,,
\end{aligned}
\tag{B.9}
$$

and the subtracted versions are obtained by adding

$$
\begin{aligned}
\Delta G_{JJ'}^{+-}\big|^{\text{1-sub}}(s,t') &= -\frac{8s\,\mathbf{q}^2}{t'^2(t'-t_\pi)}(2J'+1)\frac{2}{3}\delta_{J1}\left[\frac{d_{20}^{J'}(z_t')}{1-z_t'^2}\right]_0\,,\\
\Delta G_{JJ'}^{+-}\big|^{\text{2-sub}}(s,t') &= \Delta G_{JJ'}^{+-}\big|^{\text{1-sub}} + \frac{16s\,\mathbf{q}^4}{t'^2(t'-t_\pi)}(2J'+1)\Big(\frac{\delta_{J1}}{3}-\frac{\delta_{J2}}{5}\Big)\\
&\qquad\times\left\{\frac{1}{t'}\left[\frac{d_{20}^{J'}(z_t')}{1-z_t'^2}\right]_0+\left[\partial_t\frac{d_{20}^{J'}(z_t')}{1-z_t'^2}\right]_0\right\}\,,\\
\Delta G_{JJ'}^{-+}\big|^{\text{1-sub}}(s,t') &= -\frac{2\mathbf{q}^2}{t'^2}(2J'+1)\frac{2}{3}\delta_{J1}\left[P_{J'}(z_t')\right]_0\,,\\
\Delta G_{JJ'}^{-+}\big|^{\text{2-sub}}(s,t') &= \Delta G_{JJ'}^{-+}\big|^{\text{1-sub}} + \frac{4\mathbf{q}^4}{t'^2}(2J'+1)\Big(\delta_{J1}-\frac{\delta_{J2}}{5}\Big)\left\{\left[\partial_t P_{J'}(z_t')\right]_0+\frac{[P_{J'}(z_t')]_0}{t'}\right\}\,,\\
\Delta G_{JJ'}^{--}\big|^{\text{1-sub}}(s,t') &= -\frac{2\mathbf{q}^2}{t'^2(t'-t_\pi)}(2J'+1)\left\{t'\frac{2}{3}\delta_{J1}+2\mathbf{q}^2\Big(\delta_{J1}-\frac{\delta_{J2}}{5}\Big)\right\}\left[\frac{d_{20}^{J'}(z_t')}{1-z_t'^2}\right]_0\,,\\
\Delta G_{JJ'}^{--}\big|^{\text{2-sub}}(s,t') &= \Delta G_{JJ'}^{--}\big|^{\text{1-sub}} + \frac{4\mathbf{q}^4}{t'^2(t'-t_\pi)}(2J'+1)\left\{\frac{1}{t'}\left[\frac{d_{20}^{J'}(z_t')}{1-z_t'^2}\right]_0+\left[\partial_t\frac{d_{20}^{J'}(z_t')}{1-z_t'^2}\right]_0\right\}\\
&\qquad\times\left[t'\Big(\delta_{J1}-\frac{\delta_{J2}}{5}\Big)+2\mathbf{q}^2\Big(\frac{8}{5}\delta_{J1}-\frac{8}{15}\delta_{J2}+\frac{8}{105}\delta_{J3}\Big)\right]\,,
\end{aligned}
\tag{B.10}
$$

with

$$
\left[z_t'^2\right]_0 = 1+\frac{4a}{t'-t_\pi}\,, \qquad \left[\partial_t z_t'^2\right]_0 = \frac{4(M_\pi^2-a)}{t'(t'-t_\pi)}\,.
\tag{B.11}
$$

B.2 Kernel functions for the t-channel projection

The contributions from Born terms and subtraction constants for $J \leq 2$ are

$$\tilde{N}_0^+(t) = \frac{8M_\pi^2}{\sigma(t)t} Q_0\Big(\frac{1}{\sigma(t)}\Big) + \Delta\tilde{N}_0^+(t)\,, \qquad \tilde{N}_2^+(t) = \frac{8M_\pi^2}{\sigma(t)t}\Big\{ P_2\Big(\frac{1}{\sigma(t)}\Big) Q_0\Big(\frac{1}{\sigma(t)}\Big) - \frac{3}{2\sigma(t)}\Big\}\,,$$
$$\tilde{N}_2^-(t) = -\frac{8M_\pi^2}{\sigma(t)t}\Big\{ d_{20}^2\Big(\frac{1}{\sigma(t)}\Big) Q_0\Big(\frac{1}{\sigma(t)}\Big) + \frac{\sqrt{6}}{4\sigma(t)}\Big\} + \frac{2}{\sqrt{6}} + \Delta\tilde{N}_2^-(t)\,,$$
$$\Delta\tilde{N}_0^+\big|^{\text{0-sub}}(t) = -\frac{t}{2(M_\pi^2 - a)}\,, \qquad \Delta\tilde{N}_0^+\big|^{\text{1-sub}}(t) = \frac{M_\pi}{2\alpha}(\alpha_1 - \beta_1)t - \frac{1}{8M_\pi\alpha}(\alpha_1 + \beta_1)t^2\,,$$
$$\Delta\tilde{N}_0^+\big|^{\text{2-sub}}(t) = \frac{M_\pi}{2\alpha}(\alpha_1 - \beta_1)t + \frac{M_\pi}{24\alpha}(\alpha_2 - \beta_2)t^2 - \frac{1}{96M_\pi\alpha}(\alpha_2 + \beta_2)t^3\,,$$
$$\Delta\tilde{N}_2^-\big|^{\text{0-sub}}(t) = 0\,, \qquad \Delta\tilde{N}_2^-\big|^{\text{1-sub}}(t) = \frac{t(t - t_\pi)}{5\sqrt{6}\,M_\pi^2}\frac{M_\pi}{2\alpha}(\alpha_1 + \beta_1)\,,$$
$$\Delta\tilde{N}_2^-\big|^{\text{2-sub}}(t) = \frac{t(t - t_\pi)}{5\sqrt{6}\,M_\pi^2}\frac{M_\pi}{2\alpha}\Big(\alpha_1 + \beta_1 + \frac{t}{12}(\alpha_2 + \beta_2)\Big)\,. \tag{B.12}$$

B.2.1 s-channel

The non-vanishing kernel functions for the unsubtracted case are

$$\tilde{G}_{01}^{++}(t,s') = \frac{3t}{16s'\mathbf{q}'^2(s'-a)}\Big\{2\mathbf{q}'^2\frac{3\tilde{\gamma} + 3\tilde{\delta} - 1}{3\tilde{\gamma}} - 2(s' - M_\pi^2)\Big\}\,,$$
$$\tilde{G}_{02}^{++}(t,s') = \frac{5t}{16s'\mathbf{q}'^2(s'-a)}\Big\{2\mathbf{q}'^2\frac{20\tilde{\delta} - 6 - 15\left(\tilde{\gamma}(\tilde{\gamma}-1) + 3\tilde{\gamma}\tilde{\delta} + 2\tilde{\delta}^2\right)}{15\tilde{\gamma}^2}$$
$$+ \frac{2(s' - M_\pi^2)}{\tilde{\gamma}}\Big(\tilde{\gamma} + 2\tilde{\delta} - \frac{2}{3}\Big)\Big\}\,, \qquad \tilde{G}_{21}^{++}(t,s') = -\frac{t}{20s'(s'-a)\tilde{\gamma}}\,,$$
$$\tilde{G}_{22}^{++}(t,s') = \frac{5t}{16s'\mathbf{q}'^2(s'-a)}\Big\{2\mathbf{q}'^2\frac{2(-12 + 21\tilde{\gamma} + 28\tilde{\delta})}{105\tilde{\gamma}^2} - \frac{s' - M_\pi^2}{15\mathbf{q}'^2(s'-a)}t(t - t_\pi)\Big\}\,,$$
$$\tilde{G}_{01}^{+-}(t,s') = -\frac{3t}{4\mathbf{q}'^2(s'-a)} + \frac{3t}{4\mathbf{q}'^2 p_t q_t}Q_0(\tilde{x}_t)\,,$$
$$\tilde{G}_{02}^{+-}(t,s') = -\frac{5t}{4\mathbf{q}'^2(s'-a)}\frac{2 + 3\tilde{\gamma} - 6\tilde{\delta}}{3\tilde{\gamma}} + \frac{5t}{4\mathbf{q}'^2 p_t q_t}\Big\{\left(2\tilde{x}_t' + 1\right)Q_0(\tilde{x}_t) - \frac{2\tilde{x}_t}{\tilde{\gamma}}\Big\}\,,$$
$$\tilde{G}_{21}^{+-}(t,s') = \frac{3t}{4\mathbf{q}'^2 p_t q_t}\Big\{P_2(\tilde{x}_t)Q_0(\tilde{x}_t) - \frac{3}{2}\tilde{x}_t\Big\}\,,$$
$$\tilde{G}_{22}^{+-}(t,s') = -\frac{t}{3\mathbf{q}'^2(s'-a)\tilde{\gamma}} + \frac{5t}{4\mathbf{q}'^2 p_t q_t}\Big\{\left(2\tilde{x}_t' + 1\right)P_2(\tilde{x}_t)Q_0(\tilde{x}_t) - \Big(\frac{3}{2} - \frac{3\tilde{\delta}}{\tilde{\gamma}}\Big)\tilde{x}_t - \frac{3\tilde{x}_t^3}{\tilde{\gamma}}\Big\}\,,$$
$$\tilde{G}_{21}^{-+}(t,s') = -\frac{t\,(t - t_\pi)}{s'\mathbf{q}'^2(s'-a)}\frac{3}{20\sqrt{6}} + \frac{3p_t q_t}{s'\mathbf{q}'^2}\Big\{\left(1 - \tilde{x}_t^2\right)d_{20}^2(\tilde{x}_t)Q_0(\tilde{x}_t) + \frac{\tilde{x}_t}{2\sqrt{6}}\left(5 - 3\tilde{x}_t^2\right)\Big\}\,,$$
$$\tilde{G}_{22}^{-+}(t,s') = \frac{t(t - t_\pi)}{s'\mathbf{q}'^2(s'-a)}\frac{7\tilde{\gamma} + 14\tilde{\delta} - 2}{28\sqrt{6}\,\tilde{\gamma}} + \frac{5p_t q_t}{s'\mathbf{q}'^2}\Big\{\left(1 - \tilde{x}_t^2\right)d_{20}^2(\tilde{x}_t)\left(2\tilde{x}_t' - 1\right)Q_0(\tilde{x}_t)$$
$$- \frac{\tilde{x}_t}{\sqrt{6}\,\tilde{\gamma}}\Big(\frac{16 + 25\tilde{\gamma} + 50\tilde{\delta}}{10} - \frac{(10 + 3\tilde{\gamma} + 6\tilde{\delta})\tilde{x}_t^2}{2} + 3\tilde{x}_t^4\Big)\Big\}\,, \tag{B.13}$$

where

$$\tilde{\gamma} = \frac{8\mathbf{q}'^2(s'-a)}{t(t-t_\pi)}\,, \qquad \tilde{\delta} = \frac{(t-2M_\pi^2+2a)^2 - 4(s'-a)(2\mathbf{q}'^2+2M_\pi^2-s'-a)}{t(t-t_\pi)}\,,$$
$$z_s' = \frac{z_t^2-\tilde{\delta}}{\tilde{\gamma}}\,, \qquad \tilde{x}_t = \frac{t+2s'-2M_\pi^2}{\sqrt{t(t-t_\pi)}}\,, \qquad \tilde{x}_t' = \frac{\tilde{x}_t^2-\tilde{\delta}}{\tilde{\gamma}} = 1+\frac{t}{2\mathbf{q}'^2}\,, \tag{B.14}$$

and

$$\begin{aligned}
\Delta\tilde{G}^{++}_{JJ'}\big|^{\text{1-sub}}(t,s') &= \frac{t}{8s'\mathbf{q}'^2}(2J'+1)\delta_{J0}\Big(2\mathbf{q}'^2\big(1-\big[z_s'\big]_0\big)+t\Big)h_0(s')\left[\frac{d^{J'}_{11}(z_s')}{1+z_s'}\right]_0\,,\\
\Delta\tilde{G}^{++}_{JJ'}\big|^{\text{2-sub}}(t,s') &= \Delta\tilde{G}^{++}_{JJ'}\big|^{\text{1-sub}} + \frac{t^2}{8s'\mathbf{q}'^2}(2J'+1)\delta_{J0}\Bigg\{(t-t_\pi)\\
&\qquad\times\left\{h_0(s')\left[\partial_t\frac{d^{J'}_{11}(z_s')}{1+z_s'}\right]_0 - \frac{1}{(s'-M_\pi^2)^2}\left[\frac{d^{J'}_{11}(z_s')}{1+z_s'}\right]_0\right\}\\
&\qquad - h_0(s')\left[\partial_t(t'-t_\pi)\frac{d^{J'}_{11}(z_s')}{1+z_s'}\right]_0 + \frac{1}{(s'-M_\pi^2)^2}\left[(t'-t_\pi)\frac{d^{J'}_{11}(z_s')}{1+z_s'}\right]_0\Bigg\}\,,\\
\Delta\tilde{G}^{+-}_{JJ'}\big|^{\text{1-sub}}(t,s') &= -\frac{t}{2\mathbf{q}'^2}(2J'+1)\delta_{J0}h_0(s')\left[\frac{d^{J'}_{1,-1}(z_s')}{1-z_s'}\right]_0\,,\\
\Delta\tilde{G}^{+-}_{JJ'}\big|^{\text{2-sub}}(t,s') &= \Delta\tilde{G}^{+-}_{JJ'}\big|^{\text{1-sub}}\\
&\qquad - \frac{t^2}{2\mathbf{q}'^2}(2J'+1)\delta_{J0}\left\{h_0(s')\left[\partial_t\frac{d^{J'}_{1,-1}(z_s')}{1-z_s'}\right]_0 - \frac{1}{(s'-M_\pi^2)^2}\left[\frac{d^{J'}_{1,-1}(z_s')}{1-z_s'}\right]_0\right\}\,,\\
\Delta\tilde{G}^{-+}_{JJ'}\big|^{\text{1-sub}}(t,s') &= -\frac{t(t-t_\pi)}{2s'\mathbf{q}'^2}(2J'+1)\frac{\delta_{J2}}{5\sqrt{6}}h_0(s')\left[\frac{d^{J'}_{11}(z_s')}{1+z_s'}\right]_0\,,\\
\Delta\tilde{G}^{-+}_{JJ'}\big|^{\text{2-sub}}(t,s') &= \Delta\tilde{G}^{-+}_{JJ'}\big|^{\text{1-sub}} - \frac{t^2(t-t_\pi)}{2s'\mathbf{q}'^2}\frac{\delta_{J2}}{5\sqrt{6}}(2J'+1)\\
&\qquad\times\left\{h_0(s')\left[\partial_t\frac{d^{J'}_{11}(z_s')}{1+z_s'}\right]_0 - \frac{1}{(s'-M_\pi^2)^2}\left[\frac{d^{J'}_{11}(z_s')}{1+z_s'}\right]_0\right\}.
\end{aligned} \tag{B.15}$$

B.2.2 *t*-channel

The non-vanishing kernel functions for $J, J' \le 2$ are

$$\begin{aligned}
\tilde{K}^{++}_{00}\big|^{n\text{-sub}}(t,t') &= \frac{t^{1+n}}{t'^{1+n}(t'-t)}\,, \qquad \tilde{K}^{++}_{22}\big|^{n\text{-sub}}(t,t') = \frac{t^2(t-t_\pi)}{t'^2(t'-t_\pi)(t'-t)}\,,\\
\tilde{K}^{++}_{02}(t,t') &= \frac{5t(t+t'-t_\pi+6a)}{t'^2(t'-t_\pi)}\,, \qquad \tilde{K}^{++}_{02}\big|^{\text{1-sub}}(t,t') = \frac{5t^2}{t'^2(t'-t_\pi)}\,,\\
\tilde{K}^{++}_{02}\big|^{\text{2-sub}}(t,t') &= -\frac{10M_\pi^2t^2}{t'^3(t'-t_\pi)}\,,\\
\tilde{K}^{+-}_{02}\big|^{n\text{-sub}}(t,t') &= \frac{5\sqrt{6}\,t^{1+n}}{4t'^{1+n}(t'-t_\pi)}\,, \qquad \tilde{K}^{--}_{22}\big|^{n\text{-sub}}(t,t') = \frac{t^{1+n}(t-t_\pi)}{t'^{1+n}(t'-t_\pi)(t'-t)}\,,
\end{aligned} \tag{B.16}$$

where $n \in \{0,1,2\}$.

B.3 Muskhelishvili–Omnès solutions for the $\gamma\gamma \to \pi\pi$ partial waves

B.3.1 $I = 0$

For $0 < \delta(t_\mathrm{m}) < \pi$, which is satisfied by all $I = 0$ partial waves, the solutions are

$$
\begin{aligned}
h_{0,+}(t) &= \tilde{\Delta}_{0,+}\big|^{\text{1-sub}}(t) + \frac{M_\pi}{2\alpha}(\alpha_1-\beta_1)t\,\Omega_0(t) \\
&\quad + \frac{t^2\Omega_0(t)}{\pi}\left\{\int\limits_{t_\pi}^{t_\mathrm{m}} \mathrm{d}t' \frac{\sin\delta_0(t')\tilde{\Delta}_{0,+}\big|^{\text{1-sub}}(t')}{t'^2(t'-t)|\Omega_0(t')|} + \int\limits_{t_\mathrm{m}}^{\infty} \mathrm{d}t' \frac{\operatorname{Im} h_{0,+}(t')}{t'^2(t'-t)|\Omega_0(t')|}\right\}, \\
h_{0,+}(t) &= \tilde{\Delta}_{0,+}\big|^{\text{2-sub}}(t) + \frac{M_\pi t}{2\alpha}\Big[(\alpha_1-\beta_1)(1-t\,\dot{\Omega}_0(0)) + \frac{t}{12}(\alpha_2-\beta_2)\Big]\Omega_0(t) \\
&\quad + \frac{t^3\Omega_0(t)}{\pi}\left\{\int\limits_{t_\pi}^{t_\mathrm{m}} \mathrm{d}t' \frac{\sin\delta_0(t')\tilde{\Delta}_{0,+}\big|^{\text{2-sub}}(t')}{t'^3(t'-t)|\Omega_0(t')|} + \int\limits_{t_\mathrm{m}}^{\infty} \mathrm{d}t' \frac{\operatorname{Im} h_{0,+}(t')}{t'^3(t'-t)|\Omega_0(t')|}\right\}, \\
h_{2,+}(t) &= \tilde{\Delta}_{2,+}(t) + \frac{t^2(t-t_\pi)\Omega_2(t)}{\pi} \\
&\quad \times \left\{\int\limits_{t_\pi}^{t_\mathrm{m}} \mathrm{d}t' \frac{\sin\delta_2(t')\tilde{\Delta}_{2,+}(t')}{t'^2(t'-t_\pi)(t'-t)|\Omega_2(t')|} + \int\limits_{t_\mathrm{m}}^{\infty} \mathrm{d}t' \frac{\operatorname{Im} h_{2,+}(t')}{t'^2(t'-t_\pi)(t'-t)|\Omega_2(t')|}\right\}, \\
h_{2,-}(t) &= \tilde{\Delta}_{2,-}\big|^{\text{1-sub}}(t) + \frac{t(t-t_\pi)}{10\sqrt{6}M_\pi\alpha}(\alpha_1+\beta_1)\Omega_2(t) + \frac{t^2(t-t_\pi)\Omega_2(t)}{\pi} \\
&\quad \times \left\{\int\limits_{t_\pi}^{t_\mathrm{m}} \mathrm{d}t' \frac{\sin\delta_2(t')\tilde{\Delta}_{2,-}\big|^{\text{1-sub}}(t')}{t'^2(t'-t_\pi)(t'-t)|\Omega_2(t')|} + \int\limits_{t_\mathrm{m}}^{\infty} \mathrm{d}t' \frac{\operatorname{Im} h_{2,-}(t')}{t'^2(t'-t_\pi)(t'-t)|\Omega_2(t')|}\right\}, \\
h_{2,-}(t) &= \tilde{\Delta}_{2,-}\big|^{\text{2-sub}}(t) + \frac{t(t-t_\pi)}{10\sqrt{6}M_\pi\alpha}\Big[(\alpha_1+\beta_1)(1-t\,\dot{\Omega}_2(0)) + \frac{t}{12}(\alpha_2+\beta_2)\Big]\Omega_2(t) \\
&\quad + \frac{t^3(t-t_\pi)\Omega_2(t)}{\pi}\left\{\int\limits_{t_\pi}^{t_\mathrm{m}} \mathrm{d}t' \frac{\sin\delta_2(t')\tilde{\Delta}_{2,-}\big|^{\text{2-sub}}(t')}{t'^3(t'-t_\pi)(t'-t)|\Omega_2(t')|} + \int\limits_{t_\mathrm{m}}^{\infty} \mathrm{d}t' \frac{\operatorname{Im} h_{2,-}(t')}{t'^3(t'-t_\pi)(t'-t)|\Omega_2(t')|}\right\}.
\end{aligned}
\tag{B.17}
$$

The inhomogeneities $\tilde{\Delta}_{J,\pm}\big|^{n\text{-sub}}(t)$ are defined in (5.2) and (5.10).

B.3.2 $I = 2$

The solutions for $-\pi < \delta(t_\mathrm{m}) < 0$, which holds true for all $I = 2$ partial waves, read

$$
\begin{aligned}
h_{0,+}(t) &= \tilde{\Delta}_{0,+}\big|^{\text{1-sub}}(t) + \frac{M_\pi}{2\alpha}(\alpha_1-\beta_1)t\,\Omega_0(t)\frac{t_\mathrm{m}-t}{t_\mathrm{m}} \\
&\quad + \frac{t^2\Omega_0(t)(t_\mathrm{m}-t)}{\pi}\left\{\int\limits_{t_\pi}^{t_\mathrm{m}} \mathrm{d}t' \frac{\sin\delta_0(t')\tilde{\Delta}_{0,+}\big|^{\text{1-sub}}(t')}{t'^2(t_\mathrm{m}-t')(t'-t)|\Omega_0(t')|} + \int\limits_{t_\mathrm{m}}^{\infty} \mathrm{d}t' \frac{\operatorname{Im} h_{0,+}(t')}{t'^2(t_\mathrm{m}-t')(t'-t)|\Omega_0(t')|}\right\}, \\
h_{0,+}(t) &= \tilde{\Delta}_{0,+}\big|^{\text{2-sub}}(t) + \frac{M_\pi t}{2\alpha}\left\{(\alpha_1-\beta_1)\Big[1+\frac{t}{t_\mathrm{m}}(1-t_\mathrm{m}\,\dot{\Omega}_0(0))\Big] + \frac{t}{12}(\alpha_2-\beta_2)\right\}\Omega_0(t)\frac{t_\mathrm{m}-t}{t_\mathrm{m}}
\end{aligned}
$$

$$
\begin{aligned}
&+\frac{t^3\Omega_0(t)(t_\mathrm{m}-t)}{\pi}\left\{\int\limits_{t_\pi}^{t_\mathrm{m}}\mathrm{d}t'\frac{\sin\delta_0(t')\tilde\Delta_{0,+}\big|^{\text{2-sub}}(t')}{t'^3(t_\mathrm{m}-t')(t'-t)|\Omega_0(t')|}+\int\limits_{t_\mathrm{m}}^{\infty}\mathrm{d}t'\frac{\operatorname{Im}h_{0,+}(t')}{t'^3(t_\mathrm{m}-t')(t'-t)|\Omega_0(t')|}\right\},\\
h_{2,+}(t)&=\tilde\Delta_{2,+}(t)+\frac{t^2(t-t_\pi)\Omega_2(t)(t_\mathrm{m}-t)}{\pi}\\
&\quad\times\left\{\int\limits_{t_\pi}^{t_\mathrm{m}}\mathrm{d}t'\frac{\sin\delta_2(t')\tilde\Delta_{2,+}(t')}{t'^2(t'-t_\pi)(t_\mathrm{m}-t')(t'-t)|\Omega_2(t')|}+\int\limits_{t_\mathrm{m}}^{\infty}\mathrm{d}t'\frac{\operatorname{Im}h_{2,+}(t')}{t'^2(t'-t_\pi)(t_\mathrm{m}-t')(t'-t)|\Omega_2(t')|}\right\},\\
h_{2,-}(t)&=\tilde\Delta_{2,-}\big|^{\text{1-sub}}(t)+\frac{t(t-t_\pi)}{10\sqrt{6}M_\pi\alpha}(\alpha_1+\beta_1)\Omega_2(t)\frac{t_\mathrm{m}-t}{t_\mathrm{m}}+\frac{t^2(t-t_\pi)\Omega_2(t)(t_\mathrm{m}-t)}{\pi}\\
&\quad\times\left\{\int\limits_{t_\pi}^{t_\mathrm{m}}\mathrm{d}t'\frac{\sin\delta_2(t')\tilde\Delta_{2,-}\big|^{\text{1-sub}}(t')}{t'^2(t'-t_\pi)(t_\mathrm{m}-t')(t'-t)|\Omega_2(t')|}+\int\limits_{t_\mathrm{m}}^{\infty}\mathrm{d}t'\frac{\operatorname{Im}h_{2,-}(t')}{t'^2(t'-t_\pi)(t_\mathrm{m}-t')(t'-t)|\Omega_2(t')|}\right\},\\
h_{2,-}(t)&=\tilde\Delta_{2,-}\big|^{\text{2-sub}}(t)+\frac{t(t-t_\pi)}{10\sqrt{6}M_\pi\alpha}\Big\{(\alpha_1+\beta_1)\Big[1+\frac{t}{t_\mathrm{m}}(1-t_\mathrm{m}\,\dot\Omega_2(0))\Big]\\
&\quad+\frac{t}{12}(\alpha_2+\beta_2)\Big\}\Omega_2(t)\frac{t_\mathrm{m}-t}{t_\mathrm{m}}+\frac{t^3(t-t_\pi)\Omega_2(t)(t_\mathrm{m}-t)}{\pi}\qquad\text{(B.18)}\\
&\quad\times\left\{\int\limits_{t_\pi}^{t_\mathrm{m}}\mathrm{d}t'\frac{\sin\delta_2(t')\tilde\Delta_{2,-}\big|^{\text{2-sub}}(t')}{t'^3(t'-t_\pi)(t_\mathrm{m}-t')(t'-t)|\Omega_2(t')|}+\int\limits_{t_\mathrm{m}}^{\infty}\mathrm{d}t'\frac{\operatorname{Im}h_{2,-}(t')}{t'^3(t'-t_\pi)(t_\mathrm{m}-t')(t'-t)|\Omega_2(t')|}\right\}.
\end{aligned}
$$

The sum rules discussed in Sect. 5.1.2 are then

$$
\begin{aligned}
0&=\frac{M_\pi}{2\alpha}(\alpha_1-\beta_1)t_\mathrm{m}+\frac{t_\mathrm{m}^2}{\pi}\left\{\int\limits_{t_\pi}^{t_\mathrm{m}}\mathrm{d}t'\frac{\sin\delta_0(t')\tilde\Delta_{0,+}\big|^{\text{1-sub}}(t')}{t'^2(t'-t_\mathrm{m})|\Omega_0(t')|}+\int\limits_{t_\mathrm{m}}^{\infty}\mathrm{d}t'\frac{\operatorname{Im}h_{0,+}(t')}{t'^2(t'-t_\mathrm{m})|\Omega_0(t')|}\right\},\\
0&=\frac{M_\pi t_\mathrm{m}}{2\alpha}\Big[(\alpha_1-\beta_1)(1-t_\mathrm{m}\,\dot\Omega_0(0))+\frac{t_\mathrm{m}}{12}(\alpha_2-\beta_2)\Big]\\
&\quad+\frac{t_\mathrm{m}^3}{\pi}\left\{\int\limits_{t_\pi}^{t_\mathrm{m}}\mathrm{d}t'\frac{\sin\delta_0(t')\tilde\Delta_{0,+}\big|^{\text{2-sub}}(t')}{t'^3(t'-t_\mathrm{m})|\Omega_0(t')|}+\int\limits_{t_\mathrm{m}}^{\infty}\mathrm{d}t'\frac{\operatorname{Im}h_{0,+}(t')}{t'^3(t'-t_\mathrm{m})|\Omega_0(t')|}\right\},\\
0&=\frac{t_\mathrm{m}^2(t_\mathrm{m}-t_\pi)}{\pi}\left\{\int\limits_{t_\pi}^{t_\mathrm{m}}\mathrm{d}t'\frac{\sin\delta_2(t')\tilde\Delta_{2,+}(t')}{t'^2(t'-t_\pi)(t'-t_\mathrm{m})|\Omega_2(t')|}+\int\limits_{t_\mathrm{m}}^{\infty}\mathrm{d}t'\frac{\operatorname{Im}h_{2,+}(t')}{t'^2(t'-t_\pi)(t'-t_\mathrm{m})|\Omega_2(t')|}\right\},\\
0&=\frac{t_\mathrm{m}(t_\mathrm{m}-t_\pi)}{10\sqrt{6}M_\pi\alpha}(\alpha_1+\beta_1)\\
&\quad+\frac{t_\mathrm{m}^2(t_\mathrm{m}-t_\pi)}{\pi}\left\{\int\limits_{t_\pi}^{t_\mathrm{m}}\mathrm{d}t'\frac{\sin\delta_2(t')\tilde\Delta_{2,-}\big|^{\text{1-sub}}(t')}{t'^2(t'-t_\pi)(t'-t_\mathrm{m})|\Omega_2(t')|}+\int\limits_{t_\mathrm{m}}^{\infty}\mathrm{d}t'\frac{\operatorname{Im}h_{2,-}(t')}{t'^2(t'-t_\pi)(t'-t_\mathrm{m})|\Omega_2(t')|}\right\},\\
0&=\frac{t_\mathrm{m}(t_\mathrm{m}-t_\pi)}{10\sqrt{6}M_\pi\alpha}\Big[(\alpha_1+\beta_1)(1-t_\mathrm{m}\,\dot\Omega_2(0))+\frac{t_\mathrm{m}}{12}(\alpha_2+\beta_2)\Big]\qquad\text{(B.19)}\\
&\quad+\frac{t_\mathrm{m}^3(t_\mathrm{m}-t_\pi)}{\pi}\left\{\int\limits_{t_\pi}^{t_\mathrm{m}}\mathrm{d}t'\frac{\sin\delta_2(t')\tilde\Delta_{2,-}\big|^{\text{2-sub}}(t')}{t'^3(t'-t_\pi)(t'-t_\mathrm{m})|\Omega_2(t')|}+\int\limits_{t_\mathrm{m}}^{\infty}\mathrm{d}t'\frac{\operatorname{Im}h_{2,-}(t')}{t'^3(t'-t_\pi)(t'-t_\mathrm{m})|\Omega_2(t')|}\right\}.
\end{aligned}
$$

Appendix C

Roy–Steiner equations for pion–nucleon scattering

In Appendices C.1–C.3, we collect the various (subtracted) kernel functions and pole-term projections that contribute to the RS system in (6.39) and (6.40). For a more detail presentation we refer to [205].

C.1 Kernel functions for the *s*-channel projection

C.1.1 Nucleon pole

The s-channel projection of the nucleon pole terms may be written as

$$N_{l+}^{+}(W) = \bar{N}_{l+}^{+}(W)\,, \qquad N_{l+}^{-}(W) = \bar{N}_{l+}^{-}(W) - \frac{g^2}{4\pi}\frac{(E+m)(W-m)}{2W}\frac{\delta_{l0}}{m^2-a}\,, \tag{C.1}$$

where

$$\bar{N}_{l+}^{I}(W) = \frac{g^2}{16\pi W}\left\{(E+m)(W-m)\left[\epsilon^I\frac{Q_l(y)}{\mathbf{q}^2}+\frac{2\delta_{l0}}{m^2-s}\right]+(E-m)(W+m)\epsilon^I\frac{Q_{l+1}(y)}{\mathbf{q}^2}\right\}\,, \tag{C.2}$$

$\epsilon^I = \pm 1$ for $I = \pm$, and

$$y = 1 - \frac{s+m^2-\Sigma}{2\mathbf{q}^2}\,. \tag{C.3}$$

The Legendre functions of the second kind $Q_l(z)$ can be expressed for general complex argument as (see e.g. [253])

$$Q_l(z) = \frac{1}{2}\int_{-1}^{1}\mathrm{d}x\,\frac{P_l(x)}{z-x}\,, \tag{C.4}$$

which for $l = 0$ reduces to (B.2). In the pseudophysical region of the t-channel reaction we also need the analytic continuation for purely imaginary argument. For $z = iy$, $y > 1$, we have

$$Q_0(iy) = \frac{1}{2}\log\frac{iy+1}{iy-1} = \frac{1}{2}\log\frac{1+iy}{1-iy} - i\frac{\pi}{2} = i\left(\arctan y - \frac{\pi}{2}\right) = -Q_0(-iy)\,. \tag{C.5}$$

C.1.2 *s*-channel

The s-channel partial-wave expansion reads [254]

$$A^I(s,t) = \sum_{l=0}^{\infty} \Big\{ S^1_{l+1,l}(W,z_s) f^I_{l+}(W) - S^1_{l,l+1}(W,z_s) f^I_{(l+1)-}(W) \Big\} ,$$
$$B^I(s,t) = \sum_{l=0}^{\infty} \Big\{ S^2_{l+1,l}(W,z_s) f^I_{l+}(W) - S^2_{l,l+1}(W,z_s) f^I_{(l+1)-}(W) \Big\} , \tag{C.6}$$

with

$$S^1_{kn}(W,z_s) = 4\pi \bigg\{ \frac{W+m}{E+m} P'_k(z_s) + \frac{W-m}{E-m} P'_n(z_s) \bigg\} ,$$
$$S^2_{kn}(W,z_s) = 4\pi \bigg\{ \frac{1}{E+m}\, P'_k(z_s) - \frac{1}{E-m}\, P'_n(z_s) \bigg\} . \tag{C.7}$$

Taken together with the partial-wave projection (6.31), this ultimately leads to the kernel functions [68]

$$K^I_{ll'}(W,W') = \frac{\varphi\big[U_{ll'}\big|\delta(W,W')\big]}{s'-s} - \epsilon^I \frac{\varphi\big[V_{ll'}\big|\varrho(W,W')\big]}{2\mathbf{q}^2} - \frac{\varphi\big[U_{ll'}\big|\varkappa^I(W,W')\big]}{s'-a} , \tag{C.8}$$

where we have defined the following abbreviations: the structure

$$\varphi\big[a_{kn}\big|b(W,W')\big] = \frac{W'}{W} \Big\{ b(W,-W') a_{kn} + b(W,W') a_{k,n+1} + b(-W,-W') a_{k+1,n} + b(-W,W') a_{k+1,n+1} \Big\} , \tag{C.9}$$

for an arbitrary function $b(W,W')$, reflects MacDowell symmetry of $K^I_{ll'}(W,W')$ both with respect to W and W' and acts on

$$\delta(W,W') = \frac{E+m}{E'+m}\big[W'+W\big] , \qquad \varrho(W,W') = \frac{E+m}{E'+m}\big[W'-W+2m\big] ,$$
$$\varkappa^I(W,W') = \frac{1}{2}\Big[\delta(W,W') + \epsilon^I \varrho(W,W')\Big] , \tag{C.10}$$

as well as the angular kernels

$$U_{ll'} = \frac{1}{2}\int_{-1}^{1} \mathrm{d}z_s\; P_l(z_s) P'_{l'}(z'_s) , \qquad V_{ll'} = \frac{1}{2}\int_{-1}^{1} \mathrm{d}z_s\; \frac{P_l(z_s) P'_{l'}(z'_s)}{x_s - z_s} , \tag{C.11}$$

with

$$z'_s = \alpha z_s + \beta , \qquad \alpha = \frac{\mathbf{q}^2}{\mathbf{q}'^2}\frac{s-a}{s'-a} , \qquad \beta = 1 - \alpha - \frac{s'-s}{s'-a}\frac{s+s'-\Sigma}{2\mathbf{q}'^2} ,$$
$$x_s = 1 - \frac{s+s'-\Sigma}{2\mathbf{q}^2} , \qquad x'_s = \alpha x_s + \beta = 1 - \frac{s'+s-\Sigma}{2\mathbf{q}'^2} . \tag{C.12}$$

For the lowest kernel functions one finds

$$\begin{aligned}
&U_{l1} = \delta_{l0} \;, \qquad U_{l2} = \alpha\delta_{l1} + 3\beta\delta_{l0} \;, \qquad U_{l3} = \alpha^2\delta_{l2} + 5\alpha\beta\delta_{l1} + \frac{1}{2}\big\{5[\alpha^2+3\beta^2]-3\big\}\delta_{l0} \;, \\
&V_{l1} = Q_l(x_s) \;, \qquad V_{l2} = 3x_s'Q_l(x_s) - 3\alpha\delta_{l0} \;, \\
&V_{l3} = P_3'(x_s')Q_l(x_s) - \frac{5}{2}\alpha^2\delta_{l1} - \frac{15}{2}\alpha\big\{\alpha x_s + 2\beta\big\}\delta_{l0} \;,
\end{aligned} \tag{C.13}$$

and the calculation of higher kernel functions by means of (C.11) is straightforward, but tedious. For the numerical implementation of $K^I_{ll'}(W,W')$ it is advantageous to analytically separate the Cauchy piece of the kernel functions according to

$$\begin{aligned}
\frac{\varphi\big[U_{ll'}\big|\delta(W,W')\big]}{s'-s} &= \frac{\gamma_{ll'}(W,W')}{W'-W} + \frac{1}{W'+W}\frac{W'}{W}\left\{\frac{E+m}{E'-m}U_{ll'} - \frac{E-m}{E'+m}U_{l+1,l'+1}\right\} \;, \\
\gamma_{ll'}(W,W') &= \frac{W'}{W}\left\{\frac{E+m}{E'+m}U_{l,l'+1} - \frac{E-m}{E'-m}U_{l+1,l'}\right\} \;, \qquad \gamma_{ll'}(W,W) = \delta_{ll'} \;.
\end{aligned} \tag{C.14}$$

Asymptotically, these kernel functions behave as

$$\begin{aligned}
&K^I_{ll'}(W,W') = \mathcal{O}\big(\mathbf{q}^{2l}\big) \;, && K^I_{ll'}(-W,W') = \mathcal{O}\big(\mathbf{q}^{2l+2}\big) && \text{for } |\mathbf{q}| \to 0 \;, \\
&K^I_{ll'}(W,W') = \mathcal{O}\big(\mathbf{q}'^{-2l'}\big) \;, && K^I_{ll'}(W,-W') = \mathcal{O}\big(\mathbf{q}^{-2l'-2}\big) && \text{for } |\mathbf{q}'| \to 0 \;, \\
&K^I_{ll'}(W,W') = \mathcal{O}\big(|\mathbf{q}'|^{-2l-1}\big) && && \text{for } |\mathbf{q}'| \to \infty \;,
\end{aligned} \tag{C.15}$$

in accordance with MacDowell symmetry and the asymptotic properties of $f^I_{l\pm}(W)$.

C.1.3 t-channel

The t-channel partial-wave expansion takes the form [220]

$$\begin{aligned}
A^I(s,t) &= -\frac{4\pi}{p_t^2}\sum_J (2J+1)(p_tq_t)^J\left\{P_J(z_t)f_+^J(t) - \frac{m}{\sqrt{J(J+1)}}z_tP_J'(z_t)f_-^J(t)\right\} \;, \\
B^I(s,t) &= 4\pi\sum_J \frac{2J+1}{\sqrt{J(J+1)}}(p_tq_t)^{J-1}P_J'(z_t)f_-^J(t) \;.
\end{aligned} \tag{C.16}$$

Using the abbreviations

$$\psi\big[a_{kn}\big|d(W)\big] = d(W)a_{kn} + d(-W)a_{k+1,n} \;, \qquad \eta_J = \frac{2J+1}{4W\mathbf{q}^2}\frac{(p_t'q_t')^J}{p_t'^2} \;, \tag{C.17}$$

for an arbitrary function $d(W)$, the corresponding kernels are [68]

$$\begin{aligned}
G_{lJ}(W,t') &= -\eta_J\psi\big[A_{lJ}\big|E+m\big] \;, \\
H_{lJ}(W,t') &= \frac{\eta_J}{\sqrt{J(J+1)}}\left\{\frac{p_t'}{q_t'}\psi\big[B_{lJ}\big|(W-m)(E+m)\big] + m\psi\big[C_{lJ}\big|E+m\big]\right\} \;,
\end{aligned} \tag{C.18}$$

where $C_{lJ} = JA_{lJ} + B_{l,J-1}$, and the angular kernels for even J are defined as

$$\begin{aligned}
A_{lJ} &= \frac{1}{2}\int_{-1}^{1}\mathrm{d}z_s\;\frac{P_l(z_s)P_J(z_t')}{x_t-z_s} \;, \\
B_{lJ} &= \frac{\mu_1}{2}\int_{-1}^{1}\mathrm{d}z_s\;P_l(z_s)\frac{P_J'(z_t')}{z_t'} + \frac{\mu_2}{2}\int_{-1}^{1}\mathrm{d}z_s\;\frac{P_l(z_s)P_J'(z_t')/z_t'}{x_t-z_s} \;,
\end{aligned} \tag{C.19}$$

while one finds for odd J

$$A_{lJ} = \frac{\mu_1}{2}\int\limits_{-1}^{1} \mathrm{d}z_s\; P_l(z_s)\frac{P_J(z_t')}{z_t'} + \frac{\mu_2}{2}\int\limits_{-1}^{1} \mathrm{d}z_s\; \frac{P_l(z_s)P_J(z_t')/z_t'}{x_t - z_s}\,,$$
$$B_{lJ} = \frac{1}{2}\int\limits_{-1}^{1} \mathrm{d}z_s\; \frac{P_l(z_s)P_J'(z_t')}{x_t - z_s}\,, \tag{C.20}$$

with

$$z_t' = \sqrt{\gamma z_s + \delta}\,, \qquad \gamma = \frac{\mathbf{q}^2(s-a)}{2p_t'^2 q_t'^2}\,, \qquad \delta = \frac{(t'-\Sigma+2a)^2 - 4(s-a)(2\mathbf{q}^2+\Sigma-s-a)}{16p_t'^2 q_t'^2}\,,$$
$$\mu_1 = -\frac{\mathbf{q}^2}{2p_t'q_t'}\,, \qquad \mu_2 = \frac{2s+t'-\Sigma}{4p_t'q_t'}\,, \qquad x_t = 1 + \frac{t'}{2\mathbf{q}^2}\,. \tag{C.21}$$

It is important to note that the integrands in (C.19) and (C.20) only involve even powers of z_t', so that no square roots of z_s occur in the integrals. Explicitly, one finds for the lowest kernels

$$\begin{aligned}
G_{l0}(W,t') &= -\frac{1}{4W\mathbf{q}^2 p_t'^2}\Big\{(E+m)Q_l(x_t) - (E-m)Q_{l+1}(x_t)\Big\}\,,\\
G_{l1}(W,t') &= \frac{3}{4}\Big\{(2s+t'-\Sigma)G_{l0}(W,t') + \frac{E+m}{2Wp_t'^2}\delta_{l0}\Big\}\,,\\
H_{l1}(W,t') &= \frac{1}{\sqrt{2}}\Big\{\frac{3}{4}Z_l(W,t') - mG_{l1}(W,t')\Big\}\,,\\
G_{l2}(W,t') &= \frac{5}{16}\Big\{\Big[6s(s+t'-\Sigma) + (t'-\Sigma)^2 + 2(m^2-M_\pi^2)^2\Big]G_{l0}(W,t')\\
&\qquad + 3\frac{(E+m)(s-a)}{Wp_t'^2}\delta_{l0}\Big\}\,,\\
H_{l2}(W,t') &= \frac{15}{16\sqrt{6}}\Big\{(2s+t'-\Sigma)Z_l(W,t') - m\Big[4s(s+t'-\Sigma) + (t'-\Sigma)^2\Big]G_{l0}(W,t')\\
&\qquad - 2\frac{E+m}{W}\Big[\frac{m(s-a)}{p_t'^2} + W - m\Big]\delta_{l0}\Big\}\,,
\end{aligned} \tag{C.22}$$

where

$$Z_l(W,t') = \frac{1}{W\mathbf{q}^2}\Big\{(E+m)(W-m)Q_l(x_t) + (E-m)(W+m)Q_{l+1}(x_t)\Big\}\,. \tag{C.23}$$

In particular, they behave asymptotically according to the general relations

$$\begin{aligned}
G_{lJ}(W,t') &= \mathcal{O}\big(\mathbf{q}^{2l}\big)\,, & H_{lJ}(W,t') &= \mathcal{O}\big(\mathbf{q}^{2l}\big) && \text{for } |\mathbf{q}| \to 0\,,\\
G_{lJ}(-W,t') &= \mathcal{O}\big(\mathbf{q}^{2l+2}\big)\,, & H_{lJ}(-W,t') &= \mathcal{O}\big(\mathbf{q}^{2l+2}\big) && \text{for } |\mathbf{q}| \to 0\,,\\
G_{lJ}(W,t') &= \mathcal{O}(1)\,, & H_{lJ}(W,t') &= \mathcal{O}(1) && \text{for } q_t' \to 0\,,\\
G_{lJ}(W,t') &= \mathcal{O}\big(p_t'^{-2}\big)\,, & H_{lJ}(W,t') &= \mathcal{O}\big(p_t'^{-2}\big) && \text{for } p_t' \to 0\,,\\
G_{lJ}(W,t') &= \mathcal{O}\big(t'^{J-l-2}\big)\,, & H_{lJ}(W,t') &= \mathcal{O}\big(t'^{J-l-2}\big) && \text{for } t' \to \infty\,.
\end{aligned} \tag{C.24}$$

C.2 Kernel functions for the t-channel projection

C.2.1 Nucleon pole

The t-channel projection of the nucleon pole terms reads

$$\tilde{N}_+^J(t) = \hat{N}_+^J(t) - \frac{g^2}{4\pi}\frac{m}{3}\frac{\delta_{J1}}{m^2-a}\,, \qquad \hat{N}_+^J(t) = \frac{g^2}{4\pi}m\left\{\frac{\tilde{y}Q_J(\tilde{y})}{(p_tq_t)^J} - \delta_{J0}\right\},$$
$$\tilde{N}_-^J(t) = \hat{N}_-^J(t) - \frac{g^2}{4\pi}\frac{\sqrt{2}}{3}\frac{\delta_{J1}}{m^2-a}\,, \qquad \hat{N}_-^J(t) = \frac{g^2}{4\pi}\frac{\sqrt{J(J+1)}}{2J+1}\frac{Q_{J-1}(\tilde{y}) - Q_{J+1}(\tilde{y})}{(p_tq_t)^J}\,, \quad \text{(C.25)}$$

where

$$\tilde{y} = \frac{t-2M_\pi^2}{4p_tq_t}\,. \quad \text{(C.26)}$$

Although $\tilde{y}$ diverges at t_π and t_N, $\tilde{N}_\pm^J(t)$ itself remains finite. Expressions that allow for a stable numerical evaluation can be obtained by invoking the asymptotic form of the Legendre functions $Q_l(z)$ for $|z|\to\infty$ [253]

$$Q_l(z) \sim \frac{2^l(l!)^2}{(2l+1)!}z^{-(l+1)}\,, \quad \text{(C.27)}$$

which leads to

$$\tilde{N}_+^J(t) = \frac{g^2}{4\pi}\frac{J!}{(2J+1)!!}m\left\{\left(\frac{4}{t-2M_\pi^2}\right)^J - \delta_{J0} - \frac{\delta_{J1}}{m^2-a}\right\} + \mathcal{O}\big(p_t^2q_t^2\big)\,,$$
$$\tilde{N}_-^J(t) = \frac{g^2}{4\pi}\frac{J!}{(2J+1)!!}\sqrt{\frac{J+1}{J}}\left\{\left(\frac{4}{t-2M_\pi^2}\right)^J - \frac{\delta_{J1}}{m^2-a}\right\} + \mathcal{O}\big(p_t^2q_t^2\big)\,. \quad \text{(C.28)}$$

In contrast to the ostensible divergences for $p_tq_t\to 0$, the pole terms do involve a branch-point singularity at $t_\pi - (M_\pi^2/m)^2 \approx 3.98M_\pi^2$, where the branch cut of $Q_J(\tilde{y})$ starts.

C.2.2 s-channel

Introducing

$$\tilde{\psi}\big[a_{kn}\big|d(W')\big] = d(W')a_{k,n+1} + d(-W')a_{kn}\,, \qquad \tilde{\eta}_J = \frac{2W'}{(p_tq_t)^{J-1}}\,, \quad \text{(C.29)}$$

in analogy to (C.17), the s-channel kernel functions become

$$\tilde{G}_{Jl}(t,W') = \tilde{\eta}_J\left\{-\frac{p_t}{q_t}\tilde{\psi}\left[\tilde{A}_{Jl}\middle|\frac{W'+m}{E'+m}\right] + m\tilde{\psi}\left[\tilde{B}_{Jl}\middle|\frac{1}{E'+m}\right]\right\}\,,$$
$$\tilde{H}_{Jl}(t,W') = \tilde{\eta}_J\frac{\sqrt{J(J+1)}}{2J+1}\tilde{\psi}\left[\tilde{C}_{Jl}\middle|\frac{1}{E'+m}\right]\,, \quad \text{(C.30)}$$

with angular kernel functions

$$\tilde{A}_{Jl} = \frac{1}{p_tq_t}P_l'(\tilde{z}_s)Q_J(\tilde{x}_t) - \bar{A}_{Jl}\,, \qquad \tilde{C}_{Jl} = \tilde{A}_{J-1,l} - \tilde{A}_{J+1,l}\,,$$
$$\tilde{B}_{Jl} = \frac{1}{p_tq_t}P_l'(\tilde{z}_s)\tilde{x}_tQ_J(\tilde{x}_t) - \bar{B}_{Jl}\,, \quad \text{(C.31)}$$

their polynomial parts

$$\bar{A}_{Jl} = \frac{1}{2}\int\limits_{-1}^{1} \mathrm{d}z_t\, P_J(z_t) \left\{ \frac{1}{p_t q_t} \frac{P_l'(\tilde{z}_s) - P_l'(z_s')}{\tilde{x}_t - z_t} + \frac{1 \pm 1}{2(s'-a)} P_l'(z_s') \right\} ,$$

$$\bar{B}_{Jl} = \frac{1}{2}\int\limits_{-1}^{1} \mathrm{d}z_t\, P_J(z_t) \left\{ \frac{1}{p_t q_t} \frac{\tilde{x}_t P_l'(\tilde{z}_s) - z_t P_l'(z_s')}{\tilde{x}_t - z_t} + \frac{1 \mp 1}{2(s'-a)} z_t P_l'(z_s') \right\} , \tag{C.32}$$

where the upper/lower sign refers to even/odd J, and

$$z_s' = \frac{z_t^2 - \tilde{\delta}}{\tilde{\gamma}} , \qquad \tilde{\gamma} = \frac{\mathbf{q}'^2 (s'-a)}{2 p_t^2 q_t^2} , \qquad \tilde{\delta} = \frac{(t - \Sigma + 2a)^2 - 4(s'-a)(2\mathbf{q}'^2 + \Sigma - s' - a)}{16 p_t^2 q_t^2} ,$$
$$\tilde{x}_t = \frac{t + 2s' - \Sigma}{4 p_t q_t} , \qquad \tilde{z}_s = \frac{\tilde{x}_t^2 - \tilde{\delta}}{\tilde{\gamma}} = 1 + \frac{t}{2\mathbf{q}'^2} . \tag{C.33}$$

These kernel functions fulfill the asymptotic relations

$$\begin{aligned}
&\tilde{G}_{Jl}(t, W') = \mathcal{O}(1) , && \tilde{H}_{Jl}(t, W') = \mathcal{O}(1) && \text{for } \ p_t q_t \to 0 , \\
&\tilde{G}_{Jl}(t, W') = \mathcal{O}\big(\mathbf{q}'^{-2l}\big) , && \tilde{H}_{Jl}(t, W') = \mathcal{O}\big(\mathbf{q}'^{-2l}\big) && \text{for } \ |\mathbf{q}'| \to 0 , \\
&\tilde{G}_{Jl}(t, -W') = \mathcal{O}\big(\mathbf{q}'^{-2l-2}\big) , && \tilde{H}_{Jl}(t, -W') = \mathcal{O}\big(\mathbf{q}'^{-2l-2}\big) && \text{for } \ |\mathbf{q}'| \to 0 , \\
&\tilde{G}_{Jl}(t, W') = \mathcal{O}\big(\mathbf{q}'^{-2J}\big) , && \tilde{H}_{Jl}(t, W') = \mathcal{O}\big(\mathbf{q}'^{-2J}\big) && \text{for } \ |\mathbf{q}'| \to \infty .
\end{aligned} \tag{C.34}$$

In particular, the finite pieces for $p_t q_t \to 0$ can be derived along the lines that led to (C.28).

C.2.3 *t*-channel

The t-channel kernel functions follow from

$$\begin{pmatrix} \tilde{K}^1_{JJ'}(t,t') & \tilde{K}^2_{JJ'}(t,t') \\ 0 & \tilde{K}^3_{JJ'}(t,t') \end{pmatrix} = \frac{\zeta_{JJ'}}{t'-t} \begin{pmatrix} u_{JJ'} & v_{JJ'} \\ 0 & w_{JJ'} \end{pmatrix} , \qquad \zeta_{JJ'} = (2J'+1) \frac{(p_t' q_t')^{J'-1}}{(p_t q_t)^{J-1}} , \tag{C.35}$$

with angular kernels for even J and J'

$$u_{JJ'} = \frac{p_t q_t'}{q_t p_t'} \int\limits_0^1 \mathrm{d}z_t\; P_J(z_t) P_{J'}(z_t') ,$$

$$v_{JJ'} = \frac{m}{\sqrt{J'(J'+1)}} \frac{p_t}{q_t p_t' q_t'} \int\limits_0^1 \mathrm{d}z_t\; P_J(z_t) \Big\{ q_t^2 z_t^2 - q_t'^2 z_t'^2 \Big\} \frac{P_{J'}'(z_t')}{z_t'} ,$$

$$w_{JJ'} = \frac{1}{2J+1} \sqrt{\frac{J(J+1)}{J'(J'+1)}} \frac{p_t q_t}{p_t' q_t'} \int\limits_0^1 \mathrm{d}z_t \, \Big\{ P_{J-1}(z_t) - P_{J+1}(z_t) \Big\} z_t \frac{P_{J'}'(z_t')}{z_t'} , \tag{C.36}$$

	$p_t \to 0$	$q_t \to 0$	$t \to \infty$	$p_t' \to 0$	$q_t' \to 0$	$t' \to \infty$
$\tilde{K}^1_{JJ'}(t,t')$	$\mathcal{O}\big(p_t^2\big)$	$\mathcal{O}(1)$	$\mathcal{O}\big(t^{J'-J}\big)$	$\mathcal{O}\big(p_t'^{-2}\big)$	$\mathcal{O}(1)$	$\mathcal{O}\big(t'^{J'-J-2}\big)$
$\tilde{K}^2_{JJ'}(t,t')$	$\mathcal{O}(1)$	$\mathcal{O}(1)$	$\mathcal{O}\big(t^{J'-J}\big)$	$\mathcal{O}\big(p_t'^{-2}\big)$	$\mathcal{O}(1)$	$\mathcal{O}\big(t'^{J'-J-1}\big)$
$\tilde{K}^3_{JJ'}(t,t')$	$\mathcal{O}(1)$	$\mathcal{O}(1)$	$\mathcal{O}\big(t^{J'-J-1}\big)$	$\mathcal{O}(1)$	$\mathcal{O}(1)$	$\mathcal{O}\big(t'^{J'-J-1}\big)$

Table C.1: Asymptotic properties of the t-channel kernel functions.

and for odd J and J'

$$u_{JJ'} = \frac{p_t^2}{p_t'^2}\int_0^1 \mathrm{d}z_t\; P_J(z_t) z_t \frac{P_{J'}(z_t')}{z_t'}\,, \qquad v_{JJ'} = \frac{m}{\sqrt{J'(J'+1)}}\Big\{1-\frac{p_t^2}{p_t'^2}\Big\}\int_0^1 \mathrm{d}z_t\; P_J(z_t) z_t P'_{J'}(z_t')\,,$$
$$w_{JJ'} = \frac{1}{2J+1}\sqrt{\frac{J(J+1)}{J'(J'+1)}}\int_0^1 \mathrm{d}z_t\,\Big\{P_{J-1}(z_t) - P_{J+1}(z_t)\Big\}P'_{J'}(z_t')\,, \tag{C.37}$$

where the angles are related by

$$z_t' = \sqrt{\tilde{\alpha} z_t^2 + \tilde{\beta}}\,, \qquad \tilde{\alpha} = \frac{p_t^2 q_t^2}{p_t'^2 q_t'^2}\,, \qquad \tilde{\beta} = \frac{t'-t}{16 p_t'^2 q_t'^2}(t+t'-2\Sigma+4a)\,. \tag{C.38}$$

Again, only even powers of $z_t'^2$ appear in the angular integrals (C.36) and (C.37). Starting from these equations, one can show that for $J' < J$ all kernel functions vanish

$$\tilde{K}^1_{JJ'}(t,t') = \tilde{K}^2_{JJ'}(t,t') = \tilde{K}^3_{JJ'}(t,t') = 0 \qquad \text{for } J' < J\,, \tag{C.39}$$

while the diagonal kernels fulfill the general relations

$$\tilde{K}^1_{JJ}(t,t') = \frac{p_t^2}{p_t'^2}\frac{1}{t'-t}\,, \qquad \tilde{K}^2_{JJ}(t,t') = \sqrt{\frac{J}{J+1}}\frac{m}{4p_t'^2}\,, \qquad \tilde{K}^3_{JJ}(t,t') = \frac{1}{t'-t}\,. \tag{C.40}$$

Finally, the non-vanishing, non-diagonal kernel functions with $J \le 3$ and $J' \le 3$ read

$$\tilde{K}^1_{02}(t,t') = \frac{5}{16}\frac{p_t^2}{p_t'^2}\Big\{t+t'-2\Sigma+6a\Big\}\,, \qquad \tilde{K}^2_{02}(t,t') = \frac{5m}{16\sqrt{6}}\frac{p_t^2}{p_t'^2}\Big\{4q_t^2 - 3(t+t'-2\Sigma+4a)\Big\}\,,$$
$$\tilde{K}^1_{13}(t,t') = \frac{7}{48}\frac{p_t^2}{p_t'^2}\Big\{t+t'-2\Sigma+10a\Big\}\,, \qquad \tilde{K}^3_{13}(t,t') = \frac{7}{8\sqrt{6}}\Big\{t+t'-2\Sigma+5a\Big\}\,,$$
$$\tilde{K}^2_{13}(t,t') = \frac{7m}{64\sqrt{3}}\frac{1}{p_t'^2}\Big\{8p_t^2q_t^2 + (t'-t)(t+t'-2\Sigma+5a)\Big\}\,. \tag{C.41}$$

The general asymptotic properties of the kernels are given in Table C.1. Note, however, that exceptionally

$$\tilde{K}^2_{02}(t,t') = \mathcal{O}\big(p_t^2\big) \qquad \text{for } \; p_t \to 0\,, \qquad\qquad \tilde{K}^2_{02}(t,t') = \mathcal{O}(1) \qquad \text{for } \; t' \to \infty\,. \tag{C.42}$$

C.3 Subtractions

C.3.1 Subtracted hyperbolic dispersion relations

The sum rules for all subthreshold parameters that appear in Table 6.1 are

$$
\begin{aligned}
d_{00}^{+} &= -\frac{g^2}{m} + \frac{1}{\pi}\int\limits_{s_+}^{\infty} \mathrm{d}s'\, h_0(s') \left[\mathrm{Im}\, A^{+}\right]_{(0,0)} + \frac{1}{\pi}\int\limits_{t_\pi}^{\infty} \frac{\mathrm{d}t'}{t'} \left[\mathrm{Im}\, A^{+}\right]_{(0,0)} \ , \\
b_{00}^{-} &= \frac{g^2}{2m^2} - \frac{g^2}{m^2-a} + \frac{1}{\pi}\int\limits_{s_+}^{\infty} \mathrm{d}s'\, h_0(s') \left[\mathrm{Im}\, B^{-}\right]_{(0,0)} + \frac{1}{\pi}\int\limits_{t_\pi}^{\infty} \frac{\mathrm{d}t'}{t'} \left[\mathrm{Im}\, B^{-}\right]_{(0,0)} \ , \\
d_{01}^{+} &= \frac{1}{\pi}\int\limits_{s_+}^{\infty} \mathrm{d}s' \Big\{ h_0(s') \left[\partial_t \mathrm{Im}\, A^{+}\right]_{(0,0)} - h_2^0(s') \left[\mathrm{Im}\, A^{+}\right]_{(0,0)} \Big\} \\
&\quad + \frac{1}{\pi}\int\limits_{t_\pi}^{\infty} \frac{\mathrm{d}t'}{t'} \Big\{ \left[\partial_t \mathrm{Im}\, A^{+}\right]_{(0,0)} + \frac{1}{t'} \left[\mathrm{Im}\, A^{+}\right]_{(0,0)} \Big\} \ , \\
a_{00}^{-} &= \frac{4m}{\pi}\int\limits_{s_+}^{\infty} \mathrm{d}s'\, h_2^0(s') \left[\mathrm{Im}\, A^{-}\right]_{(0,0)} + \frac{1}{\pi}\int\limits_{t_\pi}^{\infty} \frac{\mathrm{d}t'}{t'} \left[\mathrm{Im}\, A^{-}/\nu'\right]_{(0,0)} \ , \\
b_{00}^{+} &= \frac{4m}{\pi}\int\limits_{s_+}^{\infty} \mathrm{d}s'\, h_2^0(s') \left[\mathrm{Im}\, B^{+}\right]_{(0,0)} + \frac{1}{\pi}\int\limits_{t_\pi}^{\infty} \frac{\mathrm{d}t'}{t'} \left[\mathrm{Im}\, B^{+}/\nu'\right]_{(0,0)} \ , \\
b_{01}^{-} &= \frac{1}{\pi}\int\limits_{s_+}^{\infty} \mathrm{d}s' \Big\{ h_0(s') \left[\partial_t \mathrm{Im}\, B^{-}\right]_{(0,0)} - h_2^0(s') \left[\mathrm{Im}\, B^{-}\right]_{(0,0)} \Big\} \\
&\quad + \frac{1}{\pi}\int\limits_{t_\pi}^{\infty} \frac{\mathrm{d}t'}{t'} \Big\{ \left[\partial_t \mathrm{Im}\, B^{-}\right]_{(0,0)} + \frac{1}{t'} \left[\mathrm{Im}\, B^{-}\right]_{(0,0)} \Big\} \ , \\
a_{10}^{+} &= \frac{1}{\pi}\int\limits_{s_+}^{\infty} \mathrm{d}s' \Big\{ h_0(s') \left[\partial_{\nu^2} \mathrm{Im}\, A^{+}\right]_{(0,0)} + 8m^2 h_3^0(s') \left[\mathrm{Im}\, A^{+}\right]_{(0,0)} \Big\} + \frac{1}{\pi}\int\limits_{t_\pi}^{\infty} \frac{\mathrm{d}t'}{t'} \left[\partial_{\nu^2} \mathrm{Im}\, A^{+}\right]_{(0,0)} \ , \\
a_{01}^{-} &= \frac{4m}{\pi}\int\limits_{s_+}^{\infty} \mathrm{d}s' \Big\{ h_2^0(s') \left[\partial_t \mathrm{Im}\, A^{-}\right]_{(0,0)} - h_3^0(s') \left[\mathrm{Im}\, A^{-}\right]_{(0,0)} \Big\} \\
&\quad + \frac{1}{\pi}\int\limits_{t_\pi}^{\infty} \frac{\mathrm{d}t'}{t'} \Big\{ \left[\partial_t \mathrm{Im}\, A^{-}/\nu'\right]_{(0,0)} + \frac{1}{t'} \left[\mathrm{Im}\, A^{-}/\nu'\right]_{(0,0)} \Big\} \ , \\
a_{10}^{-} &= \frac{4m}{\pi}\int\limits_{s_+}^{\infty} \mathrm{d}s' \Big\{ h_2^0(s') \left[\partial_{\nu^2} \mathrm{Im}\, A^{-}\right]_{(0,0)} + 4m^2 h_4^0(s') \left[\mathrm{Im}\, A^{-}\right]_{(0,0)} \Big\} \\
&\quad + \frac{1}{\pi}\int\limits_{t_\pi}^{\infty} \frac{\mathrm{d}t'}{t'} \left[\partial_{\nu^2} \mathrm{Im}\, A^{-}/\nu'\right]_{(0,0)} \ ,
\end{aligned}
\tag{C.43}
$$

$$b_{10}^- = \frac{1}{\pi}\int\limits_{s_+}^{\infty}\mathrm{d}s'\Big\{h_0(s')\left[\partial_{\nu^2}\mathrm{Im}\,B^-\right]_{(0,0)} + 8m^2h_3^0(s')\left[\mathrm{Im}\,B^-\right]_{(0,0)}\Big\} + \frac{1}{\pi}\int\limits_{t_\pi}^{\infty}\frac{\mathrm{d}t'}{t'}\left[\partial_{\nu^2}\mathrm{Im}\,B^-\right]_{(0,0)}\,,$$

where we have introduced the notation

$$h_0(s') = \frac{2}{s'-s_0} - \frac{1}{s'-a}\,, \qquad h_n^0(s') = \frac{1}{(s'-s_0)^n}\,. \tag{C.44}$$

Here and in the following, the dependence of the amplitudes on the internal kinematics (s',t') is suppressed and the subscript $(0,0)$ indicates evaluation at $(\nu=0,t=0)$. For that purpose, one may use the relations

$$\begin{aligned}
\left[z_s'\right]_{(0,0)} &= 1 - \frac{(s'-s_0)^2}{2\mathbf{q}'^2(s'-a)}\,, \qquad \left[\partial_t z_s'\right]_{(0,0)} = \frac{s_0-a}{2\mathbf{q}'^2(s'-a)}\,, \quad \left[\partial_{\nu^2} z_s'\right]_{(0,0)} = \frac{2m^2}{\mathbf{q}'^2(s'-a)}\,,\\
\left[z_t'^2\right]_{(0,0)} &= 1 + \frac{at' - 4m^2M_\pi^2}{4p_t'^2q_t'^2}\,, \quad \left[\partial_t z_t'^2\right]_{(0,0)} = \frac{s_0-a}{4p_t'^2q_t'^2}\,, \qquad \left[\partial_{\nu^2} z_t'^2\right]_{(0,0)} = \frac{m^2}{p_t'^2q_t'^2}\,.
\end{aligned} \tag{C.45}$$

We only quote the form of the subtracted HDRs that includes all subthreshold parameters from (C.43)

$$\begin{aligned}
A^+(s,t) = {}& d_{00}^+ + \frac{g^2}{m} + d_{01}^+ t + a_{10}^+\nu^2 + \frac{1}{\pi}\int\limits_{t_\pi}^{\infty}\mathrm{d}t'\Bigg\{\frac{\mathrm{Im}\,A^+}{t'-t} - \left(\frac{1}{t'} + \frac{t}{t'^2}\right)\left[\mathrm{Im}\,A^+\right]_{(0,0)}\\
&- \frac{t}{t'}\left[\partial_t\mathrm{Im}\,A^+\right]_{(0,0)} - \frac{\nu^2}{t'}\left[\partial_{\nu^2}\mathrm{Im}\,A^+\right]_{(0,0)}\Bigg\}\\
&+ \frac{1}{\pi}\int\limits_{s_+}^{\infty}\mathrm{d}s'\Bigg\{\left[\frac{1}{s'-s} + \frac{1}{s'-u} - \frac{1}{s'-a}\right]\mathrm{Im}\,A^+\\
&- h_0(s')\Big(t\left[\partial_t\mathrm{Im}\,A^+\right]_{(0,0)} + \nu^2\left[\partial_{\nu^2}\mathrm{Im}\,A^+\right]_{(0,0)}\Big)\\
&- \Big(h_0(s') - t\,h_2^0(s') + 8m^2\nu^2h_3^0(s')\Big)\left[\mathrm{Im}\,A^+\right]_{(0,0)}\Bigg\}\,,
\end{aligned}$$

$$\begin{aligned}
A^-(s,t) = {}& a_{00}^-\nu + a_{01}^-\nu t + a_{10}^-\nu^3 + \frac{\nu}{\pi}\int\limits_{t_\pi}^{\infty}\mathrm{d}t'\Bigg\{\frac{\mathrm{Im}\,A^-/\nu'}{t'-t} - \left(\frac{1}{t'} + \frac{t}{t'^2}\right)\left[\mathrm{Im}\,A^-/\nu'\right]_{(0,0)}\\
&- \frac{t}{t'}\left[\partial_t\mathrm{Im}\,A^-/\nu'\right]_{(0,0)} - \frac{\nu^2}{t'}\left[\partial_{\nu^2}\mathrm{Im}\,A^-/\nu'\right]_{(0,0)}\Bigg\}\\
&+ \frac{1}{\pi}\int\limits_{s_+}^{\infty}\mathrm{d}s'\Bigg\{\left[\frac{1}{s'-s} - \frac{1}{s'-u}\right]\mathrm{Im}\,A^- - 4m\nu\,h_2^0(s')\Big(t\left[\partial_t\mathrm{Im}\,A^-\right]_{(0,0)} + \nu^2\left[\partial_{\nu^2}\mathrm{Im}\,A^-\right]_{(0,0)}\Big)\\
&- 4m\nu\Big(h_2^0(s') - t\,h_3^0(s') + 4m^2\nu^2h_4^0(s')\Big)\left[\mathrm{Im}\,A^-\right]_{(0,0)}\Bigg\}\,,
\end{aligned}$$

$$B^+(s,t) = g^2\left[\frac{1}{m^2-s} - \frac{1}{m^2-u}\right] + b_{00}^+\nu + \frac{\nu}{\pi}\int\limits_{t_\pi}^{\infty}\mathrm{d}t'\Bigg\{\frac{\mathrm{Im}\,B^+/\nu'}{t'-t} - \frac{1}{t'}\left[\mathrm{Im}\,B^+/\nu'\right]_{(0,0)}\Bigg\}$$

$$+\frac{1}{\pi}\int\limits_{s_+}^{\infty}\mathrm{d}s'\left\{\left[\frac{1}{s'-s}-\frac{1}{s'-u}\right]\mathrm{Im}\,B^+-4m\nu\,h_2^0(s')\left[\mathrm{Im}\,B^+\right]_{(0,0)}\right\},$$

$$\begin{aligned}B^-(s,t)=g^2\left[\frac{1}{m^2-s}+\frac{1}{m^2-u}\right]+b_{00}^-&-\frac{g^2}{2m^2}+b_{01}^-t+b_{10}^-\nu^2+\frac{1}{\pi}\int\limits_{t_\pi}^{\infty}\mathrm{d}t'\left\{\frac{\mathrm{Im}\,B^-}{t'-t}\right.\\&\left.-\left(\frac{1}{t'}+\frac{t}{t'^2}\right)\left[\mathrm{Im}\,B^-\right]_{(0,0)}-\frac{t}{t'}\left[\partial_t\mathrm{Im}\,B^-\right]_{(0,0)}-\frac{\nu^2}{t'}\left[\partial_{\nu^2}\mathrm{Im}\,B^-\right]_{(0,0)}\right\}\\&+\frac{1}{\pi}\int\limits_{s_+}^{\infty}\mathrm{d}s'\left\{\left[\frac{1}{s'-s}+\frac{1}{s'-u}-\frac{1}{s'-a}\right]\mathrm{Im}\,B^-\right.\\&\quad-h_0(s')\Big(t\left[\partial_t\mathrm{Im}\,B^-\right]_{(0,0)}+\nu^2\left[\partial_{\nu^2}\mathrm{Im}\,B^-\right]_{(0,0)}\Big)\\&\quad\left.-\Big(h_0(s')-t\,h_2^0(s')+8m^2\nu^2h_3^0(s')\Big)\left[\mathrm{Im}\,B^-\right]_{(0,0)}\right\}.\end{aligned}\tag{C.46}$$

The reduction to the various subtraction schemes introduced in Sect. 6.3.3 may be achieved by dropping the pertinent subthreshold parameters and the terms associated with their sum rules according to (C.43).

C.3.2 *s*-channel projection

The presentation of the corrections for the various subtraction schemes will be organized in such a way that we start from the once-subtracted version and successively add the necessary amendments for the additional subtractions discussed in Sect. 6.3.3. First, we collect the contributions to the partial waves that originate from the subthreshold parameters. For convenience, we include these terms by modifying the pole terms according to

$$N_{l+}^I\big|^{n\text{-sub}}(W)=\bar{N}_{l+}^I(W)+\Delta N_{l+}^I\big|^{n\text{-sub}}(W)\,,\qquad\Delta N_{l+}^I(W)=\widehat{\Delta N}_l^I(W)-\widehat{\Delta N}_{l+1}^I(-W)\,,\tag{C.47}$$

and

$$\begin{aligned}\widehat{\Delta N}_l^+\big|^{1\text{-sub}}(W)&=\frac{\delta_{l0}}{8\pi W}(E+m)\left(d_{00}^++\frac{g^2}{m}\right),\\\widehat{\Delta N}_l^+\big|^{2\text{-sub}}(W)&=\widehat{\Delta N}_l^+\big|^{1\text{-sub}}-\frac{d_{01}^+\mathbf{q}^2\chi_l^t}{4\pi W}(E+m)+\frac{b_{00}^+\chi_l^\nu}{16\pi Wm}(E+m)(W-m)\,,\\\widehat{\Delta N}_l^+\big|^{3\text{-sub}}(W)&=\widehat{\Delta N}_l^+\big|^{2\text{-sub}}+\frac{a_{10}^+\chi_l^{\nu^2}}{32\pi Wm^2}(E+m)\,,\\\widehat{\Delta N}_l^-\big|^{1\text{-sub}}(W)&=\frac{\delta_{l0}}{8\pi W}(E+m)(W-m)\left(b_{00}^--\frac{g^2}{2m^2}\right),\\\widehat{\Delta N}_l^-\big|^{2\text{-sub}}(W)&=\widehat{\Delta N}_l^-\big|^{1\text{-sub}}+\frac{a_{00}^-\chi_l^\nu}{16\pi Wm}(E+m)-\frac{b_{01}^-\mathbf{q}^2\chi_l^t}{4\pi W}(E+m)(W-m)\,,\\\widehat{\Delta N}_l^-\big|^{3\text{-sub}}(W)&=\widehat{\Delta N}_l^-\big|^{2\text{-sub}}-\frac{a_{01}^-\mathbf{q}^2\chi_l^{\nu t}}{8\pi Wm}(E+m)\,,\\\widehat{\Delta N}_l^-\big|^{\text{ex 3-sub}}(W)&=\widehat{\Delta N}_l^-\big|^{3\text{-sub}}+\frac{a_{10}^-\chi_l^{\nu^3}}{64\pi Wm^3}(E+m)+\frac{b_{10}^-\chi_l^{\nu^2}}{32\pi Wm^2}(E+m)(W-m)\,,\end{aligned}\tag{C.48}$$

with

$$\chi_l^{\nu} = (s - s_0 - \mathbf{q}^2)\delta_{l0} + \frac{\mathbf{q}^2}{3}\delta_{l1} \ , \qquad \chi_l^{\nu t} = \left(s - s_0 - \frac{4}{3}\mathbf{q}^2\right)\delta_{l0} + (2\mathbf{q}^2 - s + s_0)\frac{\delta_{l1}}{3} - \frac{2}{15}\mathbf{q}^2\delta_{l2} \ ,$$
$$\chi_l^{\nu^2} = \left((s - s_0 - \mathbf{q}^2)^2 + \frac{\mathbf{q}^4}{3}\right)\delta_{l0} + \frac{2}{3}\mathbf{q}^2(s - s_0 - \mathbf{q}^2)\delta_{l1} + \frac{2}{15}\mathbf{q}^4\delta_{l2} \ , \qquad \chi_l^{t} = \delta_{l0} - \frac{\delta_{l1}}{3} \ ,$$
$$\chi_l^{\nu^3} = (s - s_0 - \mathbf{q}^2)\Big((s - s_0 - \mathbf{q}^2)^2 + \mathbf{q}^4\Big)\delta_{l0} + \mathbf{q}^2\left((s - s_0 - \mathbf{q}^2)^2 + \frac{\mathbf{q}^4}{5}\right)\delta_{l1}$$
$$+ \frac{2}{5}\mathbf{q}^4(s - s_0 - \mathbf{q}^2)\delta_{l2} + \frac{2}{35}\mathbf{q}^6\delta_{l3} \ . \tag{C.49}$$

Next, the s-channel kernels become

$$K_{ll'}^I\big|^{n\text{-sub}}(W, W') = K_{ll'}^I(W, W') + \Delta K_{ll'}^I\big|^{n\text{-sub}}(W, W') \ ,$$
$$\Delta K_{ll'}^I(W, W') = \widehat{\Delta K}_{ll'}^I(W, W') - \widehat{\Delta K}_{l+1,l'}^I(-W, W') \ , \tag{C.50}$$

with

$$\widehat{\Delta K}_{ll'}^+\big|^{1\text{-sub}}(W, W') = -\frac{W'}{4\pi W}(E + m)h_0(s')\left[S_{l'+1,l'}^1(W', z_s')\right]_{(0,0)}\delta_{l0} \ ,$$
$$\widehat{\Delta K}_{ll'}^+\big|^{2\text{-sub}}(W, W') = \widehat{\Delta K}_{ll'}^+\big|^{1\text{-sub}} + \frac{\mathbf{q}^2 W'}{2\pi W}\chi_l^t(E + m)$$
$$\times\left\{h_0(s')\left[\partial_t S_{l'+1,l'}^1(W', z_s')\right]_{(0,0)} - h_2^0(s')\left[S_{l'+1,l'}^1(W', z_s')\right]_{(0,0)}\right\}$$
$$- \frac{W'}{2\pi W}\chi_l^{\nu}(E + m)(W - m)h_2^0(s')\left[S_{l'+1,l'}^2(W', z_s')\right]_{(0,0)} \ ,$$
$$\widehat{\Delta K}_{ll'}^+\big|^{3\text{-sub}}(W, W') = \widehat{\Delta K}_{ll'}^+\big|^{2\text{-sub}} - \frac{W'}{16\pi W m^2}\chi_l^{\nu^2}(E + m)$$
$$\times\left\{h_0(s')\left[\partial_{\nu^2} S_{l'+1,l'}^1(W', z_s')\right]_{(0,0)} + 8m^2 h_3^0(s')\left[S_{l'+1,l'}^1(W', z_s')\right]_{(0,0)}\right\} \ ,$$
$$\widehat{\Delta K}_{ll'}^-\big|^{1\text{-sub}}(W, W') = -\frac{W'}{4\pi W}(E + m)(W - m)h_0(s')\left[S_{l'+1,l'}^2(W', z_s')\right]_{(0,0)}\delta_{l0} \ ,$$
$$\widehat{\Delta K}_{ll'}^-\big|^{2\text{-sub}}(W, W') = \widehat{\Delta K}_{ll'}^-\big|^{1\text{-sub}} + \frac{\mathbf{q}^2 W'}{2\pi W}\chi_l^t(E + m)(W - m)$$
$$\times\left\{h_0(s')\left[\partial_t S_{l'+1,l'}^2(W', z_s')\right]_{(0,0)} - h_2^0(s')\left[S_{l'+1,l'}^2(W', z_s')\right]_{(0,0)}\right\}$$
$$- \frac{W'}{2\pi W}\chi_l^{\nu}(E + m)h_2^0(s')\left[S_{l'+1,l'}^1(W', z_s')\right]_{(0,0)} \ ,$$
$$\widehat{\Delta K}_{ll'}^-\big|^{3\text{-sub}}(W, W') = \widehat{\Delta K}_{ll'}^-\big|^{2\text{-sub}} - \frac{\mathbf{q}^2 W'}{\pi W}\chi_l^{\nu t}(E + m)$$
$$\times\left\{h_3^0(s')\left[S_{l'+1,l'}^1(W', z_s')\right]_{(0,0)} - h_2^0(s')\left[\partial_t S_{l'+1,l'}^1(W', z_s')\right]_{(0,0)}\right\} \ ,$$
$$\widehat{\Delta K}_{ll'}^-\big|^{\text{ex }3\text{-sub}}(W, W') = \widehat{\Delta K}_{ll'}^-\big|^{3\text{-sub}} - \frac{W'}{8\pi W m^2}\chi_l^{\nu^3}(E + m)$$
$$\times\left\{h_2^0(s')\left[\partial_{\nu^2} S_{l'+1,l'}^1(W', z_s')\right]_{(0,0)} + 4m^2 h_4^0(s')\left[S_{l'+1,l'}^1(W', z_s')\right]_{(0,0)}\right\}$$

$$- \frac{W'}{16\pi W m^2}\chi_l^{\nu^2}(E+m)(W-m) \tag{C.51}$$
$$\times \left\{ h_0(s') \left[\partial_{\nu^2} S^2_{l'+1,l'}(W',z'_s)\right]_{(0,0)} + 8m^2 h_3^0(s') \left[S^2_{l'+1,l'}(W',z'_s)\right]_{(0,0)} \right\} .$$

Similarly, we define

$$\begin{aligned} G_{lJ}\big|^{n\text{-sub}}(W,t') &= G_{lJ}(W,t') + \Delta G_{lJ}\big|^{n\text{-sub}}(W,t') \,, \\ \Delta G_{lJ}(W,t') &= \widehat{\Delta G}_{lJ}(W,t') - \widehat{\Delta G}_{l+1,J}(-W,t') \,, \end{aligned} \tag{C.52}$$

and accordingly for $H_{lJ}(W,t')$, which yields for even J

$$\widehat{\Delta G}_{lJ}\big|^{1\text{-sub}}(W,t') = \frac{E+m}{2W}(2J+1)\frac{(p'_t q'_t)^J}{t' p'^2_t}\left[P_J(z'_t)\right]_{(0,0)}\delta_{l0} \,,$$

$$\widehat{\Delta H}_{lJ}\big|^{1\text{-sub}}(W,t') = -\frac{E+m}{2W}\frac{2J+1}{\sqrt{J(J+1)}}\frac{(p'_t q'_t)^J}{t' p'^2_t} m\left[z'_t P'_J(z'_t)\right]_{(0,0)}\delta_{l0} \,,$$

$$\widehat{\Delta G}_{lJ}\big|^{2\text{-sub}}(W,t') = \widehat{\Delta G}_{lJ}\big|^{1\text{-sub}} - \frac{E+m}{W}\mathbf{q}^2(2J+1)\frac{(p'_t q'_t)^J}{t' p'^2_t}$$
$$\times \chi_l^t \left\{ \frac{1}{t'}\left[P_J(z'_t)\right]_{(0,0)} + \left[\partial_t P_J(z'_t)\right]_{(0,0)} \right\} ,$$

$$\widehat{\Delta H}_{lJ}\big|^{2\text{-sub}}(W,t') = \widehat{\Delta H}_{lJ}\big|^{1\text{-sub}} - \frac{E+m}{2W}\frac{2J+1}{\sqrt{J(J+1)}}\frac{(p'_t q'_t)^J}{t' p'^2_t}$$
$$\times \left\{ \frac{W-m}{2q'^2_t}\chi_l^\nu \left[\frac{P'_J(z'_t)}{z'_t}\right]_{(0,0)} - 2m\mathbf{q}^2\chi_l^t\left(\frac{1}{t'}\left[z'_t P'_J(z'_t)\right]_{(0,0)} + \left[\partial_t(z'_t P'_J(z'_t))\right]_{(0,0)} \right) \right\} ,$$

$$\widehat{\Delta G}_{lJ}\big|^{3\text{-sub}}(W,t') = \widehat{\Delta G}_{lJ}\big|^{2\text{-sub}} + \frac{E+m}{8Wm^2}(2J+1)\frac{(p'_t q'_t)^J}{t' p'^2_t}\chi_l^{\nu^2}\left[\partial_{\nu^2} P_J(z'_t)\right]_{(0,0)} \,,$$

$$\widehat{\Delta H}_{lJ}\big|^{3\text{-sub}}(W,t') = \widehat{\Delta H}_{lJ}\big|^{2\text{-sub}} - \frac{E+m}{8Wm}\frac{2J+1}{\sqrt{J(J+1)}}\frac{(p'_t q'_t)^J}{t' p'^2_t}\chi_l^{\nu^2}\left[\partial_{\nu^2} z'_t P'_J(z'_t)\right]_{(0,0)} \,, \tag{C.53}$$

and for odd J

$$\widehat{\Delta H}_{lJ}\big|^{1\text{-sub}}(W,t') = -\frac{E+m}{2W}\frac{2J+1}{\sqrt{J(J+1)}}\frac{(p'_t q'_t)^{J-1}}{t'}(W-m)\left[P'_J(z'_t)\right]_{(0,0)}\delta_{l0} \,,$$

$$\widehat{\Delta G}_{lJ}\big|^{2\text{-sub}}(W,t') = \frac{E+m}{4W}(2J+1)\frac{(p'_t q'_t)^{J-1}}{t' p'^2_t}\chi_l^\nu\left[\frac{P_J(z'_t)}{z'_t}\right]_{(0,0)} \,,$$

$$\widehat{\Delta H}_{lJ}\big|^{2\text{-sub}}(W,t') = \widehat{\Delta H}_{lJ}\big|^{1\text{-sub}} - \frac{E+m}{2W}\frac{2J+1}{\sqrt{J(J+1)}}\frac{(p'_t q'_t)^{J-1}}{t' p'^2_t}$$
$$\times \left\{ \frac{m}{2}\chi_l^\nu\left[P'_J(z'_t)\right]_{(0,0)} - 2\mathbf{q}^2 p'^2_t(W-m)\chi_l^t\left(\frac{1}{t'}\left[P'_J(z'_t)\right]_{(0,0)} + \left[\partial_t P'_J(z'_t)\right]_{(0,0)} \right) \right\} ,$$

$$\widehat{\Delta G}_{lJ}\big|^{3\text{-sub}}(W,t') = \widehat{\Delta G}_{lJ}\big|^{2\text{-sub}} - \frac{E+m}{2W}(2J+1)\frac{(p'_t q'_t)^{J-1}}{t' p'^2_t}\mathbf{q}^2\chi_l^{\nu t}$$
$$\times \left\{ \frac{1}{t'}\left[\frac{P_J(z'_t)}{z'_t}\right]_{(0,0)} + \left[\partial_t \frac{P_J(z'_t)}{z'_t}\right]_{(0,0)} \right\} ,$$

$$\widehat{\Delta H}_{lJ}\big|^{\text{3-sub}}(W,t') = \widehat{\Delta H}_{lJ}\big|^{\text{2-sub}} + \frac{E+m}{2W}\frac{2J+1}{\sqrt{J(J+1)}}\frac{(p_t'q_t')^{J-1}}{t'p_t'^2}m\mathbf{q}^2\chi_l^{\nu t} \times\left\{\frac{1}{t'}\left[P_J'(z_t')\right]_{(0,0)} + \left[\partial_t P_J'(z_t')\right]_{(0,0)}\right\},$$

$$\widehat{\Delta G}_{lJ}\big|^{\text{ex 3-sub}}(W,t') = \widehat{\Delta G}_{lJ}\big|^{\text{3-sub}} + \frac{E+m}{16Wm^2}(2J+1)\frac{(p_t'q_t')^{J-1}}{t'p_t'^2}\chi_l^{\nu^3}\left[\partial_{\nu^2}\frac{P_J(z_t')}{z_t'}\right]_{(0,0)},$$

$$\widehat{\Delta H}_{lJ}\big|^{\text{ex 3-sub}}(W,t') = \widehat{\Delta H}_{lJ}\big|^{\text{3-sub}} - \frac{E+m}{16Wm}\frac{2J+1}{\sqrt{J(J+1)}}\frac{(p_t'q_t')^{J-1}}{t'p_t'^2}\left[\partial_{\nu^2}P_J'(z_t')\right]_{(0,0)} \times\left\{\chi_l^{\nu^3} + \frac{W-m}{m}2p_t'^2\chi_l^{\nu^2}\right\}. \tag{C.54}$$

C.3.3 *t*-channel projection

For the t-channel projection we consider only the once- and twice-subtracted versions as well as the partial third subtraction. Since the latter affects solely $A^{\pm}$, many kernel functions remain unaltered compared to the twice-subtracted version. We only list those kernels that actually receive further corrections.

The subthreshold-parameter contributions to the t-channel amplitudes are included by modifying the nucleon pole terms according to

$$\tilde{N}_{\pm}^J\big|^{n\text{-sub}}(t) = \hat{N}_{\pm}^J(t) + \Delta\tilde{N}_{\pm}^J\big|^{n\text{-sub}}(t), \tag{C.55}$$

and

$$\begin{aligned}
\Delta\tilde{N}_{+}^J\big|^{\text{1-sub}}(t) &= -\frac{p_t^2}{4\pi}\left(d_{00}^{+} + \frac{g^2}{m}\right)\delta_{J0} + \frac{m}{12\pi}\left(b_{00}^{-} - \frac{g^2}{2m^2}\right)\delta_{J1},\\
\Delta\tilde{N}_{+}^J\big|^{\text{2-sub}}(t) &= \Delta\tilde{N}_{+}^J\big|^{\text{1-sub}} - \frac{p_t^2}{4\pi}\left(d_{01}^{+}t - b_{00}^{+}\frac{q_t^2}{3}\right)\delta_{J0} + \frac{m}{12\pi}\left(b_{01}^{-}t - a_{00}^{-}\frac{p_t^2}{m^2}\right)\delta_{J1} + \frac{b_{00}^{+}}{30\pi}\delta_{J2},\\
\Delta\tilde{N}_{+}^J\big|^{\text{3-sub}}(t) &= \Delta\tilde{N}_{+}^J\big|^{\text{2-sub}} - \frac{p_t^2}{12\pi m}\left\{a_{01}^{-}t\,\delta_{J1} + \frac{a_{10}^{+}}{m}\left(p_t^2q_t^2\delta_{J0} + \frac{2}{5}\delta_{J2}\right)\right\},\\
\Delta\tilde{N}_{-}^J\big|^{\text{1-sub}}(t) &= \frac{\sqrt{2}}{12\pi}\left(b_{00}^{-} - \frac{g^2}{2m^2}\right)\delta_{J1},\\
\Delta\tilde{N}_{-}^J\big|^{\text{2-sub}}(t) &= \Delta\tilde{N}_{-}^J\big|^{\text{1-sub}} + \frac{\sqrt{2}}{12\pi}b_{01}^{-}t\,\delta_{J1} + \frac{b_{00}^{+}}{30\pi}\frac{\sqrt{6}}{2m}\delta_{J2}.
\end{aligned} \tag{C.56}$$

The subtracted versions of $\tilde{G}_{Jl}(t,W')$ and $\tilde{H}_{Jl}(t,W')$ can be expressed by redefining the polynomial parts of the pertinent angular kernels according to

$$\bar{A}_{Jl}\big|^{n\text{-sub}} = \bar{A}_{Jl} + \Delta\bar{A}\big|_{Jl}^{n\text{-sub}}, \tag{C.57}$$

and analogously for $\bar{B}_{Jl}$, $\bar{C}_{Jl}$. We find

$$\begin{aligned}
\Delta\bar{A}_{Jl}\big|^{\text{1-sub}} &= h_0(s')\left[P_l'(z_s')\right]_{(0,0)}\delta_{J0},\\
\Delta\bar{A}_{Jl}\big|^{\text{2-sub}} &= \Delta\bar{A}_{Jl}\big|^{\text{1-sub}} + t\Big\{h_0(s')\left[\partial_t P_l'(z_s')\right]_{(0,0)} - h_2^0(s')\left[P_l'(z_s')\right]_{(0,0)}\Big\}\delta_{J0}\\
&\quad + \frac{4}{3}p_tq_th_2^0(s')\left[P_l'(z_s')\right]_{(0,0)}\delta_{J1},
\end{aligned}$$

$$
\begin{aligned}
\Delta\bar{A}_{Jl}\big|^{\text{3-sub}} &= \Delta\bar{A}_{Jl}\big|^{\text{2-sub}} + \frac{4}{3}p_t q_t\, t\Big\{h_2^0(s')\left[\partial_t P_l'(z_s')\right]_{(0,0)} - h_3^0(s')\left[P_l'(z_s')\right]_{(0,0)}\Big\}\delta_{J1} \\
&\quad + \frac{p_t^2 q_t^2}{3m^2}\Big\{h_0(s')\left[\partial_{\nu^2} P_l'(z_s')\right]_{(0,0)} + 8m^2 h_3^0(s')\left[P_l'(z_s')\right]_{(0,0)}\Big\}\Big(\delta_{J0} + \frac{2}{5}\delta_{J2}\Big)\,, \\
\Delta\bar{B}_{Jl}\big|^{\text{1-sub}} &= \frac{1}{3}h_0(s')\left[P_l'(z_s')\right]_{(0,0)}\delta_{J1}\,, \\
\Delta\bar{B}_{Jl}\big|^{\text{2-sub}} &= \Delta\bar{B}_{Jl}\big|^{\text{1-sub}} + \frac{t}{3}\Big\{h_0(s')\left[\partial_t P_l'(z_s')\right]_{(0,0)} - h_2^0(s')\left[P_l'(z_s')\right]_{(0,0)}\Big\}\delta_{J1} \\
&\quad + \frac{4}{3}p_t q_t h_2^0(s')\left[P_l'(z_s')\right]_{(0,0)}\Big(\delta_{J0} + \frac{2}{5}\delta_{J2}\Big)\,, \\
\Delta\bar{C}_{Jl}\big|^{\text{1-sub}} &= h_0(s')\left[P_l'(z_s')\right]_{(0,0)}\delta_{J1}\,, \\
\Delta\bar{C}_{Jl}\big|^{\text{2-sub}} &= \Delta\bar{C}_{Jl}\big|^{\text{1-sub}} + t\Big\{h_0(s')\left[\partial_t P_l'(z_s')\right]_{(0,0)} - h_2^0(s')\left[P_l'(z_s')\right]_{(0,0)}\Big\}\delta_{J1} \\
&\quad + \frac{4}{3}p_t q_t h_2^0(s')\left[P_l'(z_s')\right]_{(0,0)}\delta_{J2}\,.
\end{aligned}
\tag{C.58}
$$

Finally, the modified t-channel kernels are

$$
\tilde{K}^i_{JJ'}\big|^{n\text{-sub}}(t,t') = \tilde{K}^i_{JJ'}(t,t') + \Delta\tilde{K}^i_{JJ'}\big|^{n\text{-sub}}(t,t')\,, \qquad i\in\{1,2,3\}\,, \tag{C.59}
$$

with the following corrections for even J and J'

$$
\begin{aligned}
\Delta\tilde{K}^1_{JJ'}\big|^{\text{1-sub}}(t,t') &= -(2J'+1)(p_t'q_t')^{J'}\frac{p_t^2}{p_t'^2}\frac{1}{t'}\left[P_{J'}(z_t')\right]_{(0,0)}\delta_{J0}\,, \\
\Delta\tilde{K}^1_{JJ'}\big|^{\text{2-sub}}(t,t') &= \Delta\tilde{K}^1_{JJ'}\big|^{\text{1-sub}} - (2J'+1)(p_t'q_t')^{J'}\frac{p_t^2}{p_t'^2}\frac{t}{t'} \\
&\qquad\times\Big\{\frac{1}{t'}\left[P_{J'}(z_t')\right]_{(0,0)} + \left[\partial_t P_{J'}(z_t')\right]_{(0,0)}\Big\}\delta_{J0}\,, \\
\Delta\tilde{K}^1_{JJ'}\big|^{\text{3-sub}}(t,t') &= \Delta\tilde{K}^1_{JJ'}\big|^{\text{2-sub}} - \frac{2J'+1}{3}\frac{(p_t'q_t')^{J'}p_t^2}{m^2 t' p_t'^2}\left[\partial_{\nu^2}P_{J'}(z_t')\right]_{(0,0)}\Big(p_t^2q_t^2\delta_{J0} + \frac{2}{5}\delta_{J2}\Big)\,, \\
\Delta\tilde{K}^2_{JJ'}\big|^{\text{1-sub}}(t,t') &= \frac{2J'+1}{\sqrt{J'(J'+1)}}(p_t'q_t')^{J'}\frac{p_t^2}{p_t'^2}\frac{m}{t'}\left[z_t'P_{J'}'(z_t')\right]_{(0,0)}\delta_{J0}\,, \\
\Delta\tilde{K}^2_{JJ'}\big|^{\text{2-sub}}(t,t') &= \Delta\tilde{K}^2_{JJ'}\big|^{\text{1-sub}} + \frac{2J'+1}{\sqrt{J'(J'+1)}}(p_t'q_t')^{J'}\frac{p_t^2}{p_t'^2}\frac{m}{t'} \\
&\qquad\times\Big\{t\Big[\frac{1}{t'}\left[z_t'P_{J'}'(z_t')\right]_{(0,0)} + \left[\partial_t(z_t'P_{J'}'(z_t'))\right]_{(0,0)}\Big]\delta_{J0} \\
&\qquad\qquad - \frac{1}{3}\frac{q_t^2}{q_t'^2}\left[\frac{P_{J'}'(z_t')}{z_t'}\right]_{(0,0)}\Big(\delta_{J0} + \frac{2}{5}\frac{\delta_{J2}}{p_t^2q_t^2}\Big)\Big\}\,, \\
\Delta\tilde{K}^2_{JJ'}\big|^{\text{3-sub}}(t,t') &= \Delta\tilde{K}^2_{JJ'}\big|^{\text{2-sub}} \\
&\qquad + \frac{2J'+1}{\sqrt{J'(J'+1)}}\frac{(p_t'q_t')^{J'}p_t^2}{3mt'p_t'^2}\left[\partial_{\nu^2}z_t'P_{J'}'(z_t')\right]_{(0,0)}\Big(p_t^2q_t^2\delta_{J0} + \frac{2}{5}\delta_{J2}\Big)\,, \\
\Delta\tilde{K}^3_{JJ'}\big|^{\text{2-sub}}(t,t') &= -\frac{2J'+1}{\sqrt{J'(J'+1)}}(p_t'q_t')^{J'-2}\frac{\sqrt{6}}{15}\frac{1}{t'}\left[\frac{P_{J'}'(z_t')}{z_t'}\right]_{(0,0)}\delta_{J2}\,,
\end{aligned}
\tag{C.60}
$$

and for odd J and J'

$$
\begin{aligned}
\Delta\tilde{K}^1_{JJ'}\big|^{\text{2-sub}}(t,t') &= -\frac{2J'+1}{3}(p'_tq'_t)^{J'-1}\frac{p_t^2}{p_t'^2}\frac{1}{t'}\left[\frac{P_{J'}(z'_t)}{z'_t}\right]_{(0,0)}\delta_{J1}\ ,\\
\Delta\tilde{K}^1_{JJ'}\big|^{\text{3-sub}}(t,t') &= \Delta\tilde{K}^1_{JJ'}\big|^{\text{2-sub}}\\
&\quad -\frac{2J'+1}{3}(p'_tq'_t)^{J'-1}\frac{p_t^2}{p_t'^2}\frac{t}{t'}\left\{\frac{1}{t'}\left[\frac{P_{J'}(z'_t)}{z'_t}\right]_{(0,0)}+\left[\partial_t\frac{P_{J'}(z'_t)}{z'_t}\right]_{(0,0)}\right\}\delta_{J1}\ ,\\
\Delta\tilde{K}^2_{JJ'}\big|^{\text{1-sub}}(t,t') &= -\frac{2J'+1}{\sqrt{J'(J'+1)}}(p'_tq'_t)^{J'-1}\frac{m}{t'}\left[P'_{J'}(z'_t)\right]_{(0,0)}\frac{\delta_{J1}}{3}\ ,\\
\Delta\tilde{K}^2_{JJ'}\big|^{\text{2-sub}}(t,t') &= \Delta\tilde{K}^2_{JJ'}\big|^{\text{1-sub}}-\frac{2J'+1}{\sqrt{J'(J'+1)}}(p'_tq'_t)^{J'-1}\frac{m}{t'}\\
&\quad\times\left\{\left(\frac{t}{t'}-\frac{p_t^2}{p_t'^2}\right)\left[P'_{J'}(z'_t)\right]_{(0,0)}+t\left[\partial_tP'_{J'}(z'_t)\right]_{(0,0)}\right\}\frac{\delta_{J1}}{3}\ ,\\
\Delta\tilde{K}^2_{JJ'}\big|^{\text{3-sub}}(t,t') &= \Delta\tilde{K}^2_{JJ'}\big|^{\text{2-sub}}\\
&\quad+\frac{2J'+1}{\sqrt{J'(J'+1)}}\frac{m}{3}(p'_tq'_t)^{J'-1}\frac{p_t^2}{p_t'^2}\frac{t}{t'}\left\{\frac{1}{t'}\left[P'_{J'}(z'_t)\right]_{(0,0)}+\left[\partial_tP'_{J'}(z_t)\right]_{(0,0)}\right\}\delta_{J1}\ ,\\
\Delta\tilde{K}^3_{JJ'}\big|^{\text{1-sub}}(t,t') &= -\frac{2J'+1}{\sqrt{J'(J'+1)}}(p'_tq'_t)^{J'-1}\frac{\sqrt{2}}{3}\frac{1}{t'}\left[P'_{J'}(z'_t)\right]_{(0,0)}\delta_{J1}\ ,\\
\Delta\tilde{K}^3_{JJ'}\big|^{\text{2-sub}}(t,t') &= \Delta\tilde{K}^3_{JJ'}\big|^{\text{1-sub}}\\
&\quad-\frac{2J'+1}{\sqrt{J'(J'+1)}}(p'_tq'_t)^{J'-1}\frac{\sqrt{2}}{3}\frac{t}{t'}\left\{\frac{1}{t'}\left[P'_{J'}(z'_t)\right]_{(0,0)}+\left[\partial_tP'_{J'}(z'_t)\right]_{(0,0)}\right\}\delta_{J1}\ .
\end{aligned}
\tag{C.61}
$$

Explicitly, the lowest kernel functions become

$$
\begin{aligned}
&\tilde{K}^1_{00}\big|^{\text{2-sub}}(t,t') = \frac{t}{t'}\tilde{K}^1_{00}\big|^{\text{1-sub}}(t,t') = \frac{t^2}{t'^2}\tilde{K}^1_{00}(t,t')\ ,\\
&\tilde{K}^1_{11}\big|^{\text{3-sub}}(t,t') = \frac{t}{t'}\tilde{K}^1_{11}\big|^{\text{2-sub}}(t,t') = \frac{t^2}{t'^2}\tilde{K}^1_{11}(t,t')\ ,\qquad \tilde{K}^1_{22}\big|^{\text{3-sub}}(t,t') = \frac{t}{t'}\tilde{K}^1_{22}(t,t')\ ,\\
&\tilde{K}^1_{02}\big|^{\text{1-sub}}(t,t') = \frac{5}{16}\frac{p_t^2}{p_t'^2}\left\{t+\frac{t_Nt_\pi}{2t'}\right\}\ ,\qquad \tilde{K}^1_{02}\big|^{\text{2-sub}}(t,t') = \frac{5}{8}\frac{p_t^2}{p_t'^2}\left\{\left(1+\frac{t}{t'}\right)\frac{t_Nt_\pi}{4t'}-\frac{t}{t'}s_0\right\}\ ,\\
&\tilde{K}^1_{02}\big|^{\text{3-sub}}(t,t') = \frac{5}{32}\frac{p_t^2}{p_t'^2}\frac{t(t_Nt_\pi-tt')}{t'^2}\ ,\qquad \tilde{K}^1_{13}\big|^{\text{2-sub}}(t,t') = \frac{7}{48}\frac{p_t^2}{p_t'^2}\left\{t+\frac{3t_Nt_\pi}{2t'}\right\}\ ,\\
&\tilde{K}^1_{13}\big|^{\text{3-sub}}(t,t') = \frac{7}{32}\frac{p_t^2}{p_t'^2}\frac{1}{t'^2}\left\{t_\pi t_N(t+t')-tt'(t_\pi+t_N)\right\}\ ,\\
&\tilde{K}^2_{11}\big|^{\text{3-sub}}(t,t') = \frac{t}{t_N}\tilde{K}^2_{11}\big|^{\text{2-sub}}(t,t') = \frac{t^2}{t_Nt'}\tilde{K}^2_{11}\big|^{\text{1-sub}}(t,t') = \frac{t^2}{t'^2}\tilde{K}^2_{11}(t,t')\ ,\\
&\tilde{K}^2_{22}\big|^{\text{3-sub}}(t,t') = \frac{t}{t_N}\tilde{K}^2_{22}\big|^{\text{2-sub}}(t,t') = \frac{t}{t'}\tilde{K}^2_{22}(t,t')\ ,\\
&\tilde{K}^2_{02}\big|^{\text{3-sub}}(t,t') = \frac{t}{t_N}\tilde{K}^2_{02}\big|^{\text{2-sub}}(t,t') = \frac{5m}{4\sqrt{6}}\frac{p_t^2q_t^2}{p_t'^2}\frac{t}{t'}\ ,\qquad \tilde{K}^2_{02}\big|^{\text{1-sub}}(t,t') = -\frac{5m}{8\sqrt{6}}\frac{p_t^2}{p_t'^2}\left\{t+\frac{t_\pi}{2}\right\}\ ,\\
&\tilde{K}^2_{13}\big|^{\text{1-sub}}(t,t') = \frac{7m}{16\sqrt{3}}\left\{\frac{p_t^2}{p_t'^2}\left[2q_t^2-\Big(t+t'-4s_0+5a\Big)\right]+\left[t+\frac{t_Nt_\pi}{4t'}\right]\right\}\ ,
\end{aligned}
$$

$$\tilde{K}^2_{13}\big|^{\text{2-sub}}(t,t') = \frac{7m}{16\sqrt{3}}\left\{\frac{p_t^2}{p_t'^2}\left[2q_t^2 - t - \frac{t_N t_\pi}{4t'}\right] + \left[\left(1+\frac{t}{t'}\right)\frac{t_N t_\pi}{4t'} - \frac{t}{t'}s_0\right]\right\},$$
$$\tilde{K}^2_{13}\big|^{\text{3-sub}}(t,t') = \frac{7m}{16\sqrt{3}}\left\{3\frac{p_t^2 q_t^2}{p_t'^2} - \frac{t^2}{t'^2}q_t'^2\right\}, \tag{C.62}$$
$$\tilde{K}^3_{11}\big|^{\text{2-sub}}(t,t') = \frac{t}{t'}\tilde{K}^3_{11}\big|^{\text{1-sub}}(t,t') = \frac{t^2}{t'^2}\tilde{K}^3_{11}(t,t')\,, \qquad \tilde{K}^3_{22}\big|^{\text{2-sub}}(t,t') = \frac{t}{t'}\tilde{K}^3_{22}(t,t')\,,$$
$$\tilde{K}^3_{13}\big|^{\text{1-sub}}(t,t') = \frac{7}{8\sqrt{6}}\left\{t + \frac{t_N t_\pi}{4t'}\right\}, \qquad \tilde{K}^3_{13}\big|^{\text{2-sub}}(t,t') = \frac{7}{8\sqrt{6}}\left\{\left(1+\frac{t}{t'}\right)\frac{t_N t_\pi}{4t'} - \frac{t}{t'}s_0\right\}.$$

C.4 Conventions for kaon–nucleon scattering

We define the kaon states

$$|K^+\rangle = \left|\frac{1}{2},\frac{1}{2}\right\rangle\,, \qquad |K^0\rangle = \left|\frac{1}{2},-\frac{1}{2}\right\rangle\,, \qquad |\bar{K}^0\rangle = \left|\frac{1}{2},\frac{1}{2}\right\rangle\,, \qquad |K^-\rangle = \left|\frac{1}{2},-\frac{1}{2}\right\rangle\,, \tag{C.63}$$

with crossing properties

$$C|K^+\rangle = -|K^-\rangle\,, \qquad C|K^0\rangle = |\bar{K}^0\rangle\,, \tag{C.64}$$

and choose the isospin decomposition of the amplitude as

$$T = T^+ - \boldsymbol{\tau}_N\cdot\boldsymbol{\tau}_K T^- = T^+ - 2\Big(I_s(I_s+1) - \frac{3}{2}\Big)T^-\,, \tag{C.65}$$

where $\boldsymbol{\tau}_N$ and $\boldsymbol{\tau}_K$ are the Pauli matrices associated with the nucleon and kaon isospin operators. This leads to

$$\begin{aligned} T^{I_s=0} &= T^+ + 3T^-\,, & T^{I_s=1} &= T^+ - T^-\,,\\ T^{I_u=0} &= T^+ - 3T^-\,, & T^{I_u=1} &= T^+ + T^-\,,\\ T^{I_t=0} &= 2T^+\,, & T^{I_t=1} &= 2T^-\,, \end{aligned} \tag{C.66}$$

and

$$T^{K^\pm p} = T^{K^\pm p\to K^\pm p} = T^+ \mp T^-\,. \tag{C.67}$$

In particular, (C.66) shows that the conversion factor $c_J^{KN} = 1/2$ between t-channel isospin and $I = \pm$ bases is independent of angular momentum. In complete analogy to πN scattering, the amplitude for the process $K(q) + N(p) \to K(q') + N(p')$ can be decomposed as

$$T^I(s,t) = \bar{u}(p')\left\{A^I(s,t) + \frac{\not{q}' + \not{q}}{2}B^I(s,t)\right\}u(p)\,, \qquad I = \pm\,. \tag{C.68}$$

The Born-term contributions due to hyperon pole diagrams are[1]

$$A^{K^+p}(s,t) = \sum_{Y=\Lambda,\Sigma} g^2_{KNY}\frac{m_Y - m}{u - m_Y^2}\,, \qquad B^{K^+p}(s,t) = \sum_{Y=\Lambda,\Sigma}\frac{g^2_{KNY}}{u - m_Y^2}\,,$$
$$A^{K^-p}(s,t) = \sum_{Y=\Lambda,\Sigma} g^2_{KNY}\frac{m_Y - m}{s - m_Y^2}\,, \qquad B^{K^-p}(s,t) = \sum_{Y=\Lambda,\Sigma}\frac{g^2_{KNY}}{s - m_Y^2}\,, \tag{C.69}$$

[1] We use $m_\Lambda = 1.116\,\text{GeV}$, $m_\Sigma = 1.193\,\text{GeV}$ [3], and $g^2_{KN\Lambda}/4\pi = 15.55$, $g^2_{KN\Sigma}/4\pi = 0.576$ [255] for the masses and couplings of the hyperons, respectively.

and hence

$$A^{\pm}(s,t) = \sum_{Y=\Lambda,\Sigma} g_{KNY}^2 \frac{m_Y - m}{2}\left(\frac{1}{s-m_Y^2} \pm \frac{1}{u-m_Y^2}\right),$$
$$B^{\pm}(s,t) = -\sum_{Y=\Lambda,\Sigma} \frac{g_{KNY}^2}{2}\left(\frac{1}{s-m_Y^2} \mp \frac{1}{u-m_Y^2}\right). \tag{C.70}$$

The $\bar{K}K \to \bar{N}N$ partial waves can be obtained from the invariant amplitudes by means of the projection formula (with the t-channel scattering angle $z_t = \cos\theta_t^{KN}$)

$$h_+^{J,I_t=0,1}(t) = -\frac{1}{8\pi}\int_{-1}^{1} \mathrm{d}z_t P_J(z_t)\left\{\frac{p_t^2}{(p_t k_t)^J} A^{\pm}(s,t)\Big|_{s=s(t,z_t)} - \frac{m}{(p_t k_t)^{J-1}} z_t B^{\pm}(s,t)\Big|_{s=s(t,z_t)}\right\},$$
$$h_-^{J,I_t=0,1}(t) = \frac{1}{8\pi}\frac{\sqrt{J(J+1)}}{2J+1}\frac{1}{(p_t k_t)^{J-1}}\int_{-1}^{1} \mathrm{d}z_t \big(P_{J-1}(z_t) - P_{J+1}(z_t)\big) B^{\pm}(s,t)\Big|_{s=s(t,z_t)}. \tag{C.71}$$

The main difference to the πN t-channel partial-wave projection [220] originates from the fact that due to the lack of Bose symmetry in the $\bar{K}K$ system a partial wave with given angular momentum J couples to both $I_t = 0$ and $I_t = 1$ (corresponding to $+$ and $-$ on the right-hand side of (C.71)). In the following, we are only interested in the combination where even/odd J corresponds to $I_t = 0, 1$, respectively, since only these partial waves can occur as intermediate states in $\pi\pi \to \bar{N}N$, and will therefore suppress the isospin index.[2] In these conventions, the Born terms are given by

$$h_+^J(t) = \sum_{Y=\Lambda,\Sigma} \frac{g_{KNY}^2}{8\pi}\frac{1}{(p_t k_t)^J}\left\{\Big(\frac{p_t}{k_t}(m_Y - m) + m\tilde{y}\Big) Q_J(\tilde{y}) - m\delta_{J0}\right\},$$
$$h_-^J(t) = \sum_{Y=\Lambda,\Sigma} \frac{g_{KNY}^2}{8\pi}\frac{\sqrt{J(J+1)}}{2J+1}\frac{1}{(p_t k_t)^J}\big(Q_{J-1}(\tilde{y}) - Q_{J+1}(\tilde{y})\big), \tag{C.72}$$

with

$$\tilde{y} = \frac{t - 2M_K^2 + 2(m_Y^2 - m^2)}{4 p_t k_t}. \tag{C.73}$$

The helicity amplitudes

$$H_{++}(s,t) = H_{--}(s,t) = \frac{4\pi\sqrt{t}}{k_t}\sum_{J=0}^{\infty}(2J+1) H_+^J(t) P_J(\cos\theta_t^{KN}),$$
$$H_{+-}(s,t) = -H_{-+}(s,t) = \frac{4\pi\sqrt{t}}{k_t}\sum_{J=1}^{\infty}\frac{2J+1}{\sqrt{J(J+1)}} H_-^J(t)\sin\theta_t^{KN} P_J'(\cos\theta_t^{KN}),$$
$$H_+^J(t) = \frac{k_t}{p_t}(p_t k_t)^J \frac{2}{\sqrt{t}} h_+^J(t), \qquad H_-^J(t) = \frac{k_t}{p_t}(p_t k_t)^J h_-^J(t), \tag{C.74}$$

are defined in accordance with the normalization

$$\frac{\mathrm{d}\bar{\sigma}_{K\bar{K}\to\bar{N}N}}{\mathrm{d}\Omega} = \frac{p_t}{k_t}\sum_{\bar{\lambda},\lambda}\left|\frac{H_{\bar{\lambda}\lambda}(s,t)}{8\pi\sqrt{t}}\right|^2 = \frac{2p_t}{k_t}\left\{\left|\frac{H_{++}(s,t)}{8\pi\sqrt{t}}\right|^2 + \left|\frac{H_{+-}(s,t)}{8\pi\sqrt{t}}\right|^2\right\}. \tag{C.75}$$

[2] The opposite combination features prominently in a dispersive calculation of the strangeness form factors of the nucleon, cf. [256].

C.5 Subtracted Muskhelishvili–Omnès solution

The subtracted versions of the single-channel MO solution (7.11) involve the subthreshold parameters according to Table 6.1 and the inhomogeneities

$$\tilde{\Delta}^J_\pm\big|^{n\text{-sub}}(t) = \hat{N}^J_\pm(t) + \bar{\Delta}^J_\pm\big|^{n\text{-sub}}(t)\,, \qquad \tilde{\Delta}^J_\Gamma\big|^{n\text{-sub}}(t) = m\sqrt{\frac{J}{J+1}}\tilde{\Delta}^J_-\big|^{n\text{-sub}}(t) - \tilde{\Delta}^J_+\big|^{n\text{-sub}}(t)\,, \tag{C.76}$$

where $\bar{\Delta}^J_\pm\big|^{n\text{-sub}}(t)$ is defined in analogy to (7.7) with the kernel functions replaced by the respective subtracted versions. We obtain for $J \leq 2$

$$\begin{aligned}
f^0_+(t) &= \tilde{\Delta}^0_+\big|^{1\text{-sub}}(t) - \frac{p_t^2}{4\pi}\left(d^+_{00} + \frac{g^2}{m}\right)\Omega_0(t) \\
&\quad + \frac{t(t-t_N)\Omega_0(t)}{\pi}\left\{\int\limits_{t_\pi}^{t_\mathrm{m}} \mathrm{d}t' \frac{\tilde{\Delta}^0_+\big|^{1\text{-sub}}(t')\sin\delta_0(t')}{t'(t'-t_N)(t'-t)|\Omega_0(t')|} + \int\limits_{t_\mathrm{m}}^{\infty} \mathrm{d}t' \frac{\operatorname{Im} f^0_+(t')}{t'(t'-t_N)(t'-t)|\Omega_0(t')|}\right\}, \\
f^0_+(t) &= \tilde{\Delta}^0_+\big|^{2\text{-sub}}(t) - \frac{p_t^2}{4\pi}\left\{\left[d^+_{00} + \frac{g^2}{m} + b^+_{00}\frac{M_\pi^2}{3}\right]\big(1 - t\,\dot{\Omega}_0(0)\big) + \left[d^+_{01} - \frac{b^+_{00}}{12}\right]t\right\}\Omega_0(t) \\
&\quad + \frac{t^2(t-t_N)\Omega_0(t)}{\pi}\left\{\int\limits_{t_\pi}^{t_\mathrm{m}} \mathrm{d}t' \frac{\tilde{\Delta}^0_+\big|^{2\text{-sub}}(t')\sin\delta_0(t')}{t'^2(t'-t_N)(t'-t)|\Omega_0(t')|} + \int\limits_{t_\mathrm{m}}^{\infty} \mathrm{d}t' \frac{\operatorname{Im} f^0_+(t')}{t'^2(t'-t_N)(t'-t)|\Omega_0(t')|}\right\}, \\
f^0_+(t) &= \tilde{\Delta}^0_+\big|^{3\text{-sub}}(t) - \frac{p_t^2}{4\pi}\left\{\left[d^+_{00} + \frac{g^2}{m} + \big(b^+_{00} + a^+_{10}\big)\frac{M_\pi^2}{3}\right]\big(1 - t\,\dot{\Omega}_0(0)\big)\right. \\
&\qquad\qquad \left. + \left[d^+_{01} - \frac{b^+_{00}}{12} - \frac{a^+_{10}}{12}\left(1 + \frac{M_\pi^2}{m^2}\right)\right]t\right\}\Omega_0(t) \\
&\quad + \frac{t^2(t-t_N)\Omega_0(t)}{\pi}\left\{\int\limits_{t_\pi}^{t_\mathrm{m}} \mathrm{d}t' \frac{\tilde{\Delta}^0_+\big|^{3\text{-sub}}(t')\sin\delta_0(t')}{t'^2(t'-t_N)(t'-t)|\Omega_0(t')|} + \int\limits_{t_\mathrm{m}}^{\infty} \mathrm{d}t' \frac{\operatorname{Im} f^0_+(t')}{t'^2(t'-t_N)(t'-t)|\Omega_0(t')|}\right\}, \\
\Gamma^1(t) &= \tilde{\Delta}^1_\Gamma\big|^{2\text{-sub}}(t) + \frac{p_t^2}{12\pi m}a^-_{00}\Omega_1(t) \\
&\quad + \frac{t(t-t_N)\Omega_1(t)}{\pi}\left\{\int\limits_{t_\pi}^{t_\mathrm{m}} \mathrm{d}t' \frac{\tilde{\Delta}^1_\Gamma\big|^{2\text{-sub}}(t')\sin\delta_1(t')}{t'(t'-t_N)(t'-t)|\Omega_1(t')|} + \int\limits_{t_\mathrm{m}}^{\infty} \mathrm{d}t' \frac{\operatorname{Im}\Gamma^1(t')}{t'(t'-t_N)(t'-t)|\Omega_1(t')|}\right\}, \\
\Gamma^1(t) &= \tilde{\Delta}^1_\Gamma\big|^{3\text{-sub}}(t) + \frac{p_t^2}{12\pi m}\Big\{a^-_{00}\big(1 - t\,\dot{\Omega}_1(0)\big) + a^-_{01}t\Big\}\Omega_1(t) \\
&\quad + \frac{t^2(t-t_N)\Omega_1(t)}{\pi}\left\{\int\limits_{t_\pi}^{t_\mathrm{m}} \mathrm{d}t' \frac{\tilde{\Delta}^1_\Gamma\big|^{3\text{-sub}}(t')\sin\delta_1(t')}{t'^2(t'-t_N)(t'-t)|\Omega_1(t')|} + \int\limits_{t_\mathrm{m}}^{\infty} \mathrm{d}t' \frac{\operatorname{Im}\Gamma^1(t')}{t'^2(t'-t_N)(t'-t)|\Omega_1(t')|}\right\}, \\
f^1_-(t) &= \tilde{\Delta}^1_-\big|^{1\text{-sub}}(t) + \frac{\sqrt{2}}{12\pi}\left(b^-_{00} - \frac{g^2}{2m^2}\right)\Omega_1(t) \\
&\quad + \frac{t\,\Omega_1(t)}{\pi}\left\{\int\limits_{t_\pi}^{t_\mathrm{m}} \mathrm{d}t' \frac{\tilde{\Delta}^1_-\big|^{1\text{-sub}}(t')\sin\delta_1(t')}{t'(t'-t)|\Omega_1(t')|} + \int\limits_{t_\mathrm{m}}^{\infty} \mathrm{d}t' \frac{\operatorname{Im} f^1_-(t')}{t'(t'-t)|\Omega_1(t')|}\right\},
\end{aligned}$$

$$
\begin{aligned}
f_-^1(t) &= \tilde{\Delta}_-^1\big|^{\text{2-sub}}(t) + \frac{\sqrt{2}}{12\pi}\left\{\left(b_{00}^- - \frac{g^2}{2m^2}\right)\big(1 - t\,\dot{\Omega}_1(0)\big) + b_{01}^- t\right\}\Omega_1(t) \\
&\quad + \frac{t^2\Omega_1(t)}{\pi}\left\{\int_{t_\pi}^{t_\mathrm{m}} \mathrm{d}t' \frac{\tilde{\Delta}_-^1\big|^{\text{2-sub}}(t')\sin\delta_1(t')}{t'^2(t'-t)|\Omega_1(t')|} + \int_{t_\mathrm{m}}^{\infty} \mathrm{d}t' \frac{\mathrm{Im}\, f_-^1(t')}{t'^2(t'-t)|\Omega_1(t')|}\right\}, \\
\Gamma^2(t) &= \tilde{\Delta}_\Gamma^2\big|^{\text{3-sub}}(t) + \frac{p_t^2}{30\pi m^2} a_{10}^+ \Omega_2(t) \\
&\quad + \frac{t(t-t_N)\Omega_2(t)}{\pi}\left\{\int_{t_\pi}^{t_\mathrm{m}} \mathrm{d}t' \frac{\tilde{\Delta}_\Gamma^2\big|^{\text{3-sub}}(t')\sin\delta_2(t')}{t'(t'-t_N)(t'-t)|\Omega_2(t')|} + \int_{t_\mathrm{m}}^{\infty} \mathrm{d}t' \frac{\mathrm{Im}\,\Gamma^2(t')}{t'(t'-t_N)(t'-t)|\Omega_2(t')|}\right\}, \\
f_-^2(t) &= \tilde{\Delta}_-^2\big|^{\text{2-sub}}(t) + \frac{\sqrt{6}}{60\pi m} b_{00}^+ \Omega_2(t) \\
&\quad + \frac{t\,\Omega_2(t)}{\pi}\left\{\int_{t_\pi}^{t_\mathrm{m}} \mathrm{d}t' \frac{\tilde{\Delta}_-^2\big|^{\text{2-sub}}(t')\sin\delta_2(t')}{t'(t'-t)|\Omega_2(t')|} + \int_{t_\mathrm{m}}^{\infty} \mathrm{d}t' \frac{\mathrm{Im}\, f_-^2(t')}{t'(t'-t)|\Omega_2(t')|}\right\}.
\end{aligned}
\tag{C.77}
$$

C.6 Continuity at the matching point

To prove the continuity of $\mathbf{f}(t)$ at t_m, we rewrite (7.25) in terms of a principal-value integral as

$$
\mathbf{f}(t) = \big(\mathbb{1} + i\,T(t)\Sigma(t)\big)\mathbf{\Delta}(t) + \frac{\Omega(t)}{\pi}\fint_{t_\pi}^{t_\mathrm{m}} \mathrm{d}t' \frac{\Omega^{-1}(t')T(t')\Sigma(t')\mathbf{\Delta}(t')}{t'-t} + \frac{\Omega(t)}{\pi}\int_{t_\mathrm{m}}^{\infty} \mathrm{d}t' \frac{\Omega^{-1}(t')\mathrm{Im}\,\mathbf{f}(t')}{t'-t}\,.
\tag{C.78}
$$

We only consider the case $t \to t_\mathrm{m}$ from below (continuity from above can be proven in a similar way). In this limit, the whole mass of the integral is concentrated at t_m. Using (7.30), (7.31), (7.33), and (7.39), we find

$$
\begin{aligned}
\mathbf{f}(t_\mathrm{m}) = \big(\mathbb{1} + i\,T(t_\mathrm{m})\Sigma(t_\mathrm{m})\big)\mathbf{\Delta}(t_\mathrm{m}) &+ \frac{e^{-i\pi x}}{\det\bar{\Omega}(t_\mathrm{m})}\begin{pmatrix} I_\mathrm{I} & I_\mathrm{II} \\ I_\mathrm{III} & I_\mathrm{IV}\end{pmatrix} T(t_\mathrm{m})\Sigma(t_\mathrm{m})\mathbf{\Delta}(t_\mathrm{m}) \\
&- \frac{1}{\det\bar{\Omega}(t_\mathrm{m})}\begin{pmatrix} \tilde{I}_\mathrm{I} & \tilde{I}_\mathrm{II} \\ \tilde{I}_\mathrm{III} & \tilde{I}_\mathrm{IV}\end{pmatrix} \mathrm{Im}\,\mathbf{f}(t_\mathrm{m})\,,
\end{aligned}
\tag{C.79}
$$

with

$$
\begin{aligned}
I_\mathrm{I} &= -\Big(\bar{\Omega}_{11}\bar{\Omega}_{22}\cot\pi x_{11} - \bar{\Omega}_{12}\bar{\Omega}_{21}\cot\pi x_{12}\Big)e^{i\psi}\,, & \tilde{I}_\mathrm{I} &= -\bar{\Omega}_{11}\bar{\Omega}_{22}\frac{e^{i\delta_{11}}}{\sin\pi x_{11}} + \bar{\Omega}_{12}\bar{\Omega}_{21}\frac{e^{i\delta_{12}}}{\sin\pi x_{12}}\,, \\
I_\mathrm{II} &= \bar{\Omega}_{11}\bar{\Omega}_{12}\Big(\cot\pi x_{11} - \cot\pi x_{12}\Big)e^{i\psi}\,, & \tilde{I}_\mathrm{II} &= \bar{\Omega}_{11}\bar{\Omega}_{12}\left\{\frac{e^{i\delta_{11}}}{\sin\pi x_{11}} - \frac{e^{i\delta_{12}}}{\sin\pi x_{12}}\right\}, \\
I_\mathrm{III} &= -\bar{\Omega}_{21}\bar{\Omega}_{22}\Big(\cot\pi x_{11} - \cot\pi x_{12}\Big)e^{i\psi}\,, & \tilde{I}_\mathrm{III} &= -\bar{\Omega}_{21}\bar{\Omega}_{22}\left\{\frac{e^{i\delta_{11}}}{\sin\pi x_{11}} - \frac{e^{i\delta_{12}}}{\sin\pi x_{12}}\right\}, \\
I_\mathrm{IV} &= -\Big(\bar{\Omega}_{11}\bar{\Omega}_{22}\cot\pi x_{12} - \bar{\Omega}_{12}\bar{\Omega}_{21}\cot\pi x_{11}\Big)e^{i\psi}\,, & \tilde{I}_\mathrm{IV} &= -\bar{\Omega}_{11}\bar{\Omega}_{22}\frac{e^{i\delta_{12}}}{\sin\pi x_{12}} + \bar{\Omega}_{12}\bar{\Omega}_{21}\frac{e^{i\delta_{11}}}{\sin\pi x_{11}}\,.
\end{aligned}
\tag{C.80}
$$

For the continuity condition (C.79) to be fulfilled, in particular all terms depending on $\mathbf{\Delta}(t_\mathrm{m})$ must cancel amongst themselves. Putting the coefficients of $\Delta_i(t_\mathrm{m})$ in each component f_i to zero yields four constraints on I_I–I_IV, which can be inverted to obtain

$$\begin{aligned} I_\mathrm{I} &= i \det\bar{\Omega}\, e^{i\pi x} \frac{A - e^{2i\pi x} A^*}{A + e^{2i\pi x} A^*} \,, \qquad I_\mathrm{IV} = i \det\bar{\Omega}\, e^{i\pi x} \frac{B - e^{2i\pi x} B^*}{A + e^{2i\pi x} A^*} \,, \\ I_\mathrm{II} &= \frac{\sigma^K_{t_\mathrm{m}}}{\sigma^\pi_{t_\mathrm{m}}} I_\mathrm{III} = 4 \det\bar{\Omega}\, e^{2i\pi x} \frac{|g| \sigma^K_{t_\mathrm{m}}}{A + e^{2i\pi x} A^*} \,, \end{aligned} \tag{C.81}$$

where

$$A = \eta e^{2i\pi(x-y)} - 1 \,, \qquad B = \eta e^{2i\pi y} - 1 \,. \tag{C.82}$$

Similar considerations apply to $\tilde{I}_\mathrm{I}$–$\tilde{I}_\mathrm{IV}$. By means of $\operatorname{Im}\mathbf{f} = T^* \Sigma \mathbf{f}$, the remaining pieces of (C.79) can be expressed as linear combinations of f_1 and f_2, which altogether again amounts to four constraints. The solutions are

$$\begin{aligned} \tilde{I}_\mathrm{I} &= -2i\, \det\bar{\Omega}\, e^{2i\pi x} \frac{A^*}{A + e^{2i\pi x} A^*} \,, \qquad \tilde{I}_\mathrm{IV} = -2i\, \det\bar{\Omega}\, e^{2i\pi x} \frac{B^*}{A + e^{2i\pi x} A^*} \,, \\ \tilde{I}_\mathrm{II} &= \frac{\sigma^K_{t_\mathrm{m}}}{\sigma^\pi_{t_\mathrm{m}}} \tilde{I}_\mathrm{III} = I_\mathrm{II} e^{-i\pi x} \,. \end{aligned} \tag{C.83}$$

Based on (7.43) it is straightforward to show that (C.81) and (C.83) hold as long as the following relations are fulfilled

$$\begin{aligned} \sqrt{1-z^2}\big(\bar{\Omega}_{11}\bar{\Omega}_{22} + \bar{\Omega}_{12}\bar{\Omega}_{21}\big) &= \eta \sin\pi(2y-x) \det\bar{\Omega} \,, \\ \sqrt{1-z^2}\bar{\Omega}_{11}\bar{\Omega}_{12} = -|g|\sigma^K_{t_\mathrm{m}} \det\bar{\Omega} \,, &\qquad \sqrt{1-z^2}\bar{\Omega}_{21}\bar{\Omega}_{22} = |g|\sigma^\pi_{t_\mathrm{m}} \det\bar{\Omega} \,. \end{aligned} \tag{C.84}$$

In this way, the properties (7.44) of the Omnès matrix finally ensure continuity at the matching point.

C.7 Sum rules for the threshold parameters

We only give the expressions that follow from (C.46). Together with (C.44) and

$$\begin{aligned} h_+(s') &= \frac{1}{s'-s_+} + \frac{1}{s'-s_-} - \frac{1}{s'-a} \,, \qquad h_-(s') = \frac{1}{s'-s_+} - \frac{1}{s'-s_-} \,, \\ N_\pm &= g^2 \left(\frac{1}{m^2-s_+} \pm \frac{1}{m^2-s_-} \right) , \qquad N^\pm_n = \frac{g^2}{(m^2-s_\pm)^n} \,, \qquad h^\pm_n(s') = \frac{1}{(s'-s_\pm)^n} \,, \end{aligned} \tag{C.85}$$

we find

$$\begin{aligned} \big[A^+(s,0)\big]_{\mathbf{q}^2=0} &= d^+_{00} + \frac{g^2}{m} + a^+_{10} M_\pi^2 \\ &\quad + \frac{1}{\pi} \int\limits_{t_\pi}^\infty \frac{\mathrm{d}t'}{t'} \Big\{ \big[\operatorname{Im} A^+\big]_{(M_\pi,0)} - \big[\operatorname{Im} A^+\big]_{(0,0)} - M_\pi^2 \big[\partial_{\nu^2} \operatorname{Im} A^+\big]_{(0,0)} \Big\} \\ &\quad + \frac{1}{\pi} \int\limits_{s_+}^\infty \mathrm{d}s' \Big\{ h_+(s') \big[\operatorname{Im} A^+\big]_{(M_\pi,0)} - M_\pi^2 h_0(s') \big[\partial_{\nu^2} \operatorname{Im} A^+\big]_{(0,0)} \end{aligned}$$

$$
\begin{aligned}
&\qquad - \big(h_0(s') + 8m^2 M_\pi^2 h_3^0(s')\big) \left[\operatorname{Im} A^+\right]_{(0,0)} \Bigg\} \,, \\
\left[A^-(s,0)\right]_{\mathbf{q}^2=0} &= a_{00}^- M_\pi + a_{10}^- M_\pi^3 + \frac{M_\pi}{\pi} \int\limits_{t_\pi}^{\infty} \frac{\mathrm{d}t'}{t'} \Bigg\{ \left[\operatorname{Im} A^-/\nu'\right]_{(M_\pi,0)} \\
&\qquad - \left[\operatorname{Im} A^-/\nu'\right]_{(0,0)} - M_\pi^2 \left[\partial_{\nu^2} \operatorname{Im} A^-/\nu'\right]_{(0,0)} \Bigg\} \\
&\quad + \frac{1}{\pi} \int\limits_{s_+}^{\infty} \mathrm{d}s' \Bigg\{ h_-(s') \left[\operatorname{Im} A^-\right]_{(M_\pi,0)} - 4mM_\pi^3 h_2^0(s') \left[\partial_{\nu^2} \operatorname{Im} A^-\right]_{(0,0)} \\
&\qquad - 4mM_\pi \big(h_2^0(s') + 4m^2 M_\pi^2 h_4^0(s')\big) \left[\operatorname{Im} A^-\right]_{(0,0)} \Bigg\} \,, \\
\left[B^+(s,0)\right]_{\mathbf{q}^2=0} &= N_- + b_{00}^+ M_\pi + \frac{M_\pi}{\pi} \int\limits_{t_\pi}^{\infty} \frac{\mathrm{d}t'}{t'} \Bigg\{ \left[\operatorname{Im} B^+/\nu'\right]_{(M_\pi,0)} - \left[\operatorname{Im} B^+/\nu'\right]_{(0,0)} \Bigg\} \\
&\quad + \frac{1}{\pi} \int\limits_{s_+}^{\infty} \mathrm{d}s' \Bigg\{ h_-(s') \left[\operatorname{Im} B^+\right]_{(M_\pi,0)} - 4mM_\pi h_2^0(s') \left[\operatorname{Im} B^+\right]_{(0,0)} \Bigg\} \,, \\
\left[B^-(s,0)\right]_{\mathbf{q}^2=0} &= N_+ + b_{00}^- - \frac{g^2}{2m^2} + b_{10}^- M_\pi^2 \\
&\quad + \frac{1}{\pi} \int\limits_{t_\pi}^{\infty} \frac{\mathrm{d}t'}{t'} \Bigg\{ \left[\operatorname{Im} B^-\right]_{(M_\pi,0)} - \left[\operatorname{Im} B^-\right]_{(0,0)} - M_\pi^2 \left[\partial_{\nu^2} \operatorname{Im} B^-\right]_{(0,0)} \Bigg\} \\
&\quad + \frac{1}{\pi} \int\limits_{s_+}^{\infty} \mathrm{d}s' \Bigg\{ h_+(s') \left[\operatorname{Im} B^-\right]_{(M_\pi,0)} - M_\pi^2 h_0(s') \left[\partial_{\nu^2} \operatorname{Im} B^-\right]_{(0,0)} \\
&\qquad - \big(h_0(s') + 8m^2 M_\pi^2 h_3^0(s')\big) \left[\operatorname{Im} B^-\right]_{(0,0)} \Bigg\} \,, \qquad \text{(C.86)}
\end{aligned}
$$

$$
\begin{aligned}
\left[\partial_t A^+(s,t)\right]_{t=0,\mathbf{q}^2=0} &= d_{01}^+ + a_{10}^+ \zeta_{\nu^2,t} + \frac{1}{\pi} \int\limits_{t_\pi}^{\infty} \frac{\mathrm{d}t'}{t'} \Bigg\{ \frac{1}{t'} \left[\operatorname{Im} A^+\right]_{(M_\pi,0)} + \left[\partial_t \operatorname{Im} A^+\right]_{(M_\pi,0)} \\
&\qquad - \frac{1}{t'} \left[\operatorname{Im} A^+\right]_{(0,0)} - \left[\partial_t \operatorname{Im} A^+\right]_{(0,0)} - \zeta_{\nu^2,t} \left[\partial_{\nu^2} \operatorname{Im} A^+\right]_{(0,0)} \Bigg\} \\
&\quad + \frac{1}{\pi} \int\limits_{s_+}^{\infty} \mathrm{d}s' \Bigg\{ - h_2^-(s') \left[\operatorname{Im} A^+\right]_{(M_\pi,0)} + h_+(s') \left[\partial_t \operatorname{Im} A^+\right]_{(M_\pi,0)} \\
&\qquad + h_2^0(s') \left[\operatorname{Im} A^+\right]_{(0,0)} - h_0(s') \left[\partial_t \operatorname{Im} A^+\right]_{(0,0)} \\
&\qquad - \zeta_{\nu^2,t} \Big(8m^2 h_3^0(s') \left[\operatorname{Im} A^+\right]_{(0,0)} + h_0(s') \left[\partial_{\nu^2} \operatorname{Im} A^+\right]_{(0,0)}\Big) \Bigg\} \,,
\end{aligned}
$$

$$
\begin{aligned}
\left[\partial_t A^-(s,t)\right]_{t=0,\mathbf{q}^2=0} &= \frac{a^-_{00}}{4m} + a^-_{01}M_\pi + a^-_{10}\zeta_{\nu^3,t} + \frac{1}{\pi}\int\limits_{t_\pi}^{\infty}\frac{\mathrm{d}t'}{t'}\Bigg\{\left(\frac{1}{4m}+\frac{M_\pi}{t'}\right)\left[\mathrm{Im}\,A^-/\nu'\right]_{(M_\pi,0)} \\
&\qquad + M_\pi\left[\partial_t \mathrm{Im}\,A^-/\nu'\right]_{(M_\pi,0)} - M_\pi\left[\partial_t \mathrm{Im}\,A^-/\nu'\right]_{(0,0)} \\
&\qquad - \left(\frac{1}{4m}+\frac{M_\pi}{t'}\right)\left[\mathrm{Im}\,A^-/\nu'\right]_{(0,0)} - \zeta_{\nu^3,t}\left[\partial_{\nu^2}\mathrm{Im}\,A^-/\nu'\right]_{(0,0)}\Bigg\} \\
&\quad + \frac{1}{\pi}\int\limits_{s_+}^{\infty}\mathrm{d}s'\Bigg\{h_2^-(s')\left[\mathrm{Im}\,A^-\right]_{(M_\pi,0)} + h_-(s')\left[\partial_t\mathrm{Im}\,A^-\right]_{(M_\pi,0)} - h_2^0(s')\left[\mathrm{Im}\,A^-\right]_{(0,0)} \\
&\qquad + 4mM_\pi\Big(h_3^0(s')\left[\mathrm{Im}\,A^-\right]_{(0,0)} - h_2^0(s')\left[\partial_t\mathrm{Im}\,A^-\right]_{(0,0)}\Big) \\
&\qquad - 4m\zeta_{\nu^3,t}\Big(4m^2h_4^0(s')\left[\mathrm{Im}\,A^-\right]_{(0,0)} + h_2^0(s')\left[\partial_{\nu^2}\mathrm{Im}\,A^-\right]_{(0,0)}\Big)\Bigg\}, \\
\left[\partial_t B^+(s,t)\right]_{t=0,\mathbf{q}^2=0} &= N_2^- + \frac{b^+_{00}}{4m} + \frac{1}{\pi}\int\limits_{t_\pi}^{\infty}\frac{\mathrm{d}t'}{t'}\Bigg\{\left(\frac{1}{4m}+\frac{M_\pi}{t'}\right)\left[\mathrm{Im}\,B^+/\nu'\right]_{(M_\pi,0)} \\
&\qquad + M_\pi\left[\partial_t\mathrm{Im}\,B^+/\nu'\right]_{(M_\pi,0)} - \frac{1}{4m}\left[\mathrm{Im}\,B^+/\nu'\right]_{(0,0)}\Bigg\} \\
&\quad + \frac{1}{\pi}\int\limits_{s_+}^{\infty}\mathrm{d}s'\Bigg\{h_2^-(s')\left[\mathrm{Im}\,B^+\right]_{(M_\pi,0)} + h_-(s')\left[\partial_t\mathrm{Im}\,B^+\right]_{(M_\pi,0)} - h_2^0(s')\left[\mathrm{Im}\,B^+\right]_{(0,0)}\Bigg\}, \\
\left[\partial_t B^-(s,t)\right]_{t=0,\mathbf{q}^2=0} &= -N_2^- + b^-_{01} + b^-_{10}\zeta_{\nu^2,t} + \frac{1}{\pi}\int\limits_{t_\pi}^{\infty}\frac{\mathrm{d}t'}{t'}\Bigg\{\frac{1}{t'}\left[\mathrm{Im}\,B^-\right]_{(M_\pi,0)} + \left[\partial_t\mathrm{Im}\,B^-\right]_{(M_\pi,0)} \\
&\qquad - \frac{1}{t'}\left[\mathrm{Im}\,B^-\right]_{(0,0)} - \left[\partial_t\mathrm{Im}\,B^-\right]_{(0,0)} - \zeta_{\nu^2,t}\left[\partial_{\nu^2}\mathrm{Im}\,B^-\right]_{(0,0)}\Bigg\} \\
&\quad + \frac{1}{\pi}\int\limits_{s_+}^{\infty}\mathrm{d}s'\Bigg\{-h_2^-(s')\left[\mathrm{Im}\,B^-\right]_{(M_\pi,0)} + h_+(s')\left[\partial_t\mathrm{Im}\,B^-\right]_{(M_\pi,0)} \\
&\qquad + h_2^0(s')\left[\mathrm{Im}\,B^-\right]_{(0,0)} - h_0(s')\left[\partial_t\mathrm{Im}\,B^-\right]_{(0,0)} \\
&\qquad - \zeta_{\nu^2,t}\Big(8m^2h_3^0(s')\left[\mathrm{Im}\,B^-\right]_{(0,0)} + h_0(s')\left[\partial_{\nu^2}\mathrm{Im}\,B^-\right]_{(0,0)}\Big)\Bigg\}, \qquad \text{(C.87)} \\
\left[\partial_{\mathbf{q}^2}A^+(s,0)\right]_{\mathbf{q}^2=0} &= a^+_{10}\zeta_{\nu^2,\mathbf{q}^2} + \frac{1}{\pi}\int\limits_{t_\pi}^{\infty}\frac{\mathrm{d}t'}{t'}\Big\{\left[\partial_{\mathbf{q}^2}\mathrm{Im}\,A^+\right]_{(M_\pi,0)} - \zeta_{\nu^2,\mathbf{q}^2}\left[\partial_{\nu^2}\mathrm{Im}\,A^+\right]_{(0,0)}\Big\} \\
&\quad + \frac{1}{\pi}\int\limits_{s_+}^{\infty}\mathrm{d}s'\Bigg\{\zeta_s(h_2^+(s')-h_2^-(s'))\left[\mathrm{Im}\,A^+\right]_{(M_\pi,0)} + h_+(s')\left[\partial_{\mathbf{q}^2}\mathrm{Im}\,A^+\right]_{(M_\pi,0)} \\
&\qquad - \zeta_{\nu^2,\mathbf{q}^2}\Big(8m^2h_3^0(s')\left[\mathrm{Im}\,A^+\right]_{(0,0)} + h_0(s')\left[\partial_{\nu^2}\mathrm{Im}\,A^+\right]_{(0,0)}\Big) - \frac{\zeta_{A^+}}{(s'-s_+)^{3/2}}\Bigg\},
\end{aligned}
$$

$$
\begin{aligned}
\left[\partial_{\mathbf{q}^2} A^-(s,0)\right]_{\mathbf{q}^2=0} &= a_{00}^- \frac{\zeta_s}{2m} + a_{10}^- \zeta_{\nu^3,\mathbf{q}^2} + \frac{1}{\pi}\int\limits_{t_\pi}^{\infty}\frac{\mathrm{d}t'}{t'}\Bigg\{ M_\pi \left[\partial_{\mathbf{q}^2}\mathrm{Im}\, A^-/\nu'\right]_{(M_\pi,0)} \\
&\quad + \frac{\zeta_s}{2m}\Big(\left[\mathrm{Im}\, A^-/\nu'\right]_{(M_\pi,0)} - \left[\mathrm{Im}\, A^-/\nu'\right]_{(0,0)} \Big) - \zeta_{\nu^3,\mathbf{q}^2}\left[\partial_{\nu^2}\mathrm{Im}\, A^-/\nu'\right]_{(0,0)} \Bigg\} \\
&\quad + \frac{1}{\pi}\int\limits_{s_+}^{\infty}\mathrm{d}s'\Bigg\{ \zeta_s(h_2^+(s') + h_2^-(s'))\left[\mathrm{Im}\, A^-\right]_{(M_\pi,0)} + h_-(s')\left[\partial_{\mathbf{q}^2}\mathrm{Im}\, A^-\right]_{(M_\pi,0)} \\
&\qquad - 4m\zeta_{\nu^3,\mathbf{q}^2}\Big(4m^2 h_4^0(s')\left[\mathrm{Im}\, A^-\right]_{(0,0)} + h_2^0(s')\left[\partial_{\nu^2}\mathrm{Im}\, A^-\right]_{(0,0)}\Big) \\
&\qquad - 2\zeta_s h_2^0(s')\left[\mathrm{Im}\, A^-\right]_{(0,0)} - \frac{\zeta_{A^-}}{(s'-s_+)^{3/2}}\Bigg\}, \\
\left[\partial_{\mathbf{q}^2} B^+(s,0)\right]_{\mathbf{q}^2=0} &= \zeta_s(N_2^+ + N_2^-) + b_{00}^+\frac{\zeta_s}{2m} + \frac{1}{\pi}\int\limits_{t_\pi}^{\infty}\frac{\mathrm{d}t'}{t'}\Bigg\{ M_\pi\left[\partial_{\mathbf{q}^2}\mathrm{Im}\, B^+/\nu'\right]_{(M_\pi,0)} \\
&\quad + \frac{\zeta_s}{2m}\Big(\left[\mathrm{Im}\, B^+/\nu'\right]_{(M_\pi,0)} - \left[\mathrm{Im}\, B^+/\nu'\right]_{(0,0)}\Big)\Bigg\} \\
&\quad + \frac{1}{\pi}\int\limits_{s_+}^{\infty}\mathrm{d}s'\Bigg\{ \zeta_s(h_2^+(s') + h_2^-(s'))\left[\mathrm{Im}\, B^+\right]_{(M_\pi,0)} + h_-(s')\left[\partial_{\mathbf{q}^2}\mathrm{Im}\, B^+\right]_{(M_\pi,0)} \\
&\qquad - 2\zeta_s h_2^0(s')\left[\mathrm{Im}\, B^+\right]_{(0,0)} - \frac{\zeta_{B^+}}{(s'-s_+)^{3/2}}\Bigg\}, \\
\left[\partial_{\mathbf{q}^2} B^-(s,0)\right]_{\mathbf{q}^2=0} &= \zeta_s(N_2^+ - N_2^-) + b_{10}^-\zeta_{\nu^2,\mathbf{q}^2} \\
&\quad + \frac{1}{\pi}\int\limits_{t_\pi}^{\infty}\frac{\mathrm{d}t'}{t'}\Big\{ \left[\partial_{\mathbf{q}^2}\mathrm{Im}\, B^-\right]_{(M_\pi,0)} - \zeta_{\nu^2,\mathbf{q}^2}\left[\partial_{\nu^2}\mathrm{Im}\, B^-\right]_{(0,0)}\Big\} \qquad \text{(C.88)} \\
&\quad + \frac{1}{\pi}\int\limits_{s_+}^{\infty}\mathrm{d}s'\Bigg\{ \zeta_s(h_2^+(s') - h_2^-(s'))\left[\mathrm{Im}\, B^-\right]_{(M_\pi,0)} + h_+(s')\left[\partial_{\mathbf{q}^2}\mathrm{Im}\, B^-\right]_{(M_\pi,0)} \\
&\qquad - \zeta_{\nu^2,\mathbf{q}^2}\Big(8m^2 h_3^0(s')\left[\mathrm{Im}\, B^-\right]_{(0,0)} + h_0(s')\left[\partial_{\nu^2}\mathrm{Im}\, B^-\right]_{(0,0)}\Big) - \frac{\zeta_{B^-}}{(s'-s_+)^{3/2}}\Bigg\}.
\end{aligned}
$$

In these equations the subscript $(M_\pi, 0)$ denotes evaluation at threshold ($\nu = M_\pi$, $t = 0$). The amplitudes may be calculated by summing the pertinent partial waves using

$$
\begin{aligned}
&\left[z_s'\right]_{(M_\pi,0)} = -\frac{s'+a}{s'-a}, \qquad \left[\partial_t z_s'\right]_{(M_\pi,0)} = \frac{s_+ - a}{2\mathbf{q}'^2(s'-a)}, \quad \left[\partial_{\mathbf{q}^2} z_s'\right]_{(M_\pi,0)} = \frac{2s_+}{\mathbf{q}'^2(s'-a)}, \\
&\left[z_t'^2\right]_{(M_\pi,0)} = 1 + \frac{at'}{4p_t'^2 q_t'^2}, \quad \left[\partial_t z_t'^2\right]_{(M_\pi,0)} = \frac{s_+ - a}{4p_t'^2 q_t'^2}, \qquad \left[\partial_{\mathbf{q}^2} z_t'^2\right]_{(M_\pi,0)} = \frac{s_+}{p_t'^2 q_t'^2}. \qquad \text{(C.89)}
\end{aligned}
$$

Finally, we have defined the derivatives

$$
\zeta_s = \left[\partial_{\mathbf{q}^2} s\right]_{(M_\pi,0)} = \frac{4s_+}{s_+ - s_-} = \frac{s_+}{m M_\pi},
$$

$$\zeta_{\nu^2,t} = \left[\partial_t \nu^2\right]_{(M_\pi,0)} = \frac{M_\pi}{2m}\,, \qquad \zeta_{\nu^2,\mathbf{q}^2} = \left[\partial_{\mathbf{q}^2} \nu^2\right]_{(M_\pi,0)} = \frac{s_+}{m^2}\,,$$
$$\zeta_{\nu^3,t} = \left[\partial_t \nu^3\right]_{(M_\pi,0)} = \frac{3M_\pi^2}{4m}\,, \qquad \zeta_{\nu^3,\mathbf{q}^2} = \left[\partial_{\mathbf{q}^2} \nu^3\right]_{(M_\pi,0)} = \frac{3M_\pi s_+}{2m^2}\,, \tag{C.90}$$

and removed the threshold divergence by subtracting the terms involving

$$\zeta_{A^+} = (2m+M_\pi)\zeta_{B^+} = \frac{2\pi W_+(2m+M_\pi)}{3m\sqrt{mM_\pi}}\left[\left(a_{0+}^{1/2}\right)^2 + 2\left(a_{0+}^{3/2}\right)^2\right],$$
$$\zeta_{A^-} = (2m+M_\pi)\zeta_{B^-} = \frac{2\pi W_+(2m+M_\pi)}{3m\sqrt{mM_\pi}}\left[\left(a_{0+}^{1/2}\right)^2 - \left(a_{0+}^{3/2}\right)^2\right]. \tag{C.91}$$

Bibliography

[1] H. Fritzsch, M. Gell-Mann, and H. Leutwyler, Phys. Lett. B **47** (1973) 365.

[2] D. J. Gross and F. Wilczek, Phys. Rev. Lett. **30** (1973) 1343; H. D. Politzer, Phys. Rev. Lett. **30** (1973) 1346.

[3] K. Nakamura *et al.* [Particle Data Group], J. Phys. G **37** (2010) 075021.

[4] S. Bethke, Eur. Phys. J. C **64** (2009) 689 [arXiv:0908.1135 [hep-ph]].

[5] S. Bethke *et al.*, arXiv:1110.0016 [hep-ph].

[6] R. J. Crewther, Phys. Rev. Lett. **28** (1972) 1421; M. S. Chanowitz and J. R. Ellis, Phys. Rev. D **7** (1973) 2490; J. C. Collins, A. Duncan, and S. D. Joglekar, Phys. Rev. D **16** (1977) 438; K. Fujikawa, Phys. Rev. D **23** (1981) 2262; J. F. Donoghue, E. Golowich, and B. R. Holstein, Camb. Monogr. Part. Phys. Nucl. Phys. Cosmol. **2** (1992) 1.

[7] S. Weinberg, Physica A **96** (1979) 327.

[8] H. Leutwyler, Annals Phys. **235** (1994) 165 [arXiv:hep-ph/9311274]; E. D'Hoker and S. Weinberg, Phys. Rev. D **50** (1994) 6050 [hep-ph/9409402].

[9] A. V. Manohar, arXiv:hep-ph/9606222; D. B. Kaplan, arXiv:nucl-th/0510023; D. R. Phillips, Czech. J. Phys. **52** (2002) B49 [nucl-th/0203040].

[10] G. 't Hooft, Phys. Rev. Lett. **37** (1976) 8.

[11] J. Goldstone, Nuovo Cim. **19** (1961) 154; J. Goldstone, A. Salam, and S. Weinberg, Phys. Rev. **127** (1962) 965.

[12] J. Gasser and H. Leutwyler, Annals Phys. **158** (1984) 142.

[13] J. Gasser and H. Leutwyler, Nucl. Phys. B **250** (1985) 465.

[14] U.-G. Meißner, Rept. Prog. Phys. **56** (1993) 903 [hep-ph/9302247]; G. Ecker, Prog. Part. Nucl. Phys. **35** (1995) 1 [arXiv:hep-ph/9501357]; S. Scherer, Adv. Nucl. Phys. **27** (2003) 277 [arXiv:hep-ph/0210398]; J. Gasser, Lect. Notes Phys. **629** (2004) 1 [arXiv:hep-ph/0312367]; V. Bernard and U.-G. Meißner, Ann. Rev. Nucl. Part. Sci. **57** (2007) 33 [arXiv:hep-ph/0611231]; B. Kubis, arXiv:hep-ph/0703274; V. Bernard, Prog. Part. Nucl. Phys. **60** (2008) 82 [arXiv:0706.0312 [hep-ph]]; S. Scherer and M. R. Schindler, Lect. Notes Phys. **830** (2012) 1.

[15] N. H. Fuchs, H. Sazdjian, and J. Stern, Phys. Lett. B **269** (1991) 183.

[16] G. Colangelo, J. Gasser, and H. Leutwyler, Phys. Rev. Lett. **86** (2001) 5008 [hep-ph/0103063].

[17] A. Manohar and H. Georgi, Nucl. Phys. B **234** (1984) 189.

[18] R. Urech, Nucl. Phys. B **433** (1995) 234 [arXiv:hep-ph/9405341]; U.-G. Meißner, G. Müller, and S. Steininger, Phys. Lett. B **406** (1997) 154 [Erratum-ibid. B **407** (1997) 454] [arXiv:hep-ph/9704377]; M. Knecht and R. Urech, Nucl. Phys. B **519** (1998) 329 [arXiv:hep-ph/9709348].

[19] J. Gasser, M. E. Sainio, and A. Švarc, Nucl. Phys. B **307** (1988) 779.

[20] E. E. Jenkins and A. V. Manohar, Phys. Lett. B **255** (1991) 558; V. Bernard, N. Kaiser, J. Kambor, and U.-G. Meißner, Nucl. Phys. B **388** (1992) 315.

[21] P. J. Ellis and H. B. Tang, Phys. Rev. C **57** (1998) 3356 [arXiv:hep-ph/9709354].

[22] T. Becher and H. Leutwyler, Eur. Phys. J. C **9** (1999) 643 [arXiv:hep-ph/9901384].

[23] J. L. Goity, D. Lehmann, G. Prézeau, and J. Saez, Phys. Lett. B **504** (2001) 21 [arXiv:hep-ph/0101011]; D. Lehmann and G. Prézeau, Phys. Rev. D **65** (2002) 016001 [arXiv:hep-ph/0102161].

[24] M. R. Schindler, J. Gegelia, and S. Scherer, Phys. Lett. B **586** (2004) 258 [arXiv:hep-ph/0309005]; M. R. Schindler, J. Gegelia, and S. Scherer, Nucl. Phys. B **682** (2004) 367 [arXiv:hep-ph/0310207].

[25] S. Weinberg, Phys. Lett. B **251** (1990) 288; Nucl. Phys. B **363** (1991) 3.

[26] S. Weinberg, Phys. Lett. B **295** (1992) 114 [hep-ph/9209257].

[27] U. van Kolck, Phys. Rev. C **49** (1994) 2932; C. Ordóñez, L. Ray, and U. van Kolck, Phys. Rev. Lett. **72** (1994) 1982; Phys. Rev. C **53** (1996) 2086 [hep-ph/9511380].

[28] E. Epelbaum, W. Glöckle, and U.-G. Meißner, Nucl. Phys. A **637** (1998) 107 [nucl-th/9801064]; Nucl. Phys. A **671** (2000) 295 [nucl-th/9910064].

[29] E. Epelbaum, W. Glöckle, and U.-G. Meißner, Nucl. Phys. A **747** (2005) 362 [nucl-th/0405048].

[30] D. R. Entem and R. Machleidt, Phys. Lett. B **524** (2002) 93 [nucl-th/0108057]; Phys. Rev. C **68** (2003) 041001 [nucl-th/0304018].

[31] E. Epelbaum, Prog. Part. Nucl. Phys. **57** (2006) 654 [nucl-th/0509032]; E. Epelbaum, H.-W. Hammer, and U.-G. Meißner, Rev. Mod. Phys. **81** (2009) 1773 [arXiv:0811.1338 [nucl-th]]; R. Machleidt and D. R. Entem, Phys. Rept. **503** (2011) 1 [arXiv:1105.2919 [nucl-th]].

[32] G. P. Lepage, arXiv:nucl-th/9706029; A. Nogga, R. G. E. Timmermans, and U. van Kolck, Phys. Rev. C **72** (2005) 054006 [arXiv:nucl-th/0506005]; M. C. Birse, Phys. Rev. C **74** (2006) 014003 [arXiv:nucl-th/0507077]; M. Pavón Valderrama and E. R. Arriola, Phys. Rev. C **74** (2006) 054001 [arXiv:nucl-th/0506047]; E. Epelbaum and U.-G. Meißner, arXiv:nucl-th/0609037; C.-J. Yang, C. Elster, and D. R. Phillips, Phys.

Rev. C **77** (2008) 014002 [arXiv:0706.1242 [nucl-th]]; E. Epelbaum and J. Gegelia, Eur. Phys. J. A **41** (2009) 341 [arXiv:0906.3822 [nucl-th]].

[33] V. Baru, C. Hanhart, M. Hoferichter, B. Kubis, A. Nogga, and D. R. Phillips, Phys. Lett. B **694** (2011) 473 [arXiv:1003.4444 [nucl-th]]; Nucl. Phys. A **872** (2011) 69 [arXiv:1107.5509 [nucl-th]].

[34] R. J. Eden, P. V. Landshoff, D. I. Olive, and J. C. Polkinghorne, *The analytic S-matrix*, Cambridge University Press, Cambridge, 1966.

[35] D. I. Olive, Nuovo Cim. **26** (1962) 73.

[36] N. N. Khuri and S. B. Treiman, Phys. Rev. **119** (1960) 1115; I. J. R. Aitchison and R. J. A. Golding, J. Phys. G G **4** (1978) 43; A. V. Anisovich and H. Leutwyler, Phys. Lett. B **375** (1996) 335 [hep-ph/9601237]; F. Niecknig, B. Kubis, and S. P. Schneider, arXiv:1203.2501 [hep-ph].

[37] M. Froissart, Phys. Rev. **123** (1961) 1053.

[38] A. Martin, Phys. Rev. **129** (1963) 1432.

[39] Y. S. Jin and A. Martin, Phys. Rev. **135** (1964) B1375.

[40] S. Mandelstam, Phys. Rev. **112** (1958) 1344.

[41] S. Mandelstam, Phys. Rev. **115** (1959) 1741; Phys. Rev. **115** (1959) 1752.

[42] A. Martin, Nuovo Cim. A **42** (1965) 930; Nuovo Cim. A **44** (1966) 1219.

[43] S. W. MacDowell, Phys. Rev. D **6** (1972) 3512; F. F. K. Cheung and F. S. Chen-Cheung, Phys. Rev. D **5** (1972) 970.

[44] S. M. Roy, Phys. Lett. B **36** (1971) 353.

[45] H. Lehmann, Nuovo Cim. **10** (1958) 579.

[46] C. Itzykson and J.-B. Zuber, *Quantum Field Theory*, Mc Graw-Hill Inc, New York, 1980.

[47] G. Mahoux, S. M. Roy, and G. Wanders, Nucl. Phys. B **70** (1974) 297; G. Auberson and L. Epele, Nuovo Cim. A **25** (1975) 453.

[48] L. Epele and G. Wanders, Phys. Lett. B **72** (1978) 390; Nucl. Phys. B **137** (1978) 521.

[49] J. Gasser and G. Wanders, Eur. Phys. J. C **10** (1999) 159 [arXiv:hep-ph/9903443].

[50] G. Wanders, Eur. Phys. J. C **17** (2000) 323 [arXiv:hep-ph/0005042].

[51] J. L. Basdevant, J. C. Le Guillou, and H. Navelet, Nuovo Cim. A **7** (1972) 363; J. L. Basdevant, C. D. Froggatt, and J. L. Petersen, Phys. Lett. B **41** (1972) 173; Phys. Lett. B **41** (1972) 178; Nucl. Phys. B **72** (1974) 413; C. D. Froggatt and J. L. Petersen, Nucl. Phys. B **91** (1975) 454 [Erratum-ibid. B **104** (1976) 186]; Nucl. Phys. B **129** (1977) 89; M. R. Pennington and S. D. Protopopescu, Phys. Rev. D **7** (1973) 1429; Phys. Rev. D **7** (1973) 2591.

[52] B. Ananthanarayan and P. Büttiker, Phys. Rev. D **54** (1996) 1125 [hep-ph/9601285]; Phys. Rev. D **54** (1996) 5501 [hep-ph/9604217]; Phys. Lett. B **415** (1997) 402 [hep-ph/9707305]; B. Ananthanarayan, Phys. Rev. D **58** (1998) 036002 [hep-ph/9802338].

[53] B. Ananthanarayan, G. Colangelo, J. Gasser, and H. Leutwyler, Phys. Rept. **353** (2001) 207 [hep-ph/0005297].

[54] S. Descotes-Genon, N. H. Fuchs, L. Girlanda, and J. Stern, Eur. Phys. J. C **24** (2002) 469 [hep-ph/0112088].

[55] R. García-Martín, R. Kamiński, J. R. Peláez, J. Ruiz de Elvira, and F. J. Ynduráin, Phys. Rev. D **83** (2011) 074004 [arXiv:1102.2183 [hep-ph]].

[56] B. Moussallam, Eur. Phys. J. C **71** (2011) 1814 [arXiv:1110.6074 [hep-ph]].

[57] I. Caprini, G. Colangelo, and H. Leutwyler, Eur. Phys. J. C **72** (2012) 1860 [arXiv:1111.7160 [hep-ph]]; in preparation.

[58] G. Colangelo, J. Gasser, and H. Leutwyler, Nucl. Phys. B **603** (2001) 125 [hep-ph/0103088]; Phys. Lett. B **488** (2000) 261 [hep-ph/0007112].

[59] B. Adeva *et al.* [DIRAC Collaboration], Phys. Lett. B **619** (2005) 50 [hep-ex/0504044].

[60] S. Pislak *et al.*, Phys. Rev. D **67** (2003) 072004 [Erratum-ibid. D **81** (2010) 119903] [hep-ex/0301040]; J. R. Batley *et al.* [NA48/2 Collaboration], Eur. Phys. J. C **54** (2008) 411.

[61] J. R. Batley *et al.* [NA48/2 Collaboration], Eur. Phys. J. C **70** (2010) 635.

[62] J. R. Batley *et al.* [NA48/2 Collaboration], Phys. Lett. B **633** (2006) 173 [hep-ex/0511056]; Eur. Phys. J. C **64** (2009) 589 [arXiv:0912.2165 [hep-ex]].

[63] N. Cabibbo, Phys. Rev. Lett. **93** (2004) 121801 [hep-ph/0405001]; N. Cabibbo and G. Isidori, JHEP **0503** (2005) 021 [hep-ph/0502130]; G. Colangelo, J. Gasser, B. Kubis, and A. Rusetsky, Phys. Lett. B **638** (2006) 187 [hep-ph/0604084]; J. Gasser, B. Kubis, and A. Rusetsky, Nucl. Phys. B **850** (2011) 96 [arXiv:1103.4273 [hep-ph]].

[64] M. Bissegger, A. Fuhrer, J. Gasser, B. Kubis, and A. Rusetsky, Nucl. Phys. B **806** (2009) 178 [arXiv:0807.0515 [hep-ph]]; G. Colangelo, J. Gasser, and A. Rusetsky, Eur. Phys. J. C **59** (2009) 777 [arXiv:0811.0775 [hep-ph]]; G. Colangelo, Nucl. Phys. A **827** (2009) 228C.

[65] I. Caprini, G. Colangelo, and H. Leutwyler, Phys. Rev. Lett. **96** (2006) 132001 [hep-ph/0512364].

[66] B. Ananthanarayan and P. Büttiker, Eur. Phys. J. C **19** (2001) 517 [hep-ph/0012023]; B. Ananthanarayan, P. Büttiker, and B. Moussallam, Eur. Phys. J. C **22** (2001) 133 [hep-ph/0106230].

[67] P. Büttiker, S. Descotes-Genon, and B. Moussallam, Eur. Phys. J. C **33** (2004) 409 [hep-ph/0310283].

[68] G. E. Hite and F. Steiner, Nuovo Cim. A **18** (1973) 237 [CERN-TH-1590 for appendices D and E].

[69] J. Baacke and F. Steiner, Fortsch. Phys. **18** (1970) 67; F. Steiner, Fortsch. Phys. **18** (1970) 43; Fortsch. Phys. **19** (1971) 115.

[70] N. I. Muskhelishvili, *Singular Integral Equations*, Wolters-Noordhoff Publishing, Groningen, 1953 [Dover Publications, 2nd edition, 2008].

[71] R. Omnès, Nuovo Cim. **8** (1958) 316.

[72] V. Bernard, N. Kaiser, and U.-G. Meißner, Phys. Rev. D **43** (1991) 2757; Nucl. Phys. B **357** (1991) 129.

[73] S. Descotes-Genon and B. Moussallam, Eur. Phys. J. C **48** (2006) 553 [hep-ph/0607133].

[74] S. Weinberg, Phys. Rev. Lett. **17** (1966) 616.

[75] S. R. Beane, K. Orginos, and M. J. Savage, Int. J. Mod. Phys. E **17** (2008) 1157 [arXiv:0805.4629 [hep-lat]]; A. Torok *et al.*, Phys. Rev. D **81** (2010) 074506 [arXiv:0907.1913 [hep-lat]].

[76] V. Bernard, N. Kaiser, and U.-G. Meißner, Phys. Lett. B **309** (1993) 421 [arXiv:hep-ph/9304275].

[77] A. M. Bernstein, Phys. Lett. B **442** (1998) 20 [arXiv:hep-ph/9810376]; A. M. Bernstein, M. W. Ahmed, S. Stave, Y. K. Wu, and H. R. Weller, Ann. Rev. Nucl. Part. Sci. **59** (2009) 115 [arXiv:0902.3650 [nucl-ex]].

[78] N. Fettes and U.-G. Meißner, Nucl. Phys. A **676** (2000) 311 [arXiv:hep-ph/0002162].

[79] J. Gasser, H. Leutwyler, M. P. Locher, and M. E. Sainio, Phys. Lett. B **213** (1988) 85.

[80] J. Gasser, H. Leutwyler, and M. E. Sainio, Phys. Lett. B **253** (1991) 252.

[81] M. L. Goldberger, H. Miyazawa, and R. Oehme, Phys. Rev. **99** (1955) 986.

[82] T. E. O. Ericson, B. Loiseau, and A. W. Thomas, Phys. Rev. C **66** (2002) 014005 [arXiv:hep-ph/0009312].

[83] V. V. Abaev, P. Metsä, and M. E. Sainio, Eur. Phys. J. A **32** (2007) 321 [arXiv:0704.3167 [hep-ph]].

[84] J. Gasser, V. E. Lyubovitskij, and A. Rusetsky, Phys. Rept. **456** (2008) 167 [arXiv: 0711.3522 [hep-ph]].

[85] D. Gotta *et al.*, Lect. Notes Phys. **745** (2008) 165.

[86] V. E. Lyubovitskij and A. Rusetsky, Phys. Lett. B **494** (2000) 9 [arXiv:hep-ph/0009206].

[87] D. Eiras and J. Soto, Phys. Lett. B **491** (2000) 101 [arXiv:hep-ph/0005066].

[88] P. Zemp, Thesis, University of Bern, 2004.

[89] J. Spuller *et al.*, Phys. Lett. B **67** (1977) 479.

[90] U.-G. Meißner, U. Raha, and A. Rusetsky, Eur. Phys. J. C **41** (2005) 213 [arXiv:nucl-th/0501073].

[91] T. Strauch *et al.*, Eur. Phys. J. A **47** (2011) 88 [arXiv:1011.2415 [nucl-ex]]; EPJ Web Conf. **3** (2010) 03006 [arXiv:1002.4277 [nucl-ex]].

[92] V. L. Highland *et al.*, Nucl. Phys. A **365** (1981) 333.

[93] M. Hoferichter, B. Kubis, and U.-G. Meißner, Phys. Lett. B **678** (2009) 65 [arXiv:0903.3890 [hep-ph]]; M. Hoferichter, B. Kubis, and U.-G. Meißner, Nucl. Phys. A **833** (2010) 18 [arXiv:0909.4390 [hep-ph]].

[94] J. Gasser, M. A. Ivanov, E. Lipartia, M. Mojžiš, and A. Rusetsky, Eur. Phys. J. C **26** (2002) 13 [arXiv:hep-ph/0206068].

[95] W. N. Cottingham, Annals Phys. **25** (1963) 424.

[96] J. Gasser and H. Leutwyler, Nucl. Phys. B **94** (1975) 269.

[97] J. Gasser and H. Leutwyler, Phys. Rept. **87** (1982) 77.

[98] A. Walker-Loud, C. E. Carlson, and G. A. Miller, arXiv:1203.0254 [nucl-th].

[99] H. W. Grießhammer, J. A. McGovern, D. R. Phillips, and G. Feldman, arXiv:1203.6834 [nucl-th].

[100] S. R. Beane, K. Orginos, and M. J. Savage, Nucl. Phys. B **768** (2007) 38 [arXiv:hep-lat/0605014]; T. Blum, R. Zhou, T. Doi, M. Hayakawa, T. Izubuchi, S. Uno, and N. Yamada, Phys. Rev. D **82** (2010) 094508 [arXiv:1006.1311 [hep-lat]].

[101] A. Filin, V. Baru, E. Epelbaum, J. Haidenbauer, C. Hanhart, A. E. Kudryavtsev, and U.-G. Meißner, Phys. Lett. B **681** (2009) 423 [arXiv:0907.4671 [nucl-th]].

[102] G. Colangelo *et al.*, Eur. Phys. J. C **71** (2011) 1695 [arXiv:1011.4408 [hep-lat]].

[103] J. Bijnens and J. Prades, Nucl. Phys. B **490** (1997) 239 [arXiv:hep-ph/9610360].

[104] B. Ananthanarayan and B. Moussallam, JHEP **0406** (2004) 047 [arXiv:hep-ph/0405206].

[105] B. Kubis and U.-G. Meißner, Nucl. Phys. A **699** (2002) 709 [arXiv:hep-ph/0107199].

[106] U.-G. Meißner, U. Raha, and A. Rusetsky, Phys. Lett. B **639** (2006) 478 [arXiv:nucl-th/0512035].

[107] S. R. Beane, V. Bernard, T. S. H. Lee, and U.-G. Meißner, Phys. Rev. C **57** (1998) 424 [arXiv:nucl-th/9708035].

[108] S. R. Beane, V. Bernard, E. Epelbaum, U.-G. Meißner, and D. R. Phillips, Nucl. Phys. A **720** (2003) 399 [arXiv:hep-ph/0206219].

[109] S. Liebig, V. Baru, F. Ballout, C. Hanhart, and A. Nogga, Eur. Phys. J. A **47** (2011) 69 [arXiv:1003.3826 [nucl-th]].

[110] V. Baru, C. Hanhart, A. E. Kudryavtsev, and U.-G. Meißner, Phys. Lett. B **589** (2004) 118 [arXiv:nucl-th/0402027].

[111] V. Baru, E. Epelbaum, and A. Rusetsky, Eur. Phys. J. A **42** (2009) 111 [arXiv:0905.4249 [nucl-th]].

[112] V. Lensky, V. Baru, J. Haidenbauer, C. Hanhart, A. E. Kudryavtsev, and U.-G. Meißner, Phys. Lett. B **648** (2007) 46 [arXiv:nucl-th/0608042].

[113] V. Baru, J. Haidenbauer, C. Hanhart, A. E. Kudryavtsev, V. Lensky, and U.-G. Meißner, Phys. Lett. B **659** (2008) 184 [arXiv:0706.4023 [nucl-th]].

[114] V. V. Baru and A. E. Kudryavtsev, Phys. Atom. Nucl. **60** (1997) 1475 [Yad. Fiz. **60** (1997) 1620].

[115] L. Platter and D. R. Phillips, Phys. Lett. B **641** (2006) 164 [arXiv:nucl-th/0605024]; M. Pavón Valderrama and E. R. Arriola, arXiv:nucl-th/0605078; A. Nogga and C. Hanhart, Phys. Lett. B **634** (2006) 210 [arXiv:nucl-th/0511011].

[116] J. L. Friar, U. van Kolck, G. L. Payne, and S. A. Coon, Phys. Rev. C **68** (2003) 024003 [arXiv:nucl-th/0303058].

[117] V. Bernard, N. Kaiser, J. Gasser, and U.-G. Meißner, Phys. Lett. B **268** (1991) 291.

[118] V. M. Kolybasov and V. G. Ksenzov, Zh. Eksp. Teor. Fiz. **71** (1976) 13; G. Fäldt, Phys. Scripta **16** (1977) 81.

[119] V. Lensky, V. Baru, J. Haidenbauer, C. Hanhart, A. E. Kudryavtsev, and U.-G. Meißner, Eur. Phys. J. A **26** (2005) 107 [arXiv:nucl-th/0505039].

[120] V. Bernard, N. Kaiser, and U.-G. Meißner, Nucl. Phys. A **615** (1997) 483 [arXiv:hep-ph/9611253].

[121] H. Krebs, E. Epelbaum, and U.-G. Meißner, Eur. Phys. J. A **32** (2007) 127 [arXiv:nucl-th/0703087].

[122] K. A. Brueckner, Phys. Rev. **89** (1953) 834; V. M. Kolybasov and A. E. Kudryavtsev, Nucl. Phys. B **41** (1972) 510; S. S. Kamalov, E. Oset, and A. Ramos, Nucl. Phys. A **690** (2001) 494 [arXiv:nucl-th/0010054]; U.-G. Meißner, U. Raha, and A. Rusetsky, Eur. Phys. J. C **47** (2006) 473 [arXiv:nucl-th/0603029].

[123] V. Baru, E. Epelbaum, C. Hanhart, M. Hoferichter, A. E. Kudryavtsev, and D. R. Phillips, Eur. Phys. J. A **48** (2012) 69 [arXiv:1202.0208 [nucl-th]].

[124] R. B. Wiringa, V. G. J. Stoks, and R. Schiavilla, Phys. Rev. C **51** (1995) 38 [arXiv:nucl-th/9408016].

[125] R. Machleidt, Phys. Rev. C **63** (2001) 024001 [arXiv:nucl-th/0006014].

[126] S. R. Beane and M. J. Savage, Nucl. Phys. A **717** (2003) 104 [nucl-th/0204046].

[127] D. B. Kaplan, M. J. Savage, and M. B. Wise, Phys. Lett. B **424** (1998) 390 [arXiv:nucl-th/9801034]; Nucl. Phys. B **534** (1998) 329 [arXiv:nucl-th/9802075]; J. Gegelia, Phys. Lett. B **429** (1998) 227; M. C. Birse, J. A. McGovern, and K. G. Richardson, Phys. Lett. B **464** (1999) 169 [arXiv:hep-ph/9807302]; U. van Kolck, Nucl. Phys. A **645** (1999) 273 [arXiv:nucl-th/9808007].

[128] L. Hulthén, Ark. Mat. Astron. Fys. **28 A** (1942) 5; Ark. Mat. Astron. Fys. **29 B** (1942) 1.

[129] D. R. Phillips, G. Rupak, and M. J. Savage, Phys. Lett. B **473** (2000) 209 [arXiv:nucl-th/9908054].

[130] V. Lensky, V. Baru, J. Haidenbauer, C. Hanhart, A. E. Kudryavtsev, and U.-G. Meißner, Eur. Phys. J. A **27** (2006) 37 [arXiv:nucl-th/0511054].

[131] M. Hoferichter, B. Kubis, and U.-G. Meißner, PoS **CD09** (2009) 014 [arXiv:0910.0736 [hep-ph]].

[132] R. D. Young and A. W. Thomas, Phys. Rev. D **81** (2010) 014503 [arXiv:0901.3310 [hep-lat]].

[133] J. Martin Camalich, L. S. Geng, and M. J. Vicente Vacas, Phys. Rev. D **82** (2010) 074504 [arXiv:1003.1929 [hep-lat]].

[134] S. Dürr *et al.*, Phys. Rev. D **85** (2012) 014509 [arXiv:1109.4265 [hep-lat]].

[135] G. S. Bali *et al.* [QCDSF Collaboration], arXiv:1112.0024 [hep-lat].

[136] H. Hellmann, *Einführung in die Quantenchemie*, Franz Deuticke, Leipzig, 1937; R. P. Feynman, Phys. Rev. **56** (1939) 340.

[137] A. Walker-Loud, arXiv:1112.2658 [hep-lat].

[138] T. Becher and H. Leutwyler, JHEP **0106** (2001) 017 [arXiv:hep-ph/0103263].

[139] P. Büttiker and U.-G. Meißner, Nucl. Phys. A **668** (2000) 97 [arXiv:hep-ph/9908247].

[140] J. M. Alarcón, J. Martin Camalich, and J. A. Oller, Phys. Rev. D **85** (2012) 051503 [arXiv:1110.3797 [hep-ph]].

[141] N. Fettes and U.-G. Meißner, Phys. Rev. C **63** (2001) 045201 [arXiv:hep-ph/0008181].

[142] B. Tromborg, S. Waldenstrøm, and I. Øverbø, Phys. Rev. D **15** (1977) 725.

[143] J. Gasser, A. Rusetsky, and I. Scimemi, Eur. Phys. J. C **32** (2003) 97 [arXiv:hep-ph/0305260].

[144] H. A. Bethe, Phys. Rev. **76** (1949) 38.

[145] P. U. Sauer, Phys. Rev. Lett. **32** (1974) 626; X. Kong and F. Ravndal, Phys. Lett. B **450** (1999) 320 [arXiv:nucl-th/9811076]; J. Gegelia, Eur. Phys. J. A **19** (2004) 355 [arXiv:nucl-th/0310012]; M. Pavón Valderrama and E. R. Arriola, Phys. Rev. C **80** (2009) 024001 [arXiv:0904.1120 [nucl-th]].

[146] G. Gamow, Z. Phys. **51** (1928) 204; A. Sommerfeld, *Atombau und Spektrallinien*, Volume 2, Vieweg, Braunschweig, 1939.

[147] D. V. Bugg and A. A. Carter, Phys. Lett. B **48** (1974) 67.

[148] R. A. Arndt, I. I. Strakovsky, R. L. Workman, and M. M. Pavan, Phys. Rev. C **52** (1995) 2120 [arXiv:nucl-th/9505040].

[149] M. M. Pavan, R. A. Arndt, I. I. Strakovsky, and R. L. Workman, PiN Newslett. **15** (1999) 171 [Phys. Scripta **T87** (2000) 65] [arXiv:nucl-th/9910040].

[150] M. Sainio, private communication.

[151] R. A. Arndt, W. J. Briscoe, I. I. Strakovsky, R. L. Workman, and M. M. Pavan, Phys. Rev. C **69** (2004) 035213 [arXiv:nucl-th/0311089].

[152] G. Höhler, *Pion–Nukleon-Streuung: Methoden und Ergebnisse*, in Landolt-Börnstein, **9b2**, ed. H. Schopper, Springer Verlag, Berlin, 1983.

[153] A. Donnachie and P. V. Landshoff, Phys. Lett. B **296** (1992) 227 [arXiv:hep-ph/9209205].

[154] P. Gauron and B. Nicolescu, Phys. Lett. B **486** (2000) 71 [arXiv:hep-ph/0004066].

[155] L. Montanet *et al.* [Particle Data Group], Phys. Rev. D **50** (1994) 1335.

[156] C. Caso *et al.* [Particle Data Group], Eur. Phys. J. C **3** (1998) 205.

[157] J. J. de Swart, M. C. M. Rentmeester, and R. G. E. Timmermans, PiN Newslett. **13** (1997) 96 [arXiv:nucl-th/9802084].

[158] R. A. Arndt, W. J. Briscoe, I. I. Strakovsky, and R. L. Workman, Phys. Rev. C **74** (2006) 045205 [arXiv:nucl-th/0605082].

[159] U. van Kolck, M. C. M. Rentmeester, J. L. Friar, J. T. Goldman, and J. J. de Swart, Phys. Rev. Lett. **80** (1998) 4386 [arXiv:nucl-th/9710067].

[160] N. Kaiser, Phys. Rev. C **73** (2006) 044001 [arXiv:nucl-th/0601099].

[161] T. P. Cheng and R. F. Dashen, Phys. Rev. Lett. **26** (1971) 594.

[162] L. S. Brown, W. J. Pardee, and R. D. Peccei, Phys. Rev. D **4** (1971) 2801.

[163] V. Bernard, N. Kaiser, and U.-G. Meißner, Phys. Lett. B **389** (1996) 144 [arXiv:hep-ph/9607245].

[164] J. Gasser, H. Leutwyler, and M. E. Sainio, Phys. Lett. B **253** (1991) 260.

[165] R. Koch and E. Pietarinen, Nucl. Phys. A **336** (1980) 331.

[166] M. M. Pavan, I. I. Strakovsky, R. L. Workman, and R. A. Arndt, PiN Newslett. **16** (2002) 110 [arXiv:hep-ph/0111066].

[167] P. Metsä, Eur. Phys. J. A **33** (2007) 349 [arXiv:0705.4528 [hep-ph]].

[168] U.-G. Meißner and S. Steininger, Phys. Lett. B **419** (1998) 403 [hep-ph/9709453]; G. Müller and U.-G. Meißner, Nucl. Phys. B **556** (1999) 265 [hep-ph/9903375].

[169] M. Hoferichter, D. R. Phillips, and C. Schat, Eur. Phys. J. C **71** (2011) 1743 [arXiv:1106.4147 [hep-ph]].

[170] H. Marsiske *et al.* [Crystal Ball Collaboration], Phys. Rev. D **41** (1990) 3324.

[171] J. Boyer *et al.*, Phys. Rev. D **42** (1990) 1350.

[172] H. J. Behrend *et al.* [CELLO Collaboration], Z. Phys. C **56** (1992) 381.

[173] T. Mori *et al.* [Belle Collaboration], J. Phys. Soc. Jap. **76** (2007) 074102 [arXiv:0704.3538 [hep-ex]].

[174] S. Uehara *et al.* [Belle Collaboration], Phys. Rev. D **78** (2008) 052004 [arXiv:0805.3387 [hep-ex]]; Phys. Rev. D **79** (2009) 052009 [arXiv:0903.3697 [hep-ex]].

[175] A. I. L'vov, V. A. Petrun'kin, and M. Schumacher, Phys. Rev. C **55** (1997) 359; D. Drechsel, B. Pasquini, and M. Vanderhaeghen, Phys. Rept. **378** (2003) 99 [arXiv:hep-ph/0212124]; M. Schumacher, Eur. Phys. J. C **67** (2010) 283 [arXiv:1001.0500 [hep-ph]].

[176] J. Bernabeu and J. Prades, Phys. Rev. Lett. **100** (2008) 241804 [arXiv:0802.1830 [hep-ph]].

[177] M. R. Pennington, Phys. Rev. Lett. **97** (2006) 011601.

[178] G. Mennessier, S. Narison, and W. Ochs, Phys. Lett. B **665** (2008) 205 [arXiv:0804.4452 [hep-ph]].

[179] C. Hanhart, Y. .S. Kalashnikova, A. E. Kudryavtsev, and A. V. Nefediev, Phys. Rev. D **75** (2007) 074015 [hep-ph/0701214].

[180] G. Mennessier, S. Narison, and X. G. Wang, Phys. Lett. B **696** (2011) 40 [arXiv: 1009.2773 [hep-ph]].

[181] M. Gourdin, A. Martin, Nuovo Cimento **17** (1960) 224; O. Babelon, J. L. Basdevant, D. Caillerie, M. Gourdin, and G. Mennessier, Nucl. Phys. B **114** (1976) 252; D. Morgan and M. R. Pennington, Z. Phys. C **37** (1988) 431 [Erratum-ibid. C **39** (1988) 590]; Phys. Lett. B **272** (1991) 134; J. F. Donoghue and B. R. Holstein, Phys. Rev. D **48** (1993) 137 [arXiv:hep-ph/9302203].

[182] D. Drechsel, M. Gorchtein, B. Pasquini, and M. Vanderhaeghen, Phys. Rev. C **61** (1999) 015204 [arXiv:hep-ph/9904290].

[183] L. V. Fil'kov and V. L. Kashevarov, Phys. Rev. C **73** (2006) 035210 [arXiv:nucl-th/0512047].

[184] M. R. Pennington, T. Mori, S. Uehara, and Y. Watanabe, Eur. Phys. J. C **56** (2008) 1 [arXiv:0803.3389 [hep-ph]].

[185] J. A. Oller, L. Roca, and C. Schat, Phys. Lett. B **659** (2008) 201 [arXiv:0708.1659 [hep-ph]].

[186] J. A. Oller and L. Roca, Eur. Phys. J. A **37** (2008) 15 [arXiv:0804.0309 [hep-ph]].

[187] Y. Mao, X. G. Wang, O. Zhang, H. Q. Zheng, and Z. Y. Zhou, Phys. Rev. D **79** (2009) 116008 [arXiv:0904.1445 [hep-ph]].

[188] R. García-Martín and B. Moussallam, Eur. Phys. J. C **70** (2010) 155 [arXiv:1006.5373 [hep-ph]].

[189] Yu. M. Antipov *et al.*, Phys. Lett. B **121** (1983) 445.

[190] T.A. Aybergenov *et al.*, Sov. Phys.-Lebedev Inst. Rep. **6** (1984) 32; Czech. J. Phys. B **36** (1986) 948; J. Ahrens *et al.*, Eur. Phys. J. A **23** (2005) 113 [arXiv:nucl-ex/0407011].

[191] J. Bijnens and F. Cornet, Nucl. Phys. B **296** (1988) 557; J. F. Donoghue, B. R. Holstein, and Y. C. Lin, Phys. Rev. D **37** (1988) 2423; S. Bellucci, J. Gasser, and M. E. Sainio, Nucl. Phys. B **423** (1994) 80 [Erratum-ibid. B **431** (1994) 413] [arXiv:hep-ph/9401206]; U. Bürgi, Phys. Lett. B **377** (1996) 147 [arXiv:hep-ph/9602421]; Nucl. Phys. B **479** (1996) 392 [arXiv:hep-ph/9602429].

[192] J. Gasser, M. A. Ivanov, and M. E. Sainio, Nucl. Phys. B **728** (2005) 31 [arXiv:hep-ph/0506265].

[193] J. Gasser, M. A. Ivanov, and M. E. Sainio, Nucl. Phys. B **745** (2006) 84 [arXiv:hep-ph/0602234].

[194] A. V. Guskov [COMPASS Collaboration], Phys. Part. Nucl. Lett. **7** (2010) 192; Nucl. Phys. Proc. Suppl. **198** (2010) 112.

[195] A. R. Edmonds, *Angular momentum in quantum mechanics*, Princeton University Press, Princeton, 1960.

[196] M. Jacob and G. C. Wick, Annals Phys. **7** (1959) 404 [Annals Phys. **281** (2000) 774].

[197] E. P. Wigner, *Gruppentheorie und ihre Anwendungen auf die Quantenmechanik der Atomspektren*, Vieweg Verlag, Braunschweig, 1931.

[198] D. A. Varshalovich, A. N. Moskalev, and V. K. Khersonskii, *Quantum Theory of Angular Momentum*, World-Scientific Publishing, Singapore, 1988.

[199] I. Guiaşu and E. E. Radescu, Annals Phys. **120** (1979) 145.

[200] F. E. Low, Phys. Rev. **96** (1954) 1428.

[201] K. M. Watson, Phys. Rev. **95** (1954) 228.

[202] R. García-Martín, R. Kamiński, J. R. Peláez, and J. Ruiz de Elvira, Phys. Rev. Lett. **107** (2011) 072001 [arXiv:1107.1635 [hep-ph]].

[203] I. Caprini and H. Leutwyler, private communication.

[204] C. Di Donato [KLOE/KLOE-2 Collaboration], AIP Conf. Proc. **1322** (2010) 152 [arXiv:1109.3968 [hep-ex]]; M. Mascolo [KLOE/KLOE-2 Collaboration], J. Phys. Conf. Ser. **349** (2012) 012014; F. Archilli *et al.* [KLOE/KLOE-2 Collaboration], arXiv:1107.3782 [hep-ex]; I. Prado Longhi [KLOE/KLOE-2 Collaboration], in P. Adlarson *et al.*, arXiv:1204.5509 [nucl-ex].

[205] C. Ditsche, M. Hoferichter, B. Kubis, and U.-G. Meißner, JHEP **1206** (2012) 043 [arXiv:1203.4758 [hep-ph]].

[206] J. Gasser, Annals Phys. **136** (1981) 62; V. Bernard, N. Kaiser, and U.-G. Meißner, Z. Phys. C **60** (1993) 111 [hep-ph/9303311].

[207] B. Borasoy and U.-G. Meißner, Annals Phys. **254** (1997) 192 [hep-ph/9607432].

[208] T. D. Cohen, R. J. Furnstahl, and D. K. Griegel, Phys. Rev. C **45** (1992) 1881; G.-Q. Li and C. M. Ko, Phys. Lett. B **338** (1994) 118; N. Kaiser, P. de Homont, and W. Weise, Phys. Rev. C **77** (2008) 025204 [arXiv:0711.3154 [nucl-th]].

[209] A. Bottino, F. Donato, N. Fornengo, and S. Scopel, Nucl. Phys. Proc. Suppl. **113** (2002) 50 [hep-ph/0208273]; Phys. Rev. D **78** (2008) 083520 [arXiv:0806.4099 [hep-ph]]; J. R. Ellis, K. A. Olive, and C. Savage, Phys. Rev. D **77** (2008) 065026 [arXiv:0801.3656 [hep-ph]]; N. Fornengo, S. Scopel, and A. Bottino, Phys. Rev. D **83** (2011) 015001 [arXiv:1011.4743 [hep-ph]]; O. Buchmueller *et al.*, Eur. Phys. J. C **71** (2011) 1722 [arXiv:1106.2529 [hep-ph]]; K. A. Olive, arXiv:1202.2324 [hep-ph].

[210] J. Stahov, PiN Newslett. **15** (1999) 13.

[211] J. Stahov, PiN Newslett. **16** (2002) 116.

[212] G. E. Hite, W. B. Kaufmann, and R. J. Jacob, Phys. Rev. C **71** (2005) 065201.

[213] E. Pietarinen, Preprint Series in Theoretical Physics HU-TFT-17-77, Helsinki University, unpublished.

[214] R. Koch, Z. Phys. C **15** (1982) 161.

[215] J. Stahov, PiN Newslett. **13** (1997) 174.

[216] T. W. B. Kibble, Phys. Rev. **117** (1960) 1159.

[217] D. V. Bugg, A. A. Carter, and J. R. Carter, Phys. Lett. B **44** (1973) 278.

[218] W. R. Frazer and J. R. Fulco, Phys. Rev. **119** (1960) 1420.

[219] S. W. MacDowell, Phys. Rev. **116** (1959) 774.

[220] W. R. Frazer and J. R. Fulco, Phys. Rev. **117** (1960) 1603.

[221] M. Hoferichter, C. Ditsche, B. Kubis, and U.-G. Meißner, JHEP **1206** (2012) 063 [arXiv:1204.6251 [hep-ph]].

[222] W. R. Frazer and J. R. Fulco, Phys. Rev. **117** (1960) 1609.

[223] E. Pietarinen, Nuovo Cim. A **12** (1972) 522.

[224] G. Höhler and E. Pietarinen, Nucl. Phys. B **95** (1975) 210; Phys. Lett. B **53** (1975) 471.

[225] R. Koch, Z. Phys. C **29** (1985) 597.

[226] M. E. Sainio, PoS CD **09** (2009) 013.

[227] R. A. Arndt, R. L. Workman, I. I. Strakovsky, and M. M. Pavan, nucl-th/9807087.

[228] R. A. Arndt, W. J. Briscoe, I. I. Strakovsky, and R. L. Workman, Eur. Phys. J. A **35** (2008) 311.

[229] SAID, `http://gwdac.phys.gwu.edu`.

[230] F. Huang, A. Sibirtsev, J. Haidenbauer, S. Krewald, and U.-G. Meißner, Eur. Phys. J. A **44** (2010) 81 [arXiv:0910.4275 [nucl-th]].

[231] A. V. Anisovich *et al.*, Nucl. Phys. A **662** (2000) 319 [arXiv:1109.1188 [hep-ex]].

[232] T. N. Pham and T. N. Truong, Phys. Rev. D **16** (1977) 896; I. Caprini, Rom. J. Phys. **50** (2005) 7.

[233] S. M. Flatté, Phys. Lett. B **63** (1976) 224; V. Baru, J. Haidenbauer, C. Hanhart, A. E. Kudryavtsev, and U.-G. Meißner, Eur. Phys. J. A **23** (2005) 523 [nucl-th/0410099].

[234] M. M. Nagels, T. A. Rijken, and J. J. de Swart, Phys. Rev. D **17** (1978) 768; P. M. M. Maessen, T. A. Rijken, and J. J. de Swart, Phys. Rev. C **40** (1989) 2226; V. G. J. Stoks, R. A. M. Klomp, C. P. F. Terheggen, and J. J. de Swart, Phys. Rev. C **49** (1994) 2950 [nucl-th/9406039]; T. A. Rijken, H. Polinder, and J. Nagata, Phys. Rev. C **66** (2002) 044009 [nucl-th/0201020].

[235] G. C. Oades, PiN Newslett. **15** (1999) 307; B. R. Martin and G. C. Oades, PiN Newslett. **16** (2002) 133.

[236] N. Fettes, Thesis, University of Bonn, 2000.

[237] N. Fettes, U.-G. Meißner, and S. Steininger, Nucl. Phys. A **640** (1998) 199 [hep-ph/9803266].

[238] B. Moussallam, Eur. Phys. J. C **14** (2000) 111 [arXiv:hep-ph/9909292].

[239] J. F. Donoghue, J. Gasser, and H. Leutwyler, Nucl. Phys. B **343** (1990) 341.

[240] S. Descotes-Genon, Thesis, Université de Paris–Sud, 2000.

[241] D. H. Cohen, D. S. Ayres, R. Diebold, S. L. Kramer, A. J. Pawlicki, and A. B. Wicklund, Phys. Rev. D **22** (1980) 2595; A. Etkin *et al.*, Phys. Rev. D **25** (1982) 1786.

[242] J. S. Hyslop, R. A. Arndt, L. D. Roper, and R. L. Workman, Phys. Rev. D **46** (1992) 961.

[243] B. Ananthanarayan, I. Caprini, G. Colangelo, J. Gasser, and H. Leutwyler, Phys. Lett. B **602** (2004) 218 [arXiv:hep-ph/0409222].

[244] J. A. Oller and L. Roca, Phys. Lett. B **651** (2007) 139 [arXiv:0704.0039 [hep-ph]].

[245] M. Frink, B. Kubis, and U.-G. Meißner, Eur. Phys. J. C **25** (2002) 259 [arXiv:hep-ph/0203193].

[246] J. Bijnens and P. Dhonte, JHEP **0310** (2003) 061 [hep-ph/0307044].

[247] H. Pagels and W. J. Pardee, Phys. Rev. D **4** (1971) 3335.

[248] A. Schenk, Nucl. Phys. B **363** (1991) 97.

[249] G. Wanders, Helv. Phys. Acta **39** (1966) 228; F. P. Palou and F. J. Ynduráin, Nuovo Cim. A **19** (1974) 245.

[250] K. Takeda *et al.* [JLQCD Collaboration], Phys. Rev. D **83** (2011) 114506 [arXiv: 1011.1964 [hep-lat]].

[251] S. Dinter, V. Drach, R. Frezzotti, G. Herdoiza, K. Jansen, and G. Rossi, arXiv:1202.1480 [hep-lat].

[252] W. Freeman and D. Toussaint [MILC Collaboration], arXiv:1204.3866 [hep-lat].

[253] Bateman Manuscript Project, *Higher Transcendental Functions*, **1**, ed. A. Erdélyi, McGraw-Hill, New York, 1953.

[254] G. F. Chew, M. L. Goldberger, F. E. Low, and Y. Nambu, Phys. Rev. **106** (1957) 1337.

[255] B. Holzenkamp, K. Holinde, and J. Speth, Nucl. Phys. A **500** (1989) 485.

[256] M. J. Musolf, H.-W. Hammer, and D. Drechsel, Phys. Rev. D **55** (1997) 2741 [Erratum-ibid. D **62** (2000) 079901] [hep-ph/9610402].

Acknowledgments

First of all, I would like to thank my advisor Prof. Ulf-G. Meißner for suggesting an exciting (and challenging!) thesis project, for his support and encouragement over the last three years, his unwavering belief in the viability and superiority of the Roy–Steiner approach, and last but not least for tolerating and supporting my getting distracted from the pure pion–nucleon path in one way or another. Further, I am very grateful to Prof. Hans-Werner Hammer for accepting to assess this thesis, despite the fact that some parts inevitably turned rather technical.

Part I originates predominantly from work done in collaboration with Dr. Vadim Baru, PD Christoph Hanhart, PD Bastian Kubis, Dr. Andreas Nogga, and Prof. Daniel R. Phillips (the "JOB collaboration"). Thank you all for an enjoyable collaboration, which revealed to me many facets of chiral effective field theory and the challenges in the nucleon–nucleon system that would have remained concealed otherwise.

Furthermore, I would like to express my gratitude towards Prof. Daniel R. Phillips and Dr. Carlos Schat for a pleasant collaboration during my visit at Ohio University, which led to the work presented in Part II of this thesis. Special thanks to Daniel for encouraging and supporting my stay at Ohio University, for the help in the visa and DAAD application process (thanks also to Ulf, Hans-Werner, and Bastian for support in the application), for suggesting a project that should prove remarkably beneficial for the pion–nucleon case as well, for helping me organize visits to UCSD, UW, GWU, and UMD, and above all for taking a lot of time for a project outside the group's main direction of research. Moreover, I would like to thank the whole Institute of Nuclear and Particle Physics for its hospitality during my visit, Dr. Johannes Kirscher and Stefan Kölling for help in many organizational issues in the Athens "wasteland," and last but not least Dr. Anton Wiranata for saving me from five Badminton-free months in Athens county.

Further thanks to Christoph Ditsche for a pleasurable collaboration on pion–nucleon Roy–Steiner equations—it has been quite a relief to be able to share the unavoidable periods of frustration as well as the rare moments of joy, not to mention to have cross-checks that are invaluable in a project as widespread as this one—and to Bastian for accompanying us in this process with advice, encouragement, and healthy skepticism, for finally helping to bring the notes of the calculation into a publishable form, and for proof-reading large parts of this thesis. In addition, I would like to thank Prof. Gilberto Colangelo and Dr. Bachir Moussallam for numerous helpful discussions, and acknowledge useful correspondence with M. Albaladejo, S. Descotes-Genon, D. Gotta, V. A. Nikonov, J. A. Oller, J. Peláez, H. Polinder, T. Rijken, M. Sainio, and A. V. Sarantsev.

Thanks to my long-term office mate Sebastian Schneider for many valuable discussions, in particular for exchanging workarounds for LaTeX, Mathematica, and Xmgrace bugs, to Sebastian König for help on programming issues and general IT support, and to the whole HISKP theory group for a pleasant working atmosphere.

Finally, I would like to thank my family for all the support over a long PhD work. Above all, thanks for accepting blurry pictures of what particle physics is all about, and for giving credence to my assurances that the claims of discoveries of superluminal neutrinos and suchlike that repeatably made it into the press over the last years should be taken with extreme care.

Financial support for the research presented in this thesis was provided by the DFG (SFB/TR 16, "Subnuclear Structure of Matter"), the program "Kurzstipendien für Doktorand-Innen" of the DAAD, and the Bonn–Cologne Graduate School of Physics and Astronomy.